プロジェクト 1

平成12年～平成16年 文部科学省私立大学学術研究高度化推進事業
バイオベンチャー研究開発拠点整備事業研究成果報告書

糖鎖シグナルと生体防御

平成17年4月　京都産業大学

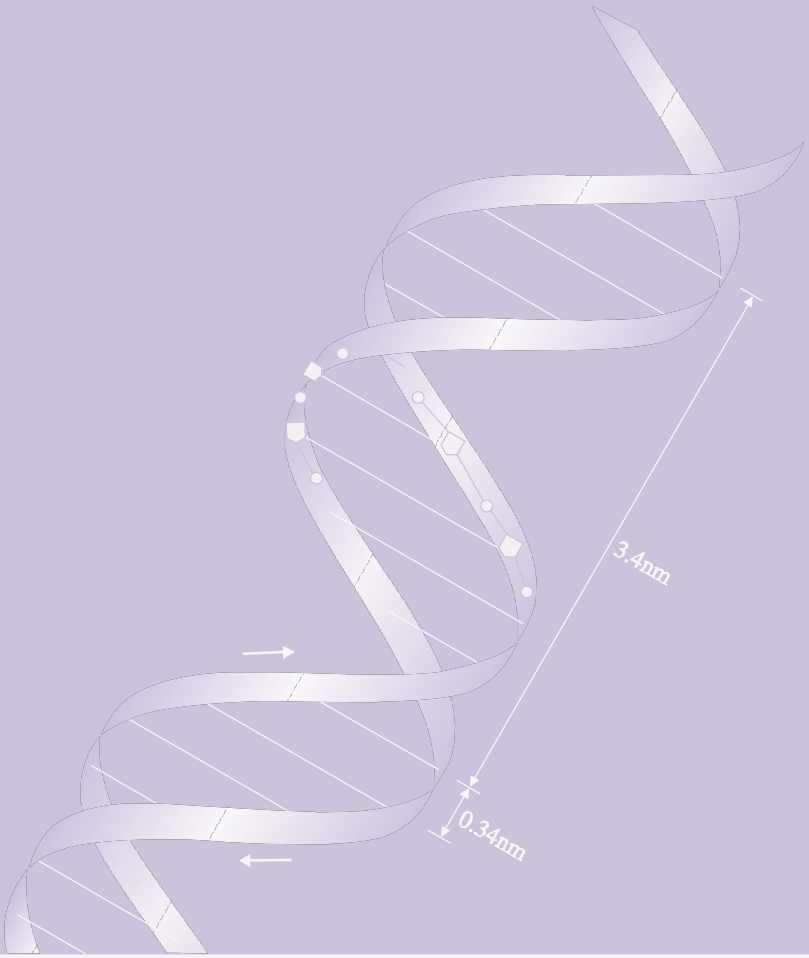

バイオ・ベンチャー　プロジェクト１

「糖鎖シグナルと生体防御」

平成 12 年度～平成 16 年度私立大学学術研究高度化推進事業

「バイオ・ベンチャー研究開発拠点整備事業」研究成果報告書

平成１７年４月

学校法人 京都産業大学

京 都 産 業 大 学

工学研究科（生物系）

中田　博（京都産業大学工学部教授）

【　目　　次　】

研究成果報告書の発刊にあたって

京都産業大学工学部生物工学科教授
バイオベンチャープロジェクト代表　中田　博

文部科学省私立大学学術研究高度化推進事業のバイオ・ベンチャー開発拠点整備事業「バイオ・ベンチャープロジェクト」に採択され、「糖鎖シグナルと生体防御」及び「高等植物のオルガネラゲノム工学」の 2 つのテーマで研究を進めてきました。最終年度にあたり、それぞれのテーマで報告書を提出する運びとなりました。21 世紀はライフサイエンスの時代と言われています。本分野においては、ヒトゲノムの解析が終了し、予防医学やテーラーメイド医療に大きな進展を見ました。その反面、新たな課題がクローズアップされ、ポストゲノム研究という形で糖鎖の研究は最重要課題の 1 つとなってきました。本学の「糖鎖シグナルと生体防御」の研究は、時代に先駆けてその問題に着手したことになり、時機を得たものでありました。

我々は、遺伝子レベルで得られた知見を背景として、あるいはその技術を利用し、あくまで生物学的現象を分子レベルでとらえるという試みを繰り返してきました。その結果、担癌状態における免疫抑制機構、癌転移における原因分子の同定と分子メカニズムの解析、及び肺癌や喫煙時のマクロファージを中心とした解析において、極めてオリジナリティーの高い特筆すべき結果を得ることが出来ました。さらに、このような分子メカニズムの解析の延長線上に、応用として免疫抑制剤や抗腫瘍剤の開発などで 2 件の特許申請がなされたことも大きな成果としてあげられます。糖鎖生物学は今後ともポストゲノムの中心課題として発展していくことが期待されています。この 5 年間で得られた成果を基礎として、糖鎖研究の拠点を形成し、さらなる発展を期す所存であります。

研 究 組 織

京都産業大学工学部生物工学科・教授 （プロジェクト１ 代表）	中田　博
京都産業大学工学部生物工学科・教授	岡山　實
京都産業大学工学部生物工学科・教授	竹内　実

共同研究者

愛知医科大学分子医科学研究所・所長	木全弘治
水谷糖質科学振興財団・事務局長	吉田圭一
愛知がんセンター研究所 第一病理学教室・室長	中西速夫
京都府立医科大学血管系老化センター 病態病理学部門・教授	伏木信次
関西医科大学第一生理学教室・講師	山本章嗣
京都府立医科大学微生物学教室・助教授	松田　修
鹿児島大学医学部公衆衛生学教室・教授	竹内　亨
㈱協和エンジニアリング・主任研究員	清水要志夫

腫瘍組織形成におけるムチンの生物学的意義と臨床的応用

要旨

上皮性癌細胞の産生するムチンが、免疫担当細胞上の受容体を介して、様々な生物学的作用をもたらし、癌細胞の増殖・進展に有利な環境を形成していることを明らかにした。

先ず、ムチンが単球／マクロファージ上のスカベンジャーリセプター（SCR）を介して、シクロオキシゲナーゼ2（COX2）を誘導し、プロスタグランジンE_2（PGE_2）の産生を亢進することを見いだした。すなわち、ヒト大腸癌由来細胞株LS 180細胞の産生するムチン（MUC2）を精製し、ヒト末梢血単球に加えると、濃度依存的にCOX2 mRNA及びCOX2酵素タンパク質が誘導され、PGE_2の産生が増加することがわかった。ムチンの単球への結合は、ポリイノシン酸やフコイダンで阻害されることから、受容体はSCRであると予想された。SCR cDNAのトランスフェクタントへのムチンの結合、あるいは可溶型SCRのムチンへの結合により、SCRがムチンの受容体であることを確認した。単球／マクロファージのCOX2誘導は、100 ng/ml程度のムチンで可能であり、in vivoでも起こりうる現象であると考えられた。事実、正常ヒト末梢血単球に担癌患者血清を加えた場合でも、同様の現象が見られた。また、ヒト大腸癌組織において、免疫組織化学的な研究結果より、ムチンの存在部位あるいは近傍に浸潤したマクロファージにおいてCOX2の誘導が観察された。

PGE_2は、血管新生、免疫抑制、アポトーシスの抑制などの生理活性をもつことが知られており、COX2の誘導は、癌組織の増殖・進展に重要な役割を果たすことが予想される。

先ず、血管新生について、マウス乳癌由来細胞株TA3の亜株であるムチン産生株のTA3-Ha細胞と非産生株のTA3-St細胞を用いて比較検討した。TA3-Haと-St細胞において、in vitroの増殖速度はほぼ同程度であったが、マウスの皮下腫瘍の場合は、TA3-Haの方が著しく早く増殖した。組織におけるCOX2 mRNA、COX2タンパク質の誘導、VEGF mRNAの誘導、活性型MMP-2の存在量を比較したところ、いずれもTA3-Haの方が有意に高い値を示した。これは、TA3-Haと-Stの腫瘍組織の組織化学的データの比較とも一致した。すなわち、組織に浸潤したマクロファージの数はほぼ同じであったが、TA3-Ha腫瘍組織のマクロファージにCOX2の誘導が観察され、血管新生も著しく亢進していた。次

に、ムチンによる免疫バランス（Th1/Th2）に対する影響について検討した。ムチンによる抗体産生能への影響について、in vitro、in vivo において羊赤血球に対する抗体産生をムチン存在下、非存在下で調べた。In vitro では、ムチンをはじめとする SCR のリガンド存在下でマウス脾細胞と羊赤血球を培養すると、抗体産生能は 2～3 倍増加した。また、この効果は、SCR ノックアウトマウスの脾細胞を用いることにより半減した。In vivo では、腹腔内へムチン及び羊赤血球を注射し、抗体産生能を見ると、～30%の増加が見られた。また、マクロファージ、CD4 陽性 T 細胞からのそれぞれ IL-12 (p70)、IFN-γの産生は、ムチンによりいずれも抑制された。また、TA3-Ha 及び TA3-St 細胞をマウス皮下に注射し、3 週間後にそれぞれの脾臓を摘出し、CD4 陽性 T 細胞の内、IL-4、IFN-γの産生細胞を FACS により検出した。その結果、IL-4 産生細胞には差は見られなかったが、IFN-γ産生細胞は、TA3-Ha 担癌マウスで減少していることがわかった。免疫バランスがムチンにより Th2 に偏ることを示唆している。

次に、腫瘍組織形成に対する可溶型 SCR の効果を検討した。すなわち、Ha 細胞に可溶型 SCR 遺伝子を導入し、マウス皮下における腫瘍形成を比較した。可溶型 SCR 強制発現細胞では、生着率や腫瘍形成速度の低下が見られた。さらに、同強制発現細胞に Ha 細胞を加えた場合でも、Ha 細胞単独よりも腫瘍組織形成は著しく遅れることがわかった。従って、腫瘍組織への可溶型 SCR の分泌は、ムチンのマクロファージへの結合をブロックし、腫瘍組織形成を抑制することがわかった。

これらの結果は、癌組織微小環境において、ムチンを起点としたカスケードが癌組織の形成に重要な役割を担っていることを示している。COX2 阻害剤が治療薬として使用されようとしていることからも、そのカスケードの上流でのブロックも有効である可能性が高い。

免疫系細胞の多くは、細胞表面にシグレックファミリーと呼ばれるレクチンを発現している。多くのシグレックファミリーは、その細胞質側に ITIM と呼ばれる免疫抑制性のシグナルを伝達するモチーフを持っている。我々は、シグレック 2，3，7，9 の可溶型を作製し、ムチンと結合することを示した。シグレック 2 に関しては、同分子の発現株であるバーキットリンパ腫の Daudi 細胞や強制発現株である K46μmλ細胞を用いて、情報伝達について検討した。ムチン存在下での B 細胞受容体を介した情報伝達において、ムチンの濃度依存的に MAPK のリン酸化が抑制されることがわかった。共焦点顕微鏡による観察から、

B 細胞受容体のラフトへの移行がムチンにより抑制されることに起因することが示唆された。他の免疫系細胞においても同様の機構が考えられ、現在検討中である。

1．序論

腫瘍細胞の増殖・進展過程には、宿主との様々な相互作用が関与している。その相互作用は、様々なサイトカインや生理活性物質が仲介していると考えられている。そのような因子が宿主の免疫系細胞などから産生されることがあり、本来、腫瘍に対して抵抗性を示す生体防御機構が逆に利用され、腫瘍細胞の増殖・進展に対して有利な環境をもたらしている可能性がある。このような機能を担う細胞として、免疫抑制マクロファージや TAM（Tumor-associated macrophage）が考えられているが、これらの細胞の実体とどのような機構でそのような因子を産生するかなどの分子的背景は明確でない。また、マクロファージ以外の免疫担当細胞にも、シグレックファミリーと呼ばれるレクチンが発現している。ムチンの場合、このレクチンに結合する可能性は十分に考えられる。加えて、これらのレクチンの細胞質側には、ITIM と呼ばれる免疫抑制性のシグナルを伝達するモチーフが存在する。これらの受容体を介した情報伝達による免疫抑制も十分に考えられる。

2．上皮性癌細胞の産生するムチンの生物学的意義

2－1．ムチンによる SCR を介した単球／マクロファージの活性化とその生物学的作用[1,2)]

我々は、ムチンと免疫系細胞の相互作用を検討する過程で、ムチンが単球／マクロファージを活性化し、PGE2 の産生を亢進することを見いだした。すな

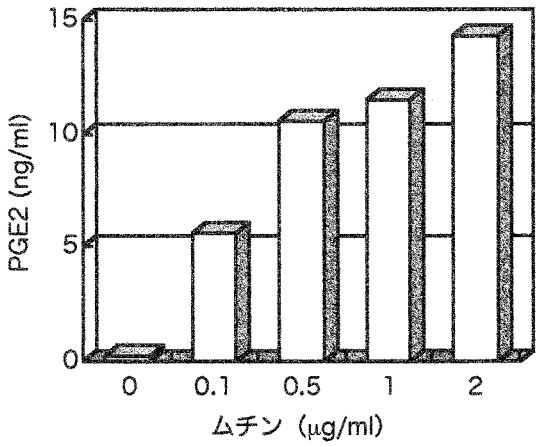

図 1　ムチンによる単球の PGE2 産生亢進

わち、ヒト大腸癌由来細胞株 LS 180 細胞の産生するムチンにより、濃度依存的にヒト末梢血単球からの PGE_2 の産生が亢進することがわかった（図 1）。受容体を検索する目的で、^{125}I で標識したムチンを用いて、単球への結合を種々の阻害剤の存在下で検討したところ、ムチン、フコイダン、ポリイノシン酸などで阻害される一方、ポリシチジル酸やオロソムコイドなどではほとんど阻害されなかった（図 2A）。この性質は、SCR のリガンドの性質に一致した。さらに、SCR cDNA の安定発現株を用いて同様の結合実験を行い、ムチンが SCR に結合することを確認した（図 2 B）。SCR は、分子上に適当な配置で陰性荷電を持つ分子と結合することが知られており [3]、ムチン上のシアル酸や硫酸基の負電荷が結合に寄与しているものと考えられる。

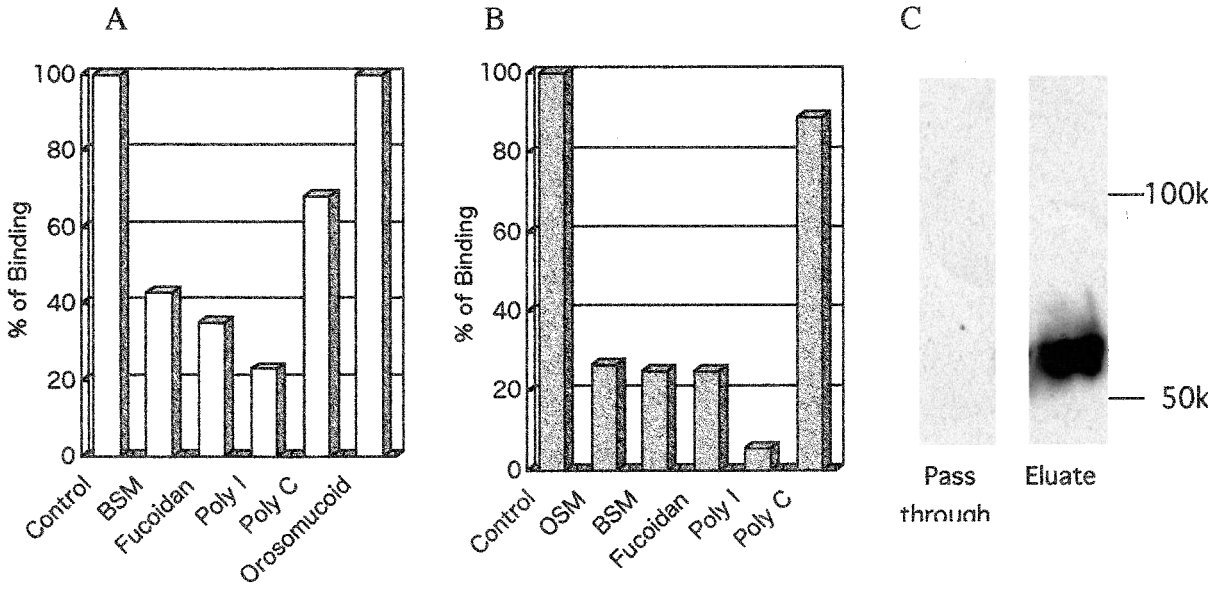

図 2 ムチンの SCR への結合
A：^{125}I 標識ムチンの単球（1 x 10^6 細胞）への結合を、様々な阻害物質存在下で 4℃、2 時間インキュベート後、測定した。
B：同様に、^{125}I 標識ムチンの結合を、SCR cDNA トランスフェクタント（1 x 10^6 細胞）を用いて検討した。
C：FLAG タグ付き可溶型 SCR を作製し、BSM-セファロースのカラムに通した。素通り及び溶出画分を回収し、電気泳動を行った。ウエスタンブロッティング後、抗 FLAG 抗体で検出した。

近年、腫瘍組織におけるシクロオキシゲナーゼ（COX）2 の誘導と PGE_2 の産生亢進が腫瘍の増殖・進展に関与することが報告されている [4-6]。しかし、腫瘍組織において最初にどの細胞で、どのような機構で COX2 が誘導され、PGE_2 の産生が亢進するかは未解明であった。我々の見いだした現象が、この機構の

一部を説明しうると考え、COX2 の誘導について検討した。その結果、単球における COX2 も、ムチンの濃度依存的に誘導されることがわかった（図 3）。また、ヒト大腸癌組織で浸潤マクロファージ、COX2、ムチンの分布を組織化学的に調べたところ、浸潤したマクロファージの近傍にムチンが存在する場合には、マクロファージに COX2 タンパク質が検出された（図 4）。従って、in vivo においても同様の現象が起こっているものと考えられる。

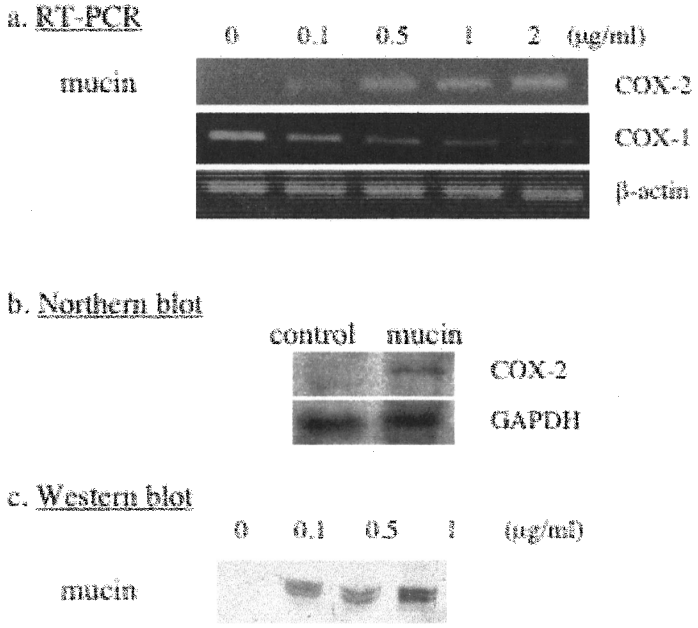

図 3 ムチンによる単球の COX2 の誘導
a：ヒト末梢血単球（5 x 10^6 細胞）をムチン（0～2 μg/ml）存在下で 2 時間培養した。RNA を調製し、RT-PCR を行った。
b：ヒト末梢血単球（2 x 10^7 細胞）をムチン（1 μg/ml）存在下で 2 時間培養した。RNA を調製し、10 μg をアガロース電気泳動し、ノーザンブロットを行った。
c：a の試料のタンパク質画分より、抗 COX-2 抗体により免疫沈降し、沈殿物を電気泳動後、ウエスタンブロッティングを行った。同じ抗体を用いて COX-2 タンパク質を検出した。

次に、マウス乳癌由来細胞株 TA3 細胞を用いて検討した。なお、TA3 細胞には、亜株としてエピグリカニンと呼ばれるムチンを産生する TA3-Ha 細胞と、非産生株の TA3-St 細胞が存在し、双方の腫瘍形成等について比較した。エピグリカニンによるマウス腹腔マクロファージからの PGE_2 の産生亢進を確認するとともに、過剰生産された PGE_2 による血管新生と Th1/Th2 の免疫バランスに対する効果を検討した。TA3-Ha、-St 細胞について、in vitro における増殖速度はほぼ同じであったが、マウス背皮下における腫瘍形成速度は TA3-Ha 細胞の方が著しく早かった（図 5）。双方の腫瘍組織について、生化学的及び免疫組織化学的手法を用いて比較検討した。組織抽出物より、COX2 mRNA、COX2 タンパク質、VEGF mRNA 及び活性型 MMP-2 などについて比較したところ、いずれも TA3-Ha 腫瘍組織の方が高い値を示した（図 6）。また、免疫組織化学による結果でも、双方の腫瘍組織に浸潤したマクロファージの数は同等であった

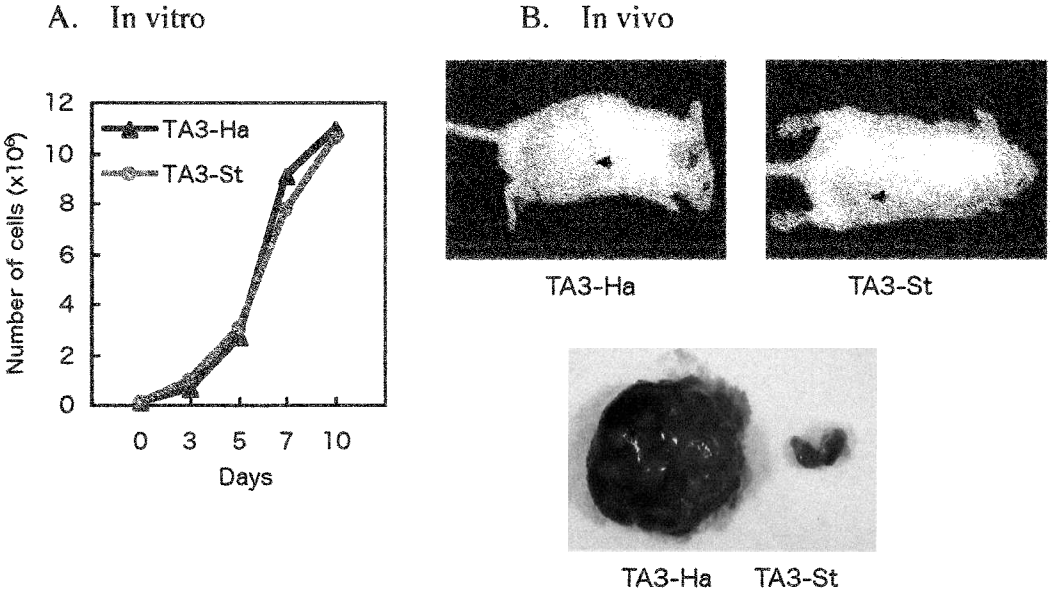

図 5 マウス乳癌細胞株 TA3-Ha、TA3-St の皮下腫瘍形成
A：TA3-Ha、-St 細胞（各々1 x 10^5 細胞）を培養した。
B：TA3-Ha、-St 細胞（各々1 x 10^5 細胞）をマウス背皮下に注射し、15 日後に腫瘍組織を摘出した。

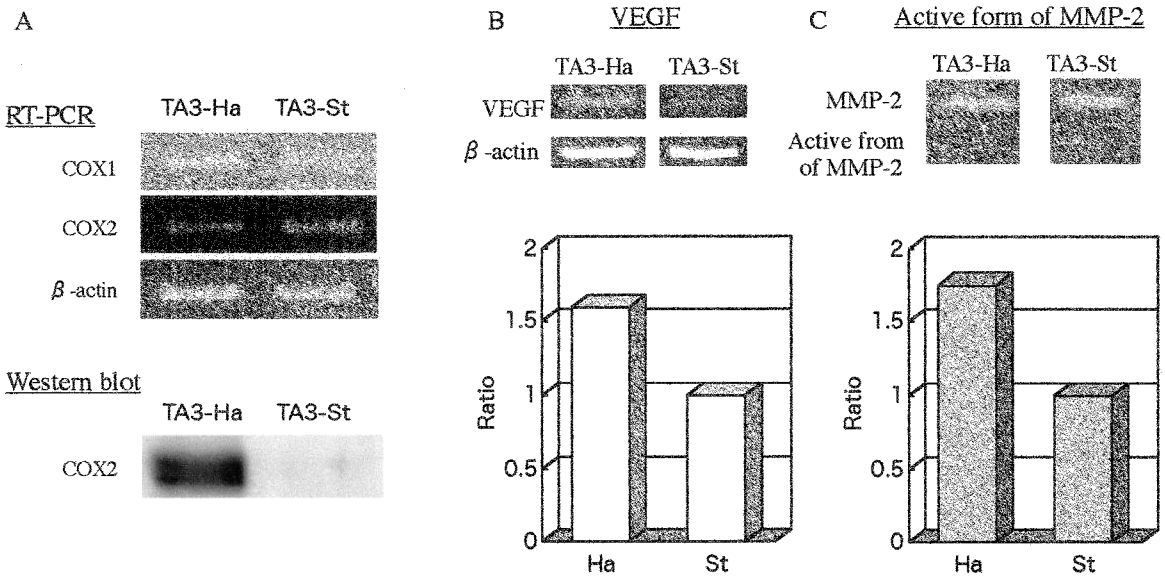

図 6 マウス乳癌細胞株 TA3-Ha、TA3-St 腫瘍組織における血管新生関連因子の誘導
A：TA3-Ha、-St 細胞（1 x 10^6 細胞）をマウス背皮下に注射し、1 週間後に腫瘍組織を摘出し、RNA 及びタンパク質画分を調製した。RT-PCR により、COX2、COX1、β-actin の発現を比較した。タンパク質画分より免疫沈降により COX2 酵素タンパク質を調製した。電気泳動後、ウエスタンブロッティングを行い、抗 COX2 抗体により検出した。
B：同様に調製した RNA を用いて、RT-PCR を行い、アガロース電気泳動後、そのバンドの濃さを数値化して VEGF mRNA の発現を比較した。
C：同様の腫瘍組織よりタンパク質画分を調製し、電気泳動後ゼラチンザイモグラフィーにより活性化型 MMP-2 酵素タンパク質を検出し、そのバンドの濃さを数値化して比較した。

が、TA3-Ha 腫瘍組織に浸潤したマクロファージに COX2 タンパク質が検出さ

れるとともに、著しい血管新生が認められた（図 7）。次に、Th1/Th2 バランスに対するムチンを起点とする PGE2 の効果について検討した。先ず、in vitro、in vivo ともにムチン処理により抗体産生能の亢進が見られた。その効果は、SCR ノックアウトマウスの脾細胞を用いることにより著しく減少した。また、マクロファージからの IL-12 の産生、あるいは CD4 陽性 T 細胞からの IFN-γの産生に関しても、ムチンの処理により産生量が低下することがわかった。これらの結果及び武藤らの報告 [7]を考慮に入れると、癌組織微小環境において、図 8 に示すようなカスケードが考えられる。すなわち、癌細胞より分泌されたムチンが、浸潤マクロファージに結合し、COX2 が誘導される。産生された PGE2 は、マクロファージや周辺の細胞に発現している EP2 リセプターを介してオートクライン、パラクラインに作用し、これらの細胞を活性化する。その結果、さらに COX2 が誘導され、PGE2 の産生が亢進する。PGE2 は、VEGF や MMP-2 の誘導を介して血管新生を促進するとともに、Th1 サイトカインの産生を抑制し、Th2 に偏った状態をもたらす。これらの状況は、マクロファージが腫瘍細胞の増殖・進展に有利な環境をもたらしていることになり、従来から指摘されている免疫抑制マクロファージあるいは TAM の実体であるとも考えられる。

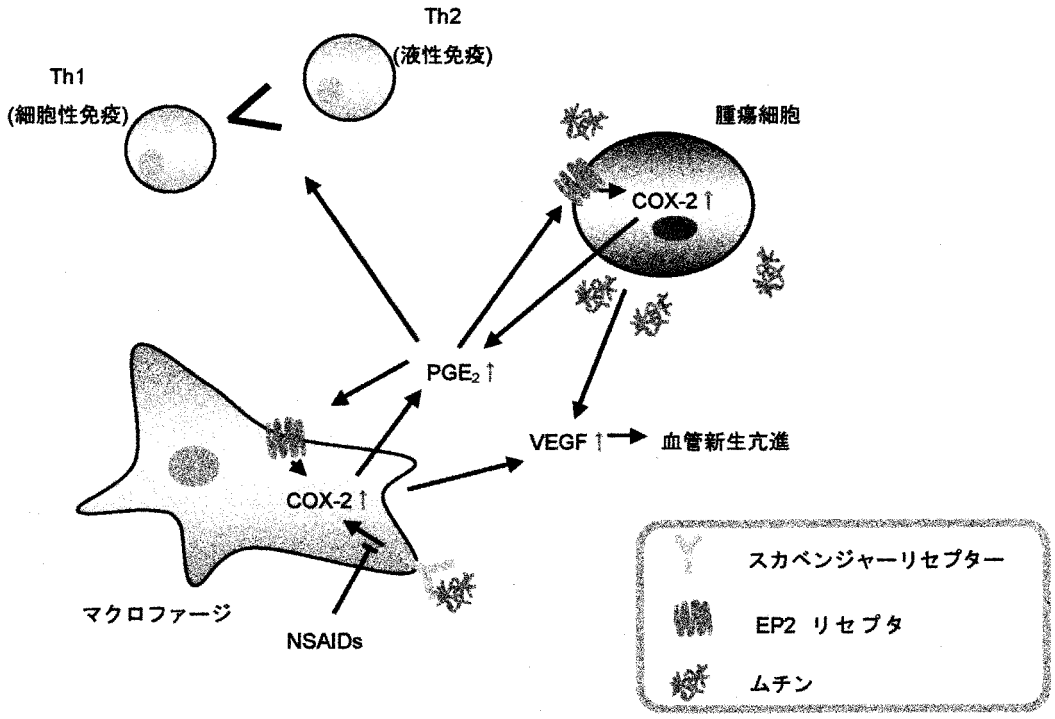

図 8　癌組織微小環境におけるムチンを起点としたカスケード

2－2．シグレックファミリー分子を介した免疫抑制機構の解析

多くのシグレックファミリーは、免疫担当細胞に発現し、細胞質側に ITIM をもつレクチン [8]であるが、生体における内在性リガンドはほとんど明らかにされていない。シグレック分子は、シアル酸を含む糖鎖を認識することから、上皮性癌細胞の産生するムチンがそのリガンドとなる可能性は十分にあると考えられた。ヒト大腸癌細胞 LS 180 の産生するムチンや BSM のシグレック 2 への結合は、シグレック 2 発現細胞であるヒトリンパ腫 Daudi 細胞やシグレック 2 cDNA 強制発現細胞を用いて明らかにした（図 9)。また、これらの細胞を用いて、ムチン存在下で B 細胞受容体を刺激すると、シグレック 2 分子のリン酸化の減少、SHP-1 のリクルートの減少、続いて MAPK のリン酸化の減少が見られた（図 10)。この一連の反応は、従来のシグレック 2 を介したシグナル伝達とは異なる結果が得られた。同様の条件で、共焦点顕微鏡を用いて B 細胞受容体の動きを観察すると、ムチン存在下ではラフトへの移行が抑制されていることがわかった（図 11)。これは、シグレック 2 に対して多数の結合部位をもつムチンが、細胞表面上のシグレック 2 分子を架橋することによる現象と考え、さらに詳細に検討中である。さらに、シグレック 3, 7 及び 9 についても可溶型シグレック分子を作製し、ムチンへの結合を確認するとともに、情報伝達及び生物学的活性への影響についても検討中である。

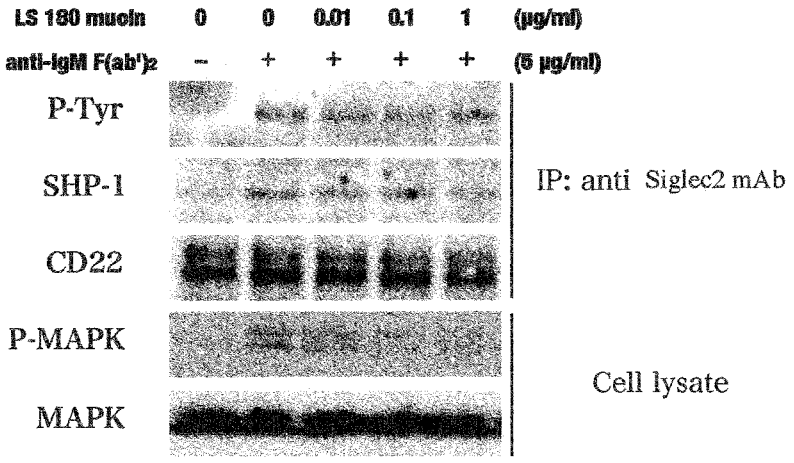

図 10 Daudi 細胞における情報伝達へのムチンの影響
図中に示すムチンの存在下で、細胞を BCR に対する抗体で刺激した。3 分後に細胞を回収し、抗シグレック 2 抗体で免疫沈降し、電気泳動、ウエスタンブロッティング後に抗 p-Tyr 抗体、抗 SHP-1 抗体で検出した。また、lysate を電気泳動し、ウエスタンブロッティング後に抗 p-MAPK 抗体で検出した。

3．考察・展望

COX2 の誘導と癌の悪性化については多くの報告があるが、その誘導メカニズムについてはほとんど研究されてこなかった。ムチンを起点とする誘導機構は、その一部を説明するものと考えられる。ムチンと癌の悪性度との関連性を示す分子的背景を明らかにしたという意味では、今後の臨床的展望を開く上で大きな意味をもつと考えている。また、SCR の様に分子パターンを認識する受容体として、Toll-like receptor などもマクロファージ／樹状細胞に存在することが知られており、同様の機構が存在する可能性は十分にある。今後の検討課題である。一方、シグレック分子による免疫抑制機構についても、正常な状態における生物学的意味は明確でないが、少なくとも担癌状態においては、ムチンにより抑制状態にあることを示した点は大きな意味があると考えている。また、その影響もそれぞれの免疫担当細胞において 20～30%の機能低下をもたらすと予想される。担癌患者における 5 年生存率の関連性を説明する数値といえる。何故なら、20～30%の機能低下でも、持続的にその状態が続くとすれば大きな意味をもつと考えられるからである。今後、分子レベルでその抑制機構をより明確にし、担癌患者における抑制の解除方法の開発及び免疫過敏状態における抑制方法の開発という 2 つの観点から研究を進めていきたい。

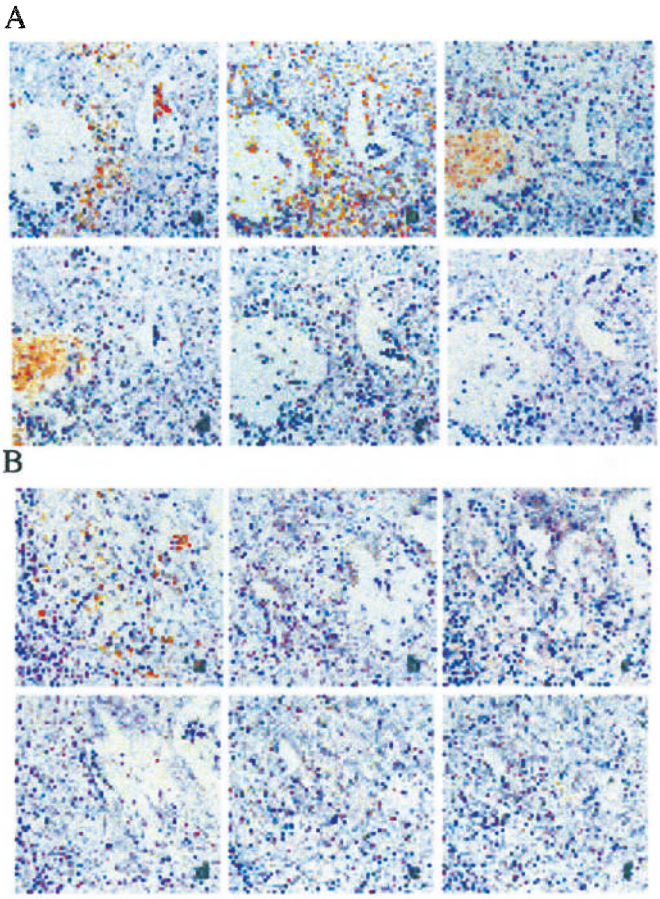

図 4 大腸癌組織におけるマクロファージ、COX2 及び癌関連糖鎖抗原の分布
A、B：a；CD68（マクロファージ）、b；COX2 タンパク質、c；Tn 抗原、d；シアリル Tn 抗原、e, f；コントロール抗体のみによる染色

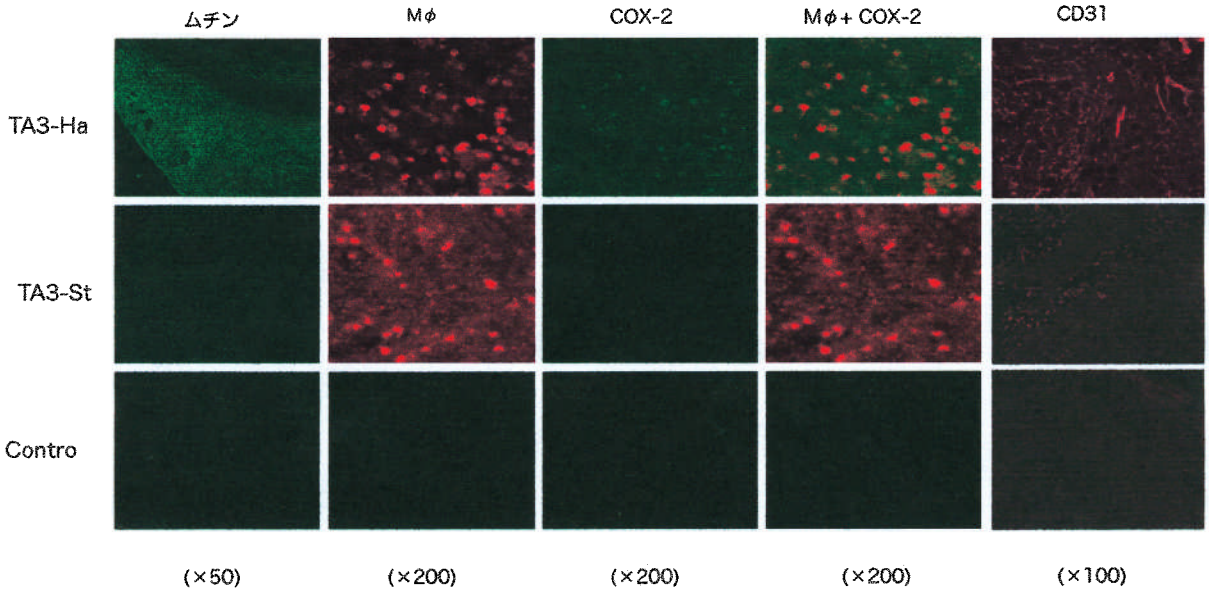

図 7 マウス乳癌細胞株 TA3-Ha、TA3-St 腫瘍組織におけるムチン、マクロファージ、COX2 及び CD31 の分布
TA3-Ha、-St 腫瘍組織を 4%パラホルムアルデヒドで固定し、凍結切片を作製した。各抗体を一次抗体として用い、FITC 又はローダミン標識二次抗体により検出した。コントロールは、一次抗体を用いずに同様の処理を行った。

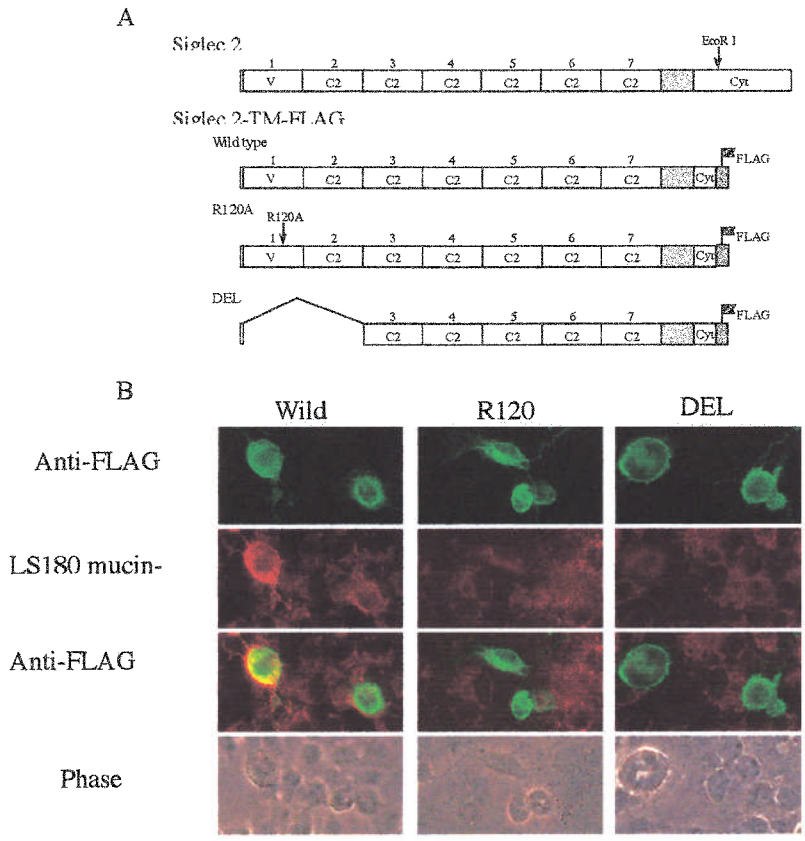

図 9 ムチンのシグレック 2 cDNA トランスフェクタントへの結合

A：3 つのシグレック 2 cDNA コンストラクトを作製した。R120A は、N 末端より 120 番目のアミノ酸である Arg を Ala に変換したものである。120 番目の Arg は、SA の結合に必須とされている。DEL は、糖鎖との結合に必要とされる領域を欠損させたコンストラクトである。

B：それぞれの cDNA トランスフェクタントへのムチン（LS 180 細胞より単離）の結合を調べた。

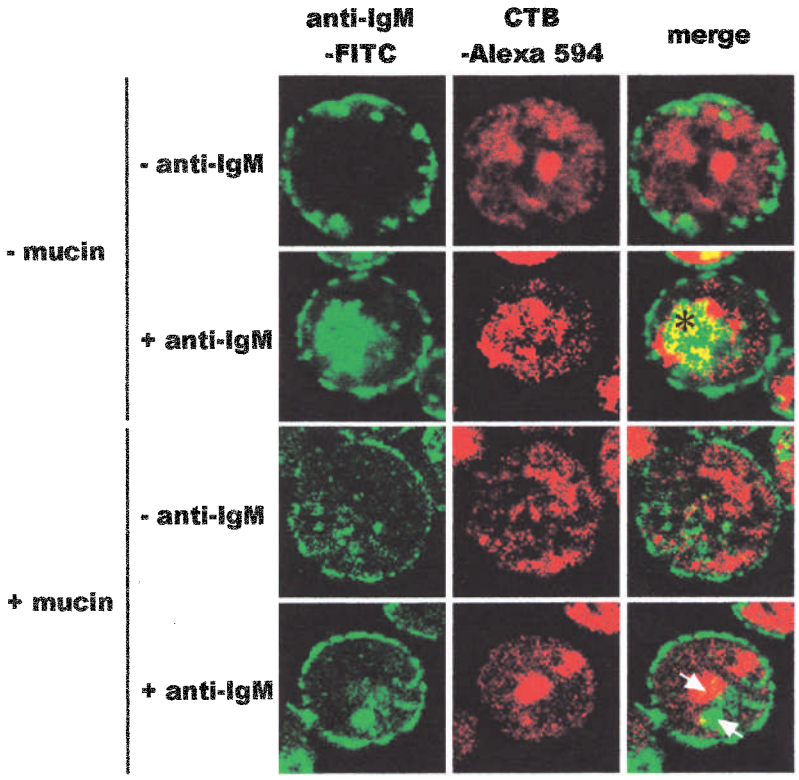

図 11 ラフトへの BCR の移行に対するムチンの影響

Anti IgM-FITC は BCR の動きを示す。CTB-Alexa 594 はラフトの位置を示す。ムチン非存在下では、BCR に抗 IgM 抗体が結合することにより、BCR はラフトに移行する（＊）。ムチン存在下では、矢印に示すようにラフトへの移行が抑制されている。

参考文献

1) Inoue, M., Fujii, H., Kaseyama, H., Yamashina, I. and Nakada, H. Stimulation of macrophages by mucins through a macrophage scavenger receptor. (1999) Biochem. Biophys. Res. Commun., **264**: 276-280.

2) Inaba, T., Sano, H., Kawahito, Y., Hla, T., Akita, K., Toda, M., Yamashina, I., Inoue, M. and Nakada, H. (2003). Induction of cyclooxygenase-2 in monocyte/macrophage by mucins secreted from colon cancer cells. Proc. Natl. Acad. Sci. USA, **100**: 2736-2741.

3) Doi, T., Higashino, K., Kurihara, Y., Miyazaki, T., Nakamura, H., Uesugi, S., Imanishi, T., Kawabe, Y., Itakura, H., Yazaki, Y., Matsumoto, A. and Kodama, T. (1993). Charged collagen structure mediates the recognition of negatively charged macromolecules by macrophage scavenger receptor. J. Biol. Chem., **268**: 2126-2133.

4) Giovannucci, E., Egan, K. M., Hunter, D. J., Stampfer, M. J., Colditz, G. A., Willett, W. C. and Speizer, F. E. (1995). Aspirin and the risk of colorectal cancer in women. N. Engl. J. Med., **333**: 609-614.

5) Giardiello, F. M., Hamilton, S. R., Krush A. J., Piantadosi S., Hylind, L. M., Celano, P., Booker, S. V., Robinson, C. R. and Offerhaus, G. J. A. (1993). Treatment of colonic and rectal adenomas with sulindac in familial adenomatous polyposis. N. Engl. J. Med., **328**: 1313-1316.

6) Oshima, M., Dinchuk, J. E., Kargman, S. L., Oshima, H., Hancock, B., Kwong, E., Trzaskos, J. M., Evans, J. F. and Taketo, M. M. (1996). Suppression of intestinal polyposis in Apc delta716 knockout mice by inhibition of cyclooxygenase 2 (COX-2). Cell, **87**: 803-809.

7) Sonoshita, M., Takaku, K., Sasaki, N., Sugimoto, Y., Ushikubi, F., Narumiya, S., Oshima, M. and Taketo, M. M. (2001). Acceleration of intestinal polyposis through prostaglandin receptor EP2 in Apc(Delta 716) knockout mice. Nat. Med., **7**: 1048-1051.

8) Crocker, P. R. and Varki, A. (2001). Siglecs, sialic acids and innate immunity. TRENDS in Immunol., **22**: 337-343.

ルイス肺癌における癌転移制御の機構的解析

工学部・生物工学科

棟居聖一、吉冨泰央、小山芳江、岡山實

緒論

がんの転移性は、その自律的な増殖性と共に癌細胞の悪性度を特徴づける重要な側面であり、その防止は癌治療において重要な問題である[1-3]。本研究室では転移の機構を癌細胞と細胞微小環境を構築する細胞外マトリックス（ECM）との相互作用の視点から明らかにすることを目的に研究が進められてきた[3-5]。この目的を達成するため、先ずマウス・ルイス肺癌から自然転移能に基づいて転移能の異なる腫瘍細胞をクローン化し、株細胞（低転移性株 P29、中転移性株 LM12-3、高転移性株 LM66-H11）として樹立した[6,5]。これらの株細胞を同系マウス（C57/BL）の皮下に移植して作らせた一次腫瘍組織を用いて、ECM を中心に転移能に共軛した組織学的特徴を解析した。その結果、P29 および LM66-H11 株細胞が生体内において全く異なる ECM-依存的腫瘍組織を形成することが示された。即ち，LM66-H11 細胞は基底膜形成能が高く、腫瘍細胞はそれを足場にした腫瘍組織形成を示した[6,8]。それに対して P29 細胞は基底膜形成能をもたず、それに代わって宿主組織に対して強い間質誘導性を示し、誘導された間質細胞の形成するフィブロネクチン（FN）に富んだ間質型 ECM 依存的な組織形成を示した[3,7,9]。この組織形成の違いを反映して、両株細胞は、培養下において FN 基質への接着に際して顕著に異なる接着応答性を示した。即ち、P29 細胞は FN 基質への接着に際してストレスファイバー（SF）形成を示すのに対して、LM66-H11 細胞においては、アクチン繊維が細胞辺縁部に局在化する皮質型アクチン（CA）の形成を示した[6,10,11]。本研究の目的は、両細胞の示す FN 基質接着依存的なアクチン細胞骨格形成誘導の違いの分子的背景を解明するとともに、両細胞が示す転移能の違いをもたらす分子的背景を明らかにすることである。

結果

転移能の異なる株細胞が示すアクチン細胞骨格形成

本研究室では腫瘍細胞としてマウス・ルイス肺癌（3LL）細胞を用い、転移能の異なる腫瘍細胞をクローン化し、株細胞として樹立した（表 1）[6,7]。これらの株細胞の中で、低転移性 P29 細胞と高転移性 LM66-H11 細胞は生体内において顕著な基底膜形成能の違いを示した。即ち、P29 細胞はラミニンの分泌能を欠如している[12]ため細胞外における基底膜形成を示さなかった。それに対して、LM66-H11 細胞は完成度の高い基底膜を腫瘍細胞間に形成し、腫瘍細胞は自ら形成した基底膜に接着した組織像を示した[6,8]。一方、基底膜形成能をもたない P29 細胞は、宿主組織に対して強い間質誘導を示し、腫瘍組織内に誘導された間質細胞は FN を主成分とする間質型 ECM を形成し、腫瘍細胞はその ECM を足場とした腫瘍組織形成を示した[3,7,9]。それに対して、LM66-H11 腫瘍組織には間質型 ECM の存在は殆ど観察されず、FN の局在は、腫瘍血管内皮基底膜に限定されていた[6,11,13]。この ECM 依存性の違いを反映して両株細胞は、FN 基質に対して全く異なる接着応答性を示した。即ち、FN 基質への接

着に際して、P29 細胞は SF を形成して伸展する（図 1A）のに対して、LM66-H11 細胞内には CA 形成が誘導された（図 1B）。SF 形成の誘導には 2 種類のシグナル、即ち、FN の Arg-Gly-Asp 配列を含む細胞結合ドメイン（Cell-I ドメイン）とインテグリンα5β1 との結合、および FN の C 末端側ヘパリン結合ドメイン（Hep-II ドメイン）と細胞膜型ヘパラン硫酸プロテオグリカンとの結合が必須であることが明らかにされた [14]。そこで我々は、この FN 基質接着依存的アクチン細胞骨格形成の誘導に関与する FN 機能ドメインを明らかにするため、FN に含まれる各種ドメインを含む組換えポリペプチド基質への接着により誘導されるアクチン細胞骨格形成を解析した。P29 細胞は、Cell-I および Hep-II ドメインの組換えポリペプチドを融合した CH-271 上で FN 基質上（図 1A）と酷似した SF 形成を示した（図 1C）が、Cell-I ドメインの組換えポリペプチド C-274 上では CA 形成を示した（図 1E)。このことは FN の Cell-I ドメインとインテグリンα5β1 との結合によって CA 形成が誘導されることを示唆している。これに加えて、P29 細胞は Hep-II ドメインの組換えポリペプチド H-271 上で糸状仮足（FP）を形成することが示された（図 1G)。このことは FN の Hep-II ドメインとヘパラン硫酸プロテオグリカンとの結合が FP 形成を誘導することを示すものである。ここで重要なことは、細胞が両ドメインに結合すると、片方だけに結合したそれぞれの場合とは異なり、SF 形成が誘導されることである。一方、LM66-H11 細胞は組換えポリペプチド基質上で P29 細胞と異なる応答性を示した。即ち、LM66-H11 細胞は CH-271 ポリペプチド基質上でも CA 形成（図 1D）を示し、その応答は C-274 ポリペプチド基質上でのそれと全く同じであった（図 1F)。また、その応答は C-274 ポリペプチド基質上での P29 細胞の応答とも同一であった（図 1E)。これらの結果は、FN 基質上の LM66-H11 細胞では、Cell-I ドメインとインテグリンα5β1 の結合しか成立していないことを示唆している。このことは、LM66-H11 細胞が H-271 ポリペプチド基質上で殆ど伸展しない事実（図 1H）からも支持された。また、これまでに本研究室において、P29 細胞が合成する細胞膜型ヘパラン硫酸プロテオグリカンの中で FN に親和性を示すプロテオグリカン分子はシンデカン-2 であるということを明らかにしている [9]。以上の結果は、LM66-H11 細胞上におけるシンデカン-2 の発現は、閾値以下であることを強く示唆している。そこで、次に両細胞におけるインテグリンα5β1 とシンデカン分子の細胞表層発現を比較した。これらのうち両細胞間で発現レベルに有意な差が認められたのはシンデカン-2 のみで、LM66-H11 細胞での発現量が有意に低かった（図示せず）[11,15]。以上の結果より、転移能の高低に拘らずインテグリンα5β1 の発現量は同じレベルであるが、シンデカン-2 の発現量が低いために LM66-H11 細胞が FN 基質上で SF 形成を示さないことが示唆された。そこで、シンデカン-2 低発現株細胞 LM66-H11 にシンデカン-2 cDNA を導入後、P29 細胞と同程度にシンデカン-2 を発現している安定発現株細胞（H11-SN2）を樹立し、FN 基質への接着応答性を解析した [11]。その結果ベクターのみを導入した H11-Vec 細胞では LM66-H11 親株細胞（図 1B）と同様に CA 形成を示した（図 2A）のに対して H11-SN2 細胞では P29 細胞（図 1A）と同様に SF 形成の誘導が観察された（図 2B)。この際、シンデカン-2 の高発現は、他のシンデカン分子およびインテグリンα5β1 の発現に影響を及ぼさなかった。(図示せず)。これらの結果を合わせて考えると、FN 基質接着に際して、細胞がインテグリンα5β1 とシンデカン-2 とで基質に結合すると、細胞内に SF 形成が誘導され、シンデカン-2 の発現が閾値以

下の場合、CA が形成されることが明らかとなった（図 3)。このことは、シンデカン-2 発現量の高い P29 細胞のシンデカン-2 の発現をシンデカン-2 アンチセンスオリゴヌクレオチドにより抑制した P29 細胞は、FN 基質接着に際して CA 形成を誘導することによっても確認された（図示せず)。

シンデカン-2 高発現細胞の示す転移能

次にシンデカン-2 高発現性の H11-SN2 細胞が FN 基質に対して P29 細胞と同様に SF 形成を示すことから、尾静脈移植によりこの細胞の転移能を測定した。P29 細胞移植マウスの肺に殆ど転移結節が認められないのに対して、LM66-H11 細胞移植マウスの肺においては非常に多くの転移結節が観察された。H11-Vec 細胞移植マウスの肺転移結節数は LM66-H11 細胞移植マウスのそれと非常に似ているが、H11-SN2 移植マウスの肺には転移結節は殆ど認められなかった（図 4)。皮下移植による自然転移においても尾静脈移植の結果と同じ結果が得られた（図示せず)。この結果は、LM66-H11 細胞のシンデカン-2 発現を人為的に高発現にすることによって、転移能が抑制されたことを示している。

シンデカン-2 発現と MMP-2 の活性化

シンデカン-2高発現による転移抑制の機構を明らかにする為に、腫瘍の転移・浸潤に直接的に関与していることが報告されているMMP[16-18]がこの腫瘍系の転移に関わっているか否かを検討した。先ず腫瘍の転移・浸潤においてその関与が明らかにされているゼラチナーゼ群であるMMP-2、9 について検討した。P29、LM66-H11、H11-SN2、H11-Vec 細胞より得られた無血清培養上清（CM）を用いたゼラチンザイモグラフィーを行った結果、シンデカン-2低発現性の高転移性LM66-H11、H11-Vec細胞ではMMP-2の活性化が見られたが、シンデカン-2高発現性の低転移性P29、H11-SN2細胞ではその活性化は観察されなかった(図 5A)。MMP-9についてはほとんど観察されなかった。MMP-2は潜在型酵素として細胞外に分泌され、細胞膜上でMT1-MMP—TIMP-2複合体に結合し[19,20]、その後、TIMP-2を結合していないMT1-MMPによりプロペプチドが切断されて中間型MMP-2となり、その後自己消化により活性型酵素となることが明らかにされている[21,22]。そこで、この活性化に関与している分子の発現量に量的な差があるか否かを検討した。P29、LM66-H11、H11-SN2、H11-Vec 細胞より得られたmRNAを用いたノーザンブロットの結果からこれらの株細胞間でMMP-2、MT1-MMP、TIMP-2 のmRNAの発現量に有意な差のないことが示された（図 5B)。これらの結果から、この腫瘍の転移過程にはMMP-2の活性化が関与しており、その活性化はシンデカン-2により制御されていることが示唆された。そこで次にシンデカン-2 がMMP-2 活性化過程へ関与している可能性について検討した。

シンデカン-2のヘパラン硫酸鎖によるMMP-2活性化の制御

シンデカン分子は、その分子の持つヘパラン硫酸鎖を介して増殖因子、あるいはECM成分に結合し、その結合シグナルを直接あるいは間接的に細胞内に伝達することが明らかにされている[23-25]。さらに、MMP-2 の持つヘモペキシン様ドメインはヘパリン結合性を示すことも明らかにされている[21,26,27]。また、本研究室においても、大腸癌細胞の産生するMMP-2がヘパリンと高い親和性を示すことを明らかにしている（図

示せず)。従って、本研究で示したシンデカン-2 の高発現によりMMP-2 の活性化が抑制される現象にはシンデカン-2 ヘパラン硫酸鎖の関与の可能性が考えられた。そこで、シンデカン-2 タンパク芯のグリコサミノグリカン鎖付加部位のセリン残基をアラニン残基に変異させた変異体を強制発現させたH11-SN2ΔGAG細胞のMMP-2 活性化、さらにはヘパリチナーゼI により細胞表層のヘパラン硫酸鎖を除去した場合のMMP-2 活性化をゼラチンザイモグラフィーにより検討した (図6)。まずP29 細胞をヘパリチナーゼI 消化することにより細胞表層からヘパラン硫酸鎖が除かれていることを抗不飽和ヘパラン硫酸抗体F58-10E4 を用いたFACS 分析により確認した (図 6A)。また、抗シンデカン-2抗体 (SN2Ab) を用いたFACS 分析により、H11-SN2ΔGAG 細胞の細胞膜表層におけるシンデカン-2 タンパク芯の発現がP29 細胞と同程度であることも確認した (図 6B)。これらの細胞から調製したCM を用いてゼラチンザイモグラフィーによりMMP-2の活性化を検討した (図 6C)。H11-SN2ΔGAG細胞の培養系ではヘパラン硫酸鎖を持つH11-SN2 細胞の培養系と比較して高いMMP-2 の活性化が観察され、これらのバンドを定量化した結果、H11-SN2 細胞による活性化の割合は、LM66-H11 細胞のそれと比較して50 % 減少していた (表2)。これに対し、H11-SN2ΔGAG 細胞による活性化はLM66-H11 細胞のそれと比較して4 % の減少しか示さず、LM66-H11 細胞とほぼ同じ程度の活性化を示した (表2)。ヘパラン硫酸鎖を持たないシンデカン-2 分子を強制発現させてもMMP-2 の活性化に対して抑制的には作用し得ないことは、MMP-2 活性化の抑制はシンデカン-2 のヘパラン硫酸鎖を介した現象であることを強く示唆している。また、シンデカン-2 高発現性のP29 細胞をヘパリチナーゼI 共存下で培養して得たCM を用いたザイモグラフィーの結果では酵素を加えないコントロールと比較して有意にMMP-2の活性化が亢進していた (図 6C)。デンシトメトリーの結果では、未処理のP29 細胞と比較してヘパリチナーゼI 消化することによりMMP-2 の活性化の割合が41 % 増加していた (表2)。この結果は先のH11-SN2ΔGAG 細胞の結果とよい一致を示している。これらの結果を総合して考えると、MMP-2の活性化はシンデカン-2のヘパラン硫酸鎖により制御されていることを強く示唆している。

考察

本研究室でのこれまでの研究で以下のことが明らかにされている。1) 培養下において、P29 細胞が FN 基質に接着すると、細胞内に SF を形成して伸展するのに対して、LM66-H11 細胞のアクチン繊維は細胞辺縁部に局在し、CA を形成する [10,11]。2) P29 細胞が合成する細胞膜型ヘパラン硫酸プロテオグリカンの中で FN に親和性を示す分子はシンデカン-2 である [9]。3) FN の Hep-II ドメインに特異的結合性を示すヘパラン硫酸鎖の最小糖鎖構造は、$[\mathrm{Ido\,(2\text{-}OSO_3)\,\alpha\,1\text{-}4GlcNSO_3\,(6\text{-}OSO_3)}]_6$ である [10]。

本研究において、P29 および LM66-H11 細胞の示す FN 基質接着時のアクチン細胞骨格形成の違いをもたらす分子的背景を明らかにするするために、FN の Cell-I ドメインを含む組換えポリペプチド (C-274)、Hep-II ドメインを含む組換えポリペプチド (H-271)、および C-274 ポリペプチドと H-271 ポリペプチドとを結合した融合組換えポリペプチド (CH-271) 基質に対する接着応答性を検討した。その結果、CH-271 ポリペプチド基質に対して P29 および LM66-H11 両細胞とも FN 基質に対する接着応答性と同一の応答性を示した。即ち、P29 細胞は SF 形成を、LM66-H11 細胞は CA

形成を示した。C-274 ポリペプチドのみを基質に用いたとき P29、LM66-H11 両細胞ともに CA を形成した。H-271 ポリペプチドのみを基質にしたときには、P29 細胞は FP 形成を示したのに対して、LM66-H11 細胞は接着性が弱く、殆ど伸展しなかった。FP 形成については、繊維芽細胞において、その形成にシンデカン-2 が関与しているという報告がなされている[28]。

次に両細胞の示す FN 基質接着依存的アクチン細胞骨格形成から考えられる両細胞の FN 受容体を解析した。Cell-I ドメインに特異的な受容体として知られているインテグリンα5β1 の細胞表層発現は両細胞ともに同じレベルであった。このことは C-274 ポリペプチド基質に両細胞を接着させたときに、両細胞共に CA を形成する事実とよく一致している。Hep-II ドメインの受容体と考えられるシンデカン-2 の発現量を比較したところ、P29 細胞のほうが LM66-H11 細胞より高い発現を示した。P29 細胞においてシンデカン-2 の発現が高いことは、H-271 ポリペプチド基質上で P29 細胞が FP 形成を示すのに対し、LM66-H11 細胞が殆ど接着を示さず、伸展しないこととよい一致を示している。さらに CH-271 ポリペプチド基質への接着に際して、P29 細胞は Cell-I ドメインと Hep-II ドメインに対し、インテグリンα5β1 とシンデカン-2 とで同時に結合することにより SF 形成を誘導する。それに対して、LM66-H11 細胞は、シンデカン-2 の発現量が閾値以下であるため、インテグリンα5β1 のみで CH-271 ポリペプチド基質に接着するため、その応答性は C-274 ポリペプチド基質上の場合と同様 CA 形成を誘導する。これらの結果は、SF 形成の誘導には一定量以上のシンデカン-2 の発現が必須であることを示している。本研究で得られた結果は以下のようにまとめるとことができる。即ち、細胞が FN 基質への接着に際して、1) Cell-I ドメインと Hep-II ドメインにインテグリンα5β1 とシンデカン-2 を介して同時に結合すると、細胞内に SF 形成が誘導される。2) Cell-I ドメインとインテグリンα5β1 との結合のみで細胞接着が起こると細胞内に CA の形成が誘導される。3) Hep-II ドメインとシンデカン-2 との結合のみで細胞接着が起こると細胞内に FP 形成が誘導される。このように FN 基質接着依存的 SF 形成の誘導にはインテグリンα5β1 とシンデカン-2 の協調作用が必須である。P29 細胞は肺胞上皮細胞由来の腫瘍細胞であるが、アクチン細胞骨格形成におけるインテグリンとシンデカンの協調作用は、繊維芽細胞の系でも観察されており、細胞種の違いを超えた一般的な現象と考えられる[29-33]。興味深いことに、繊維芽細胞においてインテグリンと協調的に作用するシンデカン分子は、シンデカン-4 と同定されている。しかし、シンデカン-4 が FN 基質に結合性をもつかどうかについては明らかにされていない。また、シンデカン-4 のノックアウトマウス由来の繊維芽細胞は、FN 基質への接着に際して SF 形成を示すことが報告されている[34]。また本研究において、SF 形成においてシンデカン-4 の作用は他の分子で代償されるが、シンデカン-2 の作用は必須であることも明らかにしている（図示せず）。これらを合わせて考えると SF 形成の誘導には、シンデカン-2 と-4 が協調的に作用することが考えられるが、その作用機構については不明である。

次に、SF 形成の誘導を示すように変換した H11-SN2 細胞の肺への転移と MMP の解析を行った。転移が成立するためには、癌細胞の一次腫瘍からの遊離、血管内侵入、転移先での血管外侵出など、癌細胞が乗り越えなければならない組織構造的障壁が多く存在する。この構造的障壁となっている ECM を分解し、がんの悪性化へ

の関与が明らかにされている分子としてマトリックス・メタロプロテアーゼ（MMP）がある[16-18]。これまでに、がんに関連するMMPとして、多くのMMPが報告されている[35]。しかし、どのMMPが、がんの浸潤、転移に作用しているかは推測の域を出ていなかった。癌転移の過程として提唱されているモデルで脈管への侵入、標的組織での脈管から標的組織への侵出など、基底膜破壊は重要なステップであると考えられてきた。基底膜の主要な構成成分であるIV型コラーゲンは基底膜の密な網目構造を形成している。このような理由からこれまでにIV型コラーゲン分解活性が癌細胞の悪性度を特徴づける一つの指標であるとして考えられている[19]。癌細胞が産生するIV型コラーゲン分解酵素としてはゼラチナーゼ群であるMMP-2、-9が主要であり、これらの癌組織での発現や局在が数多く報告されている[36]。本研究において転移能の異なる細胞で、転移能と一致したMMP-2の著しい活性化が認められた。即ち、高転移性LM66-H11細胞において高いMMP-2の活性化を示した。注目すべきはシンデカン-2を強制発現させ、転移を抑制した細胞ではMMP-2活性化が抑制されていたことである。さらに最近MMP-2活性化の抑制が観察されなかったH11-SN2ΔGAG細胞は親株H11細胞と同様に高い転移能を示す結果が得られた（未発表）。これらの結果はシンデカン-2のヘパラン硫酸鎖によりMMP-2活性化が抑制され、その結果として転移が抑制されたことを示唆している。MMP-2の活性化機構は試験管内でMT1-MMPの触媒部位を用いた実験により明らかにされている[37]。即ち、MT1-MMPが潜在型MMP-2プロペプチドのAsn37とLeu38とのペプチド結合を加水分解し、それによって生じた中間型MMP-2は自己触媒的にAsn80とTyr81のペプチド結合を加水分解し活性型MMP-2となる。Satoらは膜貫通型のMT1-MMPが細胞膜上で潜在型MMP-2を活性化することを明らかにした[19]。まず、細胞表層に発現したMT1-MMPは阻害分子であるTIMP-2と複合体を形成し、その酵素活性が阻害をうける。TIMP-2のC-末端ドメインはMMP-2のヘモペキシンドメインと親和性があるため、細胞膜表面にMT1-MMP、TIMP-2、MMP-2の３者複合体が形成される。この複合体はMMP-2を膜表面に濃縮するための受容体として機能する[38]とともに潜在型MMP-2の活性化に必須であり、この複合体構成分子間の相互作用を阻害すると活性化はおこらない。また、MT1-MMPはTIMP-2により酵素活性が阻害されているので潜在型MMP-2を分解し、活性化することができない。このため、TIMP-2を結合していない遊離のMT1-MMPがMMP-2を活性化するというモデルが考えられ、それを支持する結果が多く報告されている[21,22,39-41]。しかし、遊離のMT1-MMPが上記３者複合体の近傍にどのように存在し、それによってMMP-2の活性化がどのように調節されているのかは明らかになっていない。最近、MT1-MMPがヘモペキシン様ドメインを介してホモ二量体を形成することが明らかにされ、そのヘモペキシン様ドメインを欠損するとMMP-2を活性化できないことからホモ二量体形成が、TIMP-2非結合性のMT1-MMPを上記３者複合体の近傍に保つ役割を担っていることが推論されている[42]。本研究において、転移能の異なる株細胞P29細胞、LM66-H11細胞およびシンデカン-2を強制発現したH11-SN2細胞間で、これらMMP-2の活性化に寄与する分子群の発現量に有意な差は見いだされなかった。そこで本研究では、MMP-2の活性化抑制がシンデカン-2分子のどのような機能に基づくものかを検討した。シンデカン-2低発現性の高転移性LM66-H11株細胞にグリコサミノグリカン鎖を持たない変異シンデカン-2を強制発現させてもMMP-2活性化の抑制は観察されず、また、

シンデカン-2 高発現性の低転移性 P29 細胞から細胞表層のヘパラン硫酸鎖を酵素的に除いた培養系においては親細胞と比べ MMP-2 酵素の有意な活性化の亢進が見られた。この結果は MMP-2 活性化抑制にシンデカン-2 のヘパラン硫酸鎖が関与していることを強く示唆するものである。また、MMP-2、MT1-MMP のヘモペキシン様ドメインはヘパリンに結合性を示すことが明らかにされている [21,26,27]。これらをあわせて考えると、次に示す 2 つの可能性が考えられる（図 7）。1 つ目の可能性は、MT1-MMP、TIMP-2、MMP-2 の 3 者の活性化複合体が MMP-2 活性化の高い LM66-H11 細胞において有意に多く形成されていたことから、シンデカン-2 のヘパラン硫酸鎖が MMP-2 の活性化複合体への結合に対して抑制的に働いているという考えである。即ち、潜在型 MMP-2 活性化受容体（MT1-MMP—TIMP2 二量体）とシンデカン-2 のヘパラン硫酸側鎖は共に MMP-2 のヘモペキシンドメインに結合することから、これら二者受容体間で潜在型 MMP-2 の結合における競合が起こり、MT1-MMP に対する基質濃度が調節されていることが考えられる。細胞から分泌された潜在型 MMP-2 が MT1-MMP—TIMP-2 複合体に結合した結果 MT1-MMP により潜在領域が切断され活性化される。シンデカン-2 高発現細胞では分泌された潜在型 MMP-2 がシンデカン-2 のヘパラン硫酸鎖を介して結合することにより MT1-MMP—TIMP 複合体への結合と競合し、その結果 MMP-2 の活性化が抑制され、MMP-2 の活性化が抑制されたのではないかと考えられる。即ち、MT1-MMP—TIMP-2 複合体が MMP-2 の活性化受容体として機能しているのに対してシンデカン-2 は MMP-2 の活性化抑制受容体として機能している可能性が考えられる。今 1 つの可能性は、シンデカン-2 のヘパラン硫酸鎖が MMP-2 を活性化するのに必要な 3 者複合体の MT1-MMP と TIMP-2 非結合性の MT1-MMP との結合を阻害しているモデルである。即ち、MT1-MMP のヘモペキシン様ドメインもヘパリン結合性であることからシンデカン-2 高発現細胞においては、シンデカン-2 のヘパラン硫酸鎖が MMP-2 の活性化に必要な 3 者複合体と TIMP-2 非結合性の MT1-MMP とのホモ 2 量体形成を阻害し、結果的に MT1-MMP の活性を阻害し MMP-2 の活性化が抑制されているのではないかと考えることもできる。いずれにしても、シンデカン-2 のヘパラン硫酸依存的 MMP-2 の活性化抑制は、ヘパリンにより生体内でのがん転移が大きく抑制されるという本研究室からの報告 [43] とよい一致を示しており、臨床的研究が待たれるところである。ルイス肺癌細胞に見られた MMP-2 活性化におけるシンデカン-2 のヘパラン硫酸鎖の特異的機能が、その化学構造に基づくものか、それともシンデカン-2 の膜上における局在に基づくものなのかについては明らかではない。MMP-2 活性化制御におけるシンデカン-2 のヘパラン硫酸鎖の役割については、今後さらに詳しく解析していく必要がある。

参考文献

1. Liotta, L.A., Tryggvason, K., Garbisa, S., Hart, I., Folts, C.M. and Shafie, S. (1980) Nature, ***284***: 67-68
2. Nakajima, M., Irimura, T., DiFerrante, N. and Nicolson, G.L. (1983) Science, ***220***: 611-613
3. 岡山實, 草野由理, 小栗佳代子 (1996) 現代化学, ***308***: pp. 51-57, 東京化学同人, 東京
4. 小栗佳代子, 岡山實 (1993) 細胞社会のグリコバイオロジー (永井克孝, 箱守仙一郎, 木幡陽編) pp. 151-175, 講談社サイエンティフィック, 東京
5. 岡山實 (1997) 京都産業大学論集第 28 巻, 第 4 号, 自然科学系列 II 第 6 号, pp .1-95
6. Nakanishi, H., Oguri, K., Yoshida, K., Itano, N., Takenaga, K., Kazama, T., Yoshida, A. and Okayama, M. (1992) Biochem. J., ***288***: 215-224
7. Itano, N., Oguri, K., Nakanishi, H. and Okayama, M. (1993) J. Biochem., ***114***: 862- 873
8. Nakanishi, H., Takenaga, K., Oguri, K., Yoshida, A. and Okayama, M. (1992) Virchows, Arch. A, ***420***: 163-170
9. Itano, N., Oguri, K., Nagayasu, Y., Kusano, Y., Nakanishi, H., David, G. and Okayama, M. (1996) Biochem. J., ***315***: 925-930
10. Kusano, Y., Oguri, K., Nagayasu, Y., Munesue, S., Ishihara, M., Saiki, I.,Yonekura, H., Yamamoto, H. and Okayama, M. (2000) Exp. Cell Res., ***256***: 434-444
11. Munesue, S., Kusano, Y., Oguri, K., Itano, N., Yoshitomi, Y., Nakanishi, H., Ikuo, Y. and Okayama, M. (2002) Biochem. J., ***368***: 201-209
12. Narumi, K., Satoh, K., Isemura, M., Sakai, T., Abe, T., Kikuchi, T., Sindoh, S., Motomiya, M., Oguri, K. and Okayama, M. (1993) Cell Struct. Funct., ***18***: 183-187
13. Nakanishi, H., Oguri, K., Takenaga, K., Hosoda, S. and Okayama, M. (1994) Lab. Invest., ***70***: 324-332
14. Lenbaron, R. G., Esko, J. D., Woods, A., Johansson, S. and Hook, M. (1988) J. Cell Biol., ***106***: 945-952
15. Kusano, Y., Yoshitomi, Y., Munesue, S., Okayama, M. and Oguri, K. (2004) J. Biochem., ***135***: 129-137
16. Pyke, C., Ralfkaer, E., Huhtala, P., Hurskainen, T., Dano, K. and Tryggason, K. (1992) Cancer Res. ***52***: 1336-1341
17. Brown, P.D., Bloxidge, R.E., Anderson, E. and Howell, A. (1993) Clin. Exp. Metastasis, ***11***: 183-189
18. Stearns, M.E. and Wang, M. (1993) Cancer Res. ***53***: 878-883
19. Sato, H., Takino, T., Okada, Y., Cao, J., Shinagawa, A., Ymamoto, E. and Seiki, M. (1994) Nature, ***370***: 61-65
20. Sato, H., Kinoshita, T., Takino, T., Nakayama, K. and Seiki, M. (1996) FEBS Lett., ***393***: 101-104
21. Butler, G.S., Butler, M.J., Atkinson SJ, Will H, Tamura T, van Westrum S.S., Crabbe, T,, Clements, J., d'Ortho, M.P. and Murphy, G. (1998) J. Biol. Chem., ***273***: 871-880
22. Kinoshita, T., Sato, H., Okada, A., Ohuchi, E., Imai, K., Okada, Y. and Seiki, M. (1998) J. Biol. Chem., ***273***: 16098-16103
23. Maccarana, M., Casu, B. and Lindahl, U. (1993) J. Biol. Chem., ***268***: 23898-23905
24. Guimond, S., Maccarana, M., Olwin, B.B., Lindahl, U. and Rapraeger, A.C. (1993) J. Biol. Chem., ***268***: 23906-23914
25. McKeehan, W.L., Wang, F. and Kan, M. (1998) Prog. Nucleic Acid Res. Mol. Biol., ***59***: 135-176

26. Crabbe, T., Ioannou, C. and Docherty, A.J. (1993) Eur. J. Biochem., *218*: 431-438
27. Crabbe, T., O'Connell, J.P., Smith, B.J. and Docherty, A.J. (1994) Biochemistry, *33*: 14419-14425
28. Granes, F., Garcia, R., Casaroli-Marano, R. P., Castel, D., Rocamera, N., Reina, M., Urena, M. and Vilaro, S. (1999) Exp. Cell Res., *248*: 439-456
29. Woods, A., Couchman, J. R., Johansson, S. and Hook, M. (1986) EMBO J., *5*: 665-670
30. Woods, A., MaCarthy, J. B., Furcht, L. T. and Couchman, J. R. (1993) Mol. Biol. Cell, *4*: 605-613
31. Woods, A. and Couchman, J. R., (1994) Mol. Biol. Cell *5*: 183-192
32. Saoncella, S., Echtermeyer, F., Denhez, F., Nowlen, J. K., Mosher, D.F., Robinson, S. D., Hynes, R. O. and Goetinck, P. F. (1999) Proc. Natl. Acad. Sci. USA, *96*: 2805-2810
33. Echtermeyer, F., Baciu, P. C., Saoncella, S., Ge, Y. and Goetinck, P. F. (1999) J. Cell Sci., *112*: 3433-3441
34. Ishiguro, K., Kadomatsu, K., Kojima, Y., Muramatsu, H., Tsuzuki, S., Nakamura, E., Kusugami, K., Saito, H. and Muramatsu, T. (2000) J. Biol. Chem. *275*: 5249-5252
35. Fingleton, B. and Matrisian, L.M. (2001) in Matrix Metalloproteinase Inhibitors in Cancer Therapy. (Clendeninn NJ and Appelt K., eds.) pp. 85-112, Humana Press
36. Stetler-Stevenson, W.G. Aznavoorian, S. and Liotta, L.A. (1993) Annu. Rev. Cell Biol. *9*: 541-573
37. Will, H., Atkinson, S.J., Butler, G.S., Smith, B. and Murphy, G. (1996) J. Biol. Chem., *271*: 17119-17123
38. Strongin, A.Y., Collier, I., Bannikov, G., Marmer, B.L., Grant, G.A. and Goldberg, G.I. (1995) J. Biol. Chem., *270*: 5331-5338
39. Werb, Z. (1997) Cell., *91*: 439-442
40. Seiki, M. (1999) *APMIS*, *107*: 137-143
41. Nagase, H. and Woessner, J.F. Jr. (1999) J. Biol. Chem., *274*: 21491-21494
42. Itoh, Y., Takamura, A., Ito, N., Maru, Y., Sato, H., Suenaga, N., Aoki, T. and Seiki, M. (2001) EMBO J., *20*: 4782-4793
43. Yoshitomi, Y., Nakanishi, H., Kusano, Y., Munesue, S., Oguri, K., Tatematsu, M., Yamashina, I. and Okayama, M. (2004) Cancer Lett., *207*: 165-174

表1　ルイス肺癌由来の株細胞が示す転移能

株細胞	移植経路	移植細胞数 (x 10^5)	転移動物数 / 実験動物数	肺転移結節数	
				平均	範囲
P29	i.v.	1.0	3/7	0.4	0 - 1
LM12-3	i.v.	1.0	7/7	47.9	19 - 92
LM66-H11	i.v.	1.0	7/7	516.2	467 - 744
P29	s.c.	2.0	0/7	0	0
LM12-3	s.c.	2.0	6/7	4.5	0 - 14
LM66-H11	s.c.	2.0	7/7	35.2	23 - 56

i.v.: 静脈移植、s.c.: 皮下移植。

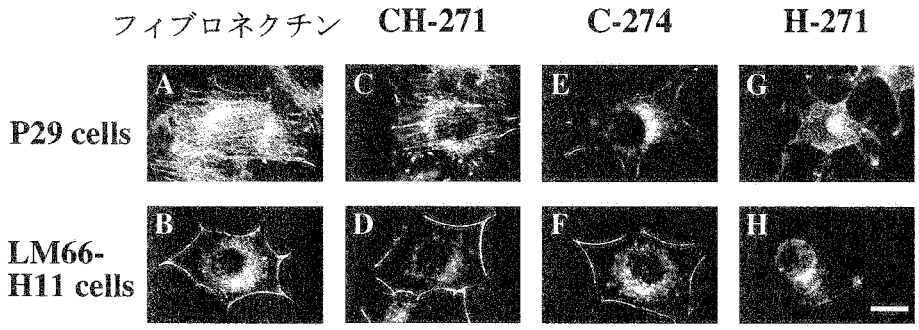

図1　転移能の異なる株細胞の基質接着依存的アクチン細胞骨格形成

フィブロネクチン（A、B）CH-271（C、D）、C-274（E、F）、H-271ポリペプチド（G、H）を被覆したカバーグラス上にP29細胞（A、C、E、G）、LM66-H11細胞（B、D、F、H）を播種し、1時間後に形成したF-アクチンをローダミン標識ファロイジンで染色した。スケールは20 μ m。

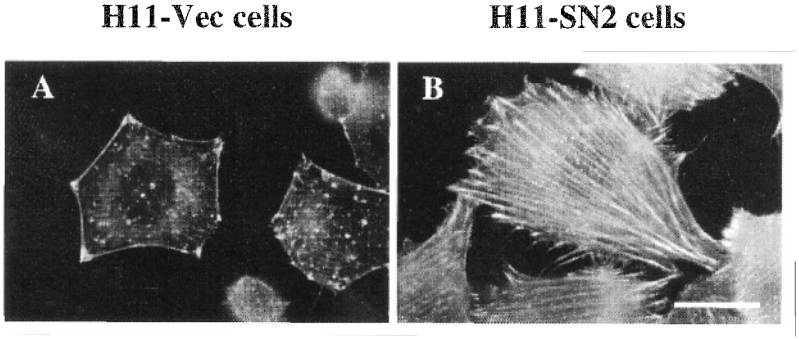

図2　シンデカン-2導入株細胞のフィブロネクチン基質に対する接着応答性

フィブロネクチンを被覆したカバーグラス上に、ベクターのみ導入H11-Vec細胞（A）および、シンデカン-2導入H11-SN2細胞（B）を播種し、1時間後に形成したF-アクチンをローダミン標識ファロイジンで染色した。スケールは20 μ m。

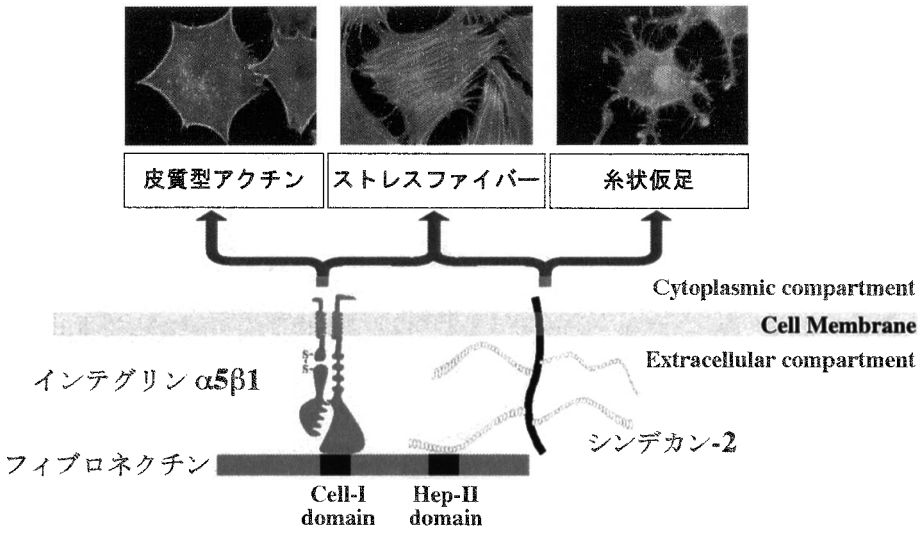

図3　インテグリンα5β1およびシンデカン-2を介したフィブロネクチン結合シグナルの伝達

細胞がインテグリンα5β1を介してフィブロネクチンのCell-Iドメインに結合した場合伸展し、皮質型アクチンを形成する。それに対してシンデカン-2を介してHep-IIドメインに結合した場合、細胞はほとんど伸展せず糸状仮足形成を示す。両方の受容体を介してフィブロネクチンに結合した場合には、細胞内にストレスファイバー形成が誘導される。このストレスファイバー形成へのシグナルはシンデカン-2の発現量に依存している。即ち、インテグリンα5β1の結合シグナルはシンデカン-2により制御されている。

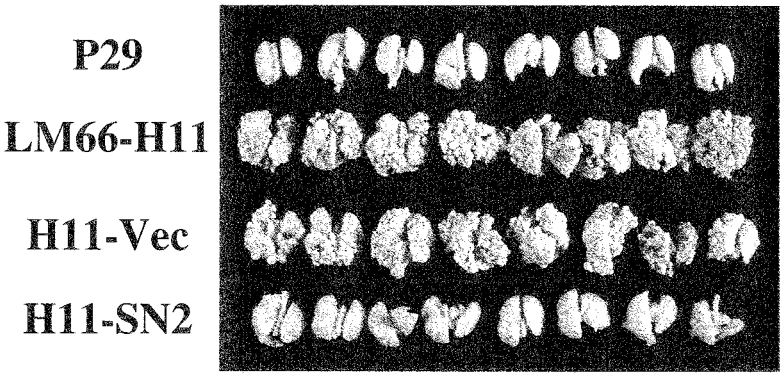

図4　シンデカン-2高発現細胞株の肺転移像

低転移性P29細胞、高転移性LM66-H11細胞、LM66-H11細胞にベクターのみを導入したH11-Vec細胞、シンデカン-2 cDNA導入H11-SN2細胞をマウス尾静脈に移植して16日後に摘出した肺における転移結節を示す。

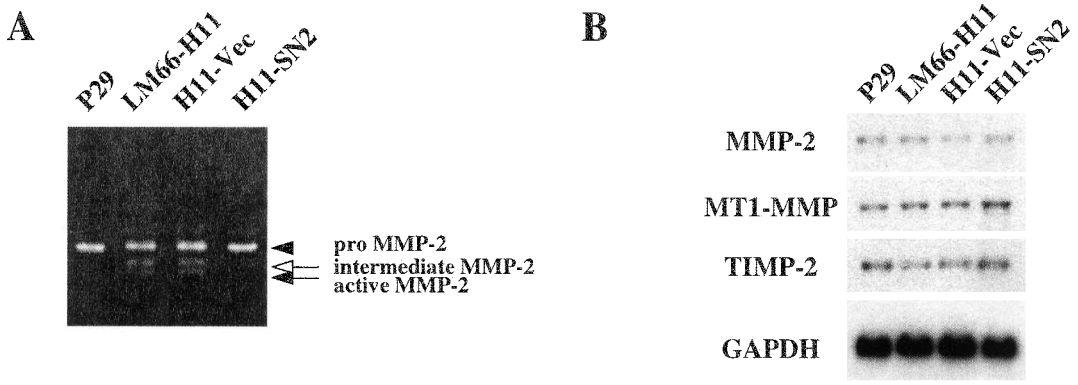

図5　MMP-2の活性化と発現量に及ぼすシンデカン-2の影響

低転移性P29細胞、高転移性LM66-H11細胞、ベクターのみを導入したH11-Vec細胞、シンデカン-2 cDNA導入H11-SN2細胞におけるMMP-2の活性化（A）、およびMMP-2活性化に関与する分子のmRNA発現量（B）を比較した。（A）各細胞5×10^5細胞から得た無血清培養上清を用いてゼラチンザイモグラフィーにより解析した。（B）各細胞より抽出したポリ$(A)^+$RNA（2μg/レーン）を用いてノ-ザンブロット法によりMMP-2, MT1-MMP, TIMP-2の発現量の比較を行った。プローブにはMMP-2（683-1484）、MT1-MMP（727-1635）、TIMP-2（415-735）を含むcDNAを用いた。

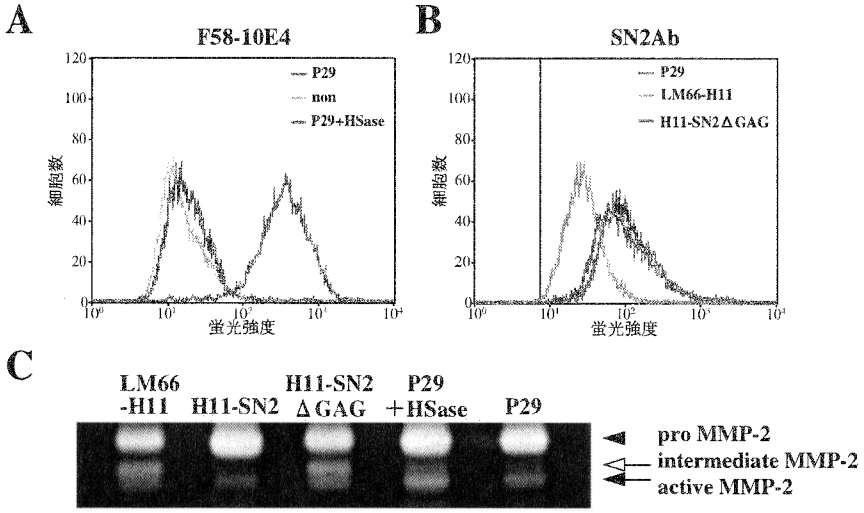

図6　MMP-2活性化における細胞表層ヘパラン硫酸、およびシンデカン-2 のヘパラン硫酸鎖に対する依存性

A, B: ヘパリチナーゼ未処理 P29細胞(P29)あるいは0.1U/mlのヘパリチナーゼIで消化したP29細胞(P29＋HSase)の細胞表層ヘパラン硫酸発現(A)、およびグリコサミノグリカン鎖を持たないシンデカン-2を高発現させたH11-SN2ΔGAG細胞、シンデカン-2高発現性P29細胞、シンデカン-2低発現性LM66-H11細胞におけるシンデカン-2の細胞表層発現(B)をFACS解析により検討した。各細胞の細胞表層発現を抗ヘパラン硫酸鎖抗体(F58-10E4)、抗シンデカン-2抗体(SN2Ab)を用いてフローサイトメーターで測定した。Aの灰色線は、非免疫血清を用いた対照を示す。C: LM66-H11細胞、H11-SN2細胞、H11-SN2ΔGAG細胞、ヘパリチナーゼI処理したP29細胞(P29＋HSase)、及び未処理のP29細胞(P29)から得た無血清培養上清を用いてゼラチンザイモグラフィーによりMMP-2活性化の解析を行った。

表2　細胞表層ヘパラン硫酸及び、シンデカン-2ヘパラン硫酸鎖によるMMP-2活性化抑制

株細胞	LM66-H11	H11-SN2	H11-SN2 ΔGAG	P29 +HSase	P29
活性化(%)	68.2	34.8	65.8	55.3	39.3
対 LM66-H11 (%)*	100	50	96	81.1	57.6
対 P29 (%)**	173.5	88.5	167.4	141	100

*LM66-H11細胞に対する各細胞の活性化の割合、**P29細胞に対する各細胞の活性化の割合を示した。

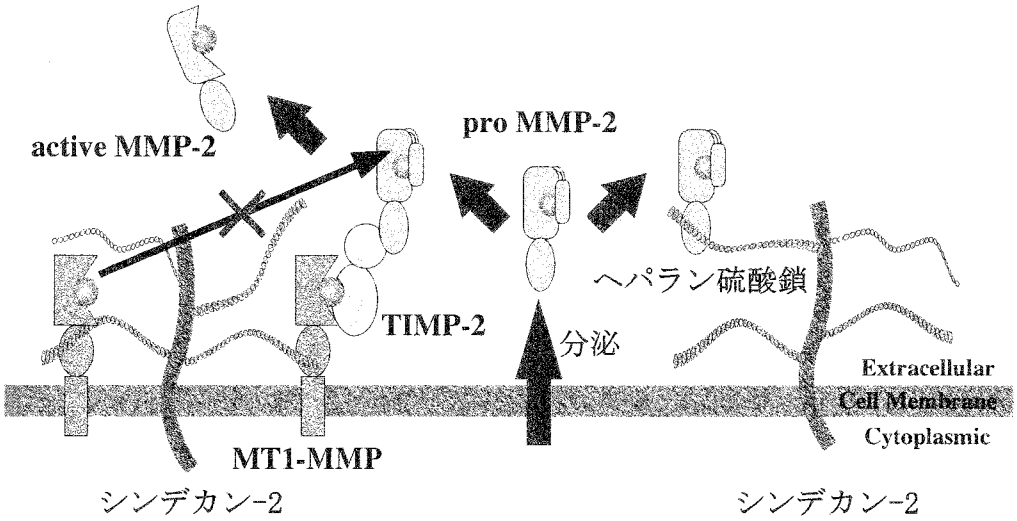

図7　シンデカン-2を介したMMP-2活性化抑制機構の仮想的模式図

細胞から分泌されたproMMP-2はTIMP-2ーMT1-MMP複合体に結合し、TIMP-2と結合していない遊離型MT1-MMPによりpro domainが切断され活性化される。シンデカン-2高発現細胞では分泌されたproMMP-2がシンデカン-2のヘパラン硫酸鎖に結合することによりTIMP-2ーMT1-MMP複合体への結合が競合的に阻害される、或はシンデカン-2がそのヘパラン硫酸鎖を介してMT1-MMPに結合することによりMT1-MMPの活性を抑制し、その結果、MMP-2の活性化が抑制される可能性が考えられる。

喫煙による生体防御機構への影響

― 肺胞マクロファージ機能の抑制機構について ―

京都産業大学・工学部・生物工学科　竹内　実

要旨

喫煙の研究は発癌、循環器系に関する研究が多く、肺の免疫系についての詳細な研究はあまりなされておらず、まだ解明されていない点も多く残されている。ヒトの喫煙研究においては、タバコの喫煙歴等に個人差があり、実験条件を統一することが難しい。また、タバコ煙には多くの汚染物質・粉塵などが含まれていることから、タバコ煙を環境分野で重要な問題である大気汚染のモデルとして着目した。本研究では、喫煙の肺免疫機能に及ぼす影響について、自動喫煙装置を用い、タバコ煙を一定量、均一にマウスに喫煙させ、喫煙の影響を正確に客観的に評価できる条件下で、肺の免疫システムにおいて重要な役割を担っている肺胞マクロファージの免疫機能への影響を検討した。

タバコ主流煙喫煙により、マウス肺胞マクロファージは、非喫煙(NS) に比べて、細胞の大型化、細胞内部の空胞変性、細胞内部構造の複雑化などの形態学的な変化が観察され、また細胞内の自動蛍光強度も喫煙(S)により強まることが認められた。肺胞マクロファージの免疫機能に関しては、喫煙により肺胞マクロファージの重要な免疫機能の一つである抗体産生に関連した抗原提示機能の抑制が認められた。また、喫煙による肺胞マクロファージの抗原提示機能の抑制機構には、抗原提示に関係した肺胞マクロファージの細胞表面抗原であるB7-1、ClassⅡ抗原の発現抑制と肺胞マクロファージの活性化サイトカインであるIL-1β、TNF-αのmRNA発現の抑制が関与していることが示された。さらに、喫煙による肺胞マクロファージがB細胞増殖機能に対して抑制を示したが、T細胞増殖機能への抑制は認められなかった。一方、成熟した抗体産生細胞に対しては抑制を示さなかったことより、喫煙による肺胞マクロファージが抗体産生の初期段階に影響を及ぼしていることが認められた。また、喫煙により肺胞マクロファージのO_2^-産生が増強されることから、肺胞マクロファージ及び肺組織のDNA損傷について検討したところ、喫煙により肺胞マクロファージのDNA損傷が認められ、また肺組織では8-OHdGの増加が認められた。

序論

喫煙の研究は、発癌、循環器系に関する研究が多く、肺の免疫系についての研究は、まだ解明されていない点が多く残されている。以前より、我々は環境分野で重要な問題として取り上げられているタバコ喫煙に着目し、喫煙の肺免疫系への影響について、気管支肺胞洗浄により得た人の肺 Natural Killer(NK)細胞活性が非喫煙者に比較して、喫煙者で低下していること、このNK活性の低下は肺胞マクロファージが産生する活性酸素によることを証明し、喫煙者における肺癌の発生の原因に肺胞マクロファージによる NK 細胞活性の低下が一つのリスクファクターとして関与していることを報告し、特に肺の免疫細胞、肺疾患と喫煙の関係について検討を加えてきた[1-10]。

タバコ喫煙により、タバコ煙は直接肺に吸入されるため、肺に存在する免疫細胞、肺組織への影響が考えられる。肺には肺胞マクロファージが存在し、肺の免疫機構に重要な役割をしている。喫煙による肺胞マクロファージ機能への影響については、種々の機能に関する詳細な報告は少なく、また一定した見解が得られていないのが現状である。ヒトにおける喫煙研究においては、タバコの吸い方等に個人差があり、実験条件を統一することが難しいのが現状である。この点を解消するため、本研究では自動喫煙装置を用い、マウスにタバコを一定量、一定期間、均一に喫煙させることが出来るための実験条件を統一し、喫煙の影響を正確に客観的に評価できる実験系を確立し、肺胞マクロファージの細胞表面抗原であるB7-1、ClassⅡ抗原の発現、抗原提示と抗体産生機能、活性酸素産生機能及びサイトカイン mRNA 発現への影響について検討した。

1．喫煙による肺胞マクロファージのBAL(Broncho Alveolar Lavage)所見に及ぼす影響

C57BL/６マウス（８～１０週齢、雌）に、ＨａｍｂｕｒｇⅡ自動喫煙装置を用いて、フィルター付きタバコ（CORESTA APROVED MONITER No.2 ：ニコチン1.5mG、タール15.2mg）の主流煙（空気：タバコ煙＝７：３）を１puff／35ml／２秒で、２０本／日、計１０回喫煙させ、１０回目の喫煙終了後、１日目に喫煙(smoking :S)群及び非喫煙non-smoking :NS)群のマウスをエーテルで犠牲死させた。その後、眼科用のハサミとピンセットで主気管支と肺を露出し、２６Ｇの注射針の付いたシリンジを用いて、ピンセットで注射針を押さえながらＰＢＳ（-）１ｍｌを気管支内に注入し、肺胞マクロファージを回収する操作を１０回行い、洗浄液を回収した肺胞マクロファージの総細胞数は、非喫煙群の2.93±0.63×10^5cells/匹に対し、喫煙群では4.02±1.05×10^5cells/匹で、喫煙による有意な($p<0.001$)総細胞数の増加が認められた。肺胞マクロファージの形態は、非喫煙群と比べて、喫煙群の肺胞マクロファージでは、細胞内に空胞変性が多数散見され、細胞の大型化が認められた。（図１）。

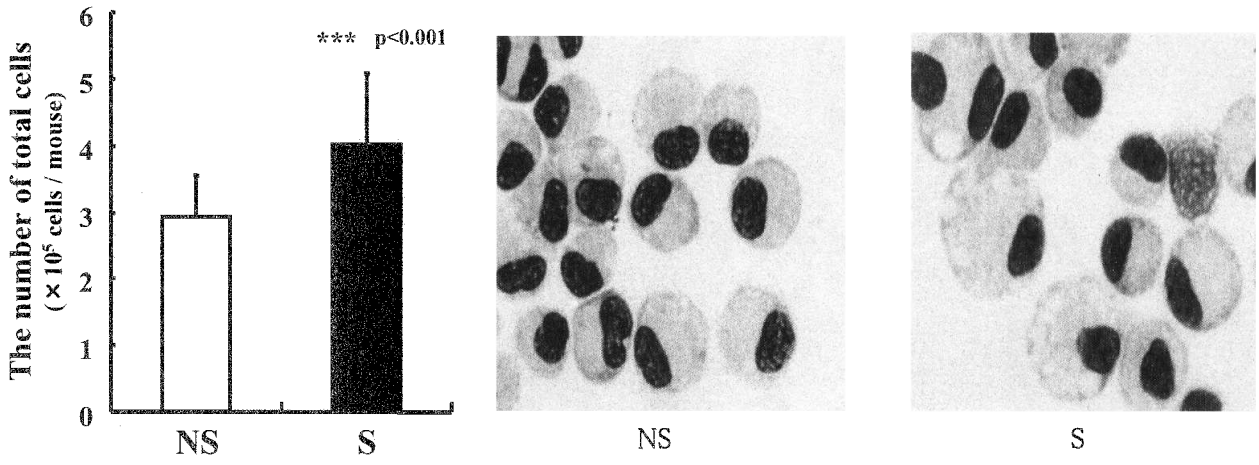

図１　喫煙による肺胞マクロファージ数と形態に及ぼす影響

2．喫煙による肺胞マクロファージの抗原提示機能に及ぼす影響

抗原提示機能は、非喫煙群及び喫煙群の肺胞マクロファージ、MHCの異なる同系マウスの脾臓細胞及び異系マウスの脾臓細胞を混合培養するリンパ球混合培養試験（MLR反応）により検討した。非喫煙群及び喫煙群の肺胞マクロファージ添加によるMLR反応のＳ．Ｉ．値は、非喫煙群の1.0に対し、喫煙群では0.54で、喫煙によるS．I．値の有意な（ｐ＜0.01）減少が認められ、非喫煙群のMLR反応を46%抑制した。この成績から、喫煙による肺胞マクロファージの抗原特異的なMLR反応の抑制が認められた。B7抗原の陽性細胞比率は、非喫煙群の35.00±2.66%に対し、喫煙群では15.60±2.64%で、喫煙による陽性細胞比率の有意な（ｐ＜0.01）減少が認められた。ｃlass Ⅱ抗原の陽性細胞比率は、非喫煙群の25.30±4.88%に対し、喫煙群では7.93±2.09%で、喫煙による陽性細胞比率の有意な（ｐ＜0.05）減少が認められた（図２）。

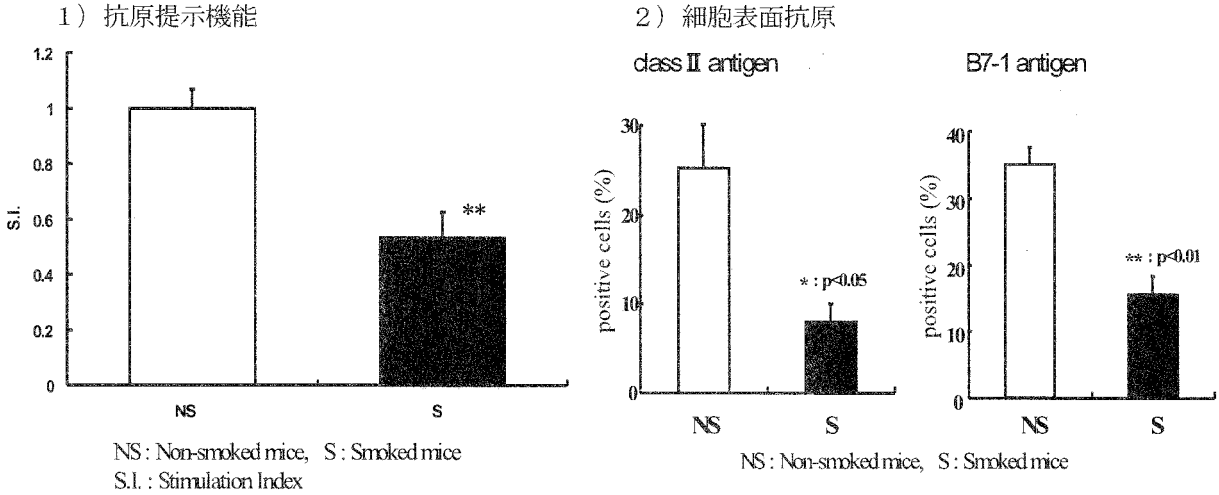

図２　喫煙による肺胞マクロファージの抗原提示機能と細胞表面抗原に及ぼす影響

３．喫煙による肺胞マクロファージのＴ，Ｂリンパ球増殖反応に及ぼす影響

Ｔ細胞、Ｂ細胞の増殖反応に及ぼす影響についてConA、LPSを用いてリンパ球を刺激増殖させ肺胞マクロファージを５%の細胞濃度で添加し増殖反応に及ぼす影響を非喫煙群と比較検討した。喫煙させた肺胞マクロファージは、Ｔ細胞の増殖には影響を及ぼさなかったが、Ｂ細胞の増殖反応だけを特異的に抑制した（図３）。

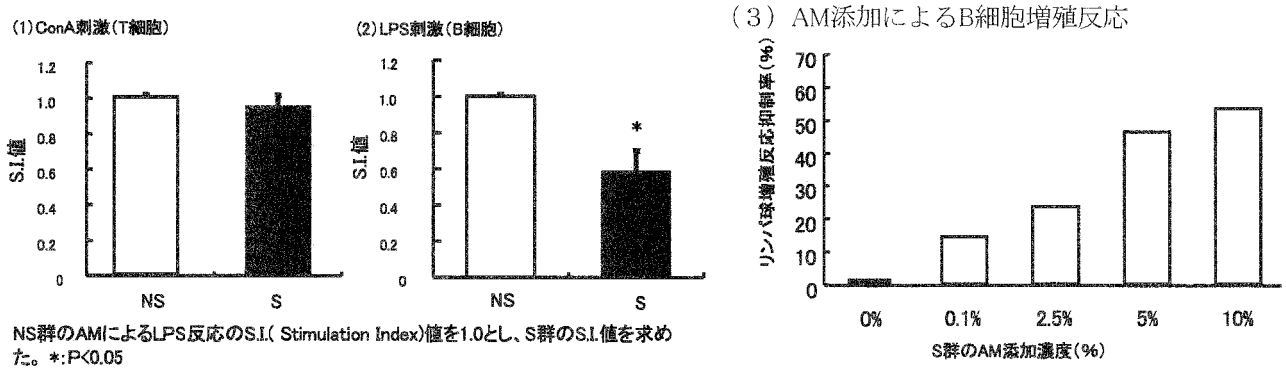

図３　喫煙による肺胞マクロファージのリンパ球増殖反応への影響

4．喫煙による肺胞マクロファージの抗体産生細胞に及ぼす影響

喫煙による肺胞マクロファージの抗体産生細胞に及ぼす影響は、SRBC 抗原に対する抗体産生細胞の PFC 活性により測定した。脾臓細胞 10^6 個当たりの PFC 数は、肺胞マクロファージ非添加では、232.5±27.5（mean±S.E.、n=2）個であったのに対して、肺胞マクロファージ添加においては、NS 群 215.5±18.5 個、S 群 204.5±16.5 個であり、喫煙による肺胞マクロファージの抗体産生細胞に及ぼす影響は、認められなかった（図４）。

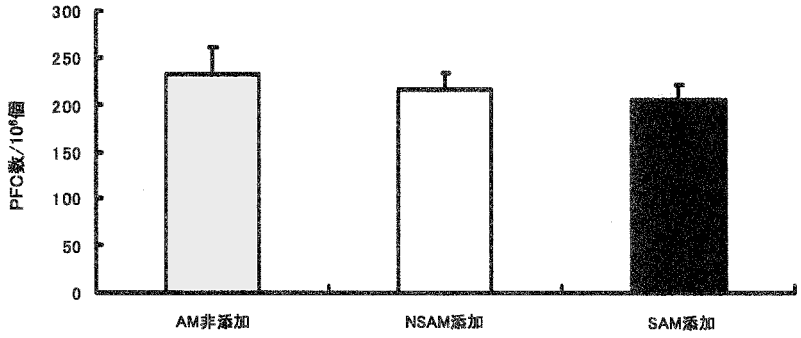

マウスに10^8個SRBCを腹腔内投与し、4日後に脾臓細胞、補体、50%SRBC、NS及びS群のAMを混合し、37℃、1時間反応後、PFC数を測定し、PFC数/10^6個脾臓細胞として表した。コントロール：脾臓細胞+補体+50%SRBC　NSAM：コントロールにNS群のAMを添加（添加濃度5%）　SAM：コントロールにS群のAMを添加（添加濃度5%）

図４　喫煙による肺胞マクロファージの抗体産生細胞への影響

5．喫煙による肺胞マクロファージのサイトカインmRNA発現に及ぼす影響

肺胞マクロファージの IL-1β mRNA 発現比(IL-1β / β-actin)は、LPS で刺激した場合、NS 群で 2.31±0.14(n=4)、S 群で 1.44±0.17(n=7)であった。肺胞マクロファージの IL-1β mRNA 発現は、NS 群に比べて S 群で有意に($p<0.01$)抑制された。肺胞マクロファージの TNF-α mRNA 発現比(TNF-α / β-actin)は、LPS で刺激した場合、NS 群で 1.81±0.33(n=4)、S 群で 1.57±0.29(n=7)であった(図５)。

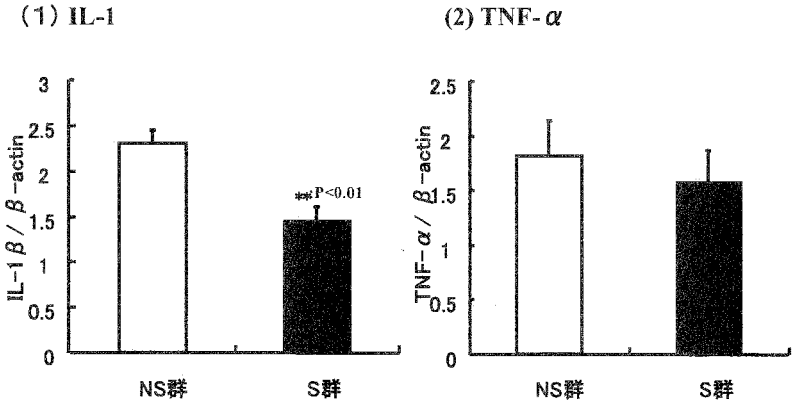

図５　喫煙による肺胞マクロファージのサイトカイン mRNA 発現

6．喫煙による肺胞マクロファージの活性酸素産生に及ぼす影響

肺胞マクロファージの O_2^- 産生の陽性細胞比率(%)は、NS 群 25.4±5.4% (mean±S.E.、n=6)、S 群 64.3±10.5%であり、喫煙による肺胞マクロファージの O_2^- 陽性細胞比率(%)の有意($p<0.001$)な増加が認められた。肺胞マクロファージの H_2O_2 産生の陽性細胞比率(%)は、NS 群で 25.5±5.0%、S 群 53.4±8.1%であり、

喫煙による肺胞マクロファージの H_2O_2 陽性細胞比率(%)の有意 ($p<0.001$)な増加が認められた。肺胞マクロファージの O_2^- H_2O_2 両産生の陽性細胞比率(%)は、NS群 8.3±4.8 (mean±S.E.、n=6)、S群 55.3±3.1 で、喫煙による肺胞マクロファージの O_2^- H_2O_2 陽性細胞比率(%)の有意な($p<0.001$)増加が認められた（図６）。

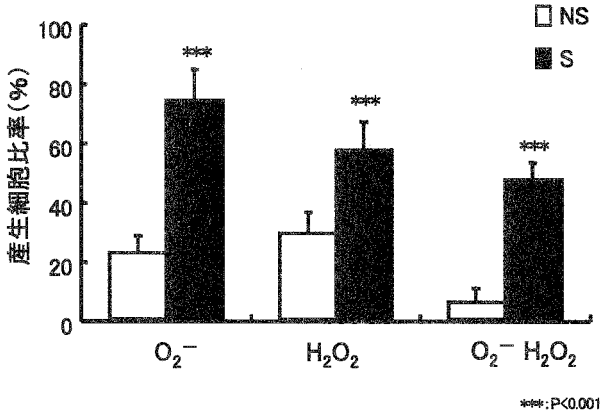

図６　喫煙による肺胞マクロファージの活性酸素産生への影響

７．喫煙による肺胞マクロファージのＢ（LPS 刺激）リンパ球増殖反応に対する活性酸素消去剤の影響

喫煙による肺胞マクロファージの LPS 刺激リンパ球増殖反応に対する活性酸素消去剤の影響は、O_2^-を消去する SOD 及び H_2O_2 を消去する catalase を用いて検討した。SOD 濃度 7.5U/ml で 17.1%、SOD 濃度 75U/ml で 20.2%の回復が認められた。catalase 濃度 6.01U/ml で 52%、catalase 濃度 60U/ml で 78.8%の有意($p<0.02$)な回復が認められた。また、SOD と catalase を使用した場合、SOD7.5U+ catalase6.01U 添加で 99.1%の有意($p<0.01$)な回復、SOD75U+ catalase60U 添加で完全に回復した($p<0.01$)。これらの成績から、喫煙による肺胞マクロファージの LPS 刺激リンパ球増殖反応の抑制は、SOD よりも catalase 添加で回復し、さらに SOD と catalase の両方添加で、完全に回復が認められた（図７）。

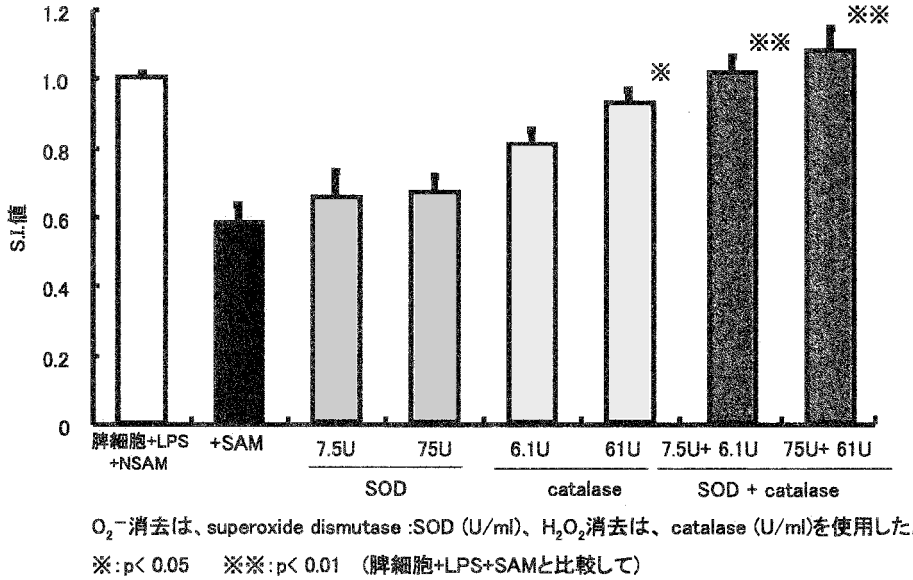

図７　喫煙による肺胞マクロファージによるＢリンパ球増殖反応に対する活性酸素消去剤の影響

総括

肺の免疫系における肺胞マクロファージの主な機能は、貪食作用、他の免疫系細胞を活性化させるサイトカインの産生、T細胞への抗原提示機能であり、肺での生体防御に中心的な役割をしている[11]。喫煙は、免疫細胞の機能に影響することが知られており、抗腫瘍細胞活性の低下、B細胞のLPS反応の増加、Con Aが誘導するIL－２産生の減少及びT細胞のMLR反応の減少などが報告されている[12-16]。しかし、喫煙の肺胞マクロファージが関与した抗原特異的（抗原提示）、抗原非特異的なリンパ球との相互反応及び肺胞マクロファージの様々な機能に及ぼす影響に関する詳細な報告は少ないのが現状である。そこで、喫煙による肺胞マクロファージの抗原提示機能とその後の抗体産生への影響を調べるために、抗原特異的なMLR法を用いて検討したところ、非喫煙群と比較して、喫煙群の肺胞マクロファージではリンパ球のMLR反応の抑制が認められた。この結果は、喫煙によって、T細胞のMLR反応が減少するという報告[14]と一致した結果であった。B7及びclassⅡ抗原は抗原提示に重要な役割をしており、クラスⅡ抗原はT細胞のTCRと接着することにより抗原提示が行なわれる。肺胞マクロファージの細胞表面抗原については、喫煙によるB7及びclass Ⅱ抗原の有意な減少が認められ、ヒトでの喫煙者の肺胞マクロファージのHLA c lass Ⅱ抗原密度が減少する報告[17]と一致していた。また、抗体産生の初期のB細胞増殖反応も喫煙により抑制され、この抑制は活性酸素消去剤により回復された結果から、B細胞増殖反応の抑制は活性酸素によることが示された。しかし、既に抗体を産生している細胞には、喫煙による影響はないことから、喫煙は肺胞マクロファージの抗原提示及びB細胞の初期増殖反応に抑制的に働き、その結果抗体産生を抑制し易感染性を増加させる可能性が示唆された（図８）。今後、この抑制機構の詳細な解明と環境タバコ煙についても同様の研究を進めることが必要であると考えられる。

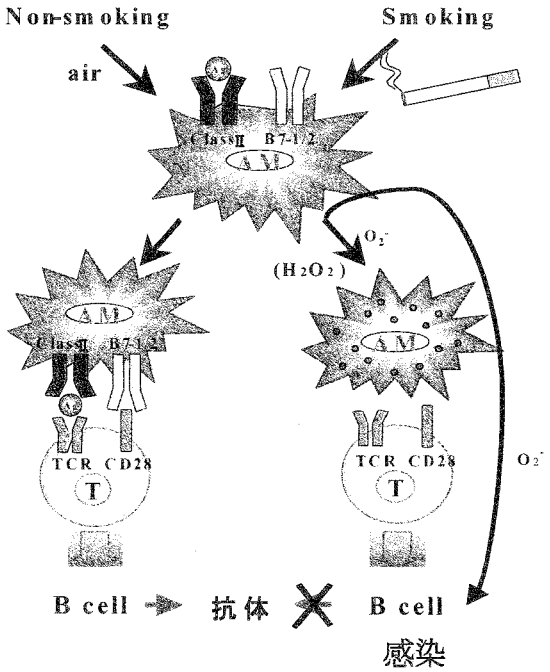

図８　喫煙による肺胞マクロファージの抗原提示機能の抑制機構

参考文献

1. M. Takeuchi, S. Nagai, and T. Izumi. Inhibition of natural killer cell activity by alveolar macrophages in smokers. In : Tobacco : The Growing Epidemic. (Rushan Lu, Judith Mackay, Shiru Niu and Richard Peto eds). Springer. pp.135-136.2000.
2. M. Takeuchi, A. Nakajima, K. Yoshikawa, M. Shinya, H. Asada, M. Yoshimura, C. Tsukano, S. Nagai and Effect of smoking on immunological functions of alveolar macrophages in mice. In : Tobacco Counters Health (A.K.Varma ed), Macmilan Ltd., pp.168-171, 2000.
3. Mikuniya T., Nagai S., Takeuchi M., Mio T., Hosono Y., Miki H., Shigematsu M., Hamada K. and Izumi T. Significance of the interleukin-1 receptor antagonist /interleukin-1β ratio as a prognostic factor in pulmonary sarcoidosis. Respiration 67: 389-396, 2000.
4. Takeuchi M., Nagai S., Nakajima A., Shinya M., Tsukano C., Asada H., Yoshikawa K., Yoshimura M. and Izumi T. Inhibition of lung natural killer (NK) cell activity by smoking : The role of alveolar macrophages. Respiration 68: 262-267, 2001.
5. 竹内実　喫煙と免疫機能.　臨床免疫　36:843-850, 2001.
6. Takeuchi M., Nagai S. and Izumi T. Effect of smoking on natural killer cell activity in the lung. CHEST 94:688-693 1988
7. Takeuchi M., Nagai S. and Izumi T. The mechanism of inhibition of alveolar macrophages on autologous blood natural killer cell activity. CHEST 95:383-387 1989
8. Nagai S., Takeuchi M., Watanabe K. Aung H. and Izumi T. Smoking and interleukin-1 activity released from human alveolar macrophages in healthy subjects. CHEST 94:694-700 1988
9. Nagai S., Aung H., Takeuchi M., Kusume K. and Izumi T. IL-1 and IL-1 inhibitory activity in the culture supernatants of alveolar macrophages from patients with interstitial lung diseases. CHEST 99:674-680 1991
10. Takeuchi M., Nagai S., Tsutsumi T., Mio T. and Izumi T. The number of interleukin-1 (IL-1) receptor on lung fibroblasts in patients with idiopathic pulmonary fibrosis. Respiration 6:236-241 1999
11. Rylander R. Pulmonary cell response to inhalted cigarette smoke Arch. Environ. Health. 29: 329-333 1974
12. Geiselhart L.A., Christian T., Minnear F., Freed B.M. The cigarette tar component p-benzoquinone blocks T-lymphocyte activation by inhibiting interleukin-□ production,but not CD25,ICAM-1 or LFA-1 expression. Toxicol Appl.Pharmacol,143: 130-136, 1997.
13. Geng Y.,Savage,S.M.,Razani-Boroujerdi,S.,Sopori,M.L. Effect of nicotine on immune response 2. Chronic nicotine treatment induces T cell anergy. The Jounal of Immunology 2384-2390, 1996.
14. Jennie C.C., Distler,S.G., Kaplan,A.M. Tobacco smoking suppresses T cell but not antigen-presenting cells in the lung-associated lymph nodes. Toxicol. Appl. Pharmacol. 102: 514-523, 1990.

15. Wayne R.T.,Holt P.G.,Keast D. Cellular immunity in mice chronically exposed to fresh cigarette smoke. Arch.Envron.Health, 27: 372-375, 1973.
16. Geng Y.,Savage,S.M.,Razani-Boroujerdi,S.,Sopori,M.L. Effect of nicotine on immune response 2. Chronic nicotine treatment induces T cell anergy. The Jounal of Immunology 2384-2390, 1996.
17. Pankow W., Neumann K., Schrer R., von Wichert P. Reduction in HLA-DR antigen density on alveolar macrophages of smokers. Lung 169(5): 255-262, 1991.

研究活動状況

〔学術論文〕

1. Akita, K., Toda, M., Hosoki, Y., Inoue, M., Fushiki, S., Oohira, A., Okayama, M., Yamashina, I. and Nakada, H. Heparan sulphate proteoglycans interact with Neurocan and promote neurite outgrowth from cerebellar granule cells. Biochem. J., 383: 129-138, 2004.

2. Nishikawa, A., Uotsu, N., Arimitsu, H., Lee, J-C., Miura, Y., Fujinaga, Y., Nakada, H., Watanabe, T., Ohyama, T., Sakano, Y. and Oguma, K. The receptor and transporter for internalization of *Clostridium botsulinum* type C progenitor toxin into HT-29 cells. Biochem. Biophys. Res. Commun., 319: 327-333, 2004.

3. Sakuraba, H., Matsuzawa, F., Aikawa, S., Doi, H., Kotani, M., Nakada, H., Fukushige, T. and Kanzaki, T. Structural and immunocytochemical studies on □-N-acetylgalactosaminidase deficiency (Schindler/Kanzaki disease). J. Hum. Genet., 49: 1-8, 2004.

4. Kusano, Y., Yoshitomi, Y., Munesue, S., Okayama, M. and Oguri, K. Cooperation of Syndecan-2 and Syndecan-4 among Cell Surface Heparan Sulfate Proteoglycans in the Actin Cytoskeletal Organization of Lewis Lung Carcinoma Cells. J. Biochem.(Tokyo), 135: 129-137, 2004

5. Yoshitomi, Y., Nakanishi, H., Kusano, Y., Munesue, S., Oguri, K., Tatematsu, M., Yamashina, I. and Okayama, M. Inhibition of experimental lung metastases of Lewis lung carcinoma cells by chemically-modified heparin with reduced anticoagulant activity. Cancer Lett., 207: 165-174, 2004

6. 棟居聖一、吉冨泰央、小山芳江、成尾英明、岡山實. シンデカン-2 を介したがん転移の制御機構の解析. 京都産業大学先端科学技術研究所所報, 第 3 号: 115-128, 平成 16 年

7. Rollin P. Tabuena, Sonoko Nagai, Takeo Tsutumi, Tomohiro Handa, Takeuchi Minoru, Takeshi Mikuniya, Michio Shigematsu, Kunio Hamada, Takateru Izumi and Michiaki Mishima. Broncholalveolar lavage fluid cell profile as a predictor of the prognosis of idiopathic pulmonary fibrosis/usual interstitial pneumonia (IPF/UIP) among japanese patients. Respiration , in press.

8. Horiguchi, N., Arimoto, K., Mizutani, A, Endo-Ichikawa, Y., Nakada, H. and Taketani, S. Galectin-1induces cell adhesion to the extracellular matrix and apoptosis of non-adherent human colon cancer Colo 201 cells. J. Biochem., 134: 869-874, 2003.

9. Inaba, T., Sano, H., Kawahito, Y., Hla, T., Akita, K., Toda, M., Yamashina, I., Inoue, M. and Nakada, H. Induction of cyclooxygenase-2 in monocyte/macrophage by mucins secreted from colon cancer cells. Proc. Natl. Acad. Sci. USA, 100: 2736-2741, 2003.

10. 吉冨泰央、棟居聖一、小山芳江、岡山實. シンデカン-2 強制発現による腫瘍の組織形成と転移、浸潤能の変化. 京都産業大学先端科学技術研究所所報, 第 2 号: 91-102, 平成 15 年

11. M. Shinya, O. Mazda, C. Tsuchihara, H. Hirai, J. Imanishi and M. Takeuchi.Interleukin-2 abolishes myeloid cell accumulation induced by Lewis lungcarcinoma. J. Interferon & Cytokine Research 23:631-638,2003.

12. Munesue, S., Kusano, Y., Oguri, K., Itano, N., Yoshitomi, Y., Nakanishi, H., Yamashina, I. and

Okayama, M. The role of syndecan-2 in regulation of actin cytoskeletal organization of Lewis lung carcinoma-derived metastatic clones. Biochemical Journal, 363: 201-20, 2002.

13. Oguri, K., Munesue, S., Kusano, Y., Yoshitomi, Y. and Okayama, M. Involvement of syndecans in actin cytoskeletal organization and tumor metastasis. Connective Tissue. 34: 283-290, 2002.

14. Asada, H., Kishida, T., Hirai, H., Satoh, E., Ohashi,.S Takeuchi, M., Kubo, T., Kita, M., Iwakura, Y., Imanishi, J. and Mazuda, O. Significant antitumor effect obtained by autologous tumor cell vaccine engineered to secrete interleukin (IL)-12 and IL-18 by means of the EBV/Lipoplex. Molecular Therapy. 5: 609-616, 2002.

15. Xu, B., Aoyama, K., Takeuchi, M., Matsushita, T. and Takeuchi, T. Expression of cytokine mRNA in mice cutaneously exposed to folmaldehyde. Immunology Letters, 84: 49-55, 2002.

16. Nakajima, A., Koga, M., Takeuchi, T., Mazuda, O., Ishida, T. and Takeuchi, M. Effect of hot water extract from agaricus blazeil murille on antibody production in mice. International Immunopharmacology, 2: 1205-1211, 2002.

17. 棟居聖一、吉冨泰央、岡山實. 細胞膜型ヘパラン硫酸プロテオグリカン，シンデカン-2 によるアクチン細胞骨格形成の制御. 京都産業大学先端科学技術研究所所報，創刊号: 95-110，平成 14 年

18. Inoue, M., Takahashi, S., Yamashina, I., Kaibori, M., Okumura, T., Kamiyama, Y., Vichier-Guerre, S., Cantacuzene, D. and Nakada, H. High density O-glycosylation of the MUC2 tandem repeat unit by N-acetylgalactosaminyltransferase-3 in colonic adenocarcinoma extracts. Cancer Res., 61: 950-956, 2001.

19. Akita, K., Fushiki, S., Fujimoto, T., Inoue, M., Oguri, K., Okayama, M., Yamashina, I. and Nakada, H. Developmental expression of a unique carbohydrate antigen, Tn antigen, in mouse central nervous tissues. J. Neurosci. Res., 65: 595-603, 2001.

20. Takeuchi, M., Nagai, S., Nakajima, A., Shinya, M., Tsukano, C., Asada, H., Yoshikawa, K., Yoshimura, M. and Izumi, T. Inhibition of lung natural killer (NK) cell activity by smoking: The role of alveolar macrophages. Respiration, 68: 262-267, 2001.

21. Oshinaga, E., Bay, S., Tello, D., Babino, A., Pritsch, O., Assemat, K., Cantacuzene, D., Nakada, H. and Alzari, P. Analysis of the fine specificity of Tn-binding proteins using synthetic glycopeptide epitopes and a biosensor based on surface plamson resonance spectroscopy. FEBS Lett., 469: 24-28, 2000.

22. Guerre, S. V., Lo-Man, R., Bay, S., Deriaud, E., Nakada, H., Leclerc, C. and Cantacuzene, D. Short synthetic glycopeptides successfully induce antibody responses to carcinoma-associated Tn antigen. J. Peptide Res., 55: 173-180, 2000.

23. Kusano, Y., Oguri, K., Nagayasu, Y., Munesue, S., Ishihara, M., Saiki, I., Yonekura, H., Yamamoto, H. and Okayama, M. Participation of syndecan 2 in the induction of stress fiber formation in cooperation with integrin □5□1: Structural characteristics of heparan sulfate chains with avidity to COOH-terminal heparin-binding domain of fibronectin. Experimental Cell Research, 256: 434-444. 2000.

24. Mikuniya, T., Nagai, S., Takeuchi, M., Mio, T., Hosono, Y., Miki, H., Shigematsu, M., Hamada, K. and Izumi, T. Significance of the interleukin-1 receptor antagonist /interleukin-1,, ratio as a prognostic factor in pulmonary sarcoidosis. Respiration, 67: 389-396, 2000.

〔学会発表〕

1. Nakada, H., Toda, M., Takagi, H., Shigenobu, T., Yoshida, M., Inaba, T., Takeuchi, N. and Inoue, M. Biological function of mucins through scavenger receptor present on monocytes/macrophages. US/JAPAN GLYCO 2004, p.14. 2004. November, [Hawaii, USA]

2. Sugihara, I., Toda, M., Inoue, M. and Nakada, H. Immunomoculatory effect of mucins produced by epithelial cancer cells. US/JAPAN GLYCO 2004, p.29. 2004. November, , [Hawaii, USA]

3. Hosoki, Y., Akita, K., Toda, M., Inoue, M., Fushiki, S., Oohira, A., Okayama, M. and Nakada, H. Heparan sulfate proteoglycans interact with neurocan and promote neurite outgrowth from cerebellar granule cells. US/JAPAN GLYCO 2004, p.29. 2004. November, [Hawaii, USA]

4. Sugihara, I., Toda, M., Inoue, M. and Nakada, H. Immunological effect of mucins produced by epithelial cancer cells. 杉原一平、戸田宗豊、井上瑞江、中田博．上皮性癌細胞より産生されるムチンの免疫学的影響．第77回日本生化学会大会、p.154、2004．10月、横浜

5. Inoue, M., Toda, M., Akita, K. and Nakada, H. Regulation of NK cell activity by mucins through Siglec 7. 井上瑞江、戸田宗豊、秋田薫、中田博．ムチンによるシグレック7を介したNK活性の制御．第77回日本生化学会大会、p.154、2004．10月、横浜

6. Hosoki, Y., Akita, K., Toda, M., Inoue, M., Fushiki, S., Oohira, A., Okayama, M., Yamashina, I. and Nakada, H. Heparan sulfate proteoglycans interact with neurocan anc promote neurite outgrowth from cerebellar granule cells. 細木由起、秋田薫、戸田宗豊、井上瑞江、伏木信次、大平敦彦、岡山實、山科郁男、中田博．小脳顆粒細胞の神経突起伸長とヘパラン硫酸プロテオグリカンのニューロカンとの相互作用．第77回日本生化学会大会、p.270、2004．10月、横浜

7. 中田博、横井川規巨、稲葉隆明、海堀昌樹、小倉徳裕、高田秀穂、井上瑞江、權雅憲、上山泰男．担癌状態におけるムチンの生物学的意義．第63回日本癌学会総会、p.97、2004．9月、福岡

8. Munesue, S., Yoshitomi, Y., Koyama, Y., Naruo, Y., Nishiyama, A., Kusano, Y., Oguri, K., Miyazaki, K. and Okayama, M. Regulation of matrix metalloproteinase-2 activation through syndecan-2 第77回日本生化学会大会（横浜）、2004.

9. 棟居聖一、吉冨泰央、小山芳江、成尾英明、草野由理、小栗佳代子、中西速夫、宮崎香、岡山實 シンデカン-2によるマウス・ルイス肺癌細胞の転移抑制 第13回日がん転移学会学術集会（東京)、2004.

10. 吉冨泰央、棟居聖一、山科郁男、岡山實、中西速夫、立松正衛、草野由理、小栗佳代子 化学修飾ヘパリンによるルイス肺がん細胞の実験肺転移抑制 第13回日がん転移学会学術集会（東京）、2004.

11. Chiharu Tsuchihara, Yoshihiro Nambu, Kazumi Mori, Taku Oikawa, Ken Nakagawa, Kazuhiro Osanai, Hirohisa Toga, Keiji Takahashi, Minoru Takeuchi and Kei-ichi Hirai. Anti-tumor effect of J103 (2-methylnaphtho[2,3-*b*]furan-4,9-dione) on lung cancer cell via Fas/Fas ligand system. ATS 100th International Conference, Am. J. Respir. Crit. Care Med., A290, 2004.

12. Hidetsugu Asada, Tsunao Kishida, Hideyo Hirai, Jiro Imanishi, Minoru Takeuchi, and Osam Mazda.

Dendritic Cell (DC) Vaccine Loaded with Apoptotic Tumor Fragments Effectively Suppress Preestablished Malignant Melanoma in Mice. The American Society of Gene Therapy, 7th Annual Meeting, p262, June, 2004.

13. 竹内実、竹林智弘、土原千春、古賀美千子、布袋義巳、浅田秀基、松田修．アガリクス茸抽出液による腫瘍増殖の予防効果とその作用機構について　第６３回日本癌学会学術総会記事 p531, 2004 年.

14. 浅田秀基，松田修，岸田綱郎，竹内実．樹状細胞へのアポトーシス誘導腫瘍細胞のパルスと naïve T 細胞を用いたワクチン細胞の作製とその抗腫瘍効果の検討．第 34 回日本免疫学会総会・学術集会．p212．2004.

15. Takeuchi Minoru, Asada Hidetsugu, Futei Yashimi, Mazda Osamu and Pinkerton Kent. The mechanism of antigen presenting activity in alveolar macrophages by main stream cigarette tobacco smoke exposure. Proceeding of the Japanease Society for Immunology, Vol. 34, p55, 2004.

16. Inaba, T., Sano, H., Kawahito, Y., Akita, K., Toda, M., Yamashina, I., Inoue, M. and Nakada, H. Induction of cyclooxygenase-2 in monocyte/macrophage by mucins secreted from colon cancer cells. XVII International symposium on Glycoconjugates, p.67, 2003.

17. Yoshitomi, Y., Munesue, S., Mizumachi, K., Kusano, Y., Oguri, K. and Okayama, M. Pathological significance of the inverse correlation between expression level of syndecan-2 and metastatic potential of Lewis lung carcinoma cells. GLYCO XVII: XVIIth International Symposium on Glycoconjugates, p.67, 2003.

18. Munesue, S., Yoshitomi, Y., Mizumachi, K., Koyama, Y., Hirose, M., Kusano, Y., Oguri, K. and Okayama, M. Regulation of Rho family proteins through Syndecan-2 and Actin Cytoskeletal Organization of Lewis Lung Carcinoma cells　第 76 回日本生化学会大会（横浜）、2003.

19. Yoshitomi, Y., Oguri, K., Kusano, Y., Nakanishi, H., Munesue, S., Koyama, Y. and Okayama, M. Signaling through Syndecan-2 Plays a Central Role in Metrastasis and Invasion of Lewis Lung Carcinoma Cells. 3rd International Conference on Proteoglycans, Italy, Parma, 2003.

20. Munesue, S., Kusano, Y., Yoshitomi, Y., Koyama, Y., Okayama, M., Funakoshi, I. and Oguri, K. Regulation of Actin Cytoskeletal Organization of Mouse Lewis Lung Carcinoma Cells through Syndecan-2. 3rd International Conference on Proteoglycans, Italy, Parma, 2003.

21. Kusano, Y., Yoshitomi, Y., Munesue, S., Koyama, Y., Okayama, M. and Oguri, K. An expression level of Syndecan-2 on Lewis lung carcinoma cells correlates inversely to metastatic potential and positively to invasive capacity. 5th Panpacific Conective Tissue, Japan, Yamaguchi, 2003.

22. Munesue, S., Yoshitomi, Y., Mizumachi, K., Koyama, Y., Hirose, M., Kusano, Y., Oguri, K. and Okayama, M. Involvement of Rho family proteins in cell adhesion-dependent actin cytoskeletal organization of Lewis lung carcinoma cells. 5th Panpacific Conective Tissue, Japan, Yamaguchi, 2003.

23. 草野由理、吉冨泰央、棟居聖一、橋本克訓、横井豊治、中西速夫、岡山實、小栗佳代子．マウスモデル系において腫瘍細胞のシンデカン-2 発現量は転移能とは逆相関を、浸潤能とは正相関を示す．第 12 回日本がん転移学会学術集会（金沢）、2003.

24. 吉冨泰央、水町弘治、廣瀬まゆみ、棟居聖一、草野由理、小栗佳代子、成宮周、岡山實．転

移能の異なる腫瘍細胞が示すアクチン細胞骨格形成における Rho ファミリー活性化の解析. 第 12 回日本がん転移学会学術集会（金沢）、2003.

25. 土原千春、南部静洋、中村佳津美、及川　卓、中川　研、長内和弘、佐久間勉、栂　博久、高橋敬治、大谷信夫、竹内　実、平井圭一 Furanonaphthoquinone(J103)の腫瘍細胞に対する抑制効果と免疫応答細胞への影響第 43 回日本呼吸器学会総会、日呼吸会誌,41:177,2003.

26. M. Takeuchi, K.R. Smith and K.E. Pinkerton. Effect of cigarette smoke exposure on immune function of alveolar macrophages in mice. 8th Tobacco-Related Disease Research Program (TRDRP) Annual Investigator Meeting, p.48, 2003.

27. 吉冨泰央、棟居聖一、草野由理、小栗佳代子、岡山　實. Overexpression of syndecan-2 supresses the metastatic phenotype of mouse Lewis lung carcinoma cells. 第 34 回日本結合組織学会. 2002.

28. 土原千春、南部静洋、中村佳津美、長内和弘、佐久間勉、栂　博久、高橋敬治、大谷信夫、竹内　実、平井圭一. 肺癌に対する Furanonaphthoquinone 誘導体の Fas を介する抗腫瘍効果と免疫応答細胞への影響第 42 回日本呼吸器学会総会、日呼吸会誌,40:143,2002

29. 土原千春、南部静洋、中村佳津美、及川　卓、長内和弘、佐久間勉、栂　博久、高橋敬治、大谷信夫、竹内　実、平井圭一. Furanonaphthoquinone 誘導体(J103)の免疫応答に関する影響第 43 回日本肺癌学会総会、肺癌,42:518,2002

30. C.Tsuchihara, Y.Nambu, K.Nakamura, K.Osanai, T.Sakuma, H.Toga, M.Takeuchi, K.Takahashi, N.Ohya, K-I.Hirai. Anti-tumor effect of furanonaphthoquinone analog(J103) on cultured lung cancer cells: up-regulation of fas receptor and induction of apoptosis via Fas/Fas ligand system. 17th Meeting of the EACR, Rev. Oncol., 4:126, 2002.

31. 草野由理、吉冨泰央、棟居聖一、岡山　實、小栗佳代子. Function of syndecan-2 as a receptor for fibronectin. 第 34 回日本結合組織学会. 2002.

32. 中田　博. 上皮性癌細胞の産生するムチンの免疫担当細胞への影響. 第 3 回関西グライコサイエンスフォーラム、p.18、2002.

33. 秋田　薫、伏木信次、宮本祐希、井上瑞江、山科郁男、棟居聖一、小栗佳代子、岡山　實、中田　博. ムチン様領域を持つシンデカン-3 のマウス中枢神経組織における発現と生物学的機能の検索. 第 49 回日本生化学会近畿支部例会、p.24、2002.

34. 草野由理、吉冨泰央、棟居聖一、岡山　實、小栗佳代子. 腫瘍細胞のシンデカン-2 発現量依存的な間質誘導能と浸潤能. 第 10 回日本がん転移学会総会、p.18、2002.

35. Takeuchi, M., Nakajima, A., Ishida, T., Koga, M. and Takeuchi, T. Effect of cigarette smoking on relationship of oxygen metabolism and cell surface antigens to antigen presenting activity in murine alveolar macrophages. Am J Respir Crit Care Med, 165: p.449, 2002.

36. 戸田宗豊、秋田　薫、井上瑞江、中田　博. ムチンによる Siglec 2 を介した B 細胞の情報伝達抑制について. 第 23 回日本糖質学会年会、p.134、2002.

37. 横井川規巨、稲葉隆明、井上瑞江、海堀昌樹、權　雅憲、上山康男、中田　博. 単球／マクロファージにおけるスカベンジャーリセプターを介したムチンによるシクロオキシゲナーゼ 2

の誘導．第 61 回日本癌学会総会、p.308、2002.

38. 竹内　実、中島敦子、佐々木洋一、古賀美千子、石田喬裕、竹内　亨．アガリクス茸抽出液投与による抗腫瘍免疫細胞への影響．第６１回日本癌学会総会、p481、2002.

39. 宮本祐希、秋田　薫、中田　博．様々な癌細胞株に発現する Tn 抗原を持つ糖タンパク質の単離と生物学的性質．第 75 回日本生化学会大会、p.723、2002.

40. 吉田匡伸、若宮伸隆、中田　博．スカベンジャーリセプター受容体へのムチンの結合を介したマウス腹腔マクロファージにおける COX-2 の誘導．第 75 回日本生化学会大会、p.723、2002.

41. 中田　博、稲葉隆明、横井川規巨、吉田匡伸、秋田　薫、戸田宗豊、山科郁男、井上瑞江．ムチンによる単球／マクロファージにおけるシクロオキシゲナーゼ 2 の誘導．第 75 回日本生化学会大会、p.723、2002.

42. 戸田宗豊、井上瑞江、山科郁男、中田　博．ムチンによる Siglec-2 (CD22) を介した B 細胞情報伝達について．第 75 回日本生化学会大会、p.723、2002.

43. 吉岡伸悟、高田美紀、石塚洋三千、里　正人、棟居聖一、小栗佳代子、岡山　實、舩越育雄．シンデカン-２、-４コアタンパク質の自己会合．第 75 回日本生化学会大会、p.731、2002.

44. 秋田　薫、伏木信次、宮本祐希、井上瑞江、山科郁男、棟居聖一、小栗佳代子、岡山　實、中田　博．シンデカン-3 のマウス中枢神経組織における発現と糖鎖を介した生物学的機能の検索．第 75 回日本生化学会大会、p.734、2002.

45. 中田　博．ムチンによる単球／マクロファージにおけるシクロオキシゲナーゼ 2 の誘導．近畿シクロオキシゲナーゼ研究会、2002.

46. 石田喬裕、古賀美千子、中島敦子、佐々木美紀、竹内　実．喫煙によるマウス肺胞マクロファージの LPS 反応抑制機序の解析．日本免疫学会総会、32：p.29、2002.

47. 古賀美千子、石田喬裕、中島敦子、佐々木美紀、竹内　実．Lewis Lung Carcinoma2 腫瘍細胞に対するエフェクター細胞の性状について．日本免疫学会総会、32：p.212、2002.

48. 井上瑞江、高橋秀司、中田　博．UDP-GalNAc: polypeptide GalNAc-T3 による Tn 抗原の形成．第２回関西グライコサイエンスフォーラム、p.4、2001.

49. 草野由理、小栗佳代子、棟居聖一、吉冨泰央、岡山　實．シンデカン-２遺伝子導入によりルイス肺癌株細胞の転移能は抑制される．第 10 回日本がん転移学会総会、p.84、2001.

50. 棟居聖一、吉冨泰央、廣瀬まゆみ、草野由理、小栗佳代子、岡山　實．腫瘍細胞の転移能を抑制するフィブロネクチン受容体、シンデカン-２の機能特異性．第 10 回日本がん転移学会総会、p.114、2001.

51. 秋田　薫、伏木信次、井上瑞江、小栗佳代子、岡山　實、中田　博．マウス胎児の中枢神経組織に発現する Tn 抗原とコアタンパク質の同定．第 22 回日本糖質学会年会、p.125、2001.

52. Fujii, H., Inaba, T., Akita, K., Inoue, M., Yamashina, I. and Nakada, H. Activation of monocytes/macrophages by mucins produced by colon cancer cells. GLYCO XVI: XVIth

International Symposium on Glycoconjugates, p.131, 2001.

53. Inoue, M., Takahashi, S., Yamashina, I. and Nakada, H. High density O-Glycosylation of the MUC2 tandem repeat unit by N-acetylgalactosaminyltransferase-3 in colonic adenocarcinoma extracts. GLYCO XVI: XVIth International Symposium on Glycoconjugates, p.131, 2001.

54. Okayama, M., Munesue, S., Yoshitomi, Y., Hirose, M., Y., Funakoshi, I., Kusano, Y. and Oguri, K. Elevated level of syndecan-2 expression suppresses the metastatic phenotype of Lewis lung carcinoma cells. GLYCO XVI: XVIth International Symposium on Glycoconjugates, p.126, 2001.

55. Oguri, K., Kusano, Y., Munesue, S., Yoshitomi, Y. and Okayama, M. Syndecan-2 acts as a regulator for actin cytoskeletal organizations in cooperation with or without integrin □5□1 on fibronectin substratum. GLYCO XVI: XVIth International Symposium on Glycoconjugates, p.28, 2001.

56. Okayama, M., Munesue, S., Yoshitomi, Y. and Hirose, M. Involvement of syndecan-2 in regulation of actin cytoskeletal organization. 53rd Harden Conference-'Proteoglycan', p.18, 2001.

57. 中田　博、佐野　統、山科郁男、井上瑞江．上皮性癌細胞の産生するムチンによる単球／マクロファージの活性化に伴う PGE2 の産生．第 60 回日本癌学会総会、p156、2001.

58. 草野由理、小栗佳代子、棟居聖一、吉冨泰央、廣瀬まゆみ、山科郁男、岡山　實．シンデカン-２強制発現による転移能の抑制．第 60 回日本癌学会総会、p.172、2001.

59. 竹内　亨、小松正治、森本兼嚢、竹内　実．酸素ストレス高感受性システムによる抗酸化物質の評価．第 60 回日本癌学会総会、p.73、2001.

60. 中島敦子、山本ひろ美、堀之内香菜子、古賀美千子、石田喬裕、竹内　亨、竹内　実．喫煙の DNA 損傷に及ぼす影響と協和アガリクス茸の効果について．第 60 回日本癌学会総会、p.273、2001.

61. 土原千春、南部静洋、高橋敬治、大谷信夫、平井圭一、竹内　実．Furanonaphthoquinone 誘導体の肺癌細胞に対する抗腫瘍効果と Fas 受容体発現誘導．第 60 回日本癌学会総会、p.583、2001.

62. 古賀美千子、石田喬裕、中島敦子、竹内　実．Lewis Lung Carcinoma2 腫瘍細胞に対するエフェクター細胞の性状について．日本免疫学会総会、31：p.163、2001.

63. 石田喬裕、古賀美千子、中島敦子、竹内　亨、竹内　実．喫煙によるマウス肺胞マクロファージの ConA 及び LPS 反応に及ぼす影響．日本免疫学会総会、31：p.239、2001.

64. 中島敦子、石田喬裕、古賀美千子、堀之内香菜子、竹内　実．協和アガリクス茸抽出液による抗体産生機能の増強機序について．日本免疫学会総会、31：p.275、2001.

65. 秋田　薫、伏木信次、宮本祐希、井上瑞江、山科郁男、棟居聖一、小栗佳代子、岡山　實、中田　博．マウス胎児の中枢神経組織における Tn 抗原の発現とコアタンパク質の同定．第 74 回日本生化学会大会、p.695、2001.

66. 稲葉隆明、吉田匡伸、秋田　薫、戸田宗豊、山科郁男、井上瑞江、中田　博．上皮性癌細胞により産生されるムチンによるヒト末梢血単球／マクロファージの活性化．第 74 回日本生化学会大会、p.695、2001.

67. 戸田宗豊、井上瑞江、秋田　薫、山科郁男、中田　博．ムチンによるCD22を介したB細胞情報伝達について．第74回日本生化学会大会、p.696、2001．

68. 吉岡伸悟、高田美紀、棟居聖一、小栗佳代子、岡山　實、舩越育雄．マウス初期胚におけるシンデカンファミリーの発現．第74回日本生化学会大会、p.702、2001．

69. 棟居聖一、吉冨泰央、廣瀬まゆみ、草野由理、小栗佳代子、舩越育雄、山科郁男、岡山　實．フィブロネクチン受容体シンデカン-2遺伝子導入による腫瘍細胞の形質転換．第74回日本生化学会大会、p.740、2001．

70. 中田　博、稲葉隆明、藤井博紹、悴山博美、山科郁男、井上瑞江．ムチンによるマクロファージの活性化．第21回日本糖質学会年会、p.74、2000．

71. Takeuchi, M., Nakajima, A., Yoshikawa, K., Shinya, M., Asada, H., Yoshikawa, M. and Tsukano, C. Functional changes in alveolar macrophages following exposure of mice to cigarette smoke. 11th World Conference On Tobacco Or Health, 2: p.430, 2000.

72. 井上瑞江、海堀昌樹、上山康男、山科郁男、中田　博．腸癌組織において発現亢進の見られる GalNAc 転移酵素と癌関連糖鎖抗原の発現との関連．第 59 回日本癌学会総会、p.304、2000．

73. 中島敦子、竹内　実．抗腫瘍性を有する協和アガリクス茸抽出液の抗体産生機能に及ぼす影響について．第59回日本癌学会総会、p.549、2000．

74. 草野由理、小栗佳代子、棟居聖一、吉冨泰央、山科郁男、岡山　實．ストレスファイバー形成におけるインテグリン □5□1とシンデカンの協調作用．第73回日本生化学会大会、p.646、2000．

75. 秋田　薫、藤本崇宏、井上瑞江、小栗佳代子、岡山　實、山科郁男、伏木信次、中田　博．マウス脳におけるTn抗原の発現と同抗原を持つ糖タンパク質の精製．第73回日本生化学会大会、p.718、2000．

76. 稲葉隆明、悴山博美、藤井博紹、山科郁男、井上瑞江、中田　博．ムチンによるヒト末梢血単球の活性化．第73回日本生化学会大会、p.718、2000．

77. 吉冨泰央、棟居聖一、草野由理、小栗佳代子、矢追義人、山科郁男、岡山　實．ストレスファイバー形成におけるシンデカン-２の作用機構．第73回日本生化学会大会、p.722、2000．

78. 棟居聖一、吉冨泰央、草野由理、小栗佳代子、山科郁男、岡山　實．細胞膜型ヘパラン硫酸プロテオグリカン、シンデカン-２遺伝子導入による形質転換．第 73 回日本生化学会大会、p.796、2000．

79. 井上瑞江、高橋秀司、山科郁男、奥村忠芳、中田　博．ムチン型糖鎖のクラスター形成に関与する UDP-GalNAc: polypeptide GalNAc-T3 について．第 73 回日本生化学会大会、p.859、2000．

80. 竹内　実、中島敦子、吉川健一、新屋政春．喫煙のマウス肺胞マクロファージの抗原提示機能と細胞表面抗原への影響．日本免疫学会総会、30：p.141、2000．

81. Takeuchi, M., Nakajima, A., Yoshikawa, K., Shinya, M., Asada, H., Yoshikawa, M., Tsukano, C.,

Nagai, S. and Izumi, T. Effect of smoking on immunological functions of Alveolar macrophages in mice. World Assembly on Tobacco Counters Health Watch-2000: p.161, 2000.

〔著書〕

1. 中田　博．上皮性癌細胞の産生するムチンの特性と腫瘍組織における生物学的意義、生化学、日本生化学会、印刷中．

2. 中田　博．上皮性癌細胞の産生するムチンの特性と機能、遺伝子医学、メディカル・ドゥ、印刷中．

3. Oguri, K. and Okayama, M. Can syndecan-1 become a prognostic factor in solid tumors? J. Gastroenterol., 39: 197-199, 2004. 3 pages

4. 中田　博．ムチンおよびムチン型糖鎖の多様性とその意義．わかる実験医学シリーズ、糖鎖生物学がわかる：pp.37-43、2002.

5. H. Nakada; Biosynthetic pathways of O-glycans. In Handbook of Glycosyltransferases and Their Related Genes (eds. N. Taniguchi, K. Honke and M. Fukuda). Springer-Verlag, Tokyo: pp.631-635, 2001.

6. 中田　博、井上瑞江．癌関連糖鎖抗原及び同抗原を持つムチン型糖タンパク質の構造、発現及び生物学的意義．京都産業大学論集、自然科学系列II、第9号：pp.1-49、2001.

7. 竹内　実．喫煙と免疫機能．臨床免疫、36：pp.843-850、2001.

8. 竹内　実、新屋政春．IL-2と癌の遺伝子治療．医歯薬出版、サイトカインと疾患：pp.158-161, 2000.

9. Takeuchi, M., Nagai, S. and Izumi, T. Inhibition of natural killer cell activity by alveolar macrophages in smokers. In: Tobacco: The Growing Epidemic. (eds. Rushan Lu, Judith Mackay, Shiru Niu and Richard Peto). Springer: pp.135-136, 2000.

10. Takeuchi, M., Nakajima, A., Yoshikawa, K., Shinya, M., Asada, H., Yoshimura, M., Tsukano, C., Nagai, S. and Izumi, T. Effect of smoking on immunological functions of alveolar macrophages in mice. In: Tobacco Counters Health (ed. A. K. Varma). Macmilan Ltd.: pp.168-171, 2000.

〈その他〉

国際シンポジウム開催；

International Symposium on Biological Science of Heparan Sulfate Proteoglycans

Kouyama Hall, Kyoto Sangyo University　　April 28-30, 2003

Organizing Committee

Minoru Okayama	*(Kyoto Sangyo University. Kyoto)*
Kayoko Oguri	*(Nagoya National Hospital, Nagoya)*
Koji kimata	*(Aichi Medical University. Nagoya)*

Kazuyuki Sugahara *(Kobe Pharmaceutical University. Kobe)*

Hiroshi Nakada *(Kyoto Sangyo University. Kyoto)*

Takashi Muramatsu *(Nagoya University. Nagoya)*

Masaki Yanagishita *(Tokyo Medical and Dental University. Tokyo)*

Foreign invited speakers

V. C. Hascall *The Cleveland Clinic Foundation, USA*

A Historical Overview of Proteoglycan Research

U. Lindahl *Uppsala University, Sweden*

Structure of Heparan Sulfate - how regulated does it need to be?

J. D. Esko *University of California, San Giego USA*

A Murine Model for Hereditary Multiple Exostoses (HME)

J. E. Turnbull *University of Birmingham, UK*

Specificity in heparan sulfate-protein interations-tools and strategies for elucidating biological functions

J. R. Couchman *Imperial College, UK*

Signalling from syndecan-4 to the cytoskeleton in cell adhesion

G. David *University of Leuven, Belgium*

Lytic controls on proteoglycan signalling

E-S. Oh *Ewha Womans University, Korea*

Syndecan-2 is a key mediator of tumorigenesis and metastasis in colon cancer

A. C. Rapraeger *University of Wisconsin-Madison, USA*

FGF and FGF receptor interactions are guided by temporal and spatial distribution of specific heparan sulfate domains during mouse development

Y. Yamaguchi *The Burnham Institute, USA*

Essential role of heparan sulfate in CNS patterning, neurogenesis, and axon guidance

学術集会開催；

"糖鎖シグナルと生体防御"公開セミナー

平成 14 年 3 月 15 日（金）　10：00ー17：40　キャンパスプラザ京都にて

演者　中田　博（京都産業大学・工学部・生物工学科、教授）

上皮性癌細胞の産生するムチンの免疫機構に対する影響

岡山　實（京都産業大学・工学部・生物工学科、教授）

シンデカン-２強制発現による癌転移の抑制

竹内　実（京都産業大学・工学部・生物工学科、教授）

喫煙と免疫

竹内　亨（鹿児島大・医学部・衛生学教室、教授）

活性酸素の生体影響とその防御

長井　苑子（京都大学・医学部・呼吸器内科、助教授）

呼吸器疾患と免疫

神奈木　玲児（愛知県がんセンター研究所・分子病態部、部長）

糖鎖による細胞間認識

川嵜　敏祐（京都大学大学院・薬学研究科、教授）

自然免疫とマンナン結合タンパク質

吉田　圭一（水谷糖質科学振興財団、事務局長）

グリコサミノグリカン糖鎖の酵素的同定法

中西　速夫（愛知県がんセンター研究所・腫瘍病理学部、室長）

不死化リンパ管内皮細胞株を用いたリンパ節転移機構の解析

木全　弘治（愛知医科大学・分子医科学研究所、所長）

硫酸化糖鎖が支配する細胞分化

Bronchoalveolar Lavage Fluid Cell Profile as a Predictor of the Prognosis of Idiopathic Pulmonary Fibrosis/Usual Interstitial Pneumonia (IPF/UIP) among Japanese Patients*

Rollin P. Tabuena M.D.[1]; Sonoko Nagai M.D., Ph.D[1]; Takeo Tsutumi M.D.[2]; Tomohiro Handa M.D.[1]; Takeuchi Minoru M.D., Ph.D[3]; Takeshi Mikuniya Ph.D[4]; Michio Shigematsu M.D., Ph.D[5]; Kunio Hamada M.D., Ph.D[6]; Takateru Izumi M.D., Ph.D[7]; Michiaki Mishima M.D., Ph.D[1]

*From the [1]Department of Respiratory Medicine, Graduate School of Medicine, Kyoto University, Kyoto, Japan

[2] National Utano Hospital, Kyoto, Japan

[3] Department of Biotechnology, Kyoto Sangyo University, Kyoto, Japan

Infectious Disease Research Laboratories, Pharmaceutical Research Department, Meiji Seika Kaisha; Ltd., Yokohama, Japan

[5] Sumitomo Hospital, Osaka, Japan

[6] Department of 1st Internal Medicine, Hokkaido University Hospital, Sapporo, Japan

[7] Central Clinic in Kyoto, Kyoto, Japan

Correspondence to:

Sonoko Nagai, M.D., PhD.

Department of Respiratory Medicine

Graduate School of Medicine

Kyoto University, Sakyo-ku, Kyoto, 606-8507, Japan

Telephone: + 81-75-751-3831; Fax: +81-75-751-3147

Email: nagai@kuhp.kyoto-u.ac.jp

Abstract

Background: The role of BALF cell profiles in predicting the clinical outcome of IPF/UIP remains to be further evaluated.

Objective: To determine whether BALF cell profiles affect the survival of patients diagnosed as UIP by surgical lung biopsy/autopsy at the early stage of IPF.

Methods: This hospital-based retrospective cohort study used 81 histologically proven IPF/UIP Japanese patients who underwent BAL examination. The BALF samples were obtained from non-current smokers: NCS (n=41) and current smokers: CS (n=40). The Kaplan-Meier and Cox's proportional hazard methods were used to estimate the survival and evaluate the risk ratio for dying among the two groups. To detect the multicollinearity, a stepwise regression was employed.

Results: A slight increase in the absolute numbers of BALF neutrophils tended to relate to an decrease in relative risk for dying among NCS patients and CS patients in the univariate analysis. In stepwise regression, the increase in %VC and the increase in BALF CD4/CD8 ratio in NCS was detected as favorable predictor; while increased BALF cells due to chronic smoking made the results unclear in CS.

Conclusions: Based on the studied bias of the biopsy-proven IPF/UIP patients with stable stages, Independent favorable variables were BALF CD4/CD8 ratio in NCS patients, while it was difficult to identify definite prognosticator in CS patients.

Keywords: Idiopathic Pulmonary Fibrosis (IPF), bronchoalveolar lavage (BAL), usual interstitial pneumonia (UIP), prognosis, survival

INTRODUCTION

Idiopathic pulmonary fibrosis (IPF) is a progressive interstitial lung disease with unknown etiology and the histological features of usual interstitial pneumonia (UIP). The clinical course of the disease can be influenced by age, smoking status, and the physiological and the radiological severity at the time of initial examination [1, 2, 3]. A recent clinical series of better defined IPF/UIP cases obtained a median survival of only 2.8 years [4], a significantly worse outcome compared to that of other chronic types of interstitial pneumonia. The bronchoalveolar lavage fluid (BALF) cell profile has been evaluated to elucidate the lung inflammatory process of IPF patients. However, there is no definite consensus regarding the potential utility of BALF cells in predicting the clinical outcome of IPF/UIP [5, 6,7]. There remains an area of uncertainty that needs to be defined.

In the BALF cell profiles of patients with IPF, a paucity of lymphocytes [8] has been shown to reflect the histological UIP pattern, and a non-specific increase in BALF neutrophils [9] and/or eosinophils has been associated with poor outcome [10, 11, 12, 13, 14,15]. On the other hand, the current evidence suggests that inflammation does not play a pivotal role in the pathogenesis of IPF [4]. The proposed epithelial/fibroblast mechanism of IPF is not suggestive of any inflammation in the lungs [16, 17,18]. In this context, the lack of inflammatory stimulus in the fibroproliferative model cannot be expected to lead to any increase in the BALF lymphocytes. This may well explain the poor response of IPF/UIP to anti-inflammatory agents such as corticosteroids.

This study uses various statistical analyses to evaluate the significance of

BALF cell parameters as prognostic factors in a retrospective cohort of IPF/UIP patients with mild to moderate disease severity, based on the study population bias that the majority of patients have been detected by routine health survey even when their signs and symptoms were subtle or mild. Clinico-pathophysiologic hints might be suggested from the study to develop a therapeutic strategy to this type of chronic progressive pulmonary fibrosis.

MATERIALS and METHODS

Subjects

Eighty-one Japanese patients with IPF/ UIP were retrospectively selected and re-reviewed from a panel of patients with ILD in the Chest Disease Research Institute of Kyoto University between 1982 and 1998. The disease severity was generally mild, ranging from a very low severity in asymptomatic patients detected by routine health surveys to moderate severity in symptomatic patients with pulmonary dysfunction. Symptomatic patients were denoted as patients who noticed an insidious onset of exertional dyspnea with or without dry cough at the time of the BAL examination. The definitive diagnosis of IPF in the presence of surgical lung biopsy showing a UIP pattern [19,20] included the following: (1) exclusion of other known causes of interstitial lung disease, (2) characteristic high resolution computed tomography (HRCT) scan, (3) restrictive pulmonary function (reduced total lung capacity (TLC), reduced vital capacity (VC) with a normal or increased forced expiratory volume in one second (FEV_1), forced vital capacity (FVC), FEV_1/FVC ratio and/or impaired gas exchange (increased alveolar-arterial pressure difference for O_2), decreased PaO_2 with rest or exercise, and decreased diffusing capacity of the lung for carbon monoxide (DL_{CO}).

Sixty-seven patients underwent either open lung biopsy (OLB) or video-assisted thoracoscopy (VATS). In 14 cases diagnosed by autopsy, the UIP lesions were found and confirmed by well-trained pathologists (M.K., C.V.T.). Patients whose conditions might have been associated with other lung diseases such as chronic hypersensitivity pneumonitis, asbestosis, chronic interstitial pneumonia associated with collagen vascular diseases, vasculitis, eosinophilic granuloma of the lungs, drug-induced interstitial pneumonia, sarcoidosis or other granulomatous diseases were excluded from the study at the time of the initial examination. No treatment with corticosteroid was administered at the time of the BAL examination, and patients had no signs or symptoms suggestive of infection.

Judging from our BAL experience in healthy subjects, chronic smoking definitely influences the BAL cell findings [1]. For this reason, we divided the IPF patients into CS and NCS groups for further analysis. The NCS group included patients who had never smoked (n=26) and ex-smokers who had quit smoking at least six months prior to the BAL examination (n=15). The CS group included patients who had smoked regularly for more than 20 years overall, including the 12 months prior to the BAL evaluation (n=40).

Informed consent was obtained from each patient and the study was approved by the Ethics committee of the Graduate School of Medicine at Kyoto University.

Chest radiograph Score Measurement

Chest radiographic scores were measured according to the method proposed by Watters *et al.* [21]. Briefly, we evaluated the standard postero-anterior chest radiographs using a quantitative score (maximum 10 points). The sum of the 3 radiographic entities was included in the overall

radiographic score: (1) regional extent and severity for parenchymal interstitial infiltrates; (2) radiographic honeycombing, and (3) radiographic evidence of pulmonary hypertension. The regional extent and severity of interstitial infiltrates were considered collectively in order to calculate the parenchymal subscore. The regional extent included six zones defined by the imaginary lines drawn one third and two thirds of the distance from the apex of the lung to the dome of the diaphragm in bilateral hemothoraces. The severity/profusion of parenchymal involvement was assessed by the combined profusion score (small, rounded opacities and/or linear, irregular densities) based on three groupings in the profusion grading system established by the International Union against Cancer Classification (UICC). Chest radiographs were taken at 135 kV under the maximum inspired condition at Kyoto University Hospital.

Chest CT evaluation

All patients underwent CT scan examination, but changes in the CT equipment over time made it difficult to strictly compare the cases at the desired level of precision. The CT patterns (UIP type versus other types) could be evaluated independently by two radiologists, both of whom used the following criteria to identify the UIP-pattern: peripheral, subpleural, and basal distribution of reticular opacities, often in association with traction bronchiectasis and honeycombing lesions. Ground glass attenuation was common but less extensive than reticular abnormality in patients with the UIP pattern.

Pulmonary Function Test

Pulmonary function assessment was performed at the start of the study before the BAL examination was contemplated using the Chestac-65V (Chest Co Ltd., Tokyo, Japan). Measurement indices included FEV_1, VC, TLC and DL_{CO}.

The DL_{CO} values were corrected for hemoglobin but not for alveolar gas volume. These values were expressed as percentages of the predicted values.

Bronchoscopy and BAL processing

BAL was performed in the Chest Disease Research Institute of Kyoto University according to our previous method and the recommendations of the BAL task group [22, 23,24]. Briefly, the subjects received an intramuscular injection of atropine (0.5 mg) and hydroxyzine (25 mg). The local anesthesia was administered 15 minutes prior to the bronchoscopy via inhalation of a 10 ml aerosol solution with 2% lidocaine. The fiberoptic bronchoscope (Olympus 200; Olympus Optical Co., Ltd., Tokyo, Japan) was inserted into the tracheobronchial tree via the oral route and wedged into the middle lobe or lingula. A sterile 0.9% saline solution (200 milliliter) pre-warmed to room temperature was instilled in four 50 ml aliquots and recovered by gentle suctioning into the siliconized containers. The recovered BALF sample was kept on ice in a siliconized tube, filtered through gauze, cytocentrifuged at 1200 rpm for 10 minutes at 4°C, and separated into cells and supernatant. The cell pellets were washed in Eagle's minimum essential medium (Nissui, Tokyo, Japan) and cytocentrifuged to adjust the total cell count. The trypan blue dye staining test confirmed a cell viability of over 95%. May-Grunwald-Giemsa was used to stain cells for the differential count of more than 300 cells.

Evaluation of lymphocyte sub-populations

Flow cytometry was performed with a dual FACScan equipped with an Ar+ laser (Becton Dickinson, Mountain View, CA, USA). BALF cells ($1x10^6$ in Eagles medium supplemented with 10% fetal calf serum) were collected en masse and analyzed using the CELLQuest program (Becton-Dickinson, Mountain View,

CA, USA). The data were examined on a logarithmic scale while the lymphocyte population was evaluated on the basis of the expression of the side scatter.

The BALF mononuclear cells were stained with monoclonal antibodies: CD4, T helper cells; CD8, T suppressor-cytotoxic cells (Becton Dickinson, Mountain View, CA, U.S.A.). Monoclonal antibodies were directly conjugated with either fluorescein isothiocyanate (FITC) (Becton Dickinson, Mountain View, CA, U.S.A.) or phycoerythrin (RDI) (Becton Dickinson, Mountain View, CA, U.S.A.), incubated for 10 minutes at 4°C using anti-CD4 or CD8 monoclonal antibodies, and analyzed within 24 hours.

Statistical and Survival Analysis

Data were analyzed using JMP statistical view software (SAS Institute Inc., SAS Campus Drive, Cary, NC, USA) running on an Apple Macintosh personal computer. Data were considered to be statistically significant if the p value was less than 0.05. The BALF cell results were expressed as median values and ranges were given using the 25^{th}-75^{th} percentiles.

To measure a frequency of distribution between two or more ordinal variables, Fisher's exact probability, chi-square test were used to evaluate the differences among the CS and NCS groups. Analysis of variance (ANOVA), Wilcoxon/Kruskal-Wallis test, and nonparametric median test were used to evaluate the relationship between two or more measured variables,

The Kaplan-Meier survival curves were derived for patients in the two groups and comparisons were made using the Log rank and Wilcoxon test. The median value of each BALF variable was used as a cut-off point for analysis and grouping. Cox's proportional hazard method was used to evaluate the risk ratio for dying of both nominal and numerical variables among the two groups. The

risk ratio and 95% confidence interval (CI) were computed for BALF variables independently associated with survival.

Multiple stepwise regression was then employed to identify an independent predictor of survival among the numerical variables, i.e., age, BALF recovery, BALF cell profiles, pulmonary function tests, and radiographic score at presentation, respectively.

Results

Study Population

Table 1 summarizes clinical demographic data on the 81 histologically proven patients at the entry of the examination. The majority of the CS patients were males without symptoms. The disease duration was defined as the month from BAL examination up to the last observation in the outpatient clinic or the patient's death. The NCS were significantly symptomatic compared to the CS (p=0.0041). No other demographic data were considered significantly different between the two groups of patients.

Some of the symptomatic patients (75% of the NCS, 25% in CS) were treated with low-dose corticosteroids and/or immunosuppressants when they needed any treatment to gradual increase in their exertional dyspnea after performing the BAL. All patients were placed on close observation (every three or six months) in the follow-up at the outpatient clinic of the Chest Disease Research Institute of Kyoto University.

Severity of pulmonary lesions at the time of BAL

Table 2 shows the severity of the pulmonary lesions as assessed by chest radiographs and pulmonary function tests. The NCS patients had significantly

higher radiologic scores using Watter's method (6.11) than the CS patients(5.44, [p=0.0063]) [25], and significantly greater volume loss (43.2%)than the CS patients(5.1%, [p=0.0001]).

BAL cellular profiles at the initial examination

Given that the BAL procedure and methods used for the cell analysis were fundamentally the same and performed in the same institute, the BALF and cell recovery profiles were considered adequate for analysis. The CS patients with IPF had a significantly higher absolute number of macrophages in the BALF than the NCS patients (p=0.034), while the NCS group had a significantly higher percentage of neutrophils in the BALF than the CS group (p=0.036), though a degree of the increase was small. No significant difference was observed between the two groups in the percentage of BALF and cell recovery. There were no significant differences between the groups in the CD4/CD8 ratio and absolute numbers and percentages of lymphocytes and eosinophils at the baseline examination (Table 3).

Kaplan Meier Survival Analysis

In the Kaplan Meier analysis performed in the NCS group, a reduced %VC was associated with an unfavorable prognosis (Fig.1), while an elevated absolute number of eosinophils (Likelihood ratio=0.008, Wilcoxon test=0.013) and elevated percentage of eosinophils (L.R.=0.008, Wilcoxon test=0.013) were associated with a favorable prognosis(Table 4). An increase in the chest radiograph score among the CS patients did seem to be related with an unfavorable survival during the follow-up of several years after the BAL examination. None of the other parameters (age, gender, CD4/CD8 ratio, BAL lymphocytes and BAL neutrophils) were significantly related to survival in either the NCS group or CS group in the

Kaplan Meier analysis (Table 4).

Univariate Analysis using Cox Proportional Hazard Model

The overall age of the patients, gender, pulmonary functions , chest radiographic scores, BALF, BALF cell percentage, and BALF and blood CD4/CD8 ratios had no significant influences on the risk for dying in both the NCS and CS group (Table 5). In the CS group, an increase in the absolute numbers of BALF neutrophils was favorable predictors (relative risk 0.487, p=0.021), while in the NCS, increase in the absolute numbers of BALF neutrophils tended to relate to favorable prognosis (relative risk 0.519, p=0.082).

Multiple Regression Analysis

Stepwise regression detected seven independent numerical variables that helped explain the clinical courses among the patients. Two independent explanatory favorable prognosticator were detected in the NCS patients : the increased BALF CD4/CD8 ratio (p=0.017) and the increased %VC (p=0.012) at the time of the BAL examination. Independent variables were detected among the CS patients: increase in BALF recovery (p=0.0068) and increase in cell recovery (p=0.0027) as favorable prognosticator, while increase in number of macrophage (p=0.0021), lymphocytes (p=0.0186), and neutrophils (p=0.0014) were identified as unfavorable prognosticator.

DISCUSSION

We reported herein a hospital-based retrospective cohort study to elucidate the significance of BALF profiles for prognosis. After dividing our entire study population into NCS and CS, our statistical analyses identified some of the

BALF parameters as prognostic variables influencing the clinical course in the 81 histology-proven patients with IPF/UIP. These variables were different between NCS and CS in this study.

The study population included IPF patients at mild to moderate stages of the disease. We should note that a substantial number of patients were detected by a routine health survey before their recognition of symptoms such as cough or exertional dyspnea manifested.

Moreover, several factors may have affected the accuracy and reliability of the methodology employed in this study. Based on our previous experience performing BAL procedures in 400 healthy Japanese subjects, the BALF cell profile in healthy subjects is clearly influenced by smoking status [24]. As such, the 81 IPF patients were divided into two populations for further survival analysis, i.e., NCS and CS. Secondly, with regard to the method used for BAL collection, the BAL procedure was basically the same and all the recovered fluid was combined and analyzed at the same time. In an earlier series we found no significant difference in the yield of differential BALF cell counts when the first aliquot was mixed in or discarded [24]. Finally, as corticosteroids and/or immunosuppressant were administered several years after the BAL examination, the treatment did not influence the BALF cell profiles.

Several studies have attempted to identify the clinical, radiologic and physiologic prognostic factors that can predict the survival of IPF patients [25,26,27,28,29,30,31,32]. Previous investigators have attempted to correlate lung function and/or radiograph with survival in IPF/UIP patients [25, 32, 33, 34]. Small sample sizes, heterogeneity in the study populations, and differences in disease severity may have lead to inconsistencies among the BALF profiles as

prognostic factors in the survival analyses. The baseline lung function in our CS patients was better preserved and less deranged than that in our NCS patients. This difference may have been due to a co-presence of an emphysematous area, a possible suppression of ongoing fibrotic processes, or an earlier detection bias due to a routine health survey in a workplace. In any case, we can point out that either numbers or percentage of neutrophils and eosinophils in our patients were lower than those in the patients reported earlier (10 %± as means or median,5 % ± as means or median) [36,37,38,39,40].

The increase in %VC in the NCS group was a favorable prognostic factor that was clearly detected through two different statistical analyses (Kaplan Meyer and multiple regression analysis). Similar results were not obtained in the CS group.

The difference in the BALF cell profiles among the IPF patients was the difference in absolute numbers of macrophages and neutrophils between the NCS and CS groups. When all the factors were combined for statistical analysis, we found that the disease severity differed completely among the groups. As such, the division of the 81 IPF patients into CS and NCS groups seemed relevant and rational. Likewise, based on the evidence of previous studies, it can be expected that a marked increase in eosinophils and/or neutrophils in the BALF of the CS patients may have been associated with a higher likelihood of disease progression and failure to respond to therapy [35, 36, 37, 38, 39,40]. Different from these reports, the data from our univariate analysis seemed to demonstrate that slight increase in BALF neutrophil counts related to favorable prognosis in the CS patients with early satge of IPF/UIP. However, it seems to be

quite difficult to identify other BALF indexes as a significant predictor in the CS patients in this study, taken into consideration the results obtained from the univariate hazard method and step regression analysis. Significance of the effects of inflammatory cells which may be accumulated through chronic smoking habit on the prognosis of IPF/UIP remains to be examined in the CS patients.

A slight increase in both the number and percentage of BALF eosinophils seemed to relate to a favorable prognosis in the NCS patients in our Kaplan-Meier survival analysis, albeit with a cut-off value of eosinophils that appeared to be lower than that reported in patients with severe disease severity. However, we should be careful to accept the result, as the Kaplan Meyer analysis are likely biased by confounding factors. In such sense, the results obtained from both multiple regression and proportional hazard analysis should be evaluated in this study.

BALF lymphocytosis was associated with more cellular biopsy, less honeycombing, and a lower responsiveness to therapy [37, 38, 39,40]. Patients with such lymphocytic patterns today are generally not considered likely candidates for IPF/UIP [18, 8]. In our study, a paucity of BALF lymphocytes was confirmed.

The increase in BALF CD4/CD8 ratio was an independent favorable prognostic factor obtained from multivariate stepwise regression in the NCS patients. The reduction of this ratio due to chronic smoking in the CS patients seemed to prevent a similarly significant result in that group. While there was no increase in the lymphocyte in the NCS patients with IPF/UIP, a small subset of CD4 T cells or CD8 T cells might have been involved in the disease progression. Only few reports have evaluated the significance of T cell subsets in BAL

samples of IPF. An elevated ratios due to infrequent increases in BALF lymphocytes have been reported in such series [39,41].

The major causes of death in this study were respiratory failure due to progression of IPF (n=45), acute exacerbation (n=6), carcinoma (n= 4), aspergillus infection (n=1) and pulmonary hypertension (n=2). None of the patients underwent lung transplantations and all had complete follow-up throughout the clinical course up to the time of death. Treatment after BAL did not relate to the outcome in the three statistical analyses.

In conclusion, in this retrospective hospital-based cohort of histology proven IPF/UIP Japanese patients with mild disease severity at the time of early stage of IPF/UIP, the significance of BALF parameters as prognostic factors differed between the NCS and CS groups. The increase in BALF CD4/CD8 ratio was identified as a favorable predictor in the NCS group, while it was difficult to identify definite prognosticator in CS patients.

Acknowledgments

The authors are grateful to Prof. T.V. Colby and Dr. M. Kitaichi for their pathological review of the slides with IPF, to Dr. M. Tsukino and Prof O.B. Danucop for their statistical advice, to Mr. Simon Johnson for editing the manuscript, and for Mrs. F. Tanioka, K. Kobayashi, and M. Yamada for their expert technical assistance in the laboratory.

This study was supported by Grants-in-Aid for the Japanese Ministry of Education and the Smoking Research Foundation of Japan.

Figure Legends

Figure 1. Significance of %VC in NCS patients with IPF estimated by Kaplan-Meier survival analysis.

A significantly better survival was seen in the IPF patients (n=41) with %VC >=72.5 (solid line) versus %VC <72.5 (thin line). Log-Rank test 0.044, Wilcoxon test 0.011.

The ordinate means the survival rate calculated by the Kaplan-Meier product limit method. The abscissa means the duration of the illness expressed in months from the detection of symptoms or to the latest observation in the survivors. The Wilcoxon and Log rank tests were used for comparison.

Abbreviations: VC- vital capacity, IPF – idiopathic pulmonary fibrosis

References:

1 Nagai S, Kitaichi M, Hamada K, Nagao T, Hoshino Y, Miki H, Izumi T: *Hospital-based cohort study of 234 histologically proven Japanese patients with* idiopathic pulmonary fibrosis. Sarcoidosis Vasc and Diffuse Lung Dis 1999; 16:209-214.

2 Nagao T, Nagai S, Hiramoto Y, Hamada K, Shigematsu M, Hayashi M, Izumi T, Mishima M: Serial evaluation of high-resolution computed tomography findings with idiopathic pulmonary fibrosis in usual interstitial pneumonia. Respiration 2002; 69:413-419.

3 King Jr TE, Tooze JA, Schwartz MI, Brown KR, Chemiack RM: Predicting survival in idiopathic pulmonary fibrosis: scoring system and survival model. Am J Respir Crit Care Med 2001; 164:1171-1181.

4 Selman M, King TE Jr, Pardo A: Idiopathic pulmonary fibrosis: prevailing and evolving hypotheses about its pathogenesis and implications to therapy. Ann Intern Med 2001; 134:136-151.

5 Veeraraghavan S, Latsi PI, Wells AU, Pantelidis, Nicholson AG, Colby TV, Haslam PL, Renzoni EA, du Bois RM: BAL findings in idiopathic nonspecific interstitial pneumonia and usual interstitial pneumonia. Eur Respir J 2003; 22:239-244.

6 King Jr TE, Costabel U, Cordier JF: Idiopathic pulmonary fibrosis: diagnosis and treatment. International consensus statement. Am J Respir Crit Care Med 2000; 161:646-664.

7 Poletti V, Chilosi M, Olivieri D. Respiration. 2004 ; 71(2):107-19. Diagnostic invasive procedures in diffuse infiltrative lung diseases.

8 Nagai S, Kitaichi M, Itoh H, Nishimura K, Izumi T, Colby TV: Idiopathic nonspecific interstitial pneumonia/fibrosis: comparison with idiopathic pulmonary fibrosis and BOOP. Eur Respir J 1998; 12:1010-1019.

9 Agusti C, Xaubet P, Luburich P, Ayuso MC, Roca J, Rodriguez-Roisin R: Computed tomography-guided bronchoalveolar lavage in idiopathic pulmonary fibrosis. Thorax 1996; 51:841-845.

10 Turner-Warwick M, Haslam P. The value of serial bronchoalveolar lavage in assessing progress of patients with cryptogenic fibrosing alveolitis: Am Rev Respir Dis 1987; 135:26-34.

11 Rudd RM, Haslam PL, Turner-Warwick M: Crytogenic fibrosing alveolitis: relationships of pulmonary physiology and bronchoalveolar lavage to response to treatment and prognosis. Am Rev Respir Dis 1981; 124:1-8.

12 Inage M, Nakamura H, Kato S, Saito H, Abe S, Hino T, Homoike H: Level of cytokeratin 19 fragments in broncholaveolar lavage fluid correlate to the intensity of neutrophil and eosinophils alveolitis in patients with idiopathic pulmonary fibrosis. Respir Med 2000; 94:155-160.

13 Wells AU, Hansell DM, Haslam PL: Bronchoalveolar lavage cellularity: lone cryptogenic fibrosing alveolitis compared with the fibrosing alveolitis of systemic sclerosis. Am J Respir Crit Care Med 1998; 157:1474-1482.

14 Peterson M, Monick M, Hunninghake GW: Prognostic role of eosinophils in pulmonary fibrosis. Chest 1992; 1:51-56.

15 Boomars KA, Wagenaar SS, Mulder PG, van Velzen-Blad H, van den Bosch JM: Relationship between cells obtained by bronchoalveolar lavage and survival in idiopathic pulmonary fibrosis. Thorax 1995; 50:1087-1092.

16 Nicholson AG, Fulford LG, Colby du Bois RM, Hansell DM, Wells AU: The relationship between individual histologic features and disease progression in

idiopathic pulmonary fibrosis. Am J Respir Crit Care Med 2002; 166:173-177.

17 King Jr TE, Schwartz MI, Brown K, Tooze JA, Colby TV, Waldron JA, Flint A, Thurlbeck W, Cherniack RM: Idiopathic pulmonary fibrosis: relationship between histopathologic features and mortality. Am J Respir Crit Care Med 2001; 164:1025-1032.

18 Collard HR, King Jr TE: Demystifying idiopathic interstitial pneumonia. Arch Intern Med 2003; 153: 17-29.

19 American Thoracic Society/European Respiratory Society: International multidisciplinary consensus classification of the idiopathic interstitial pneumonia. Am J Respir Crit Care Med 2002; 165: 277-304.

20 Costabel U, King Jr TE: International consensus statement of idiopathic pulmonary fibrosis. Eur Respir J 2001; 17: 163-167.

21 Watters LC, King Jr TE, Schwartz MI, Waldron JA, Stanford RE, Cherniack RM: A clinical, radiographic and physiologic scoring system for the longitudinal assessment of patients with idiopathic pulmonary fibrosis. Am Rev Respir Dis 1986; 133:97-103.

22 Mikuniya T, Nagai S, Shimoji T, Takeuchi M, Morita K, Mio T, Satake N, Izumi T: Quantitative evaluation of the IL-1ß and IL-1 receptor antagonist obtained from BALF macrophages in patients with interstitial lung diseases. Sarcoidosis Vasc and Diffuse Lung Dis 1997; 14:39-45.

23 Klech H, Hutter C: Current guidelines and indications for bronchoalveolar lavage (BAL): report of the European Society of Pneumology Task Force of BAL. Eur Respir J 1990; 3: 937-974.

24 Nagai S, Izumi T: Bronchoalveolar lavage: still useful in diagnosing sarcoidosis? In: Clinics in Chest Medicine Sarcoidosis. W.B. Saunders Company,

Philadelphia, Pennsylvania 1997, vol 18, pp. 787-797.

25 Collard HR, King TE JR., Bartelson BB, Vourlekis J, Schwartz MI, Brown KB: Changes in clinical and physiologic variables predict survival in idiopathic pulmonary fibrosis. Am J Respir Crit Care Med 2003; 168:538-42.

26 Mogulkoc N, Brutsche MH, Bishop PW, Greaves MS, Egan JJ: Pulmonary function in idiopathic pulmonary fibrosis and referral for lung transplantation. Am J Respir Crit Care Med 2001; 164: 103-108.

27 Hubbard R, Johnston I, Britton J: Survival in patients with cryptogenic fibrosing alveolitis: a population-based cohort study. Chest 1998; 113:396-400.

28 Mapel DW, Hunt WC, Utton R, Baumgartner K, Samet JM, Coultas DB: Idiopathic pulmonary fibrosis: survival in population based and hospital based cohorts. Thorax 1998; 53: 469-476.

29 Gay SE, Kazerooni EA, Toews GB, Lynch J III, Gross BH, Cascade PN, Spizarny DL, Flint A, Schork MA, Whyte RI: Idiopathic pulmonary fibrosis: predicting response to therapy and survival. Am J Respir Crit Care Med 1998; 157:1063-107.

30 McCormack FX, King TE Jr, Bucher BL, Nielsen L, Mason RJ: Surfactant protein A predicts survival in idiopathic pulmonary fibrosis. Am J Respir Crit Care Med 1995; 152:751-59.

31 Erbes R, Schaberg T, Loddenkemper: Lung function tests in patients with idiopathic pulmonary fibrosis. Chest 1997; 111:51-57.

32 Hanson D, Winterbauer RH, Kirtland SH, Wu R: Changes in pulmonary function test results after 1 year of therapy as predictors of survival in patients with idiopathic pulmonary fibrosis. Chest 1995; 108:305-310.

33 Flaherty KR, Mumford JA, Murray S, Kazerooni EA, Gross BH, Colby TV,

Travis WD, Flint A, Toews GB, Lynch JP III, Martinez FJ: Prognostic implications of physiologic and radiographic changes in idiopathic interstitial pneumonia. Am J Respir Crit Care Med 2003; 168:543-548.

34 Kawabata H, Nagai S, Hayashi M, Nakamura H, Nagao T, Shigematsu M, Kitaichi M, Izumi T: Significance of lung shrinkage on CXR as a prognostic factor in patients with idiopathic pulmonary fibrosis. Respirology 2003; 8: 351-358.

35 Schwartz DA, Van Fosse Scott D, Davis CS, Helmers AR, Dayton CS, Burmeister LF, Hunninghake GW: Determinants of survival in idiopathic pulmonary fibrosis. Am J Respir Crit Care Med 1994; 149: 444-9.

36 Peterson MW, Monick M, Hunninghake: Prognostic role of eosinophils in pulmonary fibrosis. Chest 1987; 92: 51-55.

37 Rudd RM, Haslam PL, Turner-Warwick M: Cryptogenic fibrosing alveolitis : relationships of pulmonary physiology and bronchoalveolar lavage to response to treatment and prognosis. Am Rev Respir Dis 1981; 124:1-8.

38 Haslam PL, Bauer W, de Rose V, Eckert H, Olivieri D, Poilter LW, Rossi GA, Teschler: The clinical role of BAL in idiopathic pulmonary fibrosis. Eur Respir Rev 1992; 2:8, 58-64.

39 Boomars KA, Wagenaar SS, Mulder PGH, Heleen van Velzen-Blad, JMM van den Bosch: Relationship between cells obtained by bronchoalveolar lavage and survival in idiopathic pulmonary fibrosis. Thorax, 1995; 50:1087-1092.

40 Watters LC, Schwartz MI, Cherniak RM: Idiopathic pulmonary fibrosis: pretreatment BAL cellular constituents and their relationships with lung histopathology and clinical response to treatment. Am Rev Respir Dis 1987; 135:696-704.

41. Ma W, Cui W, Lin Q: Improved immunophenotyping of lymphocytes in

bronchoalveolar lavage (BALF) by flow cytometry. Clinica Chimica Acta 2001; 133-138.

Table 3. BALF cell findings in Patients with IPF/UIP at initial examination

	Noncurrent smokers	Current Smokers	p value
Cases	41	40	
Fluid Recovery (%)	58.7 (39.2~69.5)*	63.7 (40~71.7)	0.266
Cell Recovery (X 10^5/ml)	1.50 (1.07~2.28)	1.99 (1.30~4.04)	0.119
Macrophage (X10^3/ml)	13.6 (7.44~19.72)	18.9 (12.0~36.4)	**0.034****
Macrophage (%)	87.2 (76.4~96.6)	94.5 (83.7~98.0)	0.152
Lymphocyte (/ml)	0.5 (0.27~1.1)	0.61 (0.26~1.06)	0.824
Lymphocyte (%)	3.5 (2.4~7.4)	2.9 (1.2~5.8)	0.435
Neutrophil (/ml)	0.21 (0~2.33)	0.099 (0~0.42)	0.266
Neutrophil (%)	1.5 (0.0~12.6)	0.5 (0.0~2.8)	**0.036****
Eosinophil (/ml)	0.09 (0~0.43)	0.06 (0~0.48)	0.653
Eosinophil (%)	0.4 (0.0~2.8)	0.4 (0.0~2.5)	0.909
CD4/CD8 ratio	1.32 (0.91~1.90)	1.43 (0.99~1.99)	0.826

*Results were expressed as median values 25th to 75th percentile

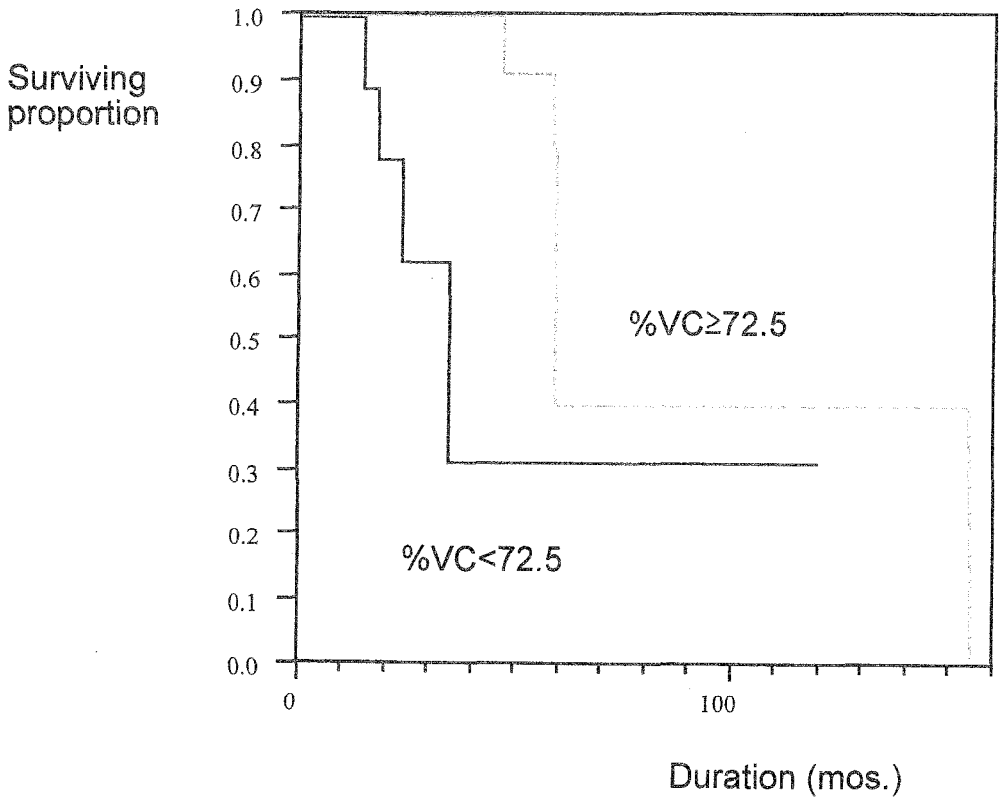

Heparan sulphate proteoglycans interact with neurocan and promote neurite outgrowth from cerebellar granule cells

Kaoru AKITA*, Munetoyo TODA*, Yuki HOSOKI*, Mizue INOUE*, Shinji FUSHIKI†, Atsuhiko OOHIRA‡, Minoru OKAYAMA*, Ikuo YAMASHINA* and Hiroshi NAKADA*[1]

*Department of Biotechnology, Faculty of Engineering, Kyoto Sangyo University, Kamigamo-Motoyama, Kita-ku, Kyoto 603-8555, Japan, †Department of Pathology and Applied Neurobiology, Kyoto Prefectural University of Medicine Graduate School of Medical Science, Kamigyo-ku, Kyoto 602-8566, Japan, and ‡Institute for Developmental Research, Aichi Human Service Center, Kasugai, Aichi 480-0392, Japan

We found that neurocan, a major brain chondroitin sulphate proteoglycan, interacts with HSPGs (heparan sulphate proteoglycans) such as syndecan-3 and glypican-1. Binding of these HSPGs to neurocan was prevented by treatment of the HSPGs with heparitinases I and II, but not by treatment of neurocan with chondroitinase ABC. Scatchard plot analysis indicated that neurocan has two binding sites for these HSPGs with different affinities. It is known that neurocan in the rodent brain is proteolytically processed with aging into N- and C-terminal fragments. When a mixture of whole neurocan and N- and C-terminal fragments prepared from neonatal mouse brains or recombinant N- and C-terminal fragments was applied to a heparin column, the whole molecule and both the N- and C-terminal fragments bound to heparin. A centrifugation cell adhesion assay indicated that both the N- and C-terminal neurocan fragments could interact with these HSPGs expressed on the cell surface. To examine the biological significance of the HSPG–neurocan interaction, cerebellar granule cells expressing these HSPGs were cultured on the recombinant neurocan substrate. A significant increase in the rate of neurite outgrowth was observed on the wells coated with the C-terminal neurocan fragment, but not with the N-terminal one. Neurite outgrowth-promoting activity was inhibited by pretreatment of neurocan substrate with heparin or the addition of heparitinase I to culture medium. These results suggest that HSPGs such as syndecan-3 and glypican-1 serve as the cell-surface receptor of neurocan, and that the interaction of these HSPGs with neurocan through its C-terminal domain is involved in the promotion of neurite outgrowth.

Key words: heparan sulphate proteoglycan, neurocan, neurite outgrowth, brain development.

INTRODUCTION

It is known that syndecan-3 is a membrane-bound HSPG (heparan sulphate proteoglycan) and has a unique mucin-like domain unlike other syndecans [1]. It has been reported that syndecan-3 interacts with some extracellular matrix components and heparin-binding growth factors through its heparan sulphate chains and that these interactions are probably involved in some biological functions such as cell adhesion, cell migration, neurite outgrowth and long-term potentiation [2–5].

In the present study, we performed a ligand overlay assay with biotinylated soluble syndecan-3 to detect binding proteins for syndecan-3. Neurocan was identified as a new binding protein for syndecan-3. The binding was prevented by the treatment of syndecan-3 with heparitinases I and II, suggesting that neurocan could bind to syndecan-3 through its heparan sulphate chains, which is consistent with the recent report that neurocan binds to heparin [6]. Similarly, we found that glypican-1 is also a neurocan-binding protein. Glypican-1, one of the GPI (glycosylphosphatidylinositol)-anchored HSPGs, is significantly expressed in the developing rodent brain similar to glypican-2 and syndecan-3 [7]. It is known that neurocan is capable of binding to various ligands including cell-surface molecules [8–10], extracellular matrix components [11–15] and growth-associated molecules [15,16], indicating that neurocan is a multi-functional component of the extracellular matrix of the brain. Syndecan-3 is expressed on the growing axonal surface during brain development [17–19]. Glypican-1 is detected on axonal projections and synaptic terminal fields in developing and adult brains [20–22]. It is well known that these cell-surface HSPGs act as co-receptors for various morphogenesis factors [23]. A recent report showed that the disruption of heparan sulphate synthesis leads to severe patterning defects in the developing mouse brain [24]. Since the HSPGs may also play some roles in the interaction between the cell and extracellular matrix [23], it is very important to determine the biological significance of cell-surface HSPG–neurocan interaction. To address this issue, cerebellar granule cells prepared from neonatal mouse cerebellum were examined, since immunohistochemical studies have revealed that syndecan-3, glypican-1 and neurocan are co-localized in the molecular layer of neonatal rodent cerebellum [17,21,25]. In the present study, we also found that the interaction of cell-surface HSPGs with neurocan substrate promoted neurite outgrowth from the cerebellar granule cells. Pretreatment of neurocan substrate with heparin or addition of heparitinase I to culture medium abolished the neurocan-induced neurite outgrowth, indicating that the heparan sulphate chain is essential for the activity. Since both soluble and cell-surface HSPGs could bind to neurocan, soluble HSPGs shed from the cell surface are probably involved in the regulation of neurocan-induced neurite outgrowth. Such a possibility will be considered in the present study.

MATERIALS AND METHODS

Animals and cells

Mice (ICR strain) and rats (Wistar strain) were purchased from SLC (Shizuoka, Japan). The animals were kept according to the ethical guidelines of the Kyoto Sangyo University animal committee. Neonatal mice aged 5–10 days were used throughout

Abbreviations used: HRP, horseradish peroxidase; HSPG, heparan sulphate proteoglycan.

[1] To whom correspondence should be addressed (email hnakada@cc.kyoto-su.ac.jp).

the experiments. N18TG-2 mouse neuroblastoma and PC12 rat pheochromocytoma cells were donated by Dr H. Higashida (Kanazawa University, Japan) and Dr M. Kurokawa-Seo (Kyoto Sangyo University, Japan) respectively.

Antibodies

An anti-mouse neurocan monoclonal antibody, designated as 3A11 (IgG2b), was generated by immunizing a female rat aged 6 weeks with proteoglycans prepared from neonatal mouse brains as described by Oohira et al. [26]. The specificity of the 3A11 monoclonal antibodies was confirmed by immunoblot analysis using purified neurocan. Goat anti-syndecan-3 and anti-glypican-1 antibodies were purchased from Santa Cruz Biotechnology (Santa Cruz, CA, U.S.A.). An antibody against rabbit cell adhesion molecule L1 was donated by Dr C. Lagenaur (University of Pittsburgh, U.S.A.). The monoclonal antibodies F69-3G10 (anti-ΔHS monoclonal antibodies) and M2 (anti-FLAG monoclonal antibodies) were obtained from Seikagaku Corp. (Tokyo, Japan) and Sigma (St. Louis, MO, U.S.A.) respectively.

Purification and identification of syndecan-3-binding protein (neurocan)

A soluble extract of neonatal mouse brains was prepared and precipitated by ammonium sulphate as described previously [27,28]. The precipitate was dissolved in a solution containing 25 mM Tris/HCl (pH 7.5), 0.1 M NaCl and 7 M urea and then dialysed against the same solution. The dialysed material was applied to a column of DEAE-Sephacel (3 cm × 15 cm; Amersham Biosciences, Piscataway, NJ, U.S.A.) equilibrated with the same solution. After washing with 25 mM Tris/HCl (pH 7.5), 0.3 M NaCl and 7 M urea, the bound proteins were eluted with 25 mM Tris/HCl (pH 7.5), 1.5 M NaCl and 7 M urea. After dialysis against 25 mM Tris/HCl (pH 7.5) and 0.15 M NaCl, the eluate was applied to a column of heparin–Sepharose (1 cm × 6 cm; Amersham Biosciences), washed with 25 mM Tris/HCl (pH 7.5) and 0.15 M NaCl and then eluted with 25 mM Tris/HCl (pH 7.5) and 0.7 M NaCl. The eluate was further fractionated by gel filtration on Sepharose CL-4B (1 cm × 110 cm; Amersham Biosciences) equilibrated with 50 mM Tris/HCl (pH 7.5), 5 mM EDTA, 0.1 % Chaps and 4 M guanidinium chloride, and then eluted with the same solution.

Syndecan-3-binding proteins were detected by the ligand overlay assay as follows. Proteins contained in each fraction were subjected to SDS/PAGE under non-reducing conditions and then transferred to a membrane. After blocking with 25 mM Tris/HCl (pH 7.5), 0.15 M NaCl, 5 mM $CaCl_2$, 5 mM $MgCl_2$ and 5 % (w/v) BSA, the membrane was incubated overnight at 4 °C with biotinylated soluble syndecan-3 (0.8 μg of protein/ml) in the blocking solution . After incubation with HRP (horseradish peroxidase)-conjugated streptavidin (Zymed, South San Francisco, CA, U.S.A.), syndecan-3-binding protein was detected with an enhanced chemiluminescence reagent (ECL®; Amersham Biosciences).

Purification of syndecan-3 and glypican-1

Soluble glypican-1 from the culture medium of PC12 cells was purified essentially by the method of Williamson et al. [29].

Soluble syndecan-3 was purified from neonatal mouse brains as described previously [28].

Neurocan–Sepharose affinity chromatography

Neurocan (450 μg of protein) purified from neonatal mouse brains was coupled with CNBr-activated Sepharose CL-4B (dry weight, 0.28 g; Amersham Biosciences) according to the manufacturer's instructions. An extract of neonatal mouse brains was fractionated first by ammonium sulphate precipitation and then on DEAE-Sephacel and heparin–Sepharose as described above. The fractions that did not bind to heparin–Sepharose were dialysed against 25 mM Tris/HCl (pH 7.5), 0.15 M NaCl, 2 mM $CaCl_2$ and 2 mM $MgCl_2$ and applied to a column of neurocan–Sepharose (0.7 cm × 2.6 cm). After extensive washing with the above buffer, the bound proteins were eluted with 25 mM Tris/HCl (pH 7.5), 0.15 M NaCl and 10 mM EDTA and then with 25 mM Tris/HCl (pH 7.5), 1.0 M NaCl and 10 mM EDTA.

Binding of labelled HSPGs to neurocan

Radioiodination of syndecan-3 and glypican-1 was performed using IODO-GEN (Pierce Biotechnology). Neurocan–Sepharose (equivalent to 0.18 μg of protein of neurocan) was incubated overnight at 4 °C with increasing concentrations (0–8 nM) of ^{125}I-syndecan-3 (2.5×10^6 c.p.m./μg) or ^{125}I-glypican-1 (5×10^6 c.p.m./μg) in 50 μl of 25 mM Tris/HCl (pH 7.5), 0.15 M NaCl, 2 mM $CaCl_2$, 2 mM $MgCl_2$, 0.5 % BSA and 0.05 % Tween 20. After washing the neurocan–Sepharose three times with the above buffer, the bound radioactivity was measured with an ARC-1000M gamma counter (Aloka Co., Tokyo, Japan). Non-specific binding was examined by incubation of ^{125}I-syndecan-3 or ^{125}I-glypican-1 with neurocan–Sepharose in the presence of a 200-fold excess of unlabelled syndecan-3 or glypican-1. ^{125}I-syndecan-3 or ^{125}I-glypican-1 (10 000 c.p.m.) was also treated with heparitinases I and II (5 m-units/ml) as described previously [28]. Neurocan–Sepharose (equivalent to 0.9 μg of protein of neurocan) was treated with protease-free chondroitinase ABC (20 m-units/ml) as described previously [28]. These materials were used for the binding experiments; for a control experiment, the radiolabelled proteoglycans were incubated with Sepharose CL-4B.

Preparation of recombinant N- and C-terminal fragments and syndecan-3 and glypican-1 cDNA transfectants

Based on the sequences of mouse neurocan (GenBank® accession no. X84727), syndecan-3 (GenBank® accession no. XM_124395) and glypican-1 (GenBank® accession no. AF185613), four pairs of primers were synthesized. Polyadenylated RNA was prepared from neonatal mouse brains using a QuickPrep® mRNA purification kit (Amersham Biosciences). First-strand cDNA, synthesized using a random primer, was amplified with four pairs of specific primers: 5′-^{128}GTGGCTGCTTCTCCTAGTCG-3′ and 5′-^{2058}CAAGTGTAGAGCGTGGCAGA-3′ and 5′-^{1942}CAGAGGCCCTAAGTGCTGTC-3′ and 5′-^{3943}GAAACGCTCTGGAGAAGGTG-3′ to produce recombinant N- and C-terminal fragments of mouse neurocan respectively and 5′-^{14}ACAAAGGCCGCCATGAAG-3′ and 5′-^{1369}GGCACTGTGGCTCTGCTAAG-3′ and 5′-^{156}ACCTTGGCTCTGCCCTTC-3′ and 5′-^{1949}AGACAGTCCTTGGGGCTAGG-3′ to obtain full-length cDNAs encoding mouse syndecan-3 and glypican-1 respectively. cDNAs encoding the N- and C-terminal fragments of neurocan were subcloned into the pFLAG-CTC expression vector (Sigma), with which BL21-CodonPlus® competent cells (Stratagene, Heidelberg, Germany) were transformed to generate C- and N-terminally FLAG-tagged recombinant fragments. Full-length cDNA encoding mouse syndecan-3 or glypican-1 was subcloned into the pcDNA 3.1 expression vector (Invitrogen, Carlsbad, CA, U.S.A.), with which N18TG-2 neuroblastoma cells were transformed using NeuroPORTER™ transfection reagent (Gene Therapy System, San Diego, CA, U.S.A.). As a control, cells were transfected with the vehicle vector only. These cells were cultured

in Dulbecco's modified Eagle's medium and 10 % (v/v) fetal calf serum in the presence of G418 (600 μg/ml). After cloning by limiting dilution, the cloned transfectants were designated as Syn3-N18TG-2 (syndecan-3 cDNA transfectants), Gly1-N18TG-2 (glypican-1 cDNA transfectants) and Mock-N18TG-2 (vehicle vector transfectants).

Binding of whole neurocan and its fragments to heparin

A mixture of whole neurocan and its fragments was prepared from neonatal mouse brains as described above. It was applied to a column of TSKgel Heparin-5PW (0.75 cm × 7.5 cm; Tosoh, Tokyo, Japan) equilibrated with 25 mM Tris/HCl (pH 7.5) and 0.15 M NaCl and eluted with a linear gradient of NaCl, from 0.15 to 1.0 M.

N- and C-terminal neurocan fragments were prepared as follows and their binding to heparin was also examined. After induction with isopropyl β-D-thiogalactoside, BL21-CodonPlus® competent cells, transformed with pFLAG CTC expression vector, were lysed by sonication in 25 mM Tris/HCl (pH 7.5), 0.15 M NaCl, 7 M urea and 1 mM PMSF and then centrifuged at 165 000 *g* for 30 min. The proteins obtained from the supernatant were mixed with heparin–Sepharose or anti-FLAG M2 monoclonal antibody-conjugated agarose (Sigma) or Sepharose CL-4B and kept overnight at 4 °C. After washing with 25 mM Tris/HCl (pH 7.5) and 0.15 M NaCl, the bound proteins were subjected to SDS/PAGE followed by electroblotting; subsequently, FLAG-tagged recombinant neurocan fragments were detected with HRP-conjugated anti-FLAG M2 monoclonal antibodies. Lysates of the transformed cells were applied to a column of TSKgel Heparin-5PW and the FLAG-tagged recombinant neurocan fragment in the eluted fractions was detected by dot-blot analysis with HRP-conjugated anti-FLAG M2 monoclonal antibodies. To confirm the binding of the N-terminal neurocan fragment to heparin, the FLAG-tagged recombinant protein was purified by affinity chromatography. The protein was applied to a column of anti-FLAG M2 monoclonal antibody-conjugated agarose (0.7 cm × 2.6 cm). After washing with 25 mM Tris/HCl (pH 7.5) and 0.15 M NaCl, the bound protein was eluted with 0.1 M glycine/HCl, pH 3.5. The wells of a Maxisorp 96-well plate (Nalge Nunc, Rochester, NY, U.S.A.) were coated with syndecan-3 or glypican-1 (0.25 μg/50 μl) overnight at 4 °C. After blocking with 30 mM $NaHCO_3$ (pH 8.0), containing 1 % BSA, purified FLAG-tagged recombinant protein (5 μg/ml) in PBS containing 1 % BSA was added to the wells, followed by incubation overnight at 4 °C. After washing with 25 mM Tris/HCl (pH 7.5) and 0.15 M NaCl containing 0.05 % Tween 20, a bound N-terminal neurocan fragment was detected with HRP-conjugated anti-FLAG M2 monoclonal antibodies using the ELISA TMB kit (Nacalai tesque, Kyoto, Japan).

Attachment of N18TG-2 cells to recombinant neurocan substrate

Cell attachment to recombinant neurocan-coated wells was examined by means of the centrifugation cell adhesion assay [30,31]. First, each well of a U-shaped 96-well plate (Nalge Nunc) was coated with 50 μl of anti-FLAG M2 monoclonal antibodies (20 μg/ml) overnight at 4 °C. After washing with 30 mM $NaHCO_3$ (pH 8.0) and blocking with 30 mM $NaHCO_3$ (pH 8.0) containing 1 % BSA, lysates of transformed *Escherichia coli* cells expressing the FLAG-tagged recombinant N- or C-terminal neurocan fragment were added to the wells, followed by incubation overnight at 4 °C. To examine the effect of heparin, wells coated with FLAG-tagged recombinant neurocan fragments were further incubated with heparin (5 μg/50 μl) in PBS containing 1 % BSA. After washing with serum-free Dulbecco's modified Eagle's medium containing 1 % BSA, Syn3-, Gly1- or Mock-N18TG-2 cells (1×10^4 cells) were added to each well and the plate was immediately centrifuged at 250 *g* for 2 min. The wells were photographed under a phase-contrast microscope. The diameter of the area to which the cells attached uniformly was measured as an index of the attachment strength by the method of Grumet et al. [31].

Neurite outgrowth assay of cerebellar granule cells

Neurite outgrowth assay was performed by using the wells of a Maxisorp 96-well plate (Nalge Nunc) treated as described for the centrifugation cell adhesion assay in the previous section. Cerebellar granule cells were prepared from neonatal mice aged 6 days by the method of Fushiki et al. [32]. The cells were planted on to the wells at a density of 5×10^3 cells/well in 100 μl of culture medium. In some experiments, heparitinase I (10 m-units) was added to the culture medium to remove cell-surface heparan sulphate chains. After culturing for 48 h, cells bearing neurites longer than the diameter of a cell body were counted as neurite-bearing cells under a phase-contrast microscope. To confirm the expression of syndecan-3, glypican-1 and cell adhesion molecule L1, the granule cells were immunostained with specific antibodies against each molecule.

Other methods

Amino acid sequencing was performed using an Applied Biosystems sequencer (Procise 492). Biotinylation of proteins was performed using EZ-Link™ Sulfo-NHS-Biotin (Pierce Biotechnology, Rockford, IL, U.S.A.). The protein concentration was determined using a BCA protein assay kit (Bio-Rad, Hercules, CA, U.S.A.) using BSA as the standard. Student's *t* test was used for statistical analysis of the experiments. $P < 0.05$ was taken as the level of significance.

RESULTS

Identification of new ligand for syndecan-3

Using the ligand overlay assay, the syndecan-3-binding protein was detected through its purification as described in the Materials and methods section. As shown in Figures 1(A) and 1(B), the syndecan-3-binding protein was recovered mainly in fractions [$K_{av} = (V_e - V_o)/(V_t - V_o) = 0.27$–$0.44$, where V_e is the elution volume, V_o the void volume and V_t the maximum elution volume] of gel filtration on Sepharose CL-4B. A control experiment using biotinylated BSA instead of syndecan-3 did not give any detectable band (results not shown). The above fractions were collected and analysed by SDS/PAGE. Treatment of the binding protein with chondroitinase ABC produced three molecular species exhibiting molecular masses of 260, 150 and 130 kDa on SDS/PAGE (Figure 1C). It was revealed that the 260 and 130 kDa components had the same N-terminal amino acid sequence, i.e. DQDTQDTTA, which coincided with that of neurocan, indicating that these core proteins correspond to the whole molecule and the N-terminal fragment of neurocan respectively. The N-terminal amino acid sequence of the 150 kDa core protein was LRAPKLWLLP, which coincided with the N-terminal sequence of the C-terminal fragment of neurocan. Anti-mouse neurocan monoclonal antibody 3A11 reacted with the 260 and 150 kDa core proteins, but not with the 130 kDa core protein (Figure 1D).

Identification of the neurocan-binding proteins

As shown in Figure 1, we found that neurocan could bind to syndecan-3. Next, we tried to confirm this binding ability using

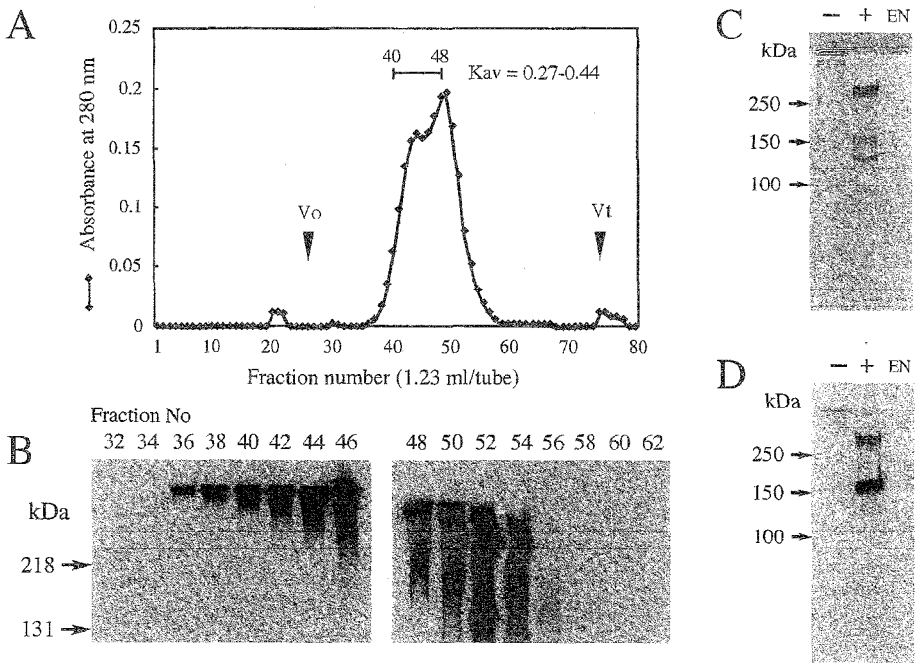

Figure 1 Purification and identification of syndecan-3-binding protein

(**A**) Syndecan-3-binding protein was fractionated by chromatography on Sepharose CL-4B and the elution profile and elution volume V_e were analysed. The void volume V_0 and the maximum elution volume V_t were measured with respect to the elution positions of Blue Dextran and *p*-nitrophenol respectively. (**B**) Aliquots of each fraction were subjected to ligand overlay assay using biotinylated soluble syndecan-3. (**C**, **D**) Positive fractions [$K_{av} = (V_e - V_0)/(V_t - V_0) = 0.27–0.44$] were collected, treated with (+) or without (−) chondroitinase ABC and then separated by SDS/PAGE (6 % gel), followed by either visualization by CBB staining (**C**) or immunochemical detection using anti-neurocan monoclonal antibody 3A11 (**D**). EN, the same amount of chondroitinase ABC used in (**C**, **D**) was subjected to SDS/PAGE followed by the same procedure as described above.

purified neurocan and asked whether neurocan is capable of binding to other HSPGs. An extract of neonatal mouse brains was fractionated by ammonium sulphate precipitation and ion-exchange chromatography on a column of DEAE-Sephacel as described in the Materials and methods section. The fractions that eluted with 0.3–1.5 M NaCl from DEAE-Sephacel were collected. Neurocan contained in these fractions was excluded using a heparin column. The pass-through fraction from the heparin column was applied to a column of neurocan–Sepharose. After extensive washing, the bound proteins were eluted with the same solution containing 10 mM EDTA and then 1 M NaCl (Figure 2A). After treatment with or without heparitinase I, eluates were subjected to SDS/PAGE followed by electroblotting. Immunoblot analysis with F69-3G10 monoclonal antibodies revealed several core proteins of HSPGs in the eluate from neurocan–Sepharose (Figure 2B). Among these bands, the core protein having a molecular mass of 62 kDa showed strong reactivity to this antibody. In the eluate with 1 M NaCl, syndecan-3 was detected on immunoblot analysis with anti-syndecan-3 antibodies (Figure 2C, lane 1). In addition, the 62 kDa core protein was identified to be glypican-1 by its immunoreactivity to anti-glypican-1 antibodies (Figure 2C, lane 2). At present, the other HSPGs that bound to neurocan–Sepharose are yet to be identified.

Binding of syndecan-3 and glypican-1 to neurocan

To examine binding properties, neurocan–Sepharose was incubated with increasing amounts of ^{125}I-syndecan-3 or ^{125}I-glypican-1. The binding of these HSPGs to neurocan was saturated (Figure 3A), and Scatchard plot analysis revealed the presence of two binding sites (Figure 3B). The calculated K_d values were 7.5 and 23.7 nM for syndecan-3 and 1.4 and 6.0 nM for glypican-1.

We examined whether the heparan sulphate chains of syndecan-3 or glypican-1 are relevant to the binding of neurocan. ^{125}I-syndecan-3 or ^{125}I-glypican-1 treated with or without heparitinases I and II was incubated with neurocan–Sepharose or Sepharose CL-4B as a control. Removal of the heparan sulphate chains of syndecan-3 and glypican-1 decreased the binding to neurocan by approx. 85 and 92 % respectively, indicating that their heparan sulphate chains were actually essential for the binding (Figure 4). A similar experiment was performed to examine the effect of the chondroitin sulphate chains of neurocan on the binding to syndecan-3 or glypican-1. As shown in Figure 4(A), removal of the chondroitin sulphate chains of neurocan had no effect on the binding to syndecan-3, and the binding of glypican-1 to neurocan increased 1.4-fold after treatment with chondroitinase ABC (Figure 4B), indicating that the neurocan core protein is responsible for the binding to the heparan sulphate chains of syndecan-3 or glypican-1. Binding of labelled HSPGs to Sepharose CL-4B was less than 1 % of the maximum binding to neurocan–Sepharose (results not shown).

Binding of neurocan fragments to heparin

As shown in Figure 1(C), the syndecan-3-binding protein is a mixture of the whole neurocan and its N- and C-terminal fragments, which is consistent with the report that neurocan is proteolytically processed with aging and cleaved its N- and C-terminal fragments [25,33]. To analyse the binding of whole neurocan and its fragments to heparin, this mixture was fractionated on a column of TSKgel Heparin-5PW (Figure 5A). After digestion with chondroitinase ABC, the eluted proteins were separated by SDS/PAGE and detected by silver staining (Figure 5B). Analysis of the N-terminal amino acid sequence revealed that the 260 kDa

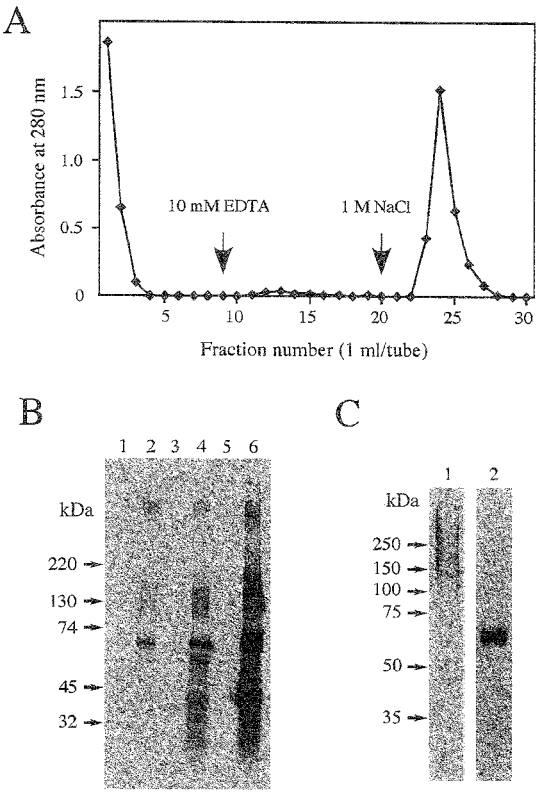

Figure 2 Identification of neurocan-binding proteins

An extract of neonatal mouse brains was fractionated by ammonium sulphate precipitation and ion-exchange chromatography on a column of DEAE-Sephacel as described in the Materials and methods section. The fractions eluted with 0.3–1.5 M NaCl from DEAE-Sephacel were applied to a column of heparin–Sepharose. (**A**) The pass-through fraction from the heparin column was applied to a column of neurocan–Sepharose. After washing, the bound components were eluted with 10 mM EDTA and then with 1.0 M NaCl. (**B**) After treatment with (lanes 2, 4 and 6) or without (lanes 1, 3 and 5) heparitinase I, aliquots of each fraction were subjected to SDS/PAGE (2–15 % gel), followed by immunoblot analysis with F69-3G10 monoclonal antibodies. Lanes 1 and 2, pass-through fraction from the heparin column; lanes 3 and 4, 10 mM EDTA eluate; lanes 5 and 6, 1 M NaCl eluate. (**C**) The eluate obtained with 1.0 M NaCl, before and after treatment with heparitinase I, was subjected to SDS/PAGE (7 % gel) followed by immunoblot analysis with anti-syndecan-3 antibodies (lane 1) and anti-glypican-1 (core protein) antibodies (lane 2) respectively.

band was the core protein of the whole neurocan, and the 150 and 130 kDa bands corresponded to its C- and N-terminal fragments respectively. The N-terminal fragment was eluted first with 0.41 M NaCl from a column of TSKgel Heparin-5PW, followed by elution of the whole neurocan and C-terminal fragment with 0.45 M NaCl. These results suggest that both the N- and C-terminal fragments of neurocan can bind to heparin and a binding site with higher affinity for heparin was located in its C-terminus, which is consistent with the finding that neurocan has two binding sites for both syndecan-3 and glypican-1, as described above. However, this result contradicts a recent report that the C-terminal fragment, but not the N-terminal one, could bind to heparin [6]. To confirm the binding of both the N- and C-terminal fragments of neurocan to heparin, we attempted to produce FLAG-tagged recombinant N- and C-terminal neurocan fragments, as shown in Figure 6(A). FLAG-tagged recombinant N- and C-terminal fragments were detected as major bands corresponding to molecular masses of 80 and 110 kDa respectively (Figure 6B, lanes 2 and 4). The molecular masses of these recombinant fragments were higher than those expected on the basis of their amino acid con-

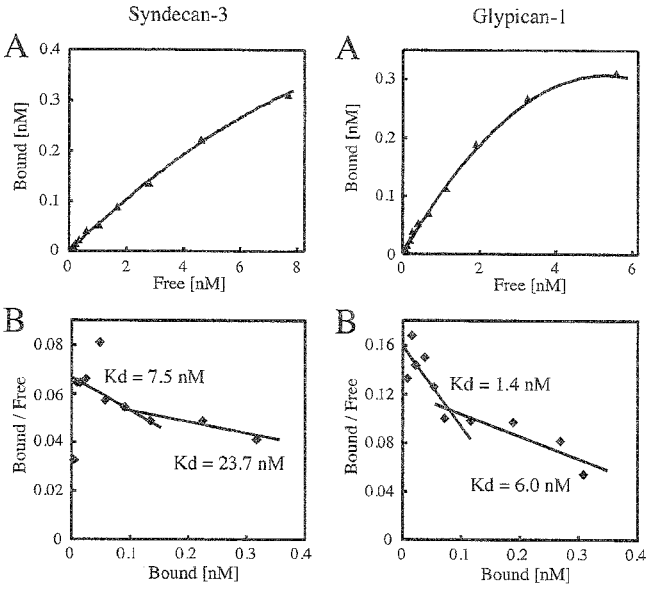

Figure 3 Binding of neurocan to syndecan-3 or glypican-1

(**A**) Neurocan–Sepharose was incubated with increasing amounts of ^{125}I-syndecan-3 (left panel) or ^{125}I-glypican-1 (right panel) as described in the Materials and methods section. Specific binding was calculated by subtracting the non-specific binding from the total binding, where total binding represents the binding with increasing concentrations of ^{125}I-syndecan-3 or ^{125}I-glypican-1 and non-specific binding represents the binding in the presence of a 200-fold excess of unlabelled syndecan-3 or glypican-1. The bound radioactivity was measured with a gamma counter. Results are expressed as the means for duplicate analyses. (**B**) Results of Scatchard plot analysis.

tents and this is probably due to the characteristic rod-like structure of neurocan, as reported by Retzler et al. [12] and Li et al. [34]. Cell lysates containing each fragment were mixed with anti-FLAG monoclonal antibody-conjugated agarose, heparin–Sepharose or Sepharose CL-4B. After washing with 25 mM Tris/HCl (pH 7.5) and 0.15 M NaCl, the bound proteins were subjected to SDS/PAGE followed by immunoblot analysis. The FLAG-tagged recombinant N- and C-terminal neurocan fragments were co-precipitated with anti-FLAG monoclonal antibody-conjugated agarose and heparin–Sepharose, but not with Sepharose CL-4B (Figure 6C). When these cell lysates were fractionated on TSKgel Heparin-5PW, both FLAG-tagged recombinant neurocan fragments bound to the heparin column (Figures 6D and 6E). To confirm further the binding of the N-terminal fragment to syndecan-3 or glypican-1, the FLAG-tagged recombinant N-terminal neurocan fragment was isolated as described in the Materials and methods section. As shown in Figure 6(F), the purified N-terminal fragment could bind to these HSPGs.

Binding of neurocan to HSPGs expressed on N18TG-2 cells

Full-length cDNA encoding mouse syndecan-3 or glypican-1 was transfected into N18TG-2 mouse neuroblastoma cells as described in the Materials and methods section. We confirmed a high level of expression of syndecan-3 or glypican-1 at mRNA and protein levels in Syn3- and Gly1-N18TG-2 cells (results not shown).

We investigated the molecular interaction between cell-surface HSPGs and neurocan using the centrifugation assay described by Friedlander et al. [30]. To determine the degree of attachment, we measured the diameter of the cell-attachment area. As shown in Table 1, the diameters of the attachment area for Syn3-N18TG-2 cells on the wells coated with the recombinant N- and C-terminal

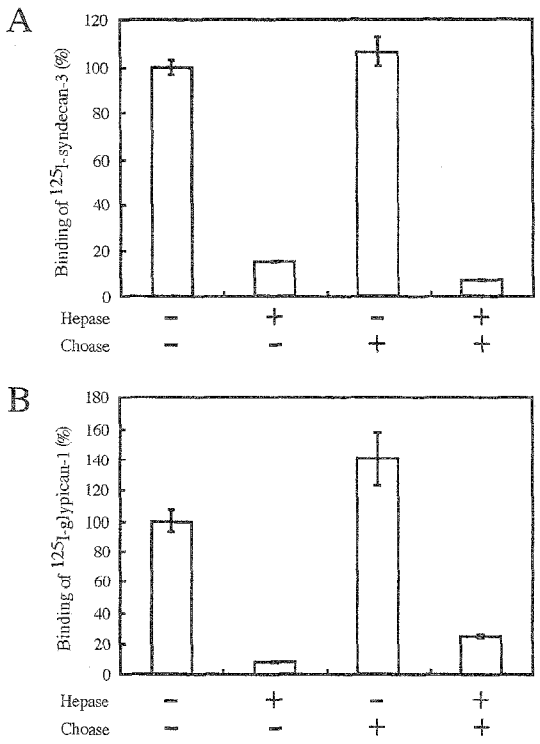

Figure 4 Involvement of glycosaminoglycans in the interaction between neurocan and syndecan-3 or glypican-1

(**A**) ^{125}I-syndecan-3 (10000 c.p.m.) was treated with (+) or without (−) heparitinases I and II (Hepase) and then mixed with neurocan–Sepharose treated with (+) or without (−) chondroitinase ABC (Choase). As a control, Sepharose CL-4B was used instead of neurocan–Sepharose CL-4B. After washing, the bound radioactivity was measured with a gamma counter. (**B**) Binding of neurocan to glypican-1 was examined similarly using ^{125}I-glypican-1 (10000 c.p.m.). Results are expressed as the averages for duplicate determinations. Error bars represent the S.E.M.

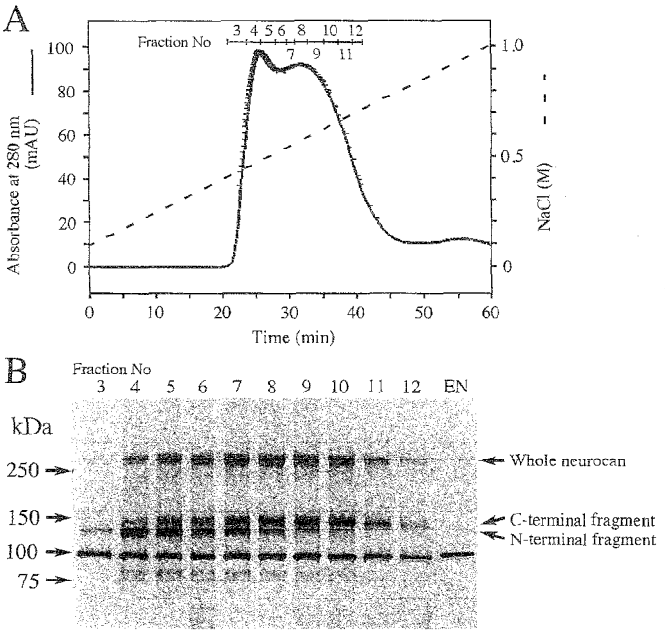

Figure 5 Elution profile of neurocan and its fragments on TSKgel Heparin-5PW

An extract of neonatal mouse brains was fractionated by ammonium sulphate precipitation and DEAE-Sepharose and heparin-affinity chromatographies as described in the Materials and methods section. (**A**) The fractions eluted from heparin–Sepharose with 0.1–0.7 M NaCl were refractionated with a linear gradient of NaCl from 0.1 to 1.0 M on TSKgel Heparin-5PW. (**B**) After digestion with chondroitinase ABC, aliquots of each fraction were subjected to SDS/PAGE (2–15 % gel), with detection by silver staining. EN, chondroitinase ABC was used for the same procedure.

neurocan fragments were 4.71 ± 0.36 and 5.14 ± 0.11 mm respectively. These areas were significantly greater than those of Mock-N18TG-2 cells. Similar results were obtained with the centrifugation assay using Gly1-N18TG-2 cells. The diameters were 4.94 ± 0.16 and 5.49 ± 0.15 mm in the wells coated with the recombinant N- and C-terminal neurocan fragments respectively. These results suggest that cell-surface HSPGs play a significant role in cell adhesion to the neurocan substrate. In the control wells coated with anti-FLAG monoclonal antibodies and blocked with BSA, the diameters of the cell-attachment areas were significantly smaller compared with those of recombinant neurocan-coated wells. The attachment of Mock-N18TG-2 cells to recombinant neurocan-coated wells was slightly promoted, probably due to other cell adhesion molecules expressed in Mock-N18TG-2 cells. The cell-attachment area in the wells incubated with heparin after coating with recombinant neurocan fragments was significantly decreased. The addition of heparin to the neurocan-uncoated wells had no effect on the binding of these transfectants.

Effect of HSPG–neurocan interaction on neurite outgrowth from cerebellar granule cells

Biological effect of neurocan on HSPG-expressing cells was investigated by using cerebellar granule cells prepared from the neonatal mouse cerebellum, since it has been reported that neurocan, syndecan-3 and glypican-1 are co-localized in the molecular layer of neonatal mouse cerebellum [17,21,25]. In the developing cerebellum, the cerebellar granule cells extend their neurites horizontally forming the parallel fibres in the molecular layer [35] where neurocan is highly expressed [25]. Syndecan-3 and glypican-1 were also detected on the growing parallel fibres in the neonatal rodent cerebellar cortex [17,21]. Approx. 80 % of the cells prepared from neonatal mouse (aged 6 days) cerebellum expressed syndecan-3 and glypican-1 in addition to cell adhesion molecule L1, a marker for cerebellar granule cells (Figure 7A). The granular cells prominently extended their neurites on the wells coated with FLAG-tagged recombinant C-terminal neurocan fragment via anti-FLAG antibody, but not on the wells coated with only anti-FLAG antibodies (Figure 7B). To examine the involvement of cell-surface HSPGs, the recombinant C-terminal neurocan fragment-coated wells were further treated with heparin before cell planting. Neurite outgrowth was significantly decreased by pretreatment with heparin (Figure 7B). In addition, neurite outgrowth was also suppressed when heparitinase I was added to culture medium (Figure 7B). These treatments with heparin or heparitinase I did not affect the cell viability (results not shown). To determine the level of neurite outgrowth-promoting activity, the neurite-bearing cells cultured under various conditions as described above were counted (Figure 7C). The C-terminal neurocan fragment increased the percentage of neurite-bearing cells by 42.8 %. In contrast, the N-terminal neurocan fragment showed little promotion of neurite outgrowth (Figures 7B and 7C).

DISCUSSION

The mechanisms that control the establishment of neuronal connection are very crucial for development of the nervous system. It is generally agreed that syndecan-3, similar to three other

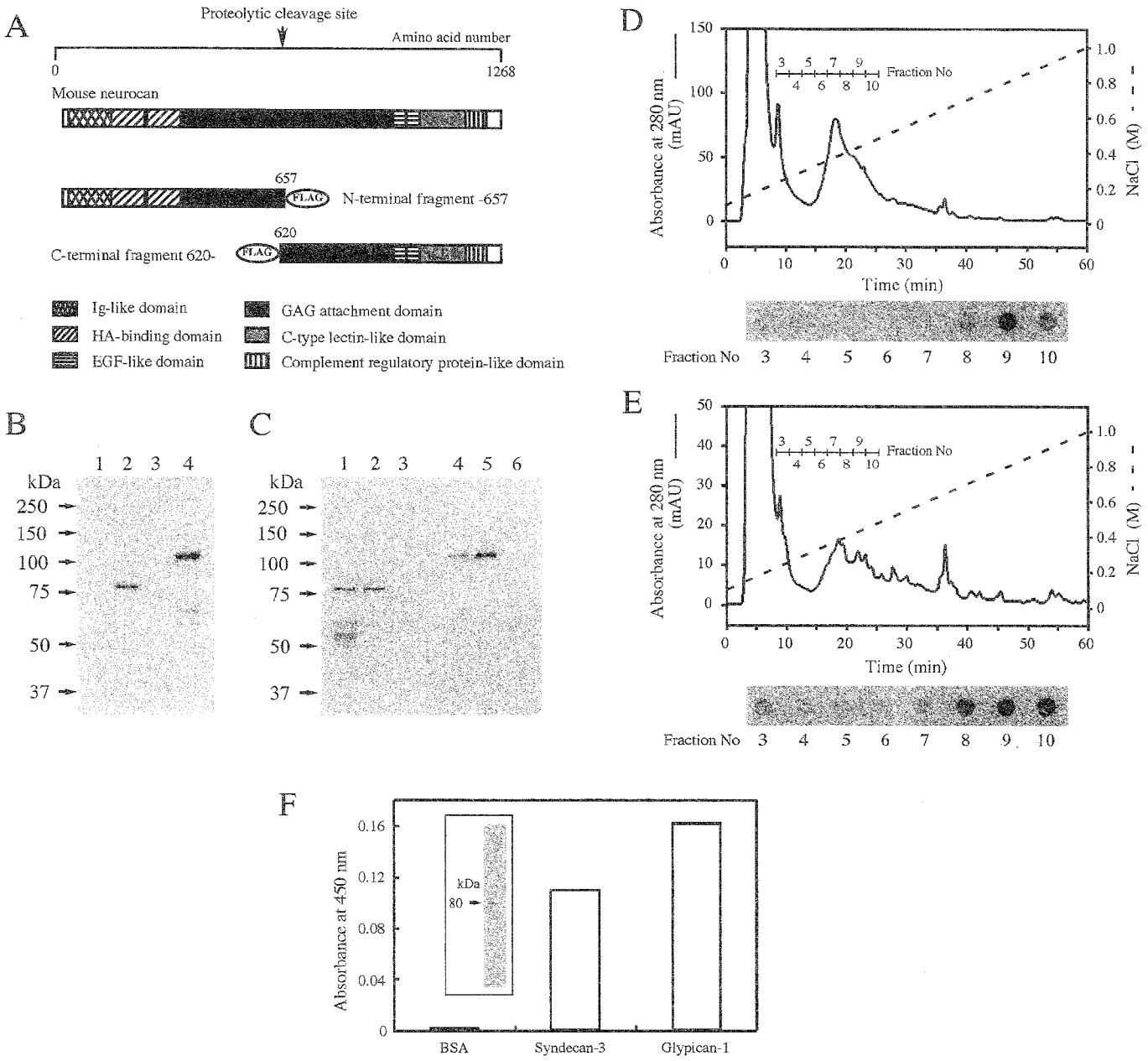

Figure 6 Binding of recombinant N- and C-terminal neurocan fragments to heparin or HSPGs

(**A**) FLAG-tagged recombinant neurocan fragments, as represented schematically, were prepared as described in the Materials and methods section. EGF, epidermal growth factor; GAG, glycosaminoglycan; HA, hyaluronic acid; Ig, immunoglobulin. (**B**) BL21 competent cells were transformed using plasmids constructed with cDNA encoding the N-terminal (lanes 1 and 2) or C-terminal fragment (lanes 3 and 4) of mouse neurocan. Before (lanes 1 and 3) and after (lanes 2 and 4) induction with isopropyl β-D-thiogalactoside, lysates of each type of cell were subjected to SDS/PAGE (7% gel) followed by immunoblot analysis. FLAG-tagged recombinant neurocan fragments were detected with HRP-conjugated anti-FLAG monoclonal antibodies. (**C**) Cell lysates containing either the FLAG-tagged recombinant N-terminal (lanes 1–3) or C-terminal (lanes 4–6) recombinant neurocan fragment were mixed with anti-FLAG monoclonal antibody-conjugated agarose (lanes 1 and 4), heparin–Sepharose (lanes 2 and 5) or Sepharose CL-4B (lanes 3 and 6). The bound proteins were subjected to SDS/PAGE and immunoblot analysis as described above. Additional bands corresponding to lower molecular masses, which were detected in (**B**) (lane 4) and (**C**) (lanes 1 and 2), were probably produced by proteolysis. (**D**, **E**) Cell lysates containing the FLAG-tagged recombinant N- (**D**) or C-terminal (**E**) neurocan fragment were applied to a column of TSKgel Heparin-5PW. The bound proteins were eluted with a linear gradient of NaCl from 0.1 to 1.0 M. FLAG-tagged recombinant neurocan fragments were detected by dot-blot analysis with HRP-conjugated anti-FLAG monoclonal antibodies. (**F**) Purified N-terminal neurocan fragment was subjected to SDS/PAGE and stained with Coomassie Brilliant Blue (inset). This fragment was added to the wells coated with syndecan-3 or glypican-1. Bound fragment was detected as described in the Materials and methods section.

syndecans, plays an important role in tissue morphogenesis and differentiation by virtue of its ability to bind to a number of extracellular matrix components and growth factors [1,23]. In the present study, we demonstrated that both soluble and cell-surface syndecan-3 and glypican-1 could bind to neurocan. Scatchard plot analysis showed that these HSPGs bound to neurocan with significantly high affinity ($K_d = 7.5$ and 23.7 nM for syndecan-3 and $K_d = 1.4$ and 6.0 nM for glypican-1). Digestion of these HSPGs with heparitinases I and II decreased their binding abilities to neurocan by 85–92%. On the other hand, the binding of these HSPGs did not decrease by the treatment of neurocan with chondroitinase ABC. These results suggest that these HSPGs bind to

Table 1 Measurement of the cell-attachment area by centrifugation assay

The centrifugation assay was performed as described in the Materials and methods section. The diameter (in mm) of the area to which the cells attached was measured as an index of the attachment strength using an internal calibrate graticule. Coating with various substrates and blocking with 1% BSA were performed as described in the Materials and methods section. Results are expressed as the means ± S.E.M. for triplicate determinations. $*P < 0.05$, $**P < 0.001$ compared with Mock-N18TG-2 on the recombinant N- or C-terminal neurocan fragment-coated wells. $\dagger P < 0.01$, $\dagger\dagger P < 0.001$ compared with each transfectant on the recombinant N- or C-terminal neurocan fragment-coated wells. FLAG Ab, anti-FLAG monoclonal antibody; N-Neuro, FLAG-tagged recombinant N-terminal neurocan fragment; C-Neuro, FLAG-tagged recombinant C-terminal neurocan fragment; Hep, heparin.

Substrate	Diameter (mm)		
	Mock-N18TG-2 cells	Syn3-N18TG-2 cells	Glyp1-N18TG-2 cells
FLAG Ab + BSA	2.77 ± 0.11	2.91 ± 0.10	2.72 ± 0.12
FLAG Ab + BSA + Hep	2.77 ± 0.10	2.96 ± 0.10	2.71 ± 0.07
FLAG Ab + BSA + N-Neuro	3.51 ± 0.10	4.71 ± 0.36*	4.94 ± 0.16**
FLAG Ab + BSA + C-Neuro	3.96 ± 0.08	5.14 ± 0.11**	5.49 ± 0.15**
FLAG Ab + BSA + N-Neuro + Hep	2.92 ± 0.15	3.29 ± 0.16†	3.33 ± 0.11††
FLAG Ab + BSA + C-Neuro + Hep	2.86 ± 0.13	3.10 ± 0.17††	2.92 ± 0.14††

the neurocan core protein through their heparan sulphate chains, which is consistent with the recent report that neurocan binds to heparin [6]. It has been reported that neurocan binds to some heparin-binding factors such as pleiotrophin/HB-GAM [15], amphoterin [15] and fibroblast growth factor-2 [16]. The binding of neurocan to these molecules is mainly mediated through its chondroitin sulphate chains [15,16]. Thus there is a possibility that the binding of neurocan to HSPGs is mediated by these heparin-binding factors, which may bridge between heparan sulphate and chondroitin sulphate chains. However, for the binding of neurocan to syndecan-3 and glypican-1, this is not the case, because treatment of neurocan with chondroitinase ABC did not cause any decrease in the binding ability.

It is known that in adult rodent brain, most neurocan is cleaved proteolytically into its C- and N-terminal fragments [25,33]. Recently, Feng et al. [6] reported that, when an extract of adult mouse brains was applied to a heparin column, the C-terminal fragment, but not the N-terminal one, could be detected in the eluate on immunoblot analysis with anti-neurocan antiserum. However, in the present study, we demonstrated that the N-terminal fragment of neurocan prepared from neonatal mouse brains, in addition to the

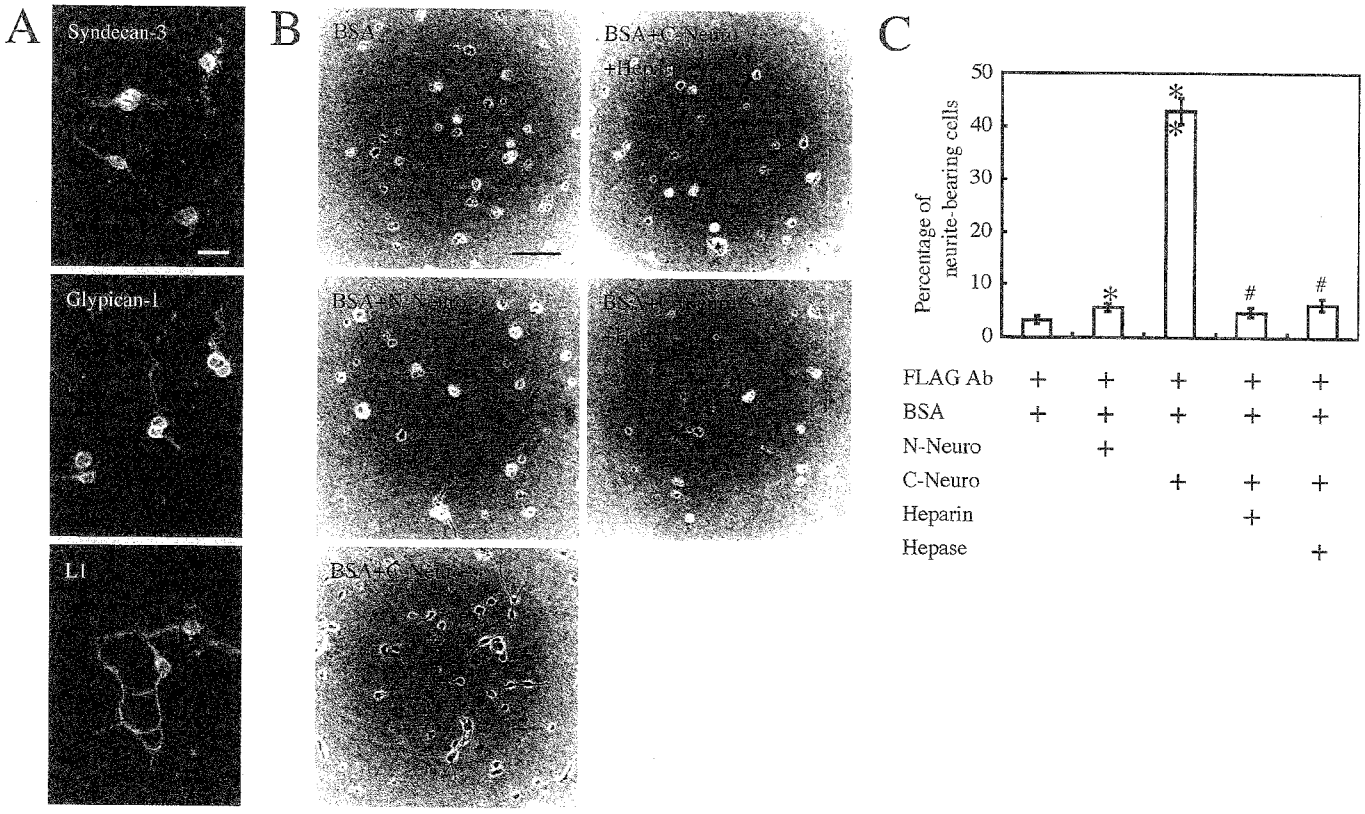

Figure 7 Neurite outgrowth from mouse cerebellar granule cells on recombinant neurocan substrate

(**A**) Cerebellar granule cells from neonatal mice aged 6 days were cultured on poly-D-lysine-coated glass slides for 48 h. The cells were immunostained with anti-syndecan-3 antibodies or anti-glypican-1 antibodies. The cells were also immunostained with antibodies against cell adhesion molecule L1, as a marker for cerebellar granule cells. As a control, the cells treated with normal goat IgG did not exhibit any positive reactivity (results not shown). Scale bar, 20 μm. (**B**) For the neurite outgrowth assay, the wells were coated with anti-FLAG antibodies only or coated with FLAG-tagged recombinant N- or C-terminal neurocan fragment via anti-FLAG antibodies. To examine further the effect of the heparan sulphate chains, the granule cells were cultured on the C-terminal neurocan fragment-substrate treated with heparin (10 μg/ml) or on the same substrate in the presence of heparitinase I (0.1 unit/ml). The granule cells from neonatal mice aged 6 days were cultured on these substrates for 48 h. These experiments were repeated three times and images from a typical experiment are shown. Scale bar, 100 μm. (**C**) The percentage of neurite-bearing cells is presented as the means for triplicate determinations. Error bars represent the S.E.M. $*P < 0.05$, $**P < 0.001$, compared with the neurocan-uncoated wells. $\#P < 0.001$, compared with recombinant C-terminal neurocan fragment-coated wells. FLAG Ab, anti-FLAG monoclonal antibody; N-Neuro, FLAG-tagged recombinant N-terminal neurocan fragment; C-Neuro, FLAG-tagged recombinant C-terminal neurocan fragment; Hepase, heparitinase I.

C-terminal fragment and whole molecule, could bind to a heparin column. To confirm this, we prepared recombinant N- and C-terminal fragments of neurocan. Using these recombinant fragments, we clearly demonstrated that both the N- and C-terminal neurocan fragments could bind to heparin, as shown in Figure 6. In addition, a higher concentration of NaCl was necessary to elute the C-terminal fragment when compared with the N-terminal fragment (Figure 5B), which is consistent with our finding that neurocan has two binding sites with different affinities for syndecan-3 and glypican-1. N-CAM (neural cell-adhesion molecule) could also bind to the N-terminal, central and C-terminal parts of neurocan [36]. Thus, by possessing multi-binding sites for ligands, neurocan may form stable molecular complexes with various extracellular and cell-surface molecules.

To examine whether neurocan could also bind to these HSPGs on the cell surface, we performed the centrifugation cell adhesion assay using N18TG-2 mouse neuroblastoma cells transfected with syndecan-3 or glypican-1 cDNA. When the wells were coated with the FLAG-tagged recombinant N- or C-terminal neurocan fragment via anti-FLAG monoclonal antibodies, the diameters of the attachment areas of Syn3- and Gly1-N18TG-2 cells were greater than those of Mock-N18TG-2 cells. These results suggest that neurocan could bind not only to soluble syndecan-3 and glypican-1 in the extracellular matrix, but also to membrane-bound ones on the neuronal cell surface.

Some experiments *in vitro* have shown that neurocan inhibits cell adhesion and neurite outgrowth and this property depends on its chondroitin sulphate chains and/or core proteins [34,37]; hence, we performed an experiment to see if the interaction between neurocan and cell-surface HSPGs has a biological effect. We examined neurite outgrowth from mouse cerebellar granule cells cultured on neurocan substrate, since immunohistochemical studies have shown that syndecan-3, glypican-1 and neurocan are co-localized in the molecular layer of neonatal rodent cerebellum [17,21,25]. When the granule cells were cultured on the wells coated with the recombinant C-terminal neurocan fragment, neurite outgrowth was significantly promoted. This neurite outgrowth-promoting activity was suppressed by pretreatment of neurocan substrate with heparin. Addition of heparitinase I into culture medium also inhibited neurite outgrowth, indicating that cell-surface HSPGs mediate this activity. Thus these results suggest that the interaction of cell-surface syndecan-3 and glypican-1 with neurocan substrate could promote neurite outgrowth. These results are consistent with the fact that the granule cells extend their neurites into the neurocan-rich molecular layer in the developing cerebellum [25,35]. In contrast with the C-terminal neurocan fragment, we could find little effect of the N-terminal fragment on neurite outgrowth, even though the cell adhesion assay showed that the N-terminal fragment could bind to cell-surface HSPGs. One possibility is that neurocan-induced neurite outgrowth needs the co-operative interactions of cell-surface HSPGs and other unidentified molecules, which could bind to the C-terminal domain of neurocan but not to the N-terminal one. As reported previously, the cerebellar granule cells express cell adhesion molecule L1, which can bind to neurocan [8] and the L1 molecule itself [38], and the L1–L1 homophilic binding promotes cell adhesion and neurite outgrowth [38]. Thus neurocan may prevent the L1–L1 homophilic binding, resulting in the inhibition of cell adhesion and neurite outgrowth [8]. However, how and what kind of effect is produced by neurocan–L1 interaction has not been demonstrated. It also remains unclear whether this interaction is co-operatively involved in the neurite outgrowth through the neurocan–cell-surface HSPG interaction. Further studies will be necessary to elucidate in detail the mechanism behind neurocan-induced neurite outgrowth.

It should also be noted that considerable amounts of these HSPGs are shed from the cell surface in the developing brain [7,18,19,28]. Soluble HSPGs shed from the cell surface may inhibit the cell-surface HSPG–neurocan interactions competitively and may regulate neurocan-induced neurite outgrowth. This possibility is currently under investigation.

This work was supported by the Foundation for Bio-venture Research Center (Ministry of Education, Culture, Sports, Science and Technology, Japan).

REFERENCES

1 Carey, D. J. (1996) N-syndecan: structure and function of a transmembrane heparan sulfate proteoglycan. Perspect. Dev. Neurobiol. **3**, 331–346
2 Chernousov, M. A., Stahl, R. C. and Carey, D. J. (1996) Schwann cells secrete a novel collagen-like adhesive protein that binds N-syndecan. J. Biol. Chem. **271**, 13844–13853
3 Kinnunen, T., Kaksonen, M., Saarinen, J., Kalkkinen, N., Peng, H. B. and Rauvala, H. (1998) Cortactin-Src kinase signaling pathway is involved in N-syndecan-dependent neurite outgrowth. J. Biol. Chem. **273**, 10702–10708
4 Lauri, S. E., Kaukinen, S., Kinnunen, T., Ylinen, A., Imai, S., Kaila, K., Taira, T. and Rauvala, H. (1999) Regulatory role and molecular interactions of a cell-surface heparan sulfate proteoglycan (N-syndecan) in hippocampal long-term potentiation. J. Neurosci. **19**, 1226–1235
5 Erdman, R., Stahl, R. C., Rothblum, K., Chernousov, M. A. and Carey, D. J. (2002) Schwann cell adhesion to a novel heparan sulfate binding site in the N-terminal domain of alpha 4 type V collagen is mediated by syndecan-3. J. Biol. Chem. **277**, 7619–7625
6 Feng, K., Arnold-Ammer, I. and Rauch, U. (2000) Neurocan is a heparin binding proteoglycan. Biochem. Biophys. Res. Commun. **272**, 449–455
7 Lander, A. D., Stipp, C. S. and Ivins, J. K. (1996) The glypican family of heparan sulfate proteoglycans: major cell-surface proteoglycans of the developing nervous system. Perspect. Dev. Neurobiol. **3**, 347–358
8 Friedlander, D. R., Milev, P., Karthikeyan, L., Margolis, R. K., Margolis, R. U. and Grumet, M. (1994) The neuronal chondroitin sulfate proteoglycan neurocan binds to the neural cell adhesion molecules Ng-CAM/L1/NILE and N-CAM, and inhibits neuronal adhesion and neurite outgrowth. J. Cell Biol. **125**, 669–680
9 Balsamo, J., Ernst, H., Zanin, M. K., Hoffman, S. and Lilien, J. (1995) The interaction of the retina cell surface N-acetylgalactosaminylphosphotransferase with an endogenous proteoglycan ligand results in inhibition of cadherin-mediated adhesion. J. Cell Biol. **129**, 1391–1401
10 Milev, P., Maurel, P., Haring, M., Margolis, R. K. and Margolis, R. U. (1996) TAG-1/axonin-1 is a high-affinity ligand of neurocan, phosphacan/protein-tyrosine phosphatase-zeta/beta, and N-CAM. J. Biol. Chem. **271**, 15716–15723
11 Grumet, M., Milev, P., Sakurai, T., Karthikeyan, L., Bourdon, M., Margolis, R. K. and Margolis, R. U. (1994) Interactions with tenascin and differential effects on cell adhesion of neurocan and phosphacan, two major chondroitin sulfate proteoglycans of nervous tissue. J. Biol. Chem. **269**, 12142–12146
12 Retzler, C., Wiedemann, H., Kulbe, G. and Rauch, U. (1996) Structural and electron microscopic analysis of neurocan and recombinant neurocan fragments. J. Biol. Chem. **271**, 17107–17113
13 Aspberg, A., Miura, R., Bourdoulous, S., Shimonaka, M., Heinegard, D., Schachner, M., Ruoslahti, E. and Yamaguchi, Y. (1997) The C-type lectin domains of lecticans, a family of aggregating chondroitin sulfate proteoglycans, bind tenascin-R by protein–protein interactions independent of carbohydrate moiety. Proc. Natl. Acad. Sci. U.S.A. **94**, 10116–10121
14 Rauch, U., Clement, A., Retzler, C., Frohlich, L., Fassler, R., Gohring, W. and Faissner, A. (1997) Mapping of a defined neurocan binding site to distinct domains of tenascin-C. J. Biol. Chem. **272**, 26905–26912
15 Milev, P., Chiba, A., Haring, M., Rauvala, H., Schachner, M., Ranscht, B., Margolis, R. K. and Margolis, R. U. (1998) High affinity binding and overlapping localization of neurocan and phosphacan/protein-tyrosine phosphatase-zeta/beta with tenascin-R, amphoterin, and the heparin-binding growth-associated molecule. J. Biol. Chem. **273**, 6998–7005
16 Milev, P., Monnerie, H., Popp, S., Margolis, R. K. and Margolis, R. U. (1998) The core protein of the chondroitin sulfate proteoglycan phosphacan is a high-affinity ligand of fibroblast growth factor-2 and potentiates its mitogenic activity. J. Biol. Chem. **273**, 21439–21442
17 Watanabe, E., Matsui, F., Keino, H., Ono, K., Kushima, Y., Noda, M. and Oohira, A. (1996) A membrane-bound heparan sulfate proteoglycan that is transiently expressed on growing axons in the rat brain. J. Neurosci. Res. **44**, 84–96

18 Carey, D. J., Conner, K., Asundi, V. K., O'Mahony, D. J., Stahl, R. C., Showalter, L., Cizmeci-Smith, G., Hartman, J. and Rothblum, L. I. (1997) cDNA cloning, genomic organization, and *in vivo* expression of rat N-syndecan. J. Biol. Chem. **272**, 2873–2879
19 Hsueh, Y. P. and Sheng, M. (1999) Regulated expression and subcellular localization of syndecan heparan sulfate proteoglycans and the syndecan-binding protein CASK/LIN-2 during rat brain development. J. Neurosci. **19**, 7415–7425
20 Litwack, E. D., Stipp, C. S., Kumbasar, A. and Lander, A. D. (1994) Neuronal expression of glypican, a cell-surface glycosylphosphatidylinositol-anchored heparan sulfate proteoglycan, in the adult rat nervous system. J. Neurosci. **14**, 3713–3724
21 Karthikeyan, L., Flad, M., Engel, M., Meyer-Puttlitz, B., Margolis, R. U. and Margolis, R. K. (1994) Immunocytochemical and *in situ* hybridization studies of the heparan sulfate proteoglycan, glypican, in nervous tissue. J. Cell Sci. **107**, 3213–3222
22 Litwack, E. D., Ivins, J. K., Kumbasar, A., Paine-Saunders, S., Stipp, C. S. and Lander, A. D. (1998) Expression of the heparan sulfate proteoglycan glypican-1 in the developing rodent. Dev. Dyn. **211**, 72–87
23 Bernfield, M., Gotte, M., Park, P. W., Reizes, O., Fitzgerald, M. L., Lincecum, J. and Zako, M. (1999) Functions of cell surface heparan sulfate proteoglycans. Annu. Rev. Biochem. **68**, 729–777
24 Inatani, M., Irie, F., Plump, A. S., Tessier-Lavigne, M. and Yamaguchi, Y. (2003) Mammalian brain morphogenesis and midline axon guidance require heparan sulfate. Science **302**, 1044–1046
25 Rauch, U., Gao, P., Janetzko, A., Flaccus, A., Hilgenberg, L., Tekotte, H., Margolis, R. K. and Margolis, R. U. (1991) Isolation and characterization of developmentally regulated chondroitin sulfate and chondroitin/keratan sulfate proteoglycans of brain identified with monoclonal antibodies. J. Biol. Chem. **266**, 14785–14801
26 Oohira, A., Matsui, F., Matsuda, M., Takida, Y. and Kuboki, Y. (1988) Occurrence of three distinct molecular species of chondroitin sulfate proteoglycan in the developing rat brain. J. Biol. Chem. **263**, 10240–10246
27 Akita, K., Fushiki, S., Fujimoto, T., Inoue, M., Oguri, K., Okayama, M., Yamashina, I. and Nakada, H. (2001) Developmental expression of a unique carbohydrate antigen, Tn antigen, in mouse central nervous tissues. J. Neurosci. Res. **65**, 595–603
28 Akita, K., Fushiki, S., Fujimoto, T., Munesue, S., Inoue, M., Oguri, K., Okayama, M., Yamashina, I. and Nakada, H. (2001) Identification of the core protein carrying the Tn antigen in mouse brain: specific expression on syndecan-3. Cell Struct. Funct. **26**, 271–278
29 Williamson, T. G., Mok, S. S., Henry, A., Cappai, R., Lander, A. D., Nurcombe, V., Beyreuther, K., Masters, C. L. and Small, D. H. (1996) Secreted glypican binds to the amyloid precursor protein of Alzheimer's disease (APP) and inhibits APP-induced neurite outgrowth. J. Biol. Chem. **271**, 31215–31221
30 Friedlander, D. R., Hoffman, S. and Edelman, G. M. (1988) Functional mapping of cytotactin: proteolytic fragments active in cell-substrate adhesion. J. Cell Biol. **107**, 2329–2340
31 Grumet, M., Flaccus, A. and Margolis, R. U. (1993) Functional characterization of chondroitin sulfate proteoglycans of brain: interactions with neurons and neural cell adhesion molecules. J. Cell Biol. **120**, 815–824
32 Fushiki, S., Matsumoto, K. and Nagata, A. (1995) Neurite outgrowth of murine cerebellar granule cells can be enhanced by aniracetam with or without alpha-amino-3-hydroxy-5-methyl-4-isoxazole propionic acid (AMPA). Neurosci. Lett. **199**, 171–174
33 Matsui, F., Watanabe, E. and Oohira, A. (1994) Immunological identification of two proteoglycan fragments derived from neurocan, a brain-specific chondroitin sulfate proteoglycan. Neurochem. Int. **25**, 425–431
34 Li, H., Leung, T. C., Hoffman, S., Balsamo, J. and Lilien, J. (2000) Coordinate regulation of cadherin and integrin function by the chondroitin sulfate proteoglycan neurocan. J. Cell Biol. **149**, 1275–1288
35 Jacobson, M. (1991) Developmental Neurobiology, 3rd edn, pp. 430–441, Plenum Press, New York and London
36 Retzler, C., Gohring, W. and Rauch, U. (1996) Analysis of neurocan structures interacting with the neural cell adhesion molecule N-CAM. J. Biol. Chem. **271**, 27304–27310
37 Talts, U., Kuhn, U., Roos, G. and Rauch, U. (2000) Modulation of extracellular matrix adhesiveness by neurocan and identification of its molecular basis. Exp. Cell. Res. **259**, 378–388
38 Lemmon, V., Farr, K. L. and Lagenaur, C. (1989) L1-mediated axon outgrowth occurs via a homophilic binding mechanism. Neuron **2**, 1597–1603

Received 8 April 2004/3 June 2004; accepted 15 June 2004
Published as BJ Immediate Publication 15 June 2004, DOI 10.1042/BJ20040585

J Hum Genet (2004) 49:1–8
DOI 10.1007/s10038-003-0098-z

ORIGINAL ARTICLE

Hitoshi Sakuraba · Fumiko Matsuzawa · Sei-ichi Aikawa
Hirofumi Doi · Masaharu Kotani · Hiroshi Nakada
Tomoko Fukushige · Tamotsu Kanzaki

Structural and immunocytochemical studies on α-*N*-acetylgalactosaminidase deficiency (Schindler/Kanzaki disease)

Received: 29 July 2003 / Accepted: 30 September 2003 / Published online: 19 December 2003

Abstract α-*N*-Acetylgalactosaminidase (α-NAGA) deficiency (Schindler/Kanzaki disease) is a clinically and pathologically heterogeneous genetic disease with a wide spectrum including an early onset neuroaxonal dystrophy (Schindler disease) and late onset angiokeratoma corporis diffusum (Kanzaki disease). In α-NAGA deficiency, there are discrepancies between the genotype and phenotype, and also between urinary excretion products (sialyl glycoconjugates) and a theoretical accumulated material (Tn-antigen; Gal NAcα1-*O*-Ser/Thr) resulting from a defect in α-NAGA. As for the former issue, previously reported genetic, biochemical and pathological data raise the question whether or not E325K mutation found in Schindler disease patients really leads to the severe phenotype of α-NAGA deficiency. The latter issue leads to the question of whether α-NAGA deficiency is associated with the basic pathogenesis of this disease. To clarify the pathogenesis of this disease, we performed structural and immunocytochemical studies. The structure of human α-NAGA deduced on homology modeling is composed of two domains, domain I, including the active site, and domain II. R329W/Q, identified in patients with Kanzaki disease have been deduced to cause drastic changes at the interface between domains I and II. The structural change caused by E325K found in patients with Schindler disease is localized on the N-terminal side of the tenth β-strand in domain II and is smaller than those caused by R329W/Q. Immunocytochemical analysis revealed that the main lysosomal accumulated material in cultured fibroblasts from patients with Kanzaki disease is Tn-antigen. These data suggest that a prototype of α-NAGA deficiency in Kanzaki disease and factors other than the defect of α-NAGA may contribute to severe neurological disorders, and Kanzaki disease is thought to be caused by a single enzyme deficiency.

Keywords α-*N*-acetylgalactosaminidase deficiency · Schindler disease · Kanzaki disease · Homology modeling · Tn-antigen

H. Sakuraba (✉) · M. Kotani
Department of Clinical Genetics,
The Tokyo Metropolitan Institute of Medical Science,
Tokyo Metropolitan Organization for Medical Research,
3-18-22 Honkomagome, Bunkyo-ku,
Tokyo 113-8613, Japan
E-mail: sakuraba@rinshoken.or.jp
Tel.: +81-3-38232105
Fax: +81-3-38236008

F. Matsuzawa · S. Aikawa · H. Doi
Celestar Lexico-Sciences,
MTG D-17, 1-3 Nakase,
Mihama-ku, Chiba 261-8501, Japan

H. Nakada
Department of Biotechnology,
Faculty of Engineering,
Kyoto Sangyo University,
Kamigamo-Motoyama,
Kita-ku, Kyoto 603-8555, Japan

T. Fukushige · T. Kanzaki
Department of Dermatology,
Faculty of Medicine,
Kagoshima University,
8-35-1 Sakuragaoka,
Kagoshima 890-8520, Japan

Introduction

α-*N*-Acetylgalactosaminidase (α-NAGA) deficiency (Schindler/Kanzaki disease) is a genetic disease characterized by deficient activity of α-NAGA (EC.3.2.1.49) and abnormal urinary excretion of glycopeptides (reviewed by Desnick and Schindler, 2001). Up to now, 12 patients from eight families with α-NAGA deficiency have been reported, and this disease is known as a clinically heterogeneous disorder (Bakker et al. 2001; Kodama et al. 2001). In 1987, two German brothers with α-NAGA deficiency were first described (van Diggelen et al. 1987). They developed an early-onset severe progressive neurological disorder pathologically characterized by an infantile neuroaxonal dystrophy

(Schindler et al. 1989), and the disease was named Schindler disease. Then, a group of adult patients with angiokeratoma corporis diffusum and vacuolization in various cell types associated with α-NAGA deficiency and glycopeptiduria identical to those in Schindler disease was reported (Kanzaki et al. 1989, 1991, 1993; Chabas et al. 1994; Kodama et al. 2001), and the disease was named Kanzaki disease. Then, α-NAGA deficiency (Schindler/Kanzaki disease) was divided into three subtypes (types I–III) in a textbook (Desnick and Schindler, 2001). According to the latter classification, type I disease, an infantile neuroaxonal dystrophy associated with α-NAGA deficiency, is an early-onset severe phenotype. Type II disease, angiokeratoma corporis diffusum associated with α-NAGA deficiency but without overt neurological manifestations, is an adult-onset mild phenotype. Type III disease is an intermediate phenotype (de Jong et al. 1994).

However, there are two paradoxes. The first one is differences between the phenotype and genotype. Keulemans et al. (1996) pointed out that vacuolization, the hallmark of lysosomal storage diseases, was observed in various cells from type II patients but not in ones from type I patients. A pathological finding in the latter cases was 'spheroid degeneration' in axons, which does not indicate a lysosomal disease. Furthermore, they found that type I patients have some residual α-NAGA activity, although the almost complete absence of α-NAGA activity was found in type II patients (Keulemans et al. 1996). Two kinds of missense mutations (R329W and R329Q) and a nonsense mutation (E193X) were identified in Type II patients, each patient being homozygous for one of the mutations (Wang et al. 1994; Kodama et al. 2001; Keulemans et al. 1996). The E193X mutation identified in Spanish patients represents a null mutation that should be associated with a severe phenotype. But their phenotype is angiokeratoma corporis diffusum. On the other hand, two affected brothers with the type I phenotype are homozygous for E325K (Wang et al. 1990). So, the E325K mutation had been thought to be associated with a severe phenotype with an infantile neuroaxonal dystrophy. However, Bakker et al. (2001) recently reported two Moroccan sibs with α-NAGA deficiency. They are homozygous for E325K alleles. The index patient, 3 years old, developed congenital cataracts and slight motor retardation, and his brother had no clinical or neurological symptoms at the age of 7 years, although it can be associated with the vegetative state of the first German brothers with Schindler disease. These data raise the question of whether or not an infantile neuroaxonal dystrophy really leads to the severe phenotype of α-NAGA deficiency.

The second paradox is a difference between urinary glycopeptides identified in patients with α-NAGA deficiency and a theoretical storage product. α-NAGA is a glycosyl hydrolase that catalyzes the hydrolysis of Tn-antigen. Tn-antigen is a glycoprotein having a structure of GalNAcα1-*O*-Ser/Thr and forms the core of *O*-linked glycoconjugates (Akita et al. 2001). It is also known as a tumor-associated antigen (Springer, 1984). A deficiency of the activity of α-NAGA should lead to the accumulation of glycoconjugates with terminal α-*N*-acetylgalactosaminyl residues. However, the major urinary excretion products are sialyl glycopeptides including NeuAcα2–3NeuAcβ 1–3 [NeuAc α2–6] GalNAcα1–*O*–Ser/Thr and NeuAcα2–3 Galβ 1–3GalNAcα1-*O*-Ser/Thr—both in Schindler disease and Kanzaki disease (Linden et al. 1989; Hirabayashi et al. 1990). This discrepancy leads to the question of whether deficient activity of α-NAGA is associated with the basic pathogenesis of this disease or not. It is very important to identify the major storage products in cells and tissues of patients with Schindler/Kanzaki disease to answer this question. But the details have not been clarified yet because there have been no autopsy cases of this disease.

In this study, we constructed a structural model of human α-NAGA by homology modeling and then characterized the molecular defects in α-NAGA caused by E325K and R329W/Q. Furthermore, we analyzed the accumulated materials in cultured fibroblasts from two patients with Kanzaki disease by means of immunocytochemical staining using an antibody against Tn-antigen and an antilysosomal-associated membrane protein-1 (LAMP-1) antibody, and lectin staining with a phytohemagglutinin purified from the seeds of *Macckia amurensis* (strongly mitogenic *Macckia amurensis* hemagglutinin, MAM),which is specific for NeuAcα2–3Gal (Kawaguchi et al. 1974). LAMP-1 is a lysosomal membrane protein. It is involved in protecting the lysosomal membrane from autodigestion and its expression is increased in lysosomal diseases (Hua et al. 1997; Meikle et al. 1998). In this study, LAMP-1 was used as a lysosomal marker. The pathogenesis of α-NAGA deficiency is discussed.

Materials and methods

Structural modeling of human wild-type and mutant α-NAGAs

Structural models of human wild-type α-NAGA and its mutants (E325K, R329W and R329Q) were built based on crystallographic structure data for chicken α-NAGA (PDB code; 1KTB) (Garman et al. 2002) exhibiting 75% amino acid identity. The modeling was performed with molecular modeling software, SYBYL/COMPOSER and BIOPOLIMER (TRIPOS, Inc., Mountain View, CA, USA). The sequence of human α-NAGA was aligned with that of chicken α-NAGA. According to the sequence alignment, the backbone structure of chicken α-NAGA was applied to the model of human α-NAGA. After each side chain had been generated and adjusted, the energy minimization procedure was performed to optimize the conformations and side-chain rotamers, as described previously (Sakuraba et al. 2002). The mutant models were built in the same way as for the wild-type but were based on the amino acid sequence with the replacements. To determine the influence of amino acid substitutions on the model structure, each mutant model was superimposed with the wild-type model based on the Cα atoms by a least-square-mean fitting method (Kabsh, 1976, 1978).

We defined the structure as being influenced by the amino acid replacement when the position of an atom of the mutant differed from that of the wild type by more than the total root-mean-square distance value, as described previously (Sakuraba H et al. 2002).

Immunocytochemical staining

Mouse monoclonal antibodies to LAMP-1 and Tn-antigen were purchased from Southern Biotechnology (Birmingham, AL, USA) and DAKO (Glostrup, Denmark), respectively. A fluorescein isothiocyanate (FITC)-conjugated MAM was purchased from Seikagaku Co. (Tokyo, Japan). FITC-conjugated goat antimouse IgM $(Fab')_2$ and Cy3-conjugated goat antimouse IgG$(Fab')_2$ were purchased from Jackson Immuno Research (West Grove, PA, USA).

Cultured skin fibroblasts from two unrelated Japanese patients with Kanzaki disease, a patient with sialidosis (lysosomal sialidase deficiency) as a pathological control, and normal control subjects were cultured in Ham's F-10 medium supplemented with 10% fetal calf serum and antibiotics at 37°C in a humidified incubator flushed continuously with a 5% CO_2-95% air mixture.

For the double staining of Tn-antigen and LAMP-1, cells grown on Lab-Tek chamber slides (Nunc, Naperville, IL, USA) were fixed with 4% paraformaldehyde in phosphate-buffered saline (PBS), pH7.4, for 5 min, followed by blocking with 1% bovine serum albumin in PBS for 30 min at room temperature. The cells were then incubated for 1 h with a mouse monoclonal antibody to Tn-antigen (1:100 diluted) in a dark place. After washing, the cells were incubated for 1 h with FITC-conjugated goat antimouse IgM $(Fab')_2$ (1:100 diluted). Then the cells were washed and incubated for 1 h with a mouse monoclonal antibody to LAMP-1 (1:100 diluted) in a dark place. After washing, the cells were reacted for 1 h with Cy3-conjugated goat antimouse IgG $(Fab')_2$ (1:200 diluted) in a dark place. The stained cells were examined under a microscope (Axiovert 100 M; Carl Zeiss, Oberkochen, Germany) equipped with a confocal laser scanning imaging system (LSM510; Carl Zeiss).

The double staining of cultured fibroblasts with FITC-MAM and an anti-LAMP-1 antibody was performed according to the modified method of Kotani et al. (submitted). Briefly, the cells were reacted for 1 h with a FITC-conjugated MAM (1:100 diluted). After washing, the cells were incubated for 1 h with an anti-LAMP-1 antibody (1:100 diluted) as the first antibody in a dark place. After washing, the cells were reacted for 1 h with Cy3-conjugated goat antimouse IgG$(Fab')_2$ (1:200 diluted) as the second antibody in a dark place.

Establishment of cultured fibroblasts was performed with informed consent from the patients, and the study was approved by the ethical committees of our institutions.

Results

Structural modeling of human wild-type and mutant α-NAGAs

We built a model of human α-NAGA based on the crystallographic structural data for chicken α-NAGA without the N-terminal 17 residues corresponding to the signal peptide. The structure corresponding to the C-terminal 7 residues has not been determined for the chicken α-NAGA structure. The model, thus, comprises 387 amino acids (i.e., residues 18–404). The modeled structure of human α-NAGA is shown in Fig. 1. The structure of human α-NAGA has two domains (domains I and II). Domain I (residues 18–311) is folded into a $(\beta/\alpha)_8$-barrel with the active site (D115 and D217), and domain II (residues 312–404) has a β sandwich fold consisting of eight antiparallel β-strands. To determine the positions of mutations, amino acid residues E325 and R329 were mapped on the monomer and dimer structures of wild-type human α-NAGA (Figs. 1 and 2). As shown in Fig. 1, the residues of E325 and R329 are located on opposite sides of the same tenth β-strand in domain II. The dimer model indicates that both E325 and R329 are not concerned with the dimer interface (Fig. 2).

To reveal the influence of the mutations, we constructed three mutant structures (R329W, R329Q and E325K) and compared them with the wild-type. R329 is located on the C-terminal side of the tenth β-strand in domain II, facing domain I (Fig. 1). In the wild-type model, the side chain of R329 fits into the domain I and forms hydrogen bonds with three residues; T274 and N306 in domain I, and I312 at the junction between the two domains (Fig. 3A). These hydrogen bonds between domains I and II are supposed to the stability of the two domains. Substitutions of R329W and R329Q cause disruption of these hydrogen bonds. In addition to the loss of the hydrogen bonds, R329W introduces a bulkier side chain that results in steric clashes. As shown in Fig. 3B and C, R329W/Q substitutions cause a drastic structural change on the interface between domains I and II. E325 is located on the N-terminal side of the tenth β-strand in domain II. The side chain is surrounded by charged residues (E234, R316, and K319) and polar residues (N230, Y327, and C343). Substitution of E325 with a positively charged K residue causes alteration of the arrangement of these residues and conformational changes of their side chains (Fig. 4). The predicted structural change is smaller than those caused by R329W/Q.

Immunocytochemical staining of cultured fibroblasts from patients with Kanzaki disease

To identify storage materials in cultured fibroblasts from Kanzaki disease patients, we tried double staining of cultured fibroblasts with an anti-Tn-antigen antibody and an anti-LAMP-1 antibody or with MAM and an anti-LAMP-1 antibody. We first performed double staining using an antibody against Tn-antigen and an anti-LAMP-1 antibody. As shown in Fig. 5, staining with the anti-LAMP-1 antibody revealed granular fluorescence, indicating lysosomes. When cells were stained with the anti-LAMP-1 antibody, both sialidosis fibroblasts and Kanzaki disease fibroblasts showed strong fluorescence, although normal controls showed weak granular fluorescence. This suggests an activated lysosomal function in these diseases. Marked fluorescence was only found in Kanzaki disease fibroblasts when the antibody against Tn-antigen was used. The localization was almost identical to that of LAMP-1 (Fig. 5A). However, only very weak fluorescence was detected in Kanzaki disease fibroblasts or in normal subjects when the cells were stained with MAM, although strong fluorescence was found in sialidosis fibroblasts in which sialylated glycoconjugates should be accumulated (Fig. 5B). The results were confirmed by three independent experiments. These results suggest that the

accumulated material in Kanzaki disease cells is Tn-antigen and not a sialyl glycoconjugate.

Discussion

α-NAGA deficiency has been shown to be a clinically and pathologically heterogeneous disease including Schindler disease and Kanzaki disease. We tried to gain an insight into the pathogenesis of α-NAGA deficiency on the basis of structural information. The modeled human α-NAGA consists of two domains, one of which has a $(\beta/\alpha)_8$-barrel structure including the active site and the other an α/β topology. This structure may be common in many lysosomal hydrolases (Mark et al. 2003). A previous study (Wang et al. 1990) demonstrated that α-NAGA formed a homodimer of a 48-kDa species in cultured fibroblasts. Structural analysis revealed that E325 and R329 are located on the N-terminal and C-terminal sides of the tenth β-strand in domain II, respectively. E325 and R329 are far from the dimer interface, and both are thus thought not to affect the dimer formation.

Among the three missense mutations (R329W, R329Q, and E325K), R329W and R329Q identified in patients with Kanzaki disease are deduced to cause drastic structural changes on the interface between domains I and II. The hydrogen bonds that R329 forms between domains I and II are supposed to contribute to the stability of the two domains. The R329W/Q substitutions causing the loss of these hydrogen bonds could destabilize the protein structure. Furthermore, the structural changes on the interface between the two

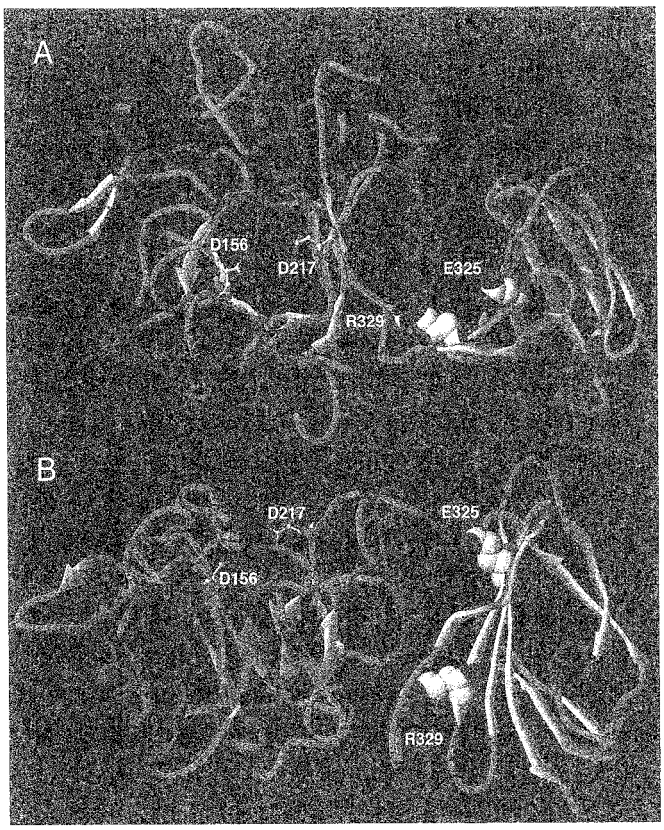

Fig. 1A, B Three-dimensional structure of human α-NAGA. **A** Front view of human α-NAGA. **B** Side view of the protein. The secondary structures are shown as tube and ribbon drawings; α-helix (*magenta*), β-sheet (*yellow*), and coil (*cyan*). Residues comprising the catalytic site (D156 and D217) are presented as a ball-and-stick model, and the localization of amino acid substitutions (E325 and R329) is presented as a space-filling model

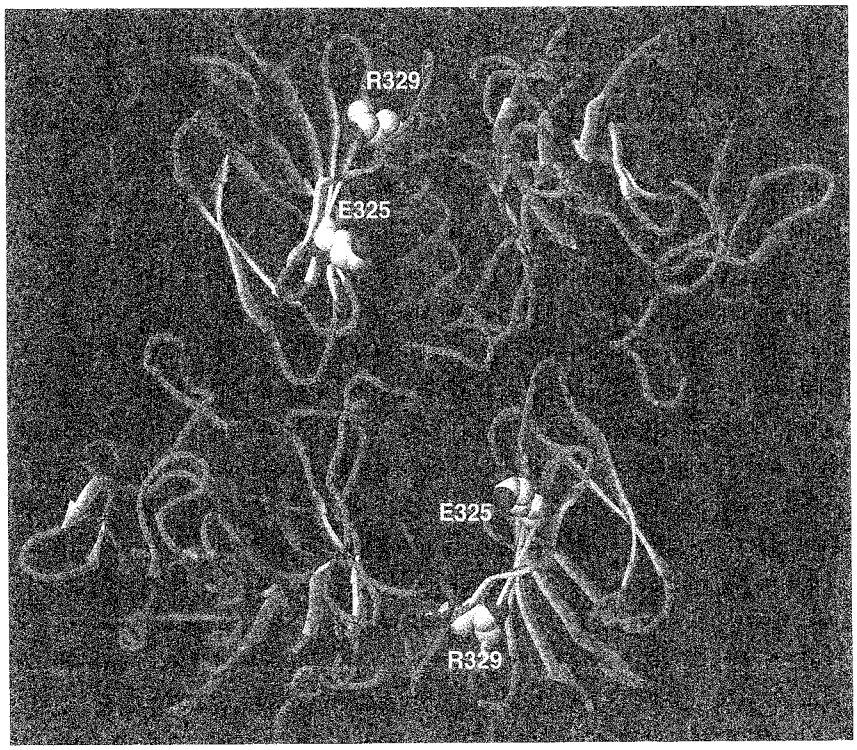

Fig. 2 Deduced structure of the dimer of human α-NAGA

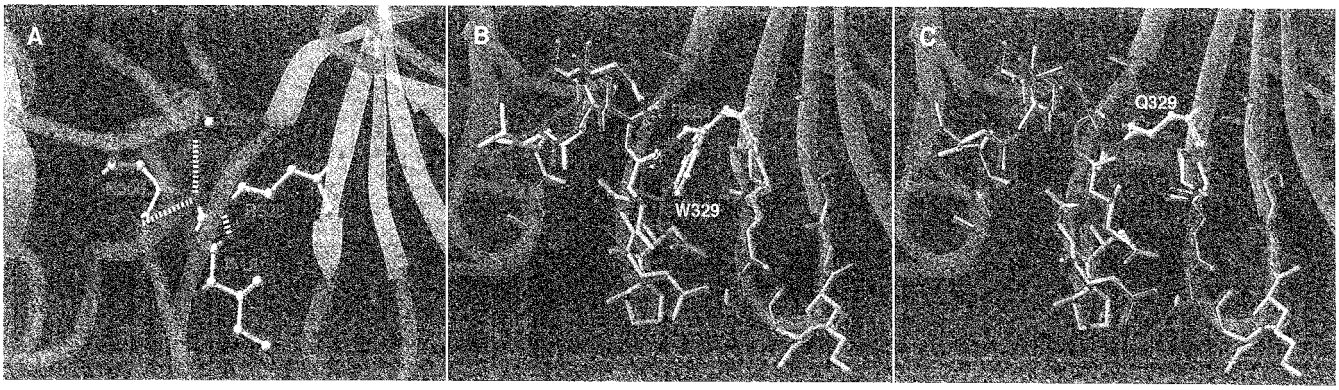

Fig. 3A–C Conformational changes of α-NAGA caused by R329W/Q. **A** Hydrogen bonds between R329 and other amino acid residues. **B** Structural change caused by R329W. **C** Structural change caused by R329Q. The residues of the wild type and mutants are colored *magenta* and *yellow*, respectively

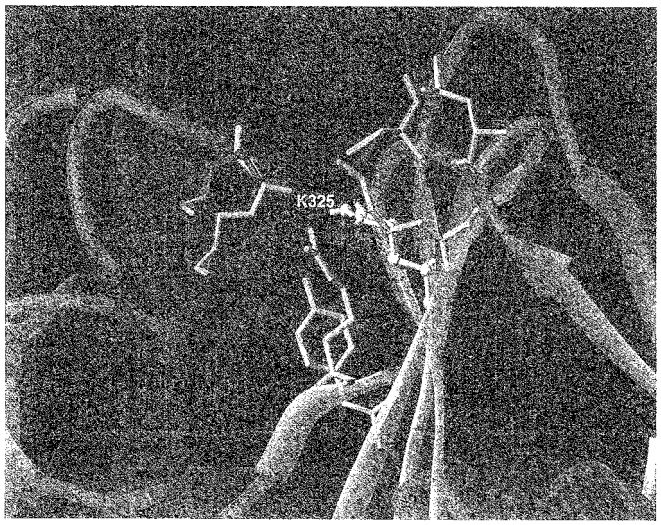

Fig. 4 Conformational changes of α-NAGA caused by E325K. The residues of the wild type and mutant are colored *magenta* and *yellow*, respectively

domains would affect the packing of the protein. These structural changes were observed not only on side chains but also on main chains forming the domain structure. Thus, the substitutions are deduced to cause a significant influence to decrease the protein stability or to cause a folding defect. α-NAGA activities in clinical samples from the patients homozygous for these mutations are both very low (below 1% of the normal control mean) (Kanzaki et al. 1991; Kodama et al. 2001), and the kinetic data could not be obtained. However, R329 is far from the active site, and it is thought not to affect the kinetic character, including Km value. Indeed, Kanzaki et al. performed immunoblotting analysis and found that no band representing the mature form of α-NAGA was detected in a patient with the R329W mutation (Kanzaki et al. 1991).

On the other hand, the deduced structural change caused by E325K was localized on the N-terminal side of the tenth β-strand and observed on only side-chain conformations.

Thus, the influence caused by E325K is deduced to be smaller than that caused by R329W/Q. Keulemans et al. (1996) reported that the synthesis of precursor α-NAGA was normal, but mature α-NAGA was not detectable with the E325K mutation, and the α-NAGA activities in patients homozygous for E325K are relatively higher (0.6–1.7% of the normal control mean) than those in Spanish Kanzaki patients homozygous for E193X (0.2% of the normal control mean). We could not obtain clinical samples from patients with Schindler disease and the kinatic data are not available. But, E325 is far from the active site. So, the structural change caused by E325K is thought to cause the expression of an unstable enzyme and the expressed protein would be degraded quickly.

Our structural data are compatible with those of comparative studies including clinical, biochemical, pathological, and genetic analyses (Keulemans et al. 1996; Bakker et al. 2001), and the results support the suggestion of Keulemans et al. (1996) and Bakker et al. (2001) that a complete α-NAGA deficiency would cause late-onset angiokeratoma corporis diffusum (Kanzaki disease), and factors other than the defect of α-NAGA may contribute to the phenotypic expression in patients with an infantile neuroaxonal dystrophy (Schindler disease). The fact that patients other than the first German sibs with the combination of α-NAGA deficiency and neuroaxonal dystrophy have not been found would support this, although extensive research to find further patients has been performed.

In α-NAGA deficiency, the main urinary excretion products (sialyl glycoconjugates) are different from a theoretical accumulation material (Tn-antigen) resulting from a defect of α-NAGA. A possible explanation is that the accumulated Tn-antigen in various kinds of cells is probably taken up from the blood by hepatocytes in the liver, where glycosyltransferases, including α2–6 sialyltransferase, are abundant, and the addition of galactose residues and *N*-acetylneuraminic acid residues could occur. As a result, excessive sialyl glycoconjugates produced in the liver would be carried to the kidneys and excreted in the urine.

To investigate the primary accumulated materials in cells, we performed immunocytochemical and lectin staining using cultured fibroblasts as the best samples because they are not influenced by the metabolism in the liver via blood. Unfortunately, we could not obtain

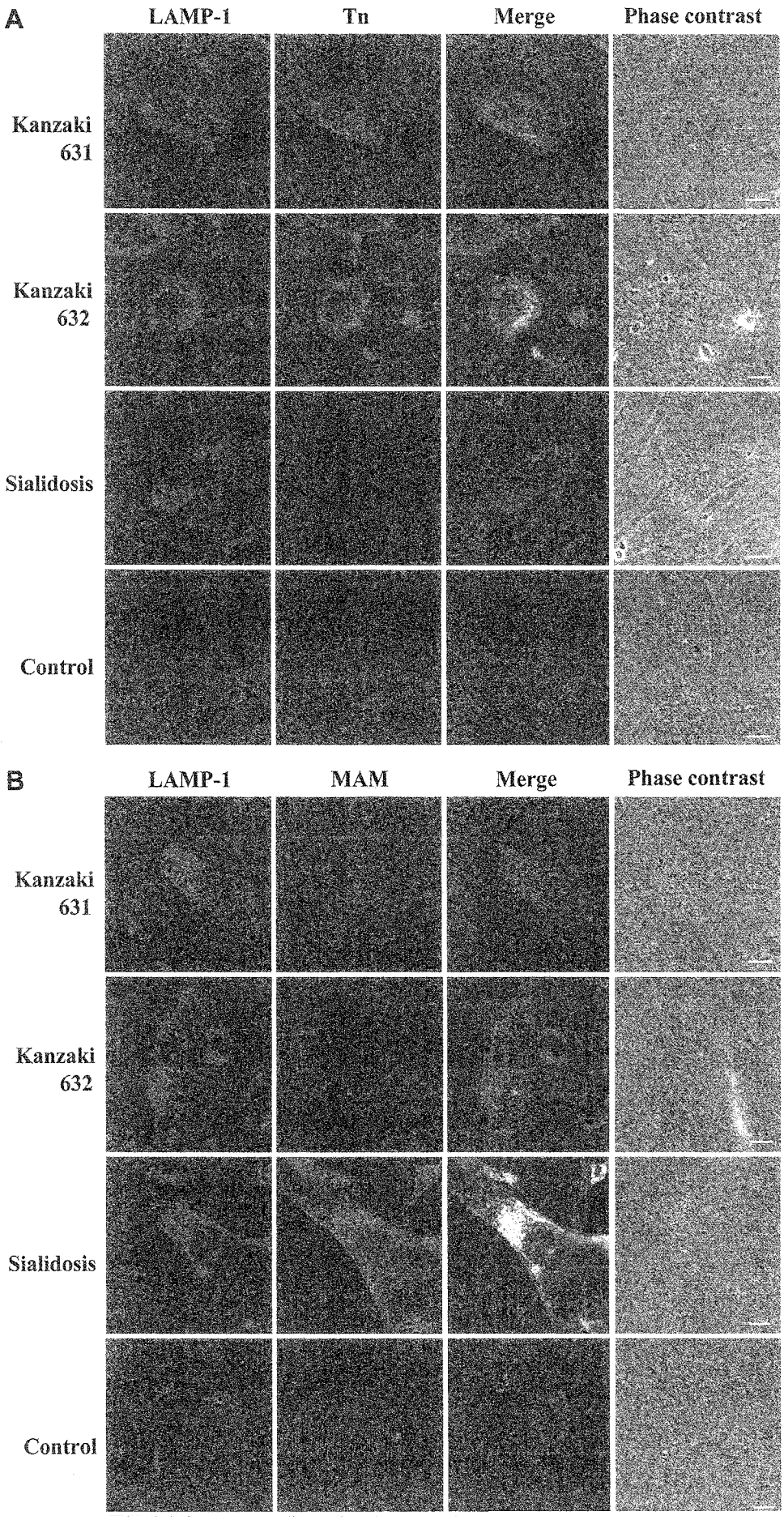

Fig. 5A, B Immunocytochemical analysis of LAMP-1 and Tn-antigen, and lectin staining with MAM using cultured fibroblasts as samples. **A** Double staining with an anti-LAMP-1 antibody (*red*) and an antibody against Tn-antigen (*green*). Lamp-1, staining with the anti-LAMP-1 antibody; Tn, staining with the antibody against Tn-antigen; Merge, double staining with these materials; Phase contrast, a phase contrast figure. **B** Double staining with the anti-LAMP-1 antibody (*red*) and MAM (*green*). Lamp-1, staining with the anti-LAMP-1 antibody; MAM, lectin staining with MAM; Merge, double staining with these materials; Phase contrast, a phase contrast figure. Kanzaki 631 and Kanzaki 632, unrelated patients with Kanzaki disease; Sialidosis, a patient with sialidosis; Control, a normal subject

fibroblasts from patients with Schindler disease. However, considering the data including those of previously reported biochemical and pathological analyses and these structural analyses, Kanzaki disease seems to be a prototype of α-NAGA deficiency. So, we used cultured fibroblasts from patients with Kanzaki disease as samples for the investigation of intracellular storage materials. The sensitive immunocytochemical analyses revealed that Tn-antigen is the major storage product. We also tried an immunoblotting analysis of Tn-antigen but could find no suitable antibodies available for that. However, Kanda et al. (2002) demonstrated that Tn-antigen was accumulated mainly in lysosomes of vascular endothelial cells, eccrine sweat gland cells, fibroblasts, and pericytes in Kanzaki disease patients using biopsied skin specimens by means of immunoelectron microscopic analyses. Considering these results, Kanzaki disease is thought to result from the defect of α-NAGA deficiency.

In conclusion, we characterized the structural and immunochemical bases of α-NAGA deficiency. The structural change caused by R329W/Q is greater than that by E325K. The main intracellular accumulated product in this disease is Tn-antigen. These findings are useful for understanding the pathogenesis of α-NAGA deficiency.

Acknowledgements This work was partly supported by grants from the Tokyo Metropolitan Government, The Japan Society for the Promotion of Science, and the Ministry of Health, Labor and Welfare of Japan.

References

Akita K, Fushiki S, Fujimoto T, Inoue M, Oguri K, Okayama M, Yamashina I, Nakada H (2001) Developmental expression of a unique carbohydrate antigen, Tn antigen, in mouse central nervous tissues. J Neurosci Res 65:595–603

Bakker HD, de Sonnaville M-LCS, Vreken P, Abeling NGGM, Groener JEM, Keulemans JLM, van Diggelen OP (2001) Human α-*N*-acetylgalactosaminidase (α-NAGA) deficiency: no association with neuroaxonal dystrophy? Eur J Hum Genet 9:91–96

Chabas A, Coll MJ, Aparicio M, Rodriguez Diaz E (1994) Mild phenotype expression of α-*N*-acetylgalactosaminidase deficiency in two adult siblings. J Inher Metab Dis 17:724–731

de Jong J, van den Berg C, Wijburg H, Willemsen R, van Diggelen O, Schindler D, Hoevenaars F, Wevers R (1994) Alpha-*N*-acetylgalactosaminidase deficiency with mild clinical manifestations and difficult biochemical diagnosis. J Pediatr 125:385–391

Desnick RJ, Schindler D (2001) α-*N*-Acetylgalactosaminidase deficiency: Schindler disease. In: Scriver CR, Beaudet AL, Sly WS, Valle D (eds) The metabolic and molecular bases of inherited disease, 8th edn. McGraw-Hill, New York, pp. 3483–3505

Garman SC, Hannick L, Zhu A, Garboczi DN (2002) The 1.9 Å structure of α-*N*-acetylgalactosaminidase: molecular basis of glycosidase deficiency diseases. Structure 10:425–434

Hirabayashi Y, Matsumoto Y, Matsumoto M, Toida T, Iida N, Matsubara T, Kanzaki T, Yokota M, Ishizuka I (1990) Isolation and characterization of major urinary amino acid *O*-glycosides and a dipeptide *O*-glycoside from a new lysosomal storage disorder (Kanzaki disease). J Biol Chem 265:1693–1701

Hua CT, Hopwood JJ, Carlsson SR, Harris RY, Meikle PJ (1998) Evaluation of the lysosome-associated membrane protein LAMP-2 as a maker for lysosomal storage disorders. Clin Chem 44:2094–2102

Kabsh W (1976) A solution for the best rotation to relate two sets of vectors. Acta Crystallogr A32:922–923

Kabsh W (1978) A discussion of the solution for the best rotation to relate two sets of vectors. Acta Crystallogr A34:827–828

Kanda A, Tsuyama S, Murata F, Kodama K, Hirabayashi Y, Kanzaki T (2002) Immunoelectron microscopic analysis of lysosomal deposits in α-*N*-acetylgalactosaminidase deficiency with angiokeratoma corporis diffusum. J Dermatol Sci 29:42–48

Kanzaki T, Yokota M, Mizuno N, Matsumoto Y, Hirabayashi Y (1989) Novel lysosomal glycoaminoacid storage disease with angiokeratoma corporis diffusum. Lancet i:875–876

Kanzaki T, Wang AM, Desnick RJ (1991) Lysosomal α-*N*-acetylgalactosaminidase deficiency, the enzymatic defect in angiokeratoma corporis diffusum with glycopeptiduria. J Clin Invest 88:707–711

Kanzaki T, Michino Y, Fumitoshi I, Hirabayashi Y, Wang AM, Desnick RJ (1993) Angiokeratoma corporis deffusum with glycopeptiduria due to deficient lysosomal α-*N*-acetylgalactosaminidase activity. Arch Dermatol 129:460–466

Kawaguchi T, Matsumoto I, Osawa T (1974) Studies on hemagglutinin from *Macckia amurensis* seeds. J Biol Chem 249:2786–2792

Keulemans JLM, Reuser AJJ, Kroos MA, Willemsen R, Hermans MMP, van den Ouweland AHW, de Jong JGN, Wevers RA, Renier WO, Schindler D, Coll MJ, Chabas A, Sakuraba H, Suzuki Y, van Diggelen OP (1996) Human α-*N*-acetylgalactosaminidase (α-NAGA) deficiency: new mutations and the paradox between genotype and phenotype. J Med Genet 33:458–464

Kodama K, Kobayashi H, Abe R, Ohkawa A, Yoshii N, Yotsumoto S, Fukushige T, Nagatsuka Y, Hirabayashi Y, Kanzaki T (2001) A new case of α-*N*-acetylgalactosaminidase deficiency with angiokeratoma corporis diffusum, with Menier's sydrome and without mental retardation. Br J Dermat 144:363–368

Linden HU, Klein RA, Egge H, Peter-Katalinic J, Dabrowski J, Schindler D (1989) Isolation and structural characterization of sialic acid-containing glycopeptides of the *O*-glycosidic type from the urine of two patients with a hereditary deficiency in α-*N*-acetylgalactosaminidase activity. Biol Chem Hoppe-Seyler 370:661–672

Mark BL, Mahuran DJ, Cherney MM, Zhao D, Knapp S, James MNG (2003) Crystal structure of human β-hexosaminidase B: Understanding the molecular basis of Sandhoff and Tay-Sachs disease. J Mol Biol 327:1093–1109

Meikle RJ, Brooks DA, Ravenscroft EM, Yan M, Williams RE, Jaunzems AE, Chataway TK, Karageorgos LE, Davey RC, Boulter CD, Carlsson SR, Hopwood JJ (1997) Diagnosis of lysosomal storage disorders: evaluation of lysosome-associated membrane protein LAMP-1 as a diagnostic marker. Clin Chem 43:1325–1335

Sakuraba H, Matsuzawa F, Aikawa S, Doi H, Kotani M, Lin H, Ohno K, Tanaka A, Yamada H, Uyama E (2002) Molecular and structural studies of the GM2 gangliosidosis 0 variant. J Hum Genet 47:176–183

Schindler D, Bishop DF, Wolfe DE, Wang AM, Egge H, Lemieux RU, Desnick RJ (1989) Neuroaxonal dystrophy due to lysosomal α-*N*-acetylgalactosaminidase deficiency. N Engl J Med 320:1735–1740

Springer GF (1984) T and Tn, general carcinoma antigens. Science 224:1198–1206

van Diggelen OP, Schindler D, Kleijer WJ, Huijmans JMG, Galjaard H, Linden HU, Peter-Katalinic J, Egge H, Dabrowski U, Cantz M (1987) Lysosomal α-*N*-acetylgalactosaminidase deficiency: a new inherited metabolic disease. Lancet 2:804

Wang AM, Bishop DF, Desnick RJ (1990) Human α-*N*-acetylgalactosaminidase: molecular cloning, nucleotide sequence, and expression of a full-length cDNA. J Biol Chem 265:21859–21866

Wang AM, Schindler D, Desnick (1990) Schindler disease: the molecular lesion in the α-*N*-acetylgalactosaminidase gene that causes an infantile neuroaxonal dystrophy. J Clin Invest 86:1752–1756

Wang AM, Kanzaki T, Desnick RJ (1994) The molecular lesion in the α-*N*-acetylgalactosaminidase gene that causes angiokeratoma corporis diffusum with glycopeptiduria. J Clin Invest 94:839–845

Available online at www.sciencedirect.com
SCIENCE DIRECT®
Biochemical and Biophysical Research Communications 319 (2004) 327–333
BBRC
www.elsevier.com/locate/ybbrc

The receptor and transporter for internalization of *Clostridium botulinum* type C progenitor toxin into HT-29 cells☆

Atsushi Nishikawa,[a,e,1] Nobuo Uotsu,[a,1] Hideyuki Arimitsu,[b] Jae-Chul Lee,[b] Yutaka Miura,[a] Yukako Fujinaga,[b,f] Hiroshi Nakada,[c] Toshihiro Watanabe,[d] Tohru Ohyama,[d] Yoshiyuki Sakano,[a] and Keiji Oguma[b,*]

[a] *Department of Applied Biological Science, and Department of Biotechnology, United Graduate School of Agricultural Science, Tokyo University of Agriculture and Technology, 3-5-8 Saiwai-cho, Fuchu-shi, Tokyo 183-8509, Japan*
[b] *Department of Bacteriology, Okayama University Graduate School of Medicine and Dentistry, 2-5-1 Shikata-cho, Okayama 700-8558, Japan*
[c] *Department of Biotechnology, Kyoto Sangyo University, Kita-ku, Kyoto 603-8555, Japan*
[d] *Department of Food Science, Faculty of Bioindustry, Tokyo University of Agriculture, 196, Yasaka, Abashiri 099-2422, Japan*
[e] *CREST, Japan Science and Technology Agency, Japan*
[f] *PREST, Japan Science and Immunology Agency, Japan*

Received 24 February 2004
Available online 18 May 2004

Abstract

Orally ingested botulinum toxin enters the circulatory system and eventually reaches the peripheral nerves, where it elicits a response of neurological dysfunction. In this study, we report the important findings concerning the mechanism of *Clostridium botulinum* type C progenitor toxin (C16S) endocytic mechanism. C16S toxin bound to high molecular weight proteins on the surface of human colon carcinoma HT-29 cells and was internalized, but not if the cells were pretreated with neuraminidase. Benzyl-GalNAc which inhibited O-glycosylation of glycoproteins also interfered in the toxin's ability to bind the cell surface. On the other hand, the toxin was internalized in spite of pretreatment of the cells with PPMP, an inhibitor of ganglioside synthesis. These results suggest that the glycoproteins, like mucin, fulfill the important roles of receptor and transporter of C16S toxin.

Keywords: *Clostridium botulinum*; Toxin binding; Hemagglutinin; Endocytic mechanisms; O-linked oligosaccharide; Mucin

Botulinum toxins are produced by the anaerobic bacterium *Clostridium botulinum* and are classified into groups A through G based upon immunological differences of neurotoxin. The molecular masses of all types of these neurotoxins are about 150 kDa. The neurotoxins associate with several kinds of protein in culture fluids to form large complexes that are designated progenitor toxins such as 900 kDa (19S), 500 kDa (16S), and 300 kDa (12S). Type C strain produces 16S and 12S toxins, C16S toxin consists of a neurotoxin, hemagglutinin components (HAs), and a non-toxic non-hemagglutinin (non-toxic non-HA) component, and C12S toxin is formed by only the neurotoxin and a single non-toxic non-HA component. On the HAs, molecular composition and size were determined based on nucleotide sequences and protein chemical analysis [1,2]. The HAs consist of four kinds of subcomponents (HA-1, HA-2, HA-3a, and HA-3b), and HA-1 and HA-3b have binding activity to erythrocyte [3]. A combination of at least HA-1, -2, and -3b is required for full hemagglutination activity of botulinum progenitor toxin, but each single HA component shows weak or no aggregation of erythrocytes [4].

☆ *Abbreviations:* C16S toxin, *Clostridium botulinum* type C progenitor toxin; HA, hemagglutinin; benzyl-GalNAc, benzyl 2-acetoamide-2-deoxy-α-D-galactopyranoside; PPMP, D,L-threo-1-phenyl-2-hexadecanoylamino-3-morpholino-propanol.

* Corresponding author. Fax: +81-86-235-7162.
E-mail addresses: nishikaw@cc.tuat.ac.jp (A. Nishikawa), uotsu@cc.tuat.ac.jp (N. Uotsu), kuma@med.okayama-u.ac.jp (K. Oguma).

[1] These authors contributed equally to this work.

0006-291X/$ - see front matter © 2004 Elsevier Inc. All rights reserved.
doi:10.1016/j.bbrc.2004.04.183

Synaptotagmin, in association with ganglioside GT1b or GD1a at the nerve terminals, is identified as the receptor for botulinum neurotoxin [5,6]. It was also reported that lipid microdomains were involved in neurospecific binding and internalization of neurotoxin [7]. Like these, neurotoxin receptors on the nerve cell surface are gradually being clarified. However, the migration mechanism of orally ingested progenitor toxin from digestive tract into body fluid circulation system is not clearly understood.

Mucins have structured various large molecular weight glycoproteins that function in vertebrates to protect epithelial cell surfaces from pathogens and digestive enzymes and also act as lubricants [8,9]. The carbohydrate content of mucin is generally more than 50% and is mainly O-linked oligosaccharides covalently linked to Ser and Thr residues. The role of O-linked oligosaccharides is less well understood. The highly glycosylated structures of mucins produce a large hydration sphere upon which the viscoelastic properties of secreted mucins and the proposed masking function of the transmembrane mucins depend [10,11].

Simpson and co-workers [12] reported that the neurotoxin of *C. botulinum* type A was absorbed from the gastrointestinal system and advanced into the general circulation. On the other hand, we reported that the C16S toxin, but not the C12S toxin, bound intensely to the microvilli of epithelial cells of guinea pig small intestine in both in vivo and in vitro tests [13], and estimated that HAs were necessary for effective binding of the progenitor toxin to epithelial cells of the small intestine. By the way the movement of the mucin in the cell surface was reported. The study reported that cell surface MUC1, one of the type I transmembrane type mucins expressed in many epithelial cells, was internalized by clathrin-dependent endocytosis and redistributed in the plasma membrane [14,15]. From this evidence, it seems that cell surface mucin plays a very important role in the migration mechanism of progenitor toxin from digestive tract into the general circulation.

In this report we demonstrate the internalization of C16S toxin into HT-29 cells, a human colon carcinoma cell line, and other well-characterized kinds of mucin expressing cells [16–19], using immunofluorescence microscopy and confocal laser scanning microscopy. We also show that the oligosaccharides of mucin at cell surface fulfill a very important role in the internalization of the toxin.

Materials and methods

Materials

Benzyl 2-acetoamide-2-deoxy-α-D-galactopyranoside (benzyl-GalNAc), Dulbecco's modified Eagle's medium (DMEM), and Dulbecco's phosphate-buffered saline (PBS) were purchased from Sigma. *Arthrobacter ureafaciens* neuraminidase was purchased from Nacalai Tesque (Japan). D,L-Threo-1-phenyl-2-hexadecanoyl-amino-3-morpholino-propanol (PPMP) was purchased from Matreya. ECL Plus Western Blotting Detection System was obtained from Amersham Biosciences. Other chemicals were from Sigma.

Toxins and antibodies

Type C16S and C12S toxins were prepared from the culture fluid of *C. botulinum* type C strain Stockholm according to the previous procedure [13]. Rabbit antiserums against type C non-toxic (anti-C non-toxic) component and against type C neurotoxin (anti-C7S) have been prepared previously [20]. Mouse monoclonal antibody against type C HA component (anti-CHA3b-6) that have been prepared previously was used in this study [21]. TRITC-labeled goat anti-rabbit IgG and FITC-labeled goat anti-mouse IgG were purchased from Molecular Probes and Becton–Dickinson, respectively.

Cell culture and cell treatment with reagents

The human colon carcinoma cell line HT-29 was purchased from the American Type Culture Collection. The cells were grown in DMEM supplemented with 10% (v/v) fetal bovine serum and 0.1 mg/ml kanamycin at 37 °C in 5% CO_2 atmosphere. In this study pH of PBS was adjusted to 6.9.

Benzyl-GalNAc treatment. The cells were precultured with 5 mM benzyl-GalNAc for 48 h [22].

Neuraminidase treatment. The cultured cells were washed with PBS and then incubated with 0.1 U neuraminidase in PBS at 37 °C for 1 h in 5% CO_2 atmosphere.

PPMP treatment. The cultured cells were washed with DMEM and then grown in the presence of DMEM containing 7.5 μM PPMP at 37 °C for 48 h [23].

Immunofluorescence microscopy

HT-29 cells were grown on glass coverslips which were precoated by collagen. The cells or pretreated cells with various reagents were washed twice with fresh DMEM, pH 7.0, and incubated with 10 nM each toxin (C16S, C12S or neurotoxin) in DMEM, pH 7.0, at 37 °C for 3 min. After incubation, the cells were washed with PBS twice, fixed with 3.7% formaldehyde for 15 min, quenched with 50 mM NH_4Cl for 10 min, and then blocked with 2% BSA for 60 min at room temperature. To observe the binding of neurotoxin, the fixed cells were treated with anti-C7S antiserum for 60 min, followed by TRITC-labeled goat anti-rabbit IgG (5.0 μg/ml in PBS). To detect the C16S toxin binding, the cells were treated with anti-CHA3b-6 antibody (4.8 μg/ml in PBS) for 60 min, followed by FITC-conjugated anti-mouse IgG antibody for 60 min.

Confocal laser scanning microscopy

HT-29 cells were grown in 8-well chamber slides (Nalge Nunc International). The cells were washed twice with fresh DMEM, pH 7.0, and incubated with 40 nM C16S toxin in DMEM, pH 7.0, at 37 °C for 5 min in 5% CO_2 atmosphere. After incubation, the cells were immediately washed with DMEM, pH 7.0, and incubated at 37 °C in 5% CO_2 atmosphere for various times. Then the cells were washed with PBS twice, fixed with 3.7% formaldehyde for 15 min, quenched with 50 mM NH_4Cl for 10 min, and then permeabilized with 0.1% saponin in 2% BSA and PBS for 60 min at room temperature. To detect C16S toxin, rabbit anti-C non-toxic component antiserum (diluted 1:10,000 with 0.1% saponin, 2% BSA) treatment for 60 min, and followed by TRITC-conjugated anti-rabbit IgG (10 μg/ml in 0.1% saponin, 2% BSA) treatment for 60 min were carried out. Confocal laser scanning microscopy analysis was then performed using Leica instrument model TCS 4D.

SDS–polyacrylamide gel electrophoresis and the toxin affinity assay

For SDS–polyacrylamide gel electrophoresis (SDS–PAGE), total cellular proteins were prepared and separated by ReadyPrep Sample Preparation Kit (Bio-Rad) according to the supplier's instructions. Briefly, the collected cells were resuspended in reagent 1, homogenized with an Ultarasonic Disruptor in ice-cold bath, and centrifuged at 6000*g* for 10 min. The supernatant (fraction 1) was removed and the pellet was resuspended in reagent 2, homogenized under the same conditions, and centrifuged at 18,000*g* for 10 min. The supernatant (fraction 2) was removed and the pellet was resuspended in reagent 3, homogenized, and centrifuged at 18,000*g* for 10 min. The supernatant was stored as fraction 3 and the residual pellet was collected as the precipitate fraction. To prepare the sample for SDS–PAGE, the precipitate fraction was dissolved by boiling with 10% SDS solution.

Each fraction was subjected to SDS–PAGE (3–15% gradient gels) under reducing conditions. Separated proteins were transferred to a PVDF membrane. The membrane was blocked with 2% horse serum in PBS for 1 h and treated with 0.4 nM of C16S toxin in PBS for 1 h, washed for 5 min with PBS containing 0.1% (w/v) Tween 20 (PBS-T) twice, and then incubated with anti-type C7S antibody solution for 1 h. After washing, the membrane was incubated with anti-rabbit Ig HRP-linked $F(ab')_2$ and subjected to ECL Plus Western Blotting Detection according to the manufacturer's instructions.

Results and discussion

Binding and internalization of toxins to HT-29 cells

HT-29 cells, a human colon carcinoma cell line, are expressing several kinds of mucin [16–19]. First HT-29 cells were exposed to C16S, C12S, and neurotoxin, respectively, and the binding of toxins to cell surface was observed using immunofluorescence microscopy. As shown in Fig. 1, only C16S toxin was observed to bind to the surface of HT-29 cells. It seems that HA components are necessary for the toxin's adsorption to the cell surface.

To examine the internalization of the toxin, HT-29 cells were exposed to C16S toxin for 5 min, incubated without toxin for several periods, and then observed using confocal laser scanning microscopy. As shown in Fig. 2, C16S toxin was clearly observed inside the plasma membrane after 4 min of incubation and later.

These results indicate that HT-29 cells have a receptor for the C16S progenitor toxin on their cell surface and a mechanism for the uptake of the toxin.

Influence of neuraminidase treatment on the binding of C16S toxin to HT-29 cells

To estimate the affinity of the HT-29 cell receptor for C16S toxin, an affinity assay was performed. HT-29 protein fractions which were separated by ReadyPrep Sample Preparation Kit were subjected to SDS–PAGE and transferred to PVDF membrane. The binding affinity of C16S toxin to blotted protein was measured using the ECL plus system (Fig. 3A). It was found that the toxin combined with four high molecular weight proteins from fraction 2. The estimated molecular weights of these bands were approximately 210, 680, 430, and 1200k, respectively. Since these high molecular weight proteins were solubilized by Preparation Kit reagent 2 which contained 4% Chaps, it would seem that these proteins were associated with membranes.

Our previous reports showed that sialic acid was an important residue for the toxins binding to erythrocyte and epithelial cells of the small intestine [3,13]. Next, we treated the protein fractions of HT-29 cells and the cells themselves with neuraminidase, and then examined the affinity for the toxin.

Four fractionated protein solutions were pre-incubated with neuraminidase at 37 °C for 8 h and subjected to the toxin binding assay. As shown in Fig. 3A, C16S toxin could not no longer combine with the high molecular membrane-associated proteins as measured by the disappearance of sialic acid. HT-29 cells which were treated with neuraminidase also lost their C16S toxin binding activity as shown in Fig. 3B.

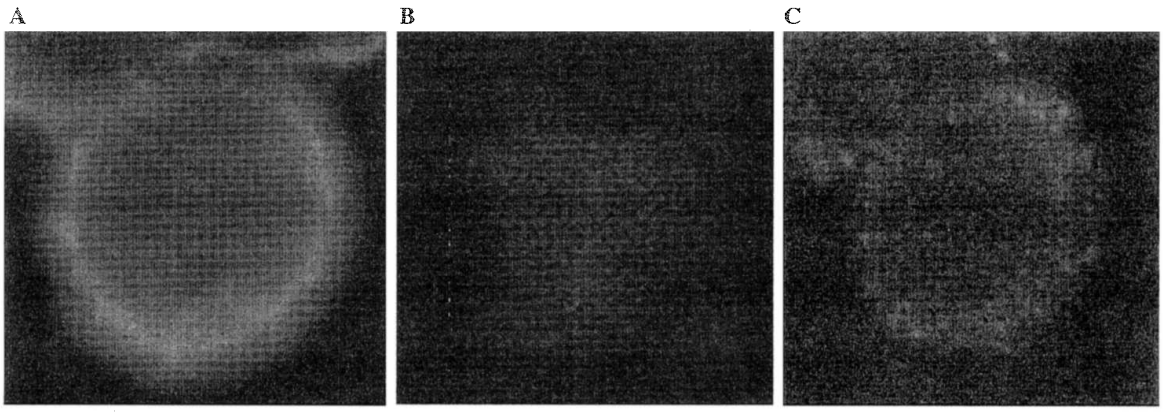

Fig. 1. C16S toxin bound to HT-29 cell surface. HT-29 cells were incubated with 10 nM each toxin at 37 °C for 3 min and then washed with PBS. The cell-associated toxins were detected by immunofluorescence microscopy using rabbit anti-C7S antiserum and TRITC-labeled anti-rabbit IgG. (A) C16S toxin; (B) C12S toxin; and (C) neurotoxin.

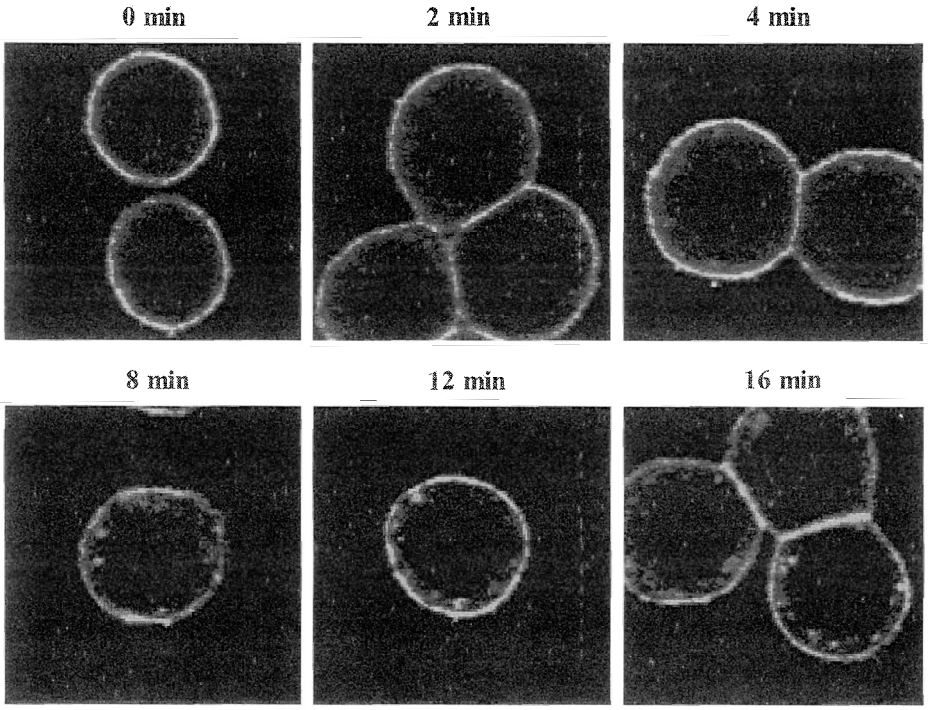

Fig. 2. Internalization of C16S toxin into HT-29 cells. HT-29 cells were incubated with 40 nM C16S toxin at 37 °C for 5 min, then washed, and incubated in toxin-free medium for various times. The cell-associated toxin and internalized toxin were analyzed by confocal laser scanning microscopy using rabbit anti-C non-toxic component antiserum and TRITC-labeled anti-rabbit IgG.

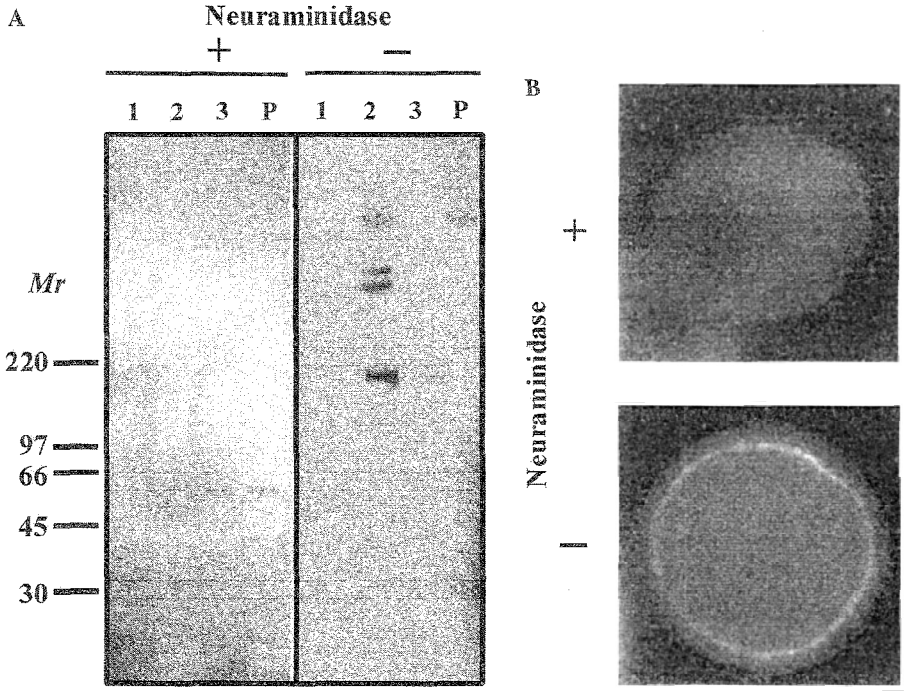

Fig. 3. Influence of neuraminidase treatment on the binding of C16S toxin to HT-29 cells. (A) Whole proteins of HT-29 cells were separated into four fractions by ReadyPrep Sample Preparation Kit. After treatment with (+) or without (−) neuraminidase, the samples were subjected to the toxin binding assay according to the methods given in Materials and methods. *Mr* indicates the migrated position of standard proteins and its relative molecular mass × 10^3. It is considered from the composition of the sample preparation reagents that fraction 1 contained mainly cytosolic proteins; 2, weakly membrane-associated proteins; 3, strongly membrane-associated proteins; and P, an unextractable fraction. (B) HT-29 cells treated with or without neuraminidase according to the method given in Materials and methods were incubated with 10 nM C16S toxin in DMEM, pH 7.0, for 3 min and then washed with PBS. The cell-associated toxins were detected by immunofluorescence microscopy using anti-CHA3b-6 antibody and FITC-labeled anti-mouse IgG.

These results indicate that C16S toxin recognizes the sialic acid residue of cell surface oligosaccharides.

Investigation of the C16S toxin receptor

We made the following experiments in order to determine whether sialic acid which fulfilled the important role for the binding of C16S toxin was derived from glycolipid or N- or O-linked oligosaccharides.

It has been reported that GT1b is a necessary component of the neurotoxin receptor in nerve cells [5,6,24]. We also reported that C16S toxin could bind to gangliosides extracted from human erythrocytes [3]. To determine whether gangliosides on the surface of HT-29

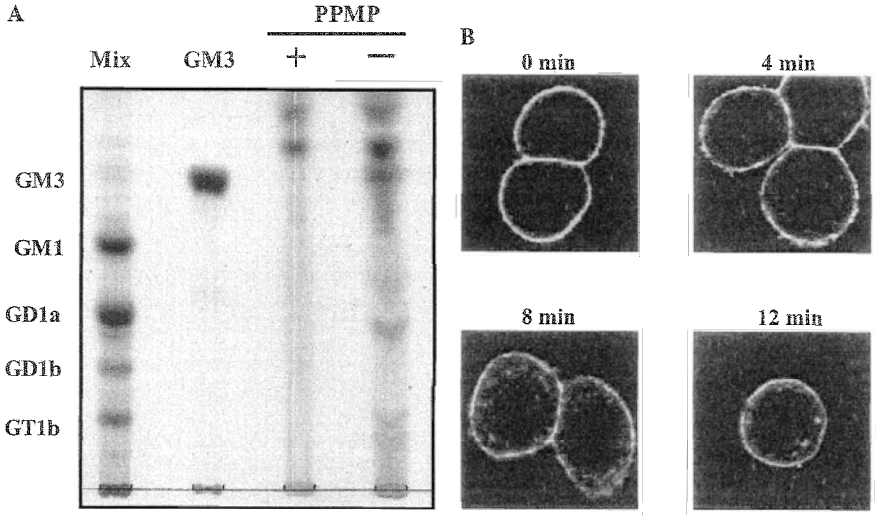

Fig. 4. Influence of PPMP treatment on C16S toxin internalization into HT-29 cells. (A) Influence of PPMP treatment on the volume of acidic gangliosides. HT-29 cells were pretreated with (+) or without (–) 7.5 μM PPMP and gangliosides were extracted with chloroform–methanol (1:2). The extracted samples were applied to the HPTLC plate, and the plate was developed in chloroform:2-propanol:50 mM KCl (2:13.4:4.6 v/v/v) [23]. Glycolipids were detected using the orcinol H_2SO_4 method. Mix and GM3 show the migration positions of the standard glycolipids mixture and GM3. (B) HT-29 cells treated with 7.5 μM PPMP were incubated with 40 nM C16S toxin at 37 °C for 5 min, then washed and incubated in toxin-free medium for various times. The cell-associated toxin and internalized toxin were analyzed by confocal laser scanning microscopy using rabbit anti-C non-toxic component antiserum and TRITC-labeled anti-rabbit IgG.

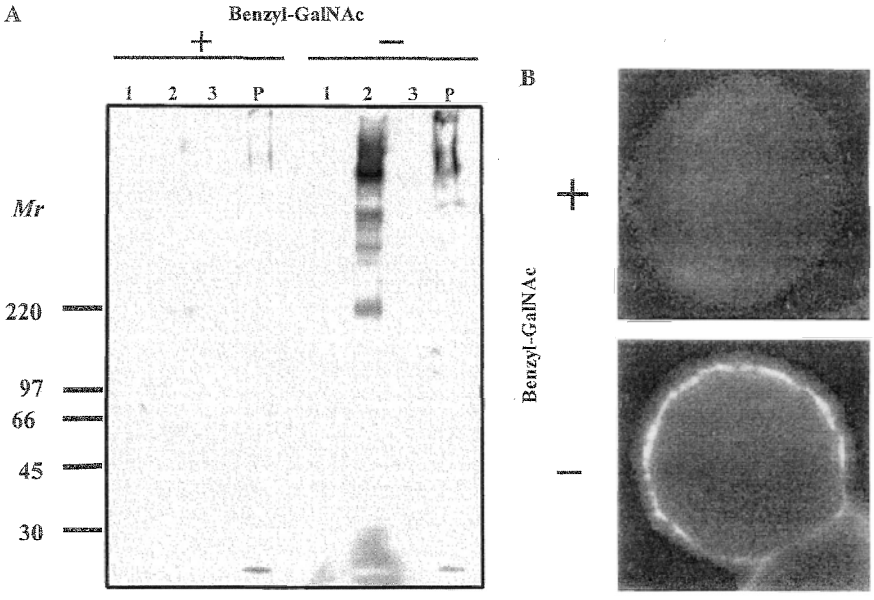

Fig. 5. The influence of benzyl-GalNAc preincubation on C16S toxin binding to cell surface. (A) HT-29 cells were pretreated with (+) of without (–) benzyl-GalNAc, and separated proteins were subjected to the toxin binding assay. C16S toxin-binding proteins on membrane were detected by the ECL plus system using rabbit anti-C7S antiserum and anti-rabbit Ig HRP-linked F(ab′)$_2$. (B) HT-29 cells treated with or without benzyl-GalNAc in DMEM were incubated with 10 nM C16S toxin for 3 min and then washed with PBS. The cell-associated toxins were detected by immunofluorescence microscopy using mouse anti-CHA3b-6 antibody and FITC-labeled anti-mouse IgG.

cells function as receptors for C16S toxin, the cells were pretreated with PPMP that reduce the level of gangliosides. PPMP is an inhibitor of glucosylceramide synthase [23]. In our experiment the amount of gangliosides in PPMP treated HT-29 cells was reduced. Examples, GM3, GM1, GD1a, GD1b, and GT1b, are shown in Fig. 4A. C16S toxin, however, could bind to the cell surface and internalize into HT-29 cells (Fig. 4B).

On the other hand the benzyl-GalNAc is well known to inhibit the O-glycosylation of mucin in colon cancer cells [22]. Then we investigated the influence of benzyl-GalNAc on toxin binding to HT-29 cells. The cells were cultured with 5 mM benzyl-GalNAc for 48 h, and then total cellular protein was fractionated by ReadyPrep Sample Preparation Kit and subjected to the toxin binding assay. As shown in Fig. 5A, there was no band which combined strongly with C16S toxin. Furthermore, C16S toxin could not be observed on benzyl-GalNAc pretreated HT-29 cells surface by immunofluorescence microscopy (Fig. 5B).

We therefore propose that C16S toxin recognizes sialic acid strongly and may be taken up into cells with O-linked oligosaccharide derived from high molecular weight glycoproteins like mucin on the surface of HT-29 cells.

The protein toxins, for example ricin, diphtheria toxin, shiga toxins, cholera toxin, and botulinum neurotoxin, bind to a variety of receptors and they use different endocytic mechanisms [25]. The receptor for botulinum progenitor toxin which is a large complex of neurotoxin, HAs, and non-toxic non-HA component, however, is not known. In addition, the toxin migration mechanism from digestive tract into body fluid circulation system is not clearly understood. Therefore, our experimental results seem to provide some useful insights into this matter.

To date, more than 15 human mucin genes have been identified. Some of them are membrane-bound and some of them are secretion types [26]. Next, we will focus on which kinds of mucin play an important role for botulinum toxin internalization.

Acknowledgment

This work has been supported by CREST of JST (Japan Science and Technology Agency).

References

[1] Y. Fujinaga, K. Inoue, S. Shimazaki, K. Tomochika, K. Tsuzuki, N. Fujii, T. Watanabe, T. Ohyama, K. Takeshi, K. Inoue, K. Oguma, Molecular construction of *Clostridium botulinum* type C progenitor toxin and its gene organization, Biochem. Biophys. Res. Commun. 205 (1994) 1291–1298.

[2] T. Watanabe, Y. Sagane, H. Kouguchi, H. Sunagawa, K. Inoue, Y. Fujinaga, K. Oguma, T. Ohyama, Molecular composition of progenitor toxin produced by *Clostridium botulinum* type C strain 6813, J. Protein Chem. 18 (1999) 753–760.

[3] K. Inoue, Y. Fujinaga, K. Honke, K. Yokota, T. Ikeda, T. Ohyama, K. Takeshi, T. Watanabe, K. Inoue, K. Oguma, Characterization of haemagglutinin activity of *Clostridium botulinum* type C and D 16S toxins, and one subcomponent of haemagglutinin (HA1), Microbiology 145 (1999) 2533–2542.

[4] H. Kouguchi, T. Watanabe, Y. Sagane, T. Ohyama, Characterization and reconstitution of functional hemagglutinin of the *Clostridium botulinum* type C progenitor toxin, Eur. J. Biochem. 268 (2001) 4019–4026.

[5] T. Nishiki, Y. Kamata, Y. Nemoto, A. Omori, T. Ito, M. Takahashi, S. Kozaki, Identification of protein receptor for *Clostridium botulinum* type B neurotoxin in rat brain synaptosomes, J. Biol. Chem. 269 (1994) 10498–10503.

[6] S. Kozaki, Y. Kamata, S. Watarai, T. Nishiki, S. Mochida, Ganglioside GT1b as a complementary receptor component for *Clostridium botulinum* neurotoxins, Microb. Pathog. 25 (1998) 91–99.

[7] J. Herreros, G. Schiavo, Lipid microdomains are involved in neurospecific binding and internalisation of clostridial neurotoxins, Int. J. Med. Microbiol. 291 (2002) 447–453.

[8] R. Yolken, J. Peterson, S. Vonderfecht, E. Fouts, K. Midthun, D. Newburg, Human milk mucin inhibits rotavirus replication and prevents experimental gastroenteritis, J. Clin. Invest. 90 (1992) 1984–1991.

[9] R.W. Walters, J.M. Pilewski, J.A. Chiorini, J. Zabner, Secreted and transmembrane mucins inhibit gene transfer with AAV4 more efficiently than AAV5, J. Biol. Chem. 277 (2002) 23709–23713.

[10] N. Jentoft, Why are proteins O-glycosylated?, Trends Biochem. Sci. 15 (1990) 291–294.

[11] R. Bansil, E. Stanley, J.T. Lamont, Mucin biophysics, Annu. Rev. Physiol. 57 (1995) 635–657.

[12] A.B. Maksymowych, M. Reinhard, C.J. Malizio, M.C. Goodnough, E.A. Johnson, L.L. Simpson, Pure botulinum neurotoxin is absorbed from the stomach and small intestine and produces peripheral neuromuscular blockade, Infect. Immun. 67 (1999) 4708–4712.

[13] Y. Fujinaga, K. Inoue, S. Watanabe, K. Yokota, Y. Hirai, E. Nagamachi, K. Oguma, The haemagglutinin of *Clostridium botulinum* type C progenitor toxin plays an essential role in binding of toxin to the epithelial cells of guinea pig small intestine, leading to the efficient absorption of the toxin, Microbiology 143 (1997) 3841–3847.

[14] R.A. Pimental, J. Julian, S.J. Gendler, D.D. Carson, Synthesis and intracellular trafficking of Muc-1 and mucins by polarized mouse uterine epithelial cells, J. Biol. Chem. 271 (1996) 28128–28137.

[15] Y. Altschuler, C.L. Kinlough, P.A. Poland, J.B. Bruns, G.. Apodaca, O.A. Weisz, R.P. Hughey, Clathrin-mediated endocytosis of MUC1 is modulated by its glycosylation state, Mol. Biol. Cell 11 (2000) 819–831.

[16] T. Lesuffleur, N. Porchet, J. Aubert, D. Swallow, J. Gum, Y. Kim, F. Real, A. Zweibaum, Differential expression of the human mucin genes MUC1 to MUC5 in relation to growth and differentiation of different mucus-secreting HT-29 cell subpopulations, J. Cell Sci. 106 (1993) 771–783.

[17] G. Huet, L. Kim, C. de Bolos, J.M. Lo-Guidice, O. Moreau, B. Hemon, C. Richet, P. Delannoy, F.X. Real, P. Degand, Characterization of mucins and proteoglycans synthesized by a mucin-secreting HT-29 cell subpopulation, J. Cell Sci. 108 (1995) 1275–1285.

[18] J.K. Sheehan, C. Brazeau, S. Kutay, H. Pigeon, S. Kirkham, M. Howard, D.J. Thornton, Physical characterization of the MUC5AC mucin: a highly oligomeric glycoprotein whether isolated from cell culture or in vivo from respiratory mucous secretions, Biochem. J. 347 (2000) 37–44.

[19] S. Truant, E. Bruyneel, V. Gouyer, O.D. Wever, F.-R. Pruvot, M. Mareel, G. Huet, Requirement of both mucins and proteoglycans in cell–cell dissociation and invasiveness of colon carcinoma HT-29 cells, Int. J. Cancer 104 (2003) 683–694.
[20] K. Oguma, B. Syuto, H. Iida, S. Kubo, Antigenic similarity of toxins produced by *Clostridium botulinum* type C and D strains, Infect. Immun. 30 (1980) 656–660.
[21] N. Mahmut, K. Inoue, Y. Fujinaga, L. Hughes, H. Arimitsu, Y. Sakaguchi, A. Ohtsuka, T. Murakami, K. Yokota, K. Oguma, J. Med. Microbiol. 51 (2002) 286–294.
[22] S. Kuan, J. Byrd, C. Basbaum, Y. Kim, Inhibition of mucin glycosylation by aryl-*N*-acetyl-alpha-galactosaminides in human colon cancer cells, J. Biol. Chem. 264 (1989) 19271–19277.
[23] B.C. Yowler, R.D. Kensinger, C.-L. Schengrund, Botulinum neurotoxin A activity is dependent upon the presence of specific gangliosides in neuroblastoma cells expressing synaptotagmin I, J. Biol. Chem. 277 (2002) 32815–32819.
[24] L. Li, B. Singh, Isolation of synaptotagmin as a receptor for types A and E botulinum neurotoxin and analysis of their comparative binding using a new microtiter plate assay, J. Nat. Toxins 7 (1998) 215–263.
[25] K. Sandvig, B.v. Deurs, Membrane traffic exploited by protein toxins, Annu. Rev. Cell Dev. Biol. 18 (2002) 1–24.
[26] L.T. Pallesen, L. Berglund, L.K. Rasmussen, T.E. Petersen, J.T. Rasmussen, Isolation and characterization of MUC15, a novel cell membrane-associated mucin, Eur. J. Biochem. 269 (2002) 2755–2763.

J. Biochem. **134**, 869–874 (2003)
DOI: 10.1093/jb/mvg213

Galectin-1 Induces Cell Adhesion to the Extracellular Matrix and Apoptosis of Non-Adherent Human Colon Cancer Colo201 Cells

Natsuko Horiguchi[1], Kei-ichiro Arimoto[1], Atsushi Mizutani[1], Yoko Endo-Ichikawa[2], Hiroshi Nakada[3] and Shigeru Taketani[*,1]

[1]Department of Biotechnology, Kyoto Institute of Technology, Kyoto 606-8585; [2]Department of Public Health, Kansai Medical University, Moriguchi 570-8506; and [3]Department of Biotechnology, Kyoto Sangyo University, Kyoto 603-8555

Received September 24, 2003; accepted October 1, 2003

To isolate cDNAs for molecules involved in cell adhesion to the extracellular matrix, expression cloning with non-adherent colon cancer Colo201 cells was carried out. Four positive clones were isolated and, when sequenced, one was found to be galectin-1, a β-galactoside-binding protein. When cultured on fibronectin-, laminin-, and collagen-coated and non-coated dishes, the adherent galectin-1 cDNA-transfected Colo201 cells increased and spread somewhat. Immunofluorescence staining revealed that galectin-1 was expressed inside and outside of Colo201 cells. The adhesion was dependent on the carbohydrate-recognition domain of galectin-1 since lactose inhibited the adhesion and exogenously-added galectin-1 caused the adhesion. PD58059, an inhibitor of mitogen-activated protein kinase, or LY294002, a phosphoinositide 3-OH kinase inhibitor, decreased the adhesion. Furthermore, the expression of galectin-1 in Colo201 cells induced apoptotic cell death, while exogenously-added galectin-1 did not cause apoptosis. These results indicate that galectin-1 plays a role in both cell–matrix interactions and the inhibition of Colo201 cell proliferation, and suggest that galectin-1 expressed in cells could be associated with apoptosis.

Key words: apoptosis, cell adhesion, Colo201 cells, expression cloning, galectin-1.

Abbreviations: ECM, extracellular matrix; CRD, carbohydrate recognition domain; kDa, kilodalton(s); FCS, fetal calf serum; SDS-PAGE, sodium dodecylsulfate–polyacrylamide gel electrophoresis; PBS, phosphate buffered saline; DTT, dithiothreitol; PMSF, phenylmethylsulfonyl fluoride; PCR, polymerase chain reaction; PVDF, poly(vinylidene difluoride); GSH, glutathione; GST, glutathione S-transferase.

Extracellular matrix (ECM) components have marked effects on cellular morphology, cell migration, growth and differentiation, suggesting the existence of transmembrane linkages and signal transduction pathways that can relay information from the ECM to the nucleus (*1*). Cells in culture adhere to ECM components and a large number of cytoplasmic proteins, some of which are likely to play a role in an intracellular response to extracellular signals (*1*, *2*). However, the necessity of generating diverse junctions on individual cells must require highly interconnected signaling cascades that can modulate responses between various pathways.

Galectin-1 is an endogenous β-galactoside binding protein (galectin family), and is produced by a variety of normal and neoplastic cells (*3*). The galectin family share jelly roll–like folding and a common topology of the carbohydrate recognition domain (CRD) with high-sequence homology among mammals (*3*, *4*). Galectins are secreted *via* a non-classical pathway, and interact with the extracellular glycans of cell-surface components including laminins, fibronectins and integrins (*3*, *4*). Galectin-1 plays a role in several biological and pathological processes, including cell growth regulation, cell–matrix interactions and T-cell apoptosis (*5*). In cells, galectins are located in the cytosol and nucleus, interacting with several signal proteins (*6*). With respect to colon tumor biology, the presence of galectin-1 and galectin-3 has so far been investigated histopathologically using different methods, the results being divergent (*7*). Namely, tumors express different levels and kinds of galectin. It is considered that galectins may be attractive targets for the development of new therapeutic strategies since most glycans are located outside cells where cell–cell or cell–matrix interactions occur and play a role in the normal maintenance of multi-cellular organisms (*4*, *7*).

Colo201 cells, which were isolated from the ascites fluid of a patient with an adenocarcinoma of the colon, are part of a unique cell line that has lost its epithelial appearance and exhibits a non-adherent morphology (*8*). Colo201 cells are a useful tool for clarifying the mechanisms involved in cell adhesion and the metastatic mobility of adenocarcinoma cells. We have screened cell adhesion–related molecules with non-adherent colon cancer Colo201 cells and found that they acquired the characteristics of adherent cells when treated with retinoic acid (*9*) and protein kinase inhibitors (*10*). The expression of constitutively active forms of GTP-binding proteins, Rac1 and Cdc42, resulted in selective increases in α6β4 integrin expression, leading to the induction of adhesion and membrane ruffles of Colo201 cells (*11*). Thus, Colo201 cells possess cytoplasmic signaling pathways that regulate integrin activation and have the ability to

*To whom correspondence should be addressed. Tel: +81-75-724-7789, Fax: +81-75-724-7760, E-mail: taketani@ipc.kit.ac.jp

become adherent cells. In a search for the molecular mechanisms responsible for the abnormal adherent properties of Colo201 cells, we carried out expression cloning to obtain factors promoting the adhesion of Colo201 cells, and isolated galectin-1 as an adhesion molecule. We here report that galectin-1 not only caused the adhesion of Colo201 cells *via* sugar-dependent interactions with extracellular proteins but also led to apoptotic cell death.

MATERIALS AND METHODS

Materials—The mammalian expression HeLa cell cDNA library (pcDNA3) was a product of Invitrogen (Carlsbad, CA). Restriction endonucleases and DNA modifying enzymes were obtained from Takara (Kyoto) and Toyobo (Tokyo). Anti–c-Myc (clone: 9E10) monoclonal and anti-caspase 3 antibodies were purchased from Sigma (St. Louis, MI) and BD Biosciences (San Jose, CA), respectively. FluoroLink-Cy2 labeled anti-mouse IgG was from Amersham-Pharmacia (Buckinghamshire, UK). Tissue culture dishes coated with collagen (type I), laminin and fibronectin were the products of BD Bioscience Co. PD58059 and LY294002 were purchased from Calbiochem-Novabiochem (San Diego, CA). Other reagents used were of analytical grade.

Cell Culture and DNA Transfection—Human colon cancer cell line Colo201, obtained from the Japan Cell Bank (Tsukuba), was grown in RPMI 1640 medium supplemented with 10% FCS (Invitrogen, Carlsbad, CA), 100 U/ml penicillin and 50 μg/ml streptomycin (*9*). The cells were transfected using SuperFector reagent (B-Bridge, San Jose, CA). Plasmids carrying various cDNAs were also transfected into Colo201 cells, by electroporation. Namely, aliquots of 10^7 cells were electroporated at 330V and 1,000 μF with 10 μg of DNA containing various amounts of appropriate plasmids, as indicated, and the pUC18 vector as a mock DNA, using an Invitrogen electroporator II according to the manufacturer's instructions.

Screening of Cell Adhesion–Related Molecules—To isolate molecules causing cell adhesion, Colo201 cells were transfected with 40 μg of the plasmid-containing cDNAs (pcDNA3) by electroporation. After incubation for 16 h, the cells were treated with 0.05% trypsin/0.2% EDTA to disperse them. The cells were then washed three times with RPMI 1640 medium, re-suspended in RPMI 1640 medium containing 10% FCS and incubated for 2 h. The medium was removed and the adherent cells were washed three times with RPMI 1640 medium to separate non-adherent cells. The adherent cells were lysed with 10 mM Tris-HCl containing 2% SDS and 10 mM EDTA (*12*). The solubilized solution was treated with phenol/chloroform/isoamylalcohol (25/24/1, v/v/v), followed by treatment with chloroform/isoamylalcohol (24/1, v/v). DNA was precipitated with ethanol. After washing with 70% ethanol, the DNA was resolved in 10 μl of sterile water, and then transformed into *E. coli* XL-1 Blue by electroporation to amplify the plasmid. These screening treatments were repeated three times. At the final screening step, plasmids were isolated from several clones. The DNA sequences obtained were analyzed by means of a computer-assisted Blast-nucleotide sequence search.

Plasmids—To replace the vector of pcDNA3-galectin-1 with pcDNA3(c-myc), pcDNA3-galectin-1 was digested with *Eco*RI and *Hin*dIII, and then the insert was ligated into *Eco*RI–*Hin*dIII–digested pcDNA3.1(–)/Myc-His B (Invitrogen). The resulting plasmid [pcDNA3(c-myc)-galectin-1] was transformed into *E. coli* XL1-Blue. To construct GST fusion protein expression plasmids, portions of human galectin-1 cDNA were amplified by PCR and the resulting fragments were ligated into the pGEX-4T vector (Amersham-Pharmacia Biotech). The primers used were AAGGATCCTGTGGTCTGGTCGCC and AAGTCGACTCAAAAGGCCACACATTTGAT. The plasmid thus constructed was pGEX/galectin-1 encoding GST-galectin-1, *i.e.* galectin-1 fused with GST. The protein was expressed in *E. coli* (strain: DH-5α) with 0.3 mM isopropyl-1-thio-β-D-galactoside at 37°C for 2 h.

Adhesion of Cells to the Cell Matrix—Bacteria expressing GST-galectin-1 were re-suspended in lysis buffer (50 mM Tris-HCl, pH 7.5, 150 mM NaCl, 0.5% Tween 20, 10% glycerol, 1mM DTT, and 0.1 mM PMSF), and then lysed by brief sonication. The GST fusion proteins were purified with GSH-Sepharose 4B beads in accordance with the manufacturer's instructions (*13*). To assay the binding of Colo201 cells to the matrix, GST and GST-galectin-1 protein were added to RPMI 1640 medium containing 1% FCS. Cells on collagen-coated dishes were incubated at 37°C for 2 h, after which they were washed five times with RPMI 1640 medium. After the final wash, the cells were treated with 0.02% trypsin and then counted.

Immunostaining—For immunostaining, adherent cells were fixed with 4% paraformaldehyde in PBS containing 1 mM $CaCl_2$ and 0.5 mM $MgCl_2$ [PBS(+)] for 20 min, and permeabilized with 0.1% Triton-X100 in PBS (+) for 30 min. The cells were then incubated with anti–c-Myc as described (*13*). After washing with PBS (+), they were incubated with fluorolink Cy2-labeled anti-mouse IgG (Amersham Pharmacia Biotech.). To stain the cell-surface, the treatment with Triton X-100 was omitted. Fluorescence microscopy was performed with a Carl-Zeiss LSM510 microscope (Tokyo).

Immunoblotting—The lysates of Colo201 cells transfected with the empty vector pcDNA3 and pcDNA3 (c-myc)-galectin-1, respectively, were also subjected to SDS-PAGE and electroblotted onto a PVDF membrane. Immunoblotting was performed with anti–c-myc-tag or anti–caspase 3. The protein concentration was estimated by Bradford's method, using bovine serum albumin as the Standard (*14*).

TUNEL Assay—To detect DNA fragmentation in apoptotic cells by direct end-labeling of cellular genomic DNA with fluorescein-conjugated dUTP using terminal deoxynucleotidyltransferase enzyme, TUNEL assays were performed with an in situ apoptosis detection kit (Takara) (*15*).

Cell-Viability Assay—After transfection of the plasmid, the cells were cultured. At indicated times, aliquots of the cell suspension were withdrawn, and the live and dead cells were counted by means of trypan blue exclusion. The percentage of dead cells relative to the control was determined.

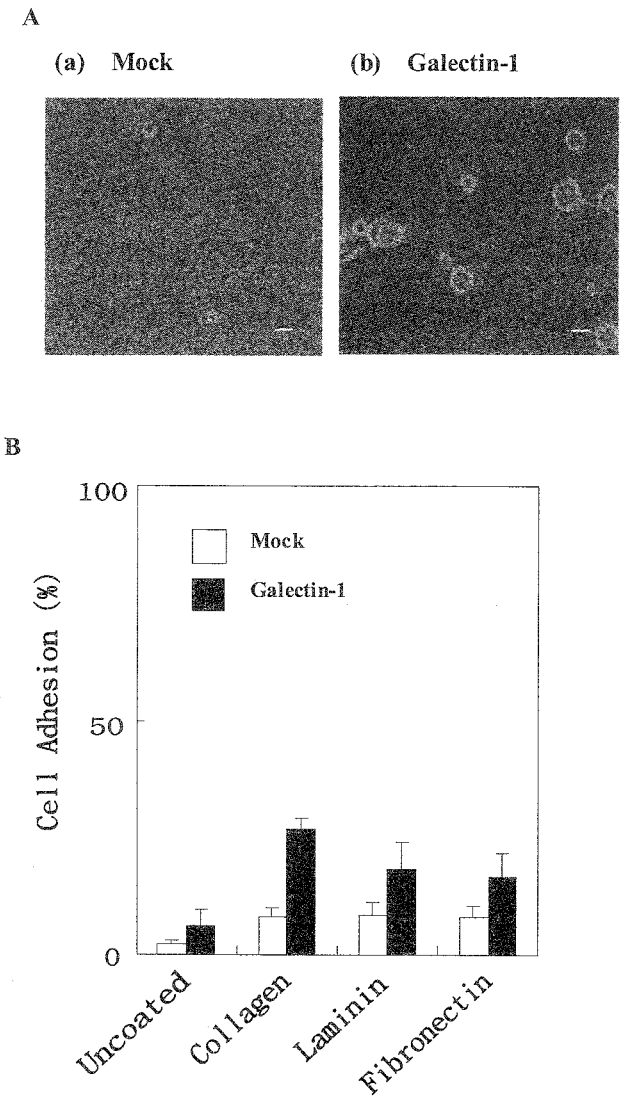

Fig. 1. **A: Morphology of adherent Colo201 cells expressing galectin-1.** Cells were transfected with 20 μg of galectin-1 (a) and mock (b) cDNA. After 16 h-incubation, the cells were washed and adherent cells were photographed at ×100. Bars = 20 mμ. **B: The cell adhesion of Colo201 cells to ECM on transfection with galectin-1 cDNA.** Galectin-1–transfected cells, seeded on uncoated, and collagen-, laminin-, and fibronectin-coated dishes, were incubated for 2 h. After the cells had been washed five times with RPMI 1640 medium, the adherent cells were counted.

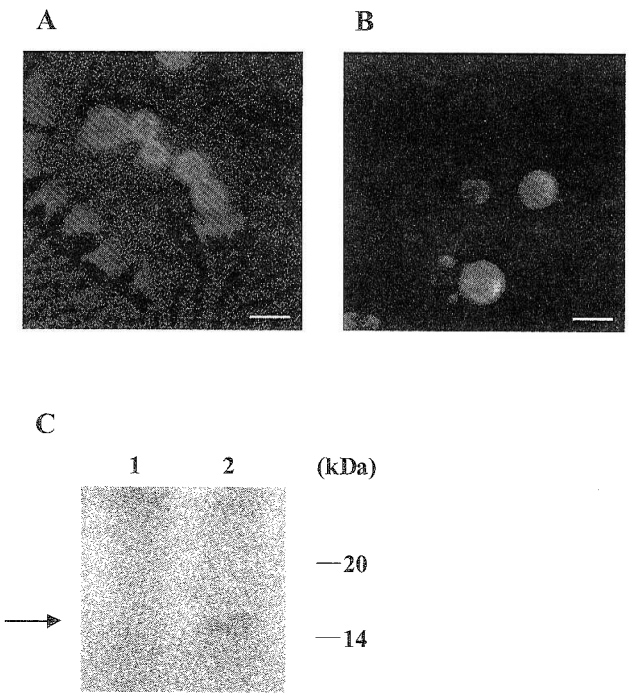

Fig. 2. **Expression of galectin-1 in Colo201 cells.** Cells were transfected with galectin-1 cDNA and the incubated for 16 h. After washing the cells, they were fixed, permeabilized and then stained with a monoclonal antibody for c-myc (A). Bars=20 mμ. The cells were also stained without permeabilization (B). (C) The cells were lysed and immunoblotting with anti–c-myc was performed after the cellular proteins had been analyzed by SDS-PAGE. The cells were transfected with mock (lane 1) and galectin-1 (lane 2) cDNA.

RESULTS

Isolation of Cell Adhesion Molecules with Non-Adherent Colon Cancer Colo201 Cells.—To isolate adhesion molecules, expression cloning was carried out by means of transfection of pcDNA3 vectors carrying human HeLa cell cDNAs into human colon cancer Colo201 cells, based on ability of adhesion of a single transfected cell to the matrix. The plasmids from pools of cDNA clones (10^4 clones) were transiently transfected into Colo201 cells. After 16h-incubation, the medium and non-adherent cells were removed, and the remaining adherent cells were treated with trypsin. After washing the cells twice with the medium, they were cultured for 2 h in RPMI 1640 medium containing 10% FCS. The plasmids from the adherent cells were recovered and amplified in *E. coli*. After three repeated screenings with 3×10^5 independent clones, four positive clones causing cell adhesion of Colo201 cells were obtained, and the DNA was isolated and sequenced. A computer-assisted blast search with the DNA sequences revealed that the four clones corresponded to galectin-1, RhoG, and ribosomal proteins L18 and 27. The cDNAs for ribosomal proteins did not contain the entire protein-coding region, but galectin-1 and RhoG did contain the entire protein-coding region. We (*11*) previously reported that the active forms of Rac-1 and Cdc42 promote the adhesion and spreading of Colo201 cells. Analogous to these GTP-binding proteins, another GTP-binding protein, RhoG, is considered to play a role in the adhesion. Here we were interested in galectin-1 cDNA as the adhesion molecule and thus further examined its properties in detail. Human galectin-1 consists of 125 amino acid residues with the CRD in the central region of the protein. Galectins are known to interact with cell-surface proteins and matrix proteins *via* the CRD (*3*, *4*). Figure 1A shows the changes in the morphology of Colo201 cells on the expression of galectin-1. When cultured on laminin-coated dishes, the cells adhered and spread somewhat. Galectin-1 cDNA was transfected into Colo201 cells, and the cells were cultured in fibronectin-, laminin-, and collagen-coated flasks. As shown in Fig. 1B, on the non-coated dishes, the numbers of adherent cells increased about 3-fold with the expression of galectin-1. On laminin-, fibronectin-, and collagen-coated dishes, the

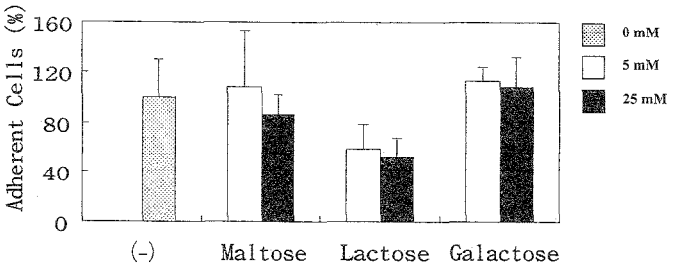

Fig. 3. **Effects of carbohydrates on the adhesion of Colo201 cells expressing galectin-1.** Cells transfected with galectin-1 cDNA were incubated for 16 h. After the cells had been collected and washed three times with RPMI 1640 medium, they were seeded onto laminin-coated dishes in RPMI 1640 medium containing the indicated concentrations of lactose, maltose and galactose, and then incubated for 2 h. The cells were washed five times with RPMI 1640 medium and then the adherent cells were counted. The concentrations of sugars used were 5 mM (open bars) and 25 mM (solid bars).

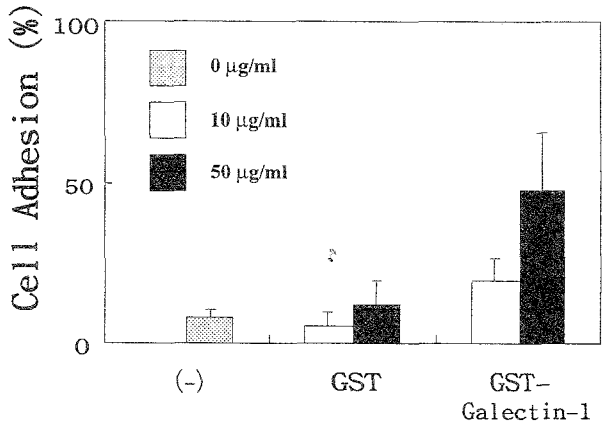

Fig. 4. **Effect of exogenously-added GST-galectin-1 fusion protein on the adhesion of Colo201 cells.** Colo201 cells were incubated in RPMI 1640 medium containing the indicated concentrations of GST or GST-galectin-1. After washing the cells with the medium, the adherent cells were counted.

numbers of adherent cells of galectin-1 cDNA transfected cells were 5- to 6-fold more than those of mock DNA transfected cells. Immunofluorescence staining revealed that galectin-1 was mainly expressed in the cytosol (Fig. 2A). Localization of galectin-1 on the cell-surface was also observed (Fig. 2B). When immunoblotting with a monoclonal antibody for anti-c-myc was performed, a specific band corresponding to a molecular mass of 17 kDa was observed for the pcDNA3-c-myc-galectin-1 cDNA transfected cells (Fig. 2C).

Involvement of Galectin-1 Expressed Inside and on the Cell Surface of Colo201 Cells in Cell Adhesion—To determine whether or not galectin-1 on the cell surface is involved in cell adhesion, the effect of various sugars on galectin-1-induced adhesion were examined. As shown in Fig. 3, of the carbohydrates tested, only lactose inhibited the adhesion in a dose-dependent manner, suggesting that the galactoside terminus of the oligosaccharide is required for the adhesion. Furthermore, to determine if exogenously-added galectin-1 induces the adhesion of Colo201 cells, the GST-galectin-1 fusion protein was synthesized in *E. coli* and purified. Figure 4 shows the

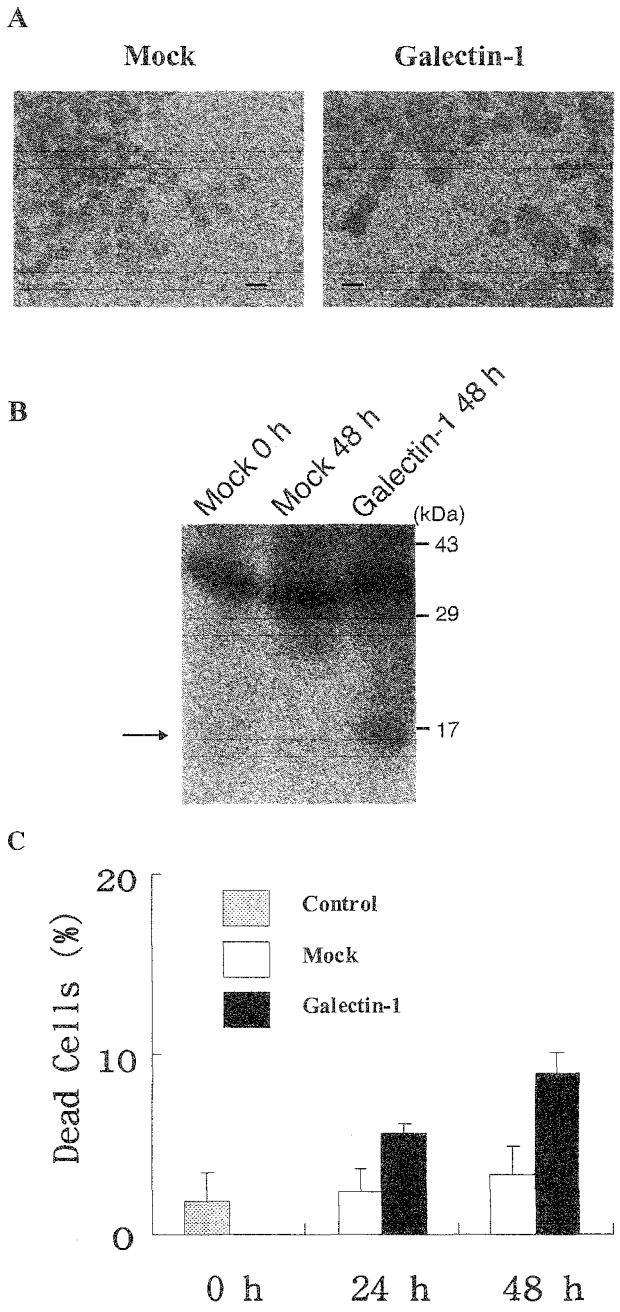

Fig. 5. **Apoptosis induced by the expression of galectin-1.** A: TUNEL assaying to detect apoptosis. Colo201 cells were transfected with pcDNA3 (c-myc)-galectin-1, and after 48 h they were assayed for DNA fragmentation by TUNEL staining. B: Immunoblotting analysis of caspase-3. Cells at 48 h after transfection were lysed, and then the cellular proteins were analyzed by SDS-PAGE. Immunoblotting with anti-caspase-3 was carried out. The arrow indicates the position of the activated caspase-3. C: Quantitative analysis of cell death. Cells after transfection with mock (open) and galectin-1 (solid) cDNA were incubated for 48 and 72 h. The total proportion of dead cells was determined by trypan blue exclusion.

changes in the adhesion of Colo201 cells on the addition of the GST-galectin-1 fusion protein. By increasing the amount of GST-galectin-1 in the medium, an increase in adherent cells was observed, while GST had no effect. It has been reported that galectin undergoes sugar-independent interactions with other proteins within cells,

suggesting that it may play a role in cell adhesion (*16, 17*). We then examined the effects of protein kinase inhibitors on the induction of cell adhesion by galectin-1. PD58059 (100 μM), an inhibitor of mitogen-activated protein kinase, decreased the cell adhesion to 25%. LY294002 (30 μM), a phosphoinositide 3-OH kinase (PI3K) inhibitor, completely abolished the adhesion. These results indicated that galectin-1 expressed both inside and outside of Colo201 cells is involved in the induction of cell adhesion.

Induction of Apoptosis by Galectin-1—Galectins have been proposed to play a role in the regulation of cellular differentiation and proliferation. Thus, we finally examined the ability of the expression of galectin-1 to induce apoptosis in Colo201 cells. Figure 5A shows the results of TUNEL assaying of apoptotic gactectin-1 cDNA-transfected Colo201 cells. At 42 h after galectin cDNA transfection, TUNEL-positive cells were observed on transfection with galectin-1 cDNA, while no apoptosis was observed in the control. When the apoptosis was examined by immunoblotting with anti-caspase 3, cleavage of the active fragment of caspase 3 in galectin-1 expressing cells was observed (Fig. 5B). To quantify the apoptotic cells, cell death was assessed by means of a dye-exclusion assay. As shown in Fig. 5C, the number of surviving cells after transfection with galectin-1 cDNA was lower than that of mock DNA-transfected cells. In separate experiments, Colo201 cells were cultured with the addition of GST-galectin-1 fusion protein (10 μg/ml), and then the effect of exogenously-added galectin-1 on apoptosis was examined by TUNEL assaying and immunoblotting with anti-caspase 3. Apoptosis was not induced on incubation with GST-galectin-1 at up to 64 h (data not shown). Thus, the function of galectin-1 in the cells was separated from those via sugar-dependent interactions outside the cells.

DISCUSSION

We isolated galectin-1 as an adhesion molecule of non-adherent colon cancer Colo201 cells by expression cloning. Increased adhesion of galectin-1–expressing Colo201 cells occurred on non-coated plates, and markedly increased adhesion was observed on collagen-, laminin-, and fibronectin-coated plates. Adhesion to the ECM is CRD-dependent since lactose inhibits the binding. Furthermore, the addition of GST-galectin-1 protein to the culture medium of Colo201 cells led to an increase in the adhesion of Colo201 cells. The expression of galectin-1 in Colo201 cells resulted in cellular apoptosis while exogenously-added galectin-1 did not cause apoptosis. These results indicated that over-expressed galectin-1 in Colo201 cells caused the inhibition of cell proliferation while only extracellular galectin was involved in adhesion.

Galectin-1, an endogenous β-galactoside–binding protein, has emerged as a potent immunomodulatory protein (*3, 5*). By virtue of its ability to interact with specific glycoconjugates, this protein has been implicated in some biological processes, including cell proliferation, cell adhesion, apoptosis, metastasis and immunoregulation (*3, 4*). Galectin-1 induced apoptosis in the activated form of mature T cells and a specific subset of immature thymocytes (*5, 18*). Due to its ability to inhibit the effector function of T cells, galectin-1 must have potent anti-flammatory and immunoregulatory effects *in vivo*. On the other hand, Van den Brule *et al.* (*19*) reported that a human melanoma cell line expresses galectin-1 in both the cytosol and plasma membrane. As galectin-1 on the cell-surface can bind preferentially to laminin to interact specifically with poly-*N*-acetyllactosamine residues (*3*), this endolectin could be a potential modulator of tumor cell-laminin interactions. These observations demonstrate that galectin-1 modulates the adhesion of melanoma cells to laminin and, therefore, could be a modulator of invasion and metastasis (*19, 20*). Colo201 cells belong to a metastatic phenotype of colon cancer (*8*). Since the expression of galectin-1 is correlated with the acquisition of the metastatic phenotype in several types of tumors, the increase in the binding of Colo201 cells caused by the cell-surface galectin-1 with CRD recognition to the ECM may reflect the invasive potential.

In addition to the well-documented function of cell-surface–located galectin-1 as a β-galactoside–binding protein, intracellular galectin-1 functions as a regulator of pre-mRNA splicing. Furthermore, it has been demonstrated that galectin-1 interacts with H-Ras and activates this small GTP-binding protein, resulting in the promotion of membrane anchoring of H-Ras (*16*). We (*11*) previously reported that when the active form of Rac1 was expressed in Colo201 cells, the adhesion and spreading of cells occurred. The expression of the constitutively-active form of Cdc42 in Colo201 cells led to the formation of lamellipodia and membrane ruffles, accompanied by actin polymerization. In this study, an increase in adherent Colo201 cells was observed when RhoG was over-expressed. We had no direct evidence of the interaction of galectin-1 with GTP-binding proteins, but the adhesion is not fully dependent on the interaction of extracellular galectin-1 with sugar chains since the adhesion caused by galectin-1 occurred on uncoated and collagen-coated plates. Collagen is not a major glycoprotein, distinct from laminin and fibronectin, which are ligands of the galectin family. The adhesion of Colo201 cells to collagen (type I) caused by galectin-1 on the cell-surface appeared to be a CRD-independent event occurring *via* an effect inside the cells. The interaction of interacellular galectin-1 with some GTP-binding proteins may trigger adhesion and spreading. Alternatively, galectin-1 may have the ability to enhance the potential of some adhesion molecules.

We previously showed that the rapid activation of PI3K or p21-activated kinase, downstream effectors of Cdc42 and Rac1, is required for the adhesion of Colo201 cells (*11*). A rapid decrease in adhesion caused by inhibitors of PI3K was also observed in Rac 1 or Cdc42-expressing Colo201 cells (*11*), suggesting that the PI3K-mediated transduction pathway involves Rac 1 and regulates the surface expression of integrin molecules. The treatment of galectin-1–expressing Colo201 cells with LY294002, a specific inhibitor of PI3K, led to the complete abolition of adhesive Colo201 cells. This study showed that PD98059, an inhibitor of MAP kinase, also inhibited the galectin-1–dependent adhesion, consistent with the observation by Paz *et al.* (*16*) that the expression of galectin-1 in 293T cells resulted in the activation of extracellular signal–regulated kinase (ERK). These results indicated that the interaction of intracellular galectin-1 with some GTP-binding proteins is linked to

both ERK and PI3K or ERK to PI3K signal transduction pathways.

In colon cancer, the expression of galectin-1 and galectin-3 remains controversial. Lotz *et al.* (*21*) and Sanjuan *et al.* (*22*) observed decreased expression of galectin-3 with the neoplastic progression of colon carcinomas. Galectin-1 in cultured colon cancer cells increased when the cells were induced to differentiate by treatment with sodium butyrate (*23*). This study showed that the overexpression of galectin-1 induced apoptosis. In contrast, marked expression of galectin-1 in epithelial tissues has been reported (*3*, *4*). Irimura *et al.* (*24*) reported increased endogenous galectin-3 expression in high-grade human colorectal carcinomas. Furthermore, it has also been reported that the expression of cytoplasmic galectin-1 and -3 markedly increased during disease progression in the human colon (*25*). Thus, malignant and dysplastic colon cancers exhibit significantly higher galectin-1 and -3 levels than normal colon tissues. In summary, changes in the expression of galectins may be due to the heterogeneity of neoplasm and cancer cell lines or their malignant and metastatic potentials. Galectins are key factors in the development of new therapeutic strategies for a wide range of analyse, including cystic diseases and metastasis. Judging from the phenotype of Colo201 cells, *i.e.* a metastatic type of colon cancer, and on the observation that galectin-1 induced apoptosis of the cells, galectin-1 may function as an inhibitory factor for the growth of metastatic colon cancers.

We wish to thank Drs. H. Mori and M. Yamao for the valuable suggestions. This study was supported in part by grants from the Ministry of Education, Science, Sports and Culture of Japan, and the Yamanouchi Foundation for Research into Metabolic Disorders.

REFERENCES

1. Ruoslahti, E. and Obrink, B. (1996). Common principles in cell adhesion. *Exp. Cell Res.* **159**, 263–273
2. Ridley, A.J., Paterson, H.F., Johnston, C.F., Diekmann, D., and Hall, A. (1992). The small GTP-binding protein rac regulates growth factor-induced membrane ruffling. *Cell* **70**, 401–410
3. Yang, R.Y. and Liu, F.T. (2003) Galectins in cell growth and apoptosis. *Cell Mol. Life Sci.* **60**, 267–276
4. Liu, F.T., Patterson, R.J., and Wang, J.L. (2002) Intracellular functions of galectins. *Biochim. Biophys. Acta.* **1572**, 263–273
5. Perillo, N.L., Pace, K.E., Seilhamer, J.J., and Baum, L.G. (1995) Apoptosis of T cells mediated by galectin-1. *Nature* **378**, 736–739
6. Rabinovich, G.A. (1999) Galectins: an evolutionarily conserved family of animal lectins with multifunctional properties; a trip from the gene to clinical therapy. *Cell Death Differ.* **6**, 711–721
7. Lahm, H., Andre, S., Hoeflich, A., Fischer, J.R., Sordat, B., Kaltner, H., Wolf, E., and Gabius, H.J. (2001) Comprehensive galectin fingerprinting in a panel of 61 human tumor cell lines by RT-PCR and its implications for diagnostic and therapeutic procedures. *J. Cancer Res. Clin. Oncol.* **127**, 375–386
8. Semple, T.U., Quinn, L.A., Woods, L.K., and Moore, G.E. (1978) Tumor and lymphoid cell lines from a patient with carcinoma of the colon for a cytotoxicity model. *Cancer Res.* **38**, 1345–1355
9. Nakagawa, K., Sogo, S., Hioki, K., Tokunaga, R., and Taketani, S. (1998). Acquisition of cell adhesion and induction of focal adhesion kinase of human colon cancer Colo 201 cells by retinoic acid-induced differentiation. *Differentiation* **62**, 249–257
10. Mohri, T., Kameshita, I., Suzuki, S., Hioki, K., Tokunaga, R., and Taketani, S. (1998). Rapid adhesion and spread of nonadherent colon cancer Colo201 cells induced by the protein kinase inhibitors, K252a and KT5720 and suppression of the adhesion by the immunosuppressants FK506 and cyclosporin A. *Cell Strutc. Funct.* **23**, 255–264
11. Mohri, T., Adachi, Y., Ikehara, S., Hioki, K., Tokunaga, R., and Taketani, S. (1999) Activated Rac1 selectively up-regulates the expression of integrin $\alpha 6\beta 4$ and induces cell adhesion and membrane ruffles of nonadherent colon cancer Colo201 cells. *Exp. Cell Res.* **253**, 533–540
12. Naglich, J.G., Metherall, J.E., Russell, D.W., and Eidels, L. (1992) Expression cloning of a diphtheria toxin receptor: identity with a heparin-binding EGF-like growth factor precursor. *Cell* **69**, 1051–1061
13. Taketani, S., Kakimoto, K., Ueta, H., Masaki, R., and Furukawa, T. (2003) Involvement of ABC7 in the biosynthesis of heme in erythroid cells: interaction of ABC7 with ferrochelatase. *Blood* **101**, 3274–3280
14. Bradford, M.M. (1976) A rapid and sensitive method for the quantitation of microgram quantities of protein utilizing the principle of protein-dye binding. *Anal. Biochem.* **72**, 248–254
15. Mizutani, A., Furukawa, T., Adachi, Y., Ikehara, S., and Taketani, S. (2002) A zinc-finger protein, PLAGL2, induces the expression of a proapoptotic protein Nip3, leading to cellular apoptosis. *J. Biol. Chem.* **277**, 15851–15858
16. Paz, A., Haklai, R., Elad-Sfadia, G., Ballan, E., and Kloog, Y. (2001) Galectin-1 binds oncogenic H-Ras to mediate Ras membrane anchorage and cell transformation. *Oncogene* **20**, 7486–7493
17. Lin, H.M., Pestell, R.G., Raz, A., and Kim, H.R. (2002) Galectin-3 enhances cyclin D(1) promoter activity through SP1 and a cAMP-responsive element in human breast epithelial cells. *Oncogene* **21**, 8001–8010
18. Perillo, N.L. and Uittenbogaart, C.H., Nguyen, J.T., and Baum, L.G. (1997) Galectin-1, an endogenous lectin produced by thymic epithelial cells, induces apoptosis of human thymocytes. *J. Exp. Med.* **185**, 1851–1858
19. Van den Brule, F.A., Buicu, C., Baldet, M., Sobel, M.E., Cooper, D.N., Marschal, P., and Castronovo, V. (1995) Galectin-1 modulates human melanoma cell adhesion to laminin. *Biochem. Biophys. Res. Commun.* **209**, 760–767
20. Rye, P.D., Fodstad, O., Emilsen, E., and Bryne, M. (1998) Invasion potential and N-acetylgalactosamine expression in a human melanoma model. *Int. J. Cancer.* **75**, 609–614
21. Lotz, M.M., Andrews, C.W. Jr., Korzelius, C.A., Lee, E.C., Steele, G.D. Jr., Clarke, A., and Mercurio, A.M. (1993) Decreased expression of Mac-2 (carbohydrate binding protein 35) and loss of its nuclear localization are associated with the neoplastic progression of colon carcinoma. *Proc. Natl. Acad. Sci. USA* **90**, 3466–3470
22. Sanjuan, X., Fernandez, P.L., Castells, A., Castronovo, V., Van den Brule, F., Liu, F.T., Cardesa, A., and Campo, E. (1997) Differential expression of galectin 3 and galectin 1 in colorectal cancer progression. *Gastroenterology* **113**, 1906–1915
23. Ohannesian, D.W., Lotan, D., and Lotan, R. (1994) Concomitant increases in galectin-1 and its glycoconjugate ligands (carcinoembryonic antigen, lamp-1, and lamp-2) in cultured human colon carcinoma cells by sodium butyrate. *Cancer Res.* **54**, 5992–6000
24. Irimura, T., Matsushita, Y., Sutton, R.C., Carralero, D., Ohannesian, D.W., Cleary, K.R., Ota, D.M., Nicolson, G.L., and Lotan, R. (1991) Increased content of an endogenous lactose-binding lectin in human colorectal carcinoma progressed to metastatic stages. *Cancer Res.* **51**, 387–393
25. Hittelet, A., Legendre, H., Nagy, N., Bronckart, Y., Pector, J.C., Salmon, I., Yeaton, P., Gabius, H.J., Kiss, R., and Camby, I. (2003) Upregulation of galectins-1 and -3 in human colon cancer and their role in regulating cell migration. *Int. J. Cancer* **103**, 370–379

JOURNAL OF INTERFERON & CYTOKINE RESEARCH 23:631–638 (2003)

Interleukin-2 Abolishes Myeloid Cell Accumulation Induced by Lewis Lung Carcinoma

MASAHARU SHIN-YA,[1,2] OSAM MAZDA,[2] CHIHARU TSUCHIHARA,[1] HIDEYO HIRAI,[2] JIRO IMANISHI,[2] and MINORU TAKEUCHI[1]

ABSTRACT

Immune aberration in cancer patients can be at least partly ascribed to an accumulation of immature myeloid cells and monocytes/macrophages with immunosuppressive functions. Mice implanted with Lewis lung carcinoma 2 (LL/2) cells show marked splenomegaly as the tumors progress, and this condition is accompanied by impaired T cell activities. We characterized the cells that accumulated in the spleens of LL/2 tumor-bearing mice and attempted to restore the normal cell population by employing interleukin-2 (IL-2). Flow cytometric analysis revealed that the cells expressing Mac1, B7, NK-K1, Gra-1, and MHC class II antigens on their surfaces drastically decreased in number when LL/2 had been engineered to produce IL-2. IL-2 also restored the concanavalin A (ConA)-mediated proliferative response and IL-2 production of the spleen cells. The *in vivo* growth of IL-2-producing tumors was significantly slower than that of parental LL/2 cells. Therefore, local IL-2 production may reverse systemic immune abnormality by stopping myeloid cell accumulation.

INTRODUCTION

IN NORMAL IMMUNOCOMPETENT INDIVIDUALS, the immune system recognizes and eliminates malignant cells. To escape immunosurveillance, tumors develop several mechanisms, such as downregulation of MHC expression, aberration in antigen-processing pathways, and lack of costimulatory molecules. Some tumors suppress the immune system of the hosts in a nonspecific manner by secreting cytokines or other soluble factors, including transforming growth factor-β (TGF-β), interleukin-10 (IL-10), and IL-4. Cellular and humoral immune responses are thereby generally hampered in many cancer patients, leading to the inability to reject the tumors.

Another important mechanism of tumor escape from host immunity is the induction of immature myeloid cells with immunosuppressive functions. Much evidence has accumulated indicating that progressive tumor growth is associated with an accumulation of immature myeloid cells and monocytes/macrophages, whereas dendritic cells (DC) decrease in number and activity.[1–3] It has been reported that the immature myeloid cells inhibit specific MHC class I-restricted cytotoxic T lymphocyte (CTL) responses.[4–6] Suppression of $CD4^+$ T cell functions has also been demonstrated in several experimental models,[7–9] although the mechanisms of immunosuppression by immature myeloid cells have not been fully elucidated. This abnormal myelopoiesis may be induced by the tumor cells through soluble factors, including granulocyte-macrophage colony-stimulating factor (GM-CSF),[10–12] macrophage CSF (M-CSF),[11,13] vascular endothelial growth factor (VEGF),[1,6,14] and IL-6.[13] GM-CSF induces expansion of the immature myeloid cells,[10,11] whereas VEGF may inhibit differentiation of DCs and facilitate generation of immature myeloid cells.[1,15] M-CSF and IL-6 may be involved in defective DC differentiation.[13,16]

Therefore, the accumulated immature myeloid cells are capable of inhibiting $CD4^+$ and $CD8^+$ T cell responses, and this may be the major factor responsible for immunosuppression in tumor-bearing hosts.[2,3,5,17,18] In this context, therapeutic intervention that regulates the immature myeloid populations should be important in improving the impaired immune responses in cancer patients.

In an attempt to regulate immunosuppressive populations in tumor-bearing hosts, we tried to apply an immunostimulatory cytokine to an experimental murine tumor model and examined the abolishment of immature myeloid cells that are otherwise induced by the tumors. We chose IL-2 as one of the most potent antitumor cytokines, having the ability to activate and propagate $CD4^+$ and $CD8^+$ T cells as well as natural killer (NK) cells. IL-2 is a promising immunotherapeutic agent for the treatment of metastatic melanoma, acute myelogenous leukemia,

[1]Department of Biotechnology, Faculty of Engineering, Kyoto Sangyo University, Kitaku, Kyoto 603-8555, Japan.
[2]Department of Microbiology, Kyoto Prefectural University of Medicine, Kamikyo, Kyoto 602-8566, Japan.

and metastatic renal cell carcinoma.[16,19,20] In the present study, we investigated the *in vivo* influence of IL-2 on the splenic myeloid cells induced by tumors, using the Lewis lung carcinoma murine model.

MATERIALS AND METHODS

Cells, plasmid, and transfection procedure

The Lewis lung carcinoma cell line LL/2[21] was cultured in Dulbecco's modified Eagle's medium (DMEM) supplemented with 10% heat-inactivated fetal bovine serum (FBS), 100 U/ml penicillin, and 100 μg/ml streptomycin (complete medium). pCMV-Neo-HuIL-2, a plasmid vector containing Neo^R and human IL-2 (HuIL-2) gene expression units, was constructed by inserting the HuIL-2 gene cDNA into the BamHI site of pCMV-Neo. Gene delivery was performed by electroporation as described previously.[22] After the transfection, cells were cultured for 3 days at 37°C in 5% CO_2/95% humidified air (standard condition). G418 (Nakalai Tesque, Kyoto, Japan) was added to the culture medium at a concentration of 0.8 mg/ml so that a G418-resistant clone was established. The resultant LL/2+IL-2 cells produced a considerable amount of HuIL-2 *in vitro* (900 ± 100 pg/ml by 10^6 cells/48 h), whereas parental LL/2 did not secrete HuIL-2 at a detectable level. MHC class I and II antigen expression was not affected by the genetic modification (data not shown).

Mice and tumor cell inoculation

Female C57BL/6 mice (7–8 weeks old) were purchased from Shimizu Laboratory Suppliers (Kyoto, Japan). They received humane care in compliance with the Guide to the Care and Use of Laboratory Animals. Five thousand LL/2 or LL/2+IL-2 cells were inoculated subcutaneously (s.c.) into the right flank of each mouse. The diameters of resultant subcutaneous tumors were measured using a digital caliper. Tumor volume was calculated as $(a^2 \times b)/2$, where a and b are the longest tumor diameter and width, respectively.

Detection of cytokine production in tumors

Twenty-one days after the tumor cell inoculation, mice were killed, and tumors were excised. Total RNA was isolated by the acid guanidinium isothiocyanate-phenol/chloroform extraction method and reverse-transcribed using 200 U Molony murine leukemia virus (MMLV) reverse transcriptase (RT) (GIBCO, Grand Island, NY). The resultant cDNA was subjected to PCR amplification using HuIL-2 gene sense (5′-ATGTACAGGATGCAACTCCTG) and antisense (5′-TCAAGTCAGTGTTGAGATGATG) primers, mouse β-actin gene sense (5′-GCATTGTTACCAACTGGGAC) and antisense (5′-TCTCCGGAGTCCATCACAAT) primers, or mouse GM-CSF gene sense (5′-GAGGCCATCAAAGAAGCCCT) and antisense (5′-GTTTCACAGTCCGTTTCCGG) primers. The PCR products were electrophoresed through an 8% polyacrylamide gel and stained with ethidium bromide. To estimate cytokine concentrations, the tumors were homogenized, and extracts were subjected to ELISA analysis using HuIL-2 and mouse GM-CSF ELISA kits (Amersham, Piscataway, NJ). To examine cytokine expression *in vitro*, total RNA was isolated from 10^6 tumor cells, and 1 μg of the RNA was subjected to RT-PCR as described. Serum cytokine levels were measured by ELISA using the GM-CSF and VEGF (R&D Systems, Minneapolis, MN) ELISA kits.

Flow cytometric analysis

The spleen cells were resuspended at a density of 1.0×10^7 cells/ml in phosphate-buffered saline ($PBS^{(+)}$) containing 0.1% NaN_3 and 2% FBS. The cells were stained with FITC-conjugated CD3, CD4, CD8, Mac1, NK-K1 (all from (PharMingen, San Diego, CA) B7, heat-stable antigen (HSA), and MHC class

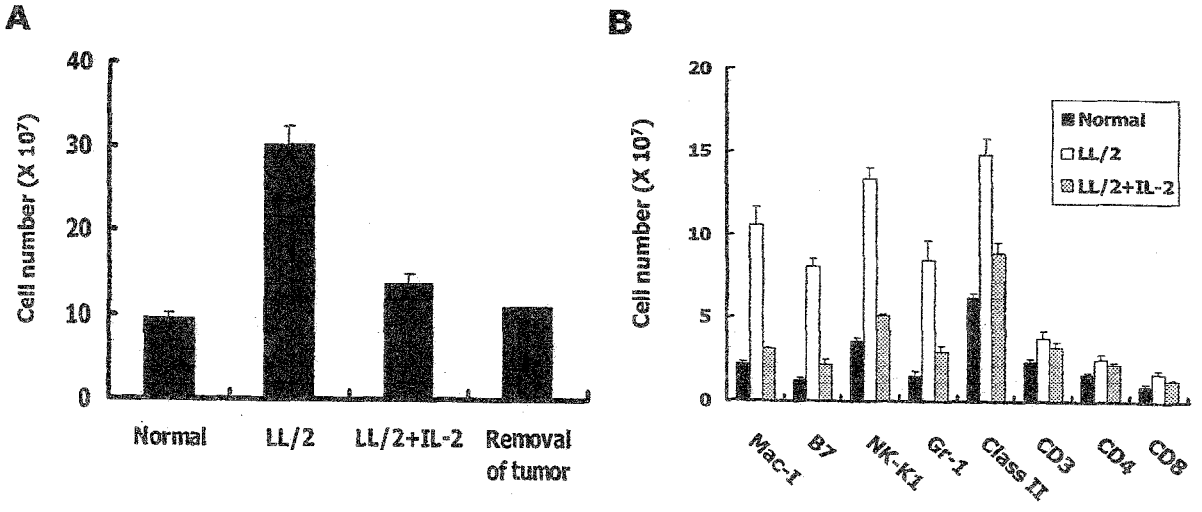

FIG. 1. Analysis of spleen cells from mice bearing LL/2 or LL/2+MuIL-2 tumors. Spleen cells were harvested 21 days after tumor cell inoculation, except that in a group in A, tumors were removed from the mice on day 21, and spleen cells were harvested 14 days thereafter (bar at right). As a control, spleen cells of normal mice were also analyzed. (A) Viable cell numbers were determined by trypan blue dye exclusion. (B) Cells were stained with the indicated antibodies, followed by flow cytometric analysis. The number of cells stained with each antibody is calculated.

II (all from Caltag Laboratories, Burlingame, CA) antibodies, and they were analyzed using a FACSort (Becton Dickinson, Mountain View, CA).

Response of splenic cells to concanavalin A (ConA)

The proliferative response to ConA was assessed by the standard ^{3}H-thymidine (^{3}H-TdR) incorporation method. Briefly, cells were seeded at a concentration of 5.0×10^5 cells/well in 96-well flat-bottom microtiter plates in the presence or absence of 1.0 μg/ml ConA. After incubation for 72 h under standard conditions as described, 18.5 kBq/well of ^{3}H-TdR was added. Cells were further cultured for 24 h, and the incorporated ^{3}H-TdR was measured with a liquid-scintillation counter. To assess mouse IL-2 (MuIL-2) production, 2.0×10^6 splenic cells/well were seeded into 24-well microtiter plates with or without 1.0 μg/ml ConA. After cells were cultivated for 24 h under standard conditions, total RNA was isolated, followed by RT-PCR analysis using MuIL-2 sense (5′-TTTTACTTGCCCAAGCAGGC) and antisense (5′-GTCCACCACAGTTGCTGACT) primers.

Statistical analyses

Statistical analyses of the results were performed using the Student's t-test. The survival difference was evaluated by the log rank test.

RESULTS

Mice implanted with LL/2 Lewis lung carcinoma cells showed marked splenomegaly as the tumors progressed. Cell counts 21 days after tumor cell implantation showed that the splenic cells from LL/2-implanted mice increased in number approximately 3-fold compared with those from normal mice ($p < 0.001$)(Fig. 1A). After the tumors were removed, the cell count decreased to the normal range within 14 days. This result strongly suggests that the aberrant population in the spleen was caused by the tumor in a reversible manner.

Flow cytometric analyses were performed to investigate the cell populations that were amplified in the spleens of the tumor-bearing mice. A population of cells with high forward and side light scattering largely accumulated in the spleen of mice

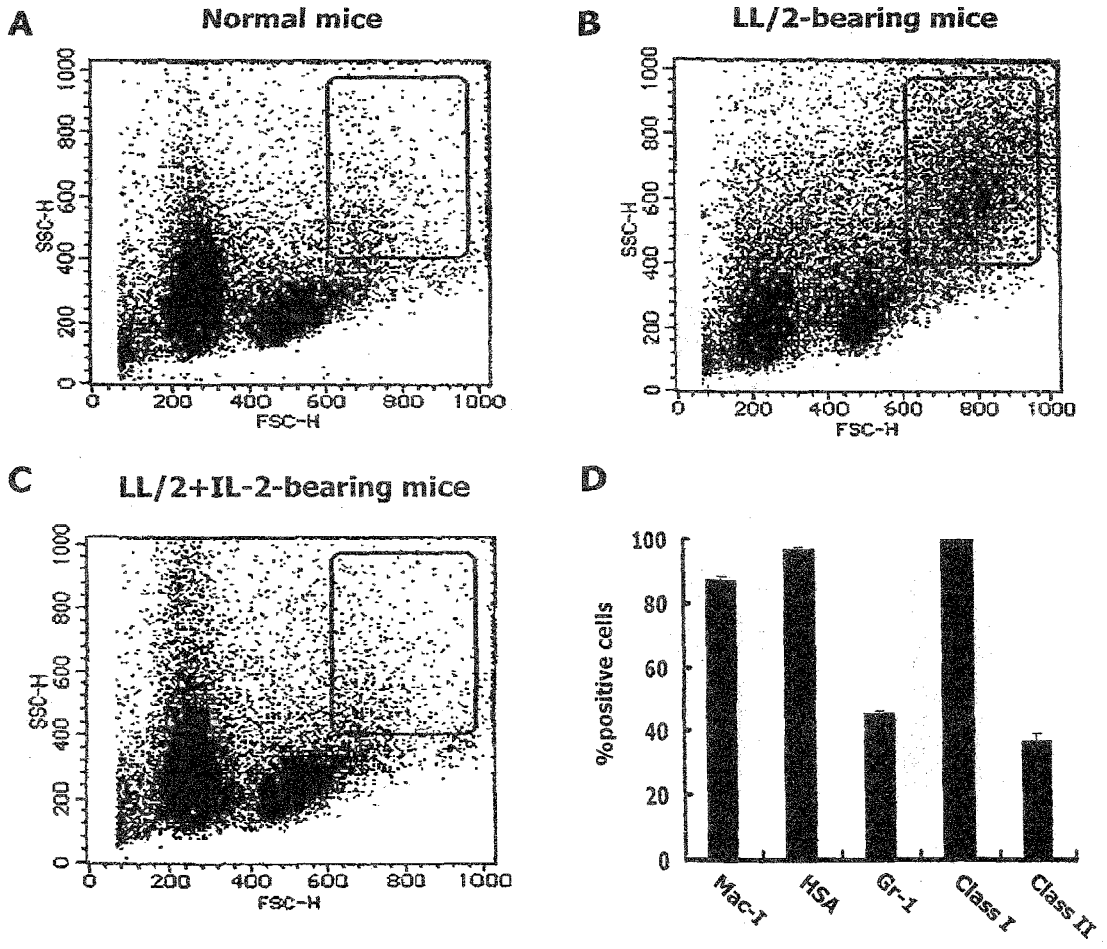

FIG. 2. HuIL-2 negated aberrant accumulation of macrophagelike cells in spleen. (A) Spleen cells were obtained from normal mice and analyzed by FACS. Representative dot plots of forward vs. side light scattering are shown. (B and C) Mice were inoculated with the LL/2 (B) or LL/2+IL-2 (C), and 21 days later, spleen cells were analyzed by FACS as in A. (D) Mice were inoculated with LL/2, and 21 days later, spleen cells were harvested. Cells were stained with the indicated antibodies, and percentages of positive cells among cells gated in B are shown.

with LL/2 tumors (Fig. 2B), although such cells were rarely observed in normal mouse spleens (Fig. 2A). The majority of the cells were regarded as myeloid cells, according to their positive staining with anti-Mac1, anti-Gra-1, and anti-HSA antibodies (Fig. 2D). The aberrant cell population disappeared after tumors were removed (data not shown).

To examine the influence of IL-2 on the splenic cell population dynamics, a group of mice were inoculated with LL/2 cells that had been genetically engineered to secrete IL-2 (LL/2+IL-2). The tumor cells successfully produced the cytokine *in vivo*, as demonstrated by ELISA and RT-PCR analyses (Fig. 3A,B). As shown in Figure 1A, the LL/2+IL-2-inoculated mice did not show a quantitative increase in the number of spleen cells, suggesting that the IL-2 restored the abnormality in the lymphoid organ that had otherwise been affected by the tumor. This is consistent with the forward vs. side light scattering profile that failed to demonstrate the myeloid cell accumulation in the spleen from LL/2+IL-2-bearing animals (Fig. 2C). Also, the percentages of myeloid marker positive cells decreased nearly to normal levels under the influence of IL-2 (Fig. 1B).

Morphologic examination indicated that neither LL/2 nor LL/2+IL-2 had metastasized to the spleen (data not shown). We suggest that the propagation or migration (or both) of the myeloid cells was induced by some soluble factor(s) secreted from the LL/2 tumors. One possibility is GM-CSF, which has been shown to be secreted from some types of tumors and which facilitates proliferation, differentiation, and activation of cells of macrophage lineage.[3,10–12] To investigate whether GM-CSF is produced by the LL/2 tumors *in vivo*, we performed ELISA and RT-PCR analyses. As shown in Figure 3C and D, LL/2 produced a significant amount of this cytokine. GM-CSF expression was also detected in the LL/2 tumor cells *in vitro* (Fig. 4A).

VEGF is another cytokine capable of inducing immature myeloid cell accumulation.[1,6,14] Thus, we examined the GM-CSF and VEGF concentrations in sera of the tumor-bearing mice. As shown in Figure 4B, the LL/2 tumor-bearing mice showed high serum levels of GM-CSF ($p < 0.01$, LL/2 vs. normal mice). The cytokine levels were significantly lower in the LL/2+IL-2 tumor bearers ($p < 0.05$, LL/2+IL-2 vs. LL/2; $p < 0.05$, LL/2+IL-2 vs. normal mouse). In contrast, serum VEGF concentrations were not elevated in the LL/2 tumor-bearing mice, and the LL/2+IL-2 tumor bearers also showed comparable levels of the cytokine. Collectively, the data suggest that GM-CSF may, at least in part, contribute to induction of the splenic myeloid cells.

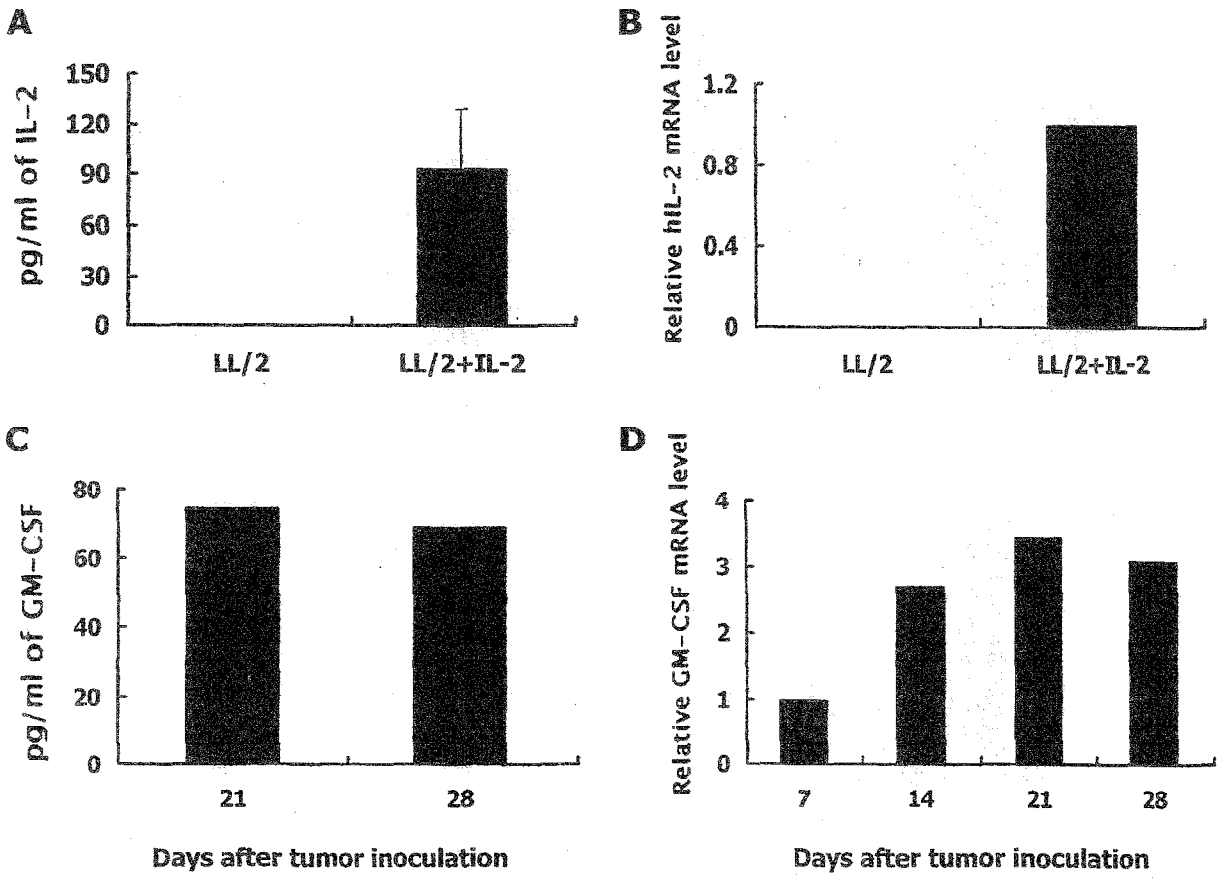

FIG. 3. Cytokine production *in vivo* by tumor cells. LL/2 and LL/2+IL-2 tumors were established in C57BL/6 mice (Fig. 1). Twenty-one days (**A** and **B**) or the indicated days (**C** and **D**) later, ELISA (**A** and **C**) and RT-PCR (**B** and **D**) analyses were performed to detect HuIL-2 (**A** and **B**) and mouse GM-CSF (**C** and **D**) expression in the tumors. In **B** and **D**, relative mRNA levels standardized by β-actin mRNA levels are shown.

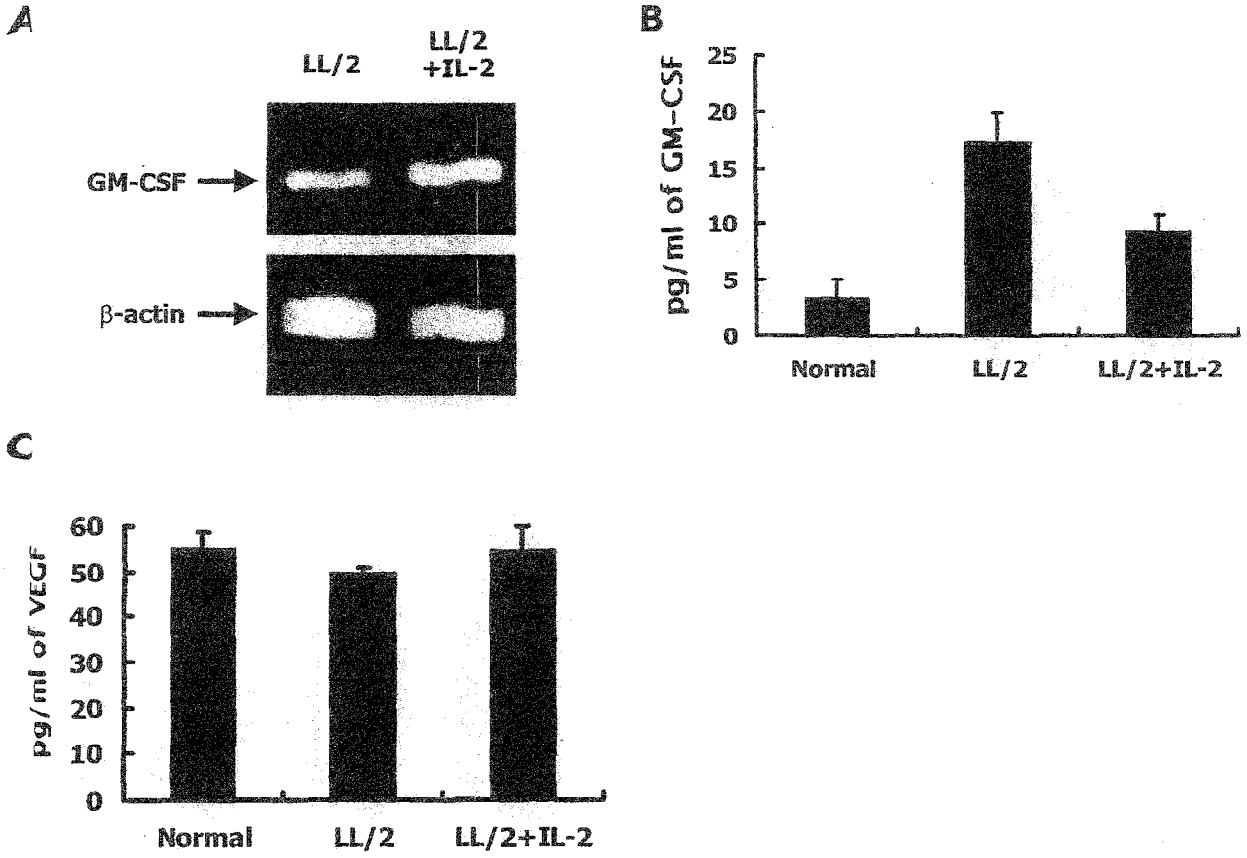

FIG. 4. GM-CSF and VEGF expression by tumor cells. (A) RNA was extracted from the LL/2 or LL/2+IL-2 cells and subjected to RT-PCR analysis using the GM-CSF or β-actin gene-specific primers. (B and C) Sera were obtained from LL/2 or LL/2+Il-2 tumor-bearing mice 21 days after tumor cell inoculation. Concentrations of GM-CSF (B) and VEGF (C) were measured by ELISA. As control, sera from normal mice were also tested.

The response of spleen cells to ConA was estimated *in vitro*. As shown in Figure 5A, spleen cells from LL/2 tumor-bearing mice showed a significantly lower proliferative response to the T cell mitogen in comparison with those from normal mice ($p < 0.001$). The mitogenic response was restored after removal of the tumor (Fig. 5C). In contrast, spleen cells from LL/2+IL-2-implanted animals exhibited a comparable level of proliferative response to that from control mice (Fig. 5A). Expression of MuIL-2 was also hampered in LL/2 tumor-bearing mice ($p < 0.05$), whereas LL/2+IL-2 implantation elevated the MuIL-2 expression by ConA-stimulated spleen cells, probably because of the HuIL-2 secreted from the tumors ($p < 0.05$)(Fig. 5B).

Spleen cells from normal mice and from LL/2 tumor-bearing mice were cocultured to assess the mechanisms of the reduction in ConA response. Proliferation of normal mouse spleen cells was significantly suppressed, and the degree of suppression depended on the sizes of the LL/2 tumors (Fig. 5D). Therefore, the splenic cells from LL/2-bearing mice may actively suppress proliferative activity of normal mouse spleen cells induced by ConA. In contrast, spleen cells from LL/2+IL-2 tumor-bearing mice did not affect the ConA response of normal spleen cells (Fig. 5D, right bar).

Finally, *in vivo* growth of LL/2 and LL/2+IL-2 tumors was compared. The proliferation rates of these two tumor cell lines were virtually the same *in vitro* (data not shown). When LL/2 cells were inoculated s.c. into syngeneic hosts, palpable tumors were established in all the mice by day 7, and tumors grew progressively thereafter. In contrast, LL/2+IL-2 tumors developed much more slowly than did the parental LL/2 tumors ($p < 0.0001$)(Fig. 6A). In addition, the mice implanted with LL/2+IL-2 survived for a significantly longer period than did the LL/2 tumor-bearing mice ($p < 0.001$)(Fig. 6B). Histologic examination of tumor tissue revealed massive infiltration of lymphoid cells in the LL/2+IL-2 tumors, whereas the lymphoid cell infiltration in the LL/2 tumors was very faint, if present at all (data not shown).

DISCUSSION

In the present study, we demonstrated that local IL-2 production in the tumor almost completely abolished the accumulation of immature myeloid cells in the spleen of LL/2 tumor-bearing mice. The results strongly suggest that cytokine gene therapy may ameliorate the impaired immunity in cancer patients, providing a useful strategy to eradicate malignancies.

Earlier studies reported the accumulation of immature myeloid or macrophagelike cells in patients with head and

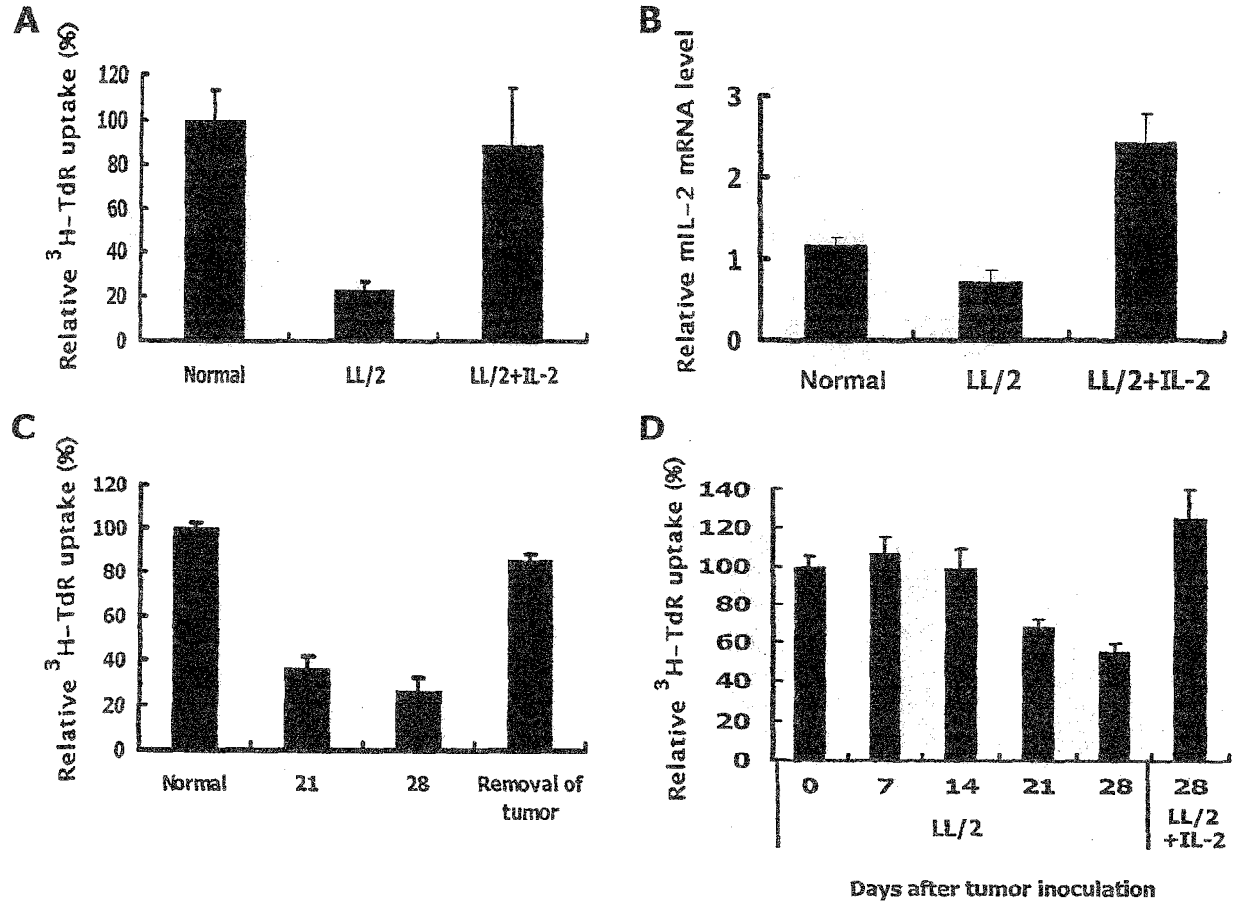

FIG. 5. HuIL-2 restored the impaired mitogenic response of spleen cells. (A, B, C) Spleen cells were harvested from the mice implanted with the indicated tumor cells (A and B) or LL/2 (C) 21 days (A and B) or on the indicated days (C) after tumor inoculation, except that in a group in C, tumor was removed from the mice 21 days after implantation, and spleen cells were obtained 2 weeks thereafter (C, right bar). As a control, spleen cells were also obtained from normal mice. ^{3}H-TdR uptake (A and C) and MuIL-2 mRNA (B) were assayed after 3 days of cultivation with ConA. (D) Spleen cells were harvested from mice on the indicated days after implantation of LL/2 or LL/2+IL-2 cells. The cells were cocultured for 3 days with normal mouse spleen cells in the presence of ConA, and ^{3}H-TdR uptake was assessed.

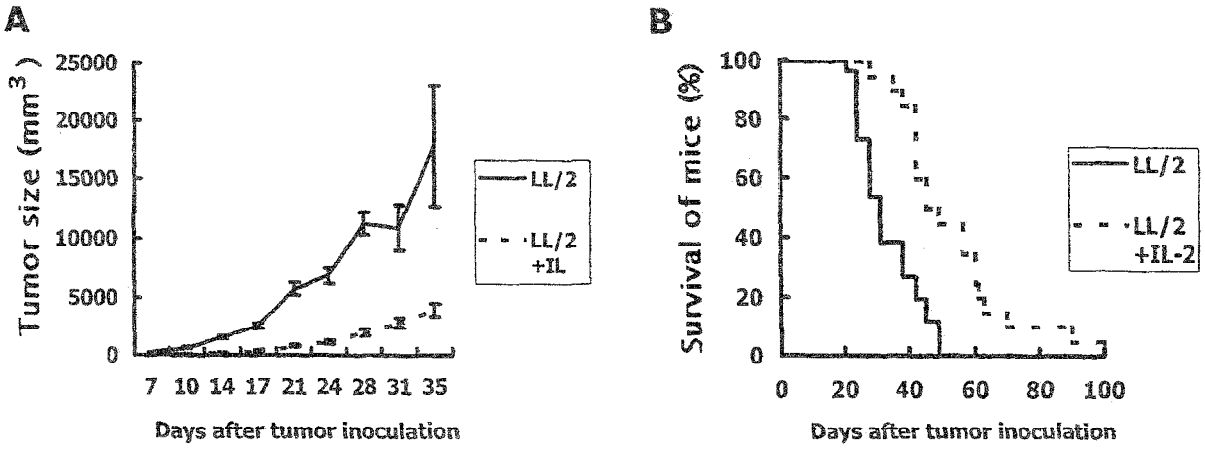

FIG. 6. IL-2 suppressed the growth of Lewis lung carcinoma in mice. LL/2 (solid lines) or LL/2+IL-2 (dotted lines) cells were inoculated s.c. into C57BL/6 mice. The volumes of subcutaneous tumors (A) and percent survival of mice (B) are shown.

neck,[1,5,23] breast,[1,5] and non-small cell lung[1,5] cancers. These cells drastically increased in number in patients with advanced cancer but dropped considerably within several weeks after surgical resection of the tumor. Similar observations have been made in mouse models bearing Lewis lung carcinoma,[24] Ehrlich carcinoma,[25,26] mammary adenocarcinoma,[18] fibrosarcoma,[5,27] and colon carcinoma.[4,17,28,29] The present findings with the LL/2 tumor model are consistent with these earlier reports.

Aberrant myeloid cell populations have been shown to suppress T cell functions *in vitro*.[1,5,23,30,31] $CD4^+$ and $CD8^+$ T cells and B cell responses may be affected in an antigen-independent and MHC-independent fashion without prior activation of the suppressor cells.[2,3,5,17,18] We have found that the spleen cells from LL/2 tumor-bearing mice significantly inhibited the ConA-stimulated proliferative response of normal mouse spleen cells *in vitro* (Fig. 5D). The results are consistent with earlier reports documenting that the immature myeloid cells suppressed the ConA response of normal T cells.[26,31] In contrast, Gabrilovich et al.[6] demonstrated that Gra-1^+ cells from tumor-bearing hosts did not affect the ConA response of normal T cells.[6] The discrepancy may be because Gabrilovich et al. used highly purified Gra-1^+ cells obtained by cell sorting. The heterogeneity of the immature myeloid cells has been suggested.[3] Different tumors may induce distinct immature myeloid cell populations.

Almand et al.[1] and Gabrilovich et al.[6] recently showed that VEGF, rather than GM-CSF, is produced from tumor cells and works as the major inducer of the immature myeloid cells. The discrepancy between their results and ours may be ascribed to the different tumor cells used in the studies, as Almand et al.[1] analyzed cancer patients with breast, head and neck, and lung cancers, and Gabrilovich et al.[6] examined MethA sarcoma and C3 tumor cells. Different tumor cells may produce different cytokines that downregulate host immune defenses. To understand and regulate immune aberration in each cancer patient, it may be particularly important to identify the immunomodulatory cytokine secreted from the tumor.

In the present study, parental and IL-2-producing tumor cells expressed comparable levels of GM-CSF *in vitro* (Fig. 4A), suggesting that the different GM-CSF serum levels in LL/2 tumor-bearing and LL/2+IL-2 tumor-bearing mice (Fig. 4B) were due to some biologic effects *in vivo* of IL-2. In this respect, T cell reactivation by IL-2 may be important.

Clonal cell death and clonal anergy (clonal paralysis) are the major causes of immune tolerance and are responsible for the nonresponsiveness of the immune system to specific tolerogens. T cells stimulated with MHC plus peptide antigen in the absence of an appropriate costimulatory signal undergo clonal anergy.[32] It has been demonstrated that supplementation of exogenous IL-2 cancels the anergy state of the T cells and restores proliferation capability and antigen-specific responses.[32,33] The present findings suggest that the immature myeloid cells suppress T cells by inducing clonal anergy rather than clonal cell death, and IL-2 may relieve T cells from the anergic state. The reactivated T cells may recognize and attack tumors, subsequently reducing the accumulated immature myeloid cells, although this hypothesis requires further experimental assessment.

High-dose IL-2 regimens have shown clinical benefit in the treatment of highly immunogenic tumors, including melanoma and renal cell carcinoma.[16,19,20] This cytokine functions as an autocrine growth factor for $CD4^+$ T cells and facilitates proliferation, differentiation, and activation of CTL and NK cells. The present data suggest that IL-2 immunotherapy may be effective in eradicating malignant tumors not only by enhancing the tumoricidal activity of the immune effector cells but also by abrogating the immunosuppression induced by tumors.

Concerning the therapeutic applications, a gene delivery system that allows IL-2 gene transfer *in vivo* into tumors may be useful. Adenoviral and retroviral vectors have been shown to enable efficient genetic transfer into tumors,[34,35] and nonviral delivery systems, such as synthetic vectors, electroporation, and naked DNA methods, may also be useful.[36,37]

ACKNOWLEDGMENTS

We thank Atsuko Nakajima, Makoto Yoshimura, and Kenichi Yoshikawa (Department of Biotechnology, Faculty of Engineering, Kyoto Sangyo University) for their helpful discussions. This work was supported by the Bio-venture project of the Ministry of Education, Culture, Sports, Science and Technology of Japan.

REFERENCES

1. ALMAND, B., RESSER, J.R., LINDMAN, B., NADAF, S., CLARK, J.I., KWON, E.D., CARBONE, D.P., and GABRILOVICH, D.I. (2000). Clinical significance of defective dendritic cell differentiation in cancer. Clin. Cancer Res. **6**, 1755–1766.
2. BRONTE, V., SERAFINI, P., APOLLONI, E., and ZANOVELLO, P. (2001). Tumor-induced immune dysfunctions caused by myeloid suppressor cells. J. Immunother. **24**, 431–446.
3. KUSMARTSEV, S., and GABRILOVICH, D.I. (2002). Immature myeloid cells and cancer-associated immune suppression. Cancer Immunol. Immunother. **51**, 293–298.
4. BRONTE, V., CHAPPELL, D.B., APOLLONI, E., CABRELLE, A., WANG, M., HWU, P., and RESTIFO, N.P. (1999). Unopposed production of granulocyte-macrophage colony-stimulating factor by tumors inhibits $CD8^+$ T cell responses by dysregulating antigen-presenting cell maturation. J. Immunol. **162**, 5728–5737.
5. ALMAND, B., CLARK, J.I., NIKITINA, E., VAN BEYNEN, J., ENGLISH, N.R., KNIGHT, S.C., CARBONE, D.P., and GABRILOVICH, D.I. (2001). Increased production of immature myeloid cells in cancer patients: a mechanism of immunosuppression in cancer. J. Immunol. **166**, 678–689.
6. GABRILOVICH, D.I., VELDERS, M.P., SOTOMAYOR, E.M., and KAST, W.M. (2001). Mechanism of immune dysfunction in cancer mediated by immature Gr-1^+ myeloid cells. J. Immunol. **166**, 5398–5406.
7. CAULEY, L.S., MILLER, E.E., YEN, M., and SWAIN, S.L. (2000). Superantigen-induced CD4 T cell tolerance mediated by myeloid cells and IFN-gamma. J. Immunol. **165**, 6056–6066.
8. DALTON, D.K., HAYNES, L., CHU, C.Q., SWAIN, S.L., and WITTMER, S. (2000). Interferon gamma eliminates responding CD4 T cells during mycobacterial infection by inducing apoptosis of activated CD4 T cells. J. Exp. Med. **192**, 117–122.
9. ATOCHINA, O., DALY-ENGEL, T., PISKORSKA, D., McGUIRE, E., and HARN, D.A. (2001). A schistosome-expressed immunomodulatory glycoconjugate expands peritoneal $Gr1^{(+)}$ macrophages that suppress naive $CD4^{(+)}$ T cell proliferation via

an IFN-gamma and nitric oxide-dependent mechanism. J. Immunol. **167**, 4293–4302.
10. FU, Y.X., WATSON, G., JIMENEZ, J.J., WANG, Y., and LOPEZ, D.M. (1990). Expansion of immunoregulatory macrophages by granulocyte-macrophage colony-stimulating factor derived from a murine mammary tumor. Cancer Res. **50**, 227–234.
11. OGHISO, Y., YAMADA, Y., ANDO, K., ISHIHARA, H., and SHIBATA, Y. (1993). Differential induction of prostaglandin E_2-dependent and -independent immune suppressor cells by tumor-derived GM-CSF and M-CSF. J. Leukocyte Biol. **53**, 86–92.
12. YOUNG, M.R., WRIGHT, M.A., MATTHEWS, J.P., MALIK, I., and PRECHEL, M. (1996). Suppression of T cell proliferation by tumor-induced granulocyte-macrophage progenitor cells producing transforming growth factor-beta and nitric oxide. J. Immunol. **156**, 1916–1922.
13. MENETRIER-CAUX, C., MONTMAIN, G., DIEU, M.C., BAIN, C., FAVROT, M.C., CAUX, C., and BLAY, J.Y. (1998). Inhibition of the differentiation of dendritic cells from $CD34^{(+)}$ progenitors by tumor cells: role of interleukin-6 and macrophage colony-stimulating factor. Blood **92**, 4778–4791.
14. SAITO, H., TSUJITANI, S., IKEGUCHI, M., MAETA, M., and KAIBARA, N. (1998). Relationship between the expression of vascular endothelial growth factor and the density of dendritic cells in gastric adenocarcinoma tissue. Br. J. Cancer **78**, 1573–1577.
15. GABRILOVICH, D.I., CHEN, H.I., GIRGIS, K.R., CUNNINGHAM, H.T., MENY, G.M., NADAF, S., KAVANAUGH, D., and CARBONE, D.P. (1996). Production of vascular endothelial growth factor by human tumors inhibits the functional maturation of dendritic cells. Nat. Med. **2**, 1096–1103.
16. ROSENBERG, S.A. (2001). Progress in the development of immunotherapy for the treatment of patients with cancer. J. Intern. Med. **250**, 462–475.
17. KUSMARTSEV, S.A., LI, Y., and CHEN, S.H. (2000). $Gr\text{-}1^+$ myeloid cells derived from tumor-bearing mice inhibit primary T cell activation induced through CD3/CD28 costimulation. J. Immunol. **165**, 779–785.
18. WATSON, G.A., FU, Y.X., and LOPEZ, D.M. (1991). Splenic macrophages from tumor-bearing mice co-expressing MAC-1 and MAC-2 antigens exert immunoregulatory functions via two distinct mechanisms. J. Leukocyte Biol. **49**, 126–138.
19. ATKINS, M.B. (2002). Interleukin-2: clinical applications. Semin. Oncol. **29**, 12–17.
20. ROSENBERG, S.A. (2001). Progress in human tumour immunology and immunotherapy. Nature **411**, 380–384.
21. BERTRAM, J.S., and JANIK, P. (1980). Establishment of a cloned line of Lewis lung carcinoma cells adapted to cell culture. Cancer Lett. **11**, 63–73.
22. MAZDA, O., SATOH, E., YASUTOMI, K., and IMANISHI, J. (1997). Extremely efficient gene transfection into lympho-hematopoietic cel lines by Epstein-Barr virus-based vectors. J. Immunol. Methods **204**, 143–151.
23. YOUNG, M.R., WRIGHT, M.A., and PANDIT, R. (1997). Myeloid differentiation treatment to diminish the presence of immune-suppressive $CD34^+$ cells within human head and neck squamous cell carcinomas. J. Immunol. **159**, 990–996.
24. YOUNG, M.R., and NEWBY, M. (1986). Differential induction of suppressor macrophages by cloned Lewis lung carcinoma variants in mice. J. Natl. Cancer Inst. **77**, 1255–1260.
25. KUSMARTSEV, S., RUIZ DE MORALES, J.M., RULLAS, J., DANILETS, M.G., and SUBIZA, J.L. (1999). Sialoadhesin expression by bone marrow macrophages derived from Ehrlich tumor-bearing mice. Cancer Immunol. Immunother. **48**, 493–398.
26. SUBIZA, J.L., VINUELA, J.E., RODRIGUEZ, R., GIL, J., FIGUEREDO, M.A., and DE LA CONCHA, E.G. (1989). Development of splenic natural suppressor (NS) cells in Ehrlich tumor-bearing mice. Int. J. Cancer **44**, 307–314.
27. ALLEVA, D.G., WALKER, T.M., and ELGERT, K.D. (1995). Induction of macrophage suppressor activity by fibrosarcoma-derived transforming growth factor-beata 1: contrasting effects on resting and activated macrophages. J. Leukocyte Biol. **57**, 919–928.
28. JAFFEE, E.M., THOMAS, M.C., HUANG, A.Y., HAUDA, K.M., LEVITSKY, H.I., and PARDOLL, D.M. (1996). Enhanced immune priming with spatial distribution of paracrine cytokine vaccines. J. Immunother. Emphasis Tumor Immunol. **19**, 176–183.
29. OTSUJI, M., KIMURA, Y., AOE, T., OKAMOTO, Y., and SAITO, T. (1996). Oxidative stress by tumor-derived macrophages suppresses the expression of CD3 zeta chain of T-cell receptor complex and antigen-specific T-cell responses. Proc. Natl. Acad. Sci. USA **93**, 13119–13124.
30. YOUNG, M.R., NEWBY, M., and WEPSIC, H.T. (1987). Hematopoiesis and suppressor bone marrow cells in mice bearing large metastatic Lewis lung carcinoma tumors. Cancer Res. **47**, 100–105.
31. ANGULO, I., RODRIGUEZ, R., GARCIA, B., MEDINA, M., NAVARRO, J., and SUBIZA, J.L. (1995). Involvement of nitric oxide in bone marrow-derived natural suppressor activity. Its dependence on IFN-gamma. J. Immunol. **155**, 15–26.
32. FIELDS, P., FITCH, F.W., and GAJEWSKI, T.F. (1996). Control of T lymphocyte signal transduction through clonal anergy. J. Mol. Med. **74**, 673–683.
33. APPLEMAN, L.J., TZACHANIS, D., GRADER-BECK, T., VAN PUIJENBROEK, A.A., and BOUSSIOTIS, V.A. (2001). Helper T cell anergy: from biochemistry to cancer pathophysiology and therapeutics. J. Mol. Med. **78**, 673–683.
34. SCUDELETTI, M., FILACI, G., IMRO, M.A., MOTTA, G., DI GAETANO, M., PIERRI, I., TONGIANI, S., INDIVERI, F., and PUPPO, F. (1993). Immunotherapy with intralesional and systemic interleukin-2 of patients with non-small cell lung cancer. Cancer Immunol. Immunother. **37**, 119–124.
35. EMTAGE, P.C., WAN, Y., MULLER, W., GRAHAM, F.L., and GAULDIE, J. (1998). Enhanced interleukin-2 gene transfer immunotherapy of breast cancer by coexpression of B7-1 and B7-2. J. Interferon Cytokine Res. **18**, 927–937.
36. MAZDA, O., SATOH, E., HIRAI, H., NOMURA, M., and IMANISHI, J. (2000). Non-viral strategies for immuno-gene therapy. In: *Recent Research Developments in Immunology*. M.P. Cancro (ed.) Trivandrum, IN: Research Signpost, pp. 273–281.
37. MAZDA, O. (2002). Improvement of nonviral gene therapy by Epstein-Barr virus (EBV)-based plasmid vectors. Curr. Gene Ther. **2**, 379–392.

Address reprint requests to:
Dr. Masaharu Shin-Ya
Department of Microbiology
Kyoto Prefectural University of Medicine
Kamikyo, Kyoto 602-8566
Japan

Tel: (+81)-75-251-5329
Fax: (+81)-75-251-5331
E-mail: masaharu@basic.kpu-m.ac.jp

Received 13 March 2003 / Accepted 10 July 2003

J. Biochem. 135, 129–137 (2004)
DOI: 10.1093/jb/mvh015

Cooperation of Syndecan-2 and Syndecan-4 among Cell Surface Heparan Sulfate Proteoglycans in the Actin Cytoskeletal Organization of Lewis Lung Carcinoma Cells

Yuri Kusano[1], Yasuo Yoshitomi[2], Seiichi Munesue[2], Minoru Okayama[2] and Kayoko Oguri[*,1]

[1]Clinical Research Center, Nagoya National Hospital, 4-1-1 Sannomaru, Naka-ku, Nagoya 460-0001; and [2]Department of Biotechnology, Faculty of Engineering, Kyoto Sangyo University, Motoyama Kamigamo, Kita-ku, Kyoto 603-8555

Received October 9, 2003; accepted November 20, 2003

Syndecan-2 cooperates with integrin α5β1 in cell adhesion to a fibronectin substratum and regulates actin cytoskeletal organization in an expression level-dependent manner; Lewis lung carcinoma-derived P29 cells with high expression form stress fibers, whereas the same tumor-derived low expressers, LM66-H11 cells, form cortex actin [Munesue, S., Kusano, Y., Oguri, K., Itano, N., Yoshitomi, Y., Nakanishi, H., Yamashina, I., and Okayama, M. (2002) *Biochem. J.* 363, 201–209]. In this study we examined the participation of other cell surface heparan sulfate proteoglycans in this signaling. The two clones expressed syndecan-1, -2 and -4, and glypican-1 at similar levels except for syndecan-2. Treatment of cells with phosphatidylinositol-specific phospholipase C or immobilized anti-syndecan-1 antibodies demonstrated that neither glypican-1 nor syndecan-1 was involved in this signaling, indicating that individual cell surface heparan sulfate proteoglycans have functional specificity. Stimulation with immobilized anti-syndecan-2 or -4 antibodies induced stress fiber formation in P29 cells but not in LM66-H11 cells, despite the similar levels of syndecan-4 expression, suggesting that stress fiber formation required a threshold expression level of syndecan-2 acting downstream of syndecan-4. This was confirmed by cells in which syndecan-2 expression was artificially suppressed by antisense mRNA oligonucleotide treatment or elevated by cDNA transfection. This is the first report demonstrating that syndecan-2 and -4 cooperate *in situ* in actin cytoskeletal organization.

Key words: actin cytoskeletal organization, cell surface heparan sulfate proteoglycans, integrin α5β1, syndecan-2, syndecan-4.

Control of cell adhesion to the surrounding extracellular matrix is important in both physiological and pathological processes, including embryonic morphogenesis, maintenance of tissue homeostasis, wound healing, and tumor cell invasion and metastasis. These processes involve a variety of extracellular ligands, their interaction with cell membrane receptors, and subsequent downstream signal cascades. One class of cell adhesion receptors is the integrins, whose roles in extracellular matrix-associated adhesion and signaling are now well established (*1–5*). Recently, the syndecans, transmembrane heparan sulfate proteoglycans, which often work in cooperation with integrins, have received much attention as another class of cell adhesion receptors (*6, 7*). The syndecan family is composed of four members and binds to a variety of soluble and solid extracellular effectors (*8, 9*). Their expression is loosely limited as to cell types, that is, syndecan-1, -2, and -3 are the major syndecans of epithelial, fibroblastic and neuronal cells, respectively, whereas syndecan-4 is ubiquitous (*10–12*). Furthermore, during embryogenesis and morphogenesis, their expression is regulated spatially and temporally, and most cells and tissues express multiple syndecans, suggesting that the respective members might have their own individual functions, whether similar or distinct. However, their functional differences or specificities are still poorly understood.

As a cell adhesion receptor, syndecan-4 has been most studied in the family. It has been demonstrated that syndecan-4 is concentrated in focal adhesions together with integrins in cultured fibroblasts (*13*), and that it activates protein kinase C by binding with phosphatidylinositol-4,5-bisphosphate (*14, 15*). Therefore, its function was suggested to be ensuring of the focal adhesion structure through recruitment of a variety of cytoplasmic proteins through protein kinase C (*16–18*). Meanwhile, we have found that syndecan-2 also acts as a cell adhesion receptor. Using mouse Lewis lung carcinoma-derived clones with different metastatic potentials, we observed that more than 85% of the heparan sulfate proteoglycans that bound to immobilized fibronectin was syndecan-2 (*19*), and demonstrated that syndecan-2 cooperates with integrin α5β1 by interacting with fibronectin through the $[IdoA(2OS)\text{-}GlcNS(6OS)]_6$ structure in its heparan sulfate side chains, and that it regulates the actin cytoskeletal organization of the cells on a fibronectin substratum (*20*). Two clones, P29 with low metastatic potential and

*To whom correspondence should be addressed. Tel: +81-52-951-1111, Fax: +81-52-951-0664, E-mail: ogurik@fbe.freeserve.ne.jp

high expression of syndecan-2, and LM66-H11 with high metastatic potential and low expression of syndecan-2, showed different actin architectures on adhesion to the fibronectin substratum; the former exhibited stress fiber formation, whereas the latter formed cortex actin. Furthermore, suppression of syndecan-2 in P29 cells, due to antisense oligonucleotide treatment, resulted in the formation of cortex actin (*20*), while overexpression of syndecan-2 on LM66-H11 cells due to cDNA transfection resulted in the formation of stress fibers (*21*). However, the level of integrin α5β1 expression did not change in either case (*20, 21*). These results indicate that syndecan-2 regulated the ligand-binding signaling through integrin α5β1 in an expression level-dependent manner. However, we also found that both clones expressed the other three syndecans at the transcriptional level although the expression of syndecan-3 was extremely low, and that the expression levels were very similar between the clones except for that of syndecan-2 (*21*). In the present study, we used these clones to investigate the involvement of cell surface heparan sulfate proteoglycans other than syndecan-2 in actin cytoskeletal organization.

EXPERIMENTAL PROCEDURES

Materials—Human plasma fibronectin was purchased from Iwaki Glass (Tokyo). A recombinant fibronectin polypeptide, C-274 (Pro^{1239}–Ser^{1515}), with an RGD-containing Cell-I domain, was generously provided by TaKaRa Biomedicals (Otsu) (*21, 22*). Monoclonal antibodies, F58–10E4 and F69–3G10, recognizing intact heparan sulfate and an epitope generated in heparitinase-digested heparan sulfate proteoglycans, respectively, along with heparitinase-I [EC 4.2.2.8] and chondroitinase ABC [EC 4.2.2.4], were purchased from Seikagaku Corp. (Tokyo). Phosphatidylinositol-specific phospholipase C [EC 3.1.4.10] from *Bacillus thuringensis* was obtained from Funakoshi (Tokyo). Antisense phosphorothioate oligonucleotides complementary to mouse syndecan-2 mRNA, and the corresponding sense and scrambled antisense phosphorothioate oligonucleotides were used as described (*20*).

Cell Culture—Low metastatic P29 and highly metastatic LM66-H11 cells cloned from mouse Lewis lung carcinoma (3LL) were maintained in Dulbecco's modified Eagle's medium (DMEM) supplemented with 10% (v/v) fetal calf serum (FCS) (GIBCO, NY), streptomycin (100 μg/ml), and penicillin (100 units/ml), as described previously (*19*). H11-SN2 and H11-Vec cells, which are LM66-H11 cells transfected with mouse syndecan-2 cDNA and the vector, respectively, were produced as described previously (*21*), and were cultured in the above medium supplemented with geneticin (800 μg/ml). Cell layers were rinsed with phosphate-buffered saline (PBS), and cells were harvested after incubation with 2 mM EDTA in PBS at 37°C for 10 min, followed by gentle flushing with a pipette. The suspended cells were subcultured or used for experiments.

Flow Cytometrical Assay—Cells [3×10^5 cells suspended in 50 μl of 0.2% bovine serum albumin (BSA)/DMEM] were incubated with antibodies or the respective non-immune sera at 4°C for 1 h with gentle agitation. After washing three times with PBS, they were exposed to FITC-conjugated second antibodies for 30 min. The labeled cells were washed, and then the fluorescence intensity was measured by flow cytometry, using an Ortho Cytoron (Ortho Diagnostic Systems).

Preparation of Antibodies to Ectodomains of Syndecan-1, -3, and -4—Rabbit antibodies, SN1Ab, SN3Ab, and SN4Ab, specific to the ectodomains of the mouse syndecan-1, -3, and -4 core proteins, respectively, were raised against the respective recombinant polypeptides, as described previously for the preparation of anti-mouse syndecan-2 (SN2Ab) (*20*). Briefly, recombinants were prepared by expressing cDNAs encoding the respective ectodomains of the mouse syndecan-1, -3, and -4 core proteins in *Escherichia coli*, XL1-Blue (Stratagene), using glutathione S-transferase (GST) gene fusion vector pGEX-2T (Amersham Pharmacia Biotech). The cDNAs were amplified by RT-PCR from polyadenylated RNA of P29 cells with primer pairs, which corresponded to the two ends of the ectodomain of each syndecan, 5′-GAGGATCCCAAATTGTGGCTGTAAATGTTCCTC-3′ and 5′-GAGAATTCTTCCTTCCTGTCCAAAAGGC-3′ for syndecan-1,5′-GAGGATCCGCTCAACGCTGGCGCAATG A-3′ and 5′-GAGAATTCCTCCTTCCGCTCTAGTATGC-3′ for syndecan-3, and 5′-GAGGATCCGAGTCGATTCGAGAGACAGAG-3′ and 5′-GAGAATTCCTCAGTTCTCTCAAAGATGTTGC-3′ for syndecan-4. GST-fused proteins were purified by glutathione-Sepharose affinity chromatography and digested with thrombin to cleave the fusion site. Recombinant proteins were separated by rechromatography on the same column and purified further on a Q-Sepharose column. Their N-terminal amino acid sequences were confirmed with a Model 492 protein sequencer (Applied Biosystems). Rabbits (Std: NZW, Japan SLC K.K., Hamamatsu) were immunized with the purified polypeptides to obtain antisera as described previously (*20*). IgG fractions precipitated with 50% ammonium sulfate from the antisera were further purified by Protein A-Sepharose 4FF chromatography. To obtain antibodies specific for each antigen, the IgGs were passed sequentially through HiTrap columns linked with the other three members of the syndecan family, and unbound fractions were finally applied to columns linked with the antigen itself. The bound materials were eluted with 0.1 M glycine HCl buffer, pH 3.0, the volumes were adjusted to the original serum volume, and the materials were then used as SN1Ab, SN3Ab, and SN4Ab. The specificities and avidities of the respective antibodies were tested by ELISA. The wells of a 96-well plate were coated with 2.5 μg/50 μl of the antigen polypeptides at 4°C overnight, and then blocked with 1% BSA/PBS at 37°C for 1 h. Antibodies at various concentrations were added and then the plates were incubated at 37°C for 1 h. After the wells had been washed with 0.05% Tween 20/PBS (PBST) 3 times, horseradish peroxidase-conjugated second antibodies were added and then the plates were incubated at 37°C for 1 h. Color was developed by the addition of H_2O_2 and TMB-ELISA (Life Technologies). The reaction was stopped by adding 2.0 M H_2SO_4, and then the absorbance at 450 nm was measured.

Western Blotting of Cell Surface Heparan Sulfate Proteoglycans—Cell surface proteoglycans were extracted from P29 and LM66-H11 cell layers with 2% Triton X-100/25 mM KCl/50 mM Tris-HCl, pH 7.3, containing 10 mM EDTA/10 mM *N*-ethylmaleimide/1 mM phenylmeth-

ylsulfonyl fluoride/0.036 mM pepstatin A as proteinase inhibitors, for 12 h on ice, and then purified as described previously (*20*). Briefly, after the removal of insoluble materials by centrifugation at 65,000 ×*g* for 30 min at 4°C, the proteoglycan fraction was obtained by DEAE-Sephacel column chromatography and then applied to an Octyl-Sepharose 4B column. The bound hydrophobic proteoglycans were eluted with a linear concentration gradient of 0–0.5% Triton X-100 in 4 M guanidinium HCl/50 mM Tris-HCl, pH 7.3. Cell surface heparan sulfate proteoglycans were purified from this fraction by immunoaffinity chromatography on an F58–10E4-linked HiTrap column. Samples were digested with heparitinase-I plus chondroitinase ABC to remove glycosaminoglycan side chains as described previously (*19*), and then subjected to SDS-PAGE followed by transfer to Hybond-P membranes (Amersham Pharmacia Biotech). The membranes were blocked with 10% skim milk in PBST for 1 h and then reacted with F69–3G10, SN1Ab, SN2Ab, SN3Ab, or SN4Ab for 1 h. After washing with PBST, the membranes were reacted with horseradish peroxidase-conjugated second antibodies for 1 h and then stained with Immunostain (Konica). Quantification of the bands was performed using the public-domain NIH Image program in a 256-gray-scale mode.

Amino Acid Sequence Analysis—The core proteins of cell surface heparan sulfate proteoglycans and recombinant polypeptides were electrophoresed, blotted onto ProBlott membranes (Applied Biosystems), and then stained with Ponceau S (Sigma-Aldrich). The stained bands were cut out and treated with 0.004% trypsin (Worthington Biochemical) at 37°C overnight. The peptides generated were separated by HPLC on a YMC-Pack AM303 column (Shimadzu, Kyoto) as described previously (*23*). The amino acid sequences of the peptide fragments were determined with a Model 492 protein sequencer (Applied Biosystems).

Treatment of Cells with Phosphatidylinositol-Specific Phospholipase C—Cells suspended in DMEM were digested with six concentrations (0, 0.5, 1, 5, 10, and 100 mU/ml) of phosphatidylinositol-specific phospholipase C at 37°C for 15 min, and then separated from the supernatants by centrifugation. The supernatants were desalted by dialysis against water and then concentrated by lyophilization. Aliquots of the cells were then inoculated onto fibronectin-coated cover glasses, incubated for 1 h in the presence or absence of the enzyme at the different concentrations, and then fixed and stained to visualize the actin cytoskeleton as described below. The hydrophobic proteoglycans were extracted from the remaining cells as described above. Samples were digested with or without heparitinase-I plus chondroitinase ABC, and the core proteins thus generated were electrophoresed and immunoblotted with F69–3G10 as described above.

Actin Cytoskeleton Staining—Cover glasses were coated with: (i) fibronectin (50 μg/ml); (ii) combinations of C-274 (500 μg/ml) and antibodies, *i.e.* SN1Ab (dilution, 1:900), SN2Ab (1:150), SN3Ab (1:150), or SN4Ab (1:15); or (iii) the individual antibodies alone overnight at 4°C, and then blocked with 0.2% BSA/PBS at room temperature for 30 min. The concentrations of the antibodies coating the cover glasses were determined as the avidity of each antibody, as calculated from the results of ELISA (Fig. 2A). Cells (5×10^3 cells in 50 μl of 0.2% BSA/DMEM) were inoculated onto the cover glasses and then incubated for 1 h at 37°C under a humidified 5% CO_2 atmosphere. They were then fixed in 3.7% paraformaldehyde containing 0.1% Tween-20 for 5 min, and treated in 0.1 M NH_4Cl for 10 min at room temperature. Actin filaments were stained with rhodamine-conjugated phalloidin (Molecular Probes) for 30 min at room temperature, and specimens were observed under a fluorescence microscope. When necessary, the number of cells per unit area was determined.

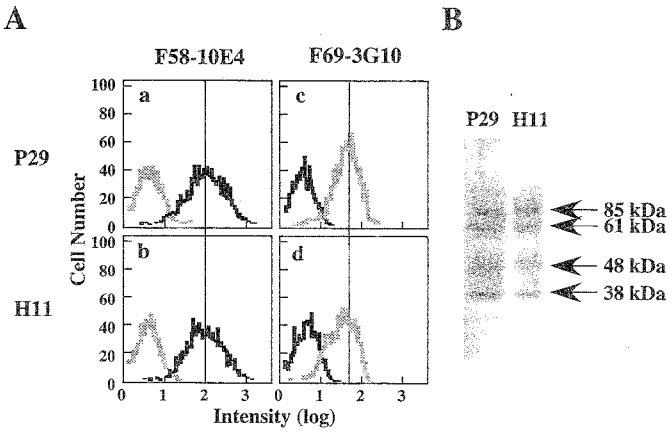

Fig. 1. **Expression of cell surface heparan sulfate proteoglycans on P29 and LM66-H11 cells.** (A) Flow cytometrical analysis. P29 (a, c) and LM66-H11 (H11) (b, d) cells were treated with (gray line) or without (black line) heparitinase-I (100 mU/ml) for 15 min at 37°C. The cells were reacted with F58-10E4 (a, b) or F69-3G10 (c, d) for 1 h at 4°C, followed by reaction with FITC-conjugated second antibodies for 30 min. The intensity of fluorescence was measured with a flow cytometer. (B) Western blot analysis. The hydrophobic heparan sulfate proteoglycans purified from P29 and LM66-H11 (H11) cells were digested with heparitinase-I (40 mU/ml) plus chondroitinase ABC (40 mU/ml) to obtain the core proteins, which were subjected to SDS-PAGE and then transferred to a membrane. The membrane was treated with F69-3G10 for 1 h, incubated with horseradish peroxidase-conjugated second antibodies for 1 h and then stained with Immunostain.

RESULTS

Identification of Cell Surface Heparan Sulfate Proteoglycan Species Expressed on P29 and LM66-H11 Cells—Our previous report (*21*) clearly demonstrated that the level of syndecan-2 expression is a primary factor in the induction of different types of actin cytoskeleton in Lewis lung carcinoma-derived cells adhered to a fibronectin substratum. However, the other members of the syndecan family were also transcribed in the two clones, although the levels in the two clones were very similar. Thus, we first analyzed the cell surface expression of all heparan sulfate proteoglycans. Flow cytometrical analysis demonstrated that the expression levels on the cell surface were not significantly different between the two clones (Fig. 1A). The epitope for F58–10E4, which recognized *N*-sulfated glucosamine in heparan sulfate (*24*), disappeared completely on heparitinase-I digestion (Fig. 1A, a and b). F69–3G10, on the other hand, only reacted after the enzyme digestion (Fig. 1A, c and d). This anti-

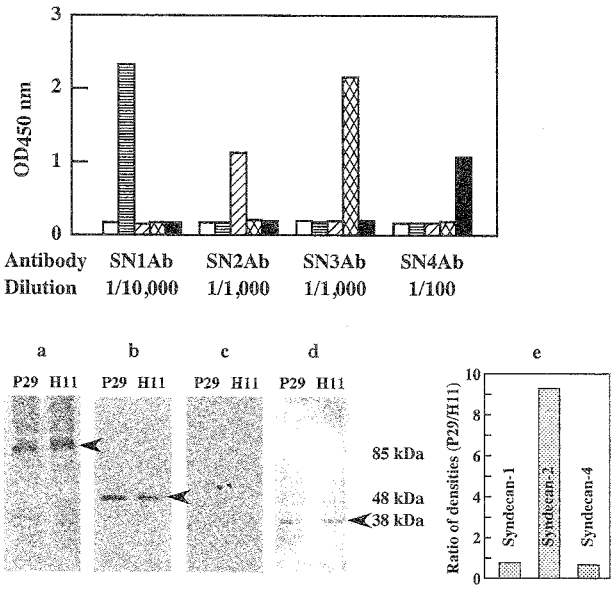

C $G^{43}FSLSDVP^{50}$
$L^{96}QA^{98}$
$T^{121}LQEAFPGAFGDLYTQN^{137}$
$L^{424}PEVMG^{429}$

Fig. 2. **Identification of cell surface heparan sulfate proteoglycans produced by P29 and LM66-H11 cells.** (A) Specificity and avidity of the synthesized antibodies against four mouse syndecans. The wells of a 96-well plate were coated with 2.5 μg of BSA (white bars), or the ectodomain of recombinant polypeptides of syndecan-1 (horizontally lined bars), -2 (slantly lined bars), -3 (crossed lined bars), or -4 (black bars). Various concentrations of SN1Ab, SN2Ab, SN3Ab and SN4Ab were reacted at 37°C for 1 h, followed by the addition of the horseradish peroxidase-conjugated second antibodies. Color was developed by TMB-ELISA. The data shown are representative in showing absorbance of around 1 to 2 at 450 nm. The fractions indicate the dilutions of the antibodies, the original serum volume being taken as 1. (B) Western blot analysis of syndecans. The proteoglycans purified from P29 and LM66-H11 (H11) cells were digested with heparitinase-I plus chondroitinase ABC to obtain the core proteins, which were subjected to SDS-PAGE, transferred to a membrane, and then immunostained with SN1Ab (a), SN2Ab (b), SN3Ab (c), or SN4Ab (d). The densities of the syndecan-1, -2, and -4 bands were quantified using the NIH Image program, and the ratios of the respective bands in P29 and LM66-H11 cells were calculated (e). (C) N-Terminal amino acid sequences of the four fragments derived from the 61 kDa protein (Fig. 1B) digested with trypsin. The numerals indicate the amino acid positions in mouse glypican-1.

body recognizes unsaturated disaccharides at the nonreducing ends of heparan sulfate chains, which are generated on heparitinase-I digestion. Therefore, its reactivity is thought to reflect the number of heparan sulfate chains. These results suggest that the difference in syndecan-2 expression between the two clones is small considering the expression of all cell surface heparan sulfate proteoglycans. We next analyzed the molecular species of cell surface heparan sulfate proteoglycans of the two clones. The core proteins generated from the hydrophobic proteoglycans on digestion with heparitinase-I plus chondroitinase ABC were separated by SDS-PAGE and then immunoblotted with F69-3G10 (Fig. 1B). Four bands corresponding to molecular masses of 85, 61, 48, and 38 kDa were detected for both clones. Among them, the 48 kDa protein exhibiting different expression levels in the two clones was identified as syndecan-2 (*25*). To identify the other materials, we produced polyclonal antibodies, SN1Ab, SN2Ab, SN3Ab, and SN4Ab, specific to recombinant polypeptides of the ectodomains of syndecan-1, -2, -3, and -4, respectively. The avidities of these four antibodies varied within a range of 10^2 in dilution (Fig. 2A). Western blot analyses with the respective antibodies revealed that the 85 and 38 kDa bands were syndecan-1 and -4, respectively (Fig. 2B, a and d), and confirmed that the 48 kDa band was syndecan-2 (Fig. 2B, b). Syndecan-3 was not detectable in either clone (Fig. 2B, c). Comparison of the individual band densities between P29 and LM66-H11 cells demonstrated that the expression levels are very similar between the two clones except for that of syndecan-2 (more than 9 times higher in P29 cells) (Fig. 2B, e), consistent with their mRNA expression levels (*21*).

To identify the 61 kDa band material, we attempted to determine its N-terminal amino acid sequence but were unable to do so, suggesting that the N-terminus of the intact molecule was blocked. Accordingly, we digested it with trypsin and obtained four fragments. As the N-terminal amino acid sequences of the fragments were homologous to partial sequences of mouse glypican-1, the 61 kDa band was identified as glypican-1 (Fig. 2C). With this procedure, using a sample prepared from 1.5×10^9 cells, the bands of syndecan-1, -2, and -4 were not detectable on separation by electrophoresis, suggesting that glypican-1 is the most abundant cell surface heparan sulfate proteoglycan. Therefore, we next examined the participation of glypican-1 in actin cytoskeletal organization.

Participation of Glypican-1 in Actin Cytoskeletal Organization—The glypican family is another type of cell surface heparan sulfate proteoglycan that anchors to the cell surface through glycosyl phosphatidylinositol. Glypicans can thus be released from the cell surface by digestion with phosphatidylinositol-specific phospholipase C (PI-PLC). To determine the possible participation of glypican-1 in actin cytoskeletal organization, cells were treated with PI-PLC to remove it. As expected, the 61 kDa band material disappeared from the cell surface on PI-PLC digestion (Fig. 3A, lanes 2 and 3), and three bands corresponding to molecular masses of 61, 59, and 56 kDa (Fig. 3A, lane 7) were observed in the supernatant. The latter two band materials were small in quantity, but were detected in the supernatant without PI-PLC-digestion (Fig. 3A, lane 6), suggesting that degradation or shedding due to proteolytic enzyme(s) occurred naturally. PI-PLC digestion affected neither stress fiber formation in P29 cells (Fig. 3B, a and c) nor cortex actin formation in LM66-H11 cells (Fig. 3B, b and d) on a fibronectin substratum. No effect was observed at any enzyme concentration (up to 100 mU/ml) (data not shown). These results indicate that glypican-1 does not play a role in the actin cytoskeletal organization in these cells on fibronectin, despite its predominance among heparan sulfate proteoglycans on the cell surface.

Ability of Each Syndecan to Cooperate with Integrin α5β1 to Induce Stress Fiber Formation—Using a mixed substratum comprising C-274 and SN2Ab, we previously demonstrated that stimulation of syndecan-2 through its core protein was equivalent to that through its heparan

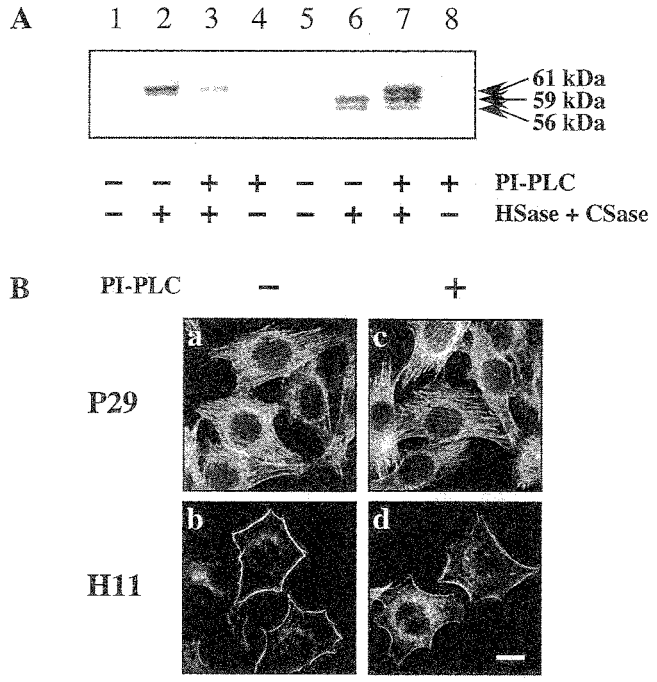

Fig. 3. **Participation of glypican-1 in actin cytoskeletal organization.** (A) Western blot analysis of glypican-1 in P29 cells before and after digestion with phosphatidylinositol-specific phospholipase C (PI-PLC). P29 cells were treated with (lanes 3, 4, 7, and 8) or without (lanes 1, 2, 5, and 6) 10 mU/ml of PI-PLC for 15 min at 37°C. Cell (lanes 1–4) and supernatant (lanes 5–8) fractions were then treated with (lanes 2, 3, 6, and 7) or without (lanes 1, 4, 5, and 8) heparitinase-I (HSase) plus chondroitinase ABC (CSase). After being subjected to SDS-PAGE, samples were immunoblotted with F69-3G10. (B) Effect of PI-PLC digestion on the actin cytoskeletal organization of P29 and LM66-H11 cells on a fibronectin substratum. P29 (a, c) and LM66-H11 (H11) (b, d) cells treated with (c, d) or without (a, b) PI-PLC as described in (A) were inoculated on cover glasses coated with fibronectin, incubated at 37°C for 1 h, fixed and then stained with rhodamine-conjugated phalloidin. Bar, 20 μm.

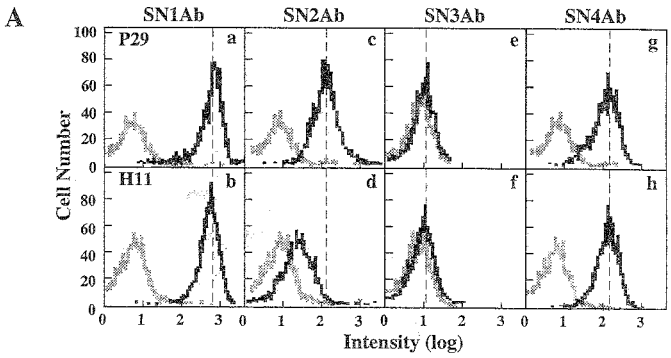

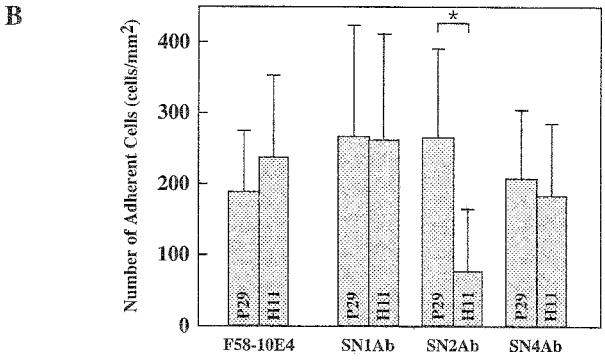

Fig. 4. **Comparison of cell surface expression of syndecans and cell adhesion to antibody-substrata between P29 and LM66-H11 cells.** (A) Flow cytometrical analyses of syndecans. P29 (a, c, e, g) and LM66-H11 (H11) (b, d, f, h) cells were treated with SN1Ab (a, b), SN2Ab (c, d), SN3Ab (e, f), or SN4Ab (g, h) for 1 h at 4°C, and then with FITC-conjugated second antibodies for 30 min. The intensity of fluorescence was measured with a flow cytometer. The peaks with gray lines are for control samples reacted with non-immune serum as the first antibodies. (B) Attachment of cells to immobilized antibodies. P29 and LM66-H11 (H11) cells were inoculated onto cover glasses coated with F58–10E4, SN1Ab, SN2Ab or SN4Ab, and then incubated at 37°C for 1 h. Cells that become attached were fixed and stained with rhodamine-conjugated phalloidin. The number of cells adhering to each substratum was determined in six randomly selected areas in two different specimens. The asterisk indicates a significant difference ($p < 0.0001$).

sulfate side chains in actin cytoskeletal organization (*21*). Therefore, we carried out a similar assay to clarify the participation of the individual syndecans in this signaling. Firstly, we examined the cell surface expression of the individual syndecans (Fig. 4A). The expression levels of syndecan-1 (Fig. 4A, a and b) and syndecan-4 (Fig. 4A, g and h) were very similar, but syndecan-3 expression was scarcely observed in either clone (Fig. 4A, e and f). Only syndecan-2 exhibited significantly different expression levels between the two clones (about 10 times higher in P29 cells) (Fig. 4A, c and d). These results are consistent with the translation (Figs. 1B and 2B) and transcription levels (*21*). Next, to verify that the immobilized antibodies were able to function as solid ligands, we carried out a cell adhesion assay (Fig. 4B). P29 cells adhered to SN1Ab, SN2Ab, and SN4Ab at the same levels as to an F58-10E4 substratum, indicating that each substratum is able to function in the binding of cells through the respective antigens. Only the adhesion of LM66-H11 cells to SN2Ab was significantly lower than that of P29 cells ($p < 0.0001$), whereas the adhesion to other substrata was similar for the two clones, suggesting that cell adhesion to the immobilized antibodies reflected the cell surface expression levels of syndecans. We then analyzed the cytoskeletal organization of the cells on substrata comprising C-274 and each antibody.

On C-274, both cell types formed cortex actin, indicating that the signal mediated by integrin α5β1 alone resulted in cortex actin formation (Fig. 5, a and b). As expected from the very low expression levels of syndecan-3, SN3Ab did not affect this signaling pathway (Fig. 5, g and h), and the cells showed similar responses to those on C-274 alone. The fact that P29 cells, which hardly express syndecan-3, form stress fibers on a fibronectin substratum indicates that syndecan-3 is not essential for stress fiber formation. In spite of the higher expression levels of syndecan-1, both cell types on the substratum containing SN1Ab (Fig. 5, c and d) showed similar responses to those on C-274 alone, indicating that the stimulation of syndecan-1 was not sufficient to modify the integrin α5β1-signaling. SN2Ab was a sufficient stimulus for the induction of stress fiber formation in P29 cells (Fig. 5e) but not in LM66-H11 cells (Fig. 5f), as shown in our previous report (*21*), indicating that the

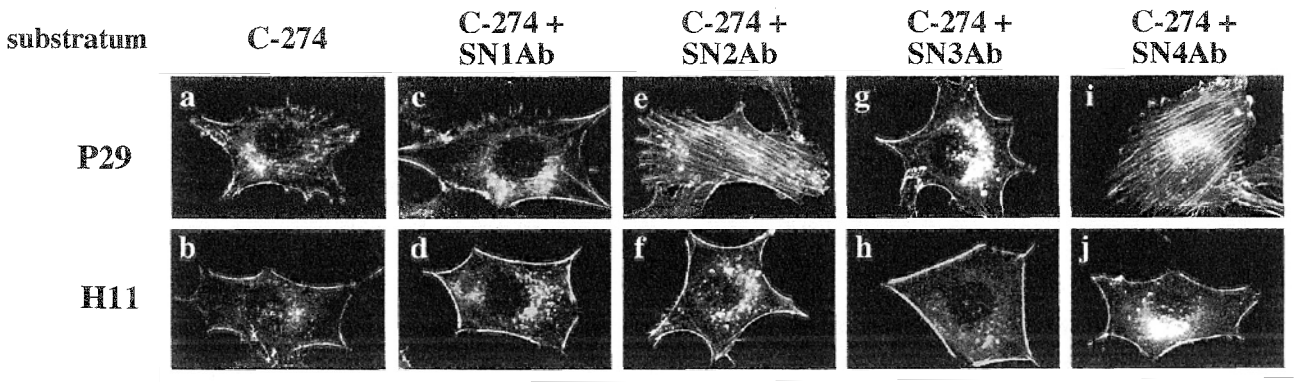

Fig. 5. **Ability of each syndecan to modify the signal through integrin α5β1 in actin cytoskeletal organization.** P29 (a, c, e, g, i) and LM66-H11 (H11) (b, d, f, h, j) cells were inoculated onto cover glasses coated with C-274 (a, b), or a mixture of C-274 and SN1Ab (c, d), SN2Ab (e, f), SN3Ab (g, h), or SN4Ab (i, j), and then incubated at 37°C for 1 h. Cells were fixed and stained with rhodamine-conjugated phalloidin. The photographs presented show typical actin cytoskeletal organization in the cells. Almost all the cells on each substratum exhibited the respective patterns in the figures.

ability of syndecan-2 to modify the signal through integrin α5β1 depends on its expression level. Although cell adhesion to SN2Ab reflected the expression level of syndecan-2 in the cells (Fig. 4B), the number of adherent cells on a mixed substratum of C-274 and SN2Ab was almost the same for the two clones (data not shown). This was expected because 91% of the P29 cells and 85% of the LM66-H11 cells adhered to the C-274 substratum (*21*).

Interestingly, the cytoskeletal organizations of the cells on a mixed substratum of C-274 and SN4Ab (Fig. 5, i and j) were very similar to those on C-274 and SN2Ab, in spite of the similar expression levels of syndecan-4 (Fig. 4A, g and h). The fact that P29 cells formed stress fibers on the mixed substratum of C-274 and SN4Ab indicated that stimulation of syndecan-4 by the antibodies was sufficient to modify the signal through integrin α5β1 (Fig.

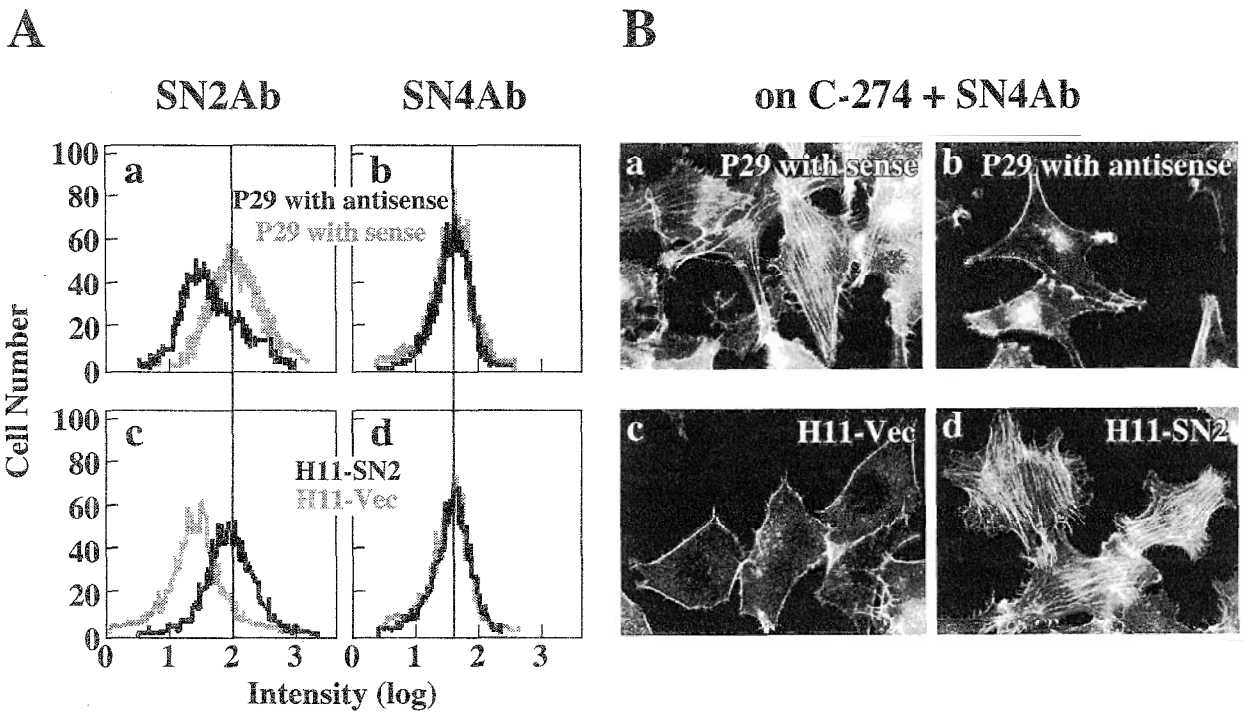

Fig. 6. **Requirement of syndecan-2 expression for stress fiber formation induced by syndecan-4-stimulation.** (A) Flow cytometrical analyses of syndecan-2 and -4 expression on cells in which syndecan-2 expression had been manipulated artificially. P29 cells (a, b) pretreated with antisense (black line) or sense (gray line) oligonucleotides of syndecan-2 mRNA for 4 days, and the cloned transfectant of LM66-H11 cells (c, d) with cDNA of syndecan-2 (H11-SN2, black line) or the vector only (H11-Vec, gray line), were treated with SN2Ab (a, c) or SN4Ab (b, d) for 1 h at 4°C, and then treated with FITC-conjugated second antibodies for 30 min. The intensity of fluorescence was measured with a flow cytometer. (B) Actin cytoskeleton in cells on a mixed substratum of C-274 and SN4Ab. P29 cells treated with sense (a) or antisense (b) oligonucleotides of syndecan-2 mRNA and H11-Vec (c) or H11-SN2 (d) were inoculated onto cover glasses coated with the mixed substratum, and then incubated at 37°C for 1 h. The cells were fixed and stained with rhodamine-conjugated phalloidin.

5i). However, LM66-H11 cells were not induced to form stress fibers (Fig. 5j), suggesting that the signal through syndecan-4 is correlated with syndecan-2 in an expression level-dependent manner, and that syndecan-2 might be situated downstream of syndecan-4. These results suggest the possibility of crosstalk between syndecan-2 and syndecan-4.

Implication of Syndecan-2 in the Syndecan-4 Signaling Pathway—To assess the possible interaction between the two species of syndecans, cells in which syndecan-2 expression was artificially regulated were plated on a substratum comprising C-274 and SN4Ab. Treatment of P29 cells with the antisense oligonucleotide of syndecan-2 mRNA for 4 days resulted in suppression of syndecan-2 expression (Fig. 6A, a), but did not significantly affect the expression of syndecan-4 (Fig. 6A, b) or syndecan-1 (data not shown). Conversely, transfection of syndecan-2 cDNA into LM66-H11 cells increased the expression of syndecan-2 (Fig. 6A, c), but not that of syndecan-4 (Fig. 6A, d) or syndecan-1 (data not shown). The cells with higher expression levels of syndecan-2, regardless of the clone or manipulation, were able to induce stress fiber formation on a mixed substratum of C-274 and SN4Ab (Fig. 6B, a and d). In contrast, the cells with low expression levels of syndecan-2 failed to form stress fibers but formed cortex actin instead (Fig. 6B, b and c). These results confirmed that the expression level of syndecan-2 regulates the signal through syndecan-4, strongly suggesting that there is crosstalk between the two syndecans, and that syndecan-2 might be situated downstream of syndecan-4.

DISCUSSION

Our previous reports (*20*, *21*) clearly demonstrated that the signal organizing the actin cytoskeleton in Lewis lung carcinoma-derived cells adhering to a fibronectin substratum is mediated through integrin $\alpha5\beta1$ and syndecan-2 in a dual receptor system. Signal transduction is possible both independently and cooperatively for each receptor. Thus, a signal mediated only by integrin $\alpha5\beta1$ or syndecan-2 resulted in either the formation of cortex actin or filopodia, whereas a signal mediated by both receptors resulted in stress fiber formation. Furthermore, it became evident that the signals had no effect when the expression level of syndecan-2 had not reached a threshold, regardless of whether syndecan-2 acts independently or cooperatively with integrin $\alpha5\beta1$. In our earlier study, we also found that other members of the syndecan family are transcribed in these cells. This prompted us to explore the possibility of their participation in this signaling pathway.

In the present study, we demonstrated that the two clones expressed four types of cell surface heparan sulfate proteoglycans; syndecan-1, syndecan-2, syndecan-4, and glypican-1. The most predominant one, glypican-1, clearly showed no participation in the signaling pathway linked to actin cytoskeletal organization in Lewis lung carcinoma cells. Functional differences between syndecans and glypicans have been demonstrated by several studies involving transfection techniques. For example, overexpression of syndecan-1, -2, or -4 on ARH-77 cells resulted in non-invasive and type I collagen-binding cells, whereas glypican-1 overexpressers were invasive and did not bind to collagen as the parent cells did (*26*). Moreover, 293T cells transfected with syndecan-2 or -4, but not glypican-1, adhered to the heparin binding domain of the laminin $\alpha3$ chain (*27*). These phenomena might be expected since signaling mediated by syndecans is thought to be transduced through their clustering, which is caused extracellularly by binding with ligands and intracellularly by binding with PDZ proteins (*28–32*), whereas glypicans are not transmembrane-type but glycosyl phosphatidylinositol-anchored proteoglycans. From these results, it is clear that glypicans perform a function(s) distinct from that/these of syndecans.

The second question is whether the individual members of the syndecan family co-existing on the same cells function differently. To clarify this, there are the following three requirements: (i) cells exhibiting expression of multiple syndecans; (ii) tools able to stimulate individual syndecans; and (iii) a bioassay system. The Lewis lung carcinoma system used here satisfies all three criteria: (i) Lewis lung carcinoma cells express syndecan-1, -2, and -4; (ii) we have prepared antibodies that can act as solid ligands for the respective syndecans; and (iii) we have already established an assay system for distinguishing different signaling. The results obtained here clearly show that each syndecan plays a different role. Syndecan-1 does not appear to be essential for the signal transduction that is dependent on substratum adhesion. The fact that syndecan-1 is located on the lateral surface of basal cells in cuboidal and columnar epithelia (*33*) would suggest that it plays a role in cell-to-cell adhesion. This idea is supported by the reports of the loss of syndecan-1 in poorly differentiated tumors (*34*, *35*).

The participation of syndecan-4 as a cell adhesion receptor in actin cytoskeletal organization is very interesting. The stimulation by immobilized C-274 and SN4Ab was sufficient to induce stress fiber formation in P29 cells but not in LM66-H11 cells, despite the similar levels of syndecan-4 expression. Furthermore, the two clones with artificially altered syndecan-2 expression levels formed converse actin cytoskeletal organizations on the same substratum. These results strongly suggest that the signal through syndecan-4 is regulated downstream by syndecan-2. Couchman and colleagues found that binding of phosphatidylinositol-4,5-bisphosphate (PIP_2) to the variable region of the cytoplasmic domain of syndecan-4, but not that of syndecan-2, regulates protein kinase Cα (PKCα) activity, and that the activated PKCα recruits cytoplasmic proteins to focal adhesions (*15*). Zimmermann *et al.* reported that the PDZ domains of syntenin, which are able to bind to the EFYA sequence common to all members of the syndecan family, concentrate PIP_2 and syndecans at the plasma membrane (*36*). It has also been reported that a synthetic peptide of the syndecan-2 cytoplasmic domain, but not that of syndecan-4, can be a substrate for PKCα, and that the level of phosphorylation is dependent on multimerization of the peptide (*37*, *38*). Furthermore, we previously demonstrated that a serine residue(s) of the syndecan-2 cytoplasmic domain purified from P29 cells is phosphorylated (*25*). Taken together, these results suggest that the signal through syndecan-4 is regulated downstream by syndecan-2 in a quantity-dependent manner, and that there may be a possible cascade in which PKCα activated by

syndecan-4 phosphorylates the cytoplasmic domain of syndecan-2. This supposition strongly supports the report (*39*) that syndecan-4-null fibroblasts form focal adhesions and stress fibers on a fibronectin substratum, even if syndecan-4 is evident in focal adhesions of normal fibroblasts, such as human and rat embryo fibroblasts (*13*). In this signal transduction, syndecan-2, rather than syndecan-4, seems to be a key molecule.

One possible origin of such a functional difference among syndecans is the specificity of the ligand binding site of heparan sulfate of each molecule. Among the cell surface heparan sulfate proteoglycans produced by P29 cells, syndecan-2 accounts for more than 85% of the syndecans that can bind to immobilized fibronectin (*19*). Furthermore, the cells bind to the Hep-II domain of fibronectin through the $[IdoA(2OS)\text{-}GlcNS(6OS)]_6$ structure in heparan sulfate chains (*20*). At least in Lewis lung carcinoma cells, this structure or cluster(s) of the structure in heparan sulfate side chains may be unique to syndecan-2. The functional specificity of syndecans can also be explained by the difference in cytoplasmic proteins bound to the cytoplasmic domain of each syndecan stimulated with extracellular ligands. Syntenin (*28*, *32*), CASK/LIN-2 (*29*, *30*), and synectin (*31*) can bind to the EFYA sequence common to all members of the syndecan family through their PDZ domains. However, as with synbindin (*40*) and ezrin (*41*, *42*) for syndecan-2 as well as syndesmos (*43*) for syndecan-4, several cytoplasmic proteins perhaps bind specifically to their cytoplasmic variable regions. Thus, the entire spectrum involving both combinations of various extracellular and intracellular binding proteins and the specific phosphorylation of their cytoplasmic domains appears to play a role in determining the functional specificity of each syndecan. In any case, this is the first report that clearly demonstrates that cell surface heparan sulfate proteoglycans expressed on the same cell function differently and clarifies the cooperation of syndecan-2 and syndecan-4 in actin cytoskeletal organization.

The authors wish to thank Takara Shuzo (TaKaRa Biomedicals) for generously providing the recombinant fibronectin polypeptide C-274. This research was supported by Grants-in-Aid for Cancer Research (11-12 and 15-13) from the Ministry of Health, Labour and Welfare (YK), and Grants-in-Aid for Bio-venture Research Center (MO) and Scientific Research on Priority Areas 1 (KO) from the Ministry of Education, Culture, Sports, Science and Technology of Japan.

REFERENCES

1. Hynes, R.O. (1987) Integrins: a family of cell surface receptors. *Cell* **48**, 549–554
2. Damsky, C.H. and Werb, Z. (1992) Signal transduction by integrin receptors for extracellular matrix: cooperative processing of extracellular information. *Curr. Opin. Cell Biol.* **4**, 772–781
3. Giancotti, F.G. and Ruoslahti, E. (1999) Integrin signaling. *Science* **285**, 1028–1032
4. Woods, A. and Couchman, J.R. (2000) Integrin modulation by lateral association. *J. Biol. Chem.* **275**, 24233–24236
5. Eliceiri, B.P. (2001) Integrin and growth factor receptor crosstalk. *Circ. Res.* **89**, 1104–1110
6. Rapraeger, A.C. (2000) Syndecan-regulated receptor signaling. *J. Cell Biol.* **149**, 995–998
7. Woods, A. (2001) Syndecans: transmembrane modulators of adhesion and matrix assembly. *J. Clin. Invest.* **107**, 935–941
8. Bernfield, M., Gotte, M., Park, P.W., Reizes, O., Fitzgerald, M.L., Lincecum, J., and Zako, M. (1999) Functions of cell surface heparan sulfate proteoglycans. *Annu. Rev. Biochem.* **68**, 729–777
9. Gallagher, J.T. (2001) Heparan sulfate: growth control with a restricted sequence menu. *J. Clin. Invest.* **108**, 357–361
10. Bernfield, M., Kokenyesi, R., Kato, M., Hinkes, M.T., Spring, J., Gallo, R.L., and Lose, E.J. (1992) Biology of the syndecans: a family of transmembrane heparan sulfate proteoglycans. *Annu. Rev. Cell. Biol.* **8**, 365–393
11. David, G., Bai, X.M., Van der Schueren, B., Marynen, P., Cassiman, J.J., and Van den Berghe, H. (1993) Spatial and temporal changes in the expression of fibroglycan (syndecan-2) during mouse embryonic development. *Development* **119**, 841–854
12. Perrimon, N. and Bernfield, M. (2000) Specificities of heparan sulphate proteoglycans in developmental processes. *Nature* **404**, 725–728
13. Woods, A. and Couchman, J.R. (1994) Syndecan-4 heparan sulfate proteoglycan is a selectively enriched and widespread focal adhesion component. *Mol. Biol. Cell* **5**, 183–192
14. Oh, E.S., Woods, A., and Couchman, J.R. (1997) Multimerization of the cytoplasmic domain of syndecan-4 is required for its ability to activate protein kinase C. *J. Biol. Chem.* **272**, 11805–11811
15. Oh, E.S., Woods, A., Lim, S.T., Theibert, A.W., and Couchman, J.R. (1998) Syndecan-4 proteoglycan cytoplasmic domain and phosphatidylinositol-4, 5-bisphosphate coordinately regulate protein kinase C activity. *J. Biol. Chem.* **273**, 10624–10629
16. Couchman, J.R. and Woods, A. (1999) Syndecan-4 and integrins: combinatorial signaling in cell adhesion. *J. Cell Sci.* **112**, 3415–3420
17. Woods, A. and Couchman, J.R. (2001) Syndecan-4 and focal adhesion function. *Curr. Opin. Cell Biol.* **13**, 578–583
18. Baciu, P.C. and Goetinck, P.F. (1995) Protein kinase C regulates the recruitment of syndecan-4 into focal contacts. *Mol. Biol. Cell* **6**, 1503–1513
19. Itano, N., Oguri, K., Nakanishi, H., and Okayama, M. (1993) Membrane-intercalated proteoglycan of a stroma-inducing clone from Lewis lung carcinoma binds to fibronectin *via* its heparan sulfate chains. *J. Biochem.* **114**, 862–873
20. Kusano, Y., Oguri, K., Nagayasu, Y., Munesue, S., Ishihara, M., Saiki, I., Yonekura, H., Yamamoto, H., and Okayama, M. (2000) Participation of syndecan 2 in the induction of stress fiber formation in cooperation with integrin $\alpha5\beta1$: structural characteristics of heparan sulfate chains with avidity to COOH-terminal heparin-binding domain of fibronectin. *Exp. Cell Res.* **256**, 434–444
21. Munesue, S., Kusano, Y., Oguri, K., Itano, N., Yoshitomi, Y., Nakanishi, H., Yamashina, I., and Okayama, M. (2002) The role of syndecan-2 in regulation of actin-cytoskeletal organization of Lewis lung carcinoma-derived metastatic clones. *Biochem. J.* **363**, 201–209
22. Makabe, T., Saiki, I., Murata, J., Ohdate, Y., Kawase, Y., Taguchi, Y., Shimojo, T., Kimizuka, F., Kato, I., and Azuma, I. (1990) Modulation of haptotactic migration of metastatic melanoma cells by the interaction between heparin and heparin-binding domain of fibronectin. *J. Biol. Chem.* **265**, 14270–14276
23. Itoh, N., Tanaka, N., Mihashi, S., and Yamashina, I. (1987) Molecular cloning and sequence analysis of cDNA for batroxobin, a thrombin-like snake venom enzyme. *J. Biol. Chem.* **262**, 3132–3135
24. David, G., Bai, X.M., Van der Schueren, B., Cassiman, J.J., and Van den Berghe, H. (1992) Developmental changes in heparan sulfate expression: *in situ* detection with mAbs. *J. Cell Biol.* **119**, 961–975
25. Itano, N., Oguri, K., Nagayasu, Y., Kusano, Y., Nakanishi, H., David, G., and Okayama, M. (1996) Phosphorylation of a membrane-intercalated proteoglycan, syndecan-2, expressed in a

stroma-inducing clone from a mouse Lewis lung carcinoma. *Biochem. J.* **315**, 925–930
26. Liu, W., Litwack, E.D., Stanley, M.J., Langford, J.K., Lander, A.D., and Sanderson, R.D. (1998) Heparan sulfate proteoglycans as adhesive and anti-invasive molecules. Syndecans and glypican have distinct functions. *J. Biol. Chem.* **273**, 22825–22832
27. Utani, A., Nomizu, M., Matsuura, H., Kato, K., Kobayashi, T., Takeda, U., Aota, S., Nielsen, P.K., and Shinkai, H. (2001) A unique sequence of the laminin α3 G domain binds to heparin and promotes cell adhesion through syndecan-2 and -4. *J. Biol. Chem.* **276**, 28779–28788
28. Grootjans, J.J., Zimmermann, P., Reekmans, G., Smets, A., Degeest, G., Durr, J., and David, G. (1997) Syntenin, a PDZ protein that binds syndecan cytoplasmic domains. *Proc. Natl Acad. Sci. USA* **94**, 13683–13688
29. Cohen, A.R. and Wood, D.F. (1998) Human CASK/LIN-2 binds syndecan-2 and protein 4.1 and localizes to the basolateral membrane of epithelial cells. *J. Cell Biol.* **142**, 129–138
30. Hsueh, Y.P., Yang, F.C., Kharazia, V., Naisbitt, S., Cohen, A.R., Weinberg, R.J., and Sheng, M. (1998) Direct interaction of CASK/LIN-2 and syndecan heparan sulfate proteoglycan and their overlapping distribution in neuronal synapses. *J. Cell Biol.* **142**, 139–151
31. Gao, Y., Li, M., Chen, W., and Simons, M. (2000) Synectin, syndecan-4 cytoplasmic domain binding PDZ protein, inhibits cell migration. *J. Cell Physiol.* **184**, 373–379
32. Zimmermann, P., Tomatis, D., Rosas, M., Grootjans, J., Leenaerts, I., Degeest, G., Reekmans, G., Coomans, C., and David, G. (2001) Characterization of syntenin, a syndecan-binding PDZ protein, as a component of cell adhesion sites and microfilaments. *Mol. Biol. Cell* **12**, 339–350
33. Hayashi, K., Hayashi, M., Jalkanen, M., Firestone, J.H., Trelstad, R.L., and Bernfield, M. (1987) Immunocytochemistry of cell surface heparan sulfate proteoglycan in mouse tissues. A light and electron microscopic study. *J. Histochem. Cytochem.* **35**, 1079–1088
34. Inki, P., Stenback, F., Grenman, S., and Jalkanen, M. (1994) Immunohistochemical localization of syndecan-1 in normal and pathological human uterine cervix. *J. Pathol.* **172**, 349–355
35. Fujiya, M., Watari, J., Ashida, T., Honda, M., Tanabe, H., Fujiki, T., Saitoh, Y., and Kohgo, Y. (2001) Reduced expression of syndecan-1 affects metastatic potential and clinical outcome in patients with colorectal cancer. *Jpn. J. Cancer Res.* **92**, 1074–1081
36. Zimmermann, P., Meerschaert, K., Reekmans, G., Leenaerts, I., Small, J.V., Vandekerckhove, J., David, G., and Gettemans, J. (2002) PIP_2-PDZ domain binding controls the association of syntenin with the plasma membrane. *Mol. Cell* **9**, 1215–1225
37. Prasthofer, T., Ek, B., Ekman, P., Owens, R., Hook, M., and Johansson, S. (1995) Protein kinase C phosphorylates two of the four known syndecan cytoplasmic domains *in vitro*. *Biochem. Mol. Biol. Int.* **36**, 793–802
38. Oh, E.S., Couchman, J.R., and Woods, A. (1997) Serine phosphorylation of syndecan-2 proteoglycan cytoplasmic domain. *Arch. Biochem. Biophys.* **344**, 67–74
39. Ishiguro, K., Kadomatsu, K., Kojima, T., Muramatsu, H., Tsuzuki, S., Nakamura, E., Kusugami, K., Saito, H., and Muramatsu, T. (2000) Syndecan-4 deficiency impairs focal adhesion formation only under restricted conditions. *J. Biol. Chem.* **275**, 5249–5252
40. Ethell, I.M., Hagihara, K., Miura, Y., Irie, F., and Yamaguchi, Y. (2000) Synbindin, a novel syndecan-2-binding protein in neuronal dendritic spines. *J. Cell Biol.* **151**, 53–68
41. Granes, F., Urena, J.M., Rocamora, N., and Vilaro, S. (2000) Ezrin links syndecan-2 to the cytoskeleton. *J. Cell Sci.* **113**, 1267–1276
42. Granes, F., Berndt, C., Roy, C., Mangeat, P., Reina, M., and Vilaro, S. (2003) Identification of a novel Ezrin-binding site in syndecan-2 cytoplasmic domain. *FEBS Lett.* **547**, 212–216
43. Baciu, P.C., Saoncella, S., Lee, S.H., Denhez, F., Leuthardt, D., and Goetinck, P.F. (2000) Syndesmos, a protein that interacts with the cytoplasmic domain of syndecan-4, mediates cell spreading and actin cytoskeletal organization. *J. Cell Sci.* **113**, 315–324

Available online at www.sciencedirect.com
SCIENCE DIRECT®
ELSEVIER
Cancer Letters 207 (2004) 165–174
CANCER Letters
www.elsevier.com/locate/canlet

Inhibition of experimental lung metastases of Lewis lung carcinoma cells by chemically modified heparin with reduced anticoagulant activity

Yasuo Yoshitomi[a], Hayao Nakanishi[b], Yuri Kusano[c], Seiichi Munesue[a], Kayoko Oguri[c], Masae Tatematsu[b], Ikuo Yamashina[a], Minoru Okayama[a,*]

[a]*Department of Biotechnology, Faculty of Engineering, Kyoto Sangyo University, Motoyama Kamigamo, Kita-ku, Kyoto 603-8555, Japan*
[b]*Division of Oncological Pathology, Aichi Cancer Center Research Institute, Chikusa-ku, Nagoya 464-8681, Japan*
[c]*Clinical Research Center, Nagoya National Hospital, Naka-ku, Nagoya 460-0001, Japan*

Received 21 October 2003; received in revised form 20 November 2003; accepted 28 November 2003

Abstract

Heparin, a widely used anticoagulant, is known to have anti-metastatic activity, although the mechanism is not fully understood. In the present study, we investigated the mechanism of this anti-metastatic activity using periodate-oxidized and borohydride-reduced heparin with low anticoagulant activity (LAC heparin). The anticoagulant activity of LAC heparin is markedly reduced to almost the control level in terms of prothrombin time in vitro, and no hemorrhagic complication was observed with injection of LAC heparin into mice in vivo. LAC heparin injected intravenously with Lewis lung carcinoma cells or 10 min before tumor cell injection significantly inhibited, to the same extent as intact heparin and in a dose- and time-dependent manner, the lung colonization that develops after intravenous injection (i.v.) of tumor cells. Flow cytometric analysis revealed that Lewis lung carcinoma cells strongly express heparan sulfate on their surface. Both the LAC heparin and intact heparin inhibited the adhesion and invasion of tumor cells to Matrigel-coated dishes in vitro without significant effect on the tumor cell growth. LAC heparin also significantly diminished tumor cell retention in the lung after i.v. of *Lac* Z gene-tagged Lewis lung carcinoma cells. These results suggest that LAC heparin may prevent tumor cells from attachment to the subendothelial matrix of lung capillaries by competitively inhibiting cell surface heparan sulfate functions and suppress lung colonization.

Keywords: Metastases; Heparin; Chemical modification; Anticoagulant activity; Lewis lung carcinoma; Mouse

1. Introduction

Heparin is a multifunctional, linear, highly sulfated polysaccharide consisting of alternating uronic acid and D-glucosamine residues [1,2]. Although heparin is best known for its anticoagulant properties [3], it affects a variety of physiological processes such as endothelial cell and smooth muscle cell growth, angiogenesis, inflammation and tumor metastasis [4]. The mechanism underlying its anti-coagulant effect is its high affinity binding to

* Corresponding author. Tel.: +81-75-705-1889; fax: +81-75-705-1914.
E-mail address: okayamam@cc.kyoto-su.ac.jp (M. Okayama).

0304-3835/$ - see front matter © 2003 Elsevier Ireland Ltd. All rights reserved.
doi:10.1016/j.canlet.2003.11.037

antithrombin III. This leads to a conformational change in antithrombin III, thereby inactivating the coagulation enzymes. Other activities are consequent on the interaction of heparin with heparin-binding proteins, including chemokines, extracellular matrix (ECM) proteins, growth factors and enzymes [5]. Introduction of chemical modifications has yielded heparins with greatly reduced anticoagulant activity but conserved non-anticoagulant effects. To date, two types of chemical modification have been reported from studies of the anti-metastatic activity of heparins with reduced anticoagulant activities. First, heparin derivatives produced by *N*- and *O*-desulfation followed by *N*-resulfation or *N*-reacetylation exhibit heparanase inhibiting activity and reduce the number of metastatic lung colonies in a murine B16F10 melanoma metastasis model [6,7]. Second group is periodate oxidized heparin or low molecular weight heparin generated by periodate oxidation followed by alkaline-degradation treatment [8,9], which are known for not having a specific pentasaccharide structure to interact with antithrombin III [10]. These periodate-oxidized, reduced [11] and non-reduced heparin [12] inhibited heparanase activity and angiogenic activity of tumor cells and thereby had anti-metastatic activity. Consequently, the anti-metastatic effect of heparin is now considered not to be primarily due to anticoagulant activity, but to result from other biological effects. Although correlations between non-anticoagulant actions of heparin derivatives with such as heparanase- or angiogenesis-inhibition activity and in vivo inhibition of metastasis have been indicated, the exact mechanism of action of these compounds remains to be elucidated.

In the present study, we investigated the effects of periodate-oxidized and borohydride-reduced heparin with low anticoagulant activity on experimental lung metastasis, focusing on its anti-adhesion activity both in vivo and in vitro.

2. Materials and methods

2.1. Animals and drugs

Six to seven week-old C57BL/6 male mice were purchased from Shizuoka Laboratory Animal Center (Hamamatsu, Japan) and maintained in an air-conditioned animal room at 25 °C. Heparin was obtained from porcine intestinal mucosa (Scientific protein laboratories (SPL) Inc, Wisconsin, USA). Heparan sulfate from bovine kidney and chondroitin sulfate A from whale cartilage were purchased from Seikagaku Corp. (Tokyo, Japan).

Chemically modified heparin with reduced antithrombin III binding activity (designated as low anticoagulant heparin; LAC-HP) was prepared by sodium periodate, followed by sodium borohydride treatment of heparin as described previously [10,13]. In brief, 20 g heparin dissolved in 400 ml of 0.1 M $NaIO_4$ in 0.05 M sodium acetate buffer (pH 5.0) was stirred at 4 °C for 72 h. Excess $NaIO_4$ was then destroyed by the addition of glycerol and the reaction mixture was subsequently dialysed against distilled water and lyophilized. The reaction product thus prepared was then resuspended with 0.2 M sodium borohydride in 0.25 M sodium bicarbonate (pH 9.5) for 3 h at 4 °C for reduction. Excess borohydride was destroyed by adding acetic acid (pH 5.0) and incubating for 30 min. The resultant periodate-oxidized and borohydride-reduced heparin was finally recovered by neutralizing with NaOH, dialysis in distilled water and lyophilization.

2.2. Cell lines

The H11 cell line was established from a Lewis lung carcinoma (3LL)-derived cell line by repeated subcutaneous transplantation of spontaneously formed lung metastatic nodules in vivo [14,15]. The 4A1-1 cell line was further established in our laboratory by *lac* Z gene transfection of the H11 cell line [16]. Briefly, H11 cells were transfected with the pCMV*lac* Z plasmid using lipofectin (GIBCO-BRL, Gaithersburg, MD). The pCMV*lac* Z expression vector used (kindly provided by Dr. Lloyd Culp) consisted of bacterial *lac* Z gene under the control of the cytomegalovirus (CMV) immediate early gene promotor and the neo resistance gene (neoR). Transfectants were isolated in selection medium supplemented with 1.0 mg/ml of G418. G418 resistant colonies were further screened for β-galactosidase activity by X-Gal staining, and one particular colony with strong blue staining was isolated, followed by single cell cloning (4A1-1). Other mouse metastatic

cell lines such as colon 26 carcinoma-derived highly metastatic clone, and FBJ, a mouse osteosarcoma cell line, were kindly provided by Dr S. Shimizu. and Dr S. Yamagata. (Aichi Cancer Center Res. Inst.) [17,18]. These cells were maintained in Dulbecco's modified Eagle's medium (DMEM) containing 10% fetal bovine serum (FBS) (GIBCO, Grand Island, NY) with 100 units/ml of penicillin, 100 μg/ml of streptomycin sulfate and 0.5 mg/ml of G418, and cultured in a humidified 5% CO_2 incubator at 37 °C.

2.3. Metastasis and micrometastasis assay

For experimental metastasis, exponentially growing metastatic tumor cells were harvested with 2 mM EDTA solution without trypsin, and aliquots (1×10^6) in 0.2 ml of Hanks' Balanced Salt Solution (HBSS) were intravenously injected into the tail veins of mice. Average 6 mice (range; 5–8) were used in each group. Heparin and its derivatives were injected intravenously at doses ranging from 0.5 to 2.0 mg/mouse, usually 10 min before tumor cell injection or co-injection with the cells. In some cases, heparin derivatives were injected subcutaneously or intraperitoneally. Mice were sacrificed at approximately 2 weeks after tumor cell inoculation and the removed lungs were weighed and fixed in Bouin's solution. The number of metastases was determined by counting visible nodules on the lung surface. Micrometastatic foci or arrested tumor cells retained in the lung were assessed by counting the number of X-Gal positive blue-staining foci under a dissecting microscope. Lungs were harvested 1 day after i.v. injection of *lac* Z transfected 4A1-1 cells (1×10^6) and were fixed and stained with X-Gal. As negative control, chondroitin sulfate A was i.v. injected into mice.

2.4. X-Gal staining

X-Gal staining was achieved with the method described previously [19]. Briefly, the lung tissues were fixed in 2% formaldehyde plus 0.2% glutaraldehyde in PBS at 4 °C for 1–2 h, and then immersed in a 0.5 mg/ml of X-Gal solution (Wako, Osaka, Japan) at 37 °C overnight and washed with PBS.

2.5. Flow cytometry

H11 cells (3×10^5 cells suspended in DMEM) were incubated with or without 0.1 U/ml of heparitinase I (EC 4.2.2.8, Seikagaku Corp., Tokyo, Japan) for 15 min at 37 °C. After washing with PBS, they were incubated with F58-10E4mAb (Seikagaku Corp.), specific to heparan sulfate, or F69-3G10 mAb (Seikagaku Corp.), specific to unsaturated non-reducing end of heparan sulfate chains, which are generated by digestion with heparitinase. After washing with PBS, they were exposed to FITC-conjugated anti-mouse IgG (MBL, Nagoya, Japan) for 30 min. The labeled cells were washed and the intensity of fluorescence was measured in a flow cytometer, FACSsort (BD Biosciences).

2.6. Assay of cell growth, attachment and invasiveness in vitro

To examine the effect of heparin species on the growth of Lewis lung carcinoma cell lines in vitro, the cells were plated at 1×10^5 cells/35 mm plastic dish in DMEM supplemented with 10% FBS in the presence or absence of heparin analogs (0.5 mg/ml). The number of viable cells was counted in triplicate with a hemocytometer for 3 days after seeding.

Cell adhesion assay was carried out with 24-well plates coated with Matrigel (IWAKI, Tokyo, Japan).The plate was preincubated in DMEM containing 0.02% bovine serum albumin (BSA) in the presence of heparin, LAC heparin and chondroitin sulfate A (all 1 mg/ml) for 15 min at 37 °C. Single tumor cell suspensions (2×10^4/100 μl HBSS) were added to each well and the dishes were incubated for 1 h at 37 °C. After removing unattached cell by two washes with HBSS, attached cells were harvested with trypsin/EDTA and counted in triplicate with a hemocytometer.

A modified Boyden chamber invasion assay was performed as follows: Culture inserts with the polycarbonate filter (pore size 8 μm) were coated with 10 μl of Matrigel solution (500 μg/ml) and set in a 24-well plate for 30 min at 37 °C. Tumor cells were then seeded at a density of 2×10^4 per well into the upper layer of the inserts in serum-free DMEM containing 0.1% BSA in the presence or absence of heparin analogs. Then DMEM containing 0.005%

Table 1
Anticoagulant activity of LAC heparin

Reagent	Anticoagulant activity[a] (second)		Hemorrhagic complication after injection into mouse[b]
	PT	APTT	
Control	10.6	41.1	−
LMW-HP	18.3	200 <	+
HP	80.0 <	200 <	++
LAC-HP	9.8	118.6	−
CSA	10.6	46.0	−

[a] PT (prothrombin time) and APTT (activated partial thromboplastin time) of human plasma containing 0.1 mg/ml LMW-HP (low molecular weight heparin), HP (heparin), LAC-HP (LAC heparin) and CSA (chondroitin sulfate A) was measured. Normal range of PT and APTT is 10–13 and 25–40 seconds, respectively.

[b] Mice are given injection i.p. (or s.c.) with reagents (1 mg/0.3 ml PBS/mouse) and hemorrhagic complication was examined 12 h post-injection.

fibronectin as a chemoattractant was filled into the lower chamber and the cells were incubated for 4 h at 37 °C. The remaining cells in the upper chamber were swabbed with cotton and penetrating cells in the lower chamber were fixed in methanol for 1 min and stained with hematoxylin. Total number of cells passing through the filter per randomly selected field (10 fields per dish) was counted using inverted microscopy. The experiment was performed in tripricate and the cell number / field was designated as an invasion index.

2.7. Statistical analysis

The statistical significance of differences in metastasis between groups was determined by applying Student's or Welch's two-tailed *t*-tests. Survival of mice treated with each reagent was analyzed by the Kaplan-Meier method and compared using the log-rank test.

3. Results

3.1. Anticoagulant activity of LAC heparin

Periodate treatment followed by reduction with sodium borohydride resulted in marked reduction of anticoagulant activity of heparin. Prothrombin time (PT) of human plasma mixed with LAC heparin decreased to the control level (10–13 seconds) (Table 1). The activated partial thromboplastin time

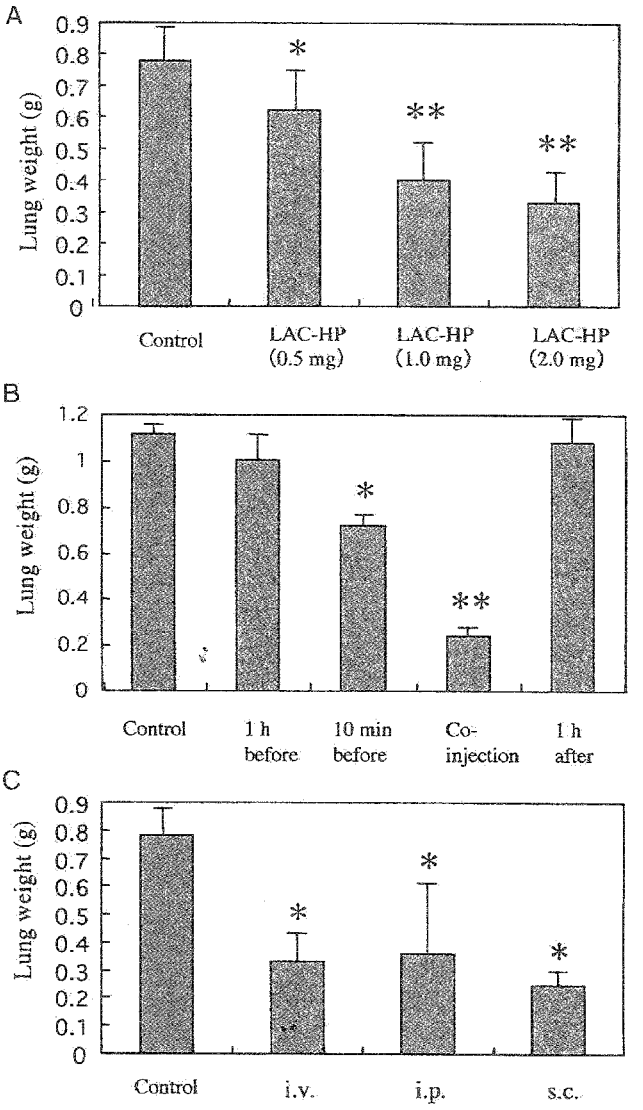

Fig. 1. Effects of dose (A), injection time (B) and injection route (C) of LAC heparin on lung colonization after intravenous injection of Lewis lung carcinoma cells into mice. (A) Mice were injected intravenously with H11 cells (1×10^6) 10 min after intravenous administration of LAC heparin at doses of 0.5–2.0 mg/mouse. (B) Mice were injected intravenously with H11 cells before and after intravenous administration of LAC heparin (1mg/mouse) at different timings. (C) Mice were injected intravenously with H11 cells 10 min after intravenous (i.v.), intraperitoneal (i.p.) and subcutaneous (s.c.) injection of LAC heparin (1 mg/mouse). Mice were sacrificed at 2 or 3 weeks post-injection and the lungs were removed and whole lung weights were measured. The data are means ± s.d. $*P < 0.01$, $**P < 0.001$ (vs Control).

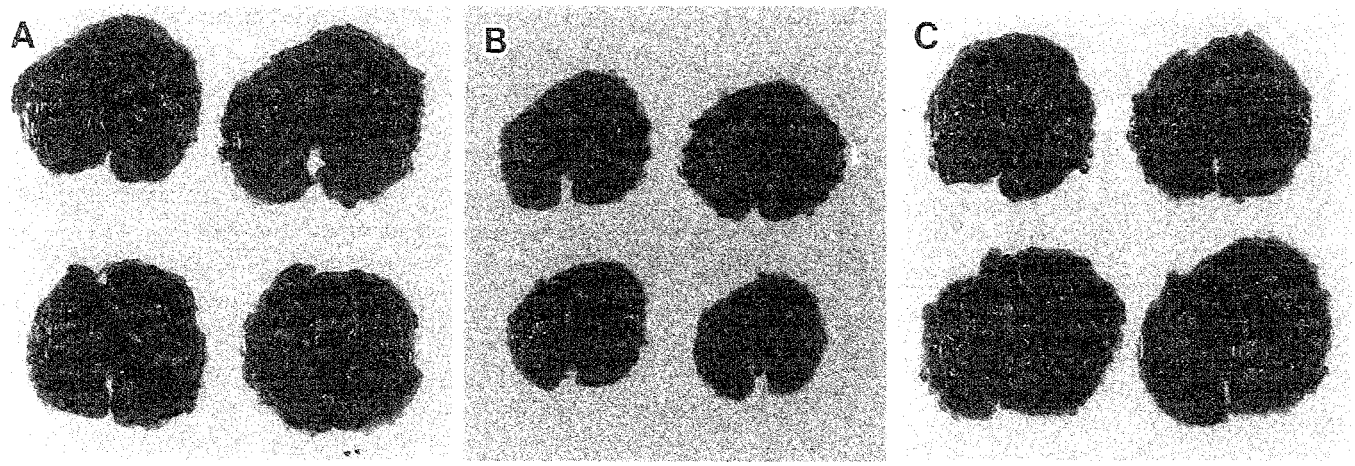

Fig. 2. Representative effects of LAC heparin on the lung colonization after intravenous injection of Lewis lung carcinoma cells into mice. Mice received i.v. injections of saline as a control (left), LAC heparin (middle) and chondroitin sulfate A (right).

(APTT) of human plasma mixed with LAC heparin also significantly reduced as compared with intact heparin, but a little bit higher than water control and chondroitin sulfate A (negative control). Therefore, we designated this compound as low anticoagulant heparin (LAC heparin). In vivo, no significant bleeding complication after intravenous, subcutaneous and intraperitoneal injection of LAC heparin into mice was observed, whereas subcutaneous and intraperitoneal injection of heparin itself into mice resulted in hematoma formation and sometimes hemorrhagic death.

3.2. Effect of dose, injection time and injection route of LAC heparin on lung colonization of tumor cells

Intravenous injection of LAC heparin at the dose of 0.5–2.0 mg/mouse significantly inhibited experimental lung metastases in a dose-dependent manner as compared with untreated controls (Fig. 1A and Fig. 2). Such inhibition of metastasis by LAC heparin was maximal when co-injected with tumor cells, followed by injection at 10 min before tumor cell inoculation. However, no significant inhibition of metastasis was observed with injection 1 h before and after tumor cell inoculation (Fig. 1B). In this study, therefore, all the experiments were done with injection of LAC heparin with 10 min before tumor cell inoculation. Intraperitoneal (i.p.) and subcutaneous (s.c.) injection(s) of LAC heparin into the left abdominal flank of mice also resulted in significant inhibition of metastasis at a comparable level to i.v. injection (Fig. 1C).

Intact heparin and other heparin derivatives including low molecular weight heparin and heparan sulfate at the dose of 1 mg/ml also showed significant inhibition of metastasis, with maximal inhibition by intact heparin. No significant inhibition was observed by chondroitin sulfate A (Fig. 3A). The generality of such inhibitory effect of LAC heparin on metastasis was confirmed by other metastasis models such as mouse B16F10 melanoma, mouse colon 26 carcinoma and FBJ mouse osteosarcoma cell lines (Fig. 3B).

3.3. Effect of LAC heparin on the survival of mice

In addition to the reduction of the number of lung colonies by chemically modified heparin, the survival of mice treated with heparin and LAC heparin was significantly longer than that of untreated control mice ($P < 0.01$ and $P < 0.05$, respectively) (Fig.3C).

3.4. FACS analysis of cell surface heparan sulfate of H11 carcinoma cells

F58-10E4, a specific mAb to heparan sulfate, strongly reacted with H11 cell surface and this was abolished by heparitinase I treatment, indicating the presence of heparan sulfate on their cell surface (Fig. 4A). This finding was confirmed by the fact that

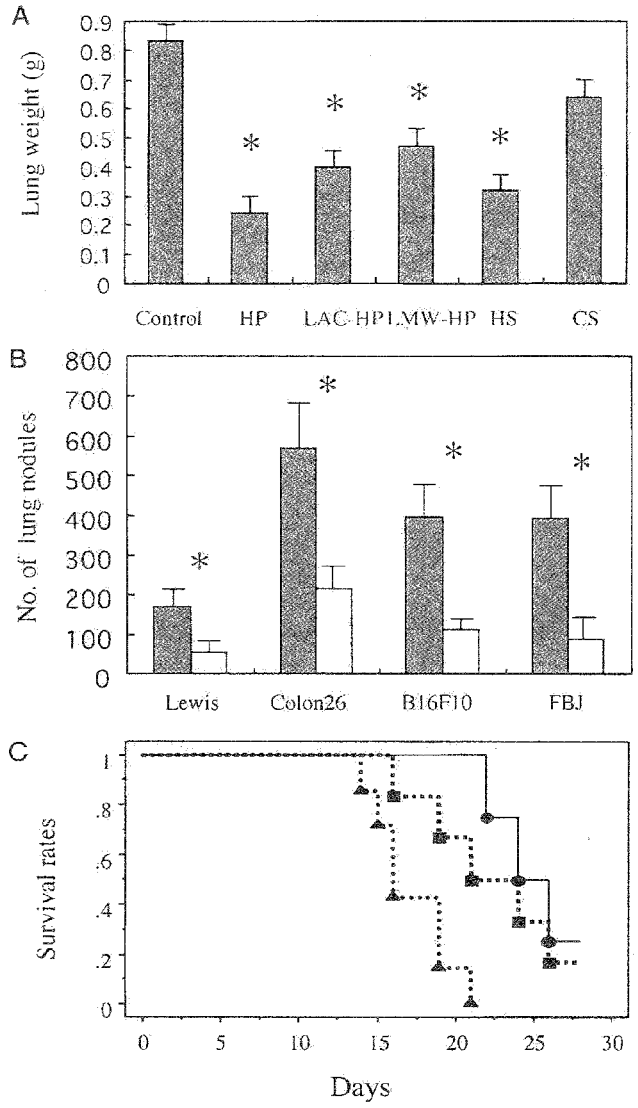

Fig. 3. Effects of species of heparin analogs on the lung colonization of Lewis lung carcinoma cells (A), effects of LAC heparin on lung colonization by various metastasis models (B) and effects of LAC heparin on the survival of mice bearing lung metastases of Lewis lung carcinoma cells (C). (A) Mice injected intravenously with H11 cells at 10 min after intravenous administration of saline (control), 1 mg/mouse of heparin (HP), LAC heparin (LAC-HP), low molecular weight heparin (LMW-HP), heparan sulfate (HS) and chondroitin sulfate A (CS). (B) Mice injected intravenously with Lewis lung carcinoma, B16F10 melanoma, colon 26 carcinoma and FBJ osteosarcoma cells at 10 min after intravenous injection of saline (closed bar) and LAC heparin (open bar). Mice were sacrificed at 2 weeks post-injection, lungs were removed, and whole lung weights (A) or the number of lung nodules (B) were measured. The data are means ± s.d. $^*P < 0.001$ (vs Control). (C) Mice injected intravenously with H11 cells 10 min after intravenous injection of saline (control, ▲), LAC heparin (LAC-HP, ■) and heparin (HP, ●). Overall survival of mice treated with each reagent was analyzed by the Kaplan–Meier method and compared using the log-rank test. Control vs LAC-HP ($P < 0.05$), Control vs HP ($P < 0.01$).

heparitinase I treatment caused enhanced reactivity of H 11 cells against F69-3G10, a specific mAb to unsaturated non-reducing end of heparan sulfate chains (Fig. 4B).

3.5. Effects of LAC heparin on the growth, adhesion and invasion of tumor cells in vitro

Heparin and LAC heparin had no substantial effect on the growth of tumor cells (Fig. 5A). However, both heparin and LAC heparin significantly inhibited the attachment of tumor cells to the Matrigel-coated dishes ($P < 0.01$) (Fig. 5B) and the tumor cells were round-shaped if attached. These reagents also inhibited invasion of Matrigel as measured by modified Boyden chamber invasion assay ($P < 0.01$) at comparable levels (Fig. 5C).

3.6. Effects of LAC heparin on the initial arrest and retention of tumor cells in the lung

Tumor cells arrested in the lungs at 1 day after i.v. injection of 4A1-1 cells into tail veins of mice could be clearly visualized as blue-stained foci under a dissecting microscope after X-Gal staining. The X-Gal positive micrometastatic foci in the lung consisted of several to dozens of tumor cells (Fig. 6A). The number of X-Gal positive foci in the lungs of mice pretreated with LAC heparin after i.v. inoculation of 4A1-1 cells was significantly decreased as compared with untreated controls in a dose-dependent manner (Fig. 6B and D), but not in those pretreated with chondroitin sulfate A (Fig. 6C and D).

4. Discussion

Metastasis in experimental animals is known to be inhibited by the widely used anticoagulant drug heparin [20,21]. Some clinical trials suggested a beneficial effect of heparin in cancer patients [22]. However, heparin therapy can be difficult to manage and of limited use because of the high risk of severe hemorrhagic complication. To overcome this problem, introduction of chemical modification to the heparin moiety to reduce its anticoagulant activity is a promising approach [7,11,12]. In the present study, we used a heparin that was chemically modified by

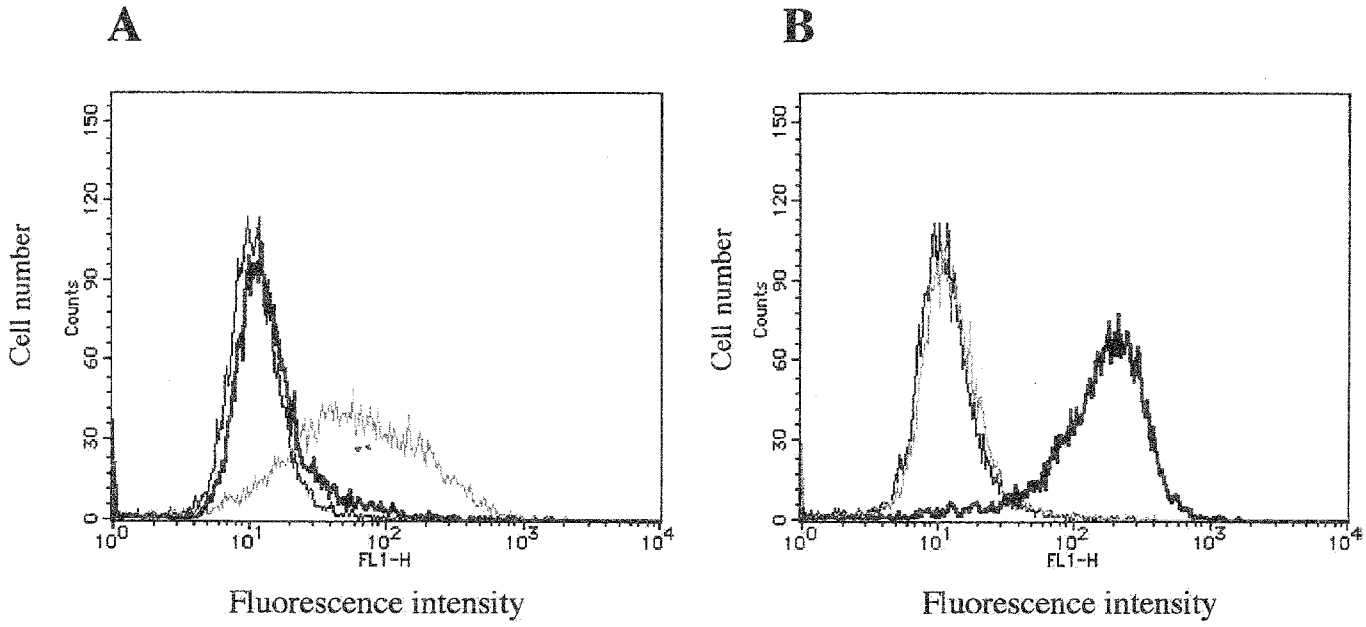

Fig. 4. Expression of heparan sulfate on Lewis lung carcinoma cells. (A) H11 cells were incubated with antibody specific to heparan sulfate, F58-10E4mAb. (B) H11 cells predigested with heparitinase I were incubated with antibody specific to unsaturated non-reducing end of heparan sulfate chains, F69-3G10mAb. After washing with PBS, they were exposed to FITC-conjugated second antibody. The labeled cells were washed and the intensity of fluorescence was measured in a flow cytometer. Green; heparitinase treatment (−), Red; heparitinase treatment (+), Black; non-immune IgG control.

periodate-oxidization and sodium borohydride-reduction. We found that the anticoagulant activity of this heparin derivative could be reduced to almost control level, allowing repetitive injection into mouse without severe bleeding complication, while its anti-metastatic activity was conserved essentially at the same level as intact heparin in experimental lung metastasis models. We confirmed the anti-metastatic activity of this heparin derivative comparable with other metastasis models including colon carcinoma, melanoma and sarcoma, suggesting the usefulness of chemically modified heparin as a potential anti-metastatic agent for a wide variety of cancer cells.

We demonstrated that the anti-metastatic effects of heparin are not primarily due to its anticoagulant activity, but to other biological effects. The anti-coagulant activity-independent mechanism of the metastasis inhibitory effect of chemically modified heparin still remains unclear. In the present study, we found that LAC heparin significantly inhibited adhesion of Lewis lung carcinoma cells to Matrigel-coated dishes in vitro and also significantly diminished retention of *lac*Z gene-tagged Lewis lung carcinoma cells in the lung after i.v. injection in vivo. Karasawa et al. previously demonstrated that chondroitin sulfate dipalmitoylphosphatidylethanolamine (CS-PE) inhibits tumor cell adhesion to Matrigel and tumor cell retention in the lung, and that this effect is due to immobilization of CS-PE onto ECM substratum [23]. In this respect, LAC heparin can also become immobilized onto the fibronectin or laminin, major basement membrane constituents, through their heparin binding domain. In this study, we showed that H11 cells express heparan sulfate on their surface. These heparan sulfate side chains on the cell surface are carried by core protein of cell surface heparan sulfate proteoglycans such as syndecan 1, 2 and 4 or glypicans [24,25]. Therefore, it is likely that LAC heparin may suppress cell adhesion and retention in the lung capillary by competitively inhibiting the interaction between syndecans or glypicans and the heparin binding domain of fibronectin and laminin in the subendothelial basement membrane as heparan sulfate analogs. On the other hand, chemically modified heparin with reduced anticoagulant activity

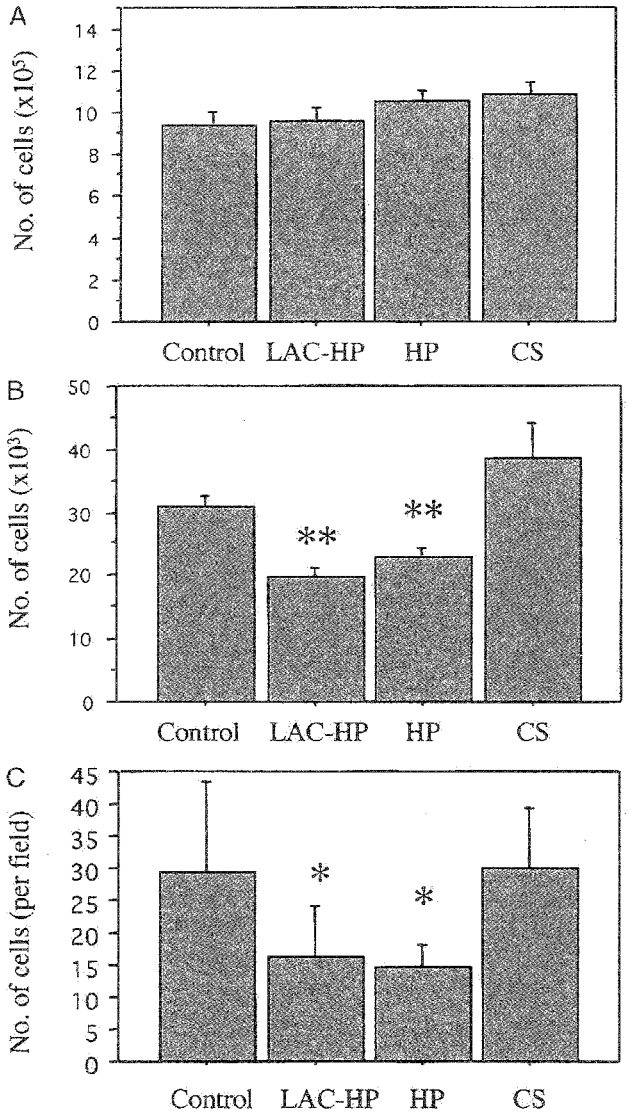

Fig. 5. Effects of LAC heparin on the growth (A), adhesion (B) and invasion (C) of tumor cells in vitro. (A) H11 cells were plated at 1×10^5 cells/35 mm plastic dish in DMEM supplemented with 10% FBS in the presence or absence of LAC heparin. The number of viable cells was counted 4 days after seeding, when all types of the cells were in a logarithmic growth phase. (B) Single cell suspensions were added to 24-well plates coated with Matrigel and were incubated for 1 h at 37 °C. After removing unattached cells by washing, attached cells were harvested and counted. The data are means ± s.d. in quadruplicate. $**P < 0.01$ (vs Control). (C) A modified Boyden chamber invasion assay using Matrigel was performed as described in Materials and Methods. The data are means ± s.d. in triplicate. $*P < 0.01$ (vs Control).

is known to be an effective inhibitor of heparanase, a heparan sulfate-degradative endo-β-glucuronidase, whose activity correlates well to tumor invasiveness and thereby the lung colonization ability of the B16F10 melanoma model [6,7,26]. In fact, periodate-oxidized and borohydride-reduced heparin is reportedly a potent heparanase inhibitor [11]. We found that tumor cells in the intact lung without heparin pretreatment appear elongated in shape and some of them migrated to the extravascular space several hours after i.v. [16], whereas tumor cells retaining in the lung with LAC heparin pretreatment seems to be round in shape and located within capillaries, suggesting impairment of adhesion and subsequent extravasation of tumor cells by LAC heparin pretreatment. In this study, we did not examine heparanase inhibitory activity of LAC heparin, however, observed inhibition of lung colonization in vivo and Matrigel invasion in vitro by LAC heparin is possibly due to both inhibition of tumor cell adhesion to subendothelial matrix and the impairment of extravasation of tumor cells from the capillary vessels via heparanase inhibition.

Chemically modified heparin with reduced anticoagulant activity is also known to inhibit tumor angiogensis [12] and the P-selectin-mediated interaction between platelets and tumor cell surface mucin ligand, thereby inhibiting formation of their complex [27]. Thus, chemically modified heparin with reduced anticoagulant activity has pleiotropic actions including anti-adhesion, anti-ECM degradation, anti-platelet tumor complex formation and anti-angiogenesis activity, suggesting multipotency in inhibition of almost all steps involved in the later phase of hematogenous metastasis development. We and others have previously demonstrated that tumor cells can be shed during surgical manipulation, and that the resultant free tumor cells released from the primary tumor have some impact on the poor outcome for cancer patients [28]. Therefore, LAC heparin therapy may be useful, for example, in the management of patients with high risk for hematogenous metastasis after surgery. The low-toxic side effects of heparin has long been proved by clinical observation in such setting as hemodialysis for a number of patients with renal insufficiency. Therefore, LAC heparin without risk of inducing acute hemorrhagic complication and other chronic toxic side effects may be a safe and effective drug as an anti-metastatic agent alone or in combination with anticancer drugs.

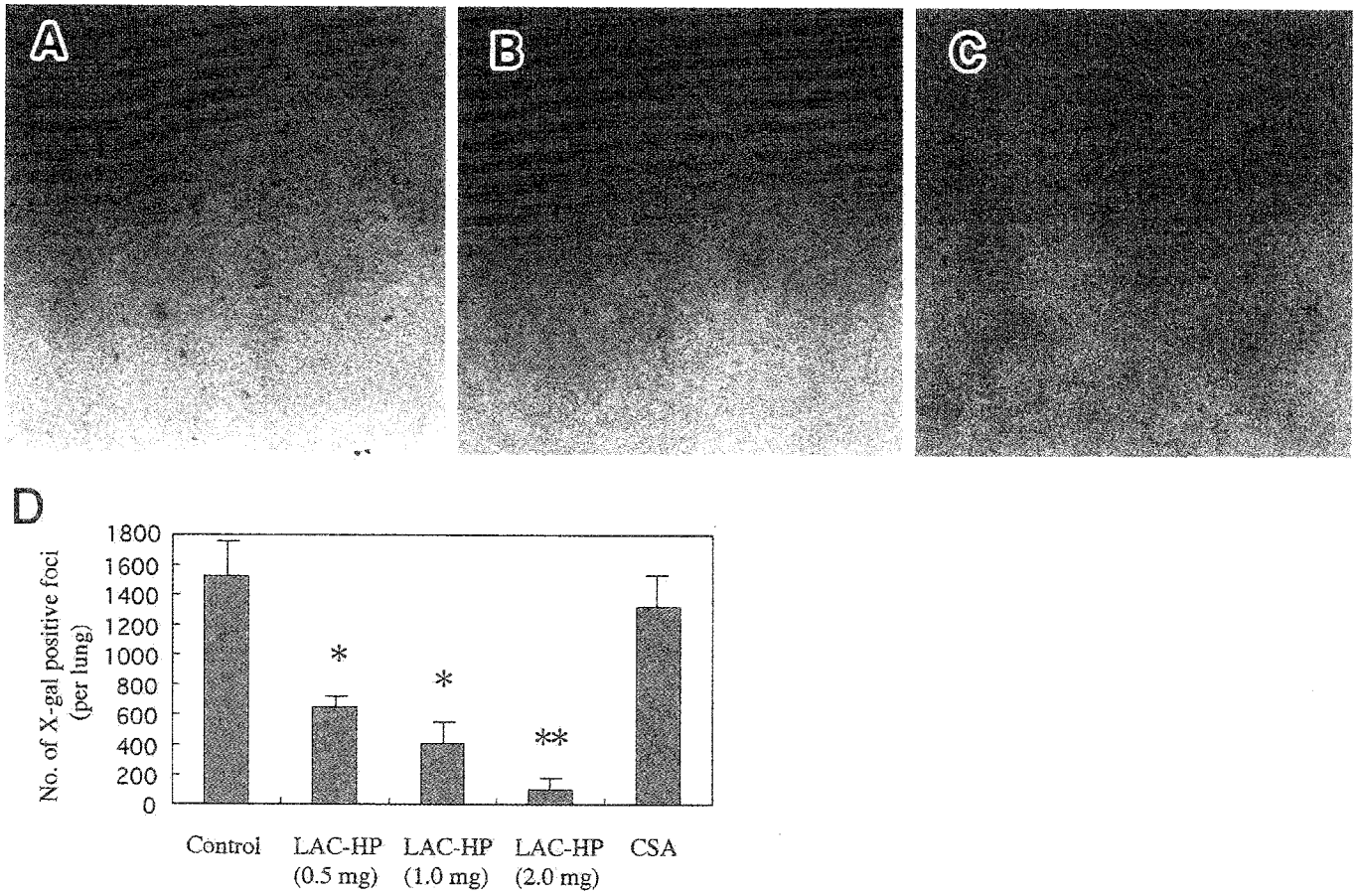

Fig. 6. Effects of LAC heparin on tumor cell arrest and retention in the lung after intravenous injection of *lac* Z gene-tagged Lewis lung carcinoma cells. Mice were injected intravenously with 4A1-1 cells 10 min after intravenous administration of LAC heparin at doses of 0.5–2.0 mg/mouse. Mice were sacrificed at 1 day post-injection and the lungs were removed and stained with X-Gal. Visualization of tumor cell retention in the lungs of mice received a single intravenous injection of saline as a control (A), LAC heparin (B) and chondroitin sulfate A (C). The number of X-Gal positive foci in the lung was compared with increasing doses of LAC heparin (D). The data are means ± s.d. $*P < 0.001$, $**P < 0.0001$.

Acknowledgements

We thank Miss N. Yamada for her expert technical assistance. This work was supported in part by a Grant-in-Aid for Scientific Research from the Ministry of Education, Science, Sports, Culture and Technology, Japan.

References

[1] D.A. Lane, U. Lindahl (Eds.), Heparin, Edward Arnold, London, 1989.
[2] K. Sugahara, H. Kitagawa, Heparin and heparan sulfate biosynthesis, IUBMB. Life 54 (2002) 163–175.
[3] R.D. Rosenberg, P.S. Damus, The purification and mechanism of action of human antithrombin-heparin cofactor, J. Biol. Chem. 248 (1973) 6490–6505.
[4] U. Lindahl, Heparin—from anticoagulant drug into the new biology, Glycoconj. J. 17 (2000) 597–605.
[5] I. Capila, R.J. Linhardt, Heparin-protein interactions, Angew. Chem. Int. Ed. Engl. 41 (2002) 391–412.
[6] T. Irimura, M. Nakajima, G.L. Nicolson, Chemically modified heparins as inhibitors of heparan sulfate specific endo-β-glucuronidase (heparanase) of metastatic melanoma cells, Biochemistry 25 (1986) 5322–5328.
[7] I. Vlodavsky, M. Mohsen, O. Lider, C.M. Svahn, H.P. Ekre, M. Vigoda, R. Ishai-Michaeli, T. Peretz, Inhibition of tumor metastasis by heparanase inhibiting species of heparin, Invasion. Metastasis. 14 (1994) 290–302.
[8] L.A. Fransson, I. Carlstedt, Alkaline and smith degradation of oxidized dermatan sulphate-chondroitin sulphate copolymers, Carbohydr. Res. 36 (1974) 349–358.

[9] L.A. Fransson, Periodate oxidation of the D-glucuronic acid residues in heparan sulphate and heparin, Carbohydr. Res. 62 (1978) 235–244.
[10] H.E. Conrad, Y. Guo, Structural analysis of periodate-oxidized heparin, in: D.A. Lane, I. Bjork, U. Lindahl (Eds.), Advances in Experimental Medicine and Biology, 313, Plenum Press, New York, 1992, pp. 31–36.
[11] F. Lapierre, K. Holme, L. Lam, R.J. Tressler, N. Storm, J. Wee, et al., Chemical modifications of heparin that diminish its anticoagulant but preserve its heparanase-inhibitory, angiostatic, anti-tumor and anti-metastatic properties, Glycobiology 6 (1996) 355–366.
[12] K. Ono, M. Ishihara, K. Ishikawa, Y. Ozeki, H. Deguchi, M. Sato, et al., Periodate-treated, non-anticoagulant heparin-carrying polystyrene (NAC-HCPS) affects angiogenesis and inhibits subcutaneous induced tumour growth and metastasis to the lung, Br. J. Cancer 86 (2002) 1803–1812.
[13] M. Ishihara, Y. Saito, H. Yura, K. Ono, K. Ishikawa, H. Hattori, et al., Heparin-carrying polystyrene to mediate cellular attachment and growth via interaction with growth factors, J. Biomed. Mater. Res. 50 (2000) 144–152.
[14] H. Nakanishi, K. Oguri, K. Yoshida, N. Itano, K. Takenaga, T. Kazama, et al., Structural differences between heparan sulphates of proteoglycan involved in the formation of basement membranes in vivo by Lewis-lung-carcinoma-derived cloned cells with different metastatic potentials, Biochem. J. 288 (Pt 1) (1992) 215–224.
[15] N. Itano, K. Oguri, H. Nakanishi, M. Okayama, Membrane-intercalated proteoglycan of a stroma-inducing clone from Lewis lung carcinoma binds to fibronectin via its heparan sulfate chains, J. Biochem. (Tokyo) 114 (1993) 862–873.
[16] K. Kobayashi, H. Nakanishi, A. Masuda, N. Tezuka, M. Mutai, M. Tatematsu, Sequential observation of micrometastasis formation by bacterial *lac* Z gene-tagged Lewis lung carcinoma cells, Cancer Lett. 112 (1997) 191–198.
[17] S. Shimizu, Y. Nishikawa, K. Kuroda, S. Takagi, K. Kozaki, S. Hyuga, S. Saga, M. Matsuyama, Involvement of transforming growth factor β1 in autocrine enhancement of gelatinase B secretion by murine metastatic colon carcinoma cells, Cancer Res. 56 (1996) 3366–3370.
[18] S. Yamagata, M. Miwa, K. Tanaka, T. Yamagata, FBJ virus-induced osteosarcoma has type V collagen consisting of A B and C-like chains in addition to type I collagen, Biochem. Biophys. Res. Commun. 105 (1982) 1208–1214.
[19] H. Nakanishi, K. Kobayashi, T. Nishimura, K. Inada, T. Tsukamoto, M. Tatematsu, Chemosensitivity of micrometastases and circulating tumor cells to uracil and tegafur as evaluated using *Lac* Z gene-tagged Lewis lung carcinoma cell, Cancer Lett. 142 (1999) 31–41.
[20] A. Amirkhosravi, S.A. Mousa, M. Amaya, J.L. Francis, Antimetastatic effect of tinzaparin, a low-molecular-weight heparin, J. Thromb. Haemost. 1 (2003) 1972–1976.
[21] H. Engelberg, Actions of heparin that may affect the malignant process, Cancer 85 (1999) 257–272.
[22] M. Hejna, M. Raderer, C.C. Zielinski, Inhibition of metastases by anticoagulants, J. Natl. Cancer Inst. 91 (1999) 22–36.
[23] K. Karasawa, N. Sugiura, Y. Hori, S. Suzuki, J. Onaya, K. Sakurai, K. Kimata, Inhibition of experimental metastasis and cell adhesion of murine melanoma cells by chondroitin sulfate-derivatized lipid, a neoproteoglycan with anti-cell adhesion activity, Clin. Exp. Metastasis. 15 (1997) 83–93.
[24] Y. Kusano, K. Oguri, Y. Nagayasu, S. Munesue, M. Ishihara, I. Saiki, et al., Participation of syndecan 2 in the induction of stress fiber formation in cooperation with integrin α5β1: structural characteristics of heparan sulfate chains with avidity to COOH-terminal heparin-binding domain of fibronectin, Exp. Cell Res. 256 (2000) 434–444.
[25] S. Munesue, Y. Kusano, K. Oguri, N. Itano, Y. Yoshitomi, H. Nakanishi, I. Yamashina, M. Okayama, The role of syndecan-2 in regulation of actin-cytoskeletal organization of Lewis lung carcinoma-derived metastatic clones, Biochem. J. 363 (2002) 201–209.
[26] C.R. Parish, D.R. Coombe, K.B. Jakobsen, F.A. Bennett, P.A. Underwood, Evidence that sulphated polysaccharides inhibit tumour metastasis by blocking tumour-cell-derived heparanases, Int. J. Cancer 40 (1987) 511–518.
[27] L. Borsig, R. Wong, J. Feramisco, D.R. Nadeau, N.M. Varki, A. Varki, Heparin and cancer revisited: mechanistic connections involving platelets, P-selectin, carcinoma mucins, and tumor metastasis, Proc. Natl. Acad. Sci. USA 98 (2001) 3352–3357.
[28] S. Ito, H. Nakanishi, T. Hirai, T. Kato, Y. Kodera, Z. Feng, et al., Quantitative detection of CEA expressing free tumor cells in the peripheral blood of colorectal cancer patients during surgery with real-time RT-PCR on a LightCycler, Cancer Lett. 183 (2002) 195–203.

J Gastroenterol 2004; 39:197–199
DOI 10.1007/s00535-004-1275-3

Journal of Gastroenterology

Editorial

Can syndecan-1 become a prognostic factor in solid tumors?

Article on page 104
Reduction of syndecan-1 expression in differentiated type early gastric cancer and background mucosa with gastric cellular phenotype
WATARI J, SAITOH Y, FUJIYA M, et al.

Syndecan is a cell-surface proteoglycan consisting of a transmembrane core protein and covalently bound heparan sulfate chains that contain ligand-binding sites. These proteoglycans comprise a family of four members of distinct gene origins. The first successful molecular cloning of the core protein was reported in 1989, by Bernfield and colleagues.[1] It was named "syndecan", from the Greek *syndein*, "to bind together", because it was thought to link the cytoskeleton to the interstitial matrix. After that, structurally related syndecans were soon identified,[2–4] and this prototype was called syndecan-1 and the others were numbered in the order of cDNA cloning.[5] Because of the structural diversity of the heparan sulfate chain, syndecans can bind a wide variety of extracellular heparin-binding molecules, both soluble and insoluble. Actually, they exhibit various functions in growth factor signaling and in cell–cell and cell–matrix adhesion.[6–8] However, it has gradually become clear that the ligand-recognition sites of heparan sulfate are considerably restricted by the sulfation pattern,[9] and that each syndecan has functional specificity and its own job. In adult tissues, the distribution of syndecans seems to be loosely regulated; syndecan-1 is expressed in epithelial cells and plasma cells; syndecan-2, in endothelial cells and fibroblasts; syndecan-3, in the central nervous system; and syndecan-4 is expressed ubiquitously in adherent cells. However, during embryogenesis and morphogenesis, syndecan expression is regulated spatially and temporally, and most cells express multiple syndecans. These facts readily lead us to assume that the expression pattern of each syndecan changes with malignant transformation.[10]

To date, around 200 reports relating to syndecan expression in cancers have been published, and considerable interest has naturally concentrated on the prognostic value of syndecan in cancer.[11–14] Most reports are related to syndecan-1, because a good antibody, B-B4, is available. B-B4 developed for CD138, a marker of multiple myeloma cells and subgroups of B-cells, recognizes a core protein of syndecan-1.[15] Because this antibody can be applied to enzyme-linked immunosorbent assay (ELISA) and immunostaining, the concentration of syndecan-1 in plasma or other body fluids and its expression in various solid tumors were examined. Comparison of syndecan-1 levels in sera drawn from patients with multiple myeloma revealed a significant difference in survival between groups; the group with "high" syndecan-1 levels had a median survival of 29 months, whereas the group with "low" levels had a median survival of 44 months.[16] In patients with multiple myeloma, this result is quite reasonable, because the syndecan-1 serum concentration is thought to reflect the number of malignant myeloma cells. However, in solid tumors, the results obtained are extremely difficult to interpret. The main reason for this difficulty is the functional redundancy of syndecan-1, which makes it complicated to understand the implications of the elevated or suppressed expression level of syndecan-1 detected by immunostaining.

According to its localization in epithelial tissues, one of the roles of syndecan-1 is considered to be the cell-cell adhesion that maintains the tissue architecture. In carcinomas, it has been reported that the reduced expression of syndecan-1 correlates with the histological differentiation grade, for example, poorly differentiated carcinoma cells often lack syndecan-1. In squamous cell carcinomas of the head and neck, positive syndecan-1 expression correlates with a more favorable prognosis.[10] However, a high level of syndecan-1 expression in breast carcinomas is related to an aggressive phenotype and poorer prognosis.[14] These seemingly inconsistent results indicate that further factors are necessary to understand the implications of syndecan-1 expression

Reprint requests to: K. Oguri

level in solid cancers. Wiksten et al.[12] found that the immunohistochemical expression of syndecan-1 in 296 gastric cancers did not correlate with the presence of metastases, peritoneal spreading, Borrmann's classification, and Lauren's classification, but correlated significantly with survival in patients with stage I disease. In this issue of the *Journal of Gastroenterology*, Watari and colleagues[17] report the expression of syndecan-1 in differentiated-type gastric cancers according to four types: gastric, ordinary, complete-intestinal, and null types.

Since 1997, they have extensively investigated the immunohistochemical expression patterns of syndecan-1 in several carcinomas, in connection with metastasis in particular.[18–22] In the study reported here,[17] they compared the alterations in syndecan-1 expression to those of E-cadherin, another class of cell adhesion molecule, and obtained the following results: (1) the immunohistochemical results of syndecan-1 expression were consistent with the results of in situ hybridization using anti-sense riboprobes; (2) syndecan-1 expression in gastric-type cancers was significantly reduced in comparison with its expression in other cancer-types, although there was no significant correlation between E-cadherin expression and these cellular phenotypes; and (3) the expression of syndecan-1 in gastric-type intestinal metaplasia surrounding the tumors was significantly lower than that in ordinary-type intestinal metaplasia, but there was no such correlation in E-cadherin expression. Although these authors do not place much emphasis on it, result (1) above is indeed important. In cancers in which the activities of degradation enzymes generally increase, the fact that the immunohistochemical expression level of syndecan-1 is consistent with its mRNA expression level strongly suggests that its reduced expression is not caused by degradation, but is, rather, a result of the downregulation of its biosynthesis. The evaluation of syndecan-1 in combination with E-cadherin is more complicated. Experimentally, it was shown by the genetic manipulation of E-cadherin that syndecan-1 expression was regulated post-transcriptionally by E-cadherin expression.[23] From the immunostainings of syndecan-1 and E-cadherin in colorectal adenoma and carcinoma, Day et al.[24] supposed that the loss of syndecan-1 occurred first, followed by the change in E-cadherin. Their results show partial agreement with the results of Watari et al.[17]

At this juncture, the prognostic value of syndecan-1 in solid cancers remains to be determined. The functions of cell adhesion molecules are regulated by extracellular binding molecules and also by cytoplasmic binding proteins downstream of signal transduction. Therefore, it may be unwarranted to expect so much from simple analyses of the immunostaining expression patterns of these cell adhesion molecules in cancers. And furthermore, as Watari et al.[17] admit, their small sample size is a limitation of this type of study. Research of this kind must have a sufficient sample size to allow for statistical processing, and for evaluation of the prognostic value of the target molecules. Cooperative multicenter studies will make it possible to obtain the large sample size required, and, to develop such pilot studies; we hope that a network will be developed.

Kayoko Oguri, PhD
Clinical Research Center, Nagoya National Hospital, 4-1-1 Sannomaru, Nakaku, Nagoya 460-0001, Japan

Minoru Okayama, PhD
Department of Biotechnology, Faculty of Engineering, Kyoto Sangyo University, Kyoto, Japan

References

1. Saunders S, Jalkanen M, O'Farrell S, Bernfield M. Molecular cloning of syndecan, an integral membrane proteoglycan. J Cell Biol 1989;108:1547–56.
2. Marynen P, Zhang J, Cassiman JJ, Van den Berghe H, David G. Partial primary structure of the 48- and 90-kilodalton core proteins of cell surface-associated heparan sulfate proteoglycans of lung fibroblasts. Prediction of an integral membrane domain and evidence for multiple distinct core proteins at the cell surface of human lung fibroblasts. J Biol Chem 1989;264:7017–24.
3. Gould SE, Upholt WB, Kosher RA. Syndecan 3: a member of the syndecan family of membrane-intercalated proteoglycans that is expressed in high amounts at the onset of chicken limb cartilage differentiation. Proc Natl Acad Sci U S A 1992;89:3271–5.
4. Kojima T, Leone CW, Marchildon GA, Marcum JA, Rosenberg RD. Isolation and characterization of heparan sulfate proteoglycans produced by cloned rat microvascular endothelial cells. J Biol Chem 1992;267:4859–69.
5. Bernfield M, Kokenyesi R, Kato M, Hinkes MT, Spring, J, Gallo RL, et al. Biology of the syndecans: a family of transmembrane heparan sulfate proteoglycans. Annu Rev Cell Biol 1992;8:365–93.
6. Bernfield M, Gotte M, Park PW, Reizes O, Fitzgerald ML, Lincecum J, et al. Functions of cell surface heparan sulfate proteoglycans. Annu Rev Biochem 1999;68:729–77.
7. Rapraeger AC. Syndecan-regulated receptor signaling. J Cell Biol 2000;149:995–8.
8. Oguri K, Munesue S, Kusano Y, Yoshitomi Y, Okayama M. Involvement of syndecans in actin cytoskeletal organization and tumor metastasis. Connect Tissue Res 2002;34:283–90.
9. Gallagher JT. Heparan sulfate: growth control with a restricted sequence menu. J Clin Invest 2001;108:357–61.
10. Inki P, Jalkanen M. The role of syndecan-1 in malignancies. Ann Med 1996;28:63–7.
11. Seidel C, Sundan A, Hjorth M, Turesson I, Dahl IM, Abildgaard N, et al. Serum syndecan-1: a new independent prognostic marker in multiple myeloma. Blood 2000;95:388–92.
12. Wiksten JP, Lundin J, Nordling S, Kokkola A, Haglund C. A prognostic value of syndecan-1 in gastric cancer. Anticancer Res 2000;20:4905–8.
13. Zellweger T, Ninck C, Mirlacher M, Annefeld M, Glass AG, Gasser TC, et al. Tissue microarray analysis reveals prognostic significance of syndecan-1 expression in prostate cancer. Prostate 2003;55:20–9.

14. Barbareschi M, Maisonneuve P, Aldovini D, Cangi MG, Pecciarini L, Angelo Mauri F, et al. High syndecan-1 expression in breast carcinoma is related to an aggressive phenotype and to poorer prognosis. Cancer 2003;93:474–83.
15. Wijdenses J, Vooijs WC, Clement C, Post J, Morard F, Vita N, et al. A plasmocyte selective monoclonal antibody (B-B4) recognizes syndecan-1. Br J Haematol 1996;94:318–23.
16. Seidel C, Sundan A, Hjorth M, Turesson I, Marie I, Dahl S, et al. Serum syndecan-1: a new independent prognostic marker in multiple myeloma. Blood 2000;95:388–92.
17. Watari J, Saitoh Y, Fujiya M, Shibata N, Tanabe H, Inaba Y, et al. Reduction of syndecan-1 expression in differentiated type early gastric cancer and background mucosa with gastric cellular phenotype. J Gastroenterol 2004;39:104–12.
18. Matsumoto A, Ono M, Fujimoto Y, Gallo RL, Bernfield M, Kohgo Y. Reduced expression of syndecan-1 in human hepatocellular carcinoma with high metastatic potential. Int J Cancer 1997;74:482–91.
19. Tanabe H, Yokota K, Kohgo Y. Localization of syndecan-1 in human gastric mucosa associated with ulceration. J Pathol 1999;187:338–44.
20. Ohtake T, Fujimoto Y, Ikuta K, Saito H, Ohhira M, Ono M, et al. Proline-rich antimicrobial peptide, PR-39 gene transduction altered invasive activity and actin structure in human hepatocelluar carcinoma cells. Br J Cancer 1999;81:393–403.
21. Toyoshima E, Ohsaki Y, Nishigaki Y, Fujimoto Y, Kohgo Y, Kikuchi K. Expression of syndecan-1 is common in human lung cancers independent of expression of epidermal growth factor receptor. Lung Cancer 2001;31:193–202.
22. Fujiya M, Watari J, Ashida T, Honda M, Tanabe H, Fujiki T, et al. Reduced expression of syndecan-1 affects metastatic potential and clinical outcome in patents with colorectal cancer. Jpn J Cancer Res 2001;92:1074–81.
23. Leppa S, Vleminckx K, Roy FV, Jalkanen M. Syndecan-1 expression in mammary epithelial tumor cells is E-cadherin-dependent. J Cell Sci 1996;109:1393–409.
24. Day RM, Hao X, Ilyas M, Daszak P, Talbot IC, Forbes A. Changes in the expression of syndecan-1 in the colorectal adenoma-carcinoma sequence. Virchows Arch 1999;434;121–5.

京 都 産 業 大 学

先端科学技術研究所所報　第3号（抜刷）

平 成 16 年 7 月 発 行

シンデカン-2を介したがん転移の制御機構の解析

棟　居　聖　一
吉　冨　泰　央
小　山　芳　江
成　尾　英　明
岡　山　　實

京 都 産 業 大 学
先端科学技術研究所

シンデカン-2を介したがん転移の制御機構の解析

棟居聖一
吉冨泰央
小山芳江
成尾英明
岡山實

要旨

マウス・ルイス肺癌から転移能の違いに基づいてクローン化した株細胞は，生体内での一次腫瘍組織形成において全く異なる細胞外マトリックス依存性を示す．即ち，低転移性P29株細胞は，宿主間質誘導能が強く，誘導された間質細胞の形成するフィブロネクチンに富んだ間質型細胞外マトリックス依存的な腫瘍組織形成を示す．それに対して高転移性LM66-H11株細胞は自らが形成する基底膜依存的な腫瘍組織形成を示す．この腫瘍組織形成の違いを反映して培養下において，これらの株細胞はフィブロネクチン基質への接着に際して異なったアクチン細胞骨格形成を示す．これまでに，この接着応答性の違いが細胞表層に存在するヘパラン硫酸プロテオグリカン・シンデカン-2の発現量に依存する現象であること，これらの株細胞の転移能とシンデカン-2発現量との間に逆相関が存在することを明らかにしてきた．

本研究ではシンデカン-2低発現性の高転移性LM66-H11株細胞にシンデカン-2を強制発現させたH11-SN2株細胞を用いて，この逆相関の背後に因果関係のあることを証明した．さらに，このシンデカン-2による転移抑制の機構を明らかにするために，がん転移に際して重要な役割を果たすことが報告されているマトリックスメタロプロテアーゼ（以下，MMPと略）とシンデカン-2との関係について検討した．その結果，MMP-2およびMMP-2活性化関連分子である膜型（以下，MTと略）1-MMP，Tissue inhibitor of metalloproteinase（以下，TIMPと略）-2の転写レベルは，シンデカン-2の発現量の高低に拘わらず，すべての株細胞間で同程度であった．しかし，その活性化はシンデカン-2低発現性・高転移性LM66-H11株細胞においては大きく亢進されているのに対して，シンデカン-2高発現性・低転移性P29およびH11-SN2株細胞においては強く抑制されていることが明らかとなった．さらに，細胞表層からヘパラン硫酸鎖を酵素的に除去したP29株細胞および，LM66-H11株細胞にシンデカン-2タンパク芯のグリコサミノグリカン鎖付加部位のセリン残基をアラニンに変異させた変異体を強制発現させたH11-SN2ΔGAG株細胞においてはMMP-2の活性化が観察された．以上の結果は，シンデカン-2がMMP-2の活性制御に直接関与していることを強く示唆している．

緒　論

癌転移の過程は，腫瘍細胞の原発巣からの遊離と浸潤，リンパ管や血管といった脈管への侵入，脈管内移動，標的臓器内毛細管の内皮細胞への接着，脈管外への浸出，組織への侵入，定着及び増殖からなると考えられている[1-3]．このような過程の各段階の機構及びそれに関わる分子の機能を明らかにすることは，がん転移の抑制の方法を考える上で極めて重要なことである．これまでに，腫瘍組織形成の視点から，がん転移を明らかにする様々な研究が行われてきた．本研究室ではこれまで，腫瘍の組織形成において細胞環境を構成する複雑な超分子複合体である細胞外マトリックスの役割に着目して研究を行ってきた．細胞外マトリックスは，主成分としてコラーゲン，糖タンパク質，プロテオグリカンからなる超分子複合体で，大きく2つに分けることができる[4-7]．1つは，上皮性の細胞が形成する基底膜で，上皮組織と結合組織との境界膜として存在し，その主要構成成分は，Ⅳ型コラーゲン，ラミニン，パールカンである．もう1つは，間質系の細胞によって形成される間質型細胞外マトリックスで，結合織細胞を取り囲む無定形の構造で，その主要構成成分は，Ⅰ型コラーゲン，フィブロネクチン，バーシカンである．これら細胞外マトリックスは，多細胞体構築に際して，細胞の足場として細胞増殖，分化，移動等の調節に機能し，組織形成に重要な役割を果たしている[9-12]．腫瘍組織形成という点でも，腫瘍細胞と細胞外マトリックスとの相互作用は，正常細胞の場合と同様に重要な役割を果たしている．しかし自然癌を用いてこの複雑な超分子複合体である細胞外マトリックスと腫瘍組織形成の関係を明らかにすることは困難である．本研究室では，単純化した解析系で腫瘍組織形成に基づくがん転移の機構を明らかにするために，マウス・ルイス肺癌から自然転移能に基づいて転移能の異なる腫瘍細胞がクローン化され，株細胞（低転移性P29，中転移性LM12-3，高転移性LM66-H11株細胞）として樹立された．これらの株細胞を同系マウス（C57/BL）の皮下に移植して作らせた一次腫瘍組織を用いて，細胞外マトリックスを中心に転移能に共軛した組織学的特徴を解析した[3,7,8]．その結果，P29およびLM66-H11株細胞が生体内において全く異なる細胞外マトリックス依存的腫瘍形成を示すことが示された．即ち，LM66-H11株細胞は基底膜形成能が高く，腫瘍細胞はそれを足場にした腫瘍組織形成を示す[14,15]．それに対してP29株細胞は基底膜形成能をもたず，それに代わって宿主組織に対して強い間質誘導性を示し，誘導された間質細胞の形成するフィブロネクチンに富んだ間質型細胞外マトリックス依存的な組織形成を示した[3,15,16]．

上記の組織形成の違いを反映して，両株細胞は，培養下においてフィブロネクチン基質への接着に際して顕著に異なる接着応答性を示す[17]．即ち，P29株細胞はフィブロネクチン基質への接着に際してストレスファイバー形成を示すのに対して，LM66-H11株細胞においては，アクチン繊維が細胞辺縁部に局在化する皮質型アクチンの形成を示す．これまでの研究において，これらの応答性の違いは細胞表層のフィブロネクチン受容体の一つ，シンデカン-2の発現

量の違いによること，シンデカン-2発現量と転移能の間に逆相関が存在することを明らかにしてきた．本研究の目的は，シンデカン-2発現量と転移能の間に存在する関係を明らかにし，シンデカン-2の転移における役割を明らかにすることである．

結　　果

マウス・ルイス肺癌（3LL）から転移能の異なる株細胞の樹立

自然癌は，ほとんど転移しない腫瘍細胞から，非常に高い転移能を示す腫瘍細胞まで多様な転移活性をもった細胞から成るキメラ組織である．転移能に共軛した腫瘍組織形成を明らかにするため，まず自然癌から転移能の異なる細胞を自然転移能の差に基づいてクローン化し，株細胞として樹立した．本研究では腫瘍細胞としてマウス・ルイス肺癌（3LL）細胞を用い転移能の異なる腫瘍細胞をクローン化し，株細胞として樹立した（表1）[13,14]．これらの株細胞を用いて以下の実験を行った．

表1　マウス・ルイス肺癌由来の株細胞が示す転移能

株細胞	移植経路	移植細胞数 ($\times 10^5$)	転移動物数	肺転移結節数	
			実験動物数	平均	範囲
P29	i.v.	1.0	3/7	0.4	0 - 1
LM12-3	i.v.	1.0	7/7	47.9	19 - 92
LM66-H11	i.v.	1.0	7/7	516.2	467 - 744
P29	s.c.	2.0	0/7	0	0
LM12-3	s.c.	2.0	6/7	4.5	0 - 14
LM66-H11	s.c.	2.0	7/7	35.2	23 - 56

i.v.: 静脈移植、s.c.: 皮下移植。

転移能の異なる株細胞の発現するシンデカンファミリー

これまでの研究で，シンデカン発現量の高い低転移性P29株細胞がフィブロネクチンに接着する際にその受容体としてインテグリン$\alpha 5\beta 1$とシンデカン-2とで結合し，協調的に作用した結果，ストレスファイバー形成を誘導することを明らかにすると同時に，高転移性LM66-H11株細胞はシンデカン-2の発現量が閾値以下であるためにインテグリンのみを介した接着の結果，皮質型アクチン形成を示すことを明らかにしてきた[17]．そこで，中転移性株細胞を含む，転移能の異なる3つの株細胞を用いて細胞表層でのシンデカンファミリーの発現量をFACSにより解析したところ，中転移性LM12-3株細胞は中程度のシンデカン-2発現量を示した（図1）．この発現はノーザンブロットによるmRNAの発現でも確認された（図示せず）．すなわち，転

移能が高くなるにつれて，シンデカン-2発現量が減少しており，シンデカン-2発現量と転移能との間には逆相関の存在することが明らかとなった．また，他のシンデカンファミリーの発現に有意な差は見られなかった．

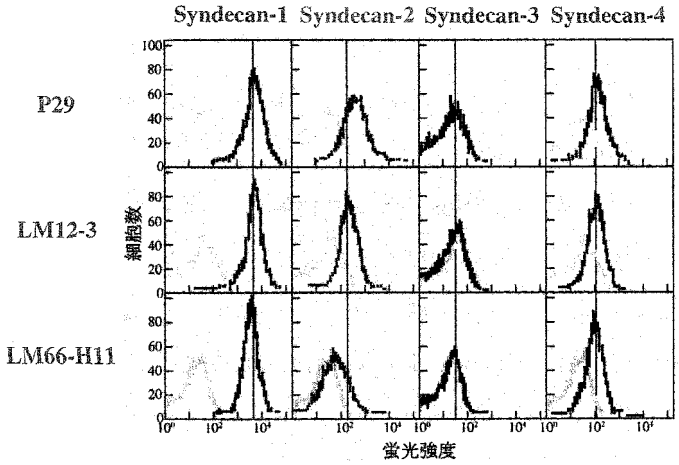

図1 転移能の異なる株細胞におけるシンデカンファミリーの細胞表層発現
低転移性P29株細胞，中転移性LM12-3株細胞，高転移性LM66-H11株細胞の細胞表層シンデカンファミリーの発現を，シンデカン-1，-2，-3および-4各々に特異的な抗体SN1，SN2，SN3およびSN4Abを用いてフローサイトメーターで測定した．これらの結果は，転移能とシンデカン-2の発現の間に逆相関のあることを示した．灰色線は非免疫血清を用いた対照を示す．

シンデカン-2強制発現株細胞の転移能

逆相関を示したシンデカン-2発現量と転移能との関係を明らかにするため，高転移性でシンデカン-2低発現性のLM66-H11株細胞にマウス・シンデカン-2 cDNAを導入し，安定高発現H11-SN2株細胞を樹立した．この細胞のシンデカン-2発現量はFACS分析（図2A），ノーザンブロット，ヘパリチナーゼⅠおよびⅡ消化によって生ずる不飽和糖を認識するF58-3G10抗体によるウエスタンブロット，シンデカン-2タンパク芯に対する抗体を用いたウエスタンブロット（図示せず）で確認した結果，低転移性でシンデカン-2高発現性P29株細胞と同程度の発現量を示した．一方，このシンデカン-2強制発現によって他のシンデカンファミリーの細胞表層発現には影響を及ぼさなかった（図2A）．このようにして樹立したH11-SN2株細胞を用いて実験転移能および自然転移能を解析した．P29，LM66-H11，H11-SN2，ベクターのみを導入したH11-Vec株細胞をマウス尾静脈に注射し，16日後の肺を摘出した（図2B）．P29株細胞注入マウスの肺に殆ど転移結節が認められないのに対して，LM66-H11株細胞注入マウスの肺においては非常に多くの転移結節が観察された．H11-Vec株細胞注入マウスの肺転移結節数はLM66-H11株細胞注入マウスのそれと非常に似ているが，H11-SN2株細胞注入マウスの肺には転移結節は殆ど認められなかった．表2に尾静脈及び皮下移植によって形成された肺転移結節の計測値を示した．また湿重量の結果（図示せず）も，肺転移像と良く一致した．この結果は，LM66-H11株細胞のシンデカン-2発現を人為的に高発現にすることによって，転移能が大きく

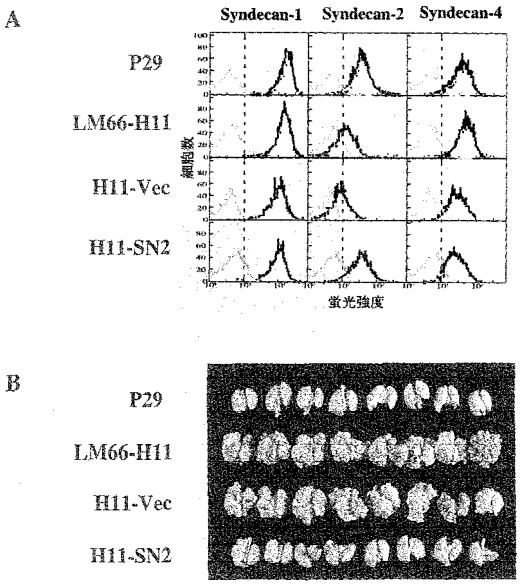

図2　シンデカン-2低発現性の高転移性H11株細胞におけるシンデカン－2高発現化の転移能への影響
A: P29株細胞，LM66-H11株細胞，LM66-H11株細胞にベクターのみを導入したH11-Vec株細胞，LM66-H11株細胞にシンデカン－2cDNAを導入し，強制発現させたH11-SN2株細胞の細胞表層シンデカンファミリーの発現を，各シンデカンのタンパク芯に対する特異抗体を用いてフローサイトメーターで測定した．灰色線は非免疫血清を用いた対照を示す．これらの結果は，シンデカン-2の高発現化は他のシンデカンの発現に影響を及ぼさないことを示している．
B: 各細胞（2×10^5細胞）をそれぞれマウス尾静脈に移植し，16日後に屠殺して肺を摘出し，ブアン・ドゥボスク固定液中で固定した後撮影した．

表2　シンデカン－2高発現性高転移細胞が示す転移能

株細胞	移植経路	移植細胞数 (x 10^5)	転移動物数	肺転移結節数	
			実験動物数	平均	範囲
P29	i.v.	2.0	6/8	2.9	0 - 9
LM66-H11	i.v.	2.0	8/8	977.9	661-1311
H11-Vec	i.v.	2.0	8/8	688.3	235 - 1405
H11-SN2	i.v.	2.0	6/8	6.8	0 - 23
P29	s.c.	2.0	3/8	0.6	0-3
LM66-H11	s.c.	2.0	7/7	29.7	3 - 69
H11-Vec	s.c.	2.0	7/7	32.1	4 - 79
H11-SN2	s.c.	2.0	1/8	0.1	0 - 1

i.v.: 静脈移植、s.c.: 皮下移植。

抑制されたことを示している．即ち，シンデカン-2の発現量と転移能との間の逆相関の背後には因果関係が存在することが明らかとなった．

ルイス肺癌細胞の示す転移能とMMP-2の活性化

この転移抑制の機構を明らかにする為の手始めとして腫瘍の転移・浸潤に直接的に関与して

いることが知られているMMPがこの腫瘍系の転移に関わっているかどうかを検討した．先ず腫瘍の転移においてその関与が多く報告されているMMP-2について検討した[17,18,19]．MMP-2は不活性の潜在型酵素として分泌され，細胞外マトリックス分解活性を発揮するには活性化の過程を経る．潜在型MMP-2（72kDa）は細胞外に分泌された後に，MT1-MMPおよびTIMP-2と活性化複合体を形成し，複合体形成に関与していないMT1-MMPにより潜在型MMP-2のプロペプチドのAsn37-Leu38間が加水分解されて中間型MMP-2（68kDa）になり，その後，自己触媒により活性型MMP-2（62kDa）となる（図3）[21-26]．低転移性P29株細胞の無血清培養上清中には72kDaの潜在型MMP-2バンドが主要バンドとして検出されるのに対して，高転移性LM66-H11株細胞の無血清培養上清中には72kDaの潜在型，68kDaの中間型および62kDaの活性型MMP-2のバンドが検出された（図4）．H11-Vec株細胞の無血清培養上清中からは，LM66-H11株細胞の無血清培養上清中と同様，潜在型，中間型および活性型MMP-2の3本のバンドが検出された．それに対して，シンデカン-2を強制発現させたH11-SN2株細胞由来の無血清培養上清中においてはP29株細胞由来の試料と同様，潜在型MMP-2が主要成分であり，中間型，活性型MMP-2は殆ど検出されなかった．この結果を定量化し，潜在型MMP-2の量に対する中間型および活性型MMP-2の割合を比較した結果，親株のLM66-H11株細胞と比べて，H11-Vec株細胞は同程度の活性化を示したのに対して，シンデカン-2強制発現H11-SN2株細胞の示す活性化は80%の減少を示した（表3）．この結果はシンデカン-2強制発現による転移の抑

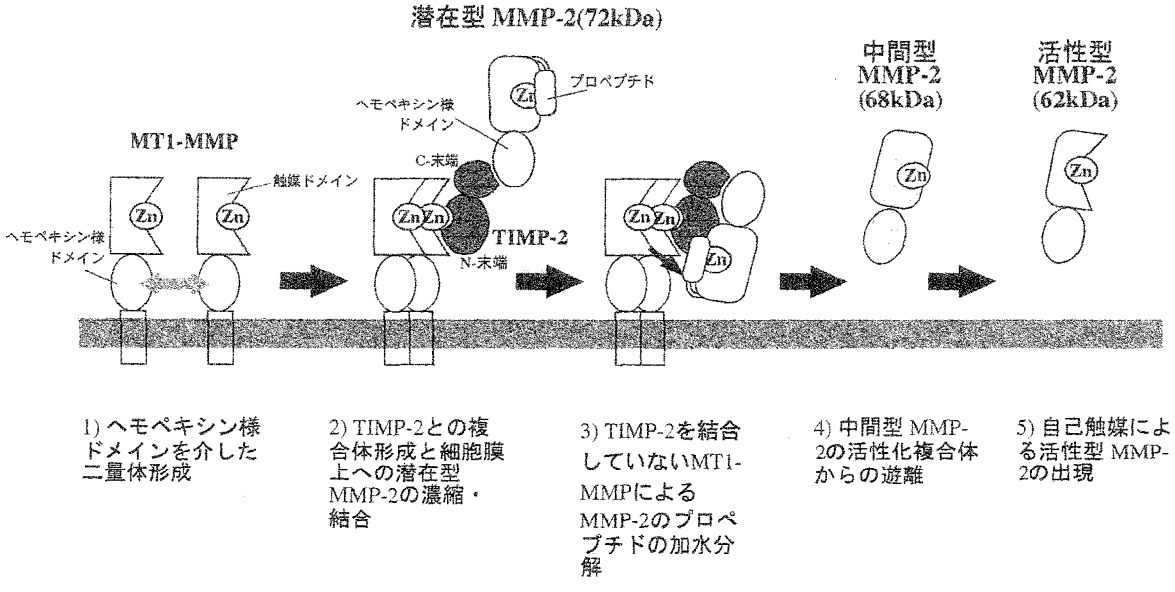

図3 MMP－2の細胞膜表面での活性化機序

MMP-2の細胞膜表面での活性化の機序は1）MT1-MMPのヘモペキシン様様ドメインを介した二量体形成に引き続き，2）TIMP-2，潜在型MMP-2が結合し活性化複合体が形成される．3）TIMP-2を結合していないMT1-MMPにより潜在型MMP-2のプロペプチドAsn37-Leu38を加水分解され，4）中間型MMP-2となり細胞膜から遊離し，5）自己触媒により活性化型MMP-2になる，という過程を経ると考えられている．（参考文献16より改変）

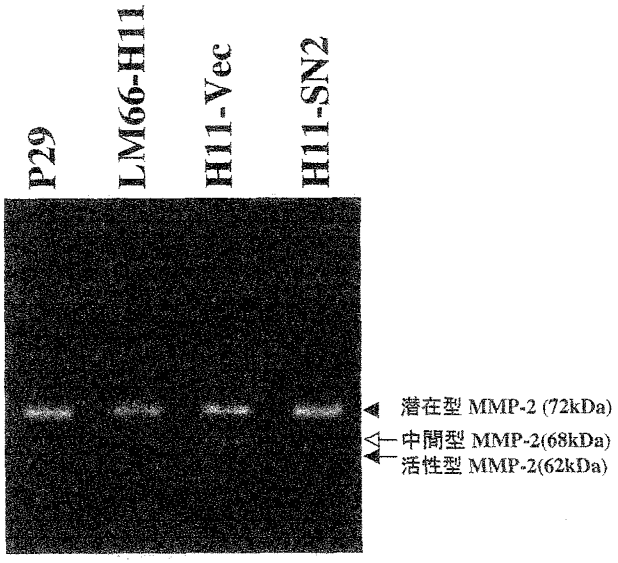

図4　ルイス肺癌細胞の産生するゼラチナーゼとその動態

P29，LM66-H11，H11-VecおよびH11-SN2株細胞より得られた無血清培養上清を，ゼラチンを基質としたザイモグラフィーによりルイス肺癌細胞の産生するMMPの分子種とその動態を検討した結果，すべての株細胞が潜在型MMP-2に相当する分子量を持つ位置（72kDa）に泳動するMMPを産生していた．更には，高転移性LM66-H11およびH11-Vec株細胞の無血清培養上清中には中間型及び活性型MMP-2に相当する位置に泳動するゼラチン分解バンドを検出した．

表3　シンデカン-2強制発現によるMMP-2活性化抑制

株細胞	P29	LM66-H11	H11-Vec	H11-SN2
活性化 (%)*	22.1	80.9	93.1	16.5
対 LM66-H11 (%)**	27.3	100	115	20

*活性化（%）は、Isnardらの方法[20]に従って計算し、MMP-2活性(%)＝
中間型バンド+活性型バンド / 潜在型バンド × 100で計算した。
**LM66-H11細胞に対する各細胞の活性化の割合を示した。

制実験の結果とよい一致を示している．

シンデカン-2発現のMMP-2活性化分子の発現に及ぼす影響

シンデカン-2高発現性株細胞の培養系におけるMMP-2活性化の抑制機構を解析するにあたって，先ず，MMP-2活性化に関与する分子群の発現に差異がないかどうかを解析した．ノーザンブロットの結果，MMP-2，MT1-MMPおよびTIMP-2の発現はシンデカン-2の発現の高低に拘わらず4つの株細胞間で有意な違いは見られなかった（図5）．そこで次にシンデカン-2がMMP-2活性化過程へ関与している可能性について検討した．

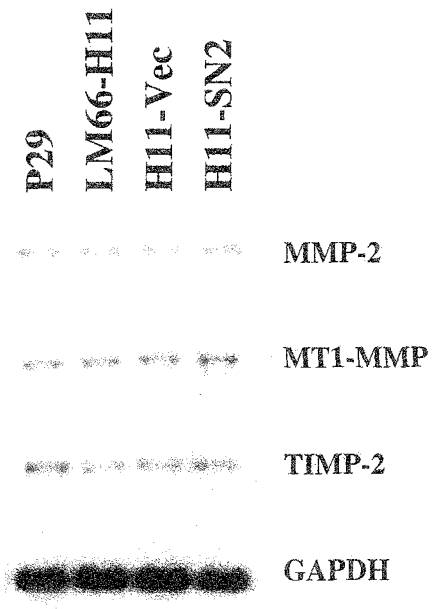

図5 転移能の異なる株細胞におけるMMP-2活性化に関与する分子群の発現P29，LM66-H11，H11-VecおよびH11-SN2株細胞から抽出したポリ(A)+RNAを用いてノーザンブロット法によりMMP-2，MT1-MMP，TIMP-2mRNAの発現量を比較した．細胞で恒常的に発現しているGAPDHの発現を対照として用いた．

MMP-2活性化におけるシンデカン-2ヘパラン硫酸鎖の関与

シンデカンの機能として，その分子の持つヘパラン硫酸鎖を介して増殖因子，あるいは細胞外マトリックス成分に結合し，その結合シグナルを直接あるいは間接的に細胞内に伝達することが明らかにされている[28-30]．これまでの研究から，MMP-2の持つヘモペキシン様ドメインはヘパリン結合性を示すことが報告されている[13,31,32]．また，MMP-2はヘパリンと結合することによりAsn80-Tyr81の間の自己消化の活性が亢進することも明らかにされている[31]．従って，本研究で示したシンデカン-2の高発現によりMMP-2の活性化が抑制される現象にはシンデカン-2ヘパラン硫酸鎖の関与の可能性が考えられた．そこで，シンデカン-2タンパク芯のグリコサミノグリカン鎖付加部位のセリン残基をアラニン残基に変異させた変異体を強制発現させたH11-SN2ΔGAG株細胞のMMP-2活性化，さらにはヘパリチナーゼⅠにより細胞表層のヘパラン硫酸鎖を除去した場合のMMP-2活性化をゼラチンザイモグラフィーにより検討した．まずP29株細胞をヘパリチナーゼⅠ消化することにより細胞表層からヘパラン硫酸鎖が除かれていることを抗不飽和ヘパラン硫酸抗体F58-10E4を用いたFACS分析により確認した（図6Aa）．また，シンデカン-2タンパク芯を認識するSN2Ab抗体を用いたFACS分析により，H11-SN2ΔGAG細胞膜表層におけるシンデカン-2タンパク芯の発現がP29細胞と同程度であることも確認した（図6Ab）．これらの細胞から調製した無血清培養上清を用いたゼラチンザイモグラフィーの結果を図6Bに示した．H11-SN2ΔGAG株細胞の培養系ではヘパラン硫酸鎖を持つH11-SN2株細胞の培養系と比較して高いMMP-2の活性化が観察され，これらのバンドを定量

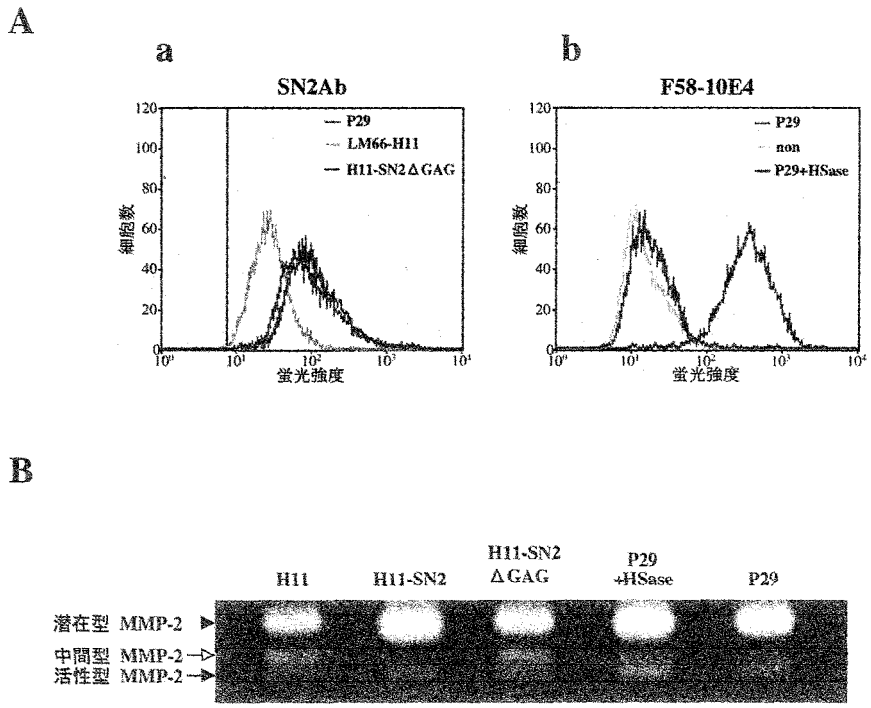

図6　MMP-2活性化における細胞表層ヘパラン硫酸鎖およびシンデカン-2ヘパラン硫酸鎖に対する依存性

A-a：未処理（P29）（濃灰色）あるいは0.1U/mlのヘパリチナーゼⅠで消化（P29+HSase）したP29細胞（赤色）を，ヘパラン硫酸鎖を特異的に認識するF58-10E4抗体と反応させ，FITC-標識二次抗体で標識した後，フローサイトメーターで蛍光強度を測定した．非免疫IgGを一次抗体として用いた結果を対照とした（non）（薄灰色）

A-b：グリコサミノグリカン鎖を持たないシンデカン-2を高発現するH11-SN2ΔGAG株細胞（赤線）を，対照としてP29株細胞（濃灰色）およびLM66-H11株細胞（薄灰色）を用い，シンデカン-2タンパク芯を特異的に認識するSN2Ab抗体と反応させ，FITC-標識二次抗体で標識した後，フローサイトメーターで蛍光強度を測定した．縦実線は非免疫IgGを一次抗体として用いた対照の蛍光強度のピークの位置を示す．

B：LM66-H11株細胞，H11-SN2株細胞，H11-SN2ΔGAG株細胞，ヘパリチナーセ処理したP29株細胞（P29+HSase）および未処理のP29株細胞（P29）のから得た無血清培養上清を用いてゼラチンザイモグラフィーによりMMP-2活性化を解析した．

表4　細胞表層ヘパラン硫酸およびシンデカン-2ヘパラン硫酸側鎖によるMMP－2活性化抑制

株細胞	LM66-H11	H11-SN2	H11-SN2 ΔGAG	P29 +HSase	P29
活性化 (%)	68.2	34.8	65.8	55.3	39.3
対 LM66-H11 (%)*	100	50	96	81.1	57.6
対 P29 (%)**	173.5	88.5	167.4	141	100

*LM66-H11細胞に対する各細胞の活性化の割合、**P29細胞に対する各細胞の活性化の割合を示した。

化した結果，H11-SN2株細胞による活性化の割合は，H11株細胞のそれと比較して50%減少していた．これに対し，H11-SN2ΔGAG株細胞による活性化はH11株細胞のそれと比較して4%の減少しか示さず，H11株細胞とほぼ同じ程度の活性化を示した（表4）．これはヘパラン硫酸鎖を持たないシンデカン-2を強制発現させてもMMP-2の活性化に対して抑制的には作用し得ないこと，すなわちMMP-2活性化の抑制はシンデカン-2のヘパラン硫酸鎖を介した現象であることを強く示唆している．また，シンデカン-2高発現性のP29株細胞をヘパリチナーゼⅠ共存下で培養して得た無血清培養上清を用いたザイモグラフィーの結果では酵素を加えないコントロールと比較して有意にMMP-2の活性化が亢進されていた（図6B）．デンシトメトリーによる定量の結果，未処理のP29株細胞と比較してヘパリチナーゼⅠ消化することによりMMP-2の活性化の割合が41%増加していた（表4）．この結果は先のH11-SN2ΔGAG株細胞の結果とよい一致を示している．以上の結果は，シンデカン-2が，MMP-2の活性抑制に直接関与していることを強く示唆している．

考　　察

本研究室でのこれまでの研究において，マウス・ルイス肺癌から自然転移能の違いに基づいてクローニングした株細胞をもちいて，これらの株細胞が，フィブロネクチン基質への接着に際して全く異なったアクチン細胞骨格形成を示し，この接着応答性の違いは細胞表層に存在するヘパラン硫酸プロテオグリカン・シンデカン-2の発現量の違いに依存していることが明らかにされている[17,33]．しかし，シンデカン-2の癌転移への関与の様式および作用の機構についてはいまだに明らかにされていない．そこで，先ず，転移能の異なる3つの株細胞を用い，転移能と細胞表層シンデカンの発現量との間に一定の関係が存在するかどうかを解析した．その結果，ルイス肺癌はシンデカンファミリーすべてのファミリーメンバーを発現していたが，そのうちシンデカン-2の発現量と転移能との間に逆相関が存在することが明らかとなった．それ以外のシンデカンは，転移能の高低に関わらず発現レベルに有意な差は観察されなかった．この実験結果に基づき，上記の逆相関の背後に因果関係があるか否かを明らかにするため，シンデカン-2低発現性の高転移性LM66-H11株細胞にシンデカン-2 cDNAを導入し強制発現させた安定高発現株H11-SN2株細胞を用い，転移能を測定したところ，シンデカン-2を高発現させることにより転移が大きく抑制された．つまりルイス肺癌においてはシンデカン-2発現量のみを人為的に変化させることにより転移能を自由にコントロールすることが可能となった．

次に，細胞表層でのシンデカン-2の強制発現が高転移性LM66-H11株細胞の転移を抑制したことから，その機構に興味が持たれた．転移が成立するためには，癌細胞の一次腫瘍からの遊離，血管内侵入，転移先での血管外侵出など，癌細胞が乗り越えなければならない生物構造的障壁が多く存在する．これらの構造的障壁となっている細胞外マトリックスを分解し，癌の悪

性化への関与が明らかにされている分子としてMMPがある．多くのMMPが，がん細胞株あるいは組織切片の解析などからがん転移に関連して報告されている[18]．しかしながらどのMMPが癌の浸潤，転移に作用しているかは明らかにされていない．がん転移の過程で脈管への侵入，標的組織での脈管から標的組織への侵入など，基底膜破壊が重要なステップであると考えられてきた．基底膜の主要な構成成分であるⅣ型コラーゲンは基底膜の密な網目構造を形成している．このような理由からこれまでにⅣ型コラーゲン分解活性が癌細胞の悪性度を特徴づける一つの指標であるとして考えられている[19]．がん細胞が産生するⅣ型コラーゲン分解酵素としてはMMP-2，MMP-9が主要であり，これらのがん組織での発現や局在が数多く報告されている[34]．本研究において転移能の異なる細胞で，転移能と一致したMMP-2の著しい活性化が認められた．すなわち，高転移性LM66-H11株細胞において高いMMP-2の活性化を示した．注目すべきはシンデカン-2を強制発現させ，転移を抑制したH11-SN2株細胞ではMMP-2活性化が抑制されていたことである．これはシンデカン-2によりMMP-2活性化が抑制され，その結果として転移が抑制されたことを示唆している．MMP-2の活性化機構は試験管内でMT1-MMPの触媒部位を用いた実験により明らかにされている[35]．即ち，MT1-MMPが潜在型MMP-2プロペプチドのAsn37とLeu38との間を加水分解し，それによって生じた中間型MMP-2は自己触媒的にAsn80とTyr81の間が加水分解され活性型MMP-2となる．Satoらは膜貫通型のMT1-MMPが細胞膜上で潜在型MMP-2を活性化することを明らかにした[21]．まず，細胞表層に発現したMT1-MMPは阻害分子であるTIMP-2と複合体を形成し，その酵素活性が阻害をうける．TIMP-2のC-末端ドメインはMMP-2のヘモペキシン様ドメインと親和性があるため，細胞膜表面にMT1-MMP，TIMP-2，MMP-2の3者複合体が形成される．この複合体はMMP-2を膜表面に濃縮するための受容体として機能する[36]とともに潜在型MMP-2の活性化に必須であり，この複合体構成分子間の相互作用を阻害すると活性化はおこらない．また，MT1-MMPはTIMP-2により酵素活性が阻害されているので潜在型MMP-2を分解し，活性化することができない．このため，TIMP-2を結合していない遊離のMT1-MMPがMMP-2を活性化するというモデルが考えられ，それを支持する結果が多く報告されている[22-26]．しかし，遊離のMT1-MMPが上記3者複合体の近傍にどのように存在し，それによってMMP-2の活性化がどのように調節されているのかは明らかになっていない．最近，MT1-MMPがヘモペキシン様ドメインを介してホモ二量体を形成することが明らかにされ，そのヘモペキシン様ドメインを欠損するとMMP-2を活性化できないことからホモ二量体形成が，TIMP-2非結合性のMT1-MMPを上記3者複合体の近傍に保つ役割を担っていることが推論されている[37]．本研究において，転移能の異なるP29，LM66-H11およびシンデカン-2を強制発現したH11-SN2株細胞間で，これらMMP-2の活性化に寄与する分子群の発現量に有意な差は見いだされなかった．そこで本研究では，MMP-2の活性化抑制がシンデカン-2のどのような機能に基づくものかを検討した．シンデカン-2低発現性の高転移性LM66-H11株細胞にグリコサミノグリカン鎖を持たない変異

シンデカン-2を強制発現させてもMMP-2活性化の抑制は観察されず，また，シンデカン-2高発現性の低転移性P29株細胞から細胞表層のヘパラン硫酸鎖を酵素的に除いた培養系においては親細胞と比べMMP-2の有意な活性化の亢進が見られた．この結果はMMP-2活性化抑制にシンデカン-2のヘパラン硫酸鎖が関与していることを強く示唆するものである．MMP-2のヘモペキシン様ドメインはヘパリンに結合性をもつことが示されているが[23,31,32]，MMP-2は，試験管内で，ヘパリン共存下においてMMP-2の自己触媒的な活性化が8倍高くなることが報告されている[31]．上記の我々の得た結果ではMMP-2活性化の高いのはシンデカン-2の発現の低いLM66-H11株細胞であり，この報告と一見矛盾するが，次に示す“抑制モデル”と“競合モデル”の2つの可能性が考えられる．一つ目の“抑制モデル”は，シンデカン-2のヘパラン硫酸鎖によって直接MMP-2活性化が抑制されているという考えで，Crabbeらは一方で，試験管内におけるヘパリンによるMMP-2の活性化の促進において，高濃度のヘパリン存在下ではMMP-2は活性化されないことも報告している．即ち，その理由として適度なヘパリン（50-200μg/ml）存在下では潜在型MMP-2と，その活性化分子との間にヘパリンが梁のように入り，お互いをそのヘパリン結合性のヘモペキシン様ドメインによって結合し，活性化する．また，高濃度のヘパリン（200μg/ml以上）存在下では，過剰なヘパリンがこの結合を競合的に阻害する可能性があるとした[31]．これらのことを考え合わせると，細胞膜表層に存在するシンデカン-2のヘパラン硫酸鎖はLM66-H11株細胞よりもP29株細胞で高濃度であるため，MMP-2活性化を抑制したと考えることができる．2つ目の“競合モデル”は，シンデカン-2の

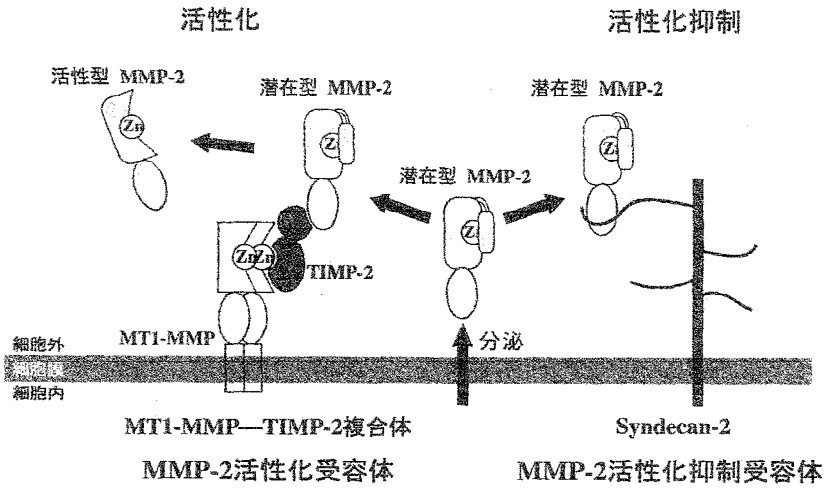

図7 シンデカン-2を介したMMP-2活性化の抑制機構の可能性
細胞から分泌された潜在型MMP-2がMT1-MMP—TIMP-2複合体に結合した結果MT1-MMPにより潜在領域が切断され活性化される．シンデカン-2高発現細胞では分泌された潜在型MMP-2がシンデカン-2のヘパラン硫酸鎖を介して結合することによりMT1-MMP—TIMP複合体への結合を競合した結果，MMP-2の活性化が抑制されたのではないかと考えられる．すなわち，MT1-MMP—TIMP-2複合体がMMP-2の活性化受容体として機能しているのに対してシンデカン-2はMMP-2の活性化抑制受容体として機能している可能性が考えられる．

ヘパラン硫酸鎖がMMP-2の活性化複合体への結合に対して抑制的に働いているという考えである．すなわち，潜在型MMP-2活性化受容体（MT1-MMP—TIMP2二量体）とシンデカン-2のヘパラン硫酸鎖は共にMMP-2のヘモペキシン様ドメインに結合することから，これら二者受容体間で潜在型MMP-2の結合における競合が起こり，MT1-MMPに対する基質濃度が調節されていることが考えられる（図7）．この“競合モデル”では，シンデカン-2が潜在型MMP-2の受容体として機能している必要があるが，最近これを裏付ける結果が得られた．細胞表層のヘパラン硫酸をヘパリチナーゼⅠで消化すると加えた酵素量に応じて潜在型MMP-2が細胞表層から遊離する（図示せず）ことが示された．すなわち，細胞表層のヘパラン硫酸鎖によって潜在型MMP-2が細胞膜上に保持されていることが明らかとなった．このような“競合モデル”の考えが正しいならば，ヘパラン硫酸鎖に結合した潜在型MMP-2はMT1-MMPの基質になり得ないような機構が存在しなければならないが，本研究ではそれを明らかにすることはできなかった．ルイス肺癌細胞に見られたMMP-2活性化におけるシンデカン-2ヘパラン硫酸鎖の特異的機能が，その化学構造に基づくものか，それともシンデカン-2の膜上における局在に基づくものなのかは今後の研究課題である．いずれにしても，MMP-2活性化制御におけるシンデカン-2のヘパラン硫酸鎖の役割については，今後さらに詳しく解析していく必要がある．

参考文献

1) Liotta, L.A., Tryggvason, K., Garbisa, S., Hart, I., Folts, C.M. and Shafie, S. (1980) Nature, ***284***: 67-68
2) Nakajima, M., Irimura, T., DiFerrante, N. and Nicolson, G.L. (1983) Science, ***220***: 611-613
3) 岡山實, 草野由理, 小栗佳代子（1996）現代化学, ***308***: pp. 51-57, 東京化学同人, 東京
4) Hedman, K. and Vaheri, A. (1989) in Fibronectin (Mosher, D.F., ed.) pp. 123-134, Academic Press, Inc. New York
5) Olsen, B.R., and Nakajima, Y. (1993) in Guidebook to the Extracellular Matrix and Adhesion Proteins (Kreis, T. and Vale, R., eds.) pp. 35-36, Oxford University Press, London
6) Farquhar, M.G. (1991) in Cell Biology of Extracellular Matrix, 2nd ed., (Hay, E.D., ed.) pp. 365-418, Prenum Press, New York
7) 小栗佳代子, 岡山實（1993）細胞社会のグリコバイオロジー（永井克孝, 箱守仙一郎, 木幡陽編）pp. 151-175, 講談社サイエンティフィック, 東京
8) 岡山實（1997）京都産業大学論集第28巻, 第4号, 自然科学系列Ⅱ第6号, pp .1-95
9) Grobstein, C. and Cohen, J. (1965) Science, 150: 626-628
10) Bernfield, M. and Banerjee, S. (1978) in Biology and Biochemistry of Basement Membrane (Kefalides, N.A., ed.) pp. 137-148, Academic Press, Inc. New York
11) Spooner, B.S., Thompson-Liestscher, H.A., Stokes, B. and Basset, K. (1986) in The Cell Surface in Development and Cancer (Steinberg, M.S., ed.) pp. 225-260, Plenum Press, New York
12) Nakanishi, Y. and Ishii, T. (1989) BioEssays, 11: 163-167

13) Nakanishi, H., Takenaga, K., Oguri, K., Yoshida, A. and Okayama, M. (1992) Virchows, Arch. A, ***420***: 163-170

14) Nakanishi, H., Oguri, K., Yoshida, K., Itano, N., Takenaga, K., Kazama, T., Yoshida, A. and Okayama, M. (1992) Biochem. J., ***288***: 215-224

15) Itano, N., Oguri, K., Nakanishi, H. and Okayama, M. (1993) J. Biochem., ***114***: 862-873

16) Itano, N., Oguri, K., Nagayasu, Y., Kusano, Y., Nakanishi, H., David, G. and Okayama, M. (1996) Biochem. J., ***315***: 925-930

17) Munesue, S., Kusano, Y., Oguri, K., Itano, N., Yoshitomi, Y., Nakanishi, H., Yamashina, I. and Okayama, M. (2002) Biochem. J., ***363***: 201-209

18) Fingleton, B. and Matrisian, L.M. (2001). Matrix metalloproteinases in cancer (Clendeninn NJ and Appelt K., ed.) pp. 85-112, Humana Press.

19) Liotta, L.A., Thorgeirsson, U.P. and Garbisa, S. (1982) Cancer Metastasis Rev, ***4***: 277-288

20) 伊藤義文. がんの浸潤・転移と細胞運動. 竹縄忠臣（編), 細胞骨格と細胞運動. シュプリンガー・フェアラーク, 2002

21) Sato, H., Takino, T., Okada, Y., Cao, J., Shinagawa, A., Yamamoto, E. and Seiki, M. (1994) Nature, ***370***: 61-65

22) Werb, Z. (1997) Cell, ***91***: pp. 439-442

23) Butler, G.S., Butler, M.J., Atkinson, S.J., Will, H., Tamura, T., van Westrum, S.S., Crabbe, T., Clements, J.,

24) d'Ortho, M.P., and Murphy, G. (1998) J Biol Chem., ***273***: 871-880, 1998.

25) Kinoshita, T., Sato, H., Okada, A., Ohuchi, E., Imai, K., Okada, Y. and Seiki, M. (1998) J. Biol. Chem., 273: 16098-16103

26) Seiki, M. (1999) APMIS, ***107***: 137-143

27) Nagase, H. and Woessner, J.F.Jr. Matrix metalloproteinases. (1999) J. Biol. Chem., ***274***: 21491-21494

28) Isnard, N., Robert, L. and Renard, G. (2003) Cell Biol. Int., ***27***: 779-784

29) Maccarana, M., Casu, B. and Lindahl U. (1993) J. Biol. Chem., ***268***: 23898-23905

30) Guimond, S., Maccarana, M., Olwin, B.B., Lindahl, U. and Rapraeger, A.C. (1993) J. Biol. Chem., ***268***: 23906-23914

31) McKeehan, W.L., Wang, F. and Kan, M. (1998) Prog. Nucleic Acid Res. Mol. Biol., ***59***: 135-176

32) Crabbe, T., Ioannou, C. and Docherty, A.J. (1993) Eur. J. Biochem., ***218***: 431-438

33) Crabbe, T., O'Connell, J.P., Smith, B.J. and Docherty, A.J. (1994) Biochemistry, ***33***: 14419-14425

34) Kusano, Y., Oguri, K., Nagayasu, Y., Munesue, S., Ishihara, M., Saiki, I., Yonekura, H., Yamamoto, H. and

35) Okayama, M. (2000) Exp. Cell. Res., ***256***: 434-444

36) Stetler-Stevenson, W.G., Aznavoorian, S. and Liotta, L.A. (1993) Annu. Rev. Cell Biol., ***9***, 541-573

37) Will, H., Atkinson, S.J., Butler, G.S., Smith, B. and Murphy, G. (1996) J. Biol. Chem., ***271***: 17119-17123

38) Strongin, A.Y., Collier, I., Bannikov, G., Marmer, B.L., Grant, G.A. and Goldberg, G.I. (1995) J. Biol. Chem., ***270***: 5331-5338

39) Itoh, Y., Takamura, A., Ito, N., Maru, Y., Sato, H., Suenaga, N., Aoki, T. and Seiki, M. (2001) EMBO J., ***20***: 4782-4793

京 都 産 業 大 学

先端科学技術研究所所報　第2号（抜刷）

平 成 15 年 7 月 発 行

シンデカン-2強制発現による腫瘍の組織形成と転移，浸潤能の変化

吉　冨　泰　央
棟　居　聖　一
小　山　芳　江
岡　山　　實

京 都 産 業 大 学
先端科学技術研究所

シンデカン-2強制発現による腫瘍の組織形成と転移，浸潤能の変化

吉冨泰央
棟居聖一
小山芳江
岡山實

要　旨

マウス・ルイス肺癌から転移能の違いに基づいてクローン化した株細胞は全く異なる一次腫瘍組織形成を示す．低転移性P29細胞は間質誘導能が強く，誘導した間質細胞の合成する間質型マトリックス依存的な腫瘍形成を示すのに対して，高転移性H11細胞は腫瘍基底膜依存的な腫瘍形成を示す．この違いを反映して培養下において，両株細胞は異なったフィブロネクチン接着応答性を示す．この応答性の違いが細胞表層に存在するシンデカン-2発現量に依存する現象であることを明らかにしてきた．

本研究ではシンデカン-2低発現性の高転移性H11細胞にシンデカン-2を強制発現させたH11-SN2細胞を樹立し，この細胞を用いて，これまで明らかにしてきた腫瘍組織形成，がん転移におけるシンデカン-2の役割を明らかにすることを目的として実験を行った．その結果，H11-SN2細胞は，増殖速度，飽和密度ともにシンデカン-2高発現性のP29細胞と同レベルを示し，驚いたことに転移能，間質誘導能ともにP29細胞と酷似した．また，H11細胞と比較してP29細胞は強い浸潤性を示し，さらに，P29腫瘍内に形成された腫瘍血管は典型的な毛細血管（capillary-like blood vessel）を形成していたのに対して，H11腫瘍に誘導された腫瘍血管は類洞様構造（sinusoid-like blood vessel）を示した．これらの一次腫瘍組織形成の違いは，がん転移，浸潤に関与することを強く示唆するものである．

緒　論

細胞と細胞外マトリックスとの相互作用は組織形成，細胞の動態を決定づける重要な役割を担っている．たとえば，上皮，内皮細胞は基底膜と相互作用し，間質細胞は間充織マトリックスと相互作用する．これらの相互作用は形態形成，創傷治癒や腫瘍形成などにおいて重要な役割を担っている[1-6]．細胞外マトリックスに急激な変化が起これば，その新しく形成された細胞外マトリックスと細胞との間に新しい相互作用が形成され，それによって細胞動態が左右さ

れる．すなわち，細胞外マトリックス内に蓄えられた情報は，細胞の受容体によって認識され，細胞内に伝達すると考えられている．がん細胞においてもまた，細胞外マトリックスとの相互作用の重要性は同じである[7-9]．

がんの転移・浸潤は，その自律的増殖性と共にがんの悪性度を特徴づける重要な側面であり，その防止はがん治療において重要な問題である．経験を積んだ病理医は腫瘍組織像からがんの悪性度を適確に判断し得る．このことから，浸潤性・転移性という腫瘍細胞の悪性度は腫瘍組織像に反映されている筈であると考え，本研究室では癌細胞と，それを取り巻く細胞外マトリックスの相互作用の視点から転移・浸潤の機構を明らかにすることを目的に研究が進められてきた[9-11]．

細胞外マトリックスは，コラーゲン，糖タンパク質，プロテオグリカンなどからなる超分子複合体で，大きく２つに分けることができる[9, 12-14]。１つは，上皮性の細胞が形成する基底膜で，上皮組織と結合組織との境界膜として存在し，その主要構成成分は，Ⅳ型コラーゲン，ラミニン，パールカンである。もう１つは，間質系の細胞によって形成される間質型ECMで，結合織細胞を取り囲む無定形の構造で，その主要構成成分は，Ⅰ型コラーゲン，フィブロネクチン，バーシカンである。

これまでの研究において，マウス・ルイス肺癌から自然転移能の違いに基づいてクローン化した転移能の異なる３つの株細胞（低転移性P29細胞，中転移性LM12-3細胞，高転移性LM66-H11細胞）を樹立した[15, 16]．これらの細胞を同系マウス（C57/BL）皮下に移植して形成した一次腫瘍の組織形成の組織学的特徴を解析した結果，転移能の異なる株細胞は全く異なった細胞外マトリックス依存性を示した[9-11]．すなわち，高転移性H11細胞は連続性の高い腫瘍基底膜を形成し，それを足場にした組織形成を示すのに対して，低転移性P29細胞は基底膜形成能を示さず，それに代わって強い間質誘導能を示し，誘導した間質細胞の形成する間質型マトリックス依存的な組織形成を示す．さらに，この違いを反映して，培養下におけるフィブロネクチン接着応答性も転移能の異なる株細胞間で明確に異なっており，P29細胞がフィブロネクチン接着依存的にストレスファイバー形成を示すのに対して，H11細胞はアクチン繊維が細胞の辺縁に集積した皮質型アクチンの形成を示す．これらの応答性の違いは細胞表層のフィブロネクチン受容体の一つ，シンデカン-2の発現量の違いによることを明らかにしてきた[17]．

本研究では，細胞外マトリックス依存性の違いをもたらした，このシンデカン-2の発現量の違いに着目して，シンデカン-2低発現性の高転移性H11細胞にシンデカン-2を強制発現させた細胞を樹立し，この細胞を用いてこれまで明らかにしてきた種々の細胞形質とシンデカン-2発現量の間に存在する関係を明らかにすることを目的に研究を行った．

結　　果

転移能の異なる3つの株細胞の発現するシンデカンファミリー

これまでの研究で，P29細胞がフィブロネクチンに接着する際にその受容体としてインテグリンα5β1とシンデカン-2とで結合し，協調的に作用した結果，ストレスファイバー形成を誘導することを明らかにすると同時に，H11細胞はシンデカン-2の発現量が閾値以下であるためにインテグリンのみを介した接着の結果，皮質型アクチン形成を示すことを明らかにしてきた[17]．そこで，中転移性細胞を含む，転移能の異なる3つの株細胞間を用いて細胞表層でのシンデカンファミリー，およびインテグリンα5β1の発現量をFACSにより解析したところ，中転移性LM12-3細胞は中程度のシンデカン-2発現量を示した（図1a）．この発現はノーザンブロットによるmRNAの発現でも確認された（図1b）．すなわち，転移能が高くなるにつれて，シンデカン-2発現量が減少しており，シンデカン-2発現量と転移能との間には逆相関の存在することが明らかとなった．

シンデカン-2強制発現株細胞の樹立

逆相関を示したシンデカン-2発現量と転移能との関係を明らかにするため，高転移性でシンデカン-2低発現性のH11細胞にマウス・シンデカン-2cDNAを導入し，安定高発現H11-SN2細胞を樹立した．この細胞のシンデカン-2発現量はノーザンブロット（図2a），ヘパリチナーゼIおよびII消化によって生ずる不飽和糖を認識するF58-3G10抗体によるウエスタンブロッ

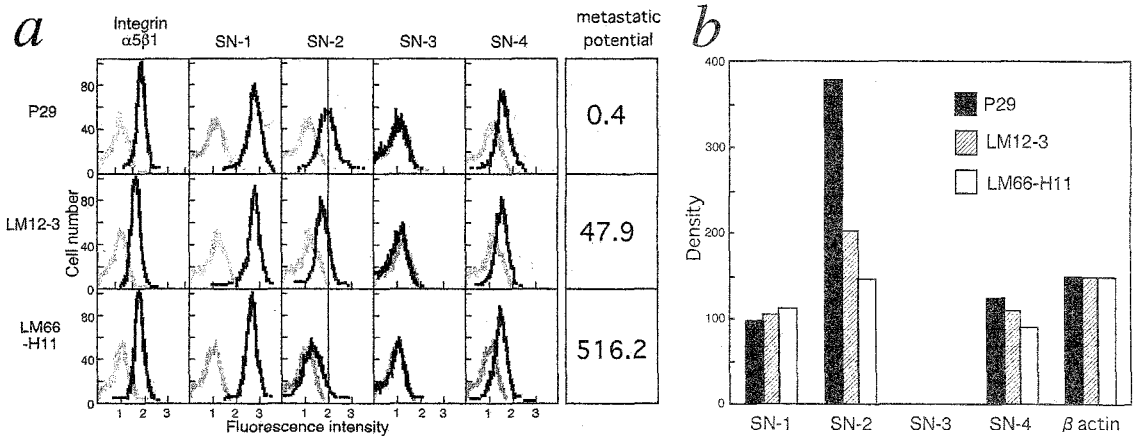

図1　転移能の異なる株細胞におけるシンデカンファミリーの細胞表層発現およびmRNAの発現量の比較
a　低転移性P29細胞，中転移性LM12-3細胞，高転移性LM66-H11細胞の細胞表層シンデカンファミリーの発現を，抗シンデカン1～4抗体，および抗インテグリンα5β1抗体を用いてフローサイトメーターで測定した．灰色線は非免疫血清を用いた対照を示す．また，各細胞をマウス（7匹／グループ）尾静脈注入し肺に転移して形成された平均腫瘍結節数を右に示した．b　各細胞より抽出したポリ（A）+RNAを用いてノーザンブロット法によりシンデカンファミリーの発現量を検出した後，デンシトメーターで定量し，βアクチンの発現量に対する各シンデカンの発現量を示した．

ト（図2b），シンデカン-2タンパク芯に対する抗体を用いたウエスタンブロット（図2c），およびFACS分析（図2d）で確認した結果，低転移性でシンデカン-2高発現性P29細胞と同程度の発現量を示した．一方，このシンデカン-2強制発現によって他のシンデカンファミリーおよびインテグリンα5β1の細胞表層発現には影響を及ぼさなかった（図2d）．このようにして樹立したH11-SN2株細胞を用いて以下の実験を行った．

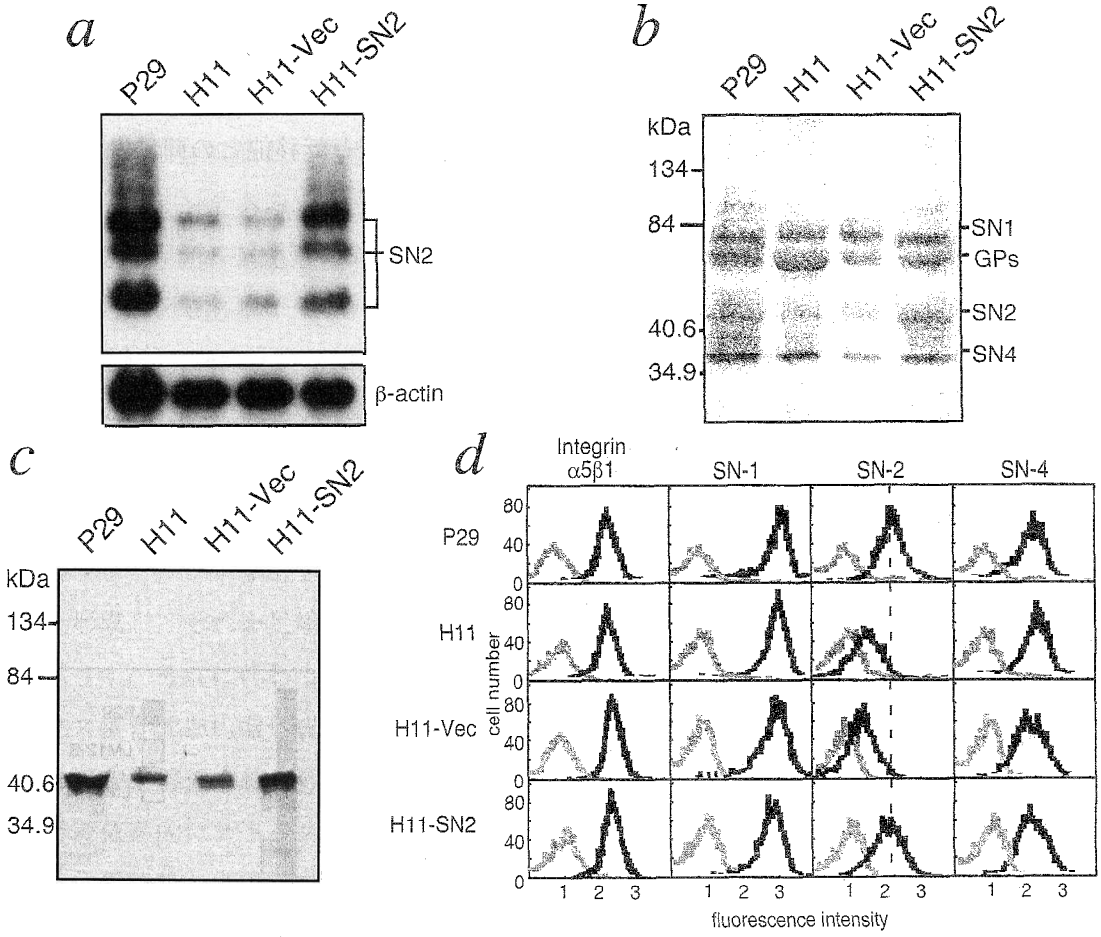

図2　シンデカン-2cDNA導入細胞のシンデカンおよびインテグリンα5β1の発現

a　各細胞より抽出したポリ(A)+RNA（2μg／レーン）を用いてノーザンブロット法によりシンデカン-2の発現量を比較した．プローブにはシンデカン-2全コード領域を含むcDNAを用いた．b　各細胞から抽出した細胞膜型プロテオグリカン画分を，ヘパリチナーゼⅠ，Ⅱおよびコンドロイチナーゼ ABC で消化し，得られたタンパク芯を SDS-PAGE により分離し，F69-3G10抗体を用いたウエスタンブロットにより細胞膜型プロテオグリカンを検出した．c　各細胞抽出液から抗シンデカン-2抗体を用いて免疫沈降した画分を，ヘパリチナーゼⅠ，Ⅱおよびコンドロイチナーゼ ABC で消化した後 SDS-PAGE により分離し，F69-3G10抗体を用いたウエスタンブロットによりシンデカン-2を検出した．d　各細胞の細胞表層シンデカンファミリーの発現を，抗シンデカン1～4抗体，および抗インテグリンα5β1抗体を用いてフローサイトメーターで測定した．灰色線は非免疫血清を用いた対照を示す．

シンデカン-2強制発現による細胞増殖能の変化

これまでの研究で転移能の異なる株細胞の増殖能を検討したところ，高転移性H11細胞の倍加時間は約12時間であるのに対して低転移性P29細胞は約9時間であった（図3a）．ベクターのみを導入したH11-Vec細胞は親株同様約12時間の倍加時間を示したのに対して，シンデカン-2を強制発現させたH11-SN2細胞はP29細胞と同様約9時間の倍加時間を示した（図3b）．また，飽和期の細胞密度，培養下での細胞の形もシンデカン-2強制発現によってP29細胞と酷似するように変化した（図3c）．

シンデカン-2強制発現細胞の示す転移能

本研究で，自然転移能の違いに基づいて株化した3つの株細胞において，転移能が高い細胞ほど細胞表層シンデカン-2の発現量が低いことを明らかにした．そこで，次にシンデカン-2発

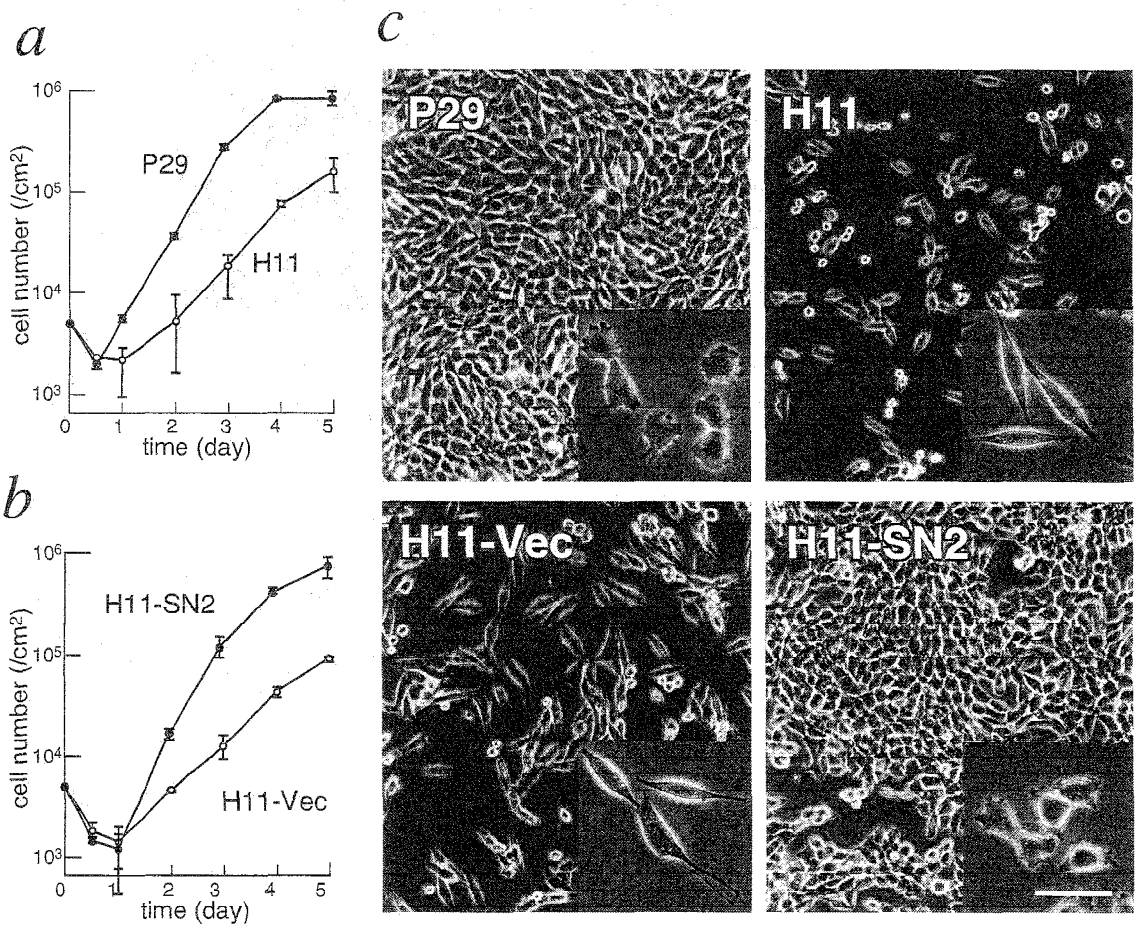

図3　シンデカン-2強制発現細胞の示す増殖能および細胞形態の変化

a　P29細胞の示す倍加時間は9時間であるのに対して，H11細胞のそれは12時間であった．b　ベクターのみを導入したH11-Vec細胞の倍加時間は親株と同じレベルであるのに対してシンデカン-2を強制発現させたH11-SN2細胞の倍加時間はP29細胞と同様，約9時間であった．c　それぞれの細胞を培養下で観察すると飽和密度に大きな違いがあり，シンデカン-2強制発現H11-SN2細胞はP29細胞の飽和密度近い値を示した．増殖期の細胞形態は各写真の右隅に示した．

現量を人為的に高発現にした細胞，H11-SN2細胞の示す実験転移能，および自然転移能を解析した．P29細胞，H11細胞，H11-Vec細胞，H11-SN2細胞をマウス尾静脈に移植し，16日後の肺を摘出し，腫瘍結節数を計測した（図4）．P29細胞移植マウスの肺に殆ど転移結節が認められないのに対して，H11細胞移植マウスの肺は全肺野にびまん性に転移結節が認められた．H11-Vec細胞移植マウスの肺転移結節はH11細胞移植マウスのそれと同様であった．驚いたことに，H11-SN2細胞移植マウスの肺に転移結節は殆ど認められなかった．湿重量（図示せず），結節数計測（表1）の結果も，臓器像と良く一致した．この結果は，H11細胞のシンデカン-2発現を人為的に高発現にすることによって，転移能が大きく抑制されたことを示している．

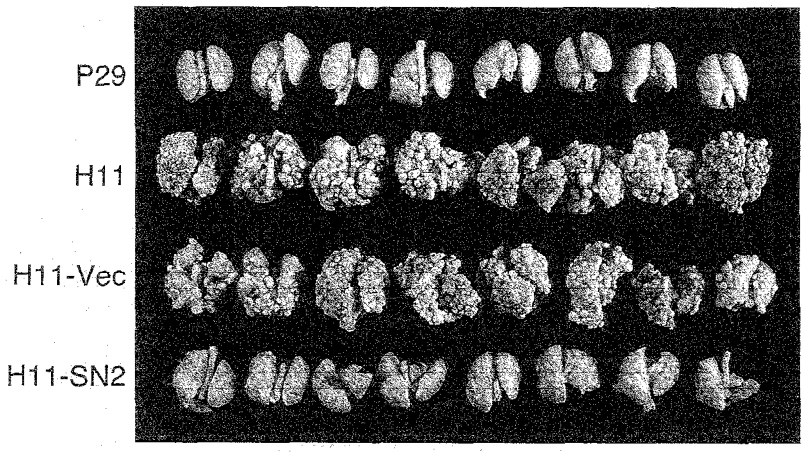

図4　シンデカン-2低発現性の高転移性H11細胞へのシンデカン-2導入の転移能への影響
P29細胞，H11細胞，H11細胞にベクターのみを導入したH11-Vec細胞，H11細胞にシンデカン-2cDNAを導入し，強制発現させたH11-SN2細胞（正）2×10^5細胞をそれぞれマウス尾静脈に移植して，16日後に摘出した肺への転移結節を示す．

表1　シンデカン-2強制発現による転移能の変化

	Route of injection	Number of Cells injected (x 10^5)	No. of animals metastasied	No. of lung nodules	
				Range	Mean
P29	i.v.	2.0	6/8	0-9	2.9
LM66-H11	i.v.	2.0	8/8	661-1311	997.9
H11-Vec	i.v.	2.0	8/8	235-1405	688.3
H11-SN2	i.v.	2.0	6/8	0-23	6.8
P29	s.c.	2.0	3/8	0-3	0.6
LM66-H11	s.c.	2.0	7/7	3-69	29.7
H11-Vec	s.c.	2.0	7/7	4-79	32.1
H11-SN2	s.c.	2.0	1/8	0-1	0.1

シンデカン-2強制発現細胞の示す一次腫瘍組織形成

これまでの研究において，低転移性P29細胞はフィブロネクチンに富んだ間質型マトリックス依存的な腫瘍組織形成を示すのに対して高転移性H11細胞は基底膜型マトリックス依存的である（図5a）ことを明らかにしてきた．この結果は培養下におけるフィブロネクチン接着応答性にも反映されており，P29細胞はフィブロネクチン基質上で伸展しストレスファイバー形成を誘導するのに対して，H11細胞はアクチン繊維が細胞辺縁に集積した皮質型アクチン形成を誘導する．これらの応答性の違いは細胞表層に存在するシンデカン-2の発現量の違いによることを明らかにしてきた．今回，シンデカン-2強制発現性のH11-SN2細胞の一次腫瘍組織形成を検討したところ，予想通り，シンデカン-2を強制発現させたH11-SN2細胞はベクターのみを導入したH11-Vec細胞と比較して明らかにフィブロネクチン染色領域が増加しており，シンデカン-2高発現のP29細胞と同程度の間質誘導能を示した（図5a）．また，誘導された間質細胞を示す1型コラーゲン陽性細胞の単位面積あたりの数もベクターのみのH11-Vec細胞と比較して有意に高い値を示した（図5b）．

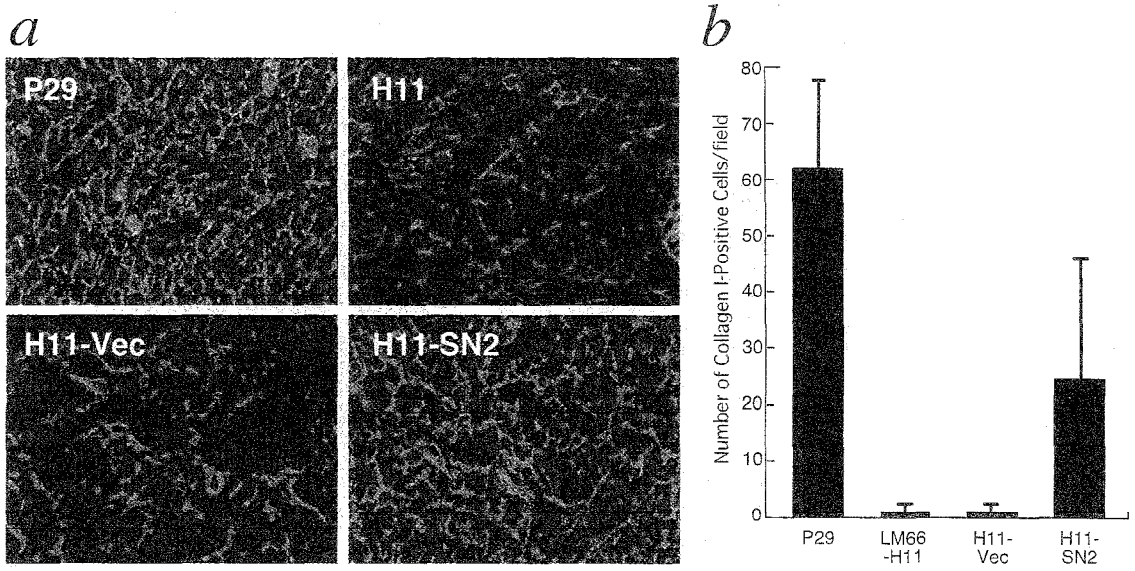

図5　シンデカン-2強制発現による一次腫瘍組織形成の変化

a　それぞれの細胞をマウス皮下に移植して作らせた一次腫瘍の組織切片を抗フィブロネクチン抗体（緑色）で染色した．強い間質誘導能を示すP29細胞が，誘導された宿主間質細胞の形成するフィブロネクチンに富んだ間質型細胞外マトリックスに取り囲まれているのに対して間質誘導能をもたないH11細胞の形成する腫瘍組織内でフィブロネクチンの存在するのは血管内皮基底膜のみである．ベクターのみを導入したH11-Vec細胞が親株の細胞と同様に間質誘導を示さないのに対してシンデカン-2強制発現のH11-SN2細胞は強い間質誘導を示す能力をもつ細胞に変化した．核はPIで対比染色した．b　宿主由来の間質細胞であるⅠ型コラーゲン陽性細胞を，抗Ⅰ型コラーゲン抗体で染色し，単位面積あたりのⅠ型コラーゲン陽性細胞数を計測した．

シンデカン-2強制発現細胞の示す浸潤能

一次腫瘍を摘出する際，P29腫瘍とその移植下部の筋肉組織との間に癒着が観察されたのに対して，H11腫瘍には全くそれが見られず，カプセル様構造を形成して筋肉組織とは明確に分離していた（図示せず）．この違いを組織学的に観察するため，一次腫瘍をヘマトキシリン・エオシンで染色し，組織像を観察した．その結果，筋肉組織への癒着が見られたP29腫瘍では，その腫瘍組織が小さい段階（移植後10日）から周辺筋肉組織への高い浸潤性を示したのに対してH11腫瘍は同じ時期に全く浸潤性を示さなかった（図6）．どちらの腫瘍も腫瘍組織が巨大に成長する移植2週間後には，圧迫に因ると思われる腫瘍塊の筋肉組織への癒着が見られた．しかしこの段階においてもH11腫瘍は筋繊維の間へ浸潤することは全く観察されなかった（図示せず）．

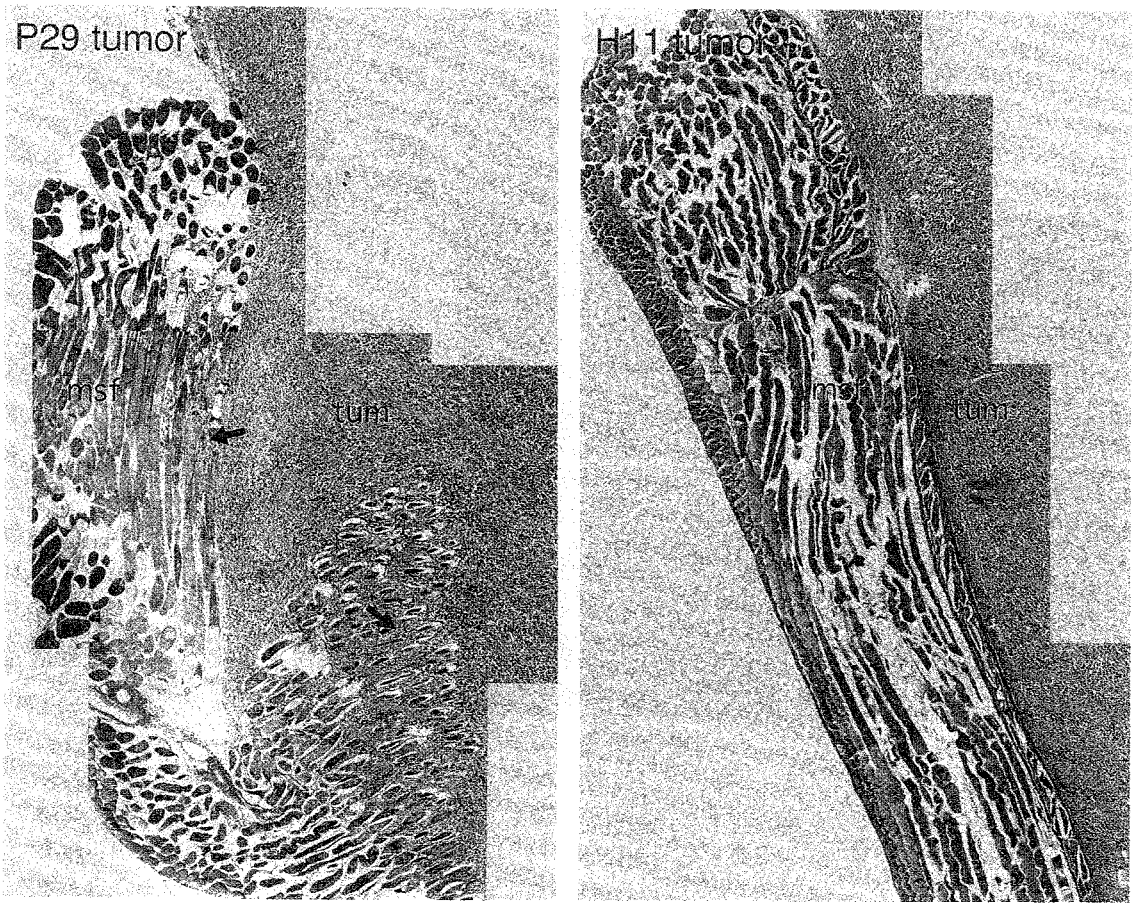

図6　各細胞の一次腫瘍における浸潤性の違い
低転移性P29細胞および高転移性H11細胞をマウス皮下に移植し，形成させた一次腫瘍をブアン固定後パラフィンに包埋し，切片をHE染色した。H11腫瘍（tum）は筋肉繊維（msf）と明確に分離しているのに対して，P29腫瘍（tum）は筋繊維（msf）の間に深く浸潤していた（矢印）．

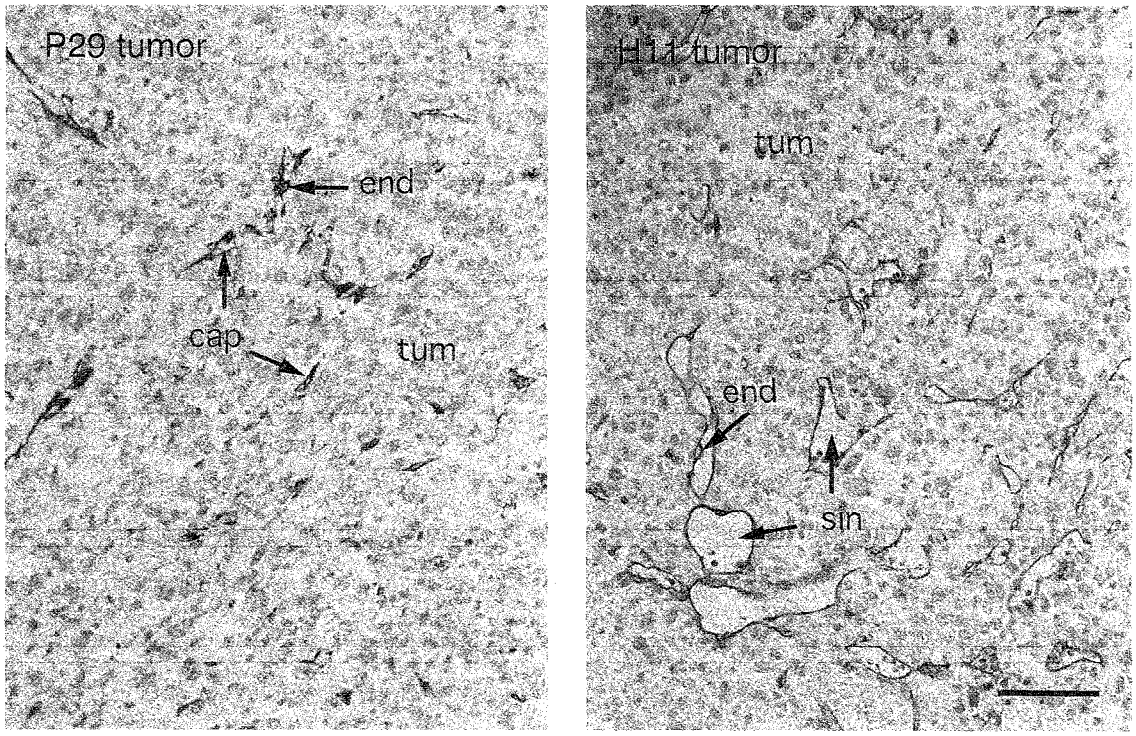

図7　転移能の異なる腫瘍組織における新生血管構造の違い
各細胞のマウス皮下移植一次腫瘍組織切片を抗CD31抗体で染色した（茶色）．核はヘマトキシリンで対比染色した（青色）．P29腫瘍の内皮細胞（end）は毛細血管（cap）を形成し，H11腫瘍組織における腫瘍血管は類洞様構造（sin）を示した．類洞の血管内皮細胞は基底膜を形成せず，径約100nmの小孔が多数開いているという特徴をもつ．スケールは100μm.

一次腫瘍における血管新生

血行性の転移能の違いを明らかにするため，一次腫瘍内に誘導された腫瘍血管に着目した．P29腫瘍に誘導された新生血管は典型的な毛細血管を形成しているのに対して，H11腫瘍における新生血管は肝臓などで見られる類洞様の血管を形成した（図7）．

考　　察

本研究室のこれまでの研究において，P29細胞は強い間質誘導能を示し，生体内においてフィブロネクチンを主要成分とする間質型マトリックスを足場とした腫瘍組織形成を示すのに対して，H11細胞は間質誘導能を示さない代わりに高い基底膜形成能を有しており，その基底膜に依存した腫瘍組織形成を示すことを明らかにしてきた[9-11]．また，これらの細胞は培養下においてフィブロネクチン基質に対して全く異なった接着応答性を示すことを明らかにしてきた．すなわち，P29細胞はインテグリンα5β1とシンデカン-2とでフィブロネクチン基質に接着し，ストレスファイバー形成を誘導すること，H11細胞はシンデカン-2の発現量が閾値以下であるためにインテグリンα5β1のみでフィブロネクチン基質に接着することにより皮質型アクチン

を形成することを明らかにしてきた．すなわち転移能の異なる株細胞の間におけるフィブロネクチン接着応答性の違いがシンデカン-2の発現量の差に依存していることを明らかにしてきた[17]．

シンデカンは細胞表層に存在した膜貫通型のタンパク芯に，ヘパラン硫酸およびコンドロイチン硫酸のグリコサミノグリカン鎖を持ったプロテオグリカンである．細胞表層ヘパラン硫酸プロテオグリカンは，近年，そのグリコサミノグリカン鎖を介した様々な増殖因子の共受容体としての役割が明らかになりつつあり[18-20]，また，シンデカンは細胞外マトリックス受容体としても注目され[21]，その膜貫通型タンパク芯の細胞内部位に特異的に結合する種々のシグナル伝達分子が明らかにされている[22, 23]．

本研究では，転移能の異なる株細胞の間で全く異なる接着応答性をもたらした原因と考えられるシンデカン-2の発現量の差に注目し，シンデカン-2低発現性の高転移性H11細胞にシンデカン-2cDNAを導入し人為的にシンデカン-2を強制発現させた株細胞H11-SN2細胞を作製し，この細胞を用いてこれまでに明らかにしてきた腫瘍組織形成およびがん転移においてシンデカン-2がどのような役割を担っているかという問題について解析した．

シンデカン-2強制発現H11-SN2細胞の形成する一次腫瘍組織形成は，予想通り間質誘導を示した．これは培養下でのフィブロネクチン基質接着応答性の違いをよく反映した結果である．また，腫瘍組織内に誘導してきた間質細胞数はP29細胞のそれと同程度であった．これらのことからシンデカン-2の高発現は高い間質誘導能の原因物質と考えられた．

間質誘導能の腫瘍学的意義はほとんど明らかにされていないが，ヒトの上皮性腫瘍の場合，程度において大きな差があるものの，ほとんどの腫瘍において間質誘導が見られ，その典型が硬癌である．硬癌は非常に強い浸潤能を示し，基底膜を破壊して周辺組織へ浸潤しやすいことが知られている．P29腫瘍はその腫瘍実質が小さい段階から周辺の筋肉組織への高い浸潤能を示したのに対してH11腫瘍は同じ時期には全く浸潤性を示さなかった．また，図示していないがシンデカン-2を強制発現させたH11-SN2細胞はP29腫瘍と同様に筋繊維の間に強い浸潤性を示した．これらの結果と先に述べたヒトの硬癌の例を考え合わせると，腫瘍の浸潤能は間質誘導能と相関関係にあると考えられる．すなわち，シンデカン-2高発現の細胞はフィブロネクチン接着応答性を反映して高い間質誘導を示し，その結果強い浸潤を示したと考えられる．また，最近，これらの細胞において，浸潤能の違いに関連すると思われる，細胞外マトリックス分解酵素であるMMP-3がP29細胞で多く発現されていることを明らかにしている（未発表）．

一方，腫瘍の転移能については，シンデカン-2を強制発現させた高転移性H11細胞，すなわち，H11-SN2細胞は大きな転移能の低下を示し，その転移能は低転移性P29細胞と同程度にまで低下した．がんの転移機構として，次の緒段階が提唱されている．原発巣からの遊離，誘導された腫瘍血管やリンパ管などの脈管への侵入，脈管内における移動，標的臓器の毛細管内皮細胞への接着あるいは物理的な停留の後，増殖し，管壁から組織へ侵入し増殖するという諸

過程を経て転移が成立すると考えられている[7, 8, 10, 24]．我々は本研究で，このモデルの一つの過程を説明し得る結果を得た．即ち，一次腫瘍内に誘導された新生血管の組織学的性質がP29およびH11腫瘍において全く異なることを見いだした．P29腫瘍内に形成される腫瘍血管は毛細血管であり，内皮細胞は内皮基底膜を形成しているのに対して，H11腫瘍内で形成された新生血管は類洞様構造を示した．類洞様血管を構成している内皮細胞の特徴として不完全な基底膜しか形成していないことがあげられる．それ故に，転移の最初の段階である脈管への侵入に際して，P29腫瘍細胞は血管内へ侵入しにくいのに対して，H11細胞は類洞様血管外へ侵出しやすいという組織学的特徴を有する．即ち，P29とH11腫瘍における転移能の大きな違いは各の腫瘍内に誘導された新生血管構造のこのような違いに基づくものと考えられた．肝障害などで肝臓に炎症が続くと線維化が進み，その結果，肝臓の類洞に血管基底膜が出現し，類洞の毛細血管化が起こり，類洞血と肝細胞間の物質交換が著しく障害されることがよく知られている．類洞形成，毛細血管形成もまた，間質誘導と深いつながりがあるのかも知れない．さらに，肝類洞を形成している伊東細胞はMMP-1, 2, 3を産生しているが，肝臓の線維化が進んだ肝硬変の患者では活性型MMP-2の産生量が低下することが明らかにされている[25]．このことは我々が最近明らかにしたH11細胞より間質誘導能の高いP29細胞の方が活性型MMP-2の産生量が低いこと（未発表）と驚くほど一致する．また間質誘導と転移能に関して別の考え方も報告されている．Barskyらは，間質型細胞外マトリックス形成を試薬を用いて阻害すると，血行性転移が大きく促進されることを示し，腫瘍細胞の増殖に伴って誘導される間質応答と，それによって腫瘍細胞間に形成される間質型マトリックスは，腫瘍細胞の血行性転移に対して障壁として働き，宿主にとって自己防御的意味を持つことを提唱している[26]．いづれにせよ，本研究では現象の記述にとどまっており，その機構的背景の解析は今後の問題として残された．

最後に，がんの転移・浸潤という2つの現象は，腫瘍の悪性度を特徴づける重要な側面であるが，非常に複雑な緒過程を含んでおり，いまだ全容は明らかにされていない．しかし，興味深いことに，本研究においてP29，H11細胞に見られたように転移能の高い細胞と浸潤能の高い細胞は必ずしも一致しないという結果を得た．すなわち，この転移・浸潤という2つの現象は，少なくともマウスルイス肺癌由来の株細胞においては，ともにシンデカン-2を介した現象であるが，それぞれは別々のシグナルカスケードの結果であり，転移能と浸潤能は相互に分離し得ることが示された．

参　考　文　献

1) Grobstein, C. and Cohen, J. (1965) Science, 150: 626-628
2) Spooner, B. S., Thompson-Letscher, H. A., Stokes, B. and Basset, K. (1986) in The Cell Surface in Development and Cancer (Steinberg, M. S., ed.), pp. 225-260

3) Ekblom, M., Klein, G., Murgrauer, G., Fecker, L., Deutzmann, R., Timpl, R. and Ekblom, P. (1990) Cell, 60: 337-346
4) Prieto, A. L., Jones, F. S., Cuningham, B. A. Crossin, K. L. and Edelman, G. M. (1990) J. Cell Biol. 111: 685-698
5) Hay, E. (1991) in Cell Biology of Extracellular Matrix (Hay, E. D. ed.) pp. 419－455, Plenum Press, New York and London
6) 小栗佳代子，岡山實 (1993) 細胞社会のグリコバイオロジー (永井克孝，箱守仙一郎，木幡陽編) pp. 151-175, 講談社サイエンティフィック，東京
7) Fidler, I. J. (1973) Nature, 242: 148-149
8) Nicolson, G. L. (1988) Biochim. Biophys. Acta, 948: 175-224
9) 小栗佳代子，岡山實 (1993) 細胞社会のグリコバイオロジー (永井克孝，箱守仙一郎，木幡陽編) pp. 151-175, 講談社サイエンティフィック，東京
10) 岡山實，草野由理，小栗佳代子 (1996) 現代化学，308: 51-57, 東京化学同人，東京
11) 岡山實 (1997) 京都産業大学論集第28巻，第4号，自然科学系列Ⅱ第6号，pp1-95
12) Hedman, K. and Vaheri, A. (1989) in Fibronectin (Mosher, D.F., ed.) pp. 123-137, Academic Press, Inc. New York
13) Olsen, B.R., and Ninomiya, Y. (1993) in Guidebook to the Extracellular Matrix and Adhesion Proteins (Kreis, T. and Vale, R., eds.) pp. 380-408, Oxford University Press, London
14) Farquhar, M.G. (1991) in Cell Biology of Extracellular Matrix, 2nd ed., (Hay, E.D., ed.) pp. 365-418, Plenum Press, New York
15) Nakanishi, H., Takenaga, K., Oguri, K., Yoshida, A. and Okayama, M. (1992) Virchows, Arch. A, 420: 163-170
16) Nakanishi, H., Oguri, K., Yoshida, K., Itano, N., Takenaga, K., Kazama, T. and Okayama, M. (1992) Biochem. J., 288: 215-224
17) Kusano, Y., Oguri, K., Nagayasy, Y., Munesue, S., Ishihara, M., Saiki, I., Yonekura, H., Yamamoto, H. and Okayama, M. (2000) Exp. Cell Res., 256:434-444
18) Maccarana, M., Casu, B. and Lindahl, U. (1993) J. Biol. Chem., 268:23898-23905
19) Guimond, S., Maccarana, M., Olwin, B. B., Lindahl, U. and Rapraeger, A. C. (1993) J. Biol. Chem., 268: 23906-23914
20) McKeehan, W. L., Wang, F. and Kan, M. (1998) Progress in Nucleic Acid Res. And Mol. Biol., 59: 135-176
21) Jalkanen, M., Elenius, K. Glycotech., 10: 211-221
22) Grootjans JJ, Reekmans G, Ceulemans H, David G. (200) J Biol Chem 30;275 (26) :19933-41
23) Cohen AR, Woods DF, Marfatia SM, Walther Z, Chishti AH, Anderson JM, Wood DF. (1998) J. Cell Biol. 13;142 (1) :129-38
24) Liotta, L. A., Tryggvason, K., Garbisa, S., Hart, I., Folts, C. M. and Shafle, S. (1980) Nature, 284: 67-68
25) Takahara T, Furui K, Funaki J, Nakayama Y, Itoh H, Miyabayashi C, Sato H, Seiki M, Ooshima A, Watanabe A. (1995) Hepatology ;21 (3) :787-95
26) Barsky, S. H. and gopalakrishna, R. (1987) Cancer Res., 47: 1663-1667

京都産業大学

先端科学技術研究所所報

創刊号（抜刷）

平成14年3月

細胞膜型ヘパラン硫酸プロテオグリカン，シンデカン-2によるアクチン細胞骨格形成の制御

棟居聖一
吉冨泰央
岡山實

細胞膜型ヘパラン硫酸プロテオグリカン，シンデカン-2によるアクチン細胞骨格形成の制御

棟居聖一
吉冨泰央
岡山實

要旨

マウス・ルイス肺癌由来の転移能の異なるクローン性株細胞は，生体内での一次腫瘍組織形成において全く異なる細胞外マトリックス依存性を示す．また，培養下においては，その違いを反映してフィブロネクチン基質への接着に際して異なったアクチン細胞骨格形成を示す．本研究の目的は，フィブロネクチン基質への接着依存的アクチン細胞骨格形成の分子的背景を明らかにすると共に，転移能の異なる株細胞で誘導される異なったアクチン細胞骨格形成をもたらす分子的背景の違いをも明らかにすることである．

緒論

がんの転移性は，その自律的な増殖性と共にがん細胞の悪性度を特徴づける重要な側面であり，その防止はがん治療において重要な問題である．本研究グループは，がん転移を腫瘍細胞と細胞微小環境を構築する細胞外マトリックス（以下，ECMと略）との相互作用の結果と位置づけ，その要因はすべて腫瘍組織形成に反映されていると仮定し，研究を行ってきた．転移は，ある環境下に位置する腫瘍細胞が原発巣から遊離，浸潤し，リンパ管や血管へ侵入し，脈管内移動，標的臓器内毛細血管の内皮細胞への接着，脈管外への浸出，組織への侵入，定着および増殖等の諸過程を経て成立すると考えられている[1-3]．

ECMは，コラーゲン，糖タンパク質，プロテオグリカンなどからなる超分子複合体で，大きく2つに分けることができる[4-7]．1つは，上皮性の細胞が形成する基底膜で，上皮組織と結合組織との境界膜として存在し，その主要構成成分は，IV型コラーゲン，ラミニン，パールカンである．もう1つは，間質系の細胞によって形成される間質型ECMで，結合織細胞を取り囲む無定形の構造で，その主要構成成分は，I型コラーゲン，フィブロネクチン，バーシカンである．

本研究室では転移の機構を癌細胞とECMとの相互作用の視点から明らかにすることを目的に研究が進められてきた．この目的を達成するため，先ずマウス・ルイス肺癌から自然転移能

に基づいて転移能の異なる腫瘍細胞がクローン化され，株細胞（低転移性株 P29，中転移性株 LM12-3，高転移性株 LM66-H11）として樹立された．これらの株細胞を同系マウス (C57/BL) の皮下に移植して作らせた一次腫瘍組織を用いて，ECM を中心に転移能に共軛した組織学的特徴を解析した．その結果，P29 および LM66-H11 株細胞が生体内において全く異なる ECM-依存的腫瘍形成を示すことが示された．即ち，LM66-H11 細胞は基底膜形成能が高く，腫瘍細胞はそれを足場にした腫瘍組織形成を示す．それに対して P29 細胞は基底膜形成能をもたず，それに代わって宿主組織に対して強い間質誘導性を示し，誘導された間質細胞の形成するフィブロネクチン（以下，FN と略）に富んだ間質型 ECM 依存的な組織形成を示した．

上記の組織形成の違いを反映して，両株細胞は，培養下において FN 基質への接着に際して顕著に異なる接着応答性を示した．即ち，P29 細胞は FN 基質への接着に際してアクチン・ストレスファイバー（以下，SF と略）形成を示すのに対して，LM66-H11 細胞においては，アクチン繊維が細胞辺縁部に局在化し，皮質型アクチン（以下，CA と略）の形成を示した．本研究の目的は，両細胞の示す FN 接着依存的なアクチン細胞骨格形成誘導の分子的背景を解明することである．

結　　果

マウス・ルイス肺癌 (3LL) 由来の異なる転移能を示す株細胞の樹立

自然癌は，ほとんど転移しない腫瘍細胞から，非常に高い転移能を示す腫瘍細胞まで多様な転移活性をもった細胞から成るキメラ組織である．転移能に共軛した腫瘍組織形成を明らかにするため，まず自然癌から転移能の異なる細胞を自然転移能の差に基づいてクローン化し，株細胞として樹立した．本研究では腫瘍細胞としてマウス・ルイス肺癌 (3LL) 細胞を用い，図 1 の方法に従って転移能の異なる腫瘍細胞をクローン化し，株細胞として樹立した（表 1）．それらの株細胞を同系マウス (C57/BL) の皮下に移植して一次腫瘍組織を作らせ，ECM を中心に組織学的特徴を解析した[3,7,8]．

腫瘍組織形成における ECM 依存性

自然転移能に基づいてクローン化した低転移性 P29 細胞と高転移性 LM66-H11 細胞は生体内において顕著な基底膜形成能の違いを示した．ルイス肺癌細胞は上皮細胞であるため両細胞ともに IV 型コラーゲン，ラミニン，パールカン等の主要基底膜成分の産生能を示すが，P29 細胞はラミニンの分泌能を欠如している[14]ため細胞外における基底膜形成能を示さなかった（図 2A）．それに対して，LM66-H11 細胞は完成度の高い基底膜を腫瘍細胞間に形成し，腫瘍細胞は自ら形成した基底膜に接着した組織像を示した[9,10]（図 2B）．一方，基底膜形成能をもたない P29 細胞は，宿主組織に対して強い間質誘導を示し，腫瘍組織内に誘導された間質細胞は

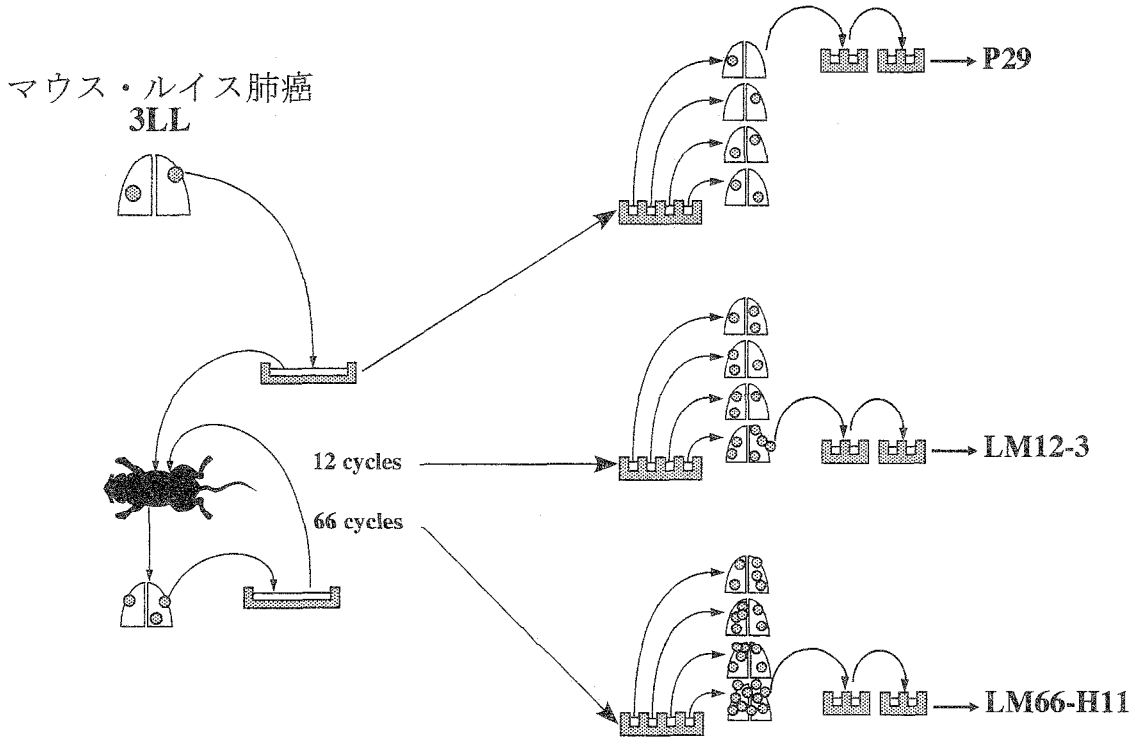

図1　マウス・ルイス肺癌 (3LL) から転移能の異なる株細胞の樹立の方法

皮下移植で継代されてきたルイス肺癌細胞を培養下に移し，2回の限界希釈により得たクローンのうち最も低い転移能を示したクローンを低転移性株細胞 P29 として実験に用いた．細胞を皮下移植し，3週間後，肺に形成された腫瘍結節を培養後，再び皮下移植することを12回，66回繰り返し，最終的に肺にできた転移巣を培養下に移し，2回の限界希釈の後にクローンを得た．これらのうち最も高い転移能を示したクローンをそれぞれ中転移性株細胞 LM12-3，高転移性株細胞 LM66-H11 として実験に用いた．

表1　マウス・ルイス肺癌由来の株細胞が示す転移能

株細胞	移植経路	移植細胞数（$\times 10^5$）	転移動物数 / 実験動物数	肺転移結節数	
				平均	範囲
P29	i.v.	1.0	3/7	0.4	0–1
LM12-3	i.v.	1.0	7/7	47.9	19–92
LM66-H11	i.v.	1.0	7/7	516.2	467–744
P29	s.c.	2.0	0/7	0	—
LM12-3	s.c.	2.0	6/7	4.5	0–14
LM66-H11	s.c.	2.0	7/7	35.2	23–56

i.v.: 静脈移植，　s.c.: 皮下移植

FNを主成分とする間質型ECMを形成し，腫瘍細胞はそのECMを足場とした腫瘍組織形成を示した[3,11,12]（図2C）．それに対して，LM66-H11腫瘍組織には間質型ECMの存在は殆ど観察されず，FNの局在は，腫瘍血管内皮基底膜に限定されていた[10,13]（図2D）．

FNおよびFN組換えポリペプチド基質接着依存的アクチン細胞骨格形成

転移能の異なる株細胞による一次腫瘍組織形成におけるECM依存性の違いを反映して両株細胞は，FN基質に対して全く異なる接着応答性を示した．即ち，FN基質への接着に際して，P29細胞はSFを形成して伸展する（図3A）のに対して，LM66-H11細胞内にはCA形成が誘導された（図3B）．SF形成の誘導には2種類のシグナル，即ち，FNのCell-Iドメインとインテグリン$\alpha5\beta1$との結合，およびFNのC-末端側のヘパリン結合ドメイン（以下，Hep-IIと略）と細胞膜型ヘパラン硫酸プロテオグリカン（以下，HSPGと略）との結合が必要であることが明らかにされている．また前者の結合が阻害されるとアクチンは糸状仮足（以下，FPと略）を形成し，後者の結合が阻害されるとCA形成が誘導される．これらの事実をリガンド側から考えると，上記の結果は3種のアクチン細胞骨格のうちいずれのアクチン細胞骨格が形成されるかはFNのCell-IおよびHep-IIドメインと上記の膜受容体との結合によって生成されるシグナルによって決定されることを示唆している．そこで，このことをFNの細胞接着ドメインを含む組換えポリペプチド（図4）を接着基質として用いることによって検証した．P29細胞は，CH-271上でFN基質上（図3A）と同一のSF形成を示した（図3C）が，C-274上ではCA形成を示した（図3E）．このことはFNのCell-Iドメインとインテグリン$\alpha5\beta1$との結合によってCA形成が誘導されることを示唆している．これに加えて，P29細胞はH-271上でFPを形成することが示された（図3G）．このことはFNのHep-IIドメインとHSPGの結合がFP形成を誘導することを示すものである．ここで重要なことは，細胞が両ドメインに結合すると，片方だけに結合したそれぞれの場合とは異なり，SF形成が誘導されることである．一方，LM66-H11細胞は組換えポリペプチド基質上でP29細胞と異なる応答性を示した．即ち，LM66-H11細胞はCH-271ポリペプチド基質上でもCA形成（図3D）を示し，その応答はC-274ポリペプチド基質上でのそれと全く同じであった（図3F）．また，その応答はC-274ポリペプチド基質上でのP29細胞の応答とも同一であった（図3E）．これらの結果は，FN基質上のLM66-H11細胞では，Cell-Iドメインとインテグリン$\alpha5\beta1$の結合しか成立していないことを示唆している．このことは，LM66-H11細胞がH-271ポリペプチド基質上で殆ど伸展しない事実（図3H）からも支持された．また，これまでに本研究室で見出されている，P29細胞が合成する細胞膜型HSPGの中でFNに親和性を示すプロテオグリカン分子はシンデカン-2であるという結果ともよい一致を示す[11]．以上の結果は，LM66-H11細胞上におけるシンデカン-2の発現は，閾値以下であることを強く示唆している．そこで，次に両細胞におけるインテグリン$\alpha5\beta1$とシンデカン-2の細胞表層発現を比較した．

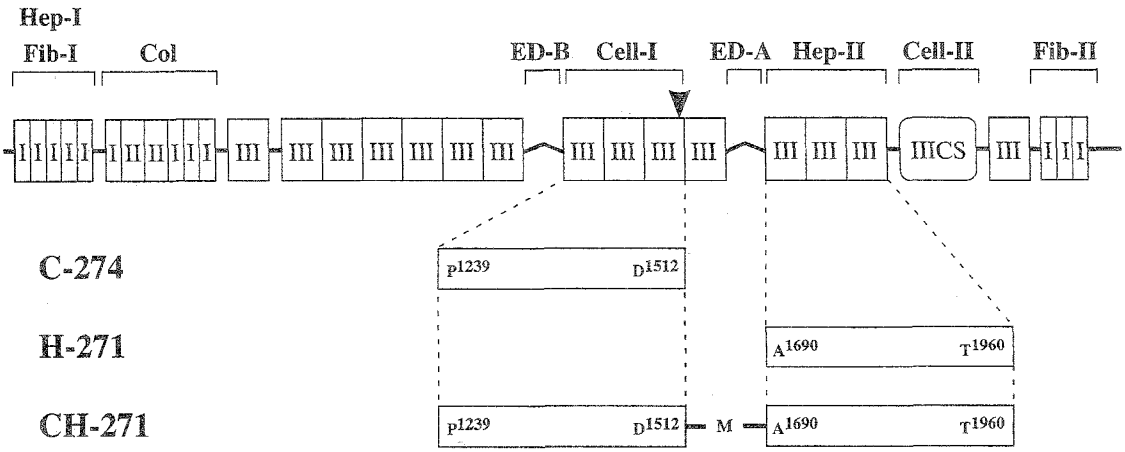

図4　フィブロネクチンおよび機能ドメインを含んだ組換え体分子の模式図
フィブロネクチンは分子量約25万のサブユニット鎖がCOOH-末端部でジスルフィド結合によって2量体を形成している（図には一つのサブユニットのみ示した）．各サブユニット鎖はI型，II型，III型繰返し配列から構成されておりインテグリン (Cell-I, Cell-II)，コラーゲン (Col)，ヘパリン (Hep-I, Hep-II)，フィブリン (Fib-I) に結合する機能ドメインを含んでいる．また，IIICS配列などの可変領域が存在する．C-274ポリペプチドはフィブロネクチンのRGD（▼）配列を含むインテグリン結合ドメイン (Cell-I; Pro1239-Ser1515) の組換え体，H-271ポリペプチドはCOOH-末端に存在するヘパリン結合ドメインII (Hep-II; Ala1690-Thr1960) の組換え体，CH-271はC-274とH-271ポリペプチドとをメチオニンを介して結合した融合型ポリペプチドを示す．ED-A, ED-Bは選択的スプライシングにより生成されるエクストラドメインを示す．

転移能の異なる株細胞が発現するFN受容体

前節でFN接着依存的SF形成の誘導には，細胞がFNのCell-IおよびHep-II両ドメインに結合することが必要であることを明らかにした．Cell-Iドメインに対する細胞表面受容体はインテグリン $\alpha5\beta1$ であり，Hep-IIドメインの受容体はシンデカン-2であることが示された．そこでP29およびLM66-H11両株細胞におけるインテグリン $\alpha5\beta1$ とシンデカン-2の細胞表層発現を検討した．抗インテグリン抗体および抗シンデカン-2抗体を用いたFACS解析の結果，インテグリン $\alpha5\beta1$ の発現レベルは，予想通り両株細胞間に有意な差を認めなかった（図5A, B）．一方，シンデカン-2の発現レベルはP29細胞の方が有意に高いことが示された（図5C, D）．さらに両細胞で発現しているシンデカン-2のFN基質への結合能の違いがアクチン細胞骨格形成の違いに影響をおよぼしているかどうか検討するため両細胞から単離・精製したシンデカン-2のFNへの結合能をFN親和性クロマトグラフィーにより比較した．その結果，両細胞が発現しているシンデカン-2のFNに対する親和性に有意な差がないことが明らかとなった（図5E, F）．

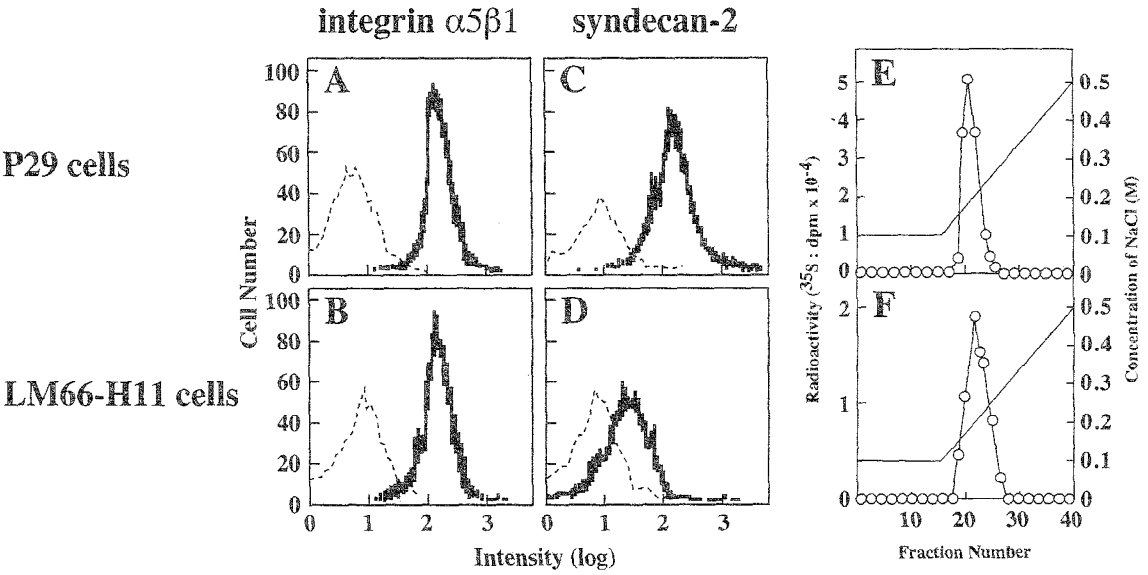

図 5　転移能の異なる株細胞におけるインテグリン α5β1 とシンデカン-2 の細胞表層発現
P29 細胞 (A, C)，LM66-H11 細胞 (B, D) の細胞表層のインテグリン α5β1 とシンデカン-2 の発現を抗インテグリン α5β1 抗体 (A, B)，抗シンデカン-2 抗体 (C, D) を用いてフローサイトメーターで計測した．点線は，非免疫血清を用いた対照を示す．P29 細胞 (E) および LM66-H11 細胞 (F) より精製した [^{35}S] 標識シンデカン-2 をフィブロネクチン結合セファロース 4B カラムに添加し，NaCl の直線的濃度勾配により溶出したときの溶出像．

転移能の異なる株細胞におけるシンデカンファミリーの発現

脊椎動物の細胞膜型 HSPG には，シンデカンファミリー 4 分子種とグリピカンファミリー 6 分子種が同定されている．グリピカンはグリコシルホスファチジルイノシトール (GPI) で細胞膜に貫入している HSPG である．それ故ホスファチジルイノシトール (PI) 特異的ホスホリパーゼ C 消化により細胞膜表面から特異的に除去することができる．PI 特異的ホスホリパーゼ C 消化した P29 細胞の FN 接着依存的アクチン細胞骨格形成を解析した結果，P29 細胞において FN 接着依存的 SF 形成に有意な変化は観察されなかった（図示せず）．この結果から，グリピカンファミリー分子は，FN 接着依存的アクチン細胞骨格形成に寄与していないことが明らかとなった．そこでシンデカンファミリー 4 分子種の mRNA の発現レベルを RT-PCR とノーザンブロットで検討した（図 6）．その結果，P29，LM66-H11 細胞ともにシンデカン-1，-2, -4 を発現していることが明らかになった．またシンデカン-3 については RT-PCR では僅かに検出されたが，ノーザンブロットでは検出されえなかった．これらのうち両細胞間で発現レベルに有意な差が認められたのはシンデカン-2 のみで，LM66-H11 細胞での発現量が有意に低かった．この結果は，シンデカン-2 の細胞表層での発現（図 5 C, D）とよい一致を示している．以上の結果より，インテグリン α5β1 の発現量は同じレベルであるが，シンデカン-2 の発現量が低い

ためにLM66-H11細胞がFN基質上でSF形成を示さないことが示唆された．そこで，次にインテグリン $\alpha5\beta1$ のリガンドとしてC-274ポリペプチドと，ヘパラン硫酸鎖に対するリガンドとしてヘパラン硫酸鎖に対する単クローン抗体F58-10E4との混合基質に対する接着依存的アクチン細胞骨格形成を解析した．この基質上でP29細胞はSF形成（図7A）を，LM66-H11細胞はCA形成（図7C）を示した．即ち，FN基質およびCH-271ポリペプチド基質上での両細胞のアクチン細胞骨格形成が再現された．この結果は，シンデカン-2を閾値以上発現しているP29細胞におけるSF形成は，ヘパラン硫酸鎖を介したシンデカン-2分子の結束化を伴った現象であることを示している．LM66-H11細胞におけるSF形成の欠如は上記結果を支持するものである．さらにインテグリン $\alpha5\beta1$ のリガンドとしてC-274ポリペプチドと，シンデカン-2に対するリガンドとして抗シンデカン-2抗体との混合基質に対する接着依存的アクチン細胞骨格形成を解析した結果，P29細胞においてはSF形成（図7B）が，LM66-H11細胞においてはCA形成（図7D）が誘導された．上に示した2つの結果は，SF形成の誘導に必要なシグナルの生成においてシンデカン-2のヘパラン硫酸鎖に対する刺激とタンパク芯に対する刺激とは等価であることを示している．

上で得られた結果を総合すると，LM66-H11細胞のFN接着依存的なSF形成の欠如は，シンデカン-2の低発現によるものであると推論された．これを検証するためLM66-H11細胞にシンデカン-2 cDNAを導入後，高発現性株細胞を樹立し，FN接着依存的アクチン細胞骨格形成を解析した．

シンデカン-2強制発現細胞の示すアクチン細胞骨格

シンデカン-2低発現株細胞LM66-H11にシンデカン-2 cDNAを導入後，P29細胞と同程度にシンデカン-2を発現している安定発現株細胞(H11-SN2)を樹立し（図8B），FN基質への接着応答性を解析した．その結果ベクターのみを導入したH11-Vec細胞（図8A）ではLM66-H11親株細胞と同様にCA形成を示した（図8C）のに対してH11-SN2細胞ではP29細胞と同様にSF形成の誘導が観察された（図8D）．この際，シンデカン-2の高発現は，他のシンデカン分子およびインテグリン $\alpha5\beta1$ の発現に影響を及ぼさなかった.（図示せず）．今回得られた結果を合わせて考えると，FN基質接着に際して，細胞がインテグリン $\alpha5\beta1$ とシンデカン-2とで基質に結合すると，細胞内にSF形成が誘導され，シンデカン-2の発現が閾値以下の場合，CAが形成される．即ち，シンデカン-2は量的閾値をもってインテグリン $\alpha5\beta1$ のFN結合情報を制御していることが明らかとなった．

考　　察

本研究室におけるこれまでの研究で，マウス・ルイス肺癌(3LL)由来の転移能の異なる株細

胞は，生体内において全く異なるECM依存的組織形成を示すことが明らかにされている．低転移性P29細胞を生体内に移植して腫瘍組織を作らせると，上皮細胞由来であるこの腫瘍細胞は基底膜成分であるIV型コラーゲン，ラミニンおよびパールカンを産生するにもかかわらず，基底膜構造を形成しない[9,13]．その原因がパールカンのヘパラン硫酸鎖の低硫酸化[10]，およびラミニンの分泌不全による[14]ことが明らかにされている．それに代わって，P29細胞は移植組織内において強い間質誘導能を示し，宿主組織から間質細胞を腫瘍組織内に誘導し，その間質細胞が形成するFNを主成分とする間質型ECMに取り囲まれて存在している[13]．即ち，P29細胞は，生体内においてFNを主成分とする間質型ECMを足場とした腫瘍組織形成を示す．それに対して，高転移性LM66-H11細胞は，間質誘導能を示さず，高い基底膜形成能を有し，基底膜に取り囲まれて存在している．即ち，LM66-H11細胞は基底膜を足場とした腫瘍組織形成を示す．本研究の目的は，同じ腫瘍組織由来の両株細胞が異なったECM足場依存的組織形成を示す分子的背景を明らかにすることである．その第一段階として，培養下における同一基質への両株細胞の接着応答性を解析対象とした．

本研究室でのこれまでの研究で以下のことが明らかにされている．1）培養下において，P29細胞がFN基質に接着すると，細胞内にSFを形成して伸展するのに対して，LM66-H11細胞のアクチン繊維は細胞辺縁部に局在し，CAを形成する[3]．2）P29細胞が合成する細胞膜型ヘパラン硫酸プロテオグリカンの中でFNに親和性を示す分子はシンデカン-2である[11,12]．3）FNのHep-IIドメインに特異的結合性を示すヘパラン硫酸鎖の最小糖鎖構造は，[Ido (2-OSO_3)α1-4GlcNSO_3 (6-OSO_3)]$_6$である[15,16]．

本研究において，P29およびLM66-H11細胞の示すFN基質接着時のアクチン細胞骨格形成（接着応答性）の違いをもたらす分子的背景を明らかにするするために，FNのCell-Iドメインを含む組換えポリペプチド (C-274)，Hep-IIドメインを含む組換えポリペプチド (H-271)，およびC-274ポリペプチドとH-271ポリペプチドとを結合した融合組換えポリペプチド (CH-271) 基質に対する接着応答性を検討した．その結果，CH-271ポリペプチド基質に対してP29およびLM66-H11両細胞ともFN基質に対する接着応答性と同一の応答性を示した．即ち，P29細胞はSF形成を，LM66-H11細胞はCA形成を示した．C-274ポリペプチドのみを基質に用いたときP29, LM66-H11両細胞ともにCAを形成した．H-271ポリペプチドのみを基質にしたときには，P29細胞はFP形成を示したのに対して，LM66-H11細胞は接着性が弱く，殆ど伸展しなかった．FP形成については，繊維芽細胞において，その形成にシンデカン-2が関与しているという報告がなされている[17]．

次に両細胞の示すFN接着依存的アクチン細胞骨格形成から考えられる両細胞のFN受容体を解析した．Cell-Iドメインに特異的な受容体として知られているインテグリン $\alpha5\beta1$ の細胞表層発現は両細胞ともに同じレベルであった．このことはC-274ポリペプチド基質に両細胞を接着させたときに，両細胞共にCAを形成する事実とよく一致している．Hep-IIドメインの受

容体と考えられるシンデカン-2の発現量を比較したところ，P29細胞のほうがLM66-H11細胞より高い発現を示した．P29細胞においてシンデカン-2の発現が高いことは，H-271ポリペプチド基質上でP29細胞がFP形成を示すのに対し，LM66-H11細胞が殆ど接着を示さず，伸展しないこととよい一致を示している．さらにCH-271ポリペプチド基質への接着に際して，P29細胞がCell-Iドメインと Hep-IIドメインに対し，インテグリン $\alpha5\beta1$ とシンデカン-2とで同時に結合することによりSF形成を誘導する．それに対して，LM66-H11細胞のシンデカン-2の発現量が閾値以下であるため，インテグリン $\alpha5\beta1$ のみでCH-271ポリペプチド基質に接着するため，その応答性はC-274ポリペプチド基質上の場合と同様であった．これらの結果は，SF形成の誘導には一定量以上のシンデカン-2の発現が必須であることを示唆している．本研究において高転移性株細胞LM66-H11は，シンデカン-2遺伝子を導入したとき以外はFN接着依存的SF形成の誘導を示さなかった．

本研究で得られた結果は図9に示すようにまとめることができる．即ち，細胞がFN基質への接着に際して，1) Cell-Iドメインと Hep-IIドメインにインテグリン $\alpha5\beta1$ とシンデカン-2を介して同時に結合すると，細胞内にSF形成が誘導される．2) Cell-Iドメインとインテグリン $\alpha5\beta1$ との結合のみで細胞接着が起こると細胞内にCAの形成が誘導される．3) Hep-IIドメインとシンデカン-2との結合のみで細胞接着が起こると細胞内にFP形成が誘導される．こ

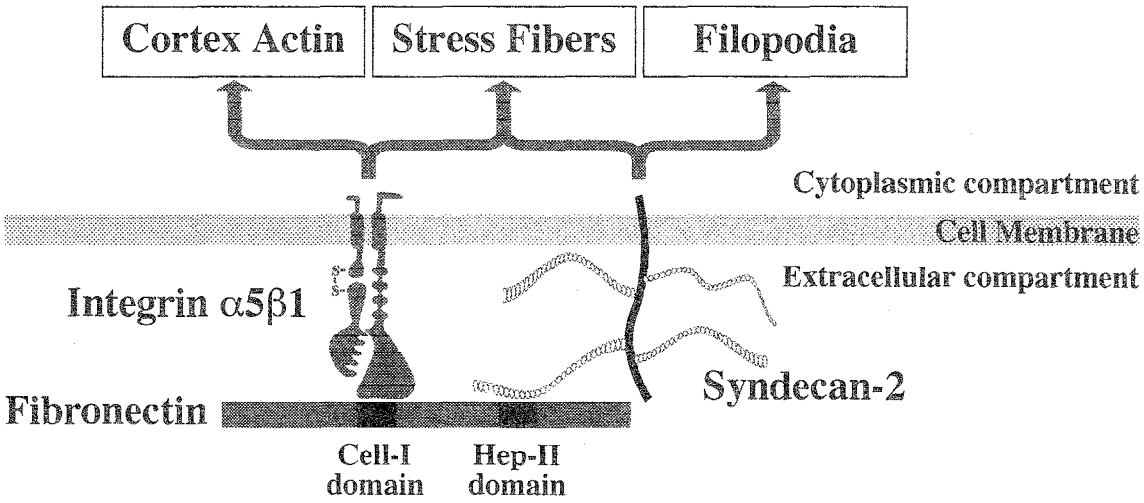

図9　インテグリン $\alpha5\beta1$ およびシンデカン-2を介したフィブロネクチン結合シグナルの伝達
細胞がインテグリン $\alpha5\beta1$ を介してフィブロネクチンのCell-Iドメインに結合した場合伸展し，皮質型アクチンを形成する．それに対してシンデカン-2を介してHep-IIドメインに結合した場合，細胞はほとんど伸展せず糸状仮足形成を示す．両方の受容体を介してフィブロネクチンに結合した場合には，細胞内にストレスファイバー形成が誘導され，伸展する．このストレスファイバー形成へのシグナルはシンデカン-2の発現量あるいは，受容体に対するリガンド結合の強さに依存している．インテグリン $\alpha5\beta1$ の結合シグナルをシンデカン-2が制御しているのである．

のようにFN接着依存的SF形成の誘導にはインテグリン $\alpha5\beta1$ とシンデカン-2の協調作用が必須である．P29細胞は肺胞上皮細胞由来の腫瘍細胞であるが，アクチン細胞骨格形成におけるインテグリンとシンデカンの協調作用は，Couchmanおよび Goetinckらにより繊維芽細胞の系でも観察されており，細胞種の違いを超えた一般的な現象と考えられる[18–22]．興味深いことに，繊維芽細胞においてインテグリンと協調的に作用するシンデカン分子は，シンデカン-4と同定されている．しかし，シンデカン-4がFN基質に結合性をもつかどうかについては明らかにされていない．また，シンデカン-4のノックアウトマウス由来の繊維芽細胞は，FN基質への接着に際してSF形成を示すことが報告されている[23]．これらと本研究結果を合わせて考えるとSF形成の誘導には，シンデカン-2と-4が協調的に作用することが考えられるが，その作用機構については不明である．本研究室で最近，SF形成においてシンデカン-4の作用は他の分子で代償されるが，シンデカン-2の作用は必須であることが明らかにされた（未発表）．

参　考　文　献

1) Liotta, L.A., Tryggvason, K., Garbisa, S., Hart, I., Folts, C.M. and Shafie, S. (1980). Metastatic potential correlates with enzymatic degradation of basement membrane collagen. Nature, **284**: 67–68.
2) Nakajima, M., Irimura, T., DiFerrante, N. and Nicolson, G.L. (1983). Heparan sulfate degradation: relation to tumor invasive and metastatic properties of mouse B16 melanoma sublines. Science, **220**: 611–613.
3) 岡山　實，草野由理，小栗佳代子 (1996)．がん転移と細胞接着分子．現代化学，**308**: pp. 51–57．東京化学同人，東京．
4) Hedman, K. and Vaheri, A. (1989). Fibronectin, (ed. Mosher, D.F.), pp. 123–134. Academic Press, Inc. New York.
5) Olsen, B.R. and Ninomiya, Y. (1999). Collagen: Guidebook to the Extracellular Matrix, Anchor, and Adhesion Proteins, (eds. Kreis, T. and Vale, R.), pp. 380–408. Oxford University Press, London.
6) Farquhar, M.G. (1991). The Glomerular Basement Membrane, A Selective Macromolecular Filter: Cell Biology of Extracellular Matrix, 2nd ed., (ed. Hay, E.D.), pp. 365–418, Prenum Press, New York and London.
7) 小栗佳代子，岡山　實 (1993)．細胞社会のグリコバイオロジー．(永井克孝，箱守仙一郎，木幡陽編)，pp. 151–175．講談社サイエンティフィック，東京．
8) 岡山　實 (1997)．京都産業大学論集第28巻，第4号，自然科学系列II第6号，pp. 1–95.
9) Nakanishi, H., Takenaga, K., Oguri, K., Yoshida, A. and Okayama, M. (1992). Morphological characteristics of tumours formed by Lewis lung carcinoma-derived cloned cell lines with different metastatic potentials: structural differences in their basement membranes formed *in vivo*. Virchows, Arch. A., **420**: 163–170.
10) Nakanishi, H., Oguri, K., Yoshida, K., Itano, N., Takenaga, K., Kazama, T., Yoshida, A. and

Okayama, M. (1992). Structural differences between heparan sulphates of proteoglycan involved in the formation of basement membranes in vivo by Lewis-lung-carcinoma-derived cloned cells with different metastatic potentials. Biochem. J., **288**: 215–224.

11) Itano, N., Oguri, K., Nakanishi, H. and Okayama, M. (1993). Membrane-intercalated proteoglycan of a stroma-inducing clone from Lewis lung carcinoma binds to fibronectin via its heparan sulfate chains. J. Biochem., **114**: 862–873.

12) Itano, N., Oguri, K., Nagayasu, Y., Kusano, Y., Nakanishi, H., David, G. and Okayama, M. (1996). Phosphorylation of a membrane-intercalated proteoglycan, syndecan-2, expressed in a stroma-inducing clone from a mouse Lewis lung carcinoma. Biochem. J., **315**: 925–930.

13) Nakanishi, H., Oguri, K., Takenaga, K., Hosoda, S. and Okayama, M. (1994). Differential fibrotic stromal responses of host tissue to low- and high-metastatic cloned Lewis lung carcinoma cells. Lab. Invest., **70**: 324–332.

14) Narumi, K., Satoh, K., Isemura, M., Sakai, T., Abe, T., Kikuchi, T., Sindoh, S., Motomiya, M., Oguri, K. and Okayama, M. (1993). Difference in laminin expression between high and low metastatic cell clones derived from murine Lewis lung carcinoma. Cell Struct. Funct., **18**: 183–187.

15) 草野（水野）由理，長安祐子，小栗佳代子，岡山　實 (1996). Biotherapy, **10**: 1318–1323.

16) Kusano, Y., Oguri, K., Nagayasu, Y., Munesue, S., Ishihara, M., Saiki, I., Yonekura, H., Yamamoto, H. and Okayama, M. (2000). Participation of syndecan 2 in the induction of stress fiber formation in cooperation with integrin $\alpha 5\beta 1$: structural characteristics of heparan sulfate chains with avidity to COOH-terminal heparin-binding domain of fibronectin. Exp. Cell Res., **256**: 434–444.

17) Granes, F., Garcia, R., Casaroli-Marano, R. P., Castel, D., Rocamera, N., Reina, M., Urena, M. and Vilaro, S. (1999). Syndecan-2 induces filopodia by active cdc42Hs. Exp. Cell Res., **248**: 439–456.

18) Woods, A., Couchman, J. R., Johansson, S. and Hook, M. (1986). Adhesion and cytoskeletal organisation of fibroblasts in response to fibronectin fragments. EMBO J., **5**: 665–670.

19) Woods, A., MaCarthy, J. B., Furcht, L. T. and Couchman, J. R. (1993). A synthetic peptide from the COOH-terminal heparin-binding domain of fibronectin promotes focal adhesion formation. Mol. Biol. Cell, **4**: 605–613.

20) Woods, A. and Couchman, J. R., (1994). Syndecan 4 heparan sulfate proteoglycan is a selectively enriched and widespread focal adhesion component. Mol. Biol. Cell, **5**: 183–192.

21) Saoncella, S., Echtermeyer, F., Denhez, F., Nowlen, J. K., Mosher, D. F., Robinson, S. D., Hynes, R. O. and Goetinck, P. F. (1999). Syndecan-4 signals cooperatively with integrins in a Rho-dependent manner in the assembly of focal adhesions and actin stress fibers. Proc. Natl. Acad. Sci. USA, **96**: 2805–2810.

22) Echtermeyer, F., Baciu, P. C., Saoncella, S., Ge, Y. and Goetinck, P. F. (1999). Syndecan-4 core protein is sufficient for the assembly of focal adhesions and actin stress fibers. J. Cell Sci., **112**: 3433–3441.

23) Ishiguro, K., Kadomatsu, K., Kojima, Y., Muramatsu, H., Tsuzuki, S., Nakamura, E., Kusugami, K., Saito, H. and Muramatsu, T. (2000). Syndecan-4 deficiency impairs focal adhesion formation only under restricted conditions. J. Biol. Chem., **275**: 5249–5252.

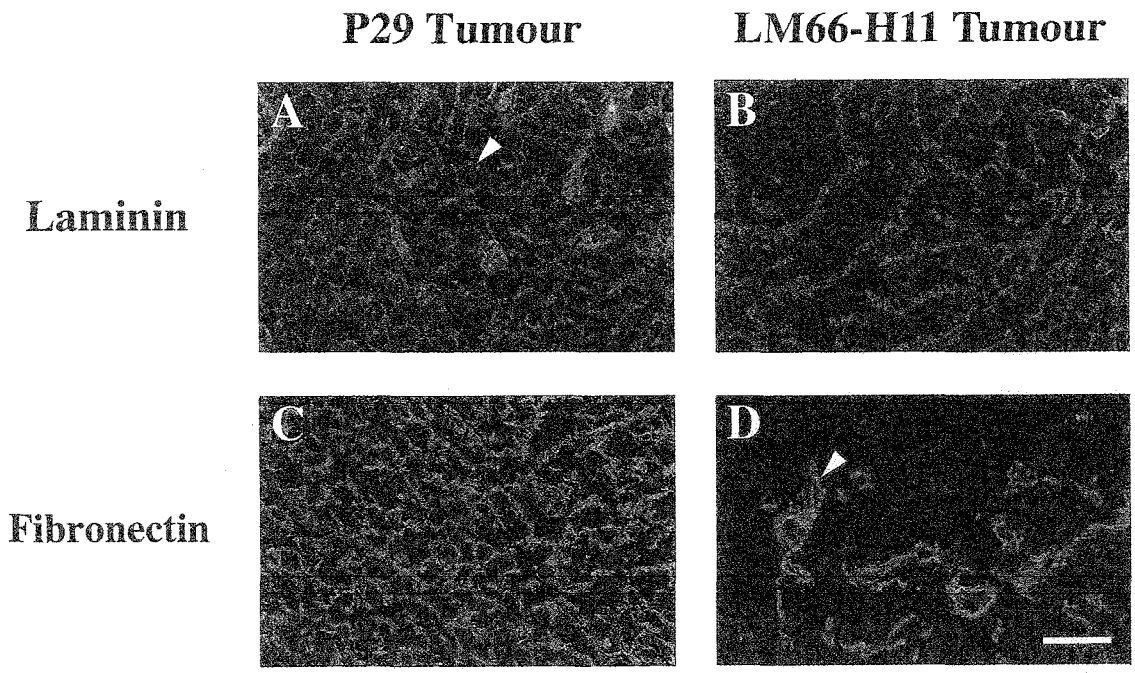

図 2　マウス・ルイス肺癌由来の転移能の異なる株細胞が形成する皮下一次腫瘍組織における細胞外マトリックスの局在

ルイス肺癌由来の転移能の異なる株細胞，低転移性 P29 株細胞 (A, C) および高転移性 LM66-H11 株細胞 (B, D) をマウス皮下に移植して作らせた一次腫瘍の組織切片を抗ラミニン抗体 (A, B) および抗フィブロネクチン抗体 (C, D) で染色した．強い間質誘導を示すP29細胞が，誘導された宿主間質細胞の形成するフィブロネクチンに富んだ間質型細胞外マトリックスに囲まれている (C) のに対して，間質誘導能をもたない LM66-H11 細胞の形成する腫瘍組織内でフィブロネクチンが存在する主要な部位は血管内皮基底膜（矢頭）である (D)．LM66-H11 細胞は自ら形成する基底膜依存的に腫瘍組織を形成する (B) が，P29 細胞の合成するラミニンは細胞内に蓄積し（矢頭），基底膜構築に寄与しない (A)．ラミニン，フィブロネクチンは FITC-標識二次抗体を使用し緑色で，核は赤色で示した．スケールは 50 μm.

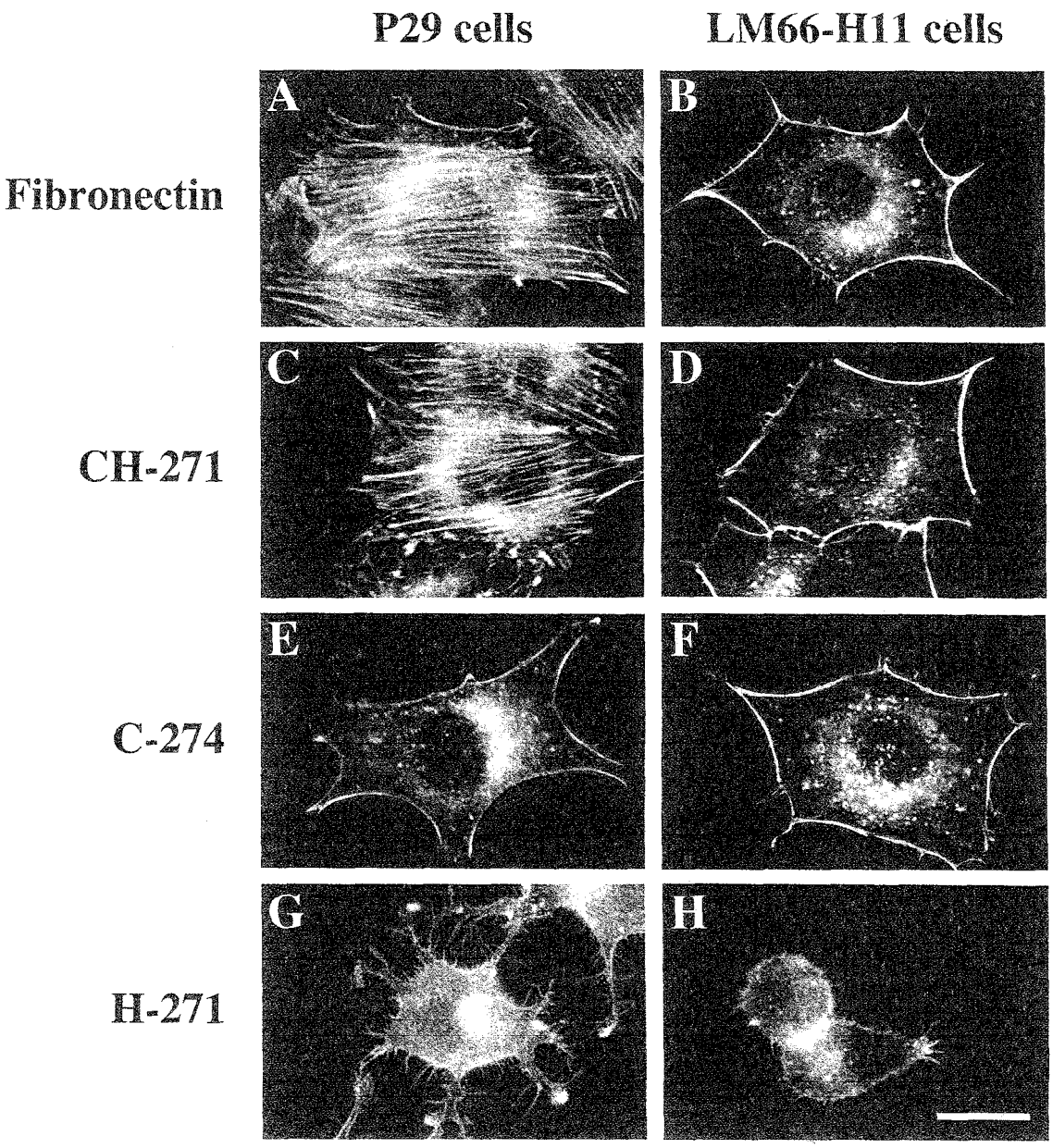

図3　転移能の異なる株細胞の基質接着依存的アクチン細胞骨格形成

フィブロネクチン (A, B), CH-271 (C, D), C-274 (E, F), H-271 (G, H) を被覆したカバーグラス上に P29 細胞 (A, C, E, G), LM66-H11 細胞 (B, D, F. H) を播種し，1時間後の F-アクチンをローダミン標識ファロイジンで染色した．スケールは 20 μm.

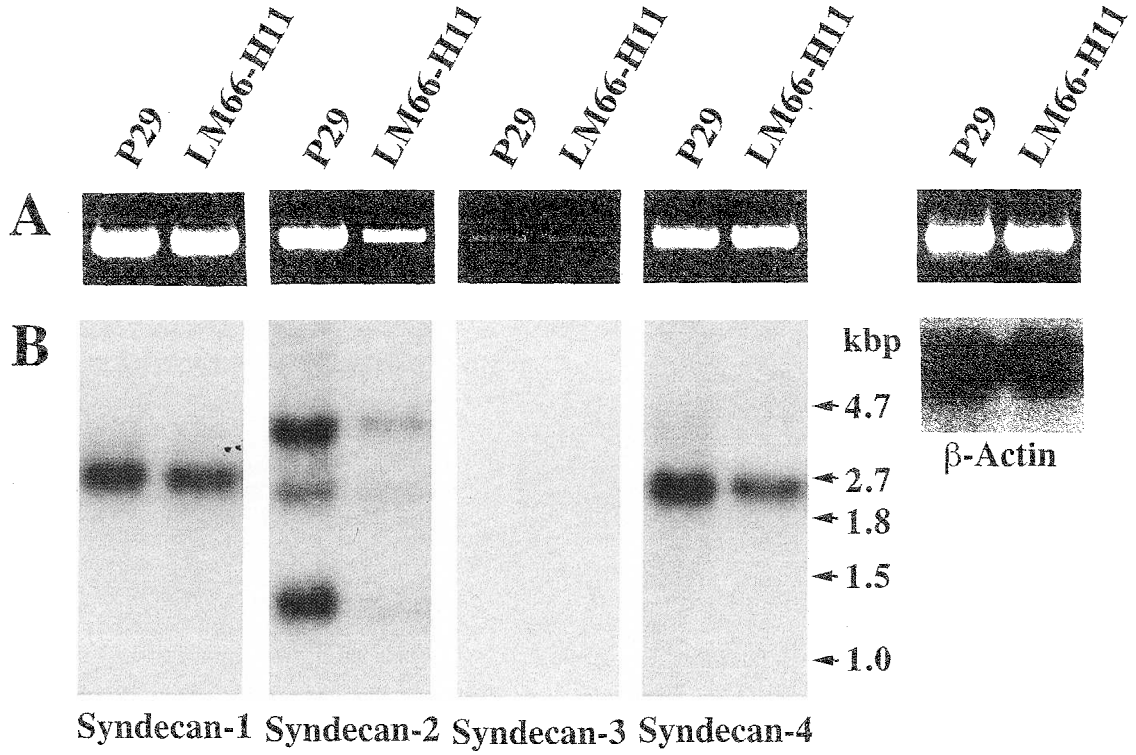

図 6　転移能の異なる株細胞が発現している細胞膜型ヘパラン硫酸プロテオグリカンの mRNA 発現
(A) P29 および LM66-H11 細胞より抽出した poly $(A)^+$ RNA を用いて RT-PCR 後，生成物を鋳型として，シンデカン-1～ -4，および β-アクチンを増幅するプライマーを用いて PCR 後，アガロースゲル電気泳動した．(B) 各細胞より抽出した poly $(A)^+$ RNA（2 μg/ レーン）を用いてノーザンブロット法によりシンデカンファミリーの発現量の比較を行った．プローブには各シンデカンの全コード域を含む 32p 標識 cDNA を用いた．

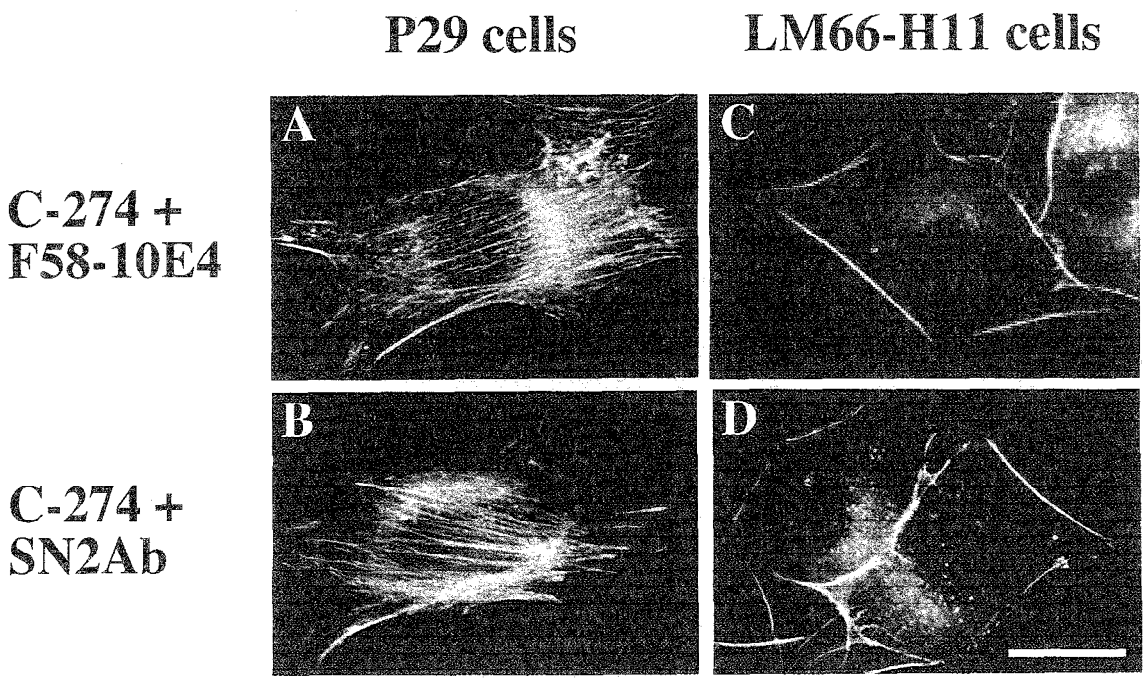

図7　C-274と抗ヘパラン硫酸抗体(F58-10E4)または抗シンデカン-2抗体(SN2A)との混合基質上における両株細胞のアクチン細胞骨格形成
C-274とF58-10E4またはSN2A抗体との混合基質を被覆したカバーグラス上にP29細胞(A, B), LM66-H11細胞(C, D)を播種し，1時間後のF-アクチンをローダミン標識ファロイジンで染色した．スケールは20 μm.

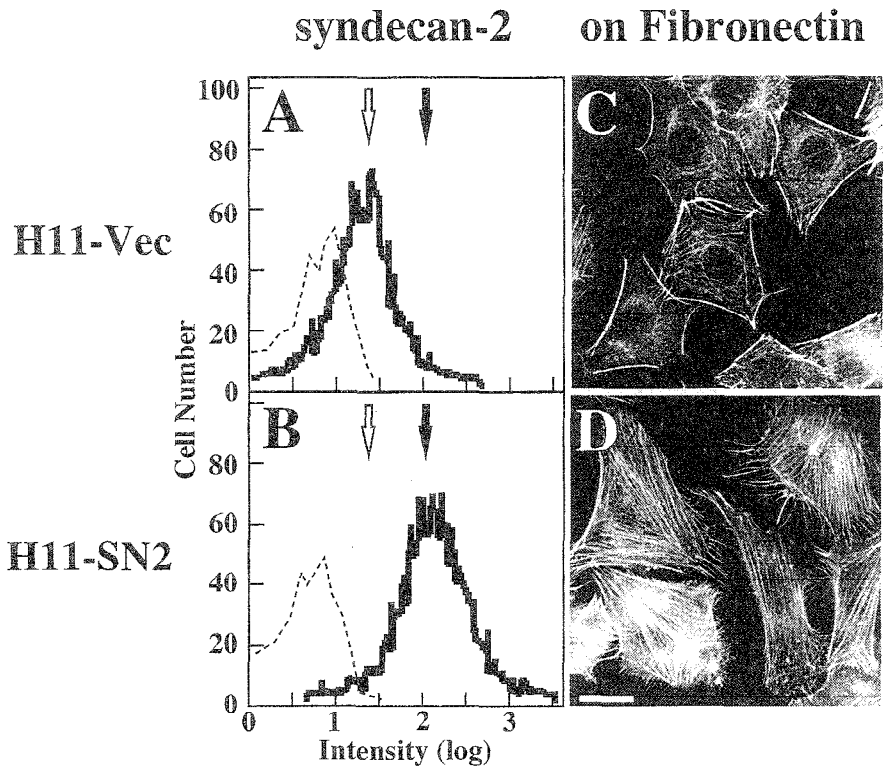

図 8　シンデカン-2 過剰発現 LM66-H11 細胞におけるストレスファイバー形成の誘導

シンデカン-2 遺伝子導入株細胞 H11-SN2 (B, D) およびベクターのみ導入した H11-Vec 株細胞 (A, C) のシンデカン-2 (A, B) 発現量を，抗シンデカン-2 抗体を用いてフローサイトメーターにより計測し，その一部を用いてフィブロネクチン基質上に播種した細胞の F-アクチンをローダミン標識ファロイジンで染色した．点線は，非免疫血清を用いた対照を示す．白抜きおよび黒の矢印はそれぞれ LM66-H11，P29 細胞のシンデカン-2 発現量の位置を示す．スケールは 20 μm.

Analysis of the fine specificity of Tn-binding proteins using synthetic glycopeptide epitopes and a biosensor based on surface plasmon resonance spectroscopy

Eduardo Osinaga[a,*], Sylvie Bay[b], Diana Tello[c], Alvaro Babino[a], Otto Pritsch[a], Karine Assemat[c], Daniele Cantacuzene[b], Hiroshi Nakada[d], Pedro Alzari[c]

[a] *Departamento de Bioquímica, Facultad de Medicina, Av. Gral. Flores 2125, CP 11800 Montevideo, Uruguay*
[b] *Unité de Chimie Organique, Institut Pasteur, 25 rue du Dr. Roux, 75724 Paris, France*
[c] *Unité de Biochimie Structurale, Institut Pasteur, 25 rue du Dr. Roux, 75724 Paris, France*
[d] *Department of Biotechnology, Faculty of Engineering, Kyoto Sangyo University, Kyoto 603, Japan*

Received 2 December 1999; received in revised form 20 January 2000

Edited by Masayuki Miyasaka

Abstract Using synthetic Tn (GalNAc-*O*-Ser/Thr) glycopeptide models and a biosensor based on surface plasmon resonance spectroscopy we have determined that isolectin B4 from *Vicia villosa* (VVLB4) binds to one Tn determinant whereas the anti-Tn monoclonal antibodies 83D4 and MLS128 require at least two Tn residues for recognition. When an unglycosylated amino acid is introduced between the Tn residues, both antibodies do not bind. MLS128 affinity was higher on a glycopeptide with three consecutive Tn residues. These results indicate that Tn residues organized in clusters are essential for the binding of these antibodies and indicate a different Tn recognition pattern for VVLB4.

Key words: Tn antigen; *O*-Glycosylation; Lectin; Monoclonal antibody; Surface plasmon resonance spectroscopy; Cancer

1. Introduction

Aberrant glycosylation of tumor mucins results in expression of unusual glycosidic structures and exposure of the peptide backbone [1]. The Tn determinant (GalNAcα-*O*-Ser/Thr), normally cryptic in mucin-type *O*-glycans, is a tumor-associated marker which has attracted particular interest in cancer biology: (a) it may be a useful diagnostic marker since it is poorly expressed in normal tissues but is widely expressed in a variety of adenocarcinomas [2]; (b) a direct correlation has been shown between carcinoma aggressiveness and the density of this antigen, e.g. extent of tissue spread and vessel invasion [3]; (c) Tn antigen can be recognized by the immune system [4] and thus provides a potentially important therapeutic target [5]; (d) Tn has been implicated in the metastasis of tumor cells [6]. Furthermore, Tn is found in the envelope glycoprotein gp120 of different HIV isolates where it constitutes an immunoneutralization epitope [7].

The Tn antigen was characterized using both monoclonal antibodies (mAb) [8–11] and lectins [12,13], but the specific reactivities displayed by these proteins are not identical. This raises questions about the exact molecular structure of the epitope. For example, it would be of interest to determine if these Tn-binding proteins require more complex epitopes than the GalNAc-Ser/Thr structure such as the involvement of other amino acids in the antigenic determinant, conformational elements or high density of Tn residues. It has been reported that clusters of Tn are an essential part of the epitope recognized by the mAb MLS128 (an IgG), which is poorly reactive or unreactive with glycopeptides bearing unclustered Tn structures [14]. Under different conditions of deglycosylation of Tn-rich mucins we have previously shown [11] that binding of mAb 83D4 (an IgM) to the mucin was much more affected by mild alkaline treatment than was the isolectin B4 from *Vicia villosa* (a lectin with specificity for Tn antigen).

Because of the potential involvement of Tn antigen in the metastatic process and its use as target for immunotherapy, a definition of the exact nature of the epitope is important. The notion of epitope is a functional concept and binding measurements are essential for the definition of the Tn epitope. In this paper we describe and measure the affinity constants of Tn clusters with two monoclonal antibodies, MLS128 and 83D4, as well as with the isolectin B4 from *Vicia villosa* (VVLB4) using well-defined glycopeptide models and a biosensor based on surface plasmon resonance spectroscopy (BIAcore™).

2. Materials and methods

2.1. Monoclonal antibodies and isolectin B4 from V. villosa

The mAb 83D4 (IgM) was produced from a mouse immunized with cell suspensions obtained from formalin-fixed paraffin-embedded sections of an invasive human breast carcinoma [15]. mAb was precipitated from ascitic fluids by dialysis against demineralized water at 4°C, dissolved in a small volume of 0.5 M NaCl in phosphate buffer saline (PBS), applied to a Sephacryl S-200 gel column (2.5×85 cm), and eluted with PBS. IgM was excluded from the gel and recovered in the first elution peak. The mAb MLS128 (IgG_1), established by immunizing mice with human colonic cancer cells (LS180) [16], was purified by affinity chromatography on protein A-Sepharose. The Tn-binding isolectin B4 from *V. villosa* seeds was purchased from Sigma Chemical Co., St Louis, MO, USA. The purity of the three anti-Tn proteins was demonstrated by SDS–PAGE analysis.

2.2. Synthesis of Tn glycopeptides

2.2.1. General methods. Reagents were purchased from Aldrich or Sigma. All the solvents were high grade and dry. CH_2Cl_2 was distilled over P_2O_5 before use. Glycosylated serine and threonine derivatives

*Corresponding author. Fax: (598)-2-924 95 63.
E-mail: eosinaga@lobbm.fmed.edu.uy

Abbreviations: mAb, monoclonal antibody; VVLB4, isolectin B4 from *Vicia villosa*

PII: S0014-5793(00)01248-5

[Fmoc-Ser(α-GalNAc(OAc)$_3$) and Fmoc-Thr(α-GalNAc(OAc)$_3$)] were prepared by classical methods [17,18] involving glycosylation of N^{α}-(fluoren-9-yl-methoxycarbonyl)-L-serine/threonine *tert*-butyl esters [19,20] with 3,4,6-tri-*O*-acetyl-2-azido-2-deoxy-β-D-galactopyranosyl chloride (obtained from tri-*O*-acetyl-D-galactal [21]) using AgOTf as catalyst [22]; this condensation was followed by the reduction/acetylation of the azido group in the 2-position [23]. At the end, the *t*-butyl esters were deprotected in formic acid [24]. For the peptide synthesis, Fmoc-protected amino acid derivatives and Wang resin were obtained from Bachem or Novabiochem. When unglycosylated, the side chains of the amino acids serine and threonine were protected by a *t*-butyl group and the lysine residues by a *t*-butyloxycarbonyl group. DMF and acetonitrile for HPLC were purchased from Merck. The final compounds were purified by reverse phase high performance liquid chromatography (HPLC) using a Perkin-Elmer pump system with a UV detector (230 nm). A column (250×10 mm) of Nucleosil C_{18} (5 mm, 300 Å) was used and the products were eluted with a gradient of MeCN/0.1% trifluoroacetic acid buffer during 20 min (flow rate 6 ml/min). Mass spectra were measured by electrospray on a Platform spectrometer (VG-Biotech-Micromass, Manchester, UK). Amino acid analyses were obtained using a Beckman 6300 analyzer, after hydrolysis of the peptides with 6 N HCl at 110°C in sealed glass tubes for 20 h.

2.2.2. Solid phase syntheses. The solid phase peptide and glycopeptide syntheses were performed manually using the standard Fmoc chemistry protocol on a polystyrene resin functionalized with *p*-benzyloxybenzyl alcohol (Wang resin) esterified with a glycine residue. The N^{α}-Fmoc amino acids (carrying standard side chain protective groups) and the glycosylated building blocks (3 equivalents) were incorporated to the peptide chain using TBTU/HOBT/DIEA 1/1/1.7 as an activating agent and DMF as solvent [25]. The couplings were monitored by the Kaiser test [26] and usually completed within 20 min. All Fmoc cleavages were carried out by treatment of the resin with 20% piperidine in DMF (2 min then 8 min). Following each deprotection, the resin was successively rinsed with DMF, CH_2Cl_2, DMF. At the end of the synthesis, the resin was extensively washed with DMF and CH_2Cl_2, dried, and treated with an aqueous TFA solution (95%) for 2 h. After filtration of the resin, the solution was concentrated and the crude product precipitated with diethyl ether. The precipitate was filtered, dissolved in water and lyophilized. The peptides were purified by HPLC (gradient from 10% to 40% in 20 min) and obtained with an overall yield of 25%. Finally the acetyl groups of the sugar moiety were removed by adding, dropwise, a solution of 1% MeONa (pH 10.8). After 8 h, methanol was evaporated and the medium neutralized to neutral pH. The peptides were purified by HPLC on a reverse phase column (C_{18}) using a gradient of 0.1% TFA in water (solution A) and acetonitrile (solution B), and characterized by mass spectrometry and amino acid analysis.

2.2.3. Characteristics of peptides. Tn0: Lys-(Gly)$_4$-Ser-Thr-Thr-(Gly)$_3$, elution with a gradient from 0% to 17% (retention time 8.4 min); ESMS: 834.47 (calc 834.38). Amino acid analysis: Lys 1.06 (1), Gly 6.66 (7), Ser 0.85 (1), Thr 2.

Tn1: Lys-(Gly)$_4$-Ser(α-GalNAc)-Thr-Thr-(Gly)$_3$, elution with a gradient from 0% to 17% (retention time 8.6 min); ESMS 1037.64 (calc 1037.46). Amino acid analysis: Lys 1, Gly 6.97 (7), Ser 0.87 (1), Thr 1.85 (2).

Tn2: Lys-(Gly)$_4$-Ser(α-GalNAc)-Thr(α-GalNAc)-Thr-(Gly)$_3$, elution with a gradient from 0% to 15% (retention time 8.8 min); ESMS 1240.41 (calc 1240.54). Amino acid analysis: Lys 1.07 (1), Gly 7, Ser 0.93 (1), Thr 1.90 (2).

Tn3: Lys-(Gly)$_4$-Ser(α-GalNAc)-Thr(α-GalNAc)-Thr(α-GalNAc)-(Gly)$_3$, elution with a gradient from 0% to 10% (retention time 11.6 min); ESMS 1443.86 (calc 1443.62). Amino acid analysis: Lys 1, Gly 6.48 (7), Ser 0.93 (1), Thr 1.74 (2).

Tn2t: Lys-(Gly)$_4$-Ser(α-GalNAc)-Thr-Thr(α-GalNAc)-(Gly)$_3$, elution with a gradient from 0% to 8% in 10 min (retention time 9.6 min); ESMS 1240.49 (calc 1240.54). Amino acid analysis: Lys 1, Gly 6.68 (7), Ser 0.89 (1), Thr 1.85 (2).

Tn2p: Lys-(Gly)$_4$-Ser(α-GalNAc)-Pro-Thr(α-GalNAc)-(Gly)$_3$, elution with a gradient from 0% to 8% (retention time 15.2 min); ESMS 1236.80 (calc 1236.55). Amino acid analysis: Lys 1, Gly 6.88 (7), Ser 0.90 (1), Thr 0.92 (1), Pro 1.03 (1).

2.3. Surface plasmon resonance studies

The BIAcore® biosensor (Pharmacia, Uppsala, Sweden), which uses surface plasmon resonance detection and permits real-time kinetic analysis of two interacting species [27], was used to measure the binding kinetics of Tn to the proteins. Immobilization of peptides on the sensor surface (a CM5 dextran sensor chip) was performed through lysine residue according to standard procedures described previously [28]. The dextran layer of the sensor chip was first activated by injecting 35 μl of 0.2 M *N*-ethyl-*N*-(3-diethylaminopropyl)carbodiimide and 0.05 M *N*-hydroxysuccinimide. Next, each peptide (30 μl) at a concentration of 2.5 mg/ml in 10 mM sodium acetate, pH 4.5, was injected. Excess reactive groups were blocked by injection of 30 μl of 1 M ethanolamine, pH 8.5. All binding analyses were conducted in HBS buffer (10 mM HEPES pH 7.4, 0.15 M NaCl, 3.4 μM EDTA, 0.005% surfactant P20) at a flow rate of 5 μl/min at 25°C. The surface was regenerated with 1 M NaCl with no loss of activity as reflected by the identical binding evidenced when an equivalent sample was reintroduced in the next cycle (data not shown). Samples for binding analysis were diluted into the binding buffer (HBS). Kinetic studies were performed by injecting 20 μl of each protein, at a flow of 5 μl/min. Each anti-Tn protein was analyzed at five different concentrations (0.062, 0.125, 0.250, 0.5, and 1.0 μM). The kinetic constants for association (K_A) and dissociation (K_D) were evaluated using BIAevaluation 3.0 software supplied by the manufacturer (Pharmacia).

3. Results and discussion

Trying to better understand the molecular structure of what is called the Tn epitope, we have performed kinetic studies by surface plasmon resonance spectroscopy to evaluate the affinities between Tn and different Tn-binding proteins. In order to analyze the clustering effect of GalNAc residues *O*-linked to serine or threonine, we have synthesized three Tn glycopeptides (Tn1, Tn2 and Tn3) as well as the Tn-free peptide (Tn0) as a control. The peptide backbone sequence is made of glycine residues to minimize steric hindrance and side chain interactions. An additional N-terminal lysine residue was introduced for binding to the sensor surface. For the kinetic analysis, each Tn-binding protein (mAbs MLS128, 83D4 and lectin VVLB4) was added at five concentrations (0.062–1.0 μM) to each flow cell; association and dissociation were monitored in real time. As can be seen in the representative sensorgrams, VVLB4 bound Tn1, Tn2 and Tn3 glycopeptides (Fig. 1A), while no binding to the GalNAc-free peptide (Tn0) was observed. Using the same flow cells we found that anti-Tn mAbs MLS128 and 83D4 did not bind to the GalNAc-free

Table 1
Kinetic parameters obtained from the interaction analysis of Tn1, Tn2 and Tn3 glycopeptides and Tn-binding proteins by a biosensor

	Tn1			Tn2			Tn3		
	K_{on} (M^{-1} s^{-1})	K_{off} (s^{-1})	K_{off}/K_{on} (M)	K_{on} (M^{-1} s^{-1})	K_{off} (s^{-1})	K_{off}/K_{on} (M)	K_{on} (M^{-1} s^{-1})	K_{off} (s^{-1})	K_{off}/K_{on} (M)
VVLB4	2.5×10^{4}	5.4×10^{-3}	2.2×10^{-7}	1.4×10^{4}	4.5×10^{-3}	3.2×10^{-7}	2.7×10^{4}	3×10^{-3}	1.1×10^{-7}
83D4	–	–	–	7.6×10^{5}	7.6×10^{-3}	1×10^{-8}	2.1×10^{5}	2.5×10^{-3}	1.2×10^{-8}
MLS128	–	–	–	2.7×10^{4}	3.6×10^{-3}	1.3×10^{-7}	4.5×10^{4}	1.1×10^{-3}	2.4×10^{-8}

Each parameter was determined as described in Section 2, evaluating each protein (mAbs MLS128, 83D4 and lectin VVLB4) at five concentrations (0.062, 0.125, 0.250, 0.5, and 1.0 μM).

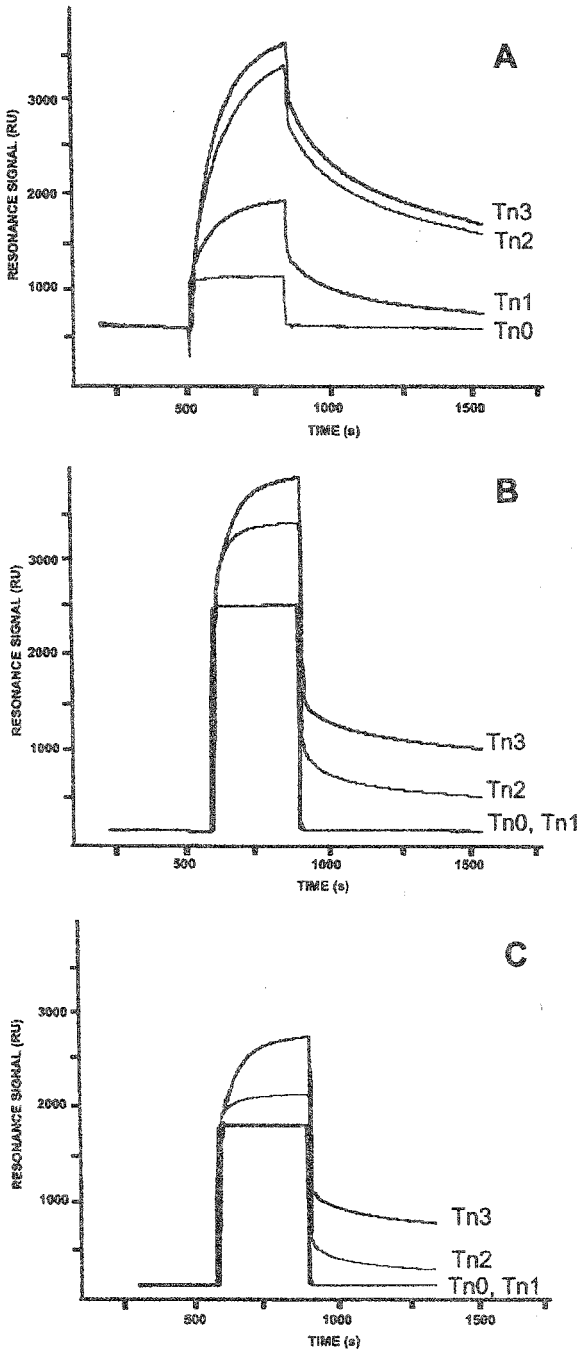

Fig. 1. Sensorgrams showing the interactions between the three Tn-binding proteins and the synthetic Tn glycopeptides. In these representative sensorgrams each protein was injected onto the surface-bound glycopeptide at 0.5 μM. A: Isolectin B4 from *V. villosa* seeds. B: mAb 83D4. C: mAb MLS128.

and the Tn1 peptides, but both did interact with the Tn2 and Tn3 peptides (Fig. 1B,C). These results indicate one Tn residue is enough for VVLB4 binding whereas the anti-Tn antibodies require at least two consecutive Tn residues for recognition.

The association, dissociation and affinity constants for the interactions between Tn glycopeptides and proteins are shown in Table 1. It appears that the VVLB4 binding does not depend on the density of the Tn determinant since the three glycopeptides Tn1, Tn2 and Tn3 show similar affinities. The mAb 83D4 recognizes both the di-Tn and the tri-Tn glycopeptides, while the mAb MLS128, although reactive with the di-Tn glycopeptide, has a higher affinity with the tri-Tn glycopeptide Tn3.

These observations suggest that a dimeric Tn cluster appears to be the 'minimum recognized structure' for MLS128 and 83D4 antibodies, and raise the question whether these monoclonal antibodies could bind to peptides where the Tn residues are not consecutive in the peptide sequence. To investigate this aspect, we synthesized glycopeptides Tn2t and Tn2p where the two Tn residues are separated by one unglycosylated amino acid. In order to evaluate the influence of the unglycosylated threonine in peptide Tn2t, proline was introduced between the two Tn units (peptide Tn2p). The results of the kinetics studies using the three Tn binding proteins are shown in the Table 2. It is observed that when an unglycosylated amino acid is introduced between the Tn residues, both MLS128 and 83D4 do not bind. This result clearly shows that two consecutive Tn structures are essential for the binding of these antibodies. By contrast, VVLB4 bound to the glycopeptides Tn2t and Tn2p with affinities similar to those observed with the glycopeptides Tn1, Tn2 and Tn3. Considering that in Tn1 glycopeptide GalNAc is *O*-linked to a serine residue, and that in both Tn2t and Tn2p glycopeptides one GalNAc is *O*-linked to serine and the other to threonine, these results indicate that the unreactivity of anti-Tn monoclonal antibodies on mono-Tn glycopeptide motifs is independent of whether GalNAc is *O*-linked to serine or threonine residues.

Our results using mAb MLS128 agree with the previous observation that this antibody preferentially binds with a cluster of three adjacent serine or threonine residues, each linked to GalNAc by a α linkage, but does not recognize mono-Tn glycopeptides [14]. Here, using synthetic model Tn glycopeptides and a biosensor based on surface plasmon resonance spectroscopy, we show that mAb MLS128 also binds glycopeptides bearing two adjacent Tn residues, although with less affinity. Furthermore, mAb 83D4 binds with similar affinity to dimeric as well as to trimeric clusters of Tn, suggesting that the fine specificity of both anti-Tn monoclonal antibodies is not the same. The clustering effect appears to be not restricted to the epitope identified by antibodies. Recently it has been reported that Tn clusters are essential for the recognition by the Tn-specific human macrophage C-type lectin, which reacts poorly with glycopeptides bearing mono-Tn motifs [29].

The clustering effect has also been reported on anti-sialyl-Tn monoclonal antibodies. Reddish et al. [30] have shown that some antibodies recognize the sialyl-Tn as an isolated structure (mAb 195.3) whereas some others need a cluster for binding (mAbs B72.3 and CC49). Recently, Tanaka et al. [31] found that a cluster composed of four sialyl-Tn antigens is the essential epitopic structure for mAb MLS132. The biological role of clustered versus single Tn or sialyl-Tn epitopes on cancer cells is still not understood. Ogata et al. [32] reported that sialyl-Tn clusters appear during malignant transformation of human colonic mucosa. The ability to synthesize monomer or cluster of Tn/sialyl-Tn structures on mucin polypeptide backbones could depend in part on the sequence of *O*-glycosylation sites of the apomucin, as well as on the repertoire and specificity of glycosyltransferases required for Tn/sialyl-Tn synthesis that exist in normal versus

Table 2
Kinetic parameters obtained from the interaction analysis of Tn2p and Tn2t glycopeptides and Tn-binding proteins by a biosensor

	Tn2p			Tn2t		
	K_{on} (M^{-1} s^{-1})	K_{off} (s^{-1})	K_{off}/K_{on} (M)	K_{on} (M^{-1} s^{-1})	K_{off} (s^{-1})	K_{off}/K_{on} (M)
VVLB4	2.2×10^{4}	3×10^{-3}	2.0×10^{-7}	1.9×10^{4}	4.3×10^{-3}	2.3×10^{-7}
83D4	–	–	–	–	–	–
MLS128	–	–	–	–	–	–

Each parameter was determined as described in Section 2, evaluating each protein (mAbs MLS128, 83D4 and lectin VVLB4) at five concentrations (0.062, 0.125, 0.250, 0.5, and 1.0 μM,)

cancerous cells. The initial transfer of GalNAc to the apomucin peptide can be performed by several UDP-GalNAc:polypeptide *N*-acetylgalactosaminyl transferases (EC 2.4.1.41) which control the *O*-linked glycosylation [33]. Studies using the MUC1 tandem repeat peptide as acceptor showed that site-specific glycosylation could regulate the addition of GalNAc to Ser/Thr at adjacent or distant positions [34], indicating that the addition of GalNAc can be affected by previous glycosylation of other sites of the peptide substrate.

The fact that Tn binding exhibited by VVLB4 is not dependent on the density of Tn determinants is in favor of different Tn recognition patterns for this lectin and the two antibodies studied, MLS128 and 83D4. These results, using model glycopeptides immobilized on a solid phase, are consistent with the reactivity observed for two plant lectins (*Salvia sclarea* and VVLB4) and mAb 83D4 using the same glycopeptides but in solution [35]. In that case also, both lectins bind similarly to Tn1, Tn2, Tn3 whereas mAb 83D4 only recognized the di- and tri-Tn glycopeptides. As part of our structural studies of Tn-binding proteins, we have constructed a single-chain Fv fragment of the anti-Tn mAb 83D4, and have demonstrated that this recombinant polypeptide retains Tn-binding properties [36]. The monoclonal antibodies directed against four sialyl-Tn and mAb 83D4 use the same V_H germline gene segment, $V_H\alpha$TAG-1 [36], indicating that the heavy chain plays a predominant role in determining the antigen binding affinity. Molecular modeling of the 83D4 molecule indicated that the antibody-combining site might be primarily defined by the CDR H1 and H2 loops. The differences in specificity between anti-Tn and anti-sialyl-Tn antibodies could be explained by significant sequence variations which occur in both the light chain and the CDR H3 loop. On the other hand, we have reported the amino acid sequence and the crystal structure of the isolectin B4 from *V. villosa* seeds [37]. The amino acid residues defining the metal- and sugar-binding sites of GalNAc-specific lectins are highly conserved in the VVLB4 structure, indicating that residues outside the carbohydrate-binding pocket and/or quaternary association determinants may modulate the affinity for the Tn glycopeptide. Crystallographic studies of these Tn-binding proteins in complex with various Tn-containing molecules are in progress, and should provide invaluable information about the specific recognition of Tn determinant. Furthermore, considering that the amino acid sequence near the *O*-linked GalNAc could participate in the determinant identified by monoclonal antibodies, we are evaluating several Tn glycopeptides in order to determine the role of the peptide moiety on their Tn-binding reactivity.

Acknowledgements: This work was partially supported by grants from the Comisión Honoraria de Lucha Contra el Cancer (Uruguay), CSIC (Universidad de la Republica, Uruguay), and ECOS France-Uruguay Program.

References

[1] Kim, Y.S., Gum, J. and Brockhausen, I. (1996) Glycoconj. J. 13, 693–707.
[2] Springer, G. (1997) J. Mol. Med. 75, 594–602.
[3] Springer, G. (1995) Crit. Rev. Oncogen. 6, 57–85.
[4] Galli-Stampino, L., Meinjohanns, E., Frische, K., Meldal, M., Jensen, T., Werdelin, O. and Mouritsen, S. (1997) Cancer Res. 57, 3214–3222.
[5] Lo-Man, R., Bay, S., Vichier-Guerre, S., Dériaud, E., Cantacuzène, D. and Leclerc, C. (1999) Cancer Res. 59, 1520–1524.
[6] Schlepper-Schafer, J. and Springer, G. (1989) Biochim. Biophys. Acta 1013, 266–272.
[7] Hansen, J.E., Nielsen, C., Arendrup, M., Olofsson, S., Mathiesen, L., Nielsen, J.O. and Clausen, H. (1991) J. Virol. 65, 6461–6467.
[8] Hirohashi, S., Clausen, H., Yamada, T., Shimosato, Y. and Hakomori, S. (1985) Proc. Natl. Acad. Sci. USA 82, 7039–7043.
[9] Takahashi, H., Metoki, R. and Hakomori, S. (1988) Cancer Res. 48, 4361–4367.
[10] Nakada, H., Numata, Y., Inoue, M., Tanaka, N., Kitagawa, H., Funakoshi, I., Fukui, S. and Yamashina, I. (1991) J. Biol. Chem. 266, 12402–12405.
[11] Osinaga, E., Pancino, G., Porchet, N., Mistro, D., Aubert, J.P. and Roseto, A. (1992) J. Tumor Marker Oncol. 7, 13–24.
[12] Tollefsen, S.E. and Kornfeld, R. (1983) J. Biol. Chem. 258, 5172–5176.
[13] Piller, V., Piller, F. and Cartron, J.-P. (1986) J. Biol. Chem. 261, 14069–14075.
[14] Nakada, H., Inoue, M., Numata, Y., Tanaka, N., Funakoshi, I., Fukui, S., Mellors, A. and Yamashina, I. (1993) Proc. Natl. Acad. Sci. USA 90, 2495–2499.
[15] Pancino, G., Osinaga, E., Vorauher, W., Kakouche, A., Mistro, D., Charpin, C. and Roseto, A. (1990) Hybridoma 9, 389–395.
[16] Numata, Y., Nakada, H., Fukui, S., Kitagawa, H., Ozaki, K., Inoue, M., Kawasaki, T., Funakoshi, I. and Yamashina, I. (1990) Biochem. Biophys. Res. Commun. 170, 980–985.
[17] Ferrari, B.P. (1980) Carbohydr. Res. 79, C1–C7.
[18] Lemieux, R.U. and Ratcliffe, R.M. (1979) Can. J. Chem. 57, 1244–1251.
[19] Schultz, M. and Kunz, H. (1993) Tetrahedron Asymm. 4, 1205–1220.
[20] Vowinkel, E. (1967) Chem. Ber. 100, 16–22.
[21] Shafizadeh, F. (1963) Methods Carbohydr. Chem. 2, 409–410.
[22] Mulard, L.A., Kovac, P. and Glaudemans, C.P. (1994) Carbohydr. Res. 259, 21–34.
[23] Paulsen, H. and Hölck, J.-P. (1982) Carbohydr. Res. 109, 89–107.
[24] Paulsen, H. and Adermann, K. (1989) Liebigs Ann. Chem. 25, 751–759.
[25] Fields, C.G., Llyod, D.H., Macdonald, R.L., Otteson, K.M. and Noble, R.M. (1991) Peptide Res. 4, 95–101.
[26] Kaiser, E., Colescott, R.L., Bossinger, C.D. and Cook, P.I. (1970) Anal. Biochem. 34, 595–598.
[27] Malmqvist, M. (1993) Nature 361, 186–187.
[28] Altschuh, D., Dubs, M.C., Weiss, E., Zeder-Lutz, G. and Van Regenmortel, M. (1992) Biochemistry 31, 6298–6304.

[29] Iida, S., Yamamoto, K. and Irimura, T. (1999) J. Biol. Chem. 274, 10697–10705.
[30] Reddish, M., Jackson, L., Koganty, R., Qiu, D., Hong, W. and Longenecker, B.M. (1997) Glycoconj. J. 14, 549–560.
[31] Tanaka, N., Nakada, H., Inoue, M. and Yamashina, I. (1999) Eur. J. Biochem. 263, 27–31.
[32] Ogata, S., Koganty, R., Reddish, M., Longenecker, B.M., Chen, A., Perez, C. and Itzkowitz, S. (1998) Glycoconj. J. 15, 29–35.
[33] Clausen, H. and Bennett, E.P. (1996) Glycobiology 6, 635–646.
[34] Hanisch, F.-G., Müller, S., Hassan, H., Clausen, H., Zachara, N., Gooley, A., Paulsen, H., Alving, K. and Peter-Katalinic, J. (1999) J. Biol. Chem. 274, 9946–9954.
[35] Medeiros, A., Bianchi, S., Calvete, J.J., Balter, H., Bay, S., Robles, A., Cantacuzène, D., Nimtz, M., Alzari, P.M. and Osinaga, E. (2000) Eur. J. Biochem. (in press).
[36] Babino, A., Pritsch, O., Oppezzo, A., Du Pasquier, R., Roseto, A., Osinaga, E. and Alzari, P.M. (1997) Hybridoma 16, 317–324.
[37] Osinaga, E., Tello, D., Batthyany, C., Bianchet, M., Tavares, G., Duran, R., Cerveñansky, C., Camoin, L., Roseto, A. and Alzari, P.M. (1997) FEBS Lett. 412, 190–196.

S. Vichier-Guerre
R. Lo-Man
S. Bay
E. Deriaud
H. Nakada
C. Leclerc
D. Cantacuzène

Short synthetic glycopeptides successfully induce antibody responses to carcinoma-associated Tn antigen

Authors' affiliations:
S. Vichier-Guerre, Unité de Chimie Organique, Institut Pasteur, Paris, France.

R. Lo-Man, Unité de Biologie des Régulations Immunitaires, Institut Pasteur, Paris, France.

S. Bay, Unité de Chimie Organique, Institut Pasteur, Paris, France.

E. Deriaud, Unité de Biologie des Régulations Immunitaires, Institut Pasteur, Paris, France.

H. Nakada, Department of Biotechnology, Faculty of Engineering, Kyoto Sangyo University, Kyoto, Japan.

C. Leclerc, Unité de Biologie des Régulations Immunitaires, Institut Pasteur, Paris, France.

D. Cantacuzène, Unité de Chimie Organique, Institut Pasteur, Paris, France.

Correspondence to:
Danièle Cantacuzène
Unité de Chimie Organique
Institut Pasteur
28 rue du Dr. Roux
75724 Paris
Cedex 15
France
Tel: 33-1-4568-8397
Fax: 33-1-4568-8404
E-mail: dcanta@pasteur.fr

Dates:
Received 15 June 1999
Revised 11 August 1999
Accepted 6 September 1999

To cite this article:
Vichier-Guerre, S., Lo-Man, R., Bay, S., Deriaud, E., Nakada, H., Leclerc, C. & Cantacuzène, D. Short synthetic glycopeptides successfully induce antibody responses to carcinoma-associated Tn antigen. *J. Peptide Res.*, 2000, 55, 173–180

ISSN 1397-002X

Key words: antigenicity; glycopeptide; immunogenicity; MLS 128; Tn antigen; tumor-associated antigen

Abstract: Glycopeptides containing a tumor-associated carbohydrate antigen (mono-, tri- or hexa-Tn antigen) as a B-cell epitope and a $CD4^+$ T-cell epitope (PV: poliovirus or TT: tetanus toxin) were prepared for immunological studies. Several Tn antigen residues [FmocSer/Thr (α-GalNAc)-OH] were successively incorporated into the peptide sequence with unprotected carbohydrate groups. The tri- and hexa-Tn glycopeptides were recognized by MLS 128, a Tn-specific monoclonal antibody. The position of the tri-Tn motif in the peptide sequence and the peptide backbone itself do not alter its antigenicity. As demonstrated by both ELISA and FACS analysis, the glycopeptides induced high titers of anti-Tn antibodies in mice, in the absence of a carrier molecule. In addition, the generated antibodies recognized the native Tn antigen on cancer cells. The antibody response obtained with a D-(Tn_3)-PV glycopeptide containing three α-GalNAc-D-serine residues is similar that obtained with the Tn_6-PV glycopeptide. These results demonstrate that short synthetic glycopeptides are able to induce anticancer antibody responses.

Abbreviations: AgOTf, trimethylsilyl trifluoromethane sulfonate; Ag_2CO_3, silver carbonate; $AgClO_4$, silver perchlorate; a-OSM, asialo ovine submaxillary mucin; CFA, complete Freund's adjuvant; DIEA, diisopropylethylamine; ESMS, electrospray mass spectroscopy; FCS, fetal calf serum; FITC, fluorescein isothiocynate; Fmoc, 9-fluorenylmethoxycarbonyl; HOBT, 1-hydroxybenzotriazole; IFA, incomplete Freund's adjuvant; MAG, multiple antigen glycopeptide; MAP, multiple antigen peptide; OSA, ovine serum albumin; PE, phycoerythrin; PFA, paraformaldehyde; Pfp, pentafluorophenyl; PV, Poliovirus; TBTU, 2-(1H-benzotriazole-1-yl)-1,1,3,3-tetramethyluronium tetrafluoroborate; TFA, trifluoroacetic acid; TT, Tetanus toxin.

As a result of aberrant glycosylation, cancer-associated carbohydrate antigens are exposed at the surface of some tumor cells, whereas they are shielded by further glycosylation or are poorly expressed in normal cells (1–3). Recent advances in immunology have renewed interest in the development of cancer vaccines, and these exposed glycosidic B-cell epitopes have been considered to be attractive targets for immunotherapy (4). Indeed, several studies have shown that efficient immune responses could be induced against different carbohydrate antigens: Tn (α-GalNAc-Ser/Thr), T (β-Gal-[1-3]-α-GalNAc-Ser/Thr), sialosyl-Tn (α-NeuAc-[2-6]-α-GalNAc-Ser/Thr) or the GM2 ganglioside (5). The immunizations have usually been performed using carbohydrate–protein conjugates (6–8).

In order to circumvent the drawbacks displayed by protein carriers, the multiple antigen glycopeptide (MAG) approach was recently developed as an alternative to present carbohydrate antigens to the immune system (9, 10). This type of immunogen is based on the multiple antigen peptide (MAP) developed by Tam and co-workers (11, 12).

In a previous paper, we described the construction of a MAG carrying the carbohydrate Tn antigen (B epitope) associated with a $CD4^+$ T-cell epitope [PV: Poliovius (13)] on a dendrimeric lysine core with four branches (10). This MAG: Tn-PV was able to induce anti-Tn IgG antibodies that recognized human tumor cell lines. Moreover therapeutic immunization with this synthetic immunogen administered with alum increased survival in tumor-bearing mice (14).

The tumor-associated glycoprotein epitope defined by the monoclonal antibody MLS 128 is expressed on most human adenocarcinomas and is minimally expressed on normal tissues. MLS 128 was raised against LS 180 cells, a human colorectal cancer cell line (15). The epitope for MLS 128 has been identified as Tn, i.e. α-GalNAc, O-linked to Ser/Thr on mucin-type glycoprotein and it seems that a cluster of α-GalNAc-Ser/Thr is essential for Tn antigenicity (8, 16–18). In LS 180 cells, the Tn antigen has been shown to be the product of glycosylation of the polypeptide encoded by the *MUC-2* gene (19). As a cluster, the Tn antigen has also been found in ovine submaxillary mucin (16), glycophorin (17) and the Jurkat cell lines (20).

In order to mimic the clustered motif encountered for the Tn antigen *in vivo*, further development of our MAG-based vaccines (10, 14) was undertaken, involving the introduction of a tri-Tn glycopeptide as the B epitope. Such an approach has already been described with di- and trimeric Tn conjugated to ovine serum albumin (OSA), Starburst dendrimers (18) and lipopeptides (21). The synthesis of linear glycopeptides (Fig. 1) was performed using Tn motifs associated with the $CD4^+$ T-cell epitope of the poliovirus (PV: KLFAVWKITYKDT). The Tn antigen was introduced in one, three or six copies and was located either in the middle or at the end of the peptide sequence. The antigenicity and immunogenicity of the resulting glycopeptides have been investigated and are described here. Since D-amino acids are known to confer proteolytic stability, D-(Tn_3)-PV glycopeptide was synthetized in order to evaluate the effect of a D-amino acid on the antigenicity and immunogenicity of this peptide [D-(Tn_3) represents three consecutive D-serine α-linked to a GalNAc residue]. Threonine was replaced in the tri-D-Tn motif by D-serine, since its β-chiral center might confer additional structural problems.

Experimental Procedures

Synthesis of the peptides and glycopeptides

The synthesis of the Tn antigens, appropriately protected, 9-fluorenylmethoxycarbonyl (Fmoc)Ser (α-GalNAc)-OH and FmocThr (α-GalNAc)-OH was performed using classical methods (22, 23) starting from tri-*O*-acetyl-D-galactal (24). *N*-(Fluorenylmethoxycarbonyl)-L-serine/threonine *tert*-butyl esters (25, 26) were used for the Koenigs-Knorr reaction with 3,4,6-tri-*O*-acetyl-2-azido-2-deoxy-β-D-galactopyranosyl chloride (27, 28). The catalyst used for the glycosylation was trimethylsilyl trifluoromethane sulfonate (AgOTf) for the L-amino acid (Ser, Thr) and silver carbonate (Ag_2CO_3)/silver perchlorate ($AgClO_4$) for the D-serine. The final deprotection of the acetyls (29) and the *t*-butyl ester afforded Tn antigens appropriately protected for the peptide synthesis.

$STTG_6KG$	STTGGGGGGKG
Tn_3G_6KG	S*T*T*GGGGGGKG
Tn_3G_6K(Biot)G	S*T*T*GGGGGGK(Biotine)G
STTG6K(Biot)G	STTGGGGGGK(Biot)G
$KG_4Tn_3G_3$	KGGGGS*T*T*GGG
PV	KLFAVWKITYKDT
Tn-PV	S*KLFAVWKITYKDT
Tn_3-PV	S*T*T*KLFAVWKITYKDT
D-(Tn_3)-PV	D-(S*)D-(S*)D-(S*)KLFAVWKITYKDT
Tn_6-PV	$(S*T*T*G)_2$KLFAVWKITYKDT
Tn_3-TT	S*T*T*QYIKANSKFIGITEL

Figure 1. Structure of the different glycopeptides. *, α-GalNAc; PV, poliovirus p 103–115; TT, tetanus toxin p 830–844; L-amino acids in single-letter code are designated by upper case letters, D-amino acids are specified by the letter D.

All the glycopeptides were assembled by the conventional solid-phase peptide methodology (Wang resin, Novabiochem) using Fmoc chemistry. The appropriately protected amino acids were incorporated manually into the peptide sequence using 2-(1H-benzotriazole-1-yl)-1,1,3,3-tetramethyluronium tetrafluoroborate (TBTU)/1-hydroxybenzotriazole (HOBT)/diisopropylethylamine (DIEA) as the coupling reagent (30, 31). Fmoc protection was removed with 20% piperidine in DMF. The glycosylated amino acids FmocSer/Thr(α-GalNAc)-OH were incorporated as their pentafluorophenyl (Pfp) esters (32); these were prepared by addition of 1,3-diisopropylcarbodiimide to the glycosylated amino acid and pentafluorophenol in dry CH_2Cl_2 (33). The reaction was followed by TLC. After concentration of the solution the Pfp-esters were used without further purification and dissolved in DMF with HOBT, as described previously (33). The peptides were cleaved from the resin with aqueous trifluoroacetic acid (TFA; 95%).

All the derivatives were purified by HPLC using a Perkin–Elmer pump system with a UV detector at 230nm; the column was a Nucleosil C_{18} (5 µm, 300A˚, 250 × 10 mm) and the gradient was performed with water (0.1‰ TFA)/acetonitrile over 20 min. The peptides and glycopeptides (Fig. 1) were all characterized by amino acid analysis and mass spectrometry.

PV

HPLC: gradient from 0 to 65%, retention time 12.6 min; FABMS: $[MH^+]$ 1613 (calcd 1611.9); amino acid analysis: Ala 1.16 (1), Asp 1.03 (1), Ile 0.96 (1), Leu 1.01 (1), Lys 2.92 (3), Phe 1 (1), Thr 1.84 (2), Tyr 0.99 (1), Val 0.94 (1).

Tn-PV

HPLC: gradient from 10 to 60%, retention time 11.2 min; electrospray mass spectroscopy (ESMS): 1903 (calcd 1903.22); amino acid analysis: Ala 1 (1), Asp 1.05 (1), Ile 1.0 (1), Leu 1.05 (1), Lys 3.12 (3), Phe 1.05 (1), Ser 0.94 (1), Thr 1.97 (2), Tyr 1.06 (1), Val 1.0 (1).

Tn_3-PV

HPLC: gradient from 10 to 60%, retention time 10.3 min; ESMS: 2512 (calcd 2511.8); amino acid analysis Ala 1 (1), Asp 1.05 (1), Ile 1.0 (1), Leu 1.05 (1), Lys 3.12 (3), Phe 1.05 (1), Ser 0.95 (1), Thr 3.74 (4), Tyr 1.06 (1), Val 1.0 (1).

D-(Tn_3)-PV

HPLC: gradient from 15 to 30%, retention time 16.9 min; ESMS: 2484 (calcd 2483.74); amino acid analysis Ala 1 (1), Asp 1.01 (1), Ile 0.96 (1), Leu 1.01 (1), Lys 3.06 (3), Phe 0.97 (1), Ser 2.7 (3), Thr 1.85 (2), Tyr 1.03 (1), Val 0.99 (1).

Tn_3-TT

HPLC: gradient from 10 to 35%, retention time 14.7 min; ESMS: 2623 (calcd 2623.56); amino acid analysis: Ala 1 (1), Asn 1.04 (1), Glu 2.16 (2), Gly 1.08 (1), Ile 2.95 (3), Leu 1.1 (1), Lys 2.04 (2), Phe 1.01 (1), Ser 1.86 (2), Thr 2.76 (3), Tyr 0.97 (1).

Tn_6-PV

HPLC: gradient from 10 to 60%, retention time 12.7 min; ESMS: 3525.0 (calcd 3524.7); amino acid analysis: Ala 1 (1), Asp 0.98 (1), Ile 0.97 (1), Leu 1.0 (1), Lys 2.91 (3), Phe 1.02 (1), Ser 2.09 (2), Thr 5.92 (6), Tyr 1.13 (1), Val 1.0 (1).

$STTG_6KG$

HPLC gradient from 0 to 17%, retention time 8.2 min; ESMS: 834.3 (calcd 834.4); amino acid analysis: Ser 0.93 (1), Thr 2 (2), Gly 7.95 (7), Lys 1.21 (1).

$STTG_6K$ (Biot)G

HPLC gradient from 0 to 20%, retention time 14.6 min; ESMS: 1060.8 (calcd 1061.1); amino acid analysis: Ser 0.93 (1), Thr 1.89 (2), Gly 7 (7), Lys 1.09 (1).

Tn_3G_6K (Biot)G

HPLC gradient from 5 to 20%, retention time 11.4 min; ESMS: 1669.7 (calcd 1670.0); amino acid analysis: Ser 1.09 (1), Thr 2 (2), Gly 6.48 (7), Lys 0.99 (1).

Tn_3G_6KG

HPLC gradient from 0 to 17%; retention time 7.6 min; ESMS: 1443.9 (calcd 1443.6); amino acid analysis: Ser 0.93 (1), Thr 1.79 (2), Gly 7 (7), Lys 1.0 (1).

$KG_4Tn_3G_3$

HPLC: gradient from 0 to 14%, retention time 9.6 min; ESMS: 1444.4 (calcd 1443.6); amino acid analysis: Ser 0.88 (1), Thr 2 (2), Gly 7.07 (7), Lys 1.03 (1).

Mice and immunization

Six to 8-week-old female BALB/c mice were from Janvier (Le Genest Saint-Isle, France). Mice were injected intraperitoneally with peptides or glycopeptides in complete Freund's adjuvant (CFA; Sigma), then boost injections were performed in incomplete Freund's adjuvant (IFA; Sigma). Sera were collected and tested to detect for the presence of

anti-Tn antibodies by enzyme-linked immunosorbant assay (ELISA) or FACS.

ELISA (for antigenicity)

The PV- and TT-glycopeptides were coated in 50 mM carbonate buffer pH 9.6 by overnight incubation at 37°C on microtiter plates; several dilutions of MLS 128 (a mouse IgG3 specific for the Tn antigen [15]) were then added for 1 h at 37°C. After washing, the MLS 128 mAb bound to the coated compound was revealed using goat antimouse IgG peroxidase conjugate (Sigma) and *O*-phenyldiamine/H_2O_2 substrates. The reaction was stopped by H_2SO_4 and the optical density (OD) read at 492 nm with an ELISA autoreader (Dynatech, Marnes la Coquette, France).

For the inhibition studies, streptavidin-coated microtiter plates (Sigma, St Louis, MO, USA) were used and incubation with the biotinylated glycopeptide Tn_3G_6K (Biot)G was performed for 1 h at 37°C. MLS 128 mAb, at 1 µg/mL, was then added to the streptavidin-coated plates with serial dilutions of the synthetic competitors (peptide or glycopeptide) for 30 min.

Results are expressed as the percentage of inhibition calculated from the values obtained without any competitor (OD_{max}) or in the presence of a competitor peptide ($OD_{comp.}$).% inhibition = $100 \times [1 - (OD_{comp.}/OD_{max})]$.

ELISA (antibody titer)

Mouse sera were tested for anti-Tn antibodies with ELISA using the synthetic glycopeptide Tn_3G_6K (Biot)G or the unglycosylated analog $STTG_6K$ (Biot)G as control. The biotinylated peptides at 1 µg/mL were incubated for 1 h at 37°C on streptavidin-coated microtiter plates. Serial dilutions of sera were then added to the plates; bound antibodies were revealed using goat antimouse IgG or IgM peroxidase conjugate (Sigma). The titers were calculated to be the $\log_{10}$ highest dilution that gave twice the signal obtained with naive mice sera tested at a dilution of 1 : 100.

Flow cytometry (FACS)

Mouse sera were tested at serial dilutions by flow cytometry on the human Jurkat tumor cell line expressing Tn. Cells were first incubated for 30 min with sera at 4°C in phosphate-buffered saline (PBS) containing 5% fetal calf serum (FCS) and 0.05% sodium azide and further incubated 30 min with goat antimouse IgM conjugated to fluorescein isothiocyanate (FITC; Pharmigen, San Diego, CA, USA) and with a mixture of biotinylated antimouse IgG1, IgG2a, IgG2b and IgG3 antibodies from goat (Amersham, Les Ulis, France). IgG binding was then revealed using streptavidin-phycoerythrin (PE; Sera-Lab). Paraformaldehyde (PFA)-fixed cells were analyzed on a FACScan flow cytometer (Becton Dickinson, Mountain View, CA, USA) and analysis performed with CellQuest software (Becton Dickinson). The titers on Jurkat cells were calculated to be the $\log_{10}$ highest dilution that gave twice the geometric mean of fluorescence obtained with unstained cells.

Results and Discussion

Synthesis

The glycopeptides were assembled by the conventional solid-phase peptide methodology using Fmoc chemistry, which is compatible with glycopeptide synthesis. The appropriately protected amino acids were incorporated into the peptide sequence using TBTU/HOBT/DIEA as the coupling reagent (30, 31). Of interest was the incorporation of three successive Tn residues, which could be achieved with the fully deprotected sugar. Several groups described the coupling of a single N-terminal glycosyl amino acid with unprotected carbohydrate hydroxyl groups (10, 34–36). However, to our knowledge, few examples of synthesis with subsequent coupling steps have been described (37–39). In our case three *O*-glycosylated Fmoc-amino acids Fmoc-Ser/Thr(α-GalNAc)-OH could be incorporated sequentially as their Pfp-esters (32, 33). This is very advantageous since it avoids potential side reactions (racemization and/or β-elimination) associated with the final deacetylation of the sugar residue, although this risk has been shown to be limited (40). Furthermore, deprotection of the acetyl groups of three sugar units is difficult to follow by HPLC when the structure is multimeric as in the case of the MAG constructs.

To synthesize the Tn_6-PV glycopeptide, a glycine residue was introduced as a spacer on the two amino groups of the N-terminal lysine residue to reduce steric hindrance (see Fig. 1 for the identification of the glycopeptides).

Antigenicity

The antigenicity of the mono-, tri- and hexa-Tn glycopeptides containing the PV sequence 103–115 (Tn-PV, Tn_3-PV, Tn_6-PV, respectively) and the tri-Tn glycopeptide with the TT sequence 830–844 (Tn_3-TT) was first evaluated by

measuring the recognition of the Tn motif using the MLS 128 mAb (Fig. 2A). The tri- and hexa-Tn peptides are efficiently recognized by MLS 128, whereas the mono-Tn-PV and the PV peptides are not. In contrast, the tri-Tn glycopeptide with three D-serine residues is also recognized by the antibody. Since the chirality of the D-(Tn_3) motif in the PV-glycopeptide does not affect recognition of the 'Tn motif' by MLS 128, the aglycone (Ser/Thr) might not be of crucial importance.

The influence, on MLS 128 binding, of the position of the tri-Tn motif within the peptide backbone was then investigated. For this purpose, an inhibition assay was performed using Tn_3G_6KG or $KG_4Tn_3G_3$ glycopeptides as competitors for the binding of MLS 128 to Tn_3G_6K(Biot)G coated on a streptavidin layer. The model polyglycine glycopeptide Tn_3G_6KG was chosen for the competition

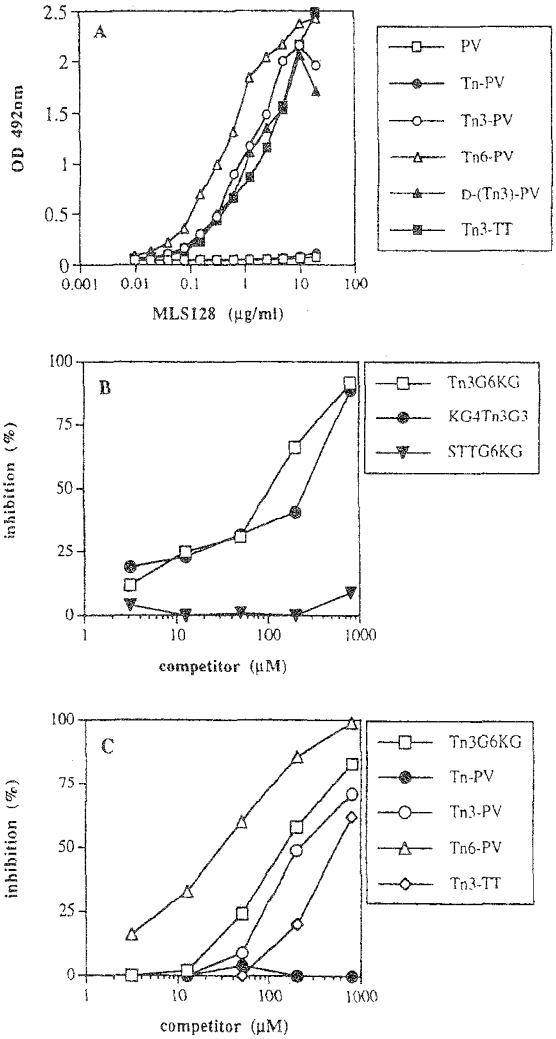

Figure 2. Antigenicity of Tn-glycopeptides using the MLS 128 mAb. MLS 128 binding to various Tn-glycopeptides was assessed by direct ELISA (A). Inhibition of MLS 128 binding to Tn3G6K(Biot)G (B, C) was performed by competitive ELISA using the indicated Tn-glycopeptides as described in Experimental Procedures.

assays because it competes efficiently with asialo ovine submaxillary mucin (a-OSM) for MLS 128 binding, whereas the unglycosylated parent peptide, $STTG_6KG$, does not (data not shown). As can be seen in Fig. 2B, the inhibition is similar whether the tri-Tn cluster is at the N-terminal end of the peptide or in the middle of the peptide chain.

Furthermore, recognition of the tri-Tn sequence by MLS 128 is affected only slightly by the nature of the adjacent peptide as shown in Fig. 2C, in inhibition studies with Tn_3-PV, Tn_3-TT or Tn_3G_6KG. These results indicate that the binding of the tri-Tn ligand to MLS 128 does not really depend on the peptide backbone. This is particularly important given the fact that the association of the Tn motif with a T-cell peptide is required for its immunogenicity.

Using MLS 128, strong immunoreactivity was observed with synthetic MUC-2 peptides (14 Thr) containing nine or 10 GalNAc residues; however, the site of glycosylation in the peptide was not clearly determined (41). In contrast, the MLS 128 mAb was shown to recognize a tri-Tn motif on glycophorin (17) suggesting that the density of the Tn motif can be a critical point for antibody recognition. This point is illustrated in Fig. 2C by the incapacity of a mono-Tn glycopeptide (Tn-PV) to inhibit MLS 128 binding.

In order to improve the antigenicity of the Tn-based glycopeptides, the density of the Tn motif was further increased by introducing one tri-Tn motif on each amino group of the N-terminal lysine residue of the PV peptide (Tn_6-PV). As shown in Fig. 2C, this strategy leads to significant enhancement of the antigenicity (measured in the competition assay) compared with the Tn_3-PV peptide.

Immunogenicity

To analyze the ability of Tn-based linear glycopeptides to induce anti-Tn antibodies, BALB/c mice received three injections of the Tn-PV, Tn_3-PV, D-(Tn_3)-PV and Tn_6-PV glycopeptides or of the control PV peptide corresponding to the T-cell epitope alone. Sera were collected after each immunization and tested for IgG and IgM anti-Tn antibodies by ELISA using a glycopeptide with a tri-Tn motif associated with a polyglycine backbone, Tn_3G_6K(Biot)G, which is unrelated to the PV sequence (Fig. 3). Another glycopeptide with an irrelevant sequence to PV was tested (Tn_3-TT) with similar results (unpublished data).

Under these conditions, anti-Tn IgM antibodies were detected after immunization with the Tn_6-PV peptide and D-(Tn_3)-PV (Fig. 3A). A slightly lower antibody response was obained when mice were immunized with Tn_3-PV. Interestingly, these three short glycopeptides also induced

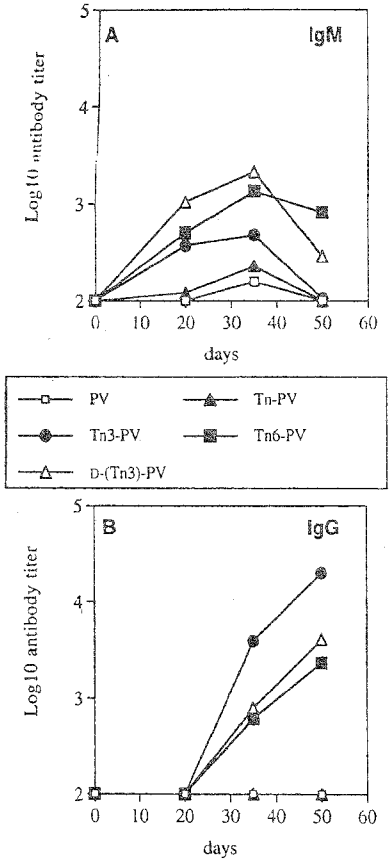

Figure 3. Anti-Tn antibodies induced in mice immunized with Tn-glycopeptides as measured by ELISA. Mice (four per group) received three injections (days 0, 21 and 42) of 50 µg PV, Tn-PV, Tn_3-PV, Tn_6-PV and D-(Tn_3)-PV in CFA for the first injection and in IFA for boost injections. After each injection, sera were collected and analyzed for anti-Tn antibody response using the Tn_3G_6K(Biot)G glycopeptide (IgM in A and IgG in B). No sera binding was observed in ELISA using the unglycosylated $STTG_6K$(Biot)G peptide as the coating antigen (data not shown). Results are expressed as the mean of individual antibody titers. Serum titers < 100 are considered negative since sera were tested at a starting dilution of 1 : 100.

anti-Tn IgG antibodies; unexpectedly however, the level was somewhat higher for the Tn_3-PV glycopeptide than for the D-(Tn_3)-PV and the Tn_6-PV homologs (Fig. 3B). This level, obtained with a linear glycopeptide in the absence of a carrier molecule, is similar to the IgG titer obtained with the dendrimeric MAG construct described earlier (10). We checked that no Tn-specific antibodies were detected after injection of the PV peptide showing the Tn specificity of the antibodies (Fig. 3B). Interestingly, the Tn-PV glycopeptide did not induce any Tn antibody. This result is in agreement with the lack of recognition of the mono-Tn glycopeptide by the MLS 128 mAb (Fig. 2C), and confirms that Tn cluster structures are required for efficient antibody production.

Peptides with contiguous B- and T epitopes have been reported to give a protective immune response in the absence of carrier molecules (42–45). However, little is known about the immunogenicity of glycopeptides as far as antibody production against the sugar moiety is concerned. Only a few examples of carbohydrate-specific antibodies raised after glycopeptide immunization have been published. Synthetic peptides containing either a pentasaccharide (46) or repeating units of 3-β-D-ribose-(1,1)-D-ribitol-5-phosphate (PRP) (47) have been shown to induce a good level of antibodies against the carbohydrate part of the glycopeptide. Other examples of immunogenic glycopeptides are known. However, the antibody specificity involves both the carbohydrate and peptide moieties (48, 49). Here we show that glycopeptides bearing a tri-Tn motif at the N-terminal end of a $CD4^+$ T-cell epitope are also able to induce the production of anti-Tn antibodies without the help of a carrier protein.

To determine whether these mouse sera were able to recognize the native Tn antigen, we titrated the anti-Tn reactivity obtained after the last immunization using human Jurkat T-lymphoma cells that express the Tn antigen (20). Figure 4 shows that sera from BALB/c mice immunized with Tn_3-PV, D-(Tn_3)-PV and Tn_6-PV bound this human cell line demonstrating that Tn-specific antibodies induced by these glycopeptides recognize the native form of

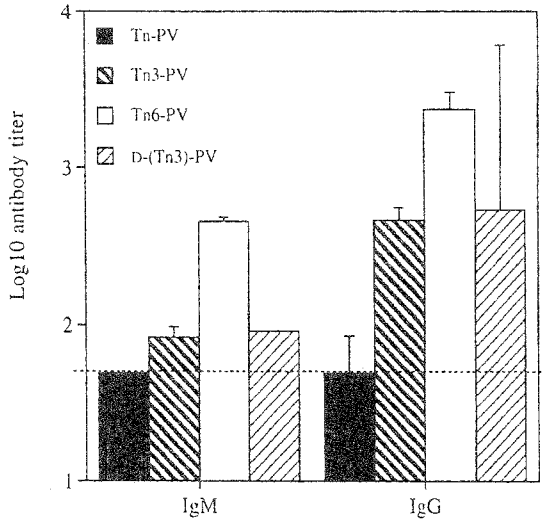

Figure 4. Anti-Tn antibodies induced in mice immunized with Tn-glycopeptides as measured by FACS using a human tumor cell line bearing the Tn antigen. Flow cytometry analysis was carried out on human Jurkat cells incubated with serial dilutions of sera from BALB/c mice (four per group) immunized on day 0 with 50 µg Tn-PV, Tn_3-PV, Tn_6-PV and D-(Tn_3)-PV in CFA, then boosted on days 21 and 42 in IFA with the same antigens. The sera are from mice bled 8 days after the last injection. Binding was detected using FITC-labeled antibodies specific for mouse IgM, and antimouse IgG biotinylated antibodies revealed with streptavidin-PE. Results are expressed as the mean of individual antibody titers calculated as indicated in Experimental Procedures. Serum titers < 50 (dashed line) are considered negative since sera were tested at a starting dilution of 1 : 50.

Tn on human tumor cells. However, the pattern of antibody titers is different whether the titration is performed by ELISA using the Tn_3G_6K (Biot)G glycopeptide (Fig. 3) or by FACS using the Jurkat cell line (Fig. 4). Recognition of the Jurkat cells was better with Tn_6-PV- than with Tn_3-PV-induced antibodies (for both IgM and IgG). Interestingly, the antibody production obtained with the tri-D-(Tn_3) glycopeptide [D-(Tn_3)-PV] containing three D-serine residues is similar to that obtained with Tn_3-PV itself. This result could be useful for the development of MAG-constructs since it would protect the tri-Tn antigen from hydrolysis by the proteases.

The choice of the tri-Tn motif (Tn_3G_6KG) for the ELISA was based on the structural motif recognized by the MLS 128 mAb [17]. Although it allows the detection of antibodies raised against the Tn_3- or Tn_6-PV glycopeptides, it only represents a Tn artificial probe. By contrast, Tn recognition measured on Jurkat cells by FACS represents a more accurate view of the natural structure available at the cell surface for antibody recognition. Under these conditions, the double tri-Tn motif (Tn_6-PV) provides a significant benefit over the single tri-Tn motif (Tn_3-PV) in the induction of anti-Tn-specific IgM and IgG antibodies.

Although the Jurkat cell may not represent the cell prototype for the Tn expression level, no carcinoma cell clones can correctly mimic the natural diversity of mucinous cancer cells. Indeed, unveiling of cryptic Tn on carcinoma cells probably leads to highly variable Tn clusters on mucin-like proteins depending on the Ser/Thr content of the amino acid sequence. We may expect that if the Tn content is high in the glycopeptidic immunogen, the antibody response will be adapted for recognition of various types of natural Tn clusters.

In conclusion, we show here that the conjugation of tri- or hexa-Tn motifs to a linear $CD4^+$ T-cell epitope successfully induces anti-Tn antibodies. These results are promising for the further development of dendrimeric MAG constructs bearing tri- or hexa-Tn clusters. Indeed, a stronger response can be expected for these tri-Tn-MAG since the mono-Tn-MAG construct itself, when used in immunotherapy, has already been shown to give some protection in tumor-bearing mice [14].

Acknowledgments: This work was supported by ARC (Association pour la Recherche contre le Cancer) and CCV (Commission Consultative de Valorisation, Institut Pasteur).

References

1. Bhavanandan, V.P. (1991) Cancer-associated mucins and mucin-type glycoproteins. *Glycobiology* **1**, 493–503.
2. Fukuda, M. (1996) Possible roles of tumor-associated carbohydrate antigens. *Cancer Res.* **56**, 2237–2244.
3. Hakomori, S. (1989) Aberrant glycosylation in tumors and tumor-associated carbohydrate antigens. *Adv. Cancer Res.* **52**, 257–331.
4. MacLean, G.D., Reddish, M.A., Bowen-Yacyshyn, M.B., Poppema, S. & Longenecker, B.M. (1994) Active specific immunotherapy against adenocarcinoma. *Cancer Invest.* **12**, 46–56.
5. Helling, F., Zhang, S., Shang, A., Adluri, S., Calves, M., Koganty, R., Longenecker, B.M., Yao, T.-J., Oettgen, H.F. & Livingston, P.O. (1995) GM2-KLH conjugate vaccine: increased immunogenicity in melanoma patients after administration with immunological adjuvant QS-21. *Cancer Res.* **55**, 2783–2788.
6. Fung, P.Y.S., Madej, M., Koganty, R.R. & Longenecker, B.M. (1990) Active specific immunotherapy of a murine mammary adenocarcinoma using a synthetic tumor-associated glycoconjugate. *Cancer Res.* **50**, 4308–4314.
7. MacLean, G.D., Bowen-Yacyshyn, M.B., Samuel, J., Meikle, A., Stuart, G., Nation, J., Poppema, S., Jerry, M., Koganty, R., Wong, T. & Longenecker, B.M. (1992) Active immunization of human ovarian cancer patients against a common carcinoma (Thomson-Friedenreich) determinant using a synthetic carbohydrate antigen. *J. Immunother.* **11**, 292–305.
8. Reddish, M.A., Jackson, L., Koganty, R.R., Qiu, D., Hong, W. & Longenecker, B.M. (1997) Specificities of an anti-sialyl-Tn and anti-Tn monoclonal antibodies generated using novel clustered synthetic glycopeptide epitopes. *Glycoconjugate J.* **14**, 549–560.
9. Lett, E., Klopfenstein, C., Klein, J.-P., Schöller, M. & Wachsmann, D. (1995) Mucosal immunogenicity of polysaccharides conjugated to a peptide or multiple-antigen peptide containing T- and B-cell epitopes. *Infect. Immun.* **63**, 2645–2651.
10. Bay, S., Lo-Man, R., Osinaga, E., Nakada, H., Leclerc, C. & Cantacuzene, D. (1997) Preparation of a multiple antigen glycopeptide (MAG) carrying the Tn antigen. *J. Peptide Res.* **49**, 620–625.
11. Posnett, D.N., McGrath, H. & Tam, J.P. (1988) A novel method for producing anti-peptide antibodies. *J. Biol. Chem.* **263**, 1719–1725.
12. Tam, J.P. (1988) Synthetic peptide vaccine design: synthesis and properties of a high-density multiple antigenic peptide system. *Proc. Natl Acad. Sci. USA* **85**, 5409–5413.
13. Leclerc, C., Deriaud, D., Mimic, V. & Van der Werf, S. (1991) Identification of a T-cell epitope adjacent to neutralization antigenic site 1 of poliovirus Type 1. *J. Virol.* **65**, 711–718.
14. Lo-Man, R., Bay, S., Vichier-Guerre, S., Deriaud, E., Cantacuzene, D. & Leclerc, C. (1999) A fully synthetic immunogen carrying a carcinoma-associated carbohydrate for active specific immunotherapy. *Cancer Res.* **59**, 1520–1524.
15. Numata, Y., Nakada, H., Fukui, S., Kitagawa, H., Ozaki, K., Inoue, M., Kawasaki, T., Funakoshi, I. & Yamashima, I. (1990) A monoclonal antibody directed to Tn antigen. *Biochem. Biophys. Res. Commun.* **170**, 981–985.

16. Nakada, H., Numata, Y., Inoue, M., Tanaka, N., Kitagawa, H., Funakoshi, I., Fukui, S. & Yamashima, I. (1991) Elucidation of an essential structure recognized by an anti-GalNAc-Ser (Thr) monoclonal antibody (MLS 128). *J. Biol. Chem.* **266**, 12402–12405.
17. Nakada, H., Inoue, M., Numata, Y., Tanaka, N., Kunakoshi, I., Fukui, S., Mellors, A. & Yamashina, I. (1993) Epitopic structure of Tn glycophorin A for an anti-Tn antibody (MLS 128). *Proc. Natl Acad. Sci. USA* **90**, 2495–2499.
18. Toyokuni, T., Dean, B., Cai, S., Boivin, D., Hakomori, S. & Singhal, A.K. (1994) Synthetic vaccines; synthesis of a dimeric Tn antigen-lipeptide conjugate that elicits immune responses against Tn-expressing glycoproteins. *J. Am. Chem. Soc.* **116**, 395–396.
19. McCool, D.J., Forstner, J.F. & Forstner, G.G. (1994) Synthesis and secretion of mucin by the human colonic tumor cell line LS 180. *Biochem. J.* **302**, 111–118.
20. Inoue, M., Nakada, H., Tanaka, N. & Yamashina, I. (1994) Tn antigen is expressed on leukosialin from T-lymphoid cells. *Cancer Res.* **54**, 85–88.
21. Toyokuni, T., Hakomori, S. & Singhal, A.K. (1994) Synthetic carbohydrate vaccines: synthesis and immunogenicity of Tn antigen conjugates. *Bioorg. Med. Chem.* **2**, 1119–1132.
22. Paulsen, H. & Hölck, J.-P. (1982) Synthese der glycopeptide *O*-β-D-galactopyranosyl-(1–3)-*O*-(2-acetamido-2-deoxy-α-D-galactopyranosyl)-(1–3)-L-serin und L-threonin. *Carbohydr. Res.* **109**, 89–107.
23. Paulsen, H. & Adermann, K. (1989) Synthesis von O-glycopeptid-sequenzen des N-terminus von Interleukin-2. *Liebigs Ann. Chem.* 751–759.
24. Shafizadeh, F. (1963) D-galactal. *Methods Carbohydr. Chem.* **2**, 409–410.
25. Schultz, M. & Kunz, H. (1993) Synthetic glycopeptides as model substrates for glycosyltransferases. *Tetrahedron Assym.* **4**, 1205–1220.
26. Vowinkel, E. (1967) Darstellung von carbonsaüreestern mittels *O*-alkyl-*N,N'*-dicylohexyl-isoharnstoffen. *Chem. Ber.* **100**, 16–22.
27. Lemieux, R.U. & Ratcliffe, R.M. (1979) The azidonitration of tri-*O*-acetyl-D-galactal. *Can. J. Chem.* **57**, 1244–1251.
28. Ferrari, B.P.A. (1980) The synthesis of derivatives of 3-*O*-(2-acetamido-2-deoxy-α-D-galactopyranosyl)-L-serine and L-threonine. *Carbohydr. Res.* **79**, C1–C7.
29. Paulsen, H., Schultz, M., Klamann, J.-D., Waller, B. & Paal, M. (1985) Synthese von *O*-glycopeptid-blöcken des glycophorin. *Liebigs Ann. Chem.* 2028–2048.
30. Knorr, R., Trzeciak, A., Bannwarth, W. & Gillessen, D. (1989) New coupling reagents in peptide chemistry. *Tetrahedron Lett.* **30**, 1927–1930.
31. Fields, C.G., Lloyd, D.H., Macdonald, R.L., Otteson, K.M. & Noble, R.M. (1991) HBTU activation for automated Fmoc solid-phase peptide synthesis. *Peptide Res.* **4**, 95–101.
32. Meldal, M. & Jensen, K.J. (1990) Pentafluorophenyl esters for the temporary protection of the α-carboxy group in solid phase glycopeptide synthesis. *J. Chem. Soc., Chem. Commun.* 483–485.
33. Elofsson, M., Roy, S., Walse, B. & Kihlberg, I. (1993) Solid phase synthesis and conformational studies of glycosylated derivatives of helper-T-cell immunogenic peptides from hen egg lysozyme. *Carbohydr. Res.* **246**, 89–103.
34. Anisfeld, S.T. & Lansbury, P.T. (1990) A convergent approach to the chemical synthesis of asparagine-linked glycopeptides. *J. Org. Chem* **55**, 5560–5562.
35. Filira, F., Biondi, L., Cavaggion, F., Scolaro, B. & Rocchi, R. (1990) Synthesis of *O*-glycosylated tuftsins by utilizing threonine derivatives containing an unprotected monosaccharide moiety. *Int. J. Peptide Protein Res.* **36**, 86–96.
36. Kates, S.A., De la Torre, B.G., Eritja, R. & Albericio, F. (1994) Solid phase *N*-glycopeptide synthesis using allyl side-chain protected Fmoc-amino acids. *Tetrahedron Lett.* **35**, 1033–1034.
37. Otvos, L., Urge, L., Hollosi, M., Wroblewski, K., Graczyk, G., Fasman, G.D. & Thurin, J. (1990) Automated solid-phase synthesis of glycopeptides. Incorporation of unprotected mono and disaccharides units of *N*-glycoprotein antennae into T-cell epitopic peptides. *Tetrahedron Lett.* **31**, 5889–5892.
38. Reimer, K.B., Meldal, M., Kusumoto, S., Fukase, K. & Bock, K. (1993) Small-scale solid phase *O*-glycopeptide synthesis of linear and cyclized hexapeptides from bood clotting factor IX containing *O*-(α-D-Xyl-1–3-α-D-Xyl-1–3β-Glc)-L-Ser. *J. Chem. Soc. Perkin Trans* **1**, 925–932.
39. Urge, L., Gorbics, L. & Otvos, L. (1992) Chemical glycosylation of peptide T at natural and artificial glycosylation sites stabilizes or rearranges the dominant reverse turn structure. *Biochem. Biophys. Res. Commun.* **184**, 1125–1132.
40. Sjölin, P., Elofsson, M. & Kihlberg, J. (1996) Removal of acyl protective groups from glycopeptides: base does not epimerize peptide stereocenters and β-elimination is slow. *J. Org. Chem.* **61**, 560–565.
41. Inoue, M., Yamashina, I. & Nakada, H. (1998) Glycosylation of tandem repeat unit of the MUC2 polypeptide leading to the synthesis of the Tn antigen. *Biochem. Biophys. Res. Commun.* **245**, 23–27.
42. Brumeanu, T.D., Casares, S., Bot, A., Bot, S. & Bona, C.A. (1997) Immunogenicity of a contiguous T-B synthetic epitope of the A/PR/8/34 influenca virus. *J. Virol.* **71**, 5473–5480.
43. Del Guercio, M.E., Alexander, J., Kubo, R.T., Arrhenius, T., Maewal, A., Appella, E., Hoffman, S.I., Jones, T., Valmori, D., Sakaguchi, K., Grey, H.M. & Sette, A. (1997) Potent immunogenic short linear peptide constructs composed of B-cell epitopes and Pan DR T helper epitopes (PADRE) for antibody responses *in vivo*. *Vaccine* **15**, 441–448.
44. Obeid, O.E., Partidos, C.D., Howard, C.R. & Steward, M.W. (1995) Protection against morbillivirus-induced encephalitis by immunization with a rationally designed synthetic peptide vaccine containing B- and T-cell epitopes from the fusion protein of measles virus. *J. Virol.* **69**, 1420–1428.
45. Partidos, C.D., Ripley, J., Delmas, A., Obeid, O.E., Denbury, A. & Steward, M.W. (1997) Fine specificity of the antibody response to a synthetic peptide from the fusion protein and protection against measles virus-induced encephalitis in a mouse model. *J. Gen. Virology* **78**, 3227–3232.
46. Meldal, M., Mouritsen, S. & Bock, K. (1993) In *Carbohydrate Antigens, ACS Symposium Ser.*, Vol. 519 (P.J. Garegg & A.A. Lindberg, eds), Academic Press, New York, pp. 19–33.
47. Chong, P., Chan, N., Kandil, A., Tripet, B., James, O., Yang, Y.-P., Shi, S.-P. & Klein, M. (1997) A strategy for rational design of fully synthetic glycopeptide conjugate vaccines. *Infect. Immun.* **65**, 4918–4925.
48. Kaumaya, P.T., Conrad, S.F., DiGeorge, A.M. & Lairmore, M.D. (1995) Glycosylation-dependent antgenic determinants of env gp46 HTLV-1. *Leukemia* **9**, S133–S138.
49. Reis, C.A., Sorensen, T., Mandel, U., David, L., Mirgorodskaya, E., Roepstorff, P., Kihlberg, J., Hansen, J.E. & Clausen, H. (1998) Development and characterization of an antibody directed to an alpha-*N*-acetyl-D-galactosamine glycosylated MUC2 peptide. *Glycoconjugate J.* **15**, 51–62.

Experimental Cell Research 256, 434–444 (2000)
doi:10.1006/excr.2000.4802, available online at http://www.idealibrary.com on IDEAL®

Participation of Syndecan 2 in the Induction of Stress Fiber Formation in Cooperation with Integrin $\alpha5\beta1$: Structural Characteristics of Heparan Sulfate Chains with Avidity to COOH-Terminal Heparin-Binding Domain of Fibronectin

Yuri Kusano,* Kayoko Oguri,* Yuko Nagayasu,* Seiichi Munesue,† Masayuki Ishihara,‡ Ikuo Saiki,§ Hideto Yonekura,¶ Hiroshi Yamamoto,¶ and Minoru Okayama†,[1]

*Clinical Research Institute, National Nagoya Hospital, Aichi, Japan; †Department of Biotechnology, Faculty of Engineering, Kyoto Sangyo University, Kyoto, Japan; ‡National Defense Medical College, Research Institute, Saitama, Japan; §Department of Pathogenic Biochemistry, Institute of Natural Medicine, Toyama Medical and Pharmaceutical University, Toyama, Japan; and ¶Department of Biochemistry, Kanazawa University School of Medicine, Kanazawa, Japan

The present study provides direct evidence that syndecan 2 participates selectively in the induction of stress fiber formation in cooperation with integrin $\alpha5\beta1$ through specific binding of its heparan sulfate side chains to the fibronectin substrate. Our previous study with Lewis lung carcinoma-derived P29 cells demonstrated that the cell surface heparan sulfate proteoglycan, which binds to fibronectin, is syndecan 2 (N. Itano *et al.*, 1996, *Biochem. J.* 315, 925–930). We here report that *in vitro* treatment of the cells by antisense oligonucleotide for syndecan 2 resulted in a failure to form stress fibers on fibronectin substrate in association with specific suppression of its cell surface expression. Instead, localization of actin filaments in the cytoplasmic cortex occurred. A similar response of the cells was observed when the cells were treated to eliminate functions of cell surface heparan sulfates, including exogenous addition of heparin and pretreatment with anti-heparan sulfate antibody, F58-10E4, and with proteinase-free heparitinase I. Size- and structure-defined oligosaccharides prepared from heparin and chemically modified heparins were utilized as competitive inhibitors to examine the structural characteristics of the cell surface heparan sulfates involved in organization of the actin cytoskeleton. Their affinity chromatography on a column linked with a recombinant H-271 peptide containing a C-terminal heparin-binding domain of fibronectin demonstrated that 2-O-sulfated iduronates were essential for the binding. Inhibition studies revealed that a heparin-derived dodecasaccharide sample enriched with an IdoA(2*O*S)-Glc*N*S(6*O*S) disaccharide completely blocked binding of the syndecan 2 ectodomain to immobilized H-271 peptide. Finally, the dodecasaccharide sample was shown to inhibit stress fiber formation, triggered by adhesion of P29 cells to a CH-271 polypeptide consisting of both the RGD cell-binding and the C-terminal heparin-binding domains of fibronectin in a fused form. All these results consistently suggest that syndecan 2 proteoglycan interacts with the C-terminal heparin-binding domain of fibronectin at the highly sulfated cluster(s), such as [IdoA(2*O*S)-Glc*N*S(6*O*S)]$_6$ present in its heparan sulfate chains, to result in the induction of stress fiber formation in cooperation with integrin $\alpha5\beta1$. © 2000 Academic Press

Key Words: heparan sulfates; syndecan 2; fibronectin; cell adhesion; stress fibers; cytoskeletal organization.

INTRODUCTION

Heparan sulfate proteoglycans on cell surfaces bind a variety of extracellular soluble and insoluble molecules via their heparan sulfate chains [1–4]. These interactions are known to modulate the biological activities of the heparin-binding molecules, such as basic fibroblast growth factor [5–9], vascular endothelial cell growth factor [10], heparin-binding epidermal growth factor-like growth factor [11], lipoprotein lipase [12–14], pleiotrophin [15], midkine [16], and fibronectin [17]. The extensive repertoire of binding interactions of cell surface heparan sulfate proteoglycans suggests that some selectivity is involved. Indeed, there is evidence that there are specific saccharide sequences of heparin responsible for the binding of antithrombin III [18, 19], basic fibroblast growth factor [20–23], fibroblast growth factor receptor [24, 25], hepatocyte growth factor [26, 27], and midkine [16]. Thus, binding selectivity is apparently dependent on the structural

[1] To whom correspondence and reprint requests should be addressed at Department of Biotechnology, Faculty of Engineering, Kyoto Sangyo University, Motoyama Kamigamo, Kitaku, Kyoto 603-8555, Japan. Fax: +81-75-705-1914. E-mail: okayamam@cc.kyoto-su.ac.jp.

0014-4827/00 $35.00

variability in the heparan sulfate chains on cell surfaces. The carbohydrate backbone of heparan sulfate consists of alternating hexuronic acid and *N*-acetylglucosamine residues. After chain elongation from the core protein, partial N-deacetylation/N-sulfation of N-acetylglucosamine, C-5 epimerization of some glucuronic acids, and incorporation of O-sulfate groups occur at various positions. The structural complexity of heparan sulfate seems to be able to generate unique domains along the chains for binding to a variety of ligands. Despite the accumulated reports of such sites in heparan sulfate chains, there is only limited information on the roles of particular proteoglycan species.

We previously demonstrated that *in vivo*-selected mouse Lewis lung carcinoma (3LL) clones with differing metastatic potential exhibit distinct variation in their extracellular matrix dependence. Thus, a low metastatic clone, P29, with a stroma-inducing capacity, shows tumorigenesis depending on the fibronectin-rich interstitial matrix formed by the induced stromal cells. On the other hand, growth of a highly metastatic clone, LM66-H11, depends on the basement membrane formed by the tumor cells themselves [28–30]. Moreover, we showed that P29 cells adhere *in vitro* to the fibronectin substrate through a dual receptor system with integrin $\alpha5\beta1$ and cell surface heparan sulfate proteoglycan(s) to result in stress fiber formation. LM66-H11 cells, in contrast, adhere to the same substrate through integrin $\alpha5\beta1$ alone, causing localization of actin filaments in the cytoplasmic cortex, suggesting that the heparan sulfate proteoglycans modulate signaling via this integrin [31]. Biochemical analysis of cell surface heparan sulfate proteoglycans produced by P29 cells demonstrated that more than 80% of the proteoglycans binding to a fibronectin affinity column is attributable to syndecan 2, a hybrid-type proteoglycan having both heparan sulfate and chondroitin sulfate, which binds to fibronectin through its heparan sulfate side chains [32, 33].

Because the N-terminal heparin-binding domain (Hep-I) of fibronectin is well established as essential for its incorporation into the extracellular matrix [34], it appears reasonable to consider that syndecan 2 expressed on the surface of P29 cells binds to the C-terminal heparin-binding domain (Hep-II) of fibronectin through its heparan sulfate chains. Thus, in the present study we intended to provide direct evidence of involvement of syndecan 2 in the induction of stress fiber formation in cooperation with integrin $\alpha5\beta1$ on cell adhesion to the fibronectin substrate, using antisense oligonucleotide for syndecan 2 core protein as its specific suppressor, and to examine the structure in the heparan sulfate chains of syndecan 2, which exhibit binding affinity for the Hep-II domain of fibronectin, using heparin- and chemically modified heparin-derived oligosaccharides as their competitive inhibitors.

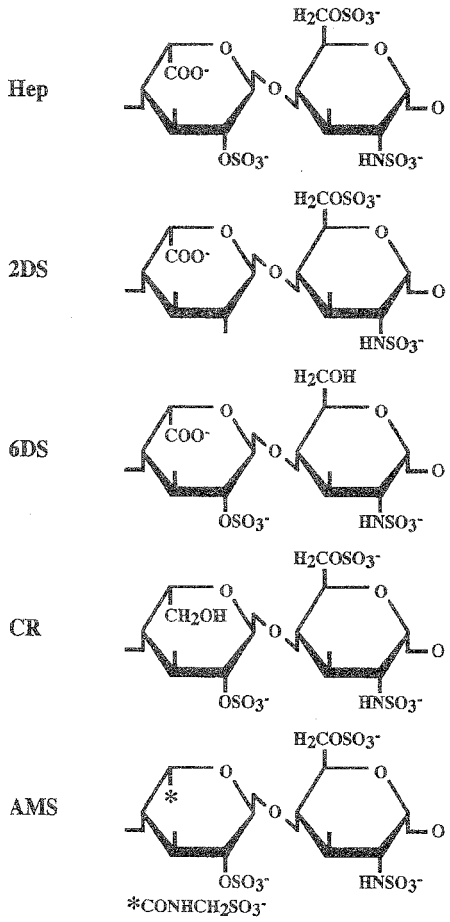

FIG. 1. Chemical structures of major disaccharides in size- and structure-defined oligosaccharide samples prepared from heparin and chemically modified heparins. Heparin (Hep) and chemically modified heparins (2DS, 2-O-desulfated; 6DS, 6-O-desulfated; CR, carboxy reduced; and AMS, carboxy-aminomethylsulfonated heparins) were partially depolymerized, and size- and structure-defined oligosaccharides were prepared by repeated gel filtration on Bio-Gel P-10, followed by ion-exchange chromatography on Q-Sepharose, as described under Methods.

METHODS

Materials. Human plasma fibronectin was purchased from Iwaki Glass (Tokyo). Three species of recombinant polypeptides of fibronectin, i.e., the RGD-containing cell-binding domain, C-274 (Pro^{1239}-Ser^{1515}); the C-terminal heparin-binding domain, H-271 (Ala^{1690}-Thr^{1960}); and a fusion peptide of C-274 and H-271 with a methionine residue, CH-271, were generously provided by TaKaRa Biomedicals (Ohtsu, Japan). Chemically modified heparins and size- and structure-defined oligosaccharides (Fig. 1) were prepared from porcine mucosal heparin (Ming Ham Co.), as described below. Some portions of the oligosaccharides were tritiated at reducing ends by reduction with [^{3}H]sodium borohydride (18.1 GBq/mmol; Du Pont-NEN Research Product). The anti-heparan sulfate monoclonal antibody, F58-10E4, and a proteinase-free heparan sulfate lyase preparation [35] from *Flavobacterium heparinum* (heparitinase I, EC 4.2.2.8) were gifts from Dr. Keiichi Yoshida of Seikagaku Corp. (Tokyo).

TABLE 1

Disaccharide Compositions (%) of Size- and Structure-Defined Oligosaccharides

	Hep				2DS				6DS			
	12 mer	10 mer	8 mer	6 mer	12 mer	10 mer	8 mer	6 mer	12 mer	10 mer	8 mer	6 mer
IdoA/GlcA–AMan	8	5	6	7	12	13	14	12	23	22	20	20
IdoA(2S)–AMan	3	2	2	1	0	0	0	1	55	56	56	52
GlcA–AMan(6S)/GlcA(2S)–AMan	1	1	2	1	6	7	5	5	6	6	7	8
IdoA–AMan(6S)	1	2	1	1	82	80	81	80	4	5	4	6
GlcA–AMan(3, 6diS)	5	7	8	7	0	0	0	0	0	0	0	0
IdoA(2S)–AMan(6S)	82	83	81	83	0	0	0	1	14	12	15	16

	CR					AMS			
	12 mer	10 mer	8 mer	6 mer		12 mer	10 mer	8 mer	6 mer
CR–IdoA(2S)–AMan(6S)	78	81	70	76	AMS–IdoA(2S)–AMan(6S)	80	76	85	82
Unknown	22	19	30	24	Unknown	20	24	15	18

Note. Abbreviations: IdoA, L-iduronic acid; IdoA(2S), L-iduronic acid (2-*O*-SO_3); GlcA, D-glucuronic acid; GlcA(2S), D-glucuronic acid (2-*O*-SO_3); AMan, anhydro-D-mannitol; AMan(6S), anhydro-D-mannitol (6-*O*-SO_3); AMan(3, 6diS), anhydro-D-mannitol (3-*O*-SO_3 and 6-*O*-SO_3); CR, carboxy reduced; AMS, carboxy-amidomethylsulfonated.

Preparation of chemically modified heparins and size- and structure-defined oligosaccharides. Four species of chemically modified heparins were prepared as described previously [36]: 2-O-desulfated (2DS) heparin by a modification of the procedure of Jaseja *et al.* [37], 6-O-desulfated (6DS) heparin by the dimethyl sulfoxide procedure of Nagasawa *et al.* [38], carboxy-reduced (CR) heparin by a modification of the procedure of Taylor *et al.* [39], and carboxy-aminomethylsulfonated (AMS) heparin by the carbodiimide procedure of Danishefsky and Siskovic [40].

The strategy for generation of size- and structure-defined oligosaccharides was detailed earlier [36, 41]. Briefly, all the samples were N-deacetylated by hydrazinolysis, followed by nitrous acid treatment at pH 4.0 for 10 min to isolate fragments that are all N-sulfated in the glucosamine residues [42]. The reaction mixtures were then incubated at pH 3.0 for another 10 min to allow partial cleavage of N-sulfated large oligosaccharides. Hydrazinolysis was omitted for AMS-heparin, since AMS groups may thereby be released. The resulting oligosaccharides were separated by gel filtration on a Bio-Gel P-10 column (1 × 200 cm) equilibrated with 0.5 M ammonium bicarbonate. The separating fractions were rechromatographed on the same column to ensure size homogeneity. Then the samples were fractionated on a Q-Sepharose (Amersham Pharmacia Biotech) column (3 × 6 cm) equilibrated with 0.2 M NaCl in 10 mM Tris–HCl, pH 7.3. The unbound oligosaccharides were removed by washing the column with equilibration buffer, and the bound oligosaccharides were eluted with a linear gradient of NaCl (0.2–1.5 M) in 10 mM Tris–HCl, pH 7.3. Fractions eluted with the highest concentrations of NaCl were dialyzed against water using 1000 molecular cutoff membranes (Spectrum, Houston, TX) and lyophilized. The disaccharide compositions of the oligosaccharide samples (Table 1) were determined with the aid of reverse-phase ion-pairing HPLC, as described previously [43].

Preparation of antibody. Rabbit antibody preparation, S2Ab, specific to the ectodomain of mouse syndecan 2 core protein, was raised against the recombinant polypeptide. Briefly, the recombinant was prepared by expressing cDNA encoding the ectodomain of mouse syndecan 2 core protein in *Escherichia coli,* XL1-Blue (Stratagene), using glutathione *S*-transferase (GST) gene fusion vector, pGEX-2 (Amersham Pharmacia Biotech). The cDNA was amplified by RT-PCR from polyadenylated RNA of P29 cells with a primer pair, 5′-GAGGATCCGAGACGAGAACAGAGCTGCA-3′ and 5′-GAGAATTCTTATTCTGTCCGTTTAAACAGATT-3′, which corresponds to its N-terminal glutamic acid to glutamic acid immediately adjacent to the transmembrane domain. The GST-fused protein obtained by glutathione–Sepharose affinity chromatography was digested with thrombin to cleave the fusion site. The recombinant polypeptide was isolated by rechromatography on a glutatione–Sepharose column and purified by Q-Sepharose, and then its N-terminal amino acid sequence was confirmed using a Model 492 protein sequencer (Applied Biosystems Inc.). One hundred micrograms of the purified polypeptide in Freund's complete adjuvant was injected into the backs of rabbits and, 3 weeks later, the same amount of the antigen in Freund's incomplete adjuvant was injected five times at 10-day intervals. IgG was obtained from the antisera by precipitation with 50% ammonium sulfate. The IgG was further purified by chromatography on Protein A–Sepharose 4FF. To obtain antibodies specific to the ectodomain of syndecan 2 core protein, the IgG was sequentially applied to HiTrap columns (Amersham Pharmacia Biotech) linked separately with the ectodomains of syndecan 1, 3, and 4. The unbound fraction was finally applied to a syndecan 2 ectodomain-linked HiTrap column, and the bound material was eluted with 0.1 M glycine HCl buffer, pH 3.0, and used as a S2Ab sample.

Cell culture. The low metastatic P29 cell line cloned from mouse Lewis lung carcinoma was routinely cultured in Dulbecco's modified Eagle's medium (DMEM) supplemented with 10% (v/v) fetal calf serum (FCS) (GIBCO), streptomycin (100 μg/ml), and penicillin (100 units/ml) at 37°C in humidified 5% CO_2 in air, as described previously [32]. The cells were harvested after incubation with 2 mM EDTA in phosphate-buffered saline (PBS) at 37°C for 10 min, followed by gentle flushing with a pipette.

Treatment of cells with antisense oligonucleotides of syndecan 2. Antisense phosphorothioate oligonucleotide complementary to the region around the initiation codon of mouse syndecan 2 mRNA (5′-CACGCGCGCTGCATATT-3′) and the corresponding sense (5′-AATATGCAGCGCGCGTG-3′) and scrambled antisense (5′-ACGTCCCTGAGCGATCT-3′) phosphorothioate oligonucleotides were synthesized using a Model 392 DNA synthesizer (Applied Biosystems Inc.). The oligodeoxynucleotides were purified by two cycles of reverse-phase HPLC.

P29 cells inoculated at a cell density of 1 × 10^3 cells/cm^2 were cultured in the presence or absence of 10 μM oligonucleotides for 4

days. The media were replaced every 48 h with fresh ones. The cells were harvested in 2 mM EDTA/PBS and suspended in 0.2% bovine serum albumin (BSA)/DMEM. A small aliquot of the cell suspension was placed on a fibronectin-coated cover glass and incubated for 1 h at 37°C, and then actin-cytoskeleton was observed as described below. The remainder was prepared by incubation with 1:100 dilution of S2Ab or preimmune rabbit serum for 1 h at 4°C with gentle agitation. After washing, cells were incubated with FITC-conjugated goat anti-rabbit IgG for 30 min at 4°C. Cells were suspended in 0.2% BSA/DMEM and analyzed using a flow cytometer, Ortho Cytoron (Ortho Diagnostic System).

Staining of cytoskeleton. Fibronectin (50 μg/ml in PBS) was placed on cover glasses at 4°C overnight. Then the glasses were blocked with 0.2% BSA/PBS at room temperature for 1 h and washed three times with DMEM. P29 cells (5×10^3 cells in 200 μl of 0.2% BSA/DMEM) were inoculated onto the fibronectin-coated glasses and incubated for 1 h at 37°C in humidified 5% CO_2 in air. After fixation in −20°C acetone for 10 min, actin filaments were stained with rhodamine-conjugated phalloidin (Molecular Probes Inc.) and the specimens were observed under a fluorescent microscope.

Affinity chromatography of size- and structure-defined oligosaccharides prepared from heparin and chemically modified heparins on an H-271-linked column. Two milligrams of H-271 polypeptide in 0.2 M $NaHCO_3$/0.5 M NaCl, pH 8.3, was coupled to an NHS-Activated HiTrap column (Amersham Pharmacia Biotech) according to the recommendations of the manufacturer. The coupling efficiency was more than 95% as monitored by absorbance at 280 nm. After the column was equilibrated with 0.1 M NaCl/0.5% Triton X-100/50 mM Tris–HCl, pH 7.3, ^{3}H-labeled oligosaccharide samples were applied to the column. The column was then washed with the equilibrating buffer and the bound oligosaccharides were eluted with a linear gradient concentration of 0.1–0.5 M NaCl/0.5% Triton X-100/50 mM Tris–HCl, pH 7.3. Radioactivity was measured in liquid scintillator by a Beckman LS-9000.

Preparation of an ectodomain from syndecan 2 isolated from P29 cells that were labeled with [^{35}S]sulfate. P29 cells were cultured in 10% FCS/DMEM to a confluent state. The medium was replaced with 10% FCS/Ham's F-12 and, after incubation for 3 h, [^{35}S]sulfate (7.4 MBq/ml, carrier free; Du Pont NEN Research Product) was added with further incubation for 24 h at 37°C in 5% CO_2 in air. After removal of the medium, the cell layer was washed three times with DMEM without FCS, and the radiolabeled macromolecules were extracted from a cell layer with 7 M urea/0.5% Triton X-100/0.15 M NaCl/50 mM Tris–HCl, pH 7.3, containing 10 mM EDTA/10 mM *N*-ethylmaleimide/1 mM phenylmethylsulfonyl fluoride/0.036 mM pepstatin A as proteinase inhibitors. The extraction was carried out continuously overnight on ice. The ^{35}S-labeled ectodomain of syndecan 2 was purified as described previously [33]. Briefly, after removal of insoluble materials in the extract by centrifugation at 65,000*g* for 30 min at 4°C, the supernatant was applied to a column (1 × 6.5 cm) of DEAE–Sephacel and washed thoroughly with the extraction buffer. The bound proteoglycan fraction was eluted with 4 M guanidinium HCl/0.05% Triton X-100/50 mM Tris–HCl, pH 7.3, and dialyzed against the elution buffer lacking Triton X-100 on ice. The dialyzate was then applied to a column (1 × 4 cm) of Octyl–Sepharose 4B and washed with 4 M guanidinium HCl/50 mM Tris–HCl, pH 7.3. The bound hydrophobic proteoglycans were eluted with a linear gradient concentration of 0–0.5% Triton X-100 in 4 M guanidinium HCl/50 mM Tris–HCl, pH 7.3, and the proteoglycan fraction was dialyzed against 50 mM NaCl/0.5% Triton X-100/50 mM Tris–HCl, pH 7.3, on ice. The sample was then applied to an anti-heparan sulfate antibody (F58-10E4)-linked HiTrap column (coupling efficiency, 82%), equilibrated with the dialyzing buffer at 4°C. After washing the column with the equilibrating solution, the bound heparan sulfate proteoglycan fraction was eluted with 0.5 M NaCl/0.5% Triton X-100/50 mM Tris–HCl, pH 7.3, and dialyzed against 0.1 M NaCl/0.5% Triton X-100/50 mM Tris–HCl, pH 7.3, on ice. Finally, the sample was applied to a fibronectin-linked Sepharose 4B column (1 × 4 cm). The bound fraction was eluted with a linear gradient concentration of NaCl (0.1–0.5 M) in 0.5% Triton X-100/50 mM Tris–HCl, pH 7.3, and the ^{35}S-labeled purified syndecan 2 thus obtained was digested with 0.005% trypsin in 0.1 M NaCl/0.5% Triton X-100/50 mM Tris–HCl, pH 7.3, at 25°C for 15 min, as described previously [33]. The digest was rechromatographed on the fibronectin-linked column, and the bound material was eluted as described above. The sample was dialyzed against 0.1 M NaCl/50 mM Tris–HCl, pH 7.3, and used as the ^{35}S-labeled ectodomain of syndecan 2 in this study.

Competitive inhibition of binding of the ^{35}S-labeled syndecan 2 ectodomain to H-271 peptide with heparin- and chemically modified heparin-derived oligosaccharides. Wells of a 96 well-plate were coated with H-271 peptide (16 μg/ml in PBS) at 4°C overnight. Plates were blocked by 1% BSA/PBS at 37°C for 1 h and, after washing with PBS, the ^{35}S-labeled syndecan 2 ectodomain in 0.1 M NaCl/50 mM Tris–HCl, pH 7.3 (1000 dpm/well) was added in the presence or absence of oligosaccharides and incubated at 37°C for 1 h. The supernatant was removed, and the wells were washed with 0.1 M NaCl/50 mM Tris–HCl, pH 7.3, the supernatant and washing solution being combined as the unbound fraction. The bound material was dissolved in 50 μl of 1 M ammonia at 37°C for 30 min with vigorous shaking. The extraction was repeated once more and the extracts were combined as the bound fraction. Radioactivity of both the fractions was measured in liquid scintillator by a Beckman LS-9000.

Inhibition of stress fiber formation in P29 cells on CH-271 substrate by heparin- and chemically modified heparin-derived oligosaccharides. CH-271 polypeptide (100 μg/ml in PBS) was placed on cover glasses at 4°C overnight. The cover glasses were blocked with 0.2% BSA/PBS at room temperature for 1 h and washed three times with DMEM. The cover glasses were then treated with various heparin-derived oligosaccharides at 200 μg/ml in 0.2% BSA/DMEM, at 37°C for 1 h. After washing the cover glasses with DMEM, P29 cells suspended in 0.2% BSA/DMEM containing the oligosaccharides (200 μg/ml) were inoculated onto the cover glasses and incubated at 37°C in humidified 5% CO_2 in air. These specimens were washed and fixed, and actin filaments were visualized with rhodamine-conjugated phalloidin, as described above.

RESULTS

Requirement of cooperation of cell surface heparan sulfate proteoglycans with integrin α5β1 for the induction of stress fiber formation. As reported previously [31], P29 cells were confirmed to adhere and spread on the fibronectin substrate in association with formation of stress fibers (Fig. 2A). When the cells were pretreated with GRGDS peptide, a minimal amino acid sequence of a cell-binding domain of fibronectin, as a ligand for integrin α5β1 [44], they adhered to the substrate but spread to a lesser extent, and stress fiber formation was not induced (Fig. 2B). Moreover, treatment of the cells with proteinase-free heparitinase-I (Fig. 2C) or with a monoclonal antibody, F58-10E4, specific to heparan sulfates [45] (Fig. 2D), before inoculation also resulted in a failure to induce the formation of stress fibers and caused localization of actin filaments in the cytoplasmic cortex, instead. A similar cellular response was observed with P29 cells on fibronectin substrate pretreated with heparin (Fig. 2E).

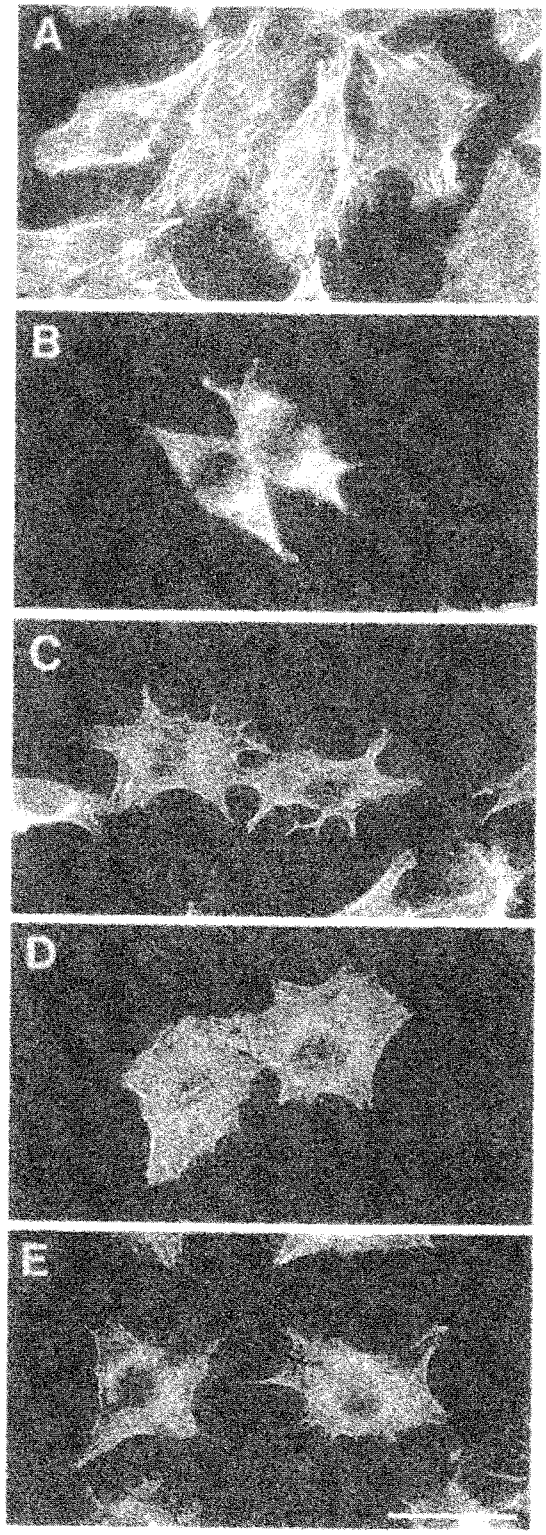

FIG. 2. Responses of P29 cells on adhesion to the fibronectin substrate under various conditions. Stress fiber formation was induced in P29 cells on adhesion to the fibronectin substrate (A). Cells pretreated with GRGDS peptide did not exhibit stress fiber formation and spread to a lesser extent, becoming spindle-like in shape (B). Proteinase-free heparitinase-I (C) or anti-heparan sulfate monoclonal antibody, F58-10E4 (D) and exogenous addition of heparin to the adhesion system (E) also resulted in a failure to form stress fibers; instead, localization of actin filaments into the cytoplasmic cortex occurred. Bar, 50 μm.

These results suggest that P29 cells adhere to the fibronectin substrate *in vitro* through two classes of fibronectin receptors, integrin $\alpha5\beta1$ and cell surface heparan sulfate proteoglycans, resulting in the induction of stress fiber formation.

Cooperation of syndecan 2 with integrin $\alpha5\beta1$ in stress fiber formation. We previously demonstrated that the fibronectin-binding proteoglycan species produced by P29 cells consists mostly of syndecan 2 [32, 33], suggesting that the proteoglycan cooperating with integrin $\alpha5\beta1$ in their adhesion to the fibronectin substrate is attributable to syndecan 2. To confirm this, the expression of syndecan 2 on P29 cells was suppressed by antisense oligonucleotide complementary to the region around the initiation codon of mouse syndecan 2 mRNA (Fig. 3). Flow cytometrical analysis using rabbit antibody specific to the ectodomain of mouse syndecan 2 (S2Ab) demonstrated that the expression level of syndecan 2 on the surface of P29 cells, which were cultured in the presence of antisense oligonucleotide for 4 days (Fig. 3B), was significantly lower than that of the cells cultured in the medium without oligonucleotides (Fig. 3A). Its expression level on the surface of the cells treated with sense oligonucleotide (Fig. 3C) was almost the same as that on the control cells. All these results indicate that treatment of the cells with the antisense oligonucleotide results in specific suppression of syndecan 2.

On cell adhesion to the fibronectin substrate, the syndecan 2-suppressed cells did not form stress fibers, and, instead, actin filaments became localized to cytoplasmic cortex (Fig. 3E). The cells incubated with sense oligonucleotide formed stress fibers (Fig. 3F), as observed in the control cells (Fig. 3D). The cells treated with scrambled antisense oligonucleotide expressed syndecan 2 at a level similar to that of the control cells and formed stress fibers on the fibronectin substrate (data not shown). These results strongly suggest that the proteoglycan cooperating with integrin $\alpha5\beta1$ is attributable to syndecan 2.

In this respect, it has been well established that fibronectin has two heparin-binding domains, named Hep-I and Hep-II domains in the N- and C-terminal regions, respectively, and that the Hep-I domain is essential for incorporation of fibronectin into the extracellular matrix [34]. The Hep-II domain acts as a ligand for cell surface heparan sulfate on cell adhesion to the fibronectin substrate [46]. Thus, it is reasonable to consider that in adhesion of P29 cells to the fibronectin

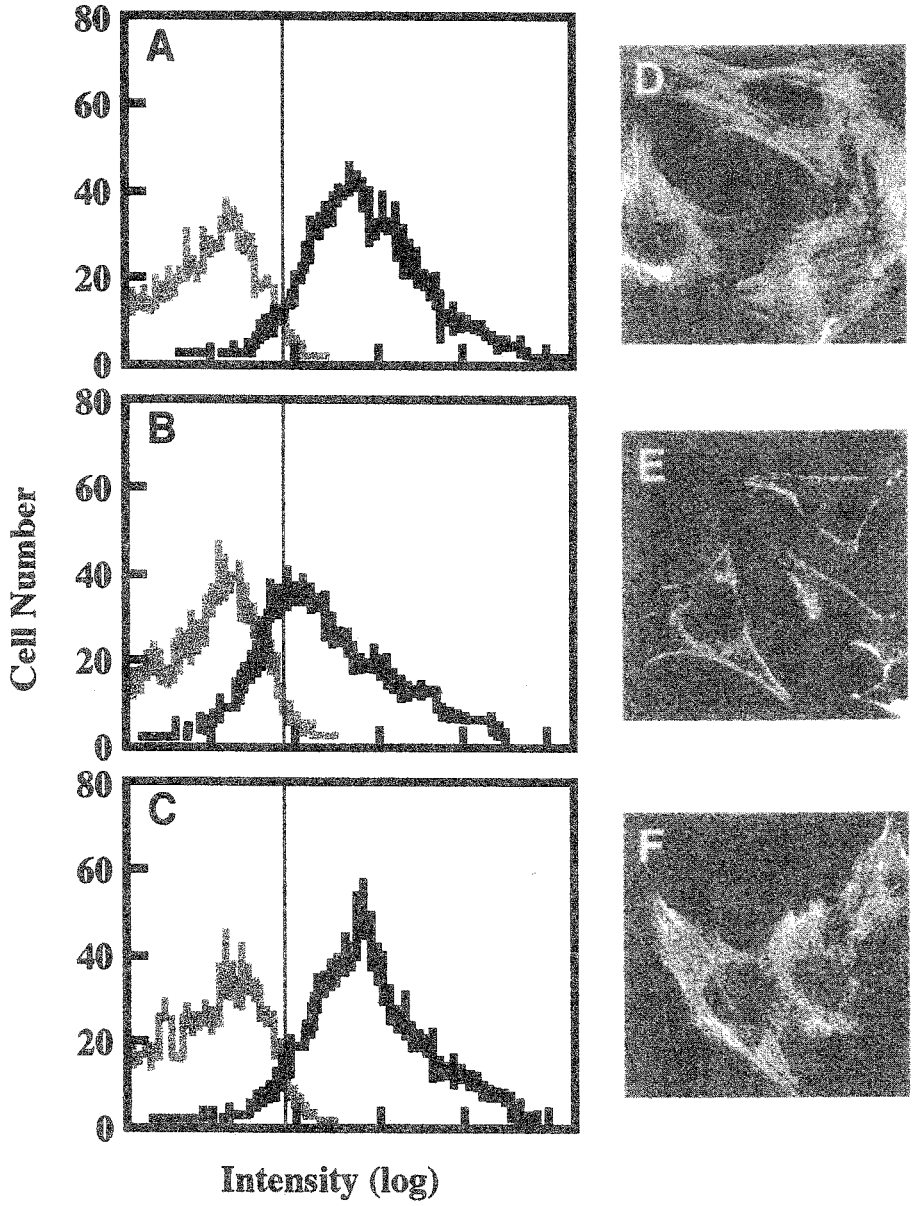

FIG. 3. Inhibition of the induction of stress fiber formation in association with specific suppression of cell surface expression of syndecan 2 in P29 cells by treatment with antisense oligonucleotide. Flow cytometrical analyses with S2Ab (black line) or preimmune rabbit serum (gray line) of P29 cells cultured for 4 days in the absence of nucleotides (A) or the presence of antisense (B) or sense oligonucleotides (C) for syndecan 2 core protein were carried out. Aliquots of the respective cell preparations were inoculated on the fibronectin-coated cover glasses and localization of actin filaments in the cells was visualized with rhodamine-conjugated phalloidin as described under Methods (D, E, F).

substrate, the heparan sulfate of syndecan 2 interacts with the Hep-II domain of fibronectin.

Binding affinity of size- and structure-defined oligosaccharides derived from heparin and chemically modified heparins to a recombinant H-271 peptide containing Hep-II domain of fibronectin. To examine the structural characteristics of the heparan sulfates of syndecan 2 cooperating with integrin $\alpha 5\beta 1$, we first tested whether size- and structure-defined oligosaccharides prepared from heparin, 2DS-, 6DS-, CR-, and AMS-heparins have some effects on the cytoskeletal organization in P29 cells. For this purpose, the binding of dodecasaccharides to an H-271 peptide affinity column was first examined (Figs. 4A–4E). Eighty-five percent of the heparin-derived dodecasaccharide sample that was enriched in IdoA(2*O*S)–Glc*N*S(6*O*S) bound to the column and eluted with 0.32 M NaCl (Fig. 4A). On affinity chromatography of the 2DS-heparin-derived dodecasaccharide sample enriched in IdoA–Glc*N*S(6*O*S) (82–89%) (Table 1), the material was

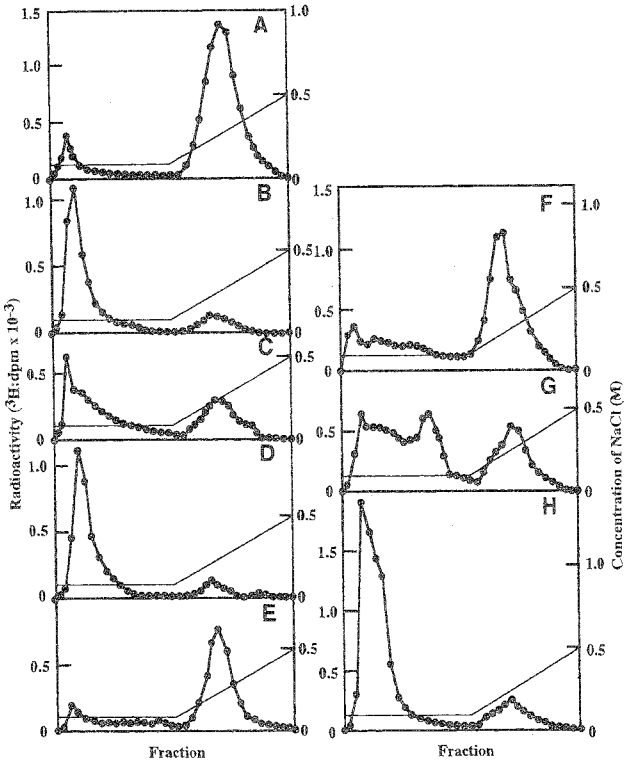

FIG. 4. Affinity chromatography of structure- and size-defined oligosaccharides, prepared from heparin and chemically modified heparins, on an H-271 peptide-linked column. Left panels show the elution profiles of the structure-defined dodecasaccharide samples prepared from heparin (A), 2DS- (B), 6DS- (C), CR- (D), and AMS- (E) heparins. Right panels show those of the size-defined oligosaccharide samples, including heparin-derived deca- (F), octa- (G), and hexasaccharides (H).

mostly excluded from the column (Fig. 4B), indicating that sulfate groups at the C-2 position of the iduronate residues are essential for binding to the H-271 peptide and sulfation at C-6 of the glucosamine residues was not sufficient for this binding. Affinity chromatography of the 6DS-heparin-derived dodecasaccharide sample showed about 50% binding to the column (Fig. 4C). The treatment for 6-O-desulfation of heparin, adopted in this study, resulted in 75% loss of 6-O-sulfate substituents in conjunction with about 25% loss of 2-O-sulfate substituents, giving a product which had a disaccharide composition of IdoA(2*O*S)–Glc*N*S (accounting for 52–56%) and IdoA–Glc*N*S/GlcA–Glc*N*S (20–23%). Therefore, the compound bound to the column can be mostly attributable to IdoA(2*O*S)–Glc*N*S. However, a possibility of the requirement of sulfation at the C-6 position of a specific glucosamine residue(s), as sulfation at the C-3 position of a glucosamine residue in the pentasaccharide specific for antithrombin III [3, 18, 19], could not be ruled out in this study. Almost all of the CR-heparin-derived dodecasaccharide sample, of which nearly 80% had three sulfate residues per disaccharide unit as the heparin-derived sample, did not bind to the column (Fig. 4D), indicating that the negative charge of the carboxy group of hexuronic acid is required for specific binding to the H-271 peptide. When the AMS-heparin-derived dodecasaccharide sample was chromatographed on the column (Fig. 4F), the amount of the bound oligosaccharides was almost the same as that for the heparin-derived bound oligosaccharides, indicating that the negative charge of the carboxy groups in hexuronic acid can be replaced by other functional groups with a negative charge, such as the aminomethyl sulfonate moiety shown here.

We next examined the size dependence in binding to the H-271 peptide column using heparin-derived dodeca-, deca-, octa-, and hexasaccharide-size classes, all with 80% of their disaccharides constituted by IdoA(2*O*S)–Glc*N*S(6*O*S). When individual samples were chromatographed on H-271 peptide column, the proportion of binding gradually decreased with reduction in size, values of 84, 68, 33, and 19% being observed for the dodeca-, deca-, octa-, and hexasaccharides, respectively (Fig. 4A and 4F–4H).

Competitive inhibition of binding of the syndecan 2 ectodomain to H-271 peptide with structure- and size-defined oligosaccharides derived from heparin and chemically modified heparins. To examine structural characteristics of the heparan sulfate chains of syndecan 2, which interact with the Hep-II domain of fibronectin, we adopted a competitive inhibition method. The binding of [^{35}S]sulfate-labeled syndecan 2 ectodomain to immobilized H-271 peptide was analyzed in the presence of structure- and size-defined oligosaccharides, of which the binding affinity to the H-271 peptide column was determined above. The heparin-derived dodecasaccharide sample enriched in IdoA(2*O*S)–Glc*N*S(6*O*S) inhibited the binding of the ectodomain in a dose-dependent manner and almost completely at a concentration of 8 μg/ml (Fig. 5A). The 2DS- and CR-heparin-derived dodecasaccharide samples did not exhibit significant inhibition of the binding and only slight competitive inhibition (about 35%) was noted with the 6DS-heparin-derived dodecasaccharide sample. The degree of the competitive inhibition with all dodecasaccharide samples except the AMS-heparin-derived one well reflected their capacity for binding to the H-271 peptide affinity column. The AMS-heparin-derived dodecasaccharide sample inhibited binding of the ectodomain to the peptide by only 50%, despite its high binding ability that was almost equal to that of the heparin-derived counterpart, suggesting that not only electrostatic but also structural interactions are important for the binding of heparan sulfates of syndecan 2 to the Hep-II domain of fibronectin.

Competitive inhibition of binding of the syndecan 2 ectodomain to H-271 peptide with the oligosaccharides

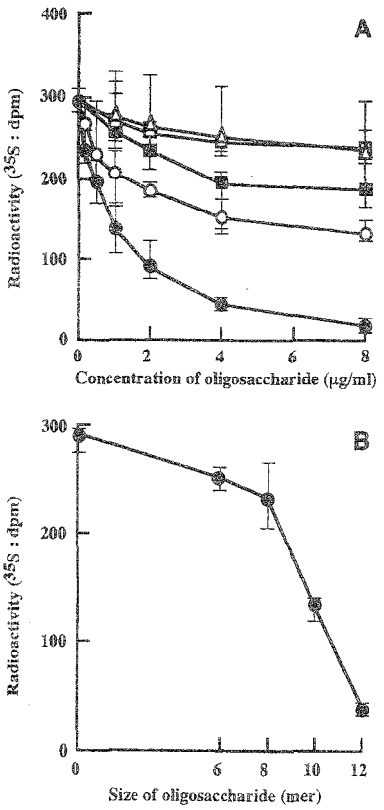

FIG. 5. Inhibitory effects of structure- and size-defined oligosaccharides on binding of the ^{35}S-labeled ectodomain of syndecan 2 to immobilized H-271 polypeptide. (A) Dose-dependent inhibition with structure-defined dodecasaccharide samples prepared from heparin (●), 2DS- (△), 6DS- (■), CR- (□), and AMS- (○) heparins. (B) Size-dependent inhibition with hexa-, octa-, deca-, and dodecasaccharides (8 μg/ml) prepared from heparin. The results show values obtained from two different experiments done in triplicate.

was found to depend on their size. When this competitive inhibition was analyzed in the presence of the heparin-derived dodeca-, deca-, octa-, and hexasaccharides at a concentration of 8 μg/ml (Fig. 5B), the hexa- and octasaccharide samples did not exhibit significant inhibition, but the decasaccharide sample reduced this binding by about 50%. The dodecasaccharide sample almost completely inhibited the binding, as did intact heparin. These results indicate that the degree of the competitive inhibition with the heparin-derived oligosaccharides having the different sizes well reflected the degree of their binding ability to the H-271 peptide affinity column.

Inhibition of stress fiber formation in P29 cells with the heparin-derived oligosaccharides of different sizes. We finally examined the inhibitory effects of the size-defined heparin-derived oligosaccharide samples on stress fiber formation. When P29 cells were inoculated onto cover glasses coated with the CH-271 peptide, a fusion form of RGD cell-binding domain (Pro^{1239}-Ser^{1515}) and Hep-II domain (Ala^{1690}-Thr^{1960}), they adhered to the substrate and spread extensively in association with stress fiber formation (Fig. 6A), as observed on intact fibronectin (see Fig. 2A). Addition of the heparin-derived hexa- (data not shown) and octasaccharides did not influence formation of stress fibers (Fig. 6B). The

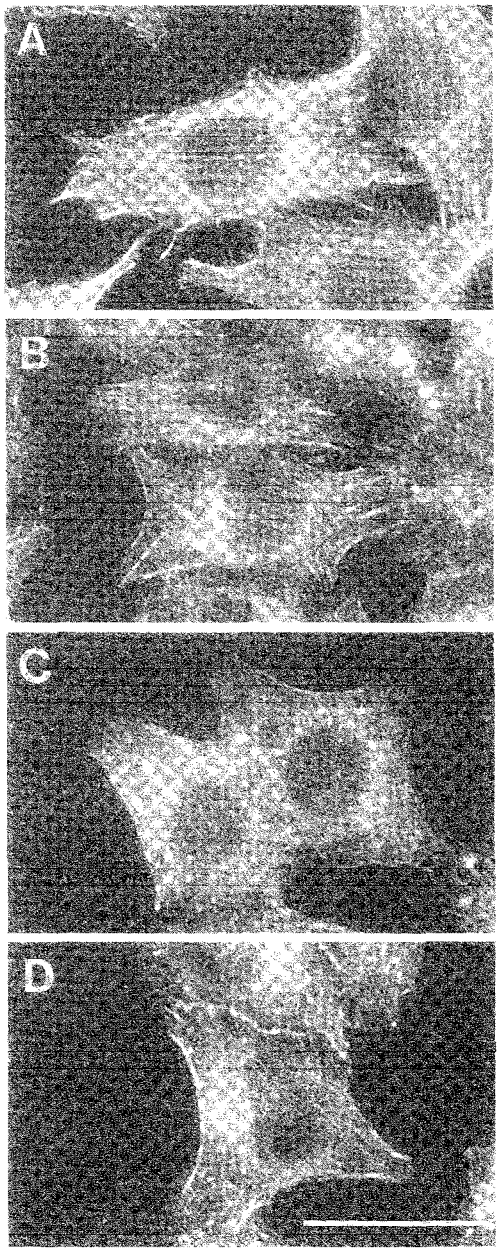

FIG. 6. Inhibitory effects of heparin-derived oligosaccharides on stress fiber formation in P29 cells triggered by adhesion to the CH-271 substrate. P29 cells were inoculated onto cover glasses coated with CH-271 polypeptide in the absence (A) or presence of heparin-derived octasaccharide sample (B), dodecasaccharide sample (C), and intact heparin (D), and incubated for 1 h, followed by staining of actin filaments with rhodamine-conjugated phalloidin. Bar, 50 μm.

decasaccharide sample exhibited only a very weak inhibitory effect with thinning of stress fibers (data not shown). The dodecasaccharide sample, in contrast, almost completely inhibited stress fiber formation (Fig. 6C), as observed with intact heparin (Fig. 6D), causing localization of actin filaments in the cytoplasmic cortex, instead. This phenotype was indistinguishable from that induced in P29 cells allowed to adhere to C-274 peptide, consisting of only the RGD cell-binding domain (data not shown). Moreover, we observed that all the 2DS-, 6DS-, CR-, and AMS-heparin-derived oligosaccharide samples did not exhibit detectable inhibitory effects on the formation of stress fibers (data not shown).

DISCUSSION

The present study clearly demonstrated that the induction of stress fiber formation triggered by adhesion of P29 cells to the immobilized fibronectin or CH-271 peptide substrate requires the cooperation of integrin $\alpha5\beta1$ with cell surface heparan sulfate proteoglycan. The stress fiber formation was thus inhibited by (1) exogenous addition of GRGDS peptide as a competitive inhibitor of the RGD cell-binding domain of fibronectin, (2) pretreatment of the cells with proteinase-free heparitinase-I or with the monoclonal antibody, F58-10E4, specific to heparan sulfate chains, and (3) exogenous addition of heparin as a competitive inhibitor of the endogenous cell surface heparan sulfate. On the other hand, these results show that in P29 cells, signaling through integrin $\alpha5\beta1$ alone cause localization of actin filaments in the cytoplasmic cortex, whereas signaling through the cell surface heparan sulfate proteoglycan causes the cells to become spindle-like in shape and not to spread. Signaling through both integrin $\alpha5\beta1$ and the cell surface proteoglycan results in the induction of stress fiber formation. These results are consistent with the observation of Couchman and his colleagues using fibroblasts [47, 48]. Thus, it appears to be common to various cell types that the fibronectin-adhesion-dependent stress fiber formation requires the dual receptor system with integrin $\alpha5\beta1$ and the cell surface heparan sulfate proteoglycan.

However, in fibroblasts the cell surface heparan sulfate proteoglycan involved in the formation of focal adhesions and stress fibers has been attributed to syndecan 4 on the basis of immunostaining indicating its localization at focal adhesions [17]. It has been recently suggested that syndecan 4 participates in regulation of focal adhesion assemblies through its phosphorylation at Ser^{183} of the cytoplasmic tail of the core protein [49, 50]. In contrast, in P29 cells, more than 80% of the fibronectin-binding cell surface proteoglycans has been identified as syndecan 2, which is shown to be involved in fibronectin-mediated stress fiber formation in the present study, but a detectable amount of syndecan 4 has not been found in the fibronectin-bound proteoglycans [32, 33]. Moreover, the present study clearly demonstrated that treatment of P29 cells with antisense oligonucleotide for syndecan 2 core protein resulted in inhibition of the induction of stress fiber formation in association with specific suppression of cell surface expression of the syndecan 2 proteoglycan. This treatment does not have a significant effect on cell surface expressions of other syndecans, syndecan 1, 3, and 4, which are produced by P29 cells [31]. In this regard, it should be noted that fibroblasts from syndecan 4 null mouse have been most recently reported to form stress fibers on cell adhesion to the fibronectin substrate [51], suggesting that the role of syndecan 4 in the organization of actin cytoskeletons could be compensated by other molecule(s). However, we could not eliminate the possibility that syndecan 4 participated in stress fiber formation of P29 cells, as shown with other cell types [17, 47]. This discrepancy may be due to the difference in cell types used in the respective experiments. Nevertheless, it is unlikely because syndecan 4 has been also shown to be a constitutent of focal adhesions of various cell types, including both mesenchymal and epithelial cell types [17]. However, it has not been elucidated whether syndecan 4 specifically binds to the C-terminal heparin-binding domain of fibronectin. That is, it is not clear at present whether the binding ability of the cell surface proteoglycan to this heparin-binding domain of fibronectin is prerequisite for its incorporation into focal adhesions. Thus, it is possible that syndecan 2 and 4 both are involved in regulation of the formation of focal adhesions and stress fibers but in different manners.

Syndecan 2 produced by P29 cells is a hybrid-type proteoglycan having three heparan sulfate chains and a single chondroitin sulfate chain on the same core protein. It binds specifically to fibronectin- or H-271 polypeptide-linked affinity column through the heparan sulfate chains [32, 33]. To elucidate chemical feature(s) of the binding site in the chains, we utilized size- and structure-defined oligosaccharides prepared from heparin and chemically modified heparins and examined (1) their binding affinity to H-271 peptide, (2) their inhibitory effect on the binding of the syndecan 2 ectodomain to H-271 peptide, and (3) their inhibitory effect on the formation of stress fibers in P29 cells. The present findings suggest that not only the electrostatic properties but also the structural configuration of the heparan sulfate chains are important for their specific binding to the Hep-II domain of fibronectin. Inhibition of binding of the syndecan 2 ectodomain to the Hep-II domain by heparin-derived oligosaccharide samples of different sizes was well reflected on inhibitory effects on stress fiber formation. The dodecasaccharide sample exhibited almost complete inhibition

against the stress fiber formation, as intact heparin showed. The disaccharide composition of this dodecasaccharide sample was similar to those of the other smaller oligosaccharide samples. The results strongly suggest that the heparan sulfate of syndecan 2 contains highly sulfated cluster(s) having the chemical structure of IdoA(2*O*S)–Glc*N*S(6*O*S). The cluster(s) is considered to be responsible for high-affinity binding to Hep-II domain of fibronectin. It is thus reasonable to draw a conclusion that the heparan sulfate chains of syndecan 2 contain highly sulfated cluster(s) ≧12 mer in size along the chains.

Heparan sulfates play many important roles in regulating a large variety of cellular physiological processes [2, 4]. Accumulated reports have indicated that heparin or heparan sulfates represent "some specificity" in interactions with biologically active proteins at their specific sites named "heparin-binding domains." It is now well established that they bind to antithrombin III through a specific pentasaccharide epitope [18, 19], and there is increasing evidence indicating the presence of specific sites in heparan sulfate chains which interact with humoral factors such as basic fibroblast growth factor, hepatocyte growth factor, and interleukin-8. Cell adhesive proteins in extracellular matrices, such as fibronectin, vitronectin, laminin, and tenascin, also have heparin-binding domains with unique amino acid sequences [2]. However, there have been few reports implicating ligand-binding specificity of heparan sulfates in functions of proteoglycan molecules [52]. The present study demonstrated that side chains with dodecasaccharide(s) enriched in the disaccharide, IdoA(2*O*S)–Glc*N*S(6*O*S), are necessary for the specific interaction of the syndecan 2 proteoglycan with the C-terminal heparin-binding domain of fibronectin. The mechanisms underlying the cooperation of syndecan 2 with integrin $\alpha5\beta1$ to induce fibronectin-mediated stress fiber formation now require elucidation.

This work was supported in part by a Grant-in-Aid for Cancer Research (9-39 and 11-13) from the Ministry of Health and Welfare, by Grants-in-Aid for Scientific Research (A-1-093080 and C-2-10680591) and Scientific Research on Priority Areas (10178222) from the Ministry of Education, Science, Sports and Culture, and by a grant from the Aichi Cancer Research Foundation.

REFERENCES

1. Bernfield, M., Kokenyesi, R., Kato, M., Hinkes, M. T., Spring, J., Gallo, R. L., and Lose, E. J. (1992). Biology of the syndecans: A family of transmembrane heparan sulphate proteoglycans. *Annu. Rev. Cell Biol.* **8,** 365–393.
2. Carey, D. J. (1997). Syndecans: Multifunctional cell-surface co-receptors. *Biochem. J.* **327,** 1–16.
3. Lindahl, U., Kusche-Gullberg, M., and Kjellen, L. (1998). Regulated diversity of heparan sulphate. *J. Biol. Chem.* **273,** 24979–24982.
4. Woods, A., Oh, E. S., and Couchman, J. R. (1998). Syndecan proteoglycans and cell adhesion. *Matrix Biol.* **17,** 477–483.
5. Klagsbrun, M., and Baird, A. (1991). A dual receptor system is required for basic fibroblast growth factor activity. *Cell* **67,** 229–231.
6. Rapraeger, A. C., Krufka, A., and Olwin, B. B. (1991). Requirement of heparan sulphate for bFGF-mediated fibroblast growth and myoblast differentiation. *Science* **252,** 1705–1708.
7. Yayon, A., Klagsbrun, M., Esko, J. D., Leder, P., and Orinits, D. M. (1991). Cell surface, heparin-like molecules are required for binding of basic fibroblast growth factor to its high affinity receptor. *Cell* **64,** 841–848.
8. Guimond, S., Maccarana, M., Olwin, B. B., Lindahl, U., and Rapraeger, A. C. (1993). Activating and inhibitory heparin sequences for FGF-2 (basic FGF): Distinct requirements for FGF-1, FGF-2 and FGF-4. *J. Biol. Chem.* **268,** 23906–23914.
9. Ishihara, M., Tyrrell, D. J., Stauber, G. B., Brown, S., Cousens, L. S., and Stack, R. J. (1993). Preparation of affinity-fractionated, heparin-derived oligosaccharides and their effects on selected biological activities mediated by basic fibroblast growth factor. *J. Biol. Chem.* **268,** 4676–4683.
10. Gitay-Goren, H., Soker, S., Vlodavsky, I., and Neufeld, G. (1992). The binding of vascular endothelial growth factor to its receptors is dependent on cell surface-associated heparin-like molecules. *J. Biol. Chem.* **267,** 6093–6098.
11. Higashiyama, S., Abraham, J. A., and Klagsbrun, M. (1993). Heparin-binding EGF-like growth factor stimulation of smooth muscle cell migration: Dependence on interactions with cell surface heparan sulfate. *J. Cell Biol.* **122,** 933–940.
12. Williams, K. J., Fless, G. M., Petrie, K. A., Snyder, M. L., Brocia, R. W., and Swenson, T. L. (1992). Mechanisms by which lipoprotein lipase alters cellular metabolism of lipoprotein(s), low density lipoprotein, and nascent lipoproteins: Roles for low density lipoprotein receptors and heparan sulphate proteoglycans. *J. Biol. Chem.* **267,** 13284–13292.
13. Mulder, M., Lombardi, P., Jansen, H., van Berkel, T. J. C., Frants, R. R., and Havekes, L. M. (1993). Low density lipoprotein receptor internalizes low density and very low density lipoproteins that are bound to heparan sulphate proteoglycans *via* lipoprotein lipase. *J. Biol. Chem.* **268,** 9369–9375.
14. Fuki, I. V., Kuhn, K. M., Lomazov, I. R., Rothman, V. L., Tuszynski, G. P., Iozzo, R. V., Swenson, T. L., Fisher, E. A., and Williams, K. J. (1997). The syndecan family of proteoglycans: Novel receptors mediating internalization of atherogenic lipoproteins *in vitro*. *J. Clin. Invest.* **100,** 1611–1622.
15. Raulo, E., Chernousov, M. A., Carey, D. J., Nolo, R., and Rauvala, H. (1994). Isolation of a neuronal cell surface receptor of heparin binding growth-associated molecule (HB-GAM): Identification and N-syndecan (syndecan-3). *J. Biol. Chem.* **269,** 12999–13004.
16. Kaneda, N., Talukder, A. H., Ishihara, M., Hara, S., Yoshida, K., and Muramatsu, T. (1996). Structural characteristics of heparin-like domain required for interaction of midkine with embryonic neurons. *Biochem. Biophys. Res. Commun.* **220,** 108–112.
17. Woods, A., and Couchman, J. R. (1994). Syndecan 4 heparan sulphate proteoglycan is a selectively enriched and widespread focal adhesion component. *Mol. Biol. Cell* **5,** 183–192.
18. Lindahl, U., Backstrom, G., and Thunberg, L. (1983). The antithrombin-binding sequence in heparin: Identification of an essential 6-*O*-sulfate group. *J. Biol. Chem.* **258,** 9826–9830.
19. Atha, D. H., Stephens, A. W., and Rosenberg, R. D. (1984). Evaluation of critical groups required for the binding of heparin to antithrombin. *Proc. Natl. Acad. Sci. USA* **81,** 1030–1034.

20. Habuchi, H., Suzuki, S., Saito, T., Tamura, T., Harada, T., Yoshida, K., and Kimata, K. (1992). Structure of a heparan sulphate oligosaccharide that binds to basic fibroblast growth factor. *Biochem. J.* **285,** 805–813.
21. Turnbull, J. E., Fernig, D. G., Ke, Y., Wilkinson, M. C., and Gallagher, J. T. (1992). Identification of the basic fibroblast growth factor binding sequence in fibroblast heparan sulphate. *J. Biol. Chem.* **267,** 10337–10341.
22. Maccarana, M., Casu, B., and Lindahl, U. (1993). Minimal sequence in heparin/heparan sulphate required for binding of basic fibroblast growth factor. *J. Biol. Chem.* **268,** 23898–23905.
23. Faham, S., Hileman, R. E., Fromm, J. R., Linhardt, R. J., and Rees, D. C. (1996). Heparin structure and interactions with basic fibroblast growth factor. *Science* **271,** 1116–1120.
24. Kan, M., Wang, R., Xu, J., Crabb, J. W., Hou, J., and McKeehan, W. L. (1993). An essential heparin-binding domain in the fibroblast growth factor receptor kinase. *Science* **259,** 1918–1921.
25. Rusnati, M., Coltrini, D., Caccia, P., Dell'Era, P., Zoppetti, G., Oreste, P., Valsasina, B., and Presta, M. (1994). Distinct role of 2-*O*-, 6-*O*-sulphate groups of heparin in the formation of the ternary complex with basic fibroblast growth factor and soluble FGF receptor-1. *Biochem. Biophys. Res. Commun.* **203,** 450–458.
26. Lyon, M., Deakin, J. A., Mizuno, K., Nakamura, T., and Gallagher, J. T. (1994). Interaction of hepatocyte growth factor with heparan sulphate: Elucidation of the major heparan sulphate structural determinants. *J. Biol. Chem.* **269,** 11216–11223.
27. Ashikari, S., Habuchi, H., and Kimata, K. (1995). Characterization of heparan sulphate oligosaccharides that bind to hepatocyte growth factor. *J. Biol. Chem.* **270,** 29586–29593.
28. Nakanishi, H., Oguri, K., Yoshida, K., Itano, N., Takenaga, K., Kazama, T., Yoshida, A., and Okayama, M. (1992). Structural differences between heparan sulphates of proteoglycan involved in the formation of basement membranes *in vivo* by Lewis-lung-carcinoma-derived cloned cells with different metastatic potentials. *Biochem. J.* **288,** 215–224.
29. Nakanishi, H., Takenaga, K., Oguri, K., Yoshida, A., and Okayama, M. (1992). Morphological characteristics of tumours formed by Lewis lung carcinoma-derived cloned cell lines with different metastatic potentials: Structural differences in their basement membranes formed *in vivo*. *Virchows Arch. [A]* **420,** 163–170.
30. Nakanishi, H., Oguri, K., Takenaga, K., Hosoda, S., and Okayama, M. (1994). Differential fibrotic stromal responses of host tissue to low- and high-metastatic cloned Lewis lung carcinoma cells. *Lab. Invest.* **70,** 324–332.
31. Oguri, K., Kusano, Y., Narumiya, S., Yamashina, I., and Okayama, M. (1997). Functional analysis of syndecan-2 acting as a receptor in co-operation with integrin $\alpha5\beta1$ on cell adhesion to fibronectin. *Glycoconj. J.* **14,** s23–s24.
32. Itano, N., Oguri, K., Nakanishi, H., and Okayama, M. (1993). Membrane-intercalated proteoglycan of a stroma-inducing clone from Lewis lung carcinoma binds to fibronectin *via* its heparan sulphate chains. *J. Biochem.* **114,** 862–873.
33. Itano, N., Oguri, K., Nagayasu, Y., Kusano, Y., Nakanishi, H., David, G., and Okayama, M. (1996). Phosphorylation of a membrane-intercalated proteoglycan, syndecan-2, expressed in a stromal-inducing clone from a mouse Lewis lung carcinoma. *Biochem. J.* **315,** 925–930.
34. Ichihara-Tanaka, K., Meda, T., and Sekiguchi, K. (1992). Matrix assembly of recombinant fibronectin polypeptide consisting of amino-terminal 70 kDa and carboxyl-terminal 37 kDa regions. *FEBS Lett.* **299,** 155–158.
35. Nakanishi, Y., Uematsu, J., Takamatsu, H., Fukuda, Y., and Yoshida, K. (1993). Removal of heparan sulfate chains halted epithelial branching morphogenesis of the developing mouse submandibular gland *in vitro*. *Dev. Growth Differ.* **35,** 371–384.
36. Ishihara, M., Shaklee, P. N., Yang, Z., Liang, W., Wei, Z., Stack, R. J., and Holme, K. (1994). Structural features in heparin which modulate specific biological activities mediated by basic fibroblast growth factor. *Glycobiology* **4,** 451–458.
37. Jaseja, M., Rej, R. N., Souriol, F., and Perlin, A. (1989). Novel regio- and stereoselective modifications of heparin in alkaline solution: Nuclear magnetic resonance spectroscopic evidence. *Can. J. Chem.* **67,** 1449–1456.
38. Nagasawa, K., Inoue, Y., and Kamata, T. (1977). Solvolytic desulfation of glycosaminoglyuronan sulfates with dimethyl sulfoxide containing water or methanol. *Carbohydr. Res.* **58,** 47–55.
39. Tayler, R. L., Shively, J. E., and Conrad, H. E. (1976). Stoichiometric reduction of uronic acid carboxyl groups in polysaccharides. *Method Carbohydr. Chem.* **7,** 149–151.
40. Danishefsky, I., and Siskovic, E. (1971). Conversion of carboxyl groups of mucopolysaccharides into amides of amino acid esters. *Carbohydr. Res.* **16,** 199–205.
41. Ishihara, M., Guo, Y., Wei, Z., Yang, Z., Swiedler, S. J., Orellans, A., and Hirschberg, C. B. (1993). Regulation of biosynthesis of the basic fibroblast growth factor binding domains of heparan sulfate by heparan sulfate-*N*-deacetylase/*N*-sulfotransferase expression. *J. Biol. Chem.* **268,** 20091–20095.
42. Guo, Y., and Conrad, H. E. (1989). The disaccharide composition of heparins and heparan sulfates. *Anal. Biochem.* **176,** 96–104.
43. Guo, Y., and Conrad, H. E. (1988). Analysis of oligosaccharides from heparin by reverse-phase ion-pairing high-performance liquid chromatography. *Anal. Biochem.* **168,** 54–62.
44. Pytela, R., Pierschbacher, M. D., Argraves, S., Suziki, S., and Ruoslahti, E. (1987). Arginine-glycine-aspartic acid adhesion receptors. *Methods Enzymol.* **144,** 475–489.
45. David, G., Bai, X. M., Van der Schueren, B., Cassiman, J. J., and Van den Berghe, H. (1992). Developmental changes in heparan sulphate expression: *in situ* detection with mAbs. *J. Cell Biol.* **119,** 961–975.
46. McCarthy, J. B., Hagen, S. T., and Furcht, L. T. (1986). Human fibronectin containing distinct adhesion- and motility-promoting domains for metastatic melanoma cells. *J. Cell Biol.* **102,** 179–188.
47. Woods, A., Couchman, J. R., Johansson, S., and Hook, M. (1986). Adhesion and cytoskeletal organization of fibroblasts in response to fibronectin fragments. *EMBO J.* **5,** 665–670.
48. Woods, A., and Couchman, J. R. (1998). Syndecans: Synergistic activators of cell adhesion. *Trends Cell Biol.* **8,** 189–192.
49. Horowitz, A., and Simons, M. (1998). Regulation of syndecan-4 phosphorylation *in vivo*. *J. Biol. Chem.* **273,** 10914–10918.
50. Horowitz, A., and Simons, M. (1998). Phosphorylation of the cytoplasmic tail of syndecan-4 regulates activation of protein kinase Cα. *J. Biol. Chem.* **273,** 25548–25551.
51. Ishiguro, K., Kadomatsu, K., Kojima, T., Tsuzuki, S., Muramatsu, H., Nakamura, E., Saito, H., and Muramatsu, T. (1999). Analysis of ryudocan/syndecan-4 function by means of gene targeting. (Abstract, P-II-II-4) International Conference on Molecular Interactions of Proteoglycan (Kanagawa, Japan).
52. Kato, M., Wang, H., Bernfield, M., Gallagher, J. T., and Turnbull, J. E. (1994). Cell surface syndecan-1 on distinct cell types differs in fine structure and ligand binding of its heparan sulphate chains. *J. Biol. Chem.* **269,** 18881–18890.

Received November 26, 1999

Clinical Investigations

Respiration

Respiration 2000;67:389–396

Received: November 30, 1998
Accepted after revision: September 5, 1999

Significance of the Interleukin-1 Receptor Antagonist/Interleukin-1β Ratio as a Prognostic Factor in Patients with Pulmonary Sarcoidosis

Takeshi Mikuniya[a] Sonoko Nagai[a] Minoru Takeuchi[b] Tadashi Mio[a]
Yuma Hoshino[a] Hiroyuki Miki[a] Michio Shigematsu[a] Kunio Hamada[a]
Takateru Izumi[a]

[a]Department of Respiratory Medicine, Graduate School of Medicine, Kyoto University, and
[b]Faculty of Bioengineering, Kyoto Sangyo University, Kyoto, Japan

Key Words

Pulmonary sarcoidosis · Interleukin-1β · Interleukin-1 receptor antagonist · Bronchoalveolar lavage fluid macrophages · Angiotensin-converting enzyme activity, serum · Chest radiographs, shadows · Pulmonary function

Abstract

Background: Various factors such as serum angiotensin-converting enzyme (sACE) activity, bronchoalveolar lavage (BAL) fluid lymphocyte percent, CD4/CD8 ratio, and shadows on chest radiograph have been identified as indexes of disease activity in patients with sarcoidosis. However, it remains to be confirmed whether these factors can predict clinical outcomes. ***Objective:*** To examine whether the interleukin-1 receptor antagonist (IL-1ra)/IL-1β ratio can predict the clinical course, we prospectively followed the clinical courses of 30 patients with pulmonary sarcoidosis 4 years after measurement of immunoreactive amounts of IL-1ra or IL-1β in the culture supernatants obtained from BAL fluid macrophages. ***Methods:*** Immunoreactive amounts of IL-1ra or IL-1β were measured using ELISA. Changes in pulmonary function, sACE activity, and shadows on chest radiographs during observation periods were evaluated as markers of changes in disease activity. ***Results:*** We found that the patients whose shadows on chest radiographs showed improvement had a higher molar IL-1ra/IL-1β ratio than the patients whose shadows persistently remained 4 years after BAL examination ($p < 0.05$). The molar ratio was found to be positively correlated with improvement of percent vital capacity ($p < 0.05$) and negatively correlated with the ratio of sACE activity at the time of the last observation to sACE activity at the time of BAL ($sACE_{LAST}/sACE_{BAL}$, $p < 0.01$). The $sACE_{LAST}/sACE_{BAL}$ ratio was significantly lower in patients whose shadows on chest radiographs decreased than in those whose shadows remained unchanged ($p < 0.005$). ***Conclusion:*** The IL-1ra/IL-1β ratio in the BAL fluid macrophage culture supernatants in patients with pulmonary sarcoidosis could be a useful marker in predicting the persistence of granulomatous lesions (chronicity).

Introduction

Clinical courses are variable in patients with pulmonary sarcoidosis, with some showing a spontaneous regression, and others showing a chronicity with functional deterioration [1]. Accordingly, there is a critical need to find factors that predict prognosis in an early stage of the disease and apply them to the management of patients [2].

KARGER

Fax + 41 61 306 12 34
E-Mail karger@karger.ch
www.karger.com

0025–7931/00/0674–0389$17.50/0

Accessible online at:
www.karger.com/journals/res

Sonoko Nagai
Department of Respiratory Medicine
Graduate School of Medicine, Kyoto University
Shogoin, Sakyo-ku, Kyoto 606-8507 (Japan)
Tel. +81 75 751 3831, Fax +81 75 751 4643, E-Mail nagai@kuhp.kyoto-u.ac.jp

Regarding intrathoracic lesions, macrophage T lymphocyte alveolitis precedes the formation of an epithelioid cell granuloma [3, 4]. Medical intervention with corticosteroids has been done for many years to suppress hyperimmune responses at the lesion sites; however, since the many attempts to clarify which patients to treat, the proper dosage, and the duration of therapy have had limited success, no general consensus has been reached on these issues [5]. Factors which reflect disease activity do not always predict prognosis [6–8]. To manage the patients appropriately in the early stages, it is critical not only to assess disease activity, but also to find prognostic factors.

Cytokine networks at the lesion sites may be deeply involved in either enhancement or suppression of inflammation [9]. Interleukin (IL)-1β, a cytokine mainly produced constitutively by macrophages, is considered to be essential for maintenance of macrophage T lymphocyte alveolitis and epithelioid cell granuloma formation [10–13]. Previous reports demonstrated that IL-1β activity in the culture supernatants of bronchoalveolar lavage fluid (BALF) macrophages tended to be higher in patients with sarcoidosis than in normal subjects [14]. Activities of IL-1β are strictly regulated by IL-1 inhibitors such as prostanoids or IL-1 receptor antagonist (IL-1ra). IL-1ra blocks IL-1 activity by occupying type I receptors without agonist activity [15].

Our previous study showed that IL-1β inhibitory activity in the culture supernatants of BALF macrophages was decreased in patients with active sarcoidosis, patients with idiopathic pulmonary fibrosis, and healthy current smokers when compared to that in healthy nonsmokers [16, 17]. Furthermore, this inhibitory activity was characterized as IL-1ra using a receptor binding assay and a chemical cross-linking method [18]. However, there was no difference of IL-1β activity among these groups. Consequently, the ratio of IL-1ra to IL-1β activity and the molar ratio of the two proteins (IL-1ra/IL-1β) were both lower in patients with interstitial lung disease and healthy current smokers than in healthy nonsmokers [19]. Given that the decrease in the IL-1ra/IL-1β ratio was prominent in the active but not the inactive sarcoidosis cases, this ratio seems to reflect disease activity in sarcoidosis.

In this prospective study, we focused on whether the molar ratio of immunoreactive amounts of IL-1ra/IL-1β in the culture supernatants of BALF macrophages predicts changes in three markers of disease activity, i.e. shadows on chest radiograph, pulmonary function test, and serum angiotensin-converting enzyme (sACE) activity in patients with pulmonary sarcoidosis.

Materials and Methods

Study Population

Our study population included 30 nonsmokers with pulmonary sarcoidosis. In all cases, sarcoidosis was histologically diagnosed as sarcoidosis by transbronchial lung biopsy. Twenty of the patients were classified as radiographic stage I (bilateral hilar lymphadenopathy, BHL), 6 as stage II (BHL with parenchymal lesions), and 4 as stage III (parenchymal lesions without BHL) at the time of BAL examination. Twenty-two cases had extrathoracic lesions, including 14 with stage I (9 uveitis, 1 skin lesions, 4 uveitis and skin lesions), 5 with stage II (2 uveitis, 2 uveitis and skin lesions, 1 uveitis, skin lesions and liver lesions) and 3 with stage III (3 uveitis). Ten healthy nonsmokers were examined as controls. No corticosteroids or immunosuppressive drugs were administered to patients with sarcoidosis. The median interval from detection to BAL was 33.5 months (range 7–87; 25th to 75th percentiles), and the patients were followed for 3–5 years after BAL (median observation period 46.0 months, range 43–50). Neither patients nor healthy subjects showed any signs or symptoms of infection. Informed consent was obtained from each patient and healthy subject. The lavage study in human subjects was approved by the Ethical Committee of the Graduate School of Medicine of the Kyoto University.

BALF Cell Preparation

BAL was performed according to the previous method with a slight modification [17]. Briefly, the upper airways were topically anesthetized with 2% lidocaine, and the fiberoptic bronchoscope was inserted into the tracheobronchial tree and wedged into the right middle lobe. The lavage was performed using a warm (37°C) sterile saline solution (50-ml aliquots to a total of 300 ml). Recovered BALF was filtered through gauze and centrifuged at 400 *g* for 10 min at 4°C. The cell pellets were resuspended in Eagle's MEM medium (Nissui, Tokyo, Japan) and centrifuged again to adjust the total cell count. Cell differentials were counted using cytospin specimens after May-Grünwald-Giemsa staining. T cell subsets which included the CD4/CD8 ratio were measured using a FACScan (Becton Dickinson) flow cytometer after staining with referred monoclonal antibodies.

Purification of BALF Macrophages

The E rosette method was used to fractionate the BALF cells into a non-rosette-forming cell fraction (macrophage-enriched) and a rosette-forming cell fraction (T-cell-enriched). The non-rosette-forming cell fraction was further purified with plastic adhesion at 37°C for 60 min. The purity of the adhesive fraction was more than 95% when stained with nonspecific esterase. Based on the cell count and cell viability determined by the trypan blue exclusion test before and after plating at 1 h of incubation, there was no difference in plating efficiency between the sarcoidosis patients and the healthy nonsmokers.

Cytokines Released from BALF Macrophages

To evaluate an in vivo condition, culture supernatants obtained from BALF macrophage-enriched fraction (1×10^6 cells/ml) were prepared in a serum-free medium (ASF 104 medium, Ajinomoto, Tokyo, Japan) with 5% CO_2 for 24 h at 37°C without lipopolysaccharide (LPS) stimulation. BALF macrophages from both sarcoidosis patients and nonsmokers checked by the trypan blue exclusion test demonstrated similar viability at 24 h. Culture supernatants were kept at –80°C after filtration. No trace amounts of LPS were

detected using the Limulus assay for LPS detection (Toxicolor System LS-6 Set, Seikagaku, Tokyo, Japan). No changes in the amounts of IL-1β or IL-1ra were shown either before or after filtration with a Millipore filter (0.45 μm, Millipore Products Division, Bedford, Mass., USA).

Measurement of the Immunoreactive Amounts of IL-1β and IL-1ra Proteins

Immunoreactive amounts of IL-1β and IL-1ra proteins in the culture supernatants were measured by a specific ELISA method using the IL-1β EASIA (Medgenix Diagnostics, Belgium) and the IL-1ra ELISA system (Biotrak, Amersham Life Science, UK). The IL-1β EASIA assay is a solid-phase enzyme-amplified sensitivity immunoassay. It is based on an oligoclonal system which uses several monoclonal antibodies directed against distinct epitopes of IL-1β. The sensitivity of this assay is 2 pg/ml. The IL-1ra ELISA system is based on a solid phase which uses a highly specific monoclonal antibody for human IL-1ra bound to the wells of a microplate together with a polyclonal antibody to human recombinant IL-1ra conjugated to horseradish peroxidase. The system has a sensitivity of 6.5 pg/ml in tissue culture media and exhibits no cross-reactivity with IL-1β or other major cytokines. Assays were done in triplicate in each ELISA. The molar ratio of IL-1ra/IL-1β was calculated according to the following formula: [immunoreactive amounts of IL-1ra (ng/ml)/24 kD (molecular weight of IL-1ra)]/[immunoreactive amounts of IL-1β (ng/ml)/17.5 kD (molecular weight of IL-1β)].

Evaluation of Changes in Disease Activities

We observed the clinical courses of patients more than 3 years after measuring the immunoreactive amounts of IL-1β and IL-1ra. We selected three markers of disease activities in this study: shadows on chest radiographs, pulmonary function tests, and sACE activity. The changes in shadows on chest radiographs 3 or 4 years after BAL were defined as: improved (disappearance or reduction of the shadows, including either BHL or parenchymal opacities), unchanged (no significant changes in either BHL or parenchymal opacities), and worsened (increase in either BHL or parenchymal opacities). Changes in sACE activity were expressed as the ratio of sACE at the last observation ($sACE_{LAST}$) to sACE at the time of BAL ($sACE_{BAL}$): $sACE_{LAST}/sACE_{BAL}$. A ratio of less than 1.0 indicated an improvement of sACE activity during the observation period, while a ratio of 1.0 or greater indicated no improvement. In addition, serial changes in the pulmonary function were also compared during the observation period [% vital capacity (%VC), forced expiratory volume 1 s (FEV1.0), FEV1.0/forced vital capacity (%), % total lung capacity (%TLC), % diffusion lung capacity for carbon monoxide (%DLCO), and % forced vital capacity (%FVC)]. BAL was not performed serially, as it is generally difficult to persuade patients to undergo the procedure twice.

Statistical Analysis

Data were analyzed with a Macintosh computer using the Statview statistical package (Abacus Concepts, Berkeley, Calif., USA) [20]. Data were compared between the two groups using the Mann-Whitney U test and the nonparametric median test. Results were expressed as median and ranges were given as 25th to 75th percentiles. The Spearman rank correlation coefficient test was used to evaluate the linear relationship among the IL-1ra/IL-1β ratio, serial changes in sACE activity, and pulmonary function tests. Data were considered to be statistically significant if the p value was less than 0.05.

Results

Study Population and BALF Cell Findings

All studied cases were nonsmokers. No difference was found between the gender ratios, but ages at the time of BAL examination tended to be higher in the sarcoidosis patients than in the healthy nonsmokers (table 1). When compared with the healthy nonsmokers, the sarcoidosis patients exhibited decreased percentages of BALF macrophages, increased percentages of BALF lymphocytes, and an elevated CD4/CD8 ratio.

Molar IL-1ra/IL-1β Ratio in the Culture Supernatants of BALF Macrophages

Though the ratio of immunological amounts of IL-1ra to IL-1β in the culture supernatants was more broadly distributed in the sarcoidosis patients, it was also significantly lower in the sarcoidosis patients [median 3.57 (25th 1.08 to 75th 10.0)] than in healthy nonsmokers [7.90 (5.9–9.2), p = 0.0305, fig. 1], as previously reported. The IL-1ra/IL-1β ratio in sarcoidosis patients was not found to be significantly correlated with the stage on chest radiographs (p = 0.658) at the time of BAL, or with age (p = 0.120), BAL lymphocyte percent (p = 0.302), BAL CD4/CD8 ratio (p = 0.774), or the presence versus absence of extrathoracic lesions (p = 0.671). In addition, among sarcoidosis patients, there was no difference in the IL-1ra/IL-1β ratio between males [2.93 (range 0.65–10.83)] and females [4.21 (range 1.43–8.94)] (p = 0.673).

Relationships between the Stage on Chest Radiographs at the Time of BAL and Clearance Rate of Abnormal Shadows

Among 20 patients assessed as radiographic stage I at the time of BAL, the shadows of BHL on the chest radiograph were reduced or cleared in 13 patients, unchanged in 6 patients, and had worsened in only 1 patients (judged by the appearance of parenchymal shadows) 4 years after BAL. Among 6 assessed as stage II, 4 showed improvement (2 with reduced shadows of BHL and 2 with reduced shadows of both BHL and parenchymal lesions), 1 patient showed no change in shadows, and 1 patient showed progression of parenchymal shadows (worsened). Three of 4 patients assessed as stage III showed no change and 1 showed progression of parenchymal shadows (worsened). The stage on chest radiographs at the time of BAL was not related to the outcome of abnormal shadows on chest radiographs 4 years after BAL (p = 0.169).

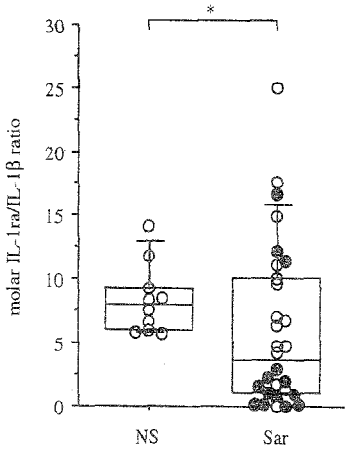

Fig. 1. The molar IL-1ra/IL-1β ratio in the culture supernatants of BALF macrophages in sarcoidosis patients (Sar) and healthy nonsmokers (NS). The box includes 50% of the observations, the bar in the center indicates the whisker box median value, and the bar outside the box indicates the 95th percentile. For sarcoidosis patients, improved cases whose shadows on chest radiograph showed regression (○) and cases whose chest radiographic shadows were either unchanged or had worsened 4 years after BAL (●) are shown. *$p < 0.05$.

Pulmonary Function Results

Pulmonary functions were compared between the results measured at the time of BAL and those measured at the last observation. The majority of patients had normal function data and the change in FEV1.0 was limited to a slight reduction ($p = 0.016$) (table 2). Improvement of sACE activity was in parallel with improvement of either %VC ($p = 0.041$) or %DLCO ($p = 0.029$). In addition, positive correlations were found between the IL-1ra/IL-1β ratio and improvement of %VC ($p = 0.027$) (table 3). However, we found no relationships between pulmonary function and the chest radiographic stages at the time of BAL or at the time of the last observation. Further, there were no correlations between the changes in the shadows on chest radiographs and the changes of pulmonary function (table 4).

Relationships of the Molar IL-1ra to IL-1β Ratio with Changes in sACE Activity and Changes in the Shadows on Chest Radiographs

The molar IL-1ra/IL-1β ratio at the time of BAL was significantly higher in patients whose shadows on chest radiographs improved 4 years after BAL [6.56 (range 3.55–10.58)] than in those whose shadows remained un-

Table 1. Study subjects and BAL cell findings

	Healthy nonsmokers	Sarcoidosis (nonsmokers)
Number of subjects	10	30
Age, years	37 (25–51)	52 (41–55)
Gender (m/f)	7/3	7/23
sACE[a], IU/l/37°C	–	24.8 (18.3–31.2)
Stage on chest radiographs	–	I (n = 20), II (n = 6), III (n = 4)
Extrathoracic lesions	–	eye (n = 21), skin (n = 8), liver (n = 1)
From detection to BAL, months	–	33.5 (7.0–87)
Observed period after BAL, months	–	46 (43–50)
BALF cell findings		
Fluid recovery, %	76.7 (71.7–81.6)	77.4 (68.7–80.0)
Recovered cells, $\times 10^5$ cells/ml	1.09 (0.75–1.20)	1.27 (0.72–1.95)
Macrophages, %	95.9 (86.7–98.8)	58.1 (50.0–92.3)**
Lymphocytes, %	4.2 (1.2–12.5)	40.9 (7.5–49.8)**
Neutrophils, %	0.0 (0.0–0.2)	0.0 (0.0–0.3)
Eosinophils, %	0.0 (0.0–0.0)	0.0 (0.0–0.0)
CD4/CD8	2.54 (0.58–3.72)	5.16 (2.88–11.6)**

Unless otherwise indicated figures represent median values with the 25th and 75th percentiles in parentheses. Stages on chest radiograph: I = BHL; II = BHL + parenchymal lesion; III = parenchymal lesion. ** $p < 0.01$ compared with nonsmokers.

[a] Normal range: 8.3–21.2.

Table 2. Changes in pulmonary function during the observation period

	At the time of BAL	At the time of last observation	At the time of BAL/last observation
%VC	101.9 (93.9–112.3)	105.0 (95.4–112.9)	1.03 (0.97–1.06)
%FVC	98.3 (87.5–110.0)	90.6 (78.7–104.0)	0.97 (0.88–1.04)
FEV1.0	2.44 (1.98–2.71)	2.36 (1.71–2.75)*	0.96 (0.92–1.01)
FEV1.0%	83.9 (76.9–87.1)	79.8 (77.0–84.4)	0.99 (0.94–1.03)
%TLC	90.9 (82.6–98.8)	86.5 (77.0–105.4)	1.03 (0.94–1.06)
%DLCO	81.1 (70.9–92.6)	75.8 (70.9–92.6)	0.99 (0.88–1.05)

Figures indicate median values with the 25th and 75th percentiles given in parentheses. * $p < 0.05$ compared with the time of BAL.

Table 3. Correlation with clinical, functional and laboratory data (Rs value)

	IL-1ra/IL-1β ratio	$sACE_{LAST}/sACE_{BAL}$ ratio	$\%VC_{LAST}/\%VC_{BAL}$ ratio	$DLCO\%_{LAST}/DLCO\%_{BAL}$ ratio
Age	–	–	–	–
sACE activity	–	−0.542**	–	–
BAL lymphocyte (%)	–	–	–	–
BAL CD4/CD8 ratio	–	–	–	–
IL-1ra/IL-1β ratio	–	−0.495**	0.700*	–
$sACE_{LAST}/sACE_{BAL}$ ratio	−0.495**	–	−0.645*	−0.692*

Age, sACE activity, BAL lymphocyte (%), BAL CD4/CD8 ratio, and IL-1ra/IL-1β ratio at the time of BAL. Data were analyzed using the Spearman rank correlation coefficient test. * $p < 0.05$; ** $p < 0.01$. – = No significant correlation.

Table 4. Relationships between clinical variable and changes in the shadows on chest radiographs

	Changes in shadows on chest radiographs			p value
	improved	unchanged	worsened	
Gender	–	–	–	0.32
Age[a]	50	52	54	0.32
sACE activity	27.1	19.6	27.2	0.017*
BAL lymphocyte, %	11.8	37.7	59.3	0.20
BAL CD4/CD8 ratio	7.18	3.90	11.1	0.56
Stage on chest radiographs	–	–	–	0.17
Extrathoracic lesions	–	–	–	0.083
IL-1ra/IL-1β ratio	6.56	0.99	2.93	0.014*
$sACE_{LAST}/sACE_{BAL}$ ratio	0.62	0.91	0.75	0.033*
$\%VC_{LAST}/\%VC_{BAL}$ ratio	1.04	1.01	0.99	0.31
$FEV1.0\%_{LAST}/FEV1.0\%_{BAL}$ ratio	0.97	0.94	0.98	0.81
$DLCO\%_{LAST}/DLCO\%_{BAL}$ ratio	0.95	0.98	1.03	0.42

Age, sACE, BAL lymphocyte (%), BAL CD4/CD8 ratio, stage on chest radiographs, extrathoracic lesions and IL-1ra/IL-1β ratio at the time of BAL. Data were analyzed using nonparametric median test. * = Statistical significance.

[a] Median value.

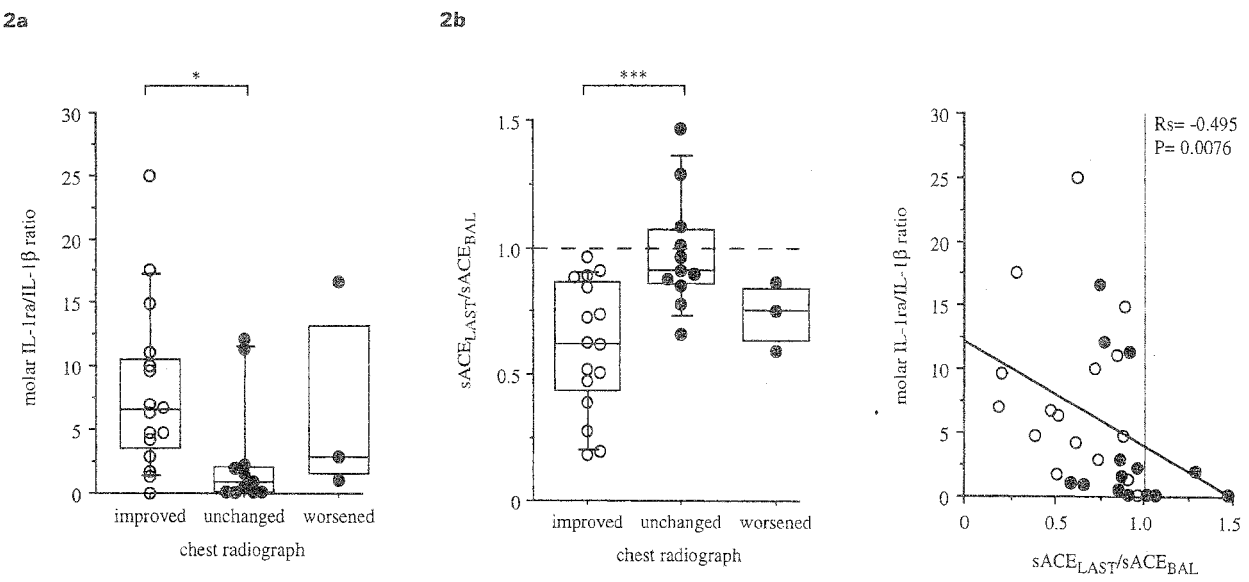

Fig. 2. Relationship between the molar IL-1ra/IL-1β ratio at the time of BAL (**a**), changes in sACE activity (sACE$_{LAST}$/sACE$_{BAL}$) (**b**), and changes on chest radiograph 4 years after BAL in sarcoidosis patients. Symbols are the same as those used in figure 1. *p < 0.05; ***p < 0.005.

Fig. 3. Correlation between the molar IL-1ra/IL-1β ratio at the time of BAL and changes in sACE activity (sACE$_{LAST}$/sACE$_{BAL}$) in sarcoidosis patients during the observation periods. Symbols are the same as those used in figure 1.

changed [0.99 (range 0.12–2.17), p = 0.017, fig. 2a]. In addition, a negative correlation was found between the IL-1ra/IL-1β ratio and changes in sACE activity (sACE$_{LAST}$/sACE$_{BAL}$: Rs = –0.495, p = 0.0076, fig. 3) during the observation periods. The sACE$_{LAST}$/sACE$_{BAL}$ ratio was lower in the patients whose chest radiographs were improved 4 years after BAL [0.623 (range 0.434–0.865)] than in those whose chest radiographs remained unchanged [0.914 (range 0.858–1.069), p = 0.0016, fig. 2b].

Correlation with Clinical Data at the Time of BAL and Changes in Disease Activity during the Observation Periods

The IL-1ra/IL-1β ratio at the time of BAL correlated well with improvements of shadows on chest radiographs (p = 0.0143), %VC (p = 0.027), and sACE activity (p = 0.0076) during the observation periods. However, age, gender, BALF lymphocyte percent, CD4/CD8 ratio, stage on chest radiographs (I, II, III), the number of patients having extrathoracic lesions, and the number of organs involved at the time of BAL showed no correlations with changes on chest radiographs, changes in sACE activity, or changes in pulmonary function (tables 3, 4).

Discussion

In this study, we prospectively evaluated the significance of the molar IL-1ra/IL-1β ratio in the culture supernatants of BALF macrophages as a prognostic factor in patients with pulmonary sarcoidosis. This ratio was more broadly distributed in sarcoidosis patients than in healthy nonsmokers. Higher ratios correlated with improvements of chest radiographic findings, %VC and sACE activity, and lower ratios correlated with a persistence of shadows and serial increases in sACE activity. Thus, unlike BALF cell findings such as cell differentials and the CD4/CD8 ratio, the molar IL-1ra/IL-1β ratio was found to be useful as a prognostic factor related to chronicity, but not to deterioration.

The following description of disease activity was drafted at the consensus conference (Los Angeles, 1993) [21]: disease activity is different from the total extent of the disease such as number of organs involved, and it should not be mistaken for the outcome of disease. However, some markers of activity may have the additional benefit of being prognostic factors indicating disease outcome. Unfortunately, there is no single test available at present which at the time of diagnosis would accurately predict the likelihood of disease progression.

The ratio of IL-1ra/IL-1β in the BALF macrophage culture supernatants was identified as a feasible marker of activity based on our previous studies [17–19]. In this study, we focused on the significance of the IL-1ra/IL-1β ratio as a putative, single prognostic marker and compared this ratio with several other established markers of activity such as chest radiographic findings, pulmonary function and sACE activity. We factored out the effect of current smoking in the parameters examined by selecting only nonsmokers.

We selected chest radiographic findings (BHL and parenchymal opacities) as traditional markers since we can cite our own evidence of the clinical courses based on the clearance rates of the shadows [22]. According to our experience, among 337 sarcoidosis patients observed for more than 10 years from the time of detection, 72% showed an improvement on chest radiographs at 5 years after detection, while 24% of the patients showed persistence of shadows at 10 years. The clearance rate of the shadows from 5 to 10 years after the detection was small (4%) [22]. Accordingly, sarcoidosis patients with pulmonary lesions with more than 5 years' duration can be evaluated as chronic cases.

The IL-1ra/IL-1β ratio predicted chronicity, but it could not easily predict a subpopulation of chronic cases likely to show deterioration. Lung function tests, particularly VC, FEV1.0, and DLCO, are useful in determining treatment indications. Baseline function tests do not yield useful information on the probability of disease progression, and there is only a loose correlation between results of lung function tests and chest radiography [21, 23]. In our study, we confirmed that while there was a positive correlation between improvement of the IL-1ra/IL-1β ratio and improvement of %VC and a negative correlation between reduced sACE activity and changes in both %VC and %DLCO, there was no correlation between the improvement of chest radiographs and improvement of pulmonary function.

sACE activity was evaluated as a macrophage/granuloma-associated marker of disease activity of sarcoidosis in the WASOG meeting in 1993 [21]. sACE levels probably reflect the total-body granuloma burden and help to maintain the inflammation [24, 25]. As ACE gene polymorphism could influence the sACE activity, sACE activity measured at one point is not a reliable marker of disease activity of sarcoidosis [26–28]. Therefore, we used the changes of sACE activity from the time of BAL to the time of final evaluation as an index.

It should be stressed that the one-point measurement of the IL-1ra/IL-1β ratio predicts changes in indexes of disease activity related to a chronicity (but not deterioration) such as chest radiographic findings, pulmonary function tests (%VC), and sACE activity in patients with pulmonary sarcoidosis. A prognostic factor which relates specifically to deterioration and not chronicity may be present. Though it is absolutely critical to know factors which predict deterioration, we should recognize that since cases which deteriorated emerge from chronic sarcoidosis cases, it is also important to recognize which patients with pulmonary sarcoidosis enter into the chronic stage within 5 years.

The roles of cytokines and their regulatory mediators in the persistence of the inflammation are still subject to debate. In our previous study, a low-grade inflammation with no detectable burst of cytokine release, a condition which cannot be found in ARDS, was found in chronic interstitial lung disease [17, 29]. In a low-grade inflammation of this type, a decrease in regulatory mediators seems to have significance.

In conclusion, the IL-1ra/IL-1β ratio at the one-point measurement was identified not only as a feasible marker of disease activity, but also as a prognostic marker predicting clinical changes in chest radiographs,%VC, and sACE activities in patients with pulmonary sarcoidosis.

Acknowledgments

We would like to express our thanks to Mr. Simon A. Johnson for checking linguistic problems, to Ms. F. Tanioka and Ms. M. Yamada for their technical help, and to Dr. N. Satake for performing BAL. This study was supported by a grant from the Smoking Research Foundation in Japan and a Grant-in-Aid for Medical Science Research (No. 06670610) from the Ministry of Education, Japan.

References

1 James DG: Clinical picture of sarcoidosis; in Schwarz MI, King TE Jr (eds): Interstitial Lung Disease. St Louis, Mosby Year Book, 1993, pp 159–178.

2 Turner-Warwick M: Treatment of pulmonary sarcoidosis. State of art; in Grassi C, Rizzato G, Pozzi E (eds): Sarcoidosis and Other Granulomatous Disorders. Amsterdam, Elsevier, 1988, pp 621–629.

3 Hunninghake GW, Gadek JE, Young R Jr, Kawanami O, Ferrans VJ, Crystal RG: Maintenance of granuloma formation in pulmonary sarcoidosis by T lymphocytes within the lung. N Engl J Med 1980;302:594–598.

4 Hunninghake GW, Crystal RG: Pulmonary sarcoidosis: A disorder mediated by excess helper T lymphocyte activity at sites of disease activity. N Engl J Med 1981;305:429–434.

5 Nagai S, Izumi T: Pulmonary sarcoidosis: Population differences and pathophysiology. South Med J 1995;88:1001–1010.

6 Newman LS, Rose CS, Marier LA: Sarcoidosis. N Engl J Med 1997;336:1224–1234.

7 Costabel U, Bross KJ, Guzman J, Nilles A, Ruhle KH, Matthys H: Predictive value of bronchoalveolar lavage T cell subsets for the course of pulmonary sarcoidosis. Ann NY Acad Sci 1986;465:418–426.

8 Ward K, O'Connor C, Odlum C, Fitzgerald MX: Prognostic value of bronchoalveolar lavage in sarcoidosis: The critical influence of disease presentation. Thorax 1989;44:6–12.

9 Mornex JF, Leroux C, Greenland T, Ecochard D: From granuloma to fibrosis in interstitial lung diseases: Molecular and cellular interactions. Eur Respir J 1994;7:779–785.

10 Hunninghake GW, Garrett KC, Richerson HB, Fantone JC, Ward PA, Rennard SI, Bitterman PB, Crystal RG: Pathogenesis of the granulomatous lung diseases. Am Rev Respir Dis 1984;130:476–496.

11 Hunninghake GW, Glazier AJ, Monick M, Dinarello CA: Interleukin-1 is a chemotactic factor for human T-lymphocytes. Am Rev Respir Dis 1987;135:66–71.

12 Kobayashi K, Allred C, Cohen S, Yoshida T: Role of interleukin-1 in experimental pulmonary granuloma in mice. J Immunol 1985;134:358–364.

13 Boros DL: Experimental granulomatosis. Clin Dermatol 1986;4:10–21.

14 Hunninghake GW: Release of interleukin-1 by alveolar macrophages of patients with active sarcoidosis. Am Rev Respir Med 1984;129:569–572.

15 Hannum CH, Wilcox CJ, Arend WP, Joslin FG, Dripps DJ, Heimdal PL, Armes LG, Sommer A, Eisenberg SP, Thompson RC: Interleukin-1 receptor antagonist activity of a human interleukin-1 inhibitor. Nature 1990;343:336–340.

16 Nagai S, Takeuchi M, Watanabe K, Aung H, Izumi T: Smoking and interleukin-1 activity released from human alveolar macrophages in healthy subjects. Chest 1988;94:694–700.

17 Nagai S, Aung H, Takeuchi M, Kusume K, Izumi T: IL-1 and IL-1 inhibitory activity in the culture supernatants of alveolar macrophages from patients with interstitial lung diseases. Chest 1991;99:674–680.

18 Takeuchi M, Nagai S, Nakada H, Aung H, Satake N, Kaneshima H, Izumi T: Characterization of interleukin-1 inhibitory factor released from human alveolar macrophages as IL-1 receptor antagonist. Clin Exp Immunol 1992;88:181–187.

19 Mikuniya T, Nagai S, Shimoji T, Takeuchi M, Morita K, Mio T, Satake N, Izumi T: Quantitative evaluation of the IL-1β and IL-1 receptor antagonist obtained from BALF macrophages in patients with interstitial lung diseases. Sarcoidosis Vasc Diffuse Lung Dis 1997;14:39–45.

20 Abacus Concepts. Statview. Berkeley, Abacus Concepts, 1992.

21 Costabel U: Consensus conference: Activity of sarcoidosis. Eur Respir J 1994;7:624–627.

22 Nagai S, Shigematsu M, Hamada K, Izumi T: Clinical courses and prognosis of pulmonary sarcoidosis. Curr Opin Pulm Med 1999;5:293–298.

23 Loddenkemper R, Kloppenborg A, Schoenfeld N, Grosser H, Costabel U: Clinical findings in 715 patients with newly detected pulmonary sarcoidosis. Sarcoidosis Vasc Diffuse Lung Dis 1998;15:178–182.

24 Nagai S, Izumi T, Takeuchi M, Watanabe K, Oshima S: The effect of angiotensin II on the accessory function of BALF macrophages – a possible autostimulatory mechanism of T lymphocyte alveolitis in sarcoidosis; in Grassi C, Rizzato G, Pozzi E (eds): Sarcoidosis and Other Granulomatous Disorders. Amsterdam, Excerpta Medica, 1988, pp 129–134.

25 Nagai S, Takeuchi M, Morita K, Mikuniya T, Satake N, Mio T, Izumi T: Angiotensin II receptor on BALF macrophages from Japanese patients with active sarcoidosis. Sarcoidosis Vasc Diffuse Lung Dis 1999;16:67–74.

26 Arbustini E, Grasso M, Leo G, Tinelli C, Fasani R, Diegoli M, Banchieri N, Cipriani A, Gorrini M, Semenzato G, Luisetti M: Polymorphism of angiotensin-converting enzyme gene in sarcoidosis. Am J Respir Crit Care Med 1996;153:851–854.

27 Maliarik MJ, Rybicki BA, Malvitz E, Sheffer RG, Major M, Popovich J Jr, Iannuzzi MC: Angiotensin-converting enzyme gene polymorphism and risk of sarcoidosis. Am J Respir Crit Care Med 1998;158:1566–1570.

28 Takemoto Y, Sakatani M, Takami S, Tachibana T, Higaki J, Ogihara T, Miki T, Katsuya T, Tsuchiyama T, Yoshida A, Yu H, Tanio Y, Umeda E: Association between angiotensin II receptor gene polymorphism and serum angiotensin converting enzyme (SACE) activity in patients with sarcoidosis. Thorax 1998;53:459–462.

29 Jacobs RF, Tabor DR, Burks AW, Campbell GD: Elevated interleukin-1 release by human alveolar macrophages during the adult respiratory distress syndrome. Am Rev Respir Dis 1989;140:1686–1692.

[CANCER RESEARCH 61, 950–956, February 1, 2001]

High Density *O*-Glycosylation of the MUC2 Tandem Repeat Unit by *N*-Acetylgalactosaminyltransferase-3 in Colonic Adenocarcinoma Extracts[1]

Mizue Inoue, Shuji Takahashi, Ikuo Yamashina, Masaki Kaibori, Tadayoshi Okumura, Yasuo Kamiyama, Sophie Vichier-Guerre, Danièle Cantacuzène, and Hiroshi Nakada[2]

Department of Biotechnology, Faculty of Engineering, Kyoto Sangyo University, Kyoto 603-8555, Japan [M. I., S. T., I. Y., H. N.]; First Department of Surgery [M. K., Y. K.] and Department of Medical Chemistry [T. O.], Kansai Medical University, Osaka 570-8506, Japan; and Unite de Chimie Organique, Institut Pasteur, Paris 75724, France [S. V-G., D. C.]

ABSTRACT

A synthetic peptide corresponding to the human MUC2 tandem repeat unit was glycosylated *in vitro* using UDP-GalNAc and extracts of colonic adenocarcinoma and paired normal mucosa, followed by fractionation of the products by reverse phase high-performance liquid chromatography. Several peaks of glycopeptides with different numbers of GalNAc residues attached were detected. It is notable that the adenocarcinoma extract was capable of glycosylating peptides to a much greater extent than was normal mucosa. The levels of mRNA for *N*-acetylgalactosaminyltransferases-1, -2, and -3 were determined by reverse transcription-PCR. Only *N*-acetylgalactosaminyltransferase-3 mRNA was expressed at a higher level in the adenocarcinoma than in the normal tissue. When the MUC2 tandem repeat peptide was glycosylated with a mixture of the normal mucosa extract and recombinant *N*-acetylgalactosaminyltransferase-3, larger amounts of glycopeptides with higher contents of GalNAc residues were produced. The MUC2 tandem repeat peptides glycosylated extensively by recombinant *N*-acetylgalactosaminyltransferase-1, -2, or -3 were prepared and characterized. Substitution at each Thr residue, as revealed by Edman degradation sequencing, in conjunction with evidence obtained on mass spectrometry indicated a heterogeneous pattern of site-specific glycosylation within the MUC2 tandem repeat. It was found that maximum numbers of 6, 8, and 11 GalNAc residues were incorporated by *N*-acetylgalactosaminyltransferases-1, -2, and -3, respectively, and that only *N*-acetylgalactosaminyltransferase-3 could completely glycosylate both consecutive sequences composed of three and five Thr residues in the MUC2 tandem repeat unit. These results suggest that *O*-glycosylation of the clustered Thr residues is a selective process controlled by *N*-acetylgalactosaminyltransferase-3 in the synthesis of clustered carbohydrate antigens.

INTRODUCTION

Mucins are high molecular weight glycoproteins characterized by many *O*-linked oligosaccharides to the core polypeptide through Ser or Thr residues. Generally, tumor-associated carbohydrate antigens are produced through incomplete synthesis of carbohydrate chains, which causes the accumulation of precursor forms, or through neosynthesis of carbohydrate chains through the activation of certain glycosyltransferases. The former involves Tn and T antigens and their sialylated counterparts, sialylTn and sialylT antigens. Carbohydrate chains related to blood group antigens are involved in the latter (1, 2).

We have prepared some monoclonal antibodies against a human colorectal cancer cell line, LS 180, and demonstrated that they are strongly reactive only with clustered *O*-glycans on peptide. For instance, the epitopic structures for anti-Tn and anti-sialylTn antibodies comprise three and four consecutive sequences of GalNAc-Ser/Thr and SAα2–6GalNAc-Ser/Thr, respectively (3–6). The clustering of a relatively common structure could lead to the formation of an uncommon structure exhibiting antigenicity. Although the roles of these truncated *O*-glycans in malignant behavior are not well understood, they are highly immunogenic and useful as a vaccine (7, 8). Therefore, it is important to elucidate a biosynthetic mechanism of clustered *O*-glycans aligned on a core peptide.

In a previous studies (3–5, 9), we reported that an extract of LS 180 cells glycosylated the MUC2 tandem repeat peptide *in vitro*, leading to the synthesis of Tn antigenic sites recognized by a monoclonal antibody (MLS 128), indicating the synthesis of clustered Thr-GalNAc.

Many mucins contain a large number of Thr and Ser residues within their tandem repeat domains, which include consecutive Thr/Ser residues except for MUC1 (10). The initial step in the regulation of *O*-glycosylation is the enzymatic transfer of GalNAc from UDP-GalNAc to Thr and Ser residues (11, 12). It is well known that there are multiple GalNAc-Ts[3] expressed in various tissues (13). Thus, GalNAc transferases that regulate the initiation of *O*-glycosylation of mucins are important for understanding some aspects of tumor-associated aberrant *O*-glycosylation.

We used a synthetic peptide of MUC2 tandem repeat unit and extracts from a human colonic adenocarcinoma and paired normal mucosa and rGalNAc-Ts as a substrate and enzyme sources, respectively. Because MUC2 is a major secreted mucin of intestinal epithelia, and its tandem repeat unit contains two consecutive parts consisting of three and five Thr residues that potentially serve as a scaffold presenting clustered carbohydrate antigens (14).

Because the *O*-glycosylation of one site of a peptide may have some effects on other acceptor sites, we used a whole unit of the MUC2 tandem repeat as a substrate. The peptide was conjugated with DABITC, which has absorbance at 436 nm, to monitor the glycosylated peptides on reverse-phase HPLC. We determined the glycosylated sites of glycopeptides with the maximum number of GalNAc residues incorporated by combining evidence from MALDI-TOF mass spectrometry with sequence data from Edman degradation. First, we found a remarkable difference between glycopeptides synthesized with extracts of colonic adenocarcinoma and with paired normal mucosa. The adenocarcinoma extract glycosylated the peptide to a greater extent than that of the normal mucosa, probably due to enhanced expression of GalNAc-T3. Next, the peptide glycosylated by rGalNAc-T1, -T2, and -T3 was prepared. Maximum numbers of 6, 8, and 11 GalNAc residues were transferred to the peptide by

Received 4/24/00; accepted 11/29/00.

The costs of publication of this article were defrayed in part by the payment of page charges. This article must therefore be hereby marked *advertisement* in accordance with 18 U.S.C. Section 1734 solely to indicate this fact.

[1] Supported in part by Grant-in-Aid for Scientific Research on Priority Areas 10178102 from the Ministry of Education, Science and Culture of Japan; by the Foundation for Bio-venture Research Center from the Ministry of Education, Science and Culture of Japan; and by the Fugaku Trust for Medicinal Research.

[2] To whom requests for reprints should be addressed, at Department of Biotechnology, Faculty of Engineering, Kyoto Sangyo University, Kita-ku, Kyoto 603-8555, Japan. Phone: 81-75-705-1897; Fax: 81-75-705-1888; E-mail: hnakada@cc.kyoto-su.ac.jp.

[3] The abbreviations used are: GalNAc-T, UDP-GalNAc:polypeptide *N*-acetylgalactosaminyltransferase; rGalNAc-T, recombinant GalNAc-T; HPLC, high-performance liquid chromatography; MALDI-TOF, matrix-assisted laser desorption/ionization time of flight mass spectrometry; DABITC, 4-*N*,*N*-dimethylaminoazobenzene-4-isothiocyanate; RT-PCR, reverse transcription-PCR; PTH, phenylthiohydantoin.

rGalNAc-T1, -T2, and -T3, respectively, and both the consecutive Thr residues were fully glycosylated by rGalNAc-T3 but not by rGalNAc-T1 or -T2.

MATERIALS AND METHODS

Materials. A synthetic peptide, AAMAPTTTPITTTTTVTPTPTPTGTQT, was obtained from Kurabo (Osaka, Japan). DABITC was purchased from Nacarai Tesque (Kyoto, Japan). Expression vector pSecTaq was from Invitrogen (San Diego, CA). A reference glycopeptide ($KGGGGS_{GalNAc}TT_{GalNAc}GGG$) was synthesized as described previously (15).

Cells. A human colorectal cancer cell line, LS 180, was obtained from the American Type Culture Collection and cultured in Eagle's MEM supplemented with 10% FCS.

Preparation of Adenocarcinoma and Normal Mucosa Extracts. A fresh colonic adenocarcinoma and normal mucosa taken at a distance of more than 10 cm from the adenocarcinoma were frozen immediately after surgery with liquid nitrogen. Five adenocarcinomas and paired normal mucosae were always processed in parallel. Extracts of adenocarcinoma and normal mucosa were obtained as follows. The tissues were homogenized in 25 mM phosphate buffer (pH 7.5) and 0.15 M NaCl with a Bio-Mixer, and the resultant lysate was centrifuged at 1,000 × *g* for 10 min. The supernatant was sonicated for 1 min and then centrifuged at 10,000 × *g* for 10 min. The supernatant was further centrifuged at 105,000 × *g* for 1 h. After solubilization with 2% octylglucoside, 2 mM phenylmethylsulfonyl fluoride, and 0.1 M Tris-HCl buffer (pH 7.4), the pellet was centrifuged at 105,000 × *g* for 1 h, and the resultant supernatant was used as the enzyme source.

RT-PCR of GalNAc-Ts. Preparation of total RNA from colonic adenocarcinoma and paired normal mucosa was performed using Isogen (Nippon Gene, Toyama, Japan) according to the manufacturer's instruction. Total RNA (1 μg) was reverse transcribed using a reaction mixture comprising 5 mM $MgCl_2$, 1 mM deoxynucleotide triphosphate mixture, 1 unit/μl RNase inhibitor, 1 μM oligodeoxythymidylic acid primer, and 0.25 unit/μl reverse transcriptase in a final volume of 20 μl. The mixture was incubated at 55°C for 40 min, at 99°C for 5 min, and then at 5°C for 5 min. The cDNA was then subjected to PCR. To obtain semiquantitative results, the cycle number and cDNA concentration were chosen so as to ensure that the amplification was not in the plateau phase. For GalNAc-T1 and -T2, 20, 26, and 30 cycles were performed, and for GalNAc-T3, 30, 35, and 40 cycles were performed. The cDNA amplification of GalNAc-Ts and β-actin was performed at the same time. The reaction mixture comprised 2.5 mM $MgCl_2$, 20 pM forward and reverse primers, and 2.5 units of TaKaRa Taq (TaKaRa, Tokyo, Japan) in a final volume of 100 μl. The forward and reverse primers used and the expected product sizes were as follows: (*a*) for GalNAc-T1, 5′-CAAAAGCCTCATGAAGGTCC-3′ and 5′-ACCCGCCATAGGTCATGT-3′, 321 bp; (*b*) for GalNAc-T2, 5′-TGGCGGGTGGATCTGCCGGC-3′ and 5′-TCTAGGTTTTCTCCTCCCCA-3′, 600 bp; (*c*) for GalNAc-T3, 5′-ACAGCAGCAGAATTGAAGCC-3′ and 5′-TTAATCATTTTGGCTAAGTA-3′, 1594 bp; and (*d*) for β-actin, 5′-ATGGATGATGATATCGCCGC-3′ and 5′-ATAGGAATCCTTCTGACCCA-3′, 291 bp. After a polymerase activation step at 94°C for 5 min, samples were amplified for the indicated numbers of cycles of denaturation at 94°C for 1 min, annealing at 55°C for 30 s, and extension at 74°C for 1 min. The amplified cDNAs were run on 1% agarose gels with 0.5 μg/ml ethidium bromide and visualized under UV light.

Preparation of rGalNAc-Ts. Total RNA was prepared from LS 180 cells using Isogen as described above. cDNAs encoding the putative ectodomains of rGalNAc-T1, -T2, and -T3 flanked by artificial sites for *Bam*HI and *Eco*RV (rGalNAc-T1) and *Bam*HI and *Xba*I (rGalNAc-T2 and -T3) were amplified by PCR. The PCR-generated DNAs were digested with *Bam*HI and *Eco*RV for rGalNAc-T1 or with *Bam*HI and *Xba*I for rGalNAc-T2 and -T3 and then inserted into expression vector pSecTag containing an immunoglobulin κ chain leader sequence, a *myc* epitope, and a polyhistidine tag. The constructed plasmid (pSecTag-rGalNAc-T1, -T2, and -T3) was introduced into TOP10F′ cells and amplified according to the manufacturer's instructions, and then COS-7 cells were transfected with pSecTag-rGalNAc-T1, -T2, and -T3 by the lipofection method. The culture medium was dialyzed against 25 mM phosphate buffer (pH 7.8) and 15 mM NaCl and then subjected to DEAE-cellulose column chromatography. This step was necessary to exclude endogenously synthesized GalNAc transferases. The excluded fraction was applied to a ProBond column, washed with 20 mM phosphate buffer (pH 7.8) and 0.5 M NaCl, and then eluted with 0.3 M imidazole, 0.5 M NaCl, and 20 mM phosphate buffer (pH 6.0). Finally, rGalNAc-Ts were prepared on an immunoaffinity column using anti-*myc*/His antibodies according to the manufacturer's instructions.

Transfer of GalNAc to a Synthetic Peptide. A synthetic peptide including 1 unit of the MUC2 tandem repeat was conjugated with DABITC as described by Chang (16). The incubation mixture comprised 5 mM $MgCl_2$, 5 mM 2-mercaptoethanol, 5 mM CDP-choline, 43 nmol of UDP-GalNAc, 4 μg of DABITC-MUC2 peptide, and an appropriate amount of a tissue extract or rGalNAc-Ts in a final volume of 100 μl. The mixture was incubated at 37°C for the times indicated in Figs. 1, 3, and 4.

Fractionation of the Glycopeptides. The glycosylated products were directly subjected to reverse phase HPLC, and elution was carried out with a linear gradient of 0–100% acetonitrile in 10 mM ammonium acetate buffer (pH 5.0) at a flow rate of 1 ml/min. Elution of the product was monitored by absorbance at 436 nm.

Mass Spectrometry of the Glycopeptides. Mass spectra of the glycopeptides were obtained by MALDI-TOF mass spectrometry (Kratos Analytical, Manchester). Samples (10 pmol) dissolved in 1 μl of distilled water were placed on a stainless steel probe tip along with 1 μl of the matrix (2,5-dihydroxybenzoin acid in 0.1% trifluoroacetic acid/acetonitrile, 7:3). Measurements were performed in the linear mode using an appropriate delay time and a potential to focus the ions of interest.

Identification of *O*-Glycosylation Sites of the Glycopeptides. The glycopeptides were degraded with cyanogen bromide (17) and then purified by the

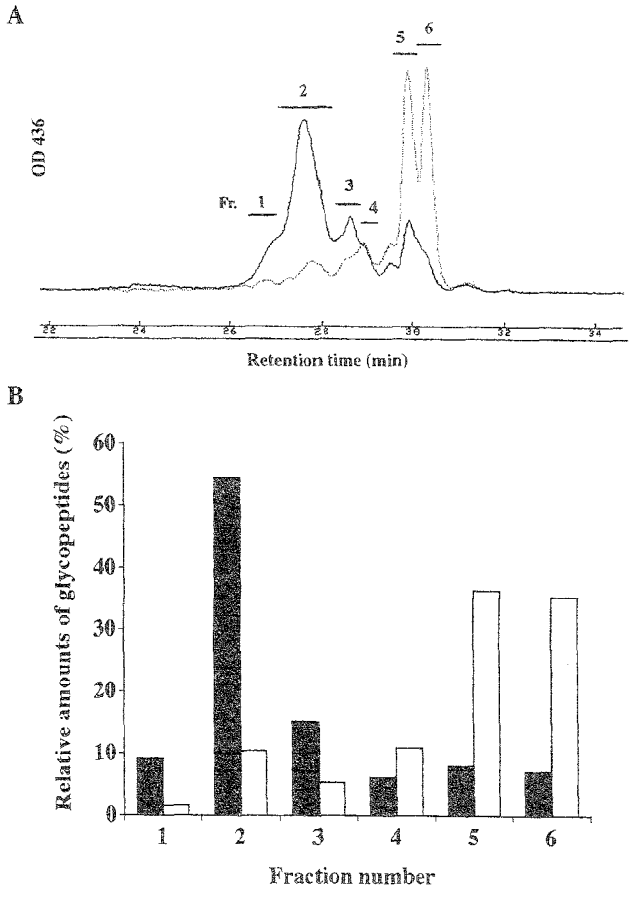

Fig. 1. Reverse phase chromatography of MUC2 peptides glycosylated by an extract of a colonic adenocarcinoma or paired normal mucosa. The MUC2 peptides were glycosylated with an extract of a colonic adenocarcinoma or paired normal mucosa at 37°C for 1 h as described in "Materials and Methods." The reaction products were directly subjected to reverse phase HPLC and fractionated (*A*; *solid line*, adenocarcinoma; *dashed line*, normal mucosa). The relative amounts of the glycopeptides in each fraction are compared (*B*). The vertical axis shows the percentage of each fraction as to the total area (■, adenocarcinoma; □, normal tissue).

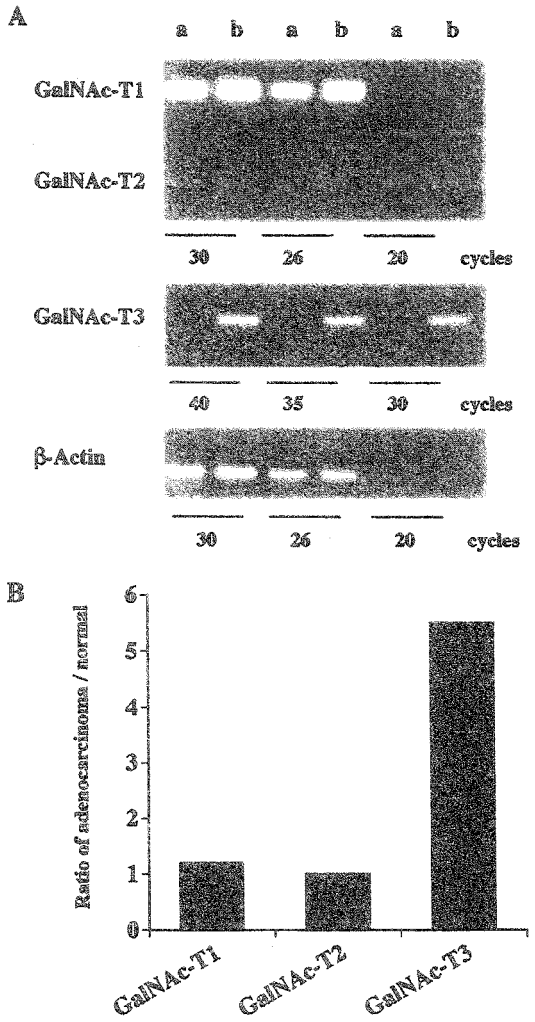

Fig. 2. RT-PCR analysis of GalNAc-T1, -T2, and -T3 mRNA expression in colonic adenocarcinoma and normal mucosa. Total RNA was prepared from a colonic adenocarcinoma (*Lanes b*) and paired normal mucosa (*Lanes a*), which are the same specimens used in Fig. 1. cDNA was amplified by various numbers of cycles. For GalNAc-T1 and -T2 and β-actin, 20, 26, and 30 cycles were performed, and for GalNAc-T3, 30, 35, and 40 cycles were performed, and these products were subjected to agarose gel electrophoresis (*A*). The mRNA levels determined with a densitometer were normalized relative to the level of β-actin mRNAs. The ratio of GalNAc-Ts mRNA prepared from the adenocarcinoma and paired normal mucosa is shown in *B*. The ratio is derived from the data obtained from the products amplified by 26 cycles for GalNAc-T1 and -T2 and β-actin and 35 cycles for GalNAc-T3.

same reverse phase HPLC. Pulsed liquid phase Edman degradation amino acid sequencing was performed with a Procise 492 protein sequencer (PE Biosystems, Foster City, CA). *O*-Glycosylation sites were determined by elution profile of PTH-Thr-GalNAc, which are eluted as two diastereotopic peaks at unique positions on the chromatogram as reported by Gerken *et al.* (18).

RESULTS

GalNAc-Ts Activity and mRNA in Colonic Adenocarcinoma and Paired Normal Mucosa. The transfer of GalNAc to the peptide was investigated *in vitro* using the MUC2 tandem repeat unit containing 14 Thr residues and extracts of colonic adenocarcinoma and normal mucosa as described in "Materials and Methods."

To detect the products directly, the synthetic peptide was conjugated with DABITC, which exhibits absorbance at 436 nm. Furthermore, as described in "Materials and Methods," four amino acids including Met were inserted between DABITC and the NH_2-terminal of the MUC2 tandem repeat to minimize the influence of DABITC and to exclude DABITC released through cyanogen bromide degradation after fractionation of the glycopeptides. The effects of various assay parameters (cell extract, MUC2 peptide, and UDP-GalNAc) were evaluated, and appropriate conditions were selected. Five colonic adenocarcinomas and paired normal mucosae were examined. Fig. 1 shows a representative elution pattern on HPLC of the glycopeptides synthesized by the adenocarcinoma or normal mucosa extract. The nonglycosylated DABITC-MUC2 peptide was eluted at 30.5 min (fraction 6). Other fractions (fractions 1–5) contained glycopeptides with various numbers of GalNAc residues transferred. The peaks that eluted faster (fractions 1 and 2) contained glycopeptides with higher contents of GalNAc residues and showed the clustered Tn antigenicity, as reported previously (9). It is notable that the adenocarcinoma extract could transfer GalNAc to the MUC2 peptide to a much higher extent compared with that of the normal paired mucosa, as shown in Fig. 1, *A* and *B*.

Expression of GalNAc-T1, -T2, and -T3 mRNA was analyzed semiquantitatively by RT-PCR. Representative results for the same specimen seen in Fig. 1 are shown in Fig. 2. The mRNA levels for all GalNAc-T probes were quantified with a densitometer and normalized relative to the level of β-actin mRNA. It was found that the level of GalNAc-T3 mRNA in an adenocarcinoma was significantly higher than that in the paired normal mucosa.

Incorporation of GalNAc to the MUC2 tandem repeat unit and level of GalNAc-T1, T2, T3 mRNA were analyzed similarly by using other four adenocarcinomas and paired normal mucosae as summarized in Table 1. Because fractions 1 and 2 in Fig. 1 contained the clustered Tn antigenicity as reported previously (9), the relative activity producing the clustered GalNAc-Thr is shown by comparing the area of fractions 1 and 2.

The area for adenocarcinomas in fractions 1 and 2 increased about 4-fold compared with that of paired normal mucosa. The relative level of GalNAc-T3 mRNA also increased significantly (about 10-fold) in adenocarcinomas, whereas the relative levels of GalNAc-T1 and -T2 mRNA increased slightly.

Characterization of the MUC2 Peptide Glycosylated by rGalNAc-Ts. It is generally agreed that there are multiple polypeptide GalNAc-Ts expressed in various tissues (13). It was interesting to determine which GalNAc-T is responsible for the synthesis of clustered carbohydrate antigens. GalNAc-T1, -T2, and -T3 have been cloned and extensively characterized (19–22). rGalNAc-Ts were prepared as described in "Materials and Methods." Each enzyme was subjected to SDS-PAGE followed by Western blotting. After staining through successive incubation with anti-*myc*/His antibodies and protein G-peroxidase, the relative amounts of the enzymes were determined with a densitometer. Bands corresponding to molecular weights of 79,000 73,000, and 85,000 were detected in the rGalNAc-T1, -T2, and -T3 lanes, respectively (data not shown). These molecular weights were larger than the sizes expected from the cDNAs inserted in the vector, and this difference was probably due to glycosylation during the synthesis in COS-7 cells.

The MUC2 tandem repeat unit conjugated with DABITC was incubated with each rGalNAc-T for up to 5 days to determine the maximal number of GalNAc residues transferred and identify the sites

Table 1 *Relative amount of glycopeptides with the Tn antigenicity and level of GalNAc-Ts mRNA in colonic adenocarcinoma and paired normal mucosa*

	Area[a]	GalNAc-T1[b]	GalNAc-T2[b]	GalNAc-T3[b]
Ratio[c]	4.16 ± 2.20	1.40 ± 0.26	1.68 ± 0.73	10.85 ± 5.66

[a] Amount of glycopeptides with the Tn antigenicity is compared by the area of fractions 1 and 2 as shown in Fig. 1. These fractions contained clustered GalNAc-Thr residue with the Tn antigenicity.
[b] Relative mRNA level is compared as shown in Fig. 2.
[c] All values (mean ± SD) are normalized relative to those of paired normal mucosa.

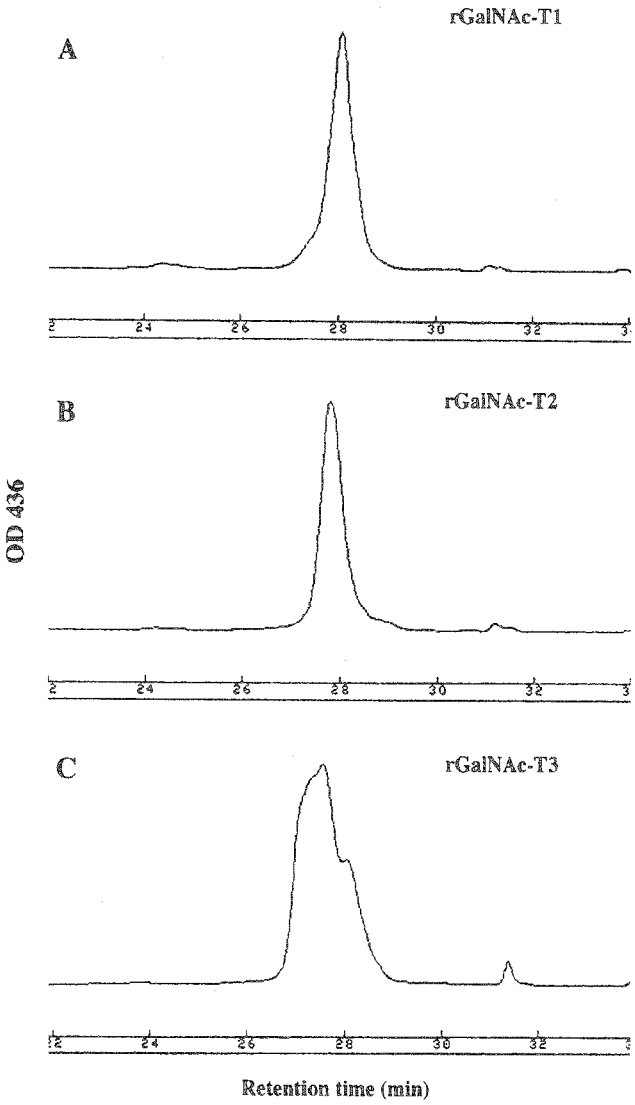

Fig. 3. Glycosylation of the MUC2 peptide by rGalNAc-T1, -T2, and -T3. The MUC2 peptide was incubated with rGalNAc-T1 (*A*), -T2 (*B*), or -T3 (*C*) for 5 days, with enzyme supplementation every day. The products were subjected to reverse phase HPLC as described in "Materials and Methods."

of *O*-glycosylation. The glycopeptides synthesized with the recombinant enzymes were directly subjected to reverse phase HPLC, as shown in Fig. 3. Although the glycopeptides synthesized with rGalNAc-T1 and -T2 gave symmetrical peaks with apparent retention times of 28.07 and 27.32 min, respectively (Fig. 3, *A* and *B*), they contained glycopeptides with a few different numbers of incorporated GalNAc residues, as described later. The elution pattern of the peptides glycosylated by rGalNAc-T3 showed a broad peak even on incubation for 5 days (Fig. 3*C*). The peak was tentatively divided into three fractions. The first fraction eluted at about 27.20 min was purified by reverse phase HPLC.

The DABITC-glycopeptides and -peptide were analyzed by MALDI-TOF mass spectrometry, as shown in Fig. 4. Peaks *a*–*c* and *d* showed DABITC-glycopeptides synthesized by GalNAc-Ts and DABITC-peptides, respectively. Peak *a*, which corresponds to the highest molecular weight synthesized by rGalNAc-T1, showed a M_r of 4177.8, corresponding to the addition of six GalNAc residues to the peptide (Fig. 4*A*). Peptides with five or four GalNAc residues attached were also observed in the lower molecular weight region. The maximum numbers of GalNAc residues incorporated by rGalNAc-T2 and -T3 were calculated to be 8 and 11 from the molecular weights of 4582.3 (peak *b*) and 5187.0 (peak *c*), respectively, as shown in Fig. 4, *B* and *C*. To exclude DABITC, the glycopeptides were degraded by cyanogen bromide treatment and purified again by the same reverse phase HPLC. To analyze the glycopeptides with a maximum number of incorporated GalNAc residues, the first peak with a symmetrical elution profile was subjected to analysis by an amino acid sequencer. It has been reported that PTH-Thr/Ser-GalNAc derivatives are eluted as two diastereotopic peaks at unique positions on the chromatogram (18). To determine the retention time of PTH-Thr-GalNAc in our system, we used a reference glycopeptide containing Ser_{GalNAc}-Thr-Thr_{GalNAc} (Fig. 5). Chromatography of PTH-Thr-GalNAc gave two peaks eluted at 5.24 min (peak *T**) and 5.94 min (peak *T***). The

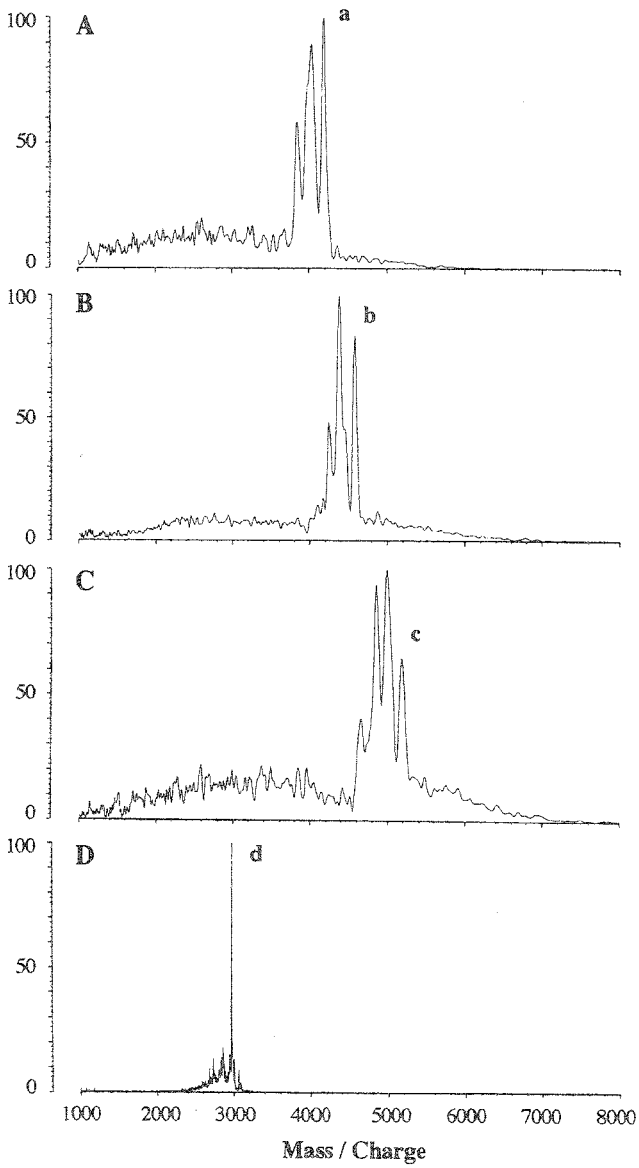

Fig. 4. MALDI-TOF mass spectra of glycopeptides. *A* and *B* show the mass spectra of the MUC2 peptide glycosylated by rGalNAc-T1 and -T2, respectively, and prepared by reverse phase HPLC as described in the Fig. 3 legend. The MUC2 peptides glycosylated by rGalNAc-T3 were subjected to reverse phase HPLC as described in the Fig. 3 legend, and the broad peak was tentatively divided into three fractions. The fraction eluted first, after rechromatography on the same column, was analyzed by MALDI-TOF mass spectrometry (*C*). The molecular weights corresponding to peaks *a*–*c*, the materials in which the maximum number of GalNAc residues incorporated, were estimated to be 4177.8, 4582.3, and 5187.0, respectively. *D* shows mass spectra of nonglycosylated DABITC-peptide (peak *d*), which was estimated to be 2964.9.

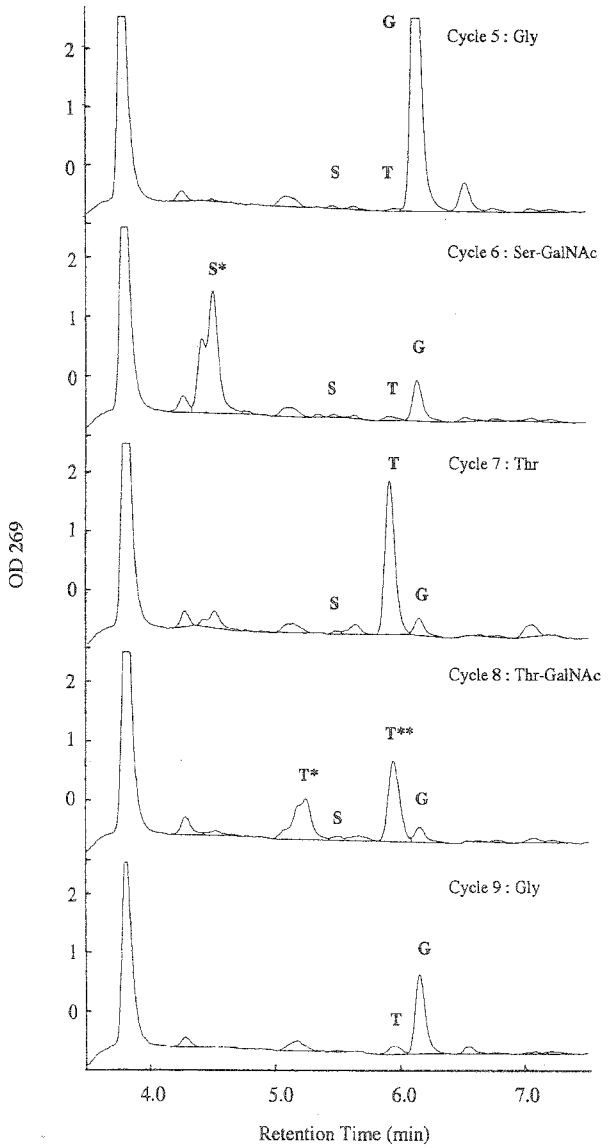

Fig. 5. Amino acid sequencing chromatography of a reference glycopeptide. A reference glycopeptide was analyzed with a Procise 492 protein sequencer. Chromatograms for cycles 6 and 8 show the elution profiles of peaks derived from PTH-Ser-GalNAc and PTH-Thr-GalNAc, respectively. PTH-Thr (*T*) was eluted at 5.91 min, and two peaks (*T** and *T***) derived from PTH-Thr-GalNAc were eluted at 5.24 and 5.94 min.

second peak was slightly behind the peak of PTH-Thr (retention time, 5.91 min) on the chromatogram. Based on these data, the sites of *O*-glycosylation were determined. Fig. 6 shows the relative areas of the peaks (T*) derived from the PTH-Thr-GalNAc at each cycle. Based on the amount of the first peak (T*) and the retention time of the second peak (T**), we determined the *O*-glycosylation sites to be the Thr-2, -4, -10, -11, -13, and –15; the Thr-2, -4, -8, -10, -11, -15, -17, and –19; and the Thr-2, -3, -4, -7, -8, -9, -10, -11, -15, -17, and -19 residues of the MUC2 peptides glycosylated by GalNAc-T1, -T2, and -T3, respectively. In addition to these *O*-glycosylation sites, two Thr residues, *i.e.*, Thr-13 (Fig. 6*B*) and Thr-21 (Fig. 6*C*), appeared to be poorly glycosylated in some cases.

DISCUSSION

Aberrant glycosylation of the core portion of *O*-glycans produces two kinds of immunogenic structures recognized by various monoclonal antibodies.

One is an unmasked core peptide produced by decreased glycosylation. MUC1 on breast cancer cells has been characterized by this unmasked core peptide and is assumed to permit preferential interaction with cytotoxic lymphocytes (23, 24). In contrast to these hypoglycosylation, Muller *et al.* (25) demonstrated that breast cancer cell line T47D glycosylates the MUC1 tandem repeat peptide at a higher density than lactating breast epithelia. This discrepancy may be explained by the finding (26) that a specific GalNAc-T named GalNAc-T4 is responsible for the glycosylation of the PDTR motif within the MUC1 tandem repeat peptide. Thus, the expression of these epitope structures seems to be dependent on the expression of particular GalNAc-Ts but not on the decrease or increase of generally expressed GalNAc-Ts.

Another is a truncated *O*-glycan, in which Tn and T antigens and their sialylated counterparts, sialylTn and sialylT antigens, are involved. Many mucins (except for MUC1) have unique tandem repeats containing consecutive Ser/Thr residues. MUC2 potentially serves as a scaffold, presenting a variety of carbohydrate epitopes on its abundant Thr residues. Byrd *et al.* (27) reported that 78% of the Thr residues are glycosylated in the LS 174T colon carcinoma cell line. However, whether or not the degree of glycosylation changes due to malignancy and how clustered *O*-glycosylation occurs have not been studied in detail. We have shown that the antigenic sites of the Tn and

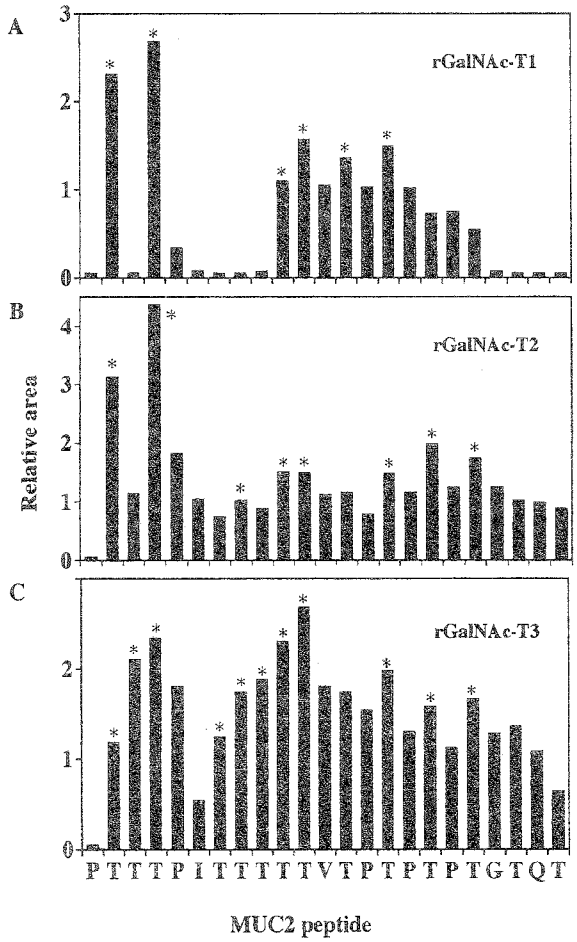

Fig. 6. Representative analysis of *O*-glycosylation sites on the MUC2 peptide. Glycopeptides prepared as described in Fig. 3 were degraded with cyanogen bromide and then subjected to rechromatography on a reverse phase column. The MUC2 peptide with the maximum number of GalNAc incorporated by rGalNAc-T1 (*A*), -T2 (*B*), or -T3 (*C*) was analyzed with a Procise 492 protein sequencer. The material in the peak derived from PTH-Thr-GalNAc with a retention time of 5.24 min was quantitated at each cycle, and its relative amount is shown as a histogram. *Asterisks* indicate *O*-glycosylation sites.

sialylTn antigens are built up clusters of GalNAc-Ser/Thr and SAα2–6GalNAc-Ser/Thr, respectively (3–6). Although the function of these antigens is not understood, their increased expression has some correlation to advanced malignancy. It has been reported that about 73% and 96% of human colon cancers express the Tn and sialylTn antigens, respectively (28).

The present study was designed to compare the glycosylation of the MUC2 peptide by extracts of colonic adenocarcinoma and paired normal mucosa and to determine which GalNAc-Ts are relevant to the synthesis of consecutive Thr-GalNAcs. Our previous work showed that microsomal membranes of LS 180 cells glycosylated the MUC2 tandem repeat peptide, leading to the synthesis of clustered Tn epitopes, and the peptide glycosylated most extensively was determined to be a glycopeptide with 11 attached GalNAc residues. It is notable that the colonic adenocarcinoma extract exhibited a higher level of enzyme activity than did the normal mucosa (Fig. 1). In addition, as judged from the elution profile of the glycopeptides on reverse phase HPLC, the colonic adenocarcinoma extract could glycosylate the peptide at the same level as the microsomal membranes of LS 180 cells, as reported previously (9).

First, we estimated the expression of GalNAc-T mRNA semiquantitatively by RT-PCR. Only GalNAc-T3 mRNA was elevated remarkably in the colonic adenocarcinoma, whereas the level of GalNAc-T1 and -T2 mRNA increased slightly (Fig. 2 and Table 1), and these findings were consistent with previous reports that in all human organs examined, GalNAc-T1 and -T2 are expressed universally at low to moderate levels, but that the expression of GalNAc-T3 mRNA is highly tissue specific (19, 21, 22, 29). GalNAc-T4 was expressed at a very low level in both adenocarcinoma and normal mucosa (data not shown). These results prompted us to examine whether or not GalNAc-T3 could glycosylate the MUC2 peptide more extensively than the other enzymes could. Although *O*-glycosylation on the MUC1 tandem repeat unit has been studied extensively (25, 30, 31), little is known about the *O*-glycosylation sites on the MUC2 peptide. Iida *et al.* (32) demonstrated the acceptor specificity of rGalNAc-T1, -T2, and -T3 toward a short peptide, PTTTLK, mimicking a part of the MUC2 tandem repeat unit, in which rGalNAc-T3 was shown to have a unique acceptor specificity differing from those of rGalNAc-T1 and -T2. Because substrate activity is significantly influenced by certain aspects of the primary amino acid sequence in the region adjoining the glycosylated position, it seems to be preferable to use a long peptide as a substrate within the range to be analyzed. In fact, Nishimori *et al.* (31) reported that the length for an enzyme-substrate interaction may extend to at least nine residues, and minimum activity is seen with substrates with one residue on the NH_2-terminal side and four residues to the COOH-terminal side. In addition, Hanisch *et al.* (33) also demonstrated that the initial glycosylation of a peptide substrate influences its subsequent glycosylation, including both vicinal and distal glycosylation sites. Therefore, we used the whole MUC2 tandem repeat composed of 23 amino acid residues as a substrate.

The MUC2 peptide was glycosylated extensively on incubation with rGalNAc-T1, -T2, and -T3 for a long period with daily supplementation of the recombinant enzymes. Although the potential glycosylation sites were glycosylated completely or almost completely, the products comprised several glycopeptides with different numbers of incorporated GalNAc residues, as shown in Fig. 4.

Muller *et al.* (25) reported that glycosylation of the tandem repeat peptides within individual MUC1 molecules is not uniform. However, the multiple Thr residues seem to be glycosylated in an ordered manner, at least under the experimental conditions used in which the peptides are glycosylated by a single enzyme *in vitro*. The fact that a preferential order for the incorporation of GalNAc to the Thr residues of the MUC2 peptide exists (32) supports this view. Although the order remains to be elucidated, it was clearly demonstrated that rGalNAc-T3 could glycosylate the MUC2 peptide most extensively, including both consecutive parts composed of three and five Thr residues (Fig. 6). This distinct substrate specificity of rGalNAc-T3 is very significant in light of the fact that in contrast to the universal expression of GalNAc-T1 and -T2 mRNA in all human organs and malignant cells, GalNAc-T3 shows a quite unique expression pattern. These results are also consistent with previous reports (30, 32), which found that although there is overlapping of acceptor-substrate specificities due to some redundant functions of these enzymes, each enzyme gives a specific pattern of glycosylated Thr residues on the MUC2 peptide.

It has been reported that GalNAc-T3 is differentially expressed by adenocarcinoma cell lines, with a tendency for more differentiated cell lines to express it more extensively (29). More detailed analysis to determine the glycosylation pattern on the MUC2 peptide by using various adenocarcinomas differentiated to various degrees is necessary.

Recently, Bennett *et al.* (34) demonstrated that a new isozyme, designated GalNAc-T6, exhibits a similar substrate specificity to GalNAc-T3. GalNAc-T3 and probably GalNAc-T6 are essential for glycosylating consecutive Thr residues, which might play significant roles in the expression of not only clustered tumor-associated carbohydrate antigens but also of carbohydrate ligands for cellular lectins.

REFERENCES

1. Hull, S. R., Bright, A., Carraway, K. L., Abe, M., Hayes, D. F., and Kufe, D. W. Oligosaccharide differences in the DF3 sialomucin antigen from normal human milk and the BT-20 human breast carcinoma cell line. Cancer Commun., *1:* 261–267, 1989.
2. Ho, S. B., and Kim, Y. S. Carbohydrate antigens on cancer-associated mucin-like molecules. Semin. Cancer Biol., *2:* 389–400, 1991.
3. Nakada, H., Numata, Y., Inoue, M., Tanaka, N., Kitagawa, H., Funakoshi, I., Fukui, S., and Yamashina, I. Elucidation of an essential structure recognized by an anti-GalNAcα-Ser(Thr) monoclonal antibody (MLS 128). J. Biol. Chem., *266:* 12402–12406, 1991.
4. Nakada, H., Inoue, M., Numata, Y., Tanaka, N., Funakoshi, I., Fukui, S., Mellors, A., and Yamashina, I. Epitopic structure of Tn glycophorin A for an anti-Tn antibody (MLS 128). Proc. Natl. Acad. Sci. USA, *90:* 2495–2499, 1993.
5. Inoue, M., Nakada, H., Tanaka, N., and Yamashina, I. Tn antigen is expressed on leukosialin from T-lymphoid cells. Cancer Res., *54:* 85–88, 1994.
6. Tanaka, N., Nakada, H., Inoue, M., and Yamashina, I. Binding characteristics of an anti-Siaα2–6GalNAcα-Ser/Thr (sialyl Tn) monoclonal antibody (MLS 132). Eur. J. Biochem., *263:* 27–32, 1999.
7. MacLean, G. D., Reddish, M., Koganty, R. R., Wong, T., Gandhi, S., Smolenski, M., Samuel, J., Nabholtz, J. M., and Longenecker, B. M. Immunization of breast cancer patients using a synthetic sialyl-Tn glycoconjugate plus Detox adjuvant. Cancer Immunol. Immunother., *36:* 215–222, 1993.
8. Lo-Man, R., Bay, S., Vichier-Guerre, S., Deriaud, E., Cantacuzene, D., and Leclerc, C. A fully synthetic immunogen carrying a carcinoma-associated carbohydrate for active specific immunotherapy. Cancer Res., *59:* 1520–1524, 1999.
9. Inoue, M., Yamashina, I., and Nakada, H. Glycosylation of the tandem repeat unit of the MUC2 polypeptide leading to the synthesis of the Tn antigen. Biochem. Biophys. Res. Commun., *245:* 23–27, 1998.
10. Kim, Y. S., Gum, J., Jr., and Brockhausen, I. Mucin glycoproteins in neoplasia. Glycoconj. J., *13:* 693–707, 1996.
11. Hagopian, S., and Eylar, E. H. Glycoprotein biosynthesis: the purification and characterization of a polypeptide: *N*-acetylgalactosaminyltransferase from bovine submaxillary glands. Arch. Biochem. Biophys., *129:* 515–524, 1969.
12. Sugiura, M., Kawasaki, T., and Yamashina, I. Purification and characterization of UDP-GalNAc:polypeptide N-acetylgalactosamine transferase from an ascites hepatoma, AH 66. J. Biol. Chem., *257:* 9501–9507, 1982.
13. Clausen, H., and Bennet, E. P. A family of UDP-GalNAc:polypeptide *N*-acetylgalactosaminyltransferases control the initiation of mucin-type *O*-linked glycosylation. Glycobiology, *6:* 635–646, 1996.
14. Gum, J. R., Byrd, J. C., Hicks, J. W., Toribara, N. W., Lamport, D. T., and Kim, Y. S. Molecular cloning of human intestinal mucin cDNAs. Sequence analysis and evidence for genetic polymorphism. J. Biol. Chem., *264:* 6480–6487, 1989.
15. Vichier-Guerre, S., Lo-Man, R., Bay, S., Deriaud, E., Nakada, H., Leclerc, C., and Cantacuzene, D. Short synthetic glycopeptides successfully induce antibody responses to carcinoma-associated Tn antigen. J. Peptide Res., *55:* 173–180, 2000.
16. Chang, J. Y. Isolation and characterization of polypeptide at the picomole level. Pre-column formation of peptide derivatives with dimethylaminoazobenzene isothiocyanate. Biochem. J., *199:* 537–545, 1981.

17. Edmundson, A. B. Cleavage of sperm whale myoglobin with cyanogen bromide. Nature (Lond.), *198:* 354–357, 1963.
18. Gerken, T. A., Owens, C. L., and Pasumarthy, M. Determination of the site-specific *O*-glycosylation pattern of the porcine submaxillary mucin tandem repeat glycopeptide. J. Biol. Chem., *272:* 9709–9719, 1997.
19. Homa, F. L., Hollander, T., Lehman, D. J., Thomsen, O. R., and Elhammer, A. P. Isolation and expression of a cDNA clone encoding a bovine UDP-GalNAc:polypeptide *N*-acetylgalactosaminyltransferase. J. Biol. Chem., *268:* 12609–12616, 1993.
20. Hagen, F. K., Van Wuyckhuyse, B., and Tabak, L. A. Purification, cloning, and expression of a bovine UDP-GalNAc:polypeptide *N*-acetyl-galactosaminyltransferase. J. Biol. Chem., *268:* 18960–18965, 1993.
21. White, T., Bennett, E. P., Takio, K., Sorensen, T., Bonding, N., and Clausen, H. Purification and cDNA cloning of a human UDP-*N*-acetyl-α-D-galactosamine: polypeptide *N*-acetylgalactosaminyltransferase. J. Biol. Chem., *270:* 24156–24165, 1995.
22. Bennett, E. P., Hassan, H., and Clausen, H. cDNA cloning and expression of a novel human UDP-*N*-acetyl-α-D-galactosamine. J. Biol. Chem., *271:* 17006–17012, 1996.
23. Barnd, D. L., Lan, M. S., Metzgar, R. S., and Finn, O. J. Specific, major histocompatibility complex-unrestricted recognition of tumor associated mucins by human cytotoxic T cells. Proc. Natl. Acad. Sci. USA, *86:* 7159–7163, 1989.
24. Gendler, S. J., Spicer, A. P., Lalani, E. N., Duhig, T., Peat, N., Burchell, J., Pemberton, L., Boshell, M., and Taylor-Papadimitriou, J. Structure and biology of a carcinoma-associated mucin, MUC1. Am. Rev. Respir. Dis., *144:* S42–S47, 1991.
25. Muller, S., Alving, K., Peter-Katalinic, J., Eachara, N., Gooley, A. A., and Hanisch, F. G. High density *O*-glycosylation on tandem repeat peptide from secretory MUC1 of T47D breast cancer cells. J. Biol. Chem., *274:* 18165–18172, 1999.
26. Bennett, E. P., Hassan, H., Mandel, U., Mirgorodskaya, E., Roepstorff, P., Burchell, J., Taylor-Papadimitriou, J., Hollingsworth, M. A., Merdx, G., van Kessel, A. G., Eiberg, H., Steffensen, R., and Clausen, H. Cloning of a human UDP-*N*-acetyl-α-D-galactosamine:polypeptide *N*-acetylgalactosaminyltransferase that complements other GalNAc-transferases in complete *O*-glycosylation of the MUC1 tandem repeat. J. Biol. Chem., *273:* 30472–30481, 1998.
27. Byrd, J. C., Nardelli, J., Siddiqui, B., and Kim, Y. S. Isolation and characterization of colon cancer mucin from xenografts of LS 174T cells. Cancer Res., *48:* 6678–6685, 1988.
28. Itkowitz, S. H., Yuan, M., Montgomery, C. K., Kjeldsen, T., Takahashi, H. K., Bigbee, W. L., and Kim, Y. S. Expression of Tn, sialosyl-Tn, and T antigens in human colon cancer. Cancer Res., *49:* 197–204, 1989.
29. Sutherlin, M. E., Nishimori, I., Caffrey, T., Bennett, E. P., Hassan, H., Mandel, U., Mack, D., Iwamura, T., Clausen, H., and Hollingsworth, M. A. Expression of three UDP-*N*-acetyl-α-D-galactosamine:polypeptide *N*-acetylgalactosaminyltransferases in adenocarcinoma cell lines. Cancer Res., *57:* 4744–4748, 1997.
30. Wandall, H. H., Hassan, H., Mirgorodskaya, I., Kristensen, A. K., Roepstorff, P., Bennett, E. P., Nielsen, P. A., Hollingsworth, M. A., Burchell, J., Taylor-Papadimitriou, J., and Clausen, H. Substrate specificities of three members of the human UDP-GalNAc:polypeptide *N*-acetylgalactosaminyltransferase family, GalNAc-T1, -T2, and -T3. J. Biol. Chem., *272:* 23503–23514, 1997.
31. Nishimori, I., Johnson, N. R., Sanderson, S. D., Perini, F., Mountjoy, K., Cerny, R. L., Gross, M. L., and Hollingsworth, M. A. Influence of acceptor substrate primary amino acid sequence on the activity of human UDP-*N*-acetylgalactosamine:polypeptide *N*-acetylgalactosaminyltransferase. J. Biol. Chem., *269:* 16123–16130, 1994.
32. Iida, S., Takeuchi, H., Hassan, H., Clausen, H., and Irimura, T. Incorporation of *N*-acetylgalactosamine into consecutive threonine residues in MUC2 tandem repeat by recombinant human *N*-acetyl-D-galactosamine transferase-T1, T2 and T3. FEBS Lett., *449:* 230–234, 1999.
33. Hanisch, F. G., Muller, S., Hassan, H., Clausen, H., Zachara, N., Gooley, A. A., Paulsen, H., Alving, K., and Peter-Katalinic, J. Dynamic epigenic regulation of initial *O*-glycosylation by UDP-*N*-acetylgalactosamine:polypeptide *N*-acetylgalactosaminyltransferases. J. Biol. Chem., *274:* 9946–9954, 1999.
34. Bennett, E. P., Hassan, H., Mande, U., Hollingsworth, M. A., Akisawa, N., Ikematsu, Y., Merkx, G., Kessel, A. G. V., Olofsson, S., and Clausen, H. Cloning and characterization of a close homologue of human UDP-*N*-acetyl-α D-galactosamine: polypeptide *N*-acetylgalactosaminyltransferase-T3 designated GalNAc-T6. J. Biol. Chem., *274:* 25362–25370, 1999.

Journal of Neuroscience Research 65:595–603 (2001)

Developmental Expression of a Unique Carbohydrate Antigen, Tn Antigen, in Mouse Central Nervous Tissues

Kaoru Akita,[1] Shinji Fushiki,[2] Takahiro Fujimoto,[1] Mizue Inoue,[1] Kayoko Oguri,[3] Minoru Okayama,[1] Ikuo Yamashina,[1] and Hiroshi Nakada[1]*

[1]Department of Biotechnology, Faculty of Engineering, Kyoto Sangyo University, Kyoto, Japan
[2]Department of Pathology and Applied Neurobiology, Research Institute for Neurological Diseases and Geriatrics, Kyoto Prefectural University of Medicine, Kyoto, Japan
[3]Clinical Research Institute, National Nagoya Hospital, Nagoya, Japan

Using an anti-Tn monoclonal antibody, the Tn antigen was detected immunohistochemically in prenatal and early postnatal central nervous tissues. On embryonic day 9 (E9), the antigen was distributed throughout the single neuroepithelial layer in the neocortex and then became more prominent in the preplate than in the ventricular zone along with formation of the preplate. Following division of the preplate and concomitant formation of the cortical plate, distinct labeling of the neocortex occurred in the marginal, subplate and intermediate zones, whereas in the cortical plate and ventricular zone were virtually not immunostained. It is notable that thalamocortical afferent fibers were also immunostained specifically on E14. After birth, the localization of the antigen became less noticeable and by 3 weeks after birth, the antigen had substantially disappeared. In the developing cerebellum, prominent labeling was also observed in the molecular layer and outskirts of the cerebellar nuclei on early postnatal days. To characterize the glycoprotein bearing the Tn antigen biochemically, immunoblot analysis was performed. The glycoprotein, most of which was extracted with a salt solution, migrated as a broad smeared band corresponding to a molecular weight of about 250 kDa on SDS-PAGE. Among the various tissues examined, this glycoprotein was only detected in the brain and its amount increased until an early postnatal stage with a peak on postnatal day 3 (P3), and then decreased gradually with age. This spatially and developmentally regulated expression of the Tn antigen suggests that this antigen plays a significant role in brain development. J. Neurosci. Res. 65: 595–603, 2001. © 2001 Wiley-Liss, Inc.

Key words: Tn antigen; neural tube; cerebral cortex; cerebellum; thalamus

During development of the mammalian central nervous system, expression of various glycoconjugates or their carbohydrate chains are spatiotemporally regulated. It has been suggested that they are involved in various events in developing brain, including cell adhesion, cell migration, cell proliferation, fasciculation, axon outgrowth, synaptogenesis, and so on (Margolis and Margolis, 1993; Friedlander et al., 1994; Rutishauser and Landmesser, 1996; Hirschberg et al., 1996; Chou et al., 1998; Varki et al., 1999). It is generally agreed that a tumorigenically transformed state exhibits some similarity to embryonic stages. Tumor-associated carbohydrate antigens are produced through incomplete synthesis of carbohydrate chains, which causes the accumulation of precursor forms, or through neosynthesis of carbohydrate chains through the activation of certain glycosyltransferases. The former involves Tn and T antigens, and their sialylated counterparts, sialyl Tn and sialyl T antigens. The T and Tn antigen are normally cryptic in mucin due to sialylation or chain elongation and branching by addition of other sugar residues. Springer et al. (1974) recognized these structures as tumor-associated antigens. Carbohydrate chains related to blood group antigens are involved in the latter. Among these carbohydrate antigens, Lewis-X (SSEA-1) has been extensively studied and revealed to play a particular role in mediating the compaction of mouse embryos (Fenderson et al., 1984).

MLS 128, a monoclonal antibody recognizing a Tn antigen, was established by immunizing mice with a human colorectal cancer cell line, LS 180 cells (Numata et al., 1990). Using Tn glycophorin A, ovine submaxillary mucin and leukosialin, which are all reactive with MLS 128, we determined the antigenic structure to comprise three consecutive N-acetylgalactosamine (GalNAc) α 1-Thr/Ser residues as a minimum antigenic site (Nakada et al.,

Contract grant sponsor: Ministry of Education, Science, and Culture of Japan; Contract grant number: 10178102; Contract grant sponsor: Fugaku Trust for Medical Research.

*Correspondence to: Dr. Hiroshi Nakada, Department of Biotechnology, Faculty of Engineering, Kyoto Sangyo University, Kamigamo-Motoyama, Kita-ku, Kyoto 603-8555, Japan. E-mail: hnakada@cc.kyoto-su.ac.jp

Received 1 December 2000; Revised 9 March 2001; Accepted 13 March 2001

1991, 1993; Inoue et al., 1994). To our knowledge, the biological significance of incompletely synthesized carbohydrate chains such as the Tn antigen has not been elucidated yet.

The expression of the glycoconjugates bearing the GalNAc or galactose (Gal) terminated carbohydrate chains has been studied mainly with plant lectins (Momoi et al., 1986; Nakagawa et al., 1987; Naegele et al., 1990). *Vicia villosa* agglutinin (VVA) and *Peanut* agglutinin (PNA) recognize the Tn and T antigens, respectively. VVA, however, recognizes not only the Tn antigen but also the terminal α GalNAc residues of blood group A type antigens and terminal β GalNAc residues (Tollefsen and Kornfeld, 1983; Scott et al., 1988). Thus, a detailed study of the Tn antigen in terms of its spatiotemporal expression and its binding specificity is required to reveal its functional significance during nervous system development.

In this study, we demonstrate that the Tn antigen was expressed in embryonic and early postnatal mouse brains, in particular, in the developing cerebral cortex and cerebellum. Immunoblot analysis revealed that MLS 128 recognized a broad smeared band corresponding to a molecular weight of about 250 kDa. The antigen was expressed throughout all embryonic stages, its amount peaking around P3 and then decreasing gradually with age. Because it is generally agreed that murine cortical neurogenesis occurs largely from E10 to E17, and gliogenesis from E15 to early postnatal age (Jacobson, 1991), the precise timing of transient expression of the Tn antigen suggests that it might be involved in developmental events.

MATERIALS AND METHODS

Antibodies

A murine anti Tn monoclonal antibody, designated as MLS 128, was prepared as described previously (Numata et al., 1990). MLS 128 recognizes a glycopeptide including a cluster of GalNAc α 1-Thr/Ser residues but not a glycolipid (Numata et al., 1990; Nakada et al., 1991, 1993; Inoue et al., 1994). A murine monoclonal antibody, MLS 132, which recognizes sialyl-Tn antigen, was established as described previously (Tanaka et al., 1999). A rabbit polyclonal antibody against the cell adhesion molecule L1 was kindly provided by Dr. Carl Lagenaur (Department of Neurobiology, University of Pittsburgh).

Histochemical Study Using MLS 128 and a Lectin

ICR strain mice (SLC Inc, Shizuoka, Japan) were mated overnight. On the following day, females were examined for vaginal plugs. The day when a vaginal plug was found was designated as E0. Pregnant mice, of gestational ages 9–18 days, were killed under general anesthesia with diethyl ether and then the embryos or fetuses were removed from their uteri by means of cesarean section. The brains were rapidly removed and fixed overnight in Bouin's fixative at 4°C. Postnatal mice aged 3- and 7-days-old were sacrificed under general anesthesia with diethyl ether. These animals were transcardially perfused with the fixative and the removed brains were re-fixed in the same fixative overnight at 4°C. Each brain was then dehydrated through a graded series of ethanol concentrations and embedded in paraffin. Paraffin sections, 4 μm thick, were obtained with a microtome. After deparaffinization, the sections were treated with 0.3% hydrogen peroxide in absolute methanol for 15 min to block endogenous peroxidase activity, and then with rabbit normal serum. After incubation with MLS 128 (10 μg/ml) at room temperature for 2 hr and subsequent rinsing with PBS, the sections were incubated with horseradish peroxidase (HRP)-conjugated rabbit anti-mouse IgG immunoglobulin (Zymed, South San Francisco, CA) at the dilution of 1:200 in 1% bovine serum albumin (BSA)-PBS for 1 hr, washed with PBS, and then visualized with 0.03% 3,3′-diaminobenzidine tetrahydrochloride (DAB), 0.003% hydrogen peroxide and 10 mM imidazole in 50 mM Tris-HCl buffer, pH 7.6. To stain cell nuclei, sections were treated with hematoxylin. Control experiments were performed similarly using normal murine IgG_3 (Zymed) instead of MLS 128. Immunohistochemical staining for cell adhesion molecule L1 was carried out using Histofine ABC Rabbit kit (Nichirei, Tokyo, Japan).

The binding specificity of MLS 128 was examined as follows. Deparaffinized sections were incubated with 0.24 U of α-*N*-acetylgalactosaminidase from chicken liver (Sigma, St. Louis, MO) in 30 mM sodium citrate buffer, pH 4.0, for 20 hr at 37°C, washed extensively with PBS, and then stained as described above. The specificity of MLS 128 was also confirmed by incubation with MLS 128 in the presence of some monosaccharides and ovine submaxillary mucin, which contains the Tn antigen. Some of the sections were stained with a HRP-conjugated VVA (E.Y. Laboratories, San Mateo, CA) according to the manufacturer's instructions. It has been reported that VVA recognizes the terminal GalNAc residues of glycoconjugates including O-linked α GalNAc (Tn antigen) residues, terminal α GalNAc residues (blood group A), and β GalNAc residues (Cad/Sda) (Tollefsen and Kornfeld, 1983; Scott et al., 1988).

Western Blotting Analysis

Embryonic and postnatal mouse tissues were homogenized in 25 mM Tris-HCl buffer, pH 7.5, 0.1 M NaCl, 2 mM EDTA, 1 mM phenylmethylsulfonyl fluoride (PMSF), pepstatin A (1 μg/ml) and leupeptin (1 μg/ml), with a Polytron homogenizer, and then centrifuged at 105,000 × *g* for 1 hr. The extract was incubated with MLS 128 at 4°C for 15 hr and then protein G-Sepharose (Amersham Pharmacia Biotech) was added. The immunoprecipitate was subjected to SDS-PAGE followed by transfer to a Zeta-probe membrane (Bio-Rad, Hercules, CA) at 20 V for 15 hr. After blocking in 50 mM Tris-HCl buffer, pH 7.5, 5% BSA and 0.15 M NaCl (blocking solution) at 50°C for 8 hr, the membrane was incubated with MLS 128 (10 μg/ml) in the blocking solution at 4°C overnight, washed with 10 mM Tris-HCl, pH 7.4, 0.15 M NaCl and 0.05% Tween-20, and then incubated with HRP-conjugated protein G (Zymed) at the dilution of 1:5,000 in the same solution for 1 hr. The membrane, after washing with the above solution, was visualized with 0.03% DAB and 0.003% hydrogen peroxide in 15 mM phosphate buffer, pH 6.8, or with an enhanced chemiluminescence kit (Amersham Pharmacia Biotech). The densities of the immunoreactive bands were determined using an application of the NIH image program (NIH Image Version 1.62). The bind-

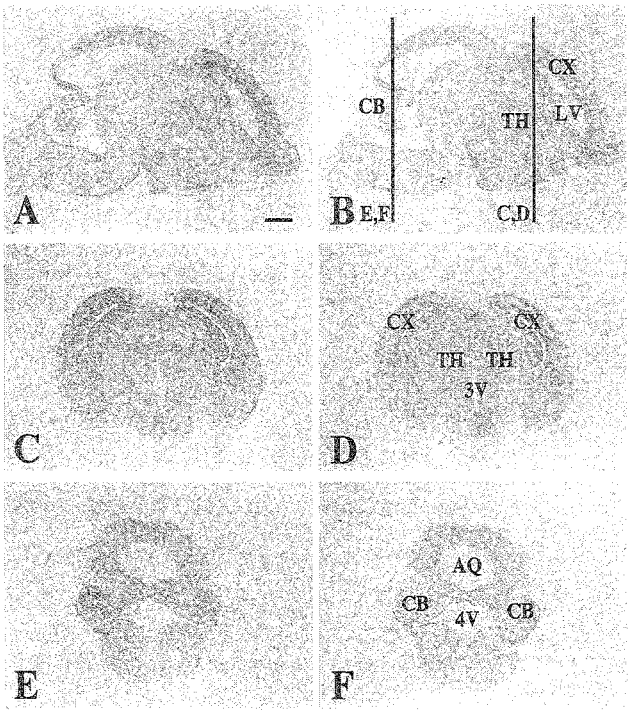

Fig. 1. Expression of the Tn antigen in E16 mouse brain. Paraffin sections of an E16 mouse brain through the parasagittal (**A**,**B**) and coronal (**C**–**F**) planes at the positions shown in B were incubated with MLS 128 (A,C,E) or normal mouse IgG (B,D,F). These sections were stained as described under Materials and Methods. Strong immunoreactivity was observed in the cerebral cortex (CX) and cerebellum (CB). The thalamus (TH) and tectum were stained moderately. The tissues were virtually not stained with normal mouse IgG (B,D,F). LV, lateral ventricle; 3V, third ventricle; 4V, fourth ventricle; AQ, aqueduct. Scale bar = 500 μm.

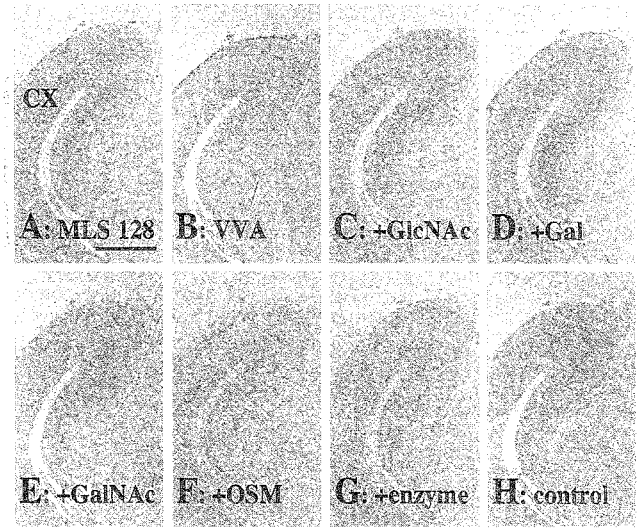

Fig. 2. Binding specificity of MLS 128 in the E16 mouse forebrain. Transverse sections through the E16 mouse forebrain were immunostained with MLS 128 in the absence (**A**) or presence of 100 mM GlcNAc (**C**), 100 mM Gal (**D**), 10 mM GalNAc (**E**), or 50 μg/ml ovine submaxillary mucin (**F**). The sections were treated with α-*N*-acetylgalactosaminidase (**G**) or digestion buffer (**H**), followed by immunostaining. To compare the staining patterns, the sections were also stained with VVA (**B**). The cerebral cortex (CX) was stained strongly with MLS 128 but only faintly with VVA. The immunostaining was hardly inhibited by GlcNAc and Gal, moderately by GalNAc, and completely by ovine submaxillary mucin. The Tn antigenicity disappeared on treatment with α-*N*-acetylgalactosaminidase. Scale bar = 500 μm.

ing of lectins to the blotted membrane was examined according to the manufacturer's instructions.

RESULTS

Immunostaining of Mouse Brains With an Anti-Tn MAb, MLS 128, and its Specificity

The expression of a couple of carbohydrate antigens was examined in mouse brains immunohistochemically using several monoclonal antibodies that recognize tumor-associated carbohydrate antigens carried by mucin-type glycoproteins. One of the monoclonal antibodies we examined, anti-Tn mAb, MLS 128, immunostained central nervous tissues. Figure 1 shows parasagittal and transverse sections of E16 mouse brains immunostained with MLS 128. It is notable that the Tn antigen was highly expressed in the cerebral cortex and cerebellum. The inferior colliculi and thalamus were immunolabeled to a moderate degree. To confirm the specificity of MLS 128, transverse sections of an E16 mouse forebrain were stained with MLS 128 and VVA (Fig. 2A,B). The cortex was stained intensely with MLS 128, as described above, but only faintly with VVA. Adjacent sections were immunostained in the presence of various sugars and ovine submaxillary mucin, which contains Tn antigenic sites, as described previously (Nakada et al., 1991). Figure 2C–F clearly show that the immunostaining was inhibited completely by ovine submaxillary mucin, partially by GalNAc, and hardly at all by *N*-acetylglucosamine (GlcNAc) and Gal, this being consistent with the fact that MLS 128 recognizes clustered GalNAc α 1-Thr/Ser residues specifically. Furthermore, immunostaining with MLS 128 significantly decreased on the treatment with α-*N*-acetylgalactosaminidase (Fig. 2G,H). These results clearly indicate that unique antigenic sites, clustered GalNAc α 1-Thr/Ser residues, are expressed in the developing mouse brain.

Localized Expression of the Tn Antigen in the Cerebral Cortex of Mouse Brains

First we investigated the cerebral cortex of mouse brains in detail, as shown in Figure 3. On E9, when the telencephalic anlage comprises a single neuroepithelial cell layer, the Tn antigen could be already detected around the neuroepithelial cells (Fig. 3A). The Tn antigen was evenly distributed throughout the layer at this stage. Immunolabeling for the Tn antigen on E12 was more prominent in the preplate than in the ventricular zone of the cerebral cortex (Fig. 3B). It is well known that the preplate splits

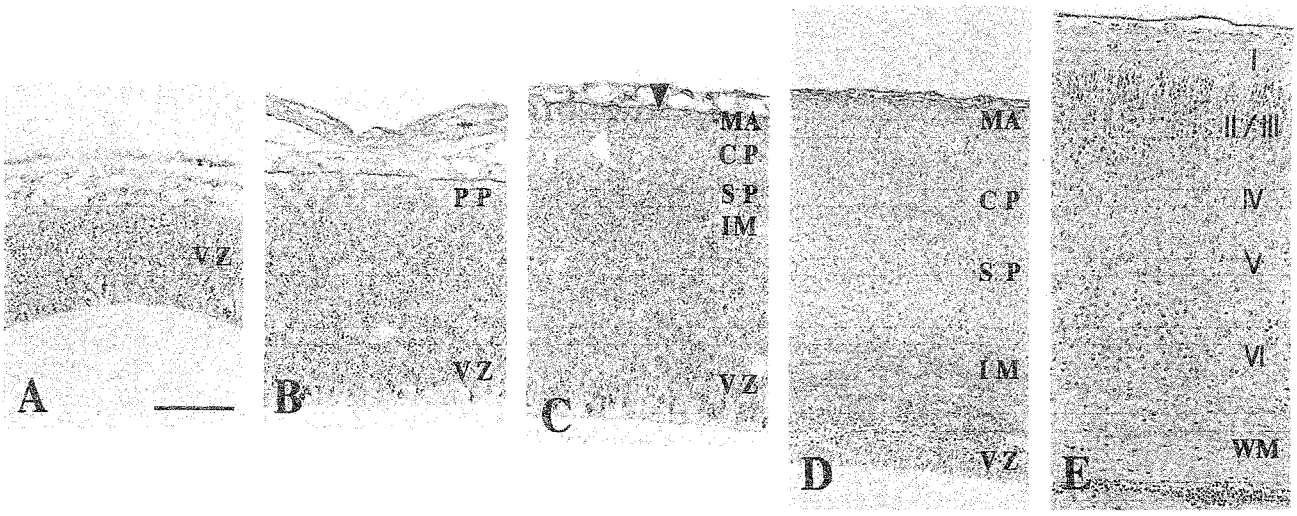

Fig. 3. Localization and temporal expression of the Tn antigen in the developing mouse cerebral cortex. On E9 (**A**), the Tn antigen was detected throughout the ventricular zone (VZ). On E12 (**B**), the immunoreactivity was prominent in the preplate (PP) and associated with fibers possibly originating from postomitotic neurons. On E14 (**C**), the Tn antigen was localized in the marginal zone (MA), subplate (SP), intermediate zone (IM), and pial membrane (arrowhead), but hardly in the cortical plate (CP) or ventricular zone. On E18 (**D**), the marginal and lower intermediate zones were strongly immunostained. On P3 (**E**), the Tn antigen had spread diffusely into all layers of the cerebral cortex, but layer I and the white matter (WM) were stained a little more intensely than the other layers. I–VI, cortical layers. Scale bar = 50 μm for A–C; 100 μm for D,E.

into the marginal zone and the subplate on cortical plate formation between these two zones. On E14, intense staining was observed in the marginal, subplate and intermediate zones (Fig. 3C). In contrast, the cortical plate and ventricular zone were virtually not immunostained. On E18, the Tn antigen was detected prominently in the marginal and lower intermediate zones (Fig. 3D). At early postnatal stages, the Tn antigen was detected mainly in the cortical layer I and the white matter, but the staining pattern was not so restricted to these particular layers as in embryonic stages (Fig. 3E).

Expression of the Tn Antigen on Thalamocortical Afferent Fibers

It is noteworthy that on E14, fibers coming from subcortical structures exhibited strong immunoreactivity for the Tn antigen (Fig. 4A,C). These fibers were distributed from the dorsal to the ventral thalamus and in the internal capsule. Association of the Tn-immunoreactivity with fiber bundles delineated the pathway of the fibers between the neocortex and thalamus, similar to that of cell adhesion molecule L1 (Fig. 4C,D). In the neocortex, these Tn-immunoreactive fibers extending from the internal capsule were found in the subplate (Fig. 4A). It appears likely that through the thalamocortical pathway on E14 mouse, Tn-bearing fibers from the thalamus invade the subplate of the neocortex and extend in the ventrolateral to dorsomedial direction within the subplate. On E18, however, the Tn antigen was barely detectable in the L1-positive thalamocortical fibers (Fig. 4B,E,F), indicating the extremely restricted expression of the Tn antigen.

Expression of the Tn Antigen in the Neural Tube

Immunostaining in developing neural tubes was also examined. On E9 neural tubes, the Tn antigen was detected in the basal lamina of lateral regions and on the cellular processes abutting lamina (data not shown). On E12, intense staining was observed in the marginal and mantle layers of the neural tube. The antigen was distributed more abundantly in dorsolateral region (Fig. 5A). Higher magnification of the lateral region, as shown in Figure 5B indicates that the antigen was mainly associated with neural projections in the marginal and mantle layers, and especially in the dorsal root entry zone. Dorsal root ganglion showed a hardly detectable level of the antigen throughout all prenatal stages. On E14, the overall staining had decreased and differences among regions were less noticeable (data not shown).

Distribution of the Tn Antigen in the Cerebellum

Tn immunoreactivity could also be found in the developing cerebellum. At prenatal stages, the Tn antigen was detected in the region adjacent to the ventricular zone and the immature molecular layer of the cerebellar primordium, but not in the ventricular and external granular layers (Fig. 6A). It is generally agreed that during postnatal stages the granular cells migrate from the external granular layer through the molecular layer to the internal granular layer. On P3, the Tn antigen was highly expressed in the molecular layer and outskirts of cerebellar nuclei (Fig. 6B,C). Some of this immunoreactivity appeared to be associated with fiber-like structures surrounding deep cer-

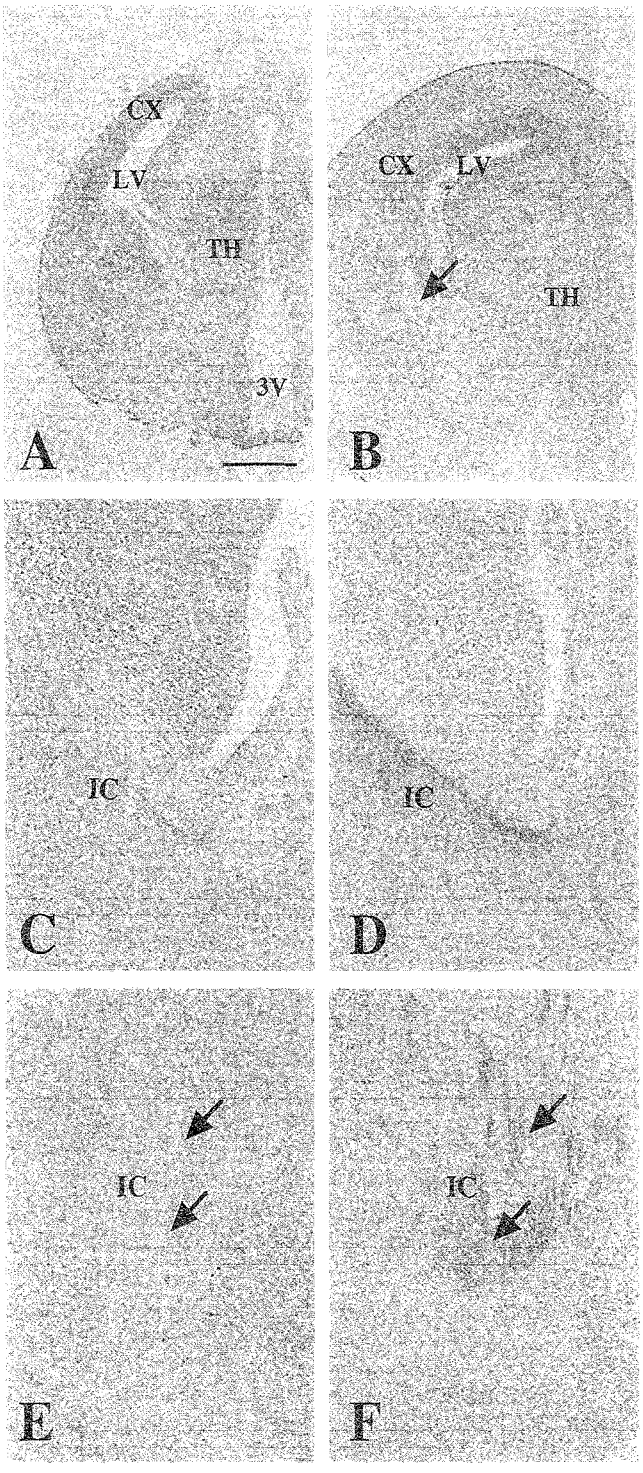

Fig. 4. Association of the Tn antigen with thalamocortical afferent fibers. Coronal sections of E14 and E18 mouse brains were immunostained with MLS 128 (**A–C,E**) and anti cell adhesion molecule L1 antibody (**D,F**). On E14, the Tn antigen was expressed on the thalamus (TH) and internal capsule (IC) in addition to the cerebral cortex (CX). The immunoreactivity was associated with the growing fiber bundle (A,C). On E18, the Tn antigen was barely detectable on the thalamocortical fiber (arrows) (B,E). Adjacent sections of C and E were immunostained with anti cell adhesion molecule L1 antibody (D,F). LV, lateral ventricle; 3V, third ventricle. Scale bar = 500 μm for A,B; 100 μm for C–F.

ebellar nuclei, and some were present in the interstitial spaces of neural cells and neuropil. On P7, the expression of this antigen in the molecular layer had decreased, but extremely restricted immunoreactivity was detected in the somata of Purkinje cells (Fig. 6D).

Immunochemical Analysis of the Glycoprotein Bearing the Tn Antigen

We demonstrated the spatiotemporal expression of the Tn antigen in mouse central nervous tissues immunohistochemically. To further characterize the component bearing the Tn antigen, immunoblot analysis was performed using extracts of various organs of early postnatal mice as described under Materials and Methods. Because MLS 128 was reactive to a mucin-type glycoprotein but not to a glycolipid as reported previously (Numata et al., 1990), the tissues were extracted by a salt solution as described under Materials and Methods. The immunoprecipitates of the extracts obtained with MLS 128 were subjected to SDS-PAGE followed by Western blotting. As shown in Figure 7, a broad smeared band corresponding to a molecular weight of about 250 kDa was only detected for the brain. Other MLS 128-reactive glycoproteins of different molecular sizes were found in the intestine but not in any other organs we examined.

Lectin Blot Analysis of the Glycoprotein Bearing the Tn Antigen in the Mouse Brain

To determine whether or not other carbohydrate chains are present on the glycoprotein and, if present, what types the carbohydrate chains are, lectin blotting was performed using the glycoprotein immunoprecipitated from the extracts of P5 mouse brains. As shown in Figure 8, the glycoprotein was reactive to *Agaricus bisporus* agglutinin-1 (ABA-1) and PNA, but not to *Concanavalin* A (Con A) and *Wheat germ* agglutinin (WGA), indicating that the glycoprotein contains sialyl-T and T antigen in addition to the Tn antigen.

Developmental Change of the Tn Antigen in the Mouse Brain

Temporal expression of the Tn antigen was investigated in the mouse cerebrum, mesencephalon, and cerebellum. These tissues were homogenized and centrifuged as described under Materials and Methods. The glycoprotein bearing the Tn antigen was immunoprecipitated from the supernatant and subjected to SDS-PAGE followed by Western blotting. Figure 9A shows the expression pattern of the Tn antigen in the cerebrum. At embryonic stages, the expression level of the Tn antigen was low. Just after birth, the expression increased, reached a maximum level around P3 and then decreased gradually with age. By 3 weeks after birth, the antigen had substantially disappeared. Similar results were obtained about the Tn antigen in the mesencephalon and cerebellum (data not shown). As shown in Figure 9B, the intensity of the band was determined with a densitometer. The developmental expression pattern of the glycoprotein bearing the Tn anti-

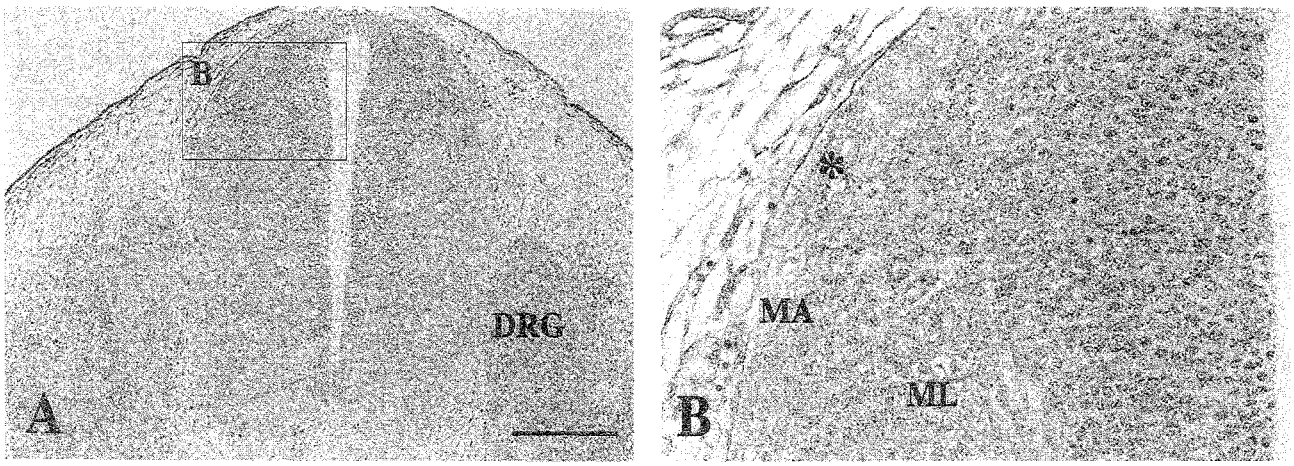

Fig. 5. Distribution of the Tn antigen in the mouse neural tube. Transverse sections were immunostained with MLS 128. The Tn antigen was observed in the marginal and mantle layers of the neural tube on E12 (**A**). The magnified region, (**B**) in (A) shows that the Tn antigen was associated with neural projections in the marginal (MA) and mantle (ML) layers. Bright staining was detected in the dorsal root entry zone (asterisk). DRG, dorsal root ganglion. Scale bar = 200 μm for A; 50 μm for B.

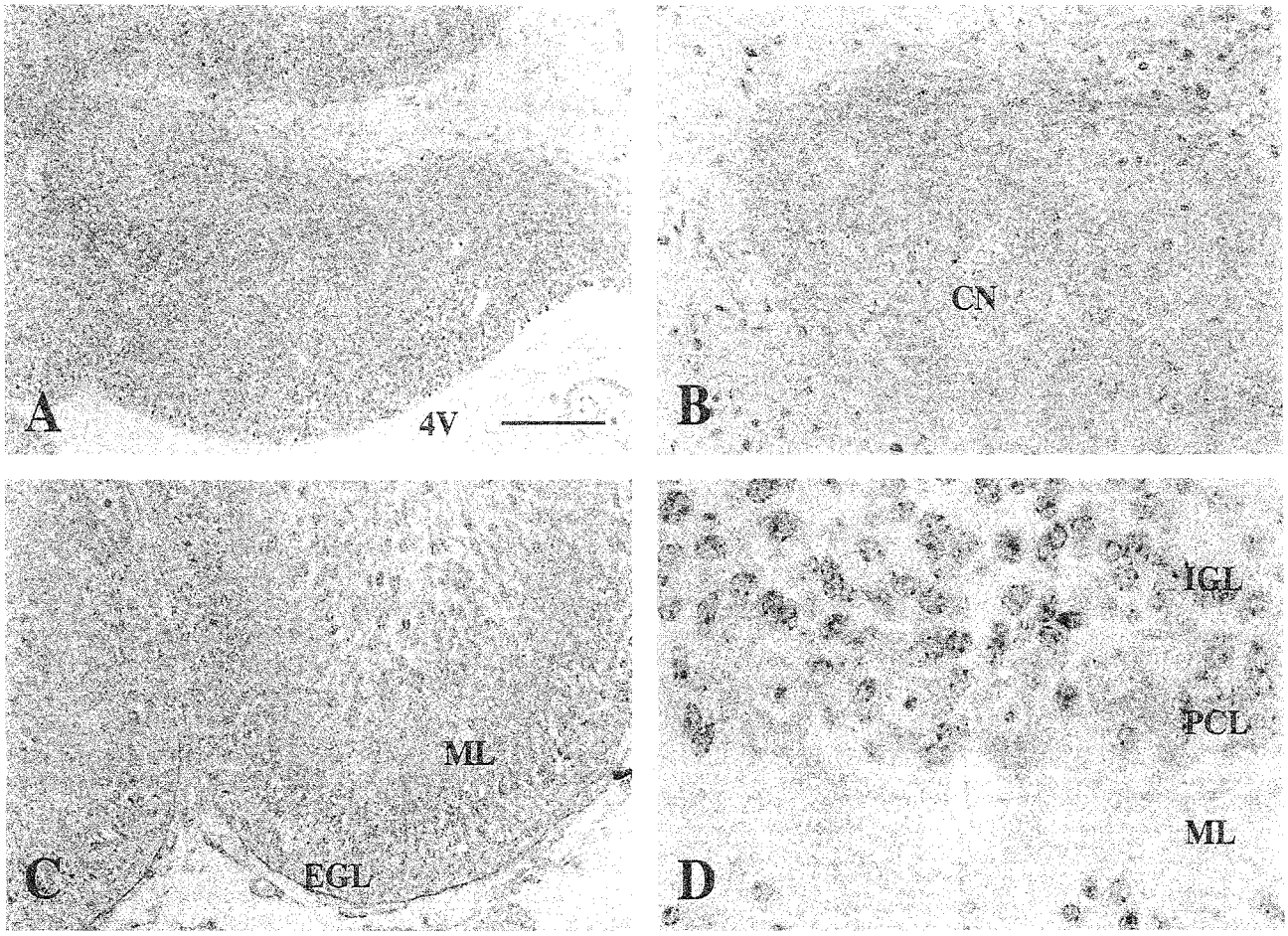

Fig. 6. Distribution of the Tn antigen in the developing mouse cerebellum. On E12 (**A**), immunoreactivity was found in the regions adjacent to the ventricular layer and the immature molecular layer of the cerebellar primordium, but not in the ventricular layer. On P3 (**B,C**), the Tn antigen was highly expressed in the molecular layer (ML) and outskirts of the cerebellar nuclei (CN). On P7 (**D**), expression of the Tn antigen in the molecular layer had decreased, but the cell bodies of Purkinje cells exhibited the immunoreactivity. 4V, fourth ventricle; EGL, external granular layer; IGL, internal granular layer; PCL, Purkinje cell layer. Scale bar = 100 μm for A; 50 μm for B,C; 20 μm for D.

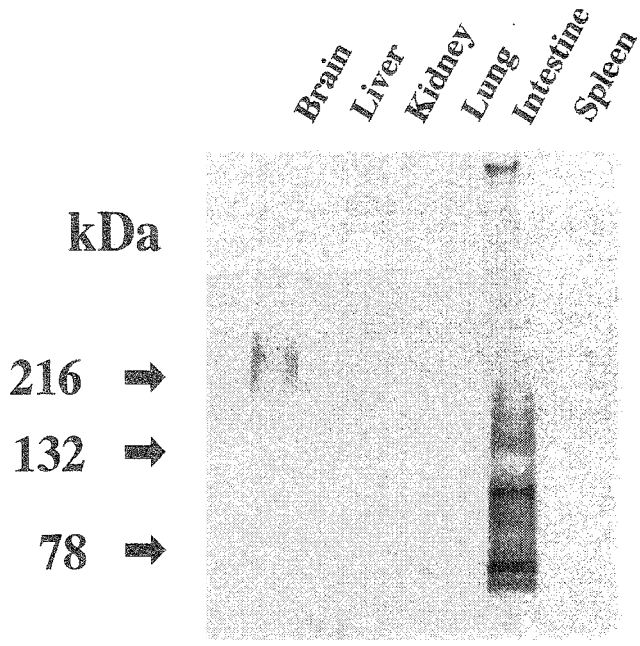

Fig. 7. Tissue distribution of the glycoproteins bearing the Tn antigen. The glycoprotein bearing the Tn antigen was examined immunochemically in extracts of various organs of P5 mice. A glycoprotein with a molecular weight of about 250 kDa was detected in the brain.

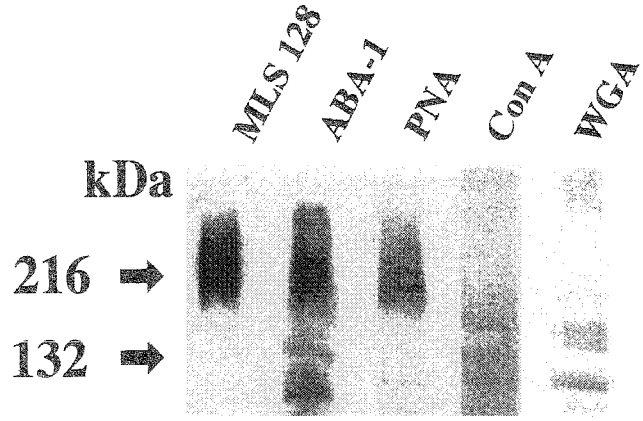

Fig. 8. Lectin blot analysis of the glycoprotein bearing the Tn antigen in P5 mouse brains. The glycoprotein immunoprecipitated with MLS 128 from the extracts of P5 mouse brain were blotted into the membrane, and reactivity with various plant lectins was examined. The smeared 250 kDa band was reactive to ABA-1 and PNA but not to Con A and WGA.

gen seems to be similar in the mouse cerebrum, mesencephalon, and cerebellum.

DISCUSSION

Restricted Expression of the Tn Antigen in Mouse Central Nervous Tissues

During histogenesis of the cerebral cortex in the mouse brain, expression of the Tn antigen appeared to be

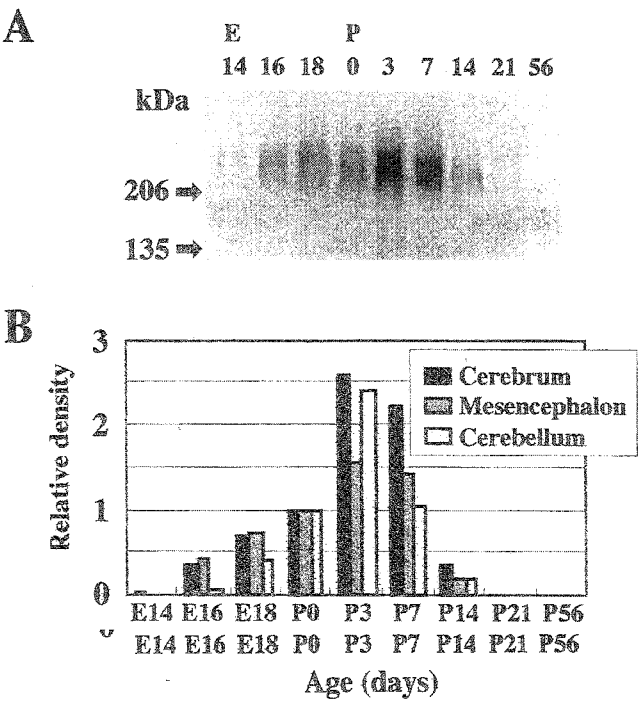

Fig. 9. Developmental changes in the glycoprotein bearing the Tn antigen in the mouse cerebrum, mesencephalon and cerebellum. (A) The glycoprotein bearing the Tn antigen from the mouse cerebrum at various developmental stages was detected by immunoblot analysis, as described under Materials and Methods. The same experiments were carried out using the extracts of developing mouse mesencephalon and cerebellum. (B) Relative amounts of the glycoprotein bearing the Tn antigen in various brain regions were determined by densitometry (NIH image program). The data were normalized as to the level on P0.

regulated both temporally and spatially. Before preplate formation, the antigen was distributed throughout the ventricular zone (Fig. 3A). As the preplate forms, the Tn antigen became more prominent in this region (Fig. 3B). The migration of cortical neurons within the preplate divides the preplate into the marginal zone and subplate. The distribution of the Tn antigen shifted along with this structural change, resulting in two immunoreactive zones, i.e., the marginal zone and subplate (Fig. 3C). It has been reported that chondroitin sulfate proteoglycan also accumulates in the preplate, the marginal zone, and subplate on early embryonic stage (Sheppard et al., 1991; Bicknese et al., 1994; Miller et al., 1995). The spatial expression of the Tn antigen on the E14 mouse neocortex is quite similar to that of chondroitin sulfate proteoglycan. At later stages, however, the distribution of the Tn antigen seems to be somewhat different from that of chondroitin sulfate proteoglycan, because the former was distributed mainly in the marginal and lower intermediate zones, and slightly in the subplate (Fig. 3D), whereas the latter was located in the marginal, subplate, and upper intermediate zones (Miller et al., 1995).

Axonal pathways are formed with great precision in the developing nervous system. The pathway taken by

afferents arriving from the thalamus is distinct from the adjacent pathway followed by axons leaving the developing neocortex. The thalamocortical afferents extend within the subplate, which is rich in chondroitin sulfate proteoglycan. In contrast, efferent axons from cortical neurons cross the subplate and extend within the intermediate zone, which contains less chondroitin sulfate proteoglycan (Catalano et al., 1991; De Carlos and O'Leary, 1992; Bicknese et al., 1994). It is notable that the staining pattern of MLS 128 on E14 delineated the pathway of fibers between the neocortex and thalamus (Fig. 4A,C). As shown in Figure 4C,D, the staining on thalamocortical afferent fibers was quite similar to that of the cell adhesion molecule L1 (Fushiki and Schachner, 1986; Fukuda et al., 1997). However, expression of the Tn antigen on these fibers was so temporally restricted that on E18, expression of the Tn antigen had already decreased unlike in the case of the cell adhesion molecule L1 (Fig. 4E,F). As reported previously, rat cortical efferent axons begin to leave the cerebral cortex and extend toward the nascent internal capsule on E14 (De Carlos and O'Leary, 1992). It is interesting to speculate that the Tn antigenicity is lost with the formation of the thalamocortical pathway. Generally, it appears likely that the Tn antigen was expressed preferentially in the regions rich in neurite-like structures, i.e., the preplate, marginal, and intermediate zones, subplate of the developing cerebral cortex (Fig. 3), and the marginal and mantle layers of the neural tube (Fig. 5), and the molecular layer of the cerebellum (Fig. 6). These observations suggest that the Tn antigen plays a significant biological role during brain development.

Biochemical Characteristics of the Glycoprotein Bearing the Tn Antigen

Immunoblot analysis was performed to characterize the glycoprotein bearing the Tn antigen. The method used for extraction of the glycoprotein from nervous tissues was examined in a solution containing either 0.3 M NaCl or 1% Triton X-100 at 4°C for 20 hr. The yield was invariant irrespective of whether or not the extraction solution contained a detergent, suggesting that the glycoprotein bearing the Tn antigen is a soluble protein. The glycoprotein was exclusively detected in the brain but not in any other organs, this being consistent with the histochemical findings (Fig. 7). Other glycoproteins of different molecular sizes detected in the intestine remain to be characterized. The developmental change of the glycoprotein bearing the Tn antigen in the mouse brain was quantitatively investigated by means of immunoblot analysis, showing a dramatic change with development (Fig. 9).

Lectin blot analysis suggested that the glycoprotein contains longer carbohydrate chains together with the Tn antigen, and that it is rich in O-glycans but poor in N-glycans (Fig. 8). In contrast, MLS 132, which is a monoclonal antibody specifically reactive with the sialyl Tn antigen (Tanaka et al., 1999), neither stained the mouse brain tissues nor reacted with the glycoprotein bearing the Tn antigen blotted on a membrane (data not shown). These results indicate that the Tn antigen was expressed in spite of the presence of glycosyltransferases that enable extension of the carbohydrate chain of GalNAc α 1-Thr/Ser residues as in tumor tissues.

Functional Possibility for the Tn Antigen

In this study, we demonstrated that the Tn antigen (GalNAc α 1-Thr/Ser) was temporally expressed in specific regions of the central nervous system. To date, some GalNAc-terminated glycoconjugates have been reported. β GalNAc-terminated saccharides are found to be concentrated in the neuromuscular junctions, and to be carried by some glycoproteins and glycolipids (Scott et al., 1988; Martin et al., 1999). Martin and Sanes (1995) reported that these glycoconjugates modulate agrin-induced clustering of acetylcholine receptors, this being relevant as to synaptic development at the neuromuscular junctions. On the other hand, the distinct biological function of the O-linked α-GalNAc structure, i.e., Tn antigen has not been proposed. Recently, it was demonstrated that a C-type lectin on the human macrophage preferentially bind clusters of GalNAc linked to Ser/Thr (Suzuki et al., 1996; Iida et al., 1999). Although the mouse homologue of this lectin is barely detectable in the brain (Mizuochi et al., 1997), there remains a possibility that the Tn antigen is a potential ligand for an endogenous lectin. In fact, we tried to isolate a binding protein for the Tn antigen. When mouse brain extracts were applied to a mucin (bearing the Tn antigen) conjugated Sepharose column, some binding proteins could be detected (data not shown). These studies and identification of the core protein bearing the Tn antigen are currently underway. It is natural that the Tn antigen disappears before appearance of immune response. The disappearance of the Tn antigen may be caused by either alteration of the antigenic carbohydrate moiety or loss of the core protein. The former may be caused by extension of the carbohydrate chain. It is tempting to speculate that a certain glycosyltransferase extends a carbohydrate chain, resulting in loss of the Tn antigen, because developmentally important events including cell migration and neurite outgrowth are supposed to be both genetically and epigenetically regulated. Expression of the Tn antigen on thalamocortical afferent fibers seems to be the case regulated by extension of the Tn antigen. Although these fibers exhibited strong immunoreactivity for the Tn antigen on E14, the antigen had disappeared barely by E18 (Fig. 4). With regard to the functional aspects of the Tn antigen, development of the thalamocortical fibers appears to be a clue to resolve this problem.

ACKNOWLEDGMENTS

This study was supported in part by a Grant-in-Aid for Scientific Research on Priority Areas, No. 10178102, from the Ministry of Education, Science and Culture of Japan, by Foundation for Bio-venture Research Center from the Ministry of Education, Science and Culture, Japan and by THE FUGAKU TRUST FOR MEDICAL RESEARCH.

REFERENCES

Bicknese AR, Sheppard AM, O'Leary DDM, Pearlman AL. 1994. Thalamocortical axons extend along a chondroitin sulfate proteoglycan-enriched pathway coincident with the neocortical subplate and distinct from the efferent path. J Neurosci 14:3500–3510.

Catalano SM, Robertson RT, Killackey HP. 1991. Early ingrowth of thalamocortical afferents to the neocortex of the prenatal rat. Proc Natl Acad Sci USA 88:2999–3003.

Chou DKH, Tobet SA, Jungalwala FB. 1998. Restoration of synthesis of sulfoglucuronylglycolipids in cerebellar granule neurons promotes dedifferentiation and neurite outgrowth. J Biol Chem 273:8508–8515.

De Carlos JA, O'Leary DDM. 1992. Growth and targeting of subplate axons and establishment of major cortical pathways. J Neurosci 12:1194–1211.

Fenderson B, Zehavi U, Hakomori S. 1984. A multivalent lacto-*N*-fucopentaose III-lysyllysine conjugate decompacts preimplantation mouse embryos, while the free oligosaccharide is ineffective. J Exp Med 160: 1591–1596.

Friedlander DR, Milev P, Karthikeyan L, Margolis RK, Margolis RU, Grumet M. 1994. The neuronal chondroitin sulfate proteoglycan neurocan binds to the neural cell adhesion molecules Ng-CAM/L1/NILE and N-CAM, and inhibits neuronal adhesion and neurite outgrowth. J Cell Biol 125:669–680.

Fukuda T, Kawano H, Ohyama K, Li HP, Takeda Y, Oohira A, Kawamura K. 1997. Immunohistochemical localization of neurocan and L1 in the formation of thalamocortical pathway of developing rats. J Comp Neurol 382:141–152.

Fushiki S, Schachner M. 1986. Immunocytological localization of cell adhesion molecules L1 and N-CAM and the shared carbohydrate epitope L2 during development of the mouse neocortex. Dev Brain Res 24:153–167.

Hirschberg K, Zisling R, van Echten G, Futerman AH. 1996. Ganglioside synthesis during the development of neuronal polarity. J Biol Chem 271:14876–14882.

Iida S, Yamamoto K, Irimura T. 1999. Interaction of human macrophage C-type lectin with O-linked *N*-acetylgalactosamine residues on mucin glycopeptides. J Biol Chem 274:10697–10705.

Inoue M, Nakada H, Tanaka N, Yamashina I. 1994. Tn antigen is expressed on leukosialin from T-lymphoid cells. Cancer Res 54:85–88.

Jacobson M. 1991. Developmental neurobiology, 3rd Ed. New York: Plenum Press. p 416–420.

Margolis RK, Margolis RU. 1993. Nervous tissue proteoglycans. Experientia 49:429–446.

Martin PT, Sanes JR. 1995. Role for a synapse-specific carbohydrate in agrin-induced clustering of acetylcholine receptors. Neuron 14:743–754.

Martin PT, Scott LJC, Porter BE, Sanes JR. 1999. Distinct structures and functions of related pre- and postsynaptic carbohydrates at the mammalian neuromuscular junction. Mol Cell Neurosci 13:105–118.

Miller B, Sheppard AM, Bicknese AR, Pearlman AL. 1995. Chondroitin sulfate proteoglycans in the developing cerebral cortex: the distribution of neurocan distinguishes forming afferent and efferent axonal pathways. J Comp Neurol 355:615–628.

Mizuochi S, Akimoto Y, Imai Y, Hirano H, Irimura T. 1997. Unique tissue distribution of a mouse macrophage C-type lectin. Glycobiology 7:137–146.

Momoi T, Yoshida-Momoi M, Kurata T. 1986. Peanut agglutinin receptor is a marker of myelin in rat brain. J Neurochem 46:229–234.

Naegele JR, Katz LC. 1990. Cell surface molecules containing *N*-acetylgalactosamine are associated with basket cells and neurogliaform cells in cat visual cortex. J Neurosci 10:540–557.

Nakada H, Numata Y, Inoue M, Tanaka N, Kitagawa H, Funakoshi I, Fukui S, Yamashina I. 1991. Elucidation of an essential structure recognized by an anti-GalNAc α-Ser(Thr) monoclonal antibody (MLS 128). J Biol Chem 266:12402–12405.

Nakada H, Inoue M, Numata Y, Tanaka N, Funakoshi I, Fukui S, Mellors A, Yamashina I. 1993. Epitopic structure of Tn glycophorin A for an anti-Tn antibody (MLS 128). Proc Natl Acad Sci USA 90:2495–2499.

Nakagawa F, Schulte BA, Wu J-Y, Spicer SS. 1987. Postnatal appearance of glycoconjugate with terminal *N*-acetylgalactosamine on the surface of selected neurons in mouse brain. Dev Neurosci 9:53–60.

Numata Y, Nakada H, Fukui S, Kitagawa H, Ozaki K, Inoue M, Kawasaki T, Funakoshi I, Yamashina I. 1990. A monoclonal antibody directed to Tn antigen. Biochem Biophys Res Commun 170:981–985.

Rutishauser U, Landmesser L. 1996. Polysialic acid in the vertebrate nervous system: a promoter of plasticity in cell-cell interactions. Trends Neurosci 19:422–427.

Scott LJC, Bacou F, Sanes JR. 1988. A synapse-specific carbohydrate at the neuromuscular junction: association with both acetylcholinesterase and a glycolipid. J Neurosci 8:932–944.

Sheppard AM, Hamilton SK, Pearlman AL. 1991. Changes in the distribution of extracellular matrix components accompany early morphogenetic events of mammalian cortical development. J Neurosci 11:3928–3942.

Springer GF, Desai PR, Banatwala I. 1974. Blood group MN specific substances and precursors in normal and malignant human breast tissues. Naturwissenschaften 61:457–458.

Suzuki N, Yamamoto K, Toyoshima S, Osawa T, Irimura T. 1996. Molecular cloning and expression of cDNA encoding human macrophage C-type lectin. J Immunol 156:128–135.

Tanaka N, Nakada H, Inoue M, Yamashina I. 1999. Binding characteristics of an anti-Sia α 2-6GalNAc α-Ser/Thr (sialyl Tn) monoclonal antibody (MLS 132). Eur J Biochem 263:27–32.

Tollefsen SE, Kornfeld R. 1983. The B_4 lectin from *Vicia villosa* seeds interacts with *N*-acetylgalactosamine residues α-linked to serine or threonine residues in cell surface glycoproteins. J Biol Chem 258:5172–5176.

Varki A, Cummings R, Esko J, Freeze H, Hart G, Marth J. 1999. Essentials of glycobiology. New York: Cold Spring Harbor Laboratory Press. p 522–524.

CELL STRUCTURE AND FUNCTION 26: 271-278 (2001)

Identification of the Core Protein Carrying the Tn Antigen in Mouse Brain: Specific Expression on Syndecan-3

Kaoru Akita[1], Shinji Fushiki[2], Takahiro Fujimoto[1], Seiichi Munesue[1], Mizue Inoue[1], Kayoko Oguri[3], Minoru Okayama[1], Ikuo Yamashina[1], and Hiroshi Nakada[1]*

[1]*Department of Biotechnology, Faculty of Engineering, Kyoto Sangyo University, Kyoto, Japan,* [2]*Department of Pathology and Applied Neurobiology, Research Institute for Neurological Diseases and Geriatrics, Kyoto Prefectural University of Medicine, Kyoto, Japan, and* [3]*Clinical Research Institute, National Nagoya Hospital, Nagoya, Japan*

ABSTRACT. **We isolated glycoproteins carrying the Tn antigen, which was expressed spatiotemporally in the developing mouse brain. The Tn antigen was expressed on two molecular species with a molecular weight from 200 to 350 kDa and 110 to 160 kDa, as judged on SDS-PAGE. Although the two glycoproteins showed different susceptibilities to heparitinase I and solubilities in a salt solution, after treatment with V8 protease they showed the same mobility corresponding to a molecular weight of 90 kDa on SDS-PAGE, suggesting that these two molecules shared a common core protein. Partial N-terminal sequences of the glycoproteins were determined, i.e. AQRXRNENFERPV and ALAAPXAPAMLP, which were identified as the sequences of the N-terminal and central portions of syndecan-3, respectively. Both glycoproteins were reactive to anti-mouse syndecan-3 antibody. These results suggest that one is a soluble syndecan-3 cleaved between mucin-like domain and transmembrane domain, and the other is a membrane-bound syndecan-3 lacking N-terminal glycosaminoglycan attachment sites, and that both glycoproteins have a mucin-like domain characteristic of syndecan-3, in which the Tn antigen may be expressed.**

Key words: syndecan-3/Tn antigen/mucin/brain development

Developing nervous tissues contain various proteoglycans, the expression of which is regulated spatiotemporally. It has been reported that these proteoglycans play important roles in nervous morphogenetic processes. Most of their functional roles seem to be derived from their binding properties to cell adhesion molecules, extracellular matrix components, growth factors and neurotrophic factors (Margolis and Margolis 1993; Oohira *et al.*, 1994). In addition to glycosaminoglycans, many proteoglycans have other types of carbohydrate chains such as N- and O-glycans. Not only glycosaminoglycans but also N- and O-glycans and core proteins seem to be involved in a variety of biological interactions (Gould *et al.*, 1992; Milev *et al.*, 1998; Herndon *et al.*, 1999; Oohira *et al.*, 2000). Syndecan-3 is known to be a heparan sulfate proteoglycan present in the developing brain. This proteoglycan has a unique mucin-like domain unlike other syndecans (Carey, 1996). We reported previously that the Tn antigen, which is one of the cancer-associated carbohydrate antigens, was expressed in developing mouse central nervous tissues, in particular, in the developing cerebral cortex and cerebellum (Akita *et al.*, 2001). To characterize the core protein, we purified glycoproteins carrying the Tn antigen from early postnatal mouse brains. Two molecular species expressed the Tn antigen. The major glycoprotein, with a molecular weight ranging from 200 to 350 kDa, exhibited similar susceptibility to glycosidases including heparitinase I to that of syndecan-3 (Chernousov and Carey, 1993; Watanabe *et al.*, 1996). Furthermore, a partial N-terminal sequence of the major glycoprotein was revealed to coincide with that of syndecan-3 (Kung *et al.*, accession No. U52826). Another glycoprotein was demonstrated to be syndecan-3 devoid of the N-terminal portion.

*To whom correspondence should be addressed: Dr. Hiroshi Nakada, Department of Biotechnology, Faculty of Engineering, Kyoto Sangyo University, Kamigamo-Motoyama, Kita-ku, Kyoto
Tel: +81-75-705-1897, Fax: +81-75-705-1888
E-mail: hnakada@cc.kyoto-su.ac.jp

Abbreviations: CHAPS, 3-[(3-cholamidopropyl) dimethylammonio]-1-propane sulfonate; E, embryonic day; HRP, horseradish peroxidase; NEM, N-ethylmaleimide; P, postnatal day; PMSF, phenylmethylsulfonyl fluoride.

Materials and Methods

Animals and antibodies

ICR strain mice (SLC Inc., Shizuoka, Japan) were used for the purification of glycoproteins carrying the Tn antigen. A murine anti-Tn monoclonal antibody, designated as MLS 128, was prepared as described previously (Numata *et al.*, 1990). MLS 128 recognizes a glycopeptide including a cluster of N-acetylgalactosamine (GalNAc) α1-Ser/Thr residues (Nakada *et al.*, 1991, 1993; Inoue *et al.*, 1994). Rabbit anti-mouse syndecan-3 core protein antibody was raised against the recombinant polypeptide of syndecan-3 according to Kusano *et al.* (2000). Monoclonal antibody 3G10, which is directed to the desaturated uronate residues produced from heparan sulfate on heparitinase treatment, was purchased from Seikagaku Kogyo (Tokyo, Japan).

Purification of glycoproteins carrying the Tn antigen from early postnatal mouse brains

The brains of postnatal mice (P5-7) were used and all procedures were carried out at 4°C or on ice unless otherwise stated. The brains (wet weight: 140 g) were homogenized in 3.5 volume of an extraction solution comprising 1% TritonX-100, 25 mM Tris-HCl buffer, pH 7.5, 0.15 M NaCl, 10 mM EDTA, 1 mM PMSF, 10 mM NEM, pepstatin-A (1μg/ml), and leupeptin (1μg/ml) with a Polytron homogenizer, extracted for 15 h, and then centrifuged at 25,000×g for 10 min, the resulting supernatant being centrifuged again at 105,000×g for 1 h. The pellet was re-homogenized in an equal volume of the extraction solution and then centrifuged as described above. The combined supernatants were fractionated by ammonium sulfate precipitation. After discarding the precipitates at 40% saturation, the glycoproteins were precipitated by further addition of solid ammonium sulfate to 85% saturation. After centrifugation at 20,000×g for 30 min, the precipitate was dissolved in a solution of 0.5% TritonX-100, 25 mM Tris-HCl buffer, pH 7.5, 0.1 M NaCl, and 0.5 mM EDTA, and then dialyzed against the same solution. The dialyzed material was applied to a column of Q-Sepharose Fast Flow column (3×15 cm) equilibrated with a solution of 0.5% TritonX-100, 25 mM Tris-HCl buffer, pH 7.5, 0.1 M NaCl, and 0.5 mM EDTA. After washing the column with 25 mM Tris-HCl buffer, pH 7.5, containing 0.25 M NaCl and 0.1% CHAPS, the glycoproteins carrying the Tn antigen were eluted with a solution of 0.1% CHAPS, 25 mM Tris-HCl buffer, pH 7.5, and 1.5 M NaCl. After dialysis of the eluate against 25 mM Tris-HCl buffer, pH 7.5, containing 0.1 M NaCl, 2 mM EDTA and 0.1% CHAPS, excessive amounts of MLS 128 and protein A-Sepharose were added, followed by mixing overnight. The immune complex was poured into a column. After extensively washing of the column with the above solution, the immune complex was eluted with 0.1 M citrate-NaOH buffer, pH 3.8, containing 0.15 M NaCl and 0.5% CHAPS. The eluate was dialyzed against 50 mM Tris-HCl buffer, pH 8.0, containing 5 mM NEM, 5 mM EDTA, 0.5% CHAPS and 4 M guanidine-HCl. After adding solid cesium chloride to a density of 1.34 mg/ml, the eluate was centrifuged at 230,000×g for 72 h and then fractionated with a density gradient fractionator, DGF-U (Hitachi, Tokyo, Japan). The fractions in which the antigen was detected were collected. The glycoproteins carrying the Tn antigen were finally purified by gel filtration on a TskgelG4000SW^{XL} column (0.78×30 cm) (Tosoh Corporation, Tokyo, Japan). In some cases, the immune complex prepared as described above was directly subjected to SDS-PAGE. Two glycoproteins corresponding to molecular weights of 200-350 kDa and 110-160 kDa were extracted from the gel.

Enzymatic treatments with glycosidases and proteases

The glycoproteins (0.1μg protein) were treated with various glycosidases and proteases. The glycoproteins were treated with 0.2 units/ml of heparitinase I or chondroitinase ABC (Seikagaku Kogyo Co., Tokyo, Japan) in 30 mM Tris-acetate buffer, pH 7.5, containing 10 mM EDTA, 10 mM NEM, 1 mM PMSF and pepstatin-A (0.25 mg/ml) at 37°C for 1 h according to Kato *et al.* (1985). Sialidase (Nacalai Tesque, Kyoto, Japan) treatment (0.06 units/ml) was performed in 30 mM sodium acetate buffer, pH 5.0, containing 5 mM EDTA, 5 mM NEM, 1 mM PMSF and pepstatin-A (0.07 mg/ml) at 37°C for 20 h. N-Glycosidase-F (Takara Shuzo, Ohtsu, Japan) treatment (0.04 units/ml) was performed at 37°C for 20 h according to manufacturer's instructions. Digestion with 0.1 units/ml of α-N-acetylgalactosaminidase (Sigma, St. Louis, MO) was carried out at 37°C for 20 h in 30 mM sodium acetate buffer, pH 4.0, containing 5 mM EDTA, 5 mM NEM, 1 mM PMSF and pepstatin-A (0.07 mg/ml). O-Sialoglycoprotein endopeptidase (Laboratories Limited, Hornby, Ontario, Canada) digestion was performed in 50 mM Hepes buffer, pH 7.2, at 37°C for 20 h, and digestion with V8 protease (Roche Molecular Biochemicals, Mannheim, Germany) was performed in 50 mM ammonium bicarbonate buffer, pH 7.8, at 37°C for 20 h. All protease digestions were carried out with a substrate/enzyme ratio of 100 : 3.

Immunoblotting

SDS-polyacrylamide gel electrophoresis on a 2–15% gradient gel was performed according to Laemmli (Laemmli, 1970). After electrophoresis, the separated proteins were transferred to a Zeta-probe membrane (Bio-Rad, Hercules, CA) at 20 V for 15 h. The membrane was incubated with 50 mM Tris-HCl buffer, pH 7.5, containing 5% BSA and 0.15 M NaCl to block nonspecific staining, followed by successive incubation with anti Tn antibody (MLS 128) or anti syndecan-3 core protein antibody and HRP-protein G (Zymed, South San Francisco, CA). The membrane was visualized with an enhanced chemiluminescence kit (Amersham Pharmacia Biotech, Buckinghamshire, England).

N-Terminal sequencing of glycoproteins carrying the Tn antigen

The N-terminal sequences of the glycoproteins were determined with an Applied Biosystems sequencer model 492.

Immunohistochemistry

Immunohistochemical staining with MLS 128 was carried out as described previously (Akita *et al.*, in 2001). The tissues were fixed overnight in Bouin's fixative at 4°C and embedded in paraffin. Paraffin sections, 4 μm thick, were obtained with a rotary microtome. After deparaffinization, the sections were treated with 0.3% hydrogen peroxide in absolute methanol for 15 min to block endogenous peroxidase activity, and then with rabbit normal serum. After incubation with MLS 128 (10 μg/ml) at room temperature for 2 h and subsequent rinsing with PBS, the sections were incubated with horseradish peroxidase (HRP)-conjugated rabbit anti-mouse IgG immunoglobulin (Zymed) at a dilution of 1:200 in 1% bovine serum albumin (BSA)-PBS for 1 h, washed with PBS, and then visualized with 0.03% 3,3'-diaminobenzidine tetrahydrochloride (DAB), 0.003% hydrogen peroxide and 10 mM imidazole in 50 mM Tris-HCl buffer, pH 7.6. To stain cell nuclei, sections were treated with hematoxylin. Control experiments were performed similarly using normal murine IgG_3 (Zymed) instead of MLS 128. Immunohistochemical staining for the syndecan-3 core protein was carried out using Histofine SAB rabbit kit (Nichirei, Tokyo, Japan).

Results

Isolation of glycoproteins carrying the Tn antigen from early postnatal mouse brains

In a previous paper, we demonstrated immunochemically that the Tn antigen was expressed in the developing mouse brain, and that a glycoprotein with a molecular weight of about 250 kDa was immunoprecipitated from a mouse brain extract with MLS 128. The glycoprotein could be extracted with a solution without any detergent as described previously (Akita *et al.*, 2001). When extracted with a solution containing 1% TritonX-100, as described under Materials and Methods, another minor glycoprotein corresponding to 140 kDa was found in addition to the major glycoprotein, as shown in Fig. 1A. To examine the developmental changes of the glycoproteins, expression of the glycoproteins was followed immunochemically in extracts of whole mouse brains from E14 to P56. The two glycoproteins showed similar expression patterns and peaked at an early postnatal stage (Fig. 1B, C). Based on these results, early postnatal brains were used as the starting material for purification of the glycoproteins. A crude extract was fractionated by ammonium sulfate precipitation and then subjected to Q-Sepharose Fast Flow anion exchange chromatography. The glycoproteins were eluted with a high salt solution containing 1.5 M NaCl, and the eluate, after dialysis, was mixed with MLS 128 and protein A-Sepharose. The immune complex was poured into a column. After extensive washing, the complex was eluted with 0.1 M citrate-NaOH buffer, pH 3.8, and then fractionated by cesium chloride density gradient centrifugation in the presence of 4 M guanidine-HCl. An

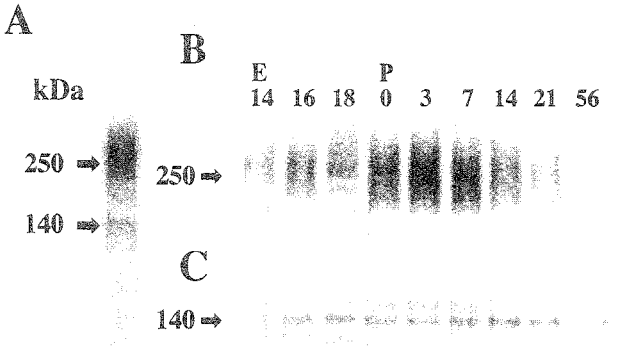

Fig. 1. Developmental changes in the glycoproteins bearing the Tn antigen in the mouse brain. The glycoproteins carrying the Tn antigen were immunoprecipitated from extracts of whole mouse brains (10 mg protein) as described under Materials and Methods. The immunoprecipitates were subjected to SDS-PAGE, followed by western blotting. A. The glycoproteins bearing the Tn antigen in mouse brains (P3). B. Developmental changes of the major glycoprotein. C. Developmental changes of the minor glycoprotein.

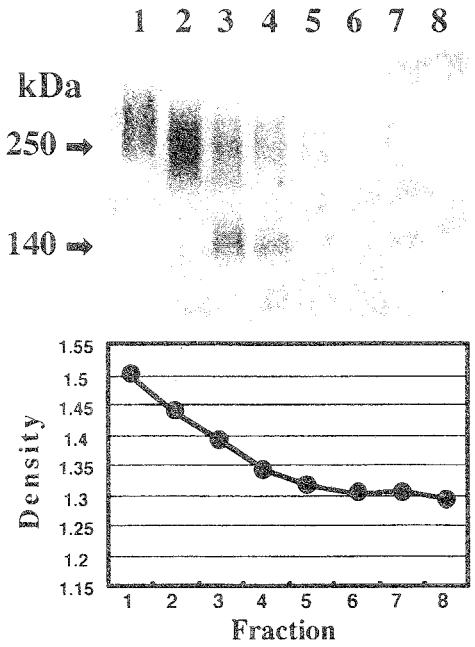

Fig. 2 Fractionation of the glycoproteins carrying the Tn antigen on cesium chloride density gradient centrifugation. The eluate obtained on immuno-affinity chromatography was subjected to CsCl density gradient centrifugation as described under Materials and Methods. An aliquot of each fraction was subjected to SDS-PAGE, followed by western blotting. The Tn antigen was detected with MLS 128 as described under Materials and Methods.

aliquot of each fraction was subjected to SDS-PAGE followed by western blotting, as shown in Fig. 2. The major glycoprotein with a molecular weight from 200 to 350 kDa was recovered in the fractions with a density of more than 1.40 g/ml. Another glycoprotein corresponding to a molecu-

lar size from 110 to 160 kDa was detected in lighter fractions. Since these molecules were not stained on silver or CBB staining, aliquots obtained at each step were biotinylated and subjected to SDS-PAGE followed by western blotting. The bands were detected by means of the streptavidin-peroxidase reaction. The finally purified glycoproteins carrying the Tn antigen gave a major smeared band and a minor one, which were clearly detected on immunochemical staining (Fig. 3B). No other contaminating proteins were detected (Fig. 3A, lane 4). From 140 g of early postnatal brain, 3.2 μg of the glycoproteins carrying the Tn antigen was obtained. In some cases, the immune complex was directly subjected to SDS-PAGE and the two glycoproteins were separated by extraction from the gel as described under Materials and Methods.

Characterization of carbohydrate moieties of glycoproteins carrying the Tn antigen

The smeared band of the major glycoprotein on SDS-PAGE suggests that it may be highly glycosylated by O-glycans

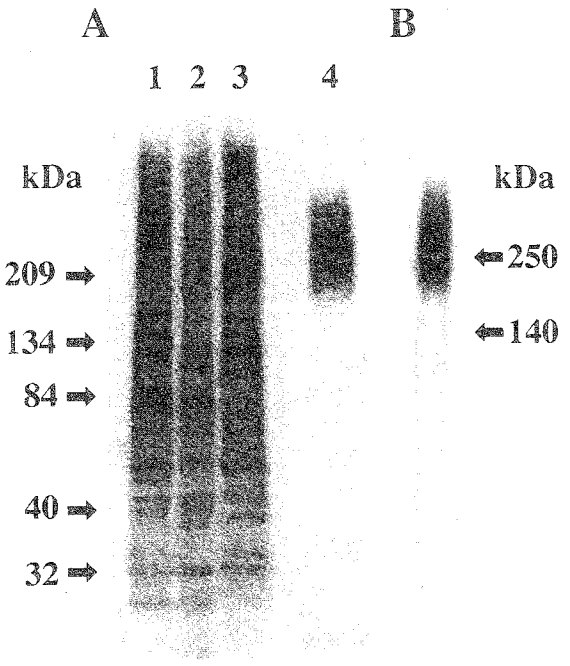

Fig. 3. SDS-PAGE of aliquots obtained at each purification step. A. Aliquots obtained at each purification step were labeled with NHS-sulfo-Biotin (Pierce) according to manufacturer's instructions. The biotinylated proteins were separated on a 2-15% SDS-polyacrylamide gel. After electroblotting onto a nylon membrane, the proteins were visualized by successive incubation with streptavidin-peroxidase and enhanced chemiluminescence reagents. Lane 1: crude extract; lane 2: aliquot obtained on ammonium sulfate fractionation; lane 3: 1.5M NaCl eluate obtained on ion exchange chromatography; lane 4: glycoproteins purified by gel filtration. B. The purified glycoproteins were detected immunochemically with MLS 128 as described in Fig. 1.

and other carbohydrate chains. To characterize the carbohydrate moieties, we treated the glycoproteins with various glycosidases. On digestion with heparitinase I, the major glycoprotein gave a less broad band corresponding to a molecular mass of 160 kDa, whereas the minor one did not show any detectable change on SDS-PAGE (Fig. 4A, lanes 4 and 5). Chondroitinase digestion did not affect the electrophoretic mobility of the major glycoprotein at all (Fig. 4A, lane 6). Monoclonal antibody 3G10, which reacts with desaturated uronate residues produced from heparan sulfate on treatment with heparitinase, recognized the major glycoprotein that had been treated with heparitinase I (data not shown). These results indicate that the major glycoprotein, but not the minor one, is a heparan sulfate proteoglycan. After heparitinase treatment, the major glycoprotein was digested with sialidase (Fig. 4A, lane 7) or N-glycanase (Fig. 4A, lane 8). Sialidase treatment increased its mobility slightly, but N-glycanase digestion did not cause any detectable change in its mobility. In addition, we demonstrated previously that the major glycoprotein was reactive to *Peanut* agglutinin and *Agaricus bisporus* agglutinin-1, but not to *wheat germ* agglutinin or *Concanavalin* A (Akita *et al.*, 2001). These results indicate that the major glycoprotein possesses heparan sulfate glycosaminoglycans and O-glycans. The Tn antigenicity was further confirmed by the fact that the antigenicity was lost on treatment with α-N-acetylgalactosaminidase (Fig. 4A, lanes 9 and 10).

Characterization of the core protein

The two glycoproteins were treated with O-sialoglycoprotein endopeptidase, which is a neutral metalloprotease and has the ability to degrade sialylated mucin-type glycoproteins. Expectedly, the Tn antigenicity was abolished upon treatment with this enzyme (Fig. 4B, lanes 3 and 4), indicating that both glycoproteins have a mucin-like domain. It should be noted that after treatment with V8 protease, these glycoproteins showed the same mobility corresponding to a molecular weight of 90 kDa (Fig. 4B, lanes 5 and 6), suggesting that they share a common core protein. After treatment with V8 protease, the major glycoprotein was not susceptible to heparitinase I, probably due to the cleavage of glycosaminoglycan attachment region (Fig. 4B, lanes 7 and 8). To further characterize the two glycoproteins, the N-terminal amino acid sequences of the glycoproteins were analyzed. The N-terminal sequence of the major glycoprotein was revealed to be AQRXRNENFERPV, which coincided with the sequence from amino acid 45 to 57 of mouse syndecan-3. Since the sequence from the N-terminus to amino acid 44 is postulated to be a signal sequence (Kung *et al.*, accession No. U52826), cleavage of the signal peptide may produce the N-terminus of the major glycoprotein. The N-terminal sequence of the minor glycoprotein was ALAAPXAPAMLP. The sequence coin-

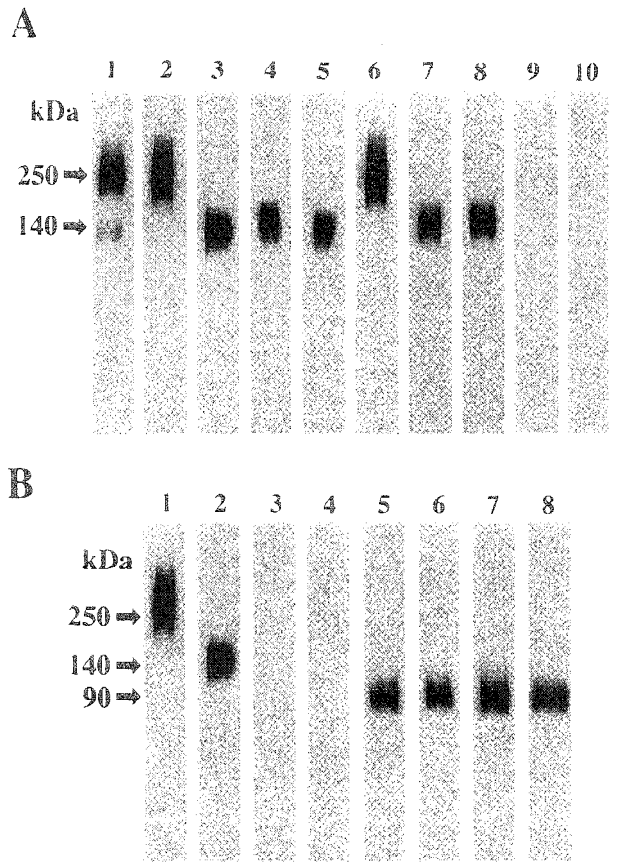

Fig. 4. Immunoreactivity of the glycoproteins treated with glycosidases (A) and proteases (B). The purified glycoproteins were digested with various glycosidases and proteases, followed by SDS-PAGE. After blotting onto a membrane, the glycoproteins were detected as described in Fig. 1. A. Lane 1: purified glycoproteins; lane 2: major glycoprotein extracted from the gel; lane 3: minor glycoprotein extracted from the gel; lane 4: major glycoprotein treated with heparitinase I; lane 5: minor glycoprotein treated with heparitinase I; lane 6: major glycoprotein treated with chondroitinase ABC; lane 7: major glycoprotein treated with heparitinase I and sialidase successively; lane 8: major glycoprotein treated with heparitinase I and N-glycanase successively; lane 9: major glycoprotein treated with α-N-acetylgalactosaminidase; lane 10: minor glycoprotein treated with α-N-acetylgalactosaminidase. B. Lane 1: major glycoprotein extracted from the gel; lane 2: minor glycoprotein extracted from the gel; lane 3: major glycoprotein treated with O-sialoglycoprotein endopeptidase; lane 4: minor glycoprotein treated with O-sialoglycoprotein endopeptidase; lane 5: major glycoprotein treated with V8 protease; lane 6: minor glycoprotein treated with V8 protease; lane 7: major glycoprotein treated with V8 protease and heparitinase I successively; lane 8: minor glycoprotein treated with V8 protease and heparitinase I successively.

cided with the central (beginning with amino acid 102) portion of syndecan-3 (Fig. 5). The amino acid residues which could not be determined, designated as X, seem to be Trp and glycosylated Thr residues based on the cDNA sequence (Kung *et al.*, accession No. U52826). Furthermore, we confirmed that the anti-mouse syndecan-3 antibody was reactive to both glycoproteins, as shown in Fig. 6.

```
  1 MKPGPPRRGT AQGQRVDTAT HAPGARGLLL PPLLLLLLAG
      AQRXRN ENFERPV
      ::: :: :::::::
 41 RAAGAQRWRN ENFERPVDLE GSGDDDSFPD DELDDLYSGS
                          ALAAPXAPA MLP
                          ::::: ::: :::
 81 GSGYFEQESG LETAMRFIPD MALAAPTAPA MLPTTVIQPV
121 DTPFEELLSE HPRPEPVTSP PLVTEVKEVV EESSQKATTI
161 STTTSTTAAT TTGAPTMATA PATAATTAPS TPEAPPATAT
201 VADVRTTGIQ GMLPLPLTTA ATAKITTPAA PSPPTTVATL
241 DTEAPTPRLV NTATSRPQSL PRPITTQEPE VAERSTLPLG
281 TTAPGPTEVA QTPTPESLLT TTQDEPEVPV SGGPSGDFEL
321 QEETTQPDTA NEVVAVEGAA AKPSPPLGTL PKGARPGLGL
361 HDNAIDSGSS AAQLLQKSIL ERKEVLVAVI VGGVVGALFA
401 AFLVTLLIYR MKKKDEGSYT LEEPKQASVT YQKPDKQEEF
441 YA
```

Fig. 5. Alignments of N-terminal amino acid sequences obtained from the two glycoproteins bearing the Tn antigen with deduced amino acid sequence of mouse syndecan-3. Aligned residues identical to mouse syndecan-3 are indicated by colons.

Expression of the Tn antigen in brain and cartilage primordium

So far, expression of syndecan-3 has been investigated in the rat brain using antibody against the core protein of syndecan-3 and *in situ* hybridization of mRNA (Watanabe *et al.*, 1996; Carey *et al.*, 1997; Hsueh and Sheng, 1999). It has been reported that syndecan-3 is present at low levels in the late embryonic brain, and that the level increases during the early postnatal period. In the present biochemical study, we showed that the Tn antigen was carried on syndecan-3 specifically. Expectedly, distribution of the Tn antigen in the postnatal mouse brain was similar to that of syndecan-3 as shown in Fig. 7C and reported by Watanabe *et al.* (1996) and Carey *et al.* (1997). The antigen was detected throughout the cerebral cortex layers and localized in the molecular layer of the cerebellar cortex as shown in Fig. 7A, B, E, F. Since syndecan-3 is also expressed during the formation of the cartilage (Gould *et al.*, 1995), we examined expression of the Tn antigen in the mouse cartilage primordium. As shown in Fig. 7G, H, the Tn antigen was detected in the mesenchymal condensed areas surrounding the mouse cartilage.

Discussion

The Tn antigen is well known as one of the tumor-associated carbohydrate antigens (Springer *et al.*, 1974). MLS 128, a monoclonal antibody recognizing the Tn antigen, was established by immunizing mice with a human colorectal cancer cell line, LS 180 cells (Numata *et al.*, 1990). Using gly-

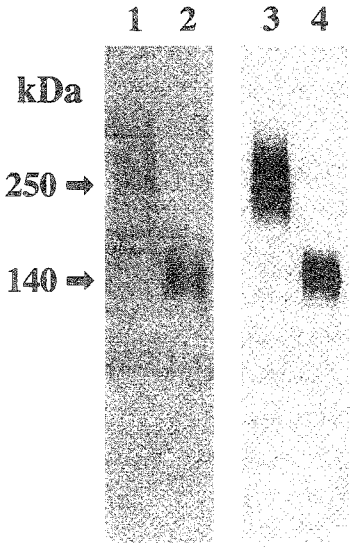

Fig. 6. Immunoreactivity of the glycoproteins with the anti-mouse syndecan-3 antibody. The major and minor glycoproteins were subjected to SDS-PAGE, blotted onto a Zeta-probe membrane, and then detected with the anti syndecan-3 antibody (lanes 1 and 2) and MLS 128 (lanes 3 and 4).

coproteins reactive to MLS 128, we elucidated the epitopic structure to consist of three consecutive residues of GalNAcα1-Ser/Thr as a minimum antigenic site (Nakada *et al.*, 1991; 1993; Inoue *et al.*, 1994). It is generally agreed that tumorigenically transformed state has some similarities to that of the embryonic stages. We demonstrated previously that the Tn antigen was expressed in embryonic and early postnatal mouse brain, in particular, in developing cerebral cortex and cerebellum (Akita *et al.*, 2001). The antigen, which was expressed throughout the embryonic stages, peaked around postnatal day 3 and decreased gradually with age as shown in Fig. 1. Expression of the antigen was also restricted temporally. In the present study, we isolated the glycoproteins carrying the Tn antigen from early postnatal mouse brains. Both the two glycoproteins corresponding to molecular weights ranging from 200 to 350 kDa and from 110 to 160 kDa were isolated and identified as syndecan-3 by amino acid sequencing and immunochemical study, these findings being consistent with the report that syndecan-3 has a mucin-like domain different from other syndecans (Carey, 1996). In fact, the mucin like-domain on syndecan-3 contains some possible Tn-antigenic sites in the form of consecutive Ser/Thr residues, which could express the Tn antigenicity if the residues Ser/Thr are substituted only by GalNAc residues. The Tn antigen is not expressed exclusively on syndecan-3 in other tissues or cancer cell lines. Among cancer cell lines we examined, the Tn antigen was carried on CD44 in a rat pancreatic cancer cell line, BSp73ASML (Nakada *et al.*, unpublished data) and CD43 in a T-lymphoid cell line, Jurkat (Inoue *et al.*, 1994), in addition to mucins in epithelial cancer cell lines. These

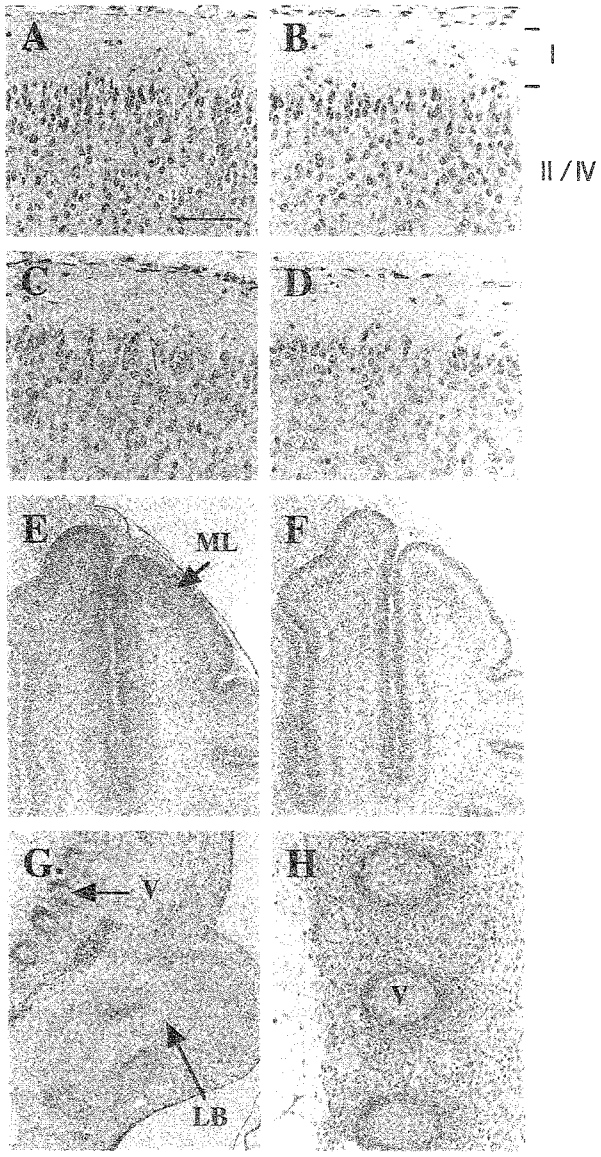

Fig. 7. Immunohistochemcal staining of mouse brain and cartilage primordium. On P4 mouse brain, the immunoreactivity was observed through the cerebral cortex layers (A) and, the molecular layer (ML) of the cerebellar cortex (E). Similar staining on P4 mouse cerebral cortex was detected with anti-mouse syndecan-3 core protein antibody as well (C). The Tn antigen was also detected in the E12 mouse cartilage primordium of vertebra (V) and limb bud (LB) (G, H). Control experiments performed using normal mouse IgG (B, F) or preimmune rabbit IgG (D) did not show any immunoreactivity. I-IV, cortical layers. Scale bar: A-D, 50 μm; E and F, 200 μm; G, 500 μm; H, 100 μm.

glycoproteins have consecutive GalNAc α1-Ser/Thr commonly. CD44 has a similar structural feature as that of syndecan-3 in respect to the fact that glycosaminoglycans and O-glycans are attached to the N-terminal and central regions of the molecule, respectively. It is reported that the O-glycans carried on CD44 play an important role in

modulating of the binding to hyaluronan (Bennett *et al.*, 1995). Gould *et al.* (1992) postulated that the multiple O-linked oligosaccharides of syndecan-3 might interact with the lectin domain of versican, since these interactions are involved in cartilage and nerve development. Thus, in the developing brain some characteristic O-glycans on syndecan-3 may modulate a biological function or interact with certain lectins. Since consecutive GalNAc α1-Ser/Thr is synthesized by a highly specific UDP-GalNAc: polypeptide N-acetylgalactosaminyltransferase (GalNAc-transferase) (Inoue *et al.*, 2001), the appearance of the Tn antigen in the developing mouse brain should be dependent on the expression of both syndecan-3 and the specific GalNAc-transferase. Disappearance of the Tn antigen may be caused by elongation of the carbohydrate chain. It would be interesting to see if the biological functions of the syndecan-3 change when some sugars are added to the Tn antigen.

It has been reported that the deduced amino acid sequence of syndecan-3 is compatible with a transmembrane proteoglycan, but syndecan-3 purified from rat brain fails to react with an antibody directed against its cytoplasmic domain (Bernfield *et al.*, 1993), indicating that most of syndecan-3 in the brain is cleaved and shed from the membrane through endoproteolytic cleavage. In fact, the major processed syndecan-3 could be extracted from mouse brains with an extraction solution not containing any detergent. The processed syndecan-3 could also be obtained from mouse brains, which had been boiled for 10 min immediately after removal from the mouse (data not shown). On the other hand, a detergent was necessary to extract the minor syndecan-3. Therefore, the minor syndecan-3 should contain its cytoplasmic domain and can be considered as an immature uncleaved form of syndecan-3 (Carey *et al.*, 1997; Hsueh and Sheng, 1999). The N-terminal sequence of the minor syndecan-3, however, coincided with that on the N-terminal side of the mucin-like domain, indicating that this form was generated through endoproteolytic cleavage at the C-terminal side of a methionine residue (amino acid 101), which is located on the N-terminal side of the mucin-like domain. The minor syndecan-3 could also be obtained from mouse brains boiled immediately after removal from the mice (data not shown). The possibility that syndecan-3 had been degraded by some proteases derived from other subcellular compartments such as the lysosome during the isolation procedure seems to be ruled out, being consistent with the report by Hsueh and Sheng (1999). Although it is generally agreed that syndecans are primary signaling cell surface receptors (Carey, 1997), syndecan-3 seems to be processed rapidly after its synthesis. Fig. 8 shows the two processed syndecan-3 schematically based on our results and deduced amino acid sequences (Kung *et al.*, accession No. U52826). Thus, two syndecan-3 ectodomains containing N-terminal glycosaminoglycan attachment sites can be shed from the membrane. One is the major syndecan-3 described above, and the other is a syndecan-3 fragment cleaved on the N-terminal side of the mucin-like domain, the residual portion of which is the minor syndecan-3 bound to the membrane. These soluble fragments of syndecan-3 may contribute to the structure of the extracellular matrix, and/or retention and storage of heparin-binding factors via their heparan sulfate glycosaminoglycans.

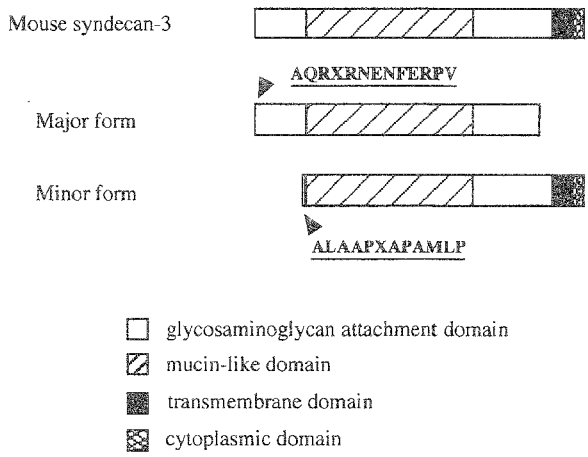

Fig. 8. Schematic structure of processed mouse syndecan-3. The major and minor forms are devoid of the transmembrane and cytoplasmic domain, and N-terminal glycosaminoglycan attachment domain, respectively.

Acknowledgments. This study was supported in part by a Grant-in-Aid for Scientific Research on Priority Areas, No. 10178102, from the Ministry of Education, Science and Culture of Japan, by the Foundation for Bio-venture Research Center from the Ministry of Education, Science and Culture of Japan, and by the Fugaku Trust for Medical Research.

References

Akita, K., Fushiki, S., Fujimoto, T., Inoue, M., Oguri, K., Okayama, M., Yamashina, I., and Nakada, H. 2001. Developmental expression of a unique carbohydrate antigen, Tn antigen, in mouse central nervous tissues. *J. Neurosci. Res.*, **65**: 595-603.

Bennett, K.L., Modrell, B., Greenfield, B., Bartolazzi, A., Stamenkovic, I., Peach, R., Jackson, D.G., Spring, F., and Aruffo, A. 1995. Regulation of CD44 binding to hyaluronan by glycosylation of variably spliced exons. *J. Cell. Biol.*, **131**: 1623–1633.

Bernfield, M., Hinkes, M.T., and Gallo, R.L. 1993. Developmental expression of the syndecans: possible function and regulation. *Dev. Suppl.*, **1993**: 205–212.

Carey, D.J. 1996. N-syndecan: structure and function of a transmembrane heparan sulfate proteoglycan. *Perspect. Dev. Neurobiol.*, **3**: 331–346.

Carey, D.J. 1997. Syndecans: multifunctional cell-surface co-receptors. *Biochem. J.*, **327**: 1–16.

Carey, D.J., Conner, K., Asundi, V.K., O'Mahony, D.J., Stahl, R.C., Showalter, L., Cizmeci-Smith, G., Hartman, J., and Rothblum, L.I. 1997. cDNA cloning, genomic organization, and in vivo expression of rat N-syndecan. *J. Biol. Chem.*, **272**: 2873–2879.

Chernousov, M.A. and Carey, D.J. 1993. N-syndecan (Syndecan 3) from neonatal rat brain binds basic fibroblast growth factor. *J. Biol. Chem.*, **268**: 16810–16814.

Gould, S.E., Upholt, W.B., and Kosher, R.A. 1992. Syndecan-3: a member of the syndecan family of membrane-intercalated proteoglycans that is expressed in high amounts at the onset of chicken limb cartilage differentiation. *Proc. Natl. Acad. Sci. USA*, **89**: 3271–3275.

Gould, S.E., Upholt, W.B., Kosher, R.A. 1995. Characterization of chicken syndecan-3 as a heparan sulfate proteoglycan and its expression during embryogenesis. *Dev. Biol.*, **168**: 438–451.

Herndon, M.E., Stipp, C.S., and Lander, A.D. 1999. Interactions of neural glycosaminoglycans and proteoglycans with protein ligands: assessment of selectivity, heterogeneity and the participation of core proteins in binding. *Glycobiology*, **9**: 143–155.

Hsueh, Y-P. and Sheng, M. 1999. Regulated expression and subcellular localization of syndecan heparan sulfate proteoglycans and the syndecan-binding protein CASK/LIN-2 during rat brain development. *J. Neurosci.*, **19**: 7415–7425.

Inoue, M., Nakada, H., Tanaka, N., and Yamashina, I. 1994. Tn antigen is expressed on leukosialin from T-lymphoid cells. *Cancer. Res.*, **54**: 85–88.

Inoue, M., Takahashi, S., Yamashina, I., Kaibori, M., Okumura, T., Kamiyama, Y., Vichier-Guerre, S., Cantacuzene, D., and Nakada, H. 2001. High density O-glycosylation of the MUC2 tandem repeat unit by N-acetylgalactosaminyltransferase-3 in colonic adenocarcinoma extracts. *Cancer Res.*, **61**: 950–956.

Kato, M., Oike, Y., Suzuki, S., and Kimata, K. 1985. Selective removal of heparan sulfate chains from proteoheparan sulfate with a commercial preparation of heparitinase. *Anal. Biochem.*, **148**: 479–484.

Kusano, Y., Oguri, K., Nagayasu, Y., Munesue, S., Ishihara, M., Saiki, I., Yonekura, H., Yamamoto, H., and Okayama, M. 2000. Participation of syndecan 2 in the induction of stress fiber formation in cooperation with integrin $\alpha5\beta1$: structural characteristics of heparan sulfate chains with avidity to COOH-terminal heparin-binding domain of fibronectin. *Exp. Cell. Res.*, **256**: 434–444.

Laemmli, U.K. 1970. Cleavage of structural proteins during the assembly of the head of bacteriophage T4. *Nature*, **227**: 680–685.

Margolis, R.K., and Margolis, R.U. 1993. Nervous tissue proteoglycans. *Experientia*, **49**: 429–446.

Milev, P., Chiba, A., Häring, M., Rauvala, H., Schachner, M., Ranscht, B., Margolis, R.K., and Margolis, R.U. 1998. High affinity binding and overlapping localization of neurocan and phosphacan/protein-tyrosine phosphatase-ζ/βwith tenascin-R, amphoterin, and the heparin-binding growth-associated molecule. *J. Biol. Chem.*, **273**: 6998–7005.

Nakada, H., Numata, Y., Inoue, M., Tanaka, N., Kitagawa, H., Funakoshi, I., Fukui, S., and Yamashina, I. 1991. Elucidation of an essential structure recognized by an anti-GalNAcα-Ser(Thr) monoclonal antibody (MLS 128). *J. Biol. Chem.*, **266**: 12402–12405.

Nakada, H., Inoue, M., Numata, Y., Tanaka, N., Funakoshi, I., Fukui, S., Mellors, A., and Yamashina, I. 1993. Epitopic structure of Tn glycophorin A for an anti-Tn antibody (MLS 128). *Proc. Natl. Acad. Sci. USA*, **90**: 2495–2499.

Numata, Y., Nakada, H., Fukui, S., Kitagawa, H., Ozaki, K., Inoue, M., Kawasaki, T., Funakoshi, I., and Yamashina, I. 1990. A monoclonal antibody directed to Tn antigen. *Biochem. Biophys. Res. Commun.*, **170**: 981–985.

Oohira, A., Katoh-Semba, R., Watanabe, E., and Matsui, F. 1994. Brain development and multiple molecular species of proteoglycan. *Neurosci. Res.*, **20**: 195–207.

Oohira, A., Matsui, F., Tokita, Y., Yamauchi, S., and Aono, S. 2000. Molecular interactions of neural chondroitin sulfate proteoglycans in the brain development. *Arch. Biochem. Biophys.*, **374**: 24–34.

Springer, G.F., Desai, P.R., and Banatwala, I. 1974. Blood group MN specific substances and precursors in normal and malignant human breast tissues. *Naturwissenschaften*, **61**: 457–458.

Watanabe, E., Matsui, F., Keino, H., Ono, K., Kushima, Y., Noda, M., and Oohira, A. 1996. A membrane-bound heparan sulfate proteoglycan that is transiently expressed on growing axons in the rat brain. *J. Neurosci. Res.*, **44**: 84–96.

(*Received for publication. July 3. 2001*
and in revised form. September 11. 2001)

Clinical Investigations

Respiration

Respiration 2001;68:262–267

Received: July 19, 1999
Accepted after revision: September 26, 2000

Inhibition of Lung Natural Killer Cell Activity by Smoking: The Role of Alveolar Macrophages

M. Takeuchi[a] S. Nagai[b] A. Nakajima[a] M. Shinya[a] C. Tsukano[a] H. Asada[a]
K. Yoshikawa[a] M. Yoshimura[a] T. Izumi[b]

[a]Department of Biotechnology, Faculty of Engineering, Kyoto Sangyo University, and
[b]Chest Disease Research Institute, Kyoto University, Kyoto, Japan

Key Words
Smoking · Natural killer cell activity · Alveolar macrophages · Lung

Abstract
Background: It is known that natural killer (NK) cell activity in the lung of smokers (SM) is lower than in non-smokers (NS). However, little is known about the underlying mechanisms. ***Objective:*** The purpose of this work was to investigate the mechanisms of the inhibition of NK cell activity by alveolar macrophages (AM) in SM. ***Methods:*** Lung effector cells and AM were obtained using bronchoalveolar lavage. The NK cell activity was assayed by ^{51}Cr release method after incubation of 4 and 24 h, using K562 as target cell. AM were added at a concentration of 25% to effector cells. ***Results:*** Following 24-hour culture, NK cell activity significantly increased in the NS but not in the SM. Lung NK cell activity was significantly augmented by interleukin-2 in the NS but not in the SM. Addition of AM to the NK cell preparation from SM exerted a significantly greater suppressive effect on autologous blood NK cell activity than in the NS. Indomethacin, catalase or thiourea did not prevent AM-mediated suppression of NK cell activity, in contrast to superoxide dismutase. ***Conclusions:*** These results suggest that the suppression of NK cell activity by AM in SM may be caused by O_2^- release rather than by prostaglandins, H_2O_2 or OH release from AM.

Introduction

Cigarette smoking causes an impairment in the immune system. Cigarette smokers (SM) have decreased helper/suppresser T cell ratios, decreased serum immunoglobulin levels and suppressed natural killer (NK) cell activity [1]. NK cells are large granular lymphocytes capable of destroying target cells without prior sensitization. Since the NK cell activity is most evident against neoplastic and virus-infected targets, it is believed that the major role of NK cells is to provide surveillance against cancer and viral infections [2]. NK cell activity is reduced in SM, but these studies have mainly focused on peripheral blood and lymphoid organs [3]. Little is known about NK cells in the lung. We have previously reported that the NK cell activity in the lung of SM is lower than in non-smokers (NS) [4]. Alveolar macrophages (AM) play a major role in lung defense mechanisms. Cigarette smoking induces various changes in the metabolism of AM [5]. In addition, AM have been shown to inhibit the expression of NK cell

KARGER
Fax + 41 61 306 12 34
E-Mail karger@karger.ch
www.karger.com

0025–7931/01/0683–0262$17.50/0

Accessible online at:
www.karger.com/journals/res

Minoru Takeuchi
Department of Biotechnology, Faculty of Engineering
Kyoto Sangyo University
Motoyama, Kamigamo, Kita-ku, Kyoto 603-8555 (Japan)
Tel. +81 75 705 1926, Fax +81 75 705 1926, E-Mail mtakex@cc.kyoto-su.ac.jp

activity [6]. It is known that prostaglandins (PG) and oxygen radicals are produced by AM and monocytes, and that PG and oxygen radicals from monocytes may suppress NK cell activity [7, 8]. Also, the NK cell activity of the lung in SM is reduced [4]. Little, however, is known about the mechanisms of cell-mediated down-regulation of NK cell activity. To evaluate a possible role for PG or oxygen radicals in AM-mediated inhibition of NK cell activity in SM, we examined the effect of a PG synthetase inhibitor and antioxidants on AM-mediated inhibition of NK cell activity in smokers. This study was designed to evaluate the suppressive effect of smoking on NK cell activity in the human lung and to investigate the mechanism of the inhibition of NK cell activity by AM in smokers.

Material and Methods

Subjects. Forty-five healthy male individuals were studied. There were 23 non-smokers (NS) ranging in age from 24 to 56 years (34.2 ± 6.1, mean ± SE) and 22 smokers (SM) ranging in age from 27 to 57 years (35.4 ± 6.3). All individuals had normal physical examination results, chest roentgenograms, and lung function tests. The smoking history ranged from 4 to 30 years (13.4 ± 6.0), and from 15 to 50 cigarettes/day (27.0 ± 6.2). Pack years ranged from 4 to 50 (22.8 ± 7.3). Informed consent was obtained from healthy volunteers. The lavage study of human subjects was approved by the Kyoto University.

Bronchoalveolar Lavage (BAL). BAL was performed by instillation of 300 ml of 0.9% saline solution in six 50-ml aliquots into the middle lobe or the lingula through a flexible bronchoscope under topical anesthesia. The fluid retrieved by suctioning was filtered through gauze and placed on ice.

Isolation of BAL and Blood Effector Cells. The recovered cells were separated from the BAL fluid by centrifugation and washed twice in RPMI-1640 medium. Blood mononuclear cells were separated from the peripheral blood by Ficoll-Hypaque centrifugation. To obtain purified preparations of BAL and blood lymphocytes, mononuclear cells were suspended in culture medium (RPMI-1640 suspended with 50 m*M* glutamine, 100 μg/ml streptomycin, 100 U/ml penicillin and 10% FCS) and were depleted of adherent cells by adherence to plastic tissue culture dishes for 60 min at 37°C, followed by passage through nylon columns. Nonadherent cells were eluted from the nylon wool columns at 2 ml/min at 37°C using culture medium. The resulting lymphocyte populations (referred to throughout as lymphocytes) were routinely of ≥98% purity as determined by morphology and nonspecific esterase staining.

Isolation of AM. The recovered cells were separated from the BAL fluid by centrifugation and washed twice in RPMI-1640 medium. AM were purified from the mononuclear cell populations by adherence to plastic dishes for 1 h at 37°C in culture medium, then removed using a disposable cell scraper. The resulting AM were 98% pure as determined by morphology and nonspecific esterase staining. The viability of AM was >90% as measured by 0.2% trypan blue exclusion test.

Target Cells. The cultured human cell line used as target was the K562 erythroleukemia cell line; 5×10^6 cells were labeled by addition of 100 μCi $Na^{51}CrO_4$ and incubated for 1 h at 37°C with occasional shaking. The cells were then washed three times and were resuspended at a concentration of 1×10^5 cells/ml in culture medium.

NK Cell Cytotoxicity Assay. The cytotoxicity assay was performed as described previously [9]. Briefly, 100 μl effector cells (1×10^5 cells) and 100 μl labeled target cells (1×10^4 cells) at an effector to target (E/T) ratio of 10:1 were added to wells of round-bottom microtiter plates. The plates were then centrifuged and incubated at 37°C for 4 h in a humidified atmosphere of 5% CO_2 in air, after which supernatants were removed using a supernatant collection system. Supernatants from triplicate wells were counted in a γ-counter for 1 min. Spontaneous ^{51}Cr release was determined in wells containing target cells and medium, and maximum release by the addition of Triton X-100. The percentage of cytotoxicity for each assay was calculated from the following formula:

$$\text{NK cell activity (\%)} = \frac{\text{experimental release} - \text{spontaneous release}}{\text{maximum release} - \text{spontaneous release}} \times 100$$

The range of spontaneous release from the target cells was 5–10% of maximum release.

Treatment with Interleukin-2 (IL-2). Effector cells (1×10^6/ml) in BAL were precultured with IL-2 at a dose of 50 U/ml in culture medium for 24 h at 37°C in 5% CO_2 and air before the addition of target cells. Effector cells were washed with 50 ml of PBS before the ^{51}Cr release assay (E/T = 10) was performed.

Effect of AM. To determine if AM could inhibit NK cell activity, AM were added at a final concentration of 25% to blood effector cells in the NK cell activity (E/T = 10). Percent inhibition of additional AM (AM-A) NK cell activity was calculated from the following formula:

$$\text{inhibition (\%)} = \left(1 - \frac{\text{AM-A NK cell activity}}{\text{non-AM-A NK cell activity}}\right) \times 100$$

Effect of Indomethacin or Antioxidants. To evaluate a possible role for PG or oxygen radicals in AM-mediated inhibition of NK cell activity, indomethacin or antioxidants were added to the 25% additional concentration of the AM coculture NK cell assay as described above at final concentrations of 2.5×10^{-7} to 2.5×10^{-5} m*M* of indomethacin, 1.4–1,400 U/ml of catalase, 2.5 and 25 m*M* of thiourea or 7.5–750 U/ml of superoxide dismutase (SOD).

Statistics. All data were expressed as means ± SE of the mean. Statistical significance was assessed by a two-tailed Student's *t* test. Any p value <0.05 was considered significant.

Results

Recovery of BAL Fluid and Cells from NS and SM

The total number of cells recovered was significantly ($p < 0.05$) increased in SM compared with that in NS (table 1). This was due to an increase in proportion of AM recovered from SM. The percentage of lymphocytes in SM was significantly ($p < 0.05$) lower than in NS. The percentage of BAL fluid recovery and granulocytes of SM was similar to that of NS.

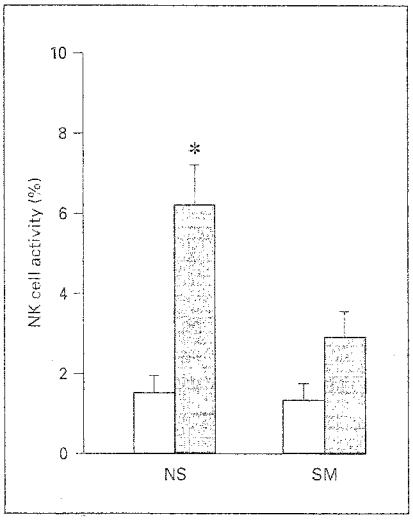

Fig. 1. NK cell activity of the lung in healthy NS and SM. □ = Before culture; ▨ = after 24 h of culture. The data are shown as means ± SE. * $p < 0.05$, vs. before culture.

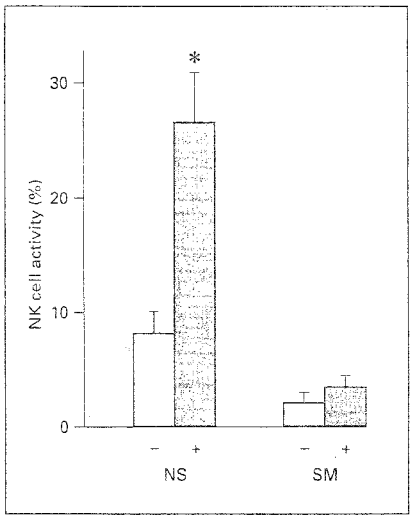

Fig. 2. Effect of IL-2 on lung NK cell activity in healthy NS and SM. − = No treatment; + = IL-2 50 U/ml treatment. The data are shown as means ± SE. * $p < 0.05$, vs. no IL-2 treatment.

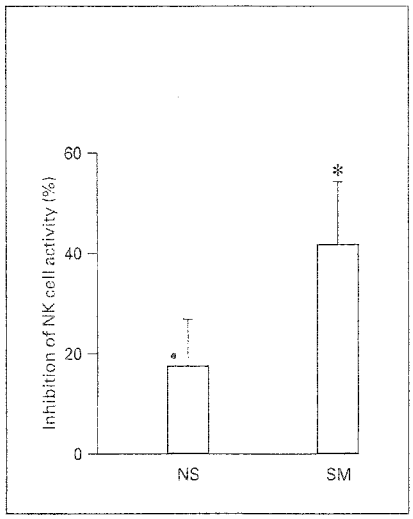

Fig. 3. Effect of AM in healthy NS and SM on autologous blood NK cell activity at 25% AM additional concentration. The data are shown as means ± SE. * $p < 0.05$, vs. NS.

Table 1. Recovery of BAL fluid and cells in NS and SM

	Fluid recovery, %	Total cells, n		AM, %	Lympho-cytes, %	Granulo-cytes, %
		× 10^6/ml	× 10^3/ml			
NS (n = 23)	76.2 ± 2.3	10.1 ± 3.7	43.5 ± 7.0	86.9 ± 5.6	12.5 ± 4.0	0.6 ± 0.2
SM (n = 22)	71.0 ± 4.2	29.8 ± 4.3[a]	147.8 ± 5.2[b]	97.0 ± 2.0[a]	4.6 ± 0.7[a]	0.4 ± 0.2

Means ± SE. [a] $p < 0.05$, [b] $p < 0.01$ vs. NS.

NK Cell Activity of Lung in NS and SM

NK cells in SM lungs had low levels of cytotoxicity against K562 target cells before and after 24 h of incubation. Lung NK cell activity in NS were initially very low (1.5 ± 0.4%, mean ± SE), but after 24 h of incubation in medium alone, NK cell activity values were 6.1 ± 1.1%. This represented a significant ($p < 0.05$) increase in NK cell activity at an E/T ratio of 10:1. In smokers, lung NK cell activity levels were initially 1.3 ± 0.5% and increased after 24 h to 2.9 ± 0.7%. The difference was not statistically significant (fig. 1).

Responsiveness to IL-2 of Lung Effector Cells in NS and SM

NK cell activity was very low in the lung of NS and SM, but this activity could be augmented in medium alone after 24 h of incubation in NS but not in SM (fig. 2). The NK cell activity of lung after 24 h of culture was significantly ($p < 0.05$) augmented by IL-2 in vitro in NS, but not in SM.

Inhibition of Autologous Blood NK Cell Activity by Addition of AM in NS and SM

Blood E/T ratio of 10:1 was usually kept constant, whereas the concentration of AM-A to blood effector cells was 25%. The AM was inhibited 18 ± 5.4% (mean ± SE)

in NS and 42 ± 8.9% in SM at a 25% concentration of AM-A to autologous blood effector cells (fig. 3). There was a difference between NS and SM in the inhibitory activity of AM on autologous blood NK cell activity. AM in SM significantly ($p < 0.05$) inhibited autologous blood NK cell activity compared to NS.

Effect of Indomethacin, Catalase, Thiourea or SOD on AM-Mediated Inhibition of Autologous Blood NK Cell Activity in SM

To evaluate the possibility that the AM-mediated inhibition of NK cell activity in SM might be caused by PG and oxygen radicals produced by AM, indomethacin, catalase, thiourea or SOD were added to AM-blood effector cell co-cultivation NK cell assay at 25% AM additional concentration (fig. 4). The AM in SM caused a 42 ± 8.9% (mean ± SE) inhibition of NK cell activity. Final concentrations of 2.5×10^{-7} to 2.5×10^{-5} m*M* of indomethacin failed to reverse AM-mediated inhibition of NK cell activity. At concentrations of 1.4–1,400 U/ml of catalase or 2.5, 25 m*M* of thiourea, inhibition of NK cell activity by AM was not reversed. However, SOD at final concentrations of 75 or 750 U/ml prevented AM-mediated inhibition of NK cell activity, and NK cell activity recovered to the level of non-AM-A NK cell activity. Indomethacin, catalase or thiourea did not prevent AM-mediated suppression of NK cell activity in SM, but SOD prevented this suppression. SOD did not cause cytotoxicity on AM.

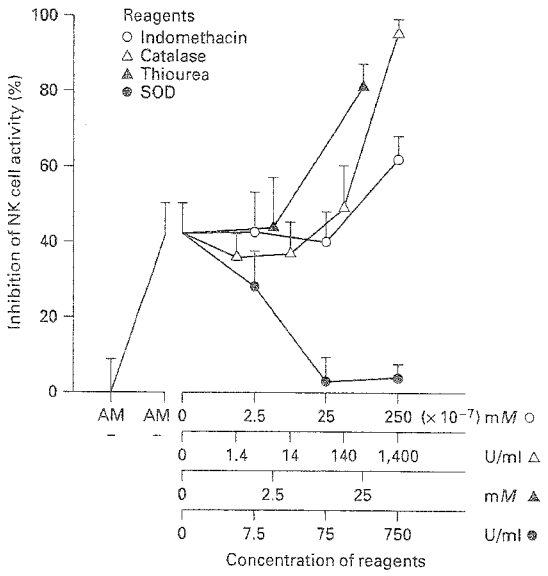

Fig. 4. Effect of indomethacin, catalase, thiourea or SOD on AM-mediated inhibition of autologous blood NK cell activity in healthy SM. – = No addition of AM from SM; + = 25% addition of AM from SM. The data are shown as means ± SE.

Discussion

We have demonstrated that NK cell activity in the lung is impaired in SM. Furthermore, these NK cells respond poorly to IL-2. In addition, AM from SM exert a significantly greater suppressive effect on autologous NK cell activity than AM from NS. We also examined the effect of indomethacin, a PG synthetase inhibitor, catalase, a H_2O_2 scavenger, thiourea, an OH scavenger, and SOD, an O_2^- scavenger on AM-mediated inhibition of NK cell activity in smokers. Our results showed that in contrast to indomethacin, catalase and thiourea, SOD prevented the inhibition of NK cell activity by AM in smokers. NK cell activity recovered to the baseline level before the addition of AM. Our results suggest that the AM-mediated inhibition of NK cell activity in SM may be caused by O_2^- production from AM, but not by PG, H_2O_2 or OH.

NK cells are large granular lymphoid cells which play an important role in immune surveillance against tumors and resistance against certain microbial infections [10]. Immunologic alterations due to smoking include an increase in peripheral leukocyte count, a decrease in circulating immunoglobulin levels, and the formation of serum precipitins against tobacco antigens [11, 12]. Results of peripheral blood lymphocyte responsiveness to mitogens are conflicting [12], and range from an enhancement, no effect, to suppression in SM. Miller et al. [13] observed that heavy smokers have a significantly lower percentage of CD4+ lymphocytes and a higher percentage of CD8+ lymphocytes in blood, with a resultant lower CD4:CD8 ratio. Costabel et al. [14] also reported a markedly decreased ratio of CD4+/CD8+ lymphocytes in the bronchoalveolar lavage fluid of SM.

Blood NK cell activity in SM was examined in two studies; both reported depressed levels of activity in SM [3, 15]. Phillips et al. [3] noted that heavy SM (79 pack-years) had decreased NK cell activity, but light SM (27 pack-years) had normal NK cell activity in blood. Our previous data are similar, particularly in light SM. Hughes et al. [15] also concluded that heavy SM as a group had low NK cell activity, while little is known about NK cells in the lung. In lung NK cell activity, Robinson et al. [16] using BAL reported that NK cells were present in the normal human lung but expressed little NK cell activity com-

pared with blood. Our previous reports are in agreement with the report which found NK cell activity in NS to be lower in BAL fluid than in blood [4]. The present investigation shows that NK cell activity in the NS lung significantly increases after 24 h of culture. However, in SM, no increase in NK cell activity was noted. We observed differences between NS and SM with regard to NK cell activity of the lung but not that of blood. This indicates that alterations in NK cells induced by smoking are localized. In earlier studies, NK cell activity was augmented by IL-2 [17]. Our study confirms previous reports of augmented NK cell activity by IL-2 in the lung NS. However, lung NK cell activity in SM was not augmented by IL-2. Our data show that the function of NK cells in the lung of SM is damaged by smoking.

Human AM reportedly are better producers of PG than other mononuclear phagocytes [18]. AM can also release superoxide anions (O_2^-) and other forms of reduced O_2 species [7]. It is known that E-series PG and oxygen radicals from human monocytes can suppress NK cell activity [8]. Robinson et al. [16], using BAL fluid from healthy NS, reported that neither indomethacin nor antioxidants prevented the AM-mediated suppression of NK cell activity. However, Weissler et al. [19], using AM from patients with lung cancer, reported that the cultured supernatant of lipopolysaccharide-stimulated AM suppressed NK cell activity, and this suppression was blocked if indomethacin was present in AM cultures, suggesting that PG released by AM might inhibit NK cell activity. This is due to a difference in culture conditions. The data presented suggest that under lipopolysaccharide-stimulated conditions, PG produced by AM may partially suppress NK cell activity. Seaman et al. [8] demonstrated that suppression of NK cell activity was mediated by human monocytes or polymorphonuclear leukocytes and that suppression was dependent on the generation of reactive forms of molecular oxygen, particularly hydrogen peroxide (H_2O_2). However, the mechanisms by which AM inhibit NK cell activity remain unclear. To evaluate a possible role for PG or oxygen radicals in AM-mediated inhibition of NK cell activity in smokers, we examined the effect of a PG synthetase inhibitor (indomethacin) or antioxidants (catalase: H_2O_2 scavenger, thiourea: OH scavenger, and SOD: O_2^- scavenger) on AM-mediated inhibition of NK cell activity in smokers. Our results show that indomethacin, catalase or thiourea at various concentration did not prevent, but SOD prevented the AM-mediated inhibition of NK cell activity, so NK cell activity recovered to the non-AM-A level. In our opinion, the lack of agreement between our results and previous reports may be due to differences in materials and culture conditions. Our results suggest that the AM-mediated inhibition of autologous blood NK cell activity in smokers may be caused by O_2^- production from AM, but not PG, H_2O_2 or OH. Additionally, the release of O_2^- by AM could result in the low NK cell activity in the lung.

SM are known to have an increased number of AM [20]. Our results are similar in this regard. It is also known that AM from healthy cigarette smokers release more O_2^- than NS [20]. Hoidal et al. [7] reported that AM from SM were cytocidal to fibroblasts in culture, and lysis of fibroblasts by AM from SM was completely prevented by the addition of SOD and catalase. Our study also shows that the AM-mediated inhibition of NK cell activity in SM was prevented by SOD. These findings suggest that the increased O_2^- production by AM from smokers was completely prevented by the addition of SOD and catalase.

In summary, we have demonstrated that NK cell activity in the lung is impaired in SM. Furthermore, these NK cells respond poorly to IL-2. Also, AM in SM exerted significantly greater suppressive effect on autologous NK cell activity than AM in NS. The AM-mediated inhibition of NK cell activity in SM may be caused by O_2^- production from AM, but not PG, H_2O_2 or OH.

Acknowledgments

This study was supported by a grant-in-aid for Scientific Research C (No. 09680537) and a bio-venture project of academic frontier science from the Ministry of Education, Science, Sports and Culture, Japan.

References

1 Barbour SE, Nakashima K, Zhang JB, Tangada S, Hahn CL, Schenkein HA, Tew JG: Tobacco and smoking. Rev Oral Biol Med 1997;8:437–460.

2 Herberman RB, Djeu JK, Kay HD, Ortaldo JR, Ricardi C, Bonnard CD: Natural killer cells. J Immunol 1979;44:43–70.

3 Phillips B, Marshall ME, Brown S, Thomspon JS: Effect of smoking on human natural killer cell activity. Cancer 1985;56:2789–2792.

4 Takeuchi M, Nagai S, Izumi T: Effect of smoking on natural killer cell activity in the lung. Chest 1988;94:688–693.

5 McCrea KA, Ensor JE, Nall K, Bleecker ER, Hasday JD: Altered cytokine regulation in the lungs of cigarette smokers. Am J Respir Crit Care Med 1994;150:696–703.

6 Takeuchi M, Nagai S, Izumi T: The mechanism of inhibition of alveolar macrophages on autologous blood natural killer cell activity. Chest 1989;95:383–387.

7 Hoidal JR, Beall GD, Repine JE: Production of hydroxyl radical by human alveolar macrophages. Infect Immun 1979;26:1088–1094.

8 Seaman WE, Gindhart TD, Blackman MA, Dalal B, Tolol N, Werb Z: Suppression of natural killing in vitro by monocytes and polymorphonuclear leukocytes. J Clin Invest 1982;69:876–888.

9 Ortaldo JR, Oldham RK, Cannon GC, Herberman RB: Specificity of natural cytotoxic reactivity of normal human lymphocytes against a myeloid leukemia cell line. J Natl Cancer Inst 1977;59:77–82.

10 Herberman RB: Natural killer cells and their possible roles in resistance against disease. Clin Immunol Rev 1981;1:1–65.

11 Gerard JW, Heiner PC, Mink J, Meyers A, Dosman JA: Immunoglobulin levels in smokers and non-smokers. Ann Allergy 1980;44:261–262.

12 Johnson JD, Houchens DP, Kluwe WM, Craig DK, Fisher GL: Effects of mainstream and environmental tobacco smoke on the immune system in animals and humans. Toxicology 1990;20:369–395.

13 Miller LG, Goldstein G, Murphy M, Ginns LC: Reversible alterations in immunoregulatory T cells in smoking. Chest 1982;82:526–529.

14 Costabel U, Bross KJ, Reuter C, Ruhle KH, Matthys H: Alterations in immunoregulatory T-cell subsets in cigarette smokers. Chest 1986;90:39–44.

15 Hughes DA, Haslam PL, Townshend PJ, Turner-Warwick M: Numerical and function alterations in circulatory lymphocytes in cigarette smokers. Clin Exp Immunol 1985;61:459–466.

16 Robinson BWS, Pinkston P, Crystal RG: Natural killer cells are present in the normal human lung but are functionally impotent. J Clin Invest 1984;74:942–950.

17 Itoh K, Shiba K, Shimizu Y, Suzuki R, Kumagai K: Generation of activated killer cells by recombinant interleukin 2 in collaboration with interferon-γ. J Immunol 1985;134:3124–3129.

18 Morley J, Bray MA, Jones RW, Nugteren DH, Dorp DA: Prostaglandin and thromboxane production by human and guinea-pig macrophages and leukocytes. Prostaglandins 1979;17:730–736.

19 Weissler JC, Nicod LP, Toews GB: Pulmonary natural killer cell activity is reduced in patients with bronchogenic carcinoma. Am Rev Respir Dis 1987;135:1353–1357.

20 Richter AM, Abboud RT, Johal SS, Fera TA: Acute effect of smoking on superoxide production by pulmonary alveolar macrophages. Lung 1986;164:233–242.

The role of syndecan-2 in regulation of actin-cytoskeletal organization of Lewis lung carcinoma-derived metastatic clones

Seiichi MUNESUE*, Yuri KUSANO†, Kayoko OGURI†, Naoki ITANO†[1], Yasuo YOSHITOMI*, Hayao NAKANISHI‡, Ikuo YAMASHINA* and Minoru OKAYAMA*[2]

*Department of Biotechnology, Faculty of Engineering, Kyoto Sangyo University, Kyoto 603-8555, Japan, †Clinical Research Institute, National Nagoya Hospital, Nagoya 460-0001, Japan, and ‡Division of Oncological Pathology, Aichi Cancer Center Research Institute, Nagoya 464-8681, Japan

Syndecans, a family of transmembrane heparan sulphate proteoglycans, contribute to various biological processes, including adhesion, motility, proliferation, differentiation and morphogenesis. We document here the involvement of syndecan-2 acting alone or co-operatively with integrin $\alpha5\beta1$, for regulation of actin-cytoskeletal organization on cell adhesion to fibronectin, using fibronectin-recombinant polypeptides containing the ligands for either or both of these receptors as substrata. Lewis lung carcinoma-derived low-metastatic P29 cells binding to the substrata by both receptors formed actin stress fibres, whereas those binding by syndecan-2 or integrin $\alpha5\beta1$ alone formed filopodia or cortex actin. In contrast, higher metastatic LM66-H11 cells formed cortex actin even on substrata containing both ligands. Northern-blot and flow-cytometric analyses revealed that syndecan-2 expression in LM66-H11 cells was significantly lower (1/4.5 in mRNA and 1/8 in cell-surface expression) than in P29 cells, whereas expression levels of integrin $\alpha5\beta1$ and other syndecans were similar in both cell types. These results suggest that the failure of LM66-H11 to form stress fibres is due to a lower expression of syndecan-2 than that due to a threshold for its function. This was confirmed by the finding that overexpression of syndecan-2 by transfection of its cDNA into LM66-H11 cells caused the formation of stress fibres on the fibronectin substratum. These *in vitro* cellular responses of the two clones might reflect their *in vivo* situation in primary tumours in which P29 cells with a stroma-inducing capacity were immediately surrounded by fibronectin-rich matrix formed by the induced stromal cells, whereas LM66-H11 cells without such capacity were not surrounded by a similar matrix.

Key words: actin stress fibres, cell adhesion, fibronectin-recombinant polypeptides, heparan sulphate proteoglycans, integrin $\alpha5\beta1$.

INTRODUCTION

The extracellular matrix (ECM) is an extremely complex supramolecular structure. each of its components comprises several domains to allow them to interact with each other or with other ECM constituents and with cells. Cells generally interact with the ECM formed by themselves; epithelial cells interact with basement membranes and mesenchymal and stromal cells with interstitial-type matrix, but occasionally with allogenic ECM. Epithelial–mesenchymal or epithelial–stromal interactions play an important role in both physiological and pathological situations such as embryonic morphogenesis [1,2], wound healing [3] and tumorigenesis [4], and are accompanied by dynamic changes of ECM [5,6] to generate new cell–matrix interactions. In a metastatic process, tumour cells are always forced to interact with allogenic ECMs and these interactions are presumed to be important for the completion of metastasis.

The information encoded in an ECM is revealed by the interaction between individual ECM components and their respective receptors on the cell surface. It is well established that cell contact with a single ECM component initiates multiple signals affecting both cell behaviour and gene expression [7,8]. The interactions between fibronectin and integrin $\alpha5\beta1$ have been studied extensively [9–11]. Their binding triggers the assembly of many cytoplasmic signalling proteins to form focal adhesions and re-organize actin cytoskeletons [12,13]. Recently, it has become clear that syndecans, a family of transmembrane heparan sulphate proteoglycans whose external glycosaminoglycan chains can bind various extracellular soluble and insoluble ligands and whose core protein cytoplasmic domain can transduce signals into intracellular events, can modify signals generated by integrin-mediated cell adhesion to fibronectin [14]. Syndecan-4 signals co-operatively with integrins for the assembly of focal adhesions in fibroblasts inoculated on a fibronectin substratum [15,16] in a Rho-dependent manner [17]. Although details of the signalling processes remain to be determined, several components, which appear to be involved in the signalling, have been identified. Couchman and co-workers [18–20] have demonstrated that the variable region in the cytoplasmic domain of syndecan-4 binds phosphatidylinositol 4,5-bisphosphate and protein kinase Cα (PKCα), and this interaction mediates its own multimerization, with resultant regulation of the intracellular distribution and activity of PKCα. Screening of a yeast two-hybrid library with a syndecan cytoplasmic domain identified several PDZ-containing proteins, syntenin [21], CASK/LIN-2 [22], synectin [23] and synbindin [24], which bind to the COOH-terminal EFYA sequence of syndecans, and syndesmos, which binds to both the membrane proximal and the variable regions [25].

Recently, we demonstrated that Lewis lung carcinoma-derived low-metastatic P29 cells induced actin stress-fibre formation on adhesion to a fibronectin substratum [26]. The formation of actin

Abbreviations used: ECM, extracellular matrix; PKCα, protein kinase Cα; DMEM, Dulbecco's modified Eagle's medium; FCS, foetal calf serum; RT, reverse transcription.

[1] Present address: Institute for Molecular Science of Medicine, Aichi Medical University, Nagakute, Aichi, Japan.

[2] To whom correspondence should be addressed (e-mail: okayamam@cc.kyoto-su.ac.jp).

stress fibres was completely inhibited by the addition of GRGDS peptide, heparin, anti-heparan sulphate monoclonal antibody or heparan sulphate oligomer [IdoA(2-OSO_3)-GlcNSO_3(6-OSO_3)]$_6$, or treatment of the cells with heparitinase-I, suggesting that the signal to form actin stress fibres was transduced by a dual-receptor system with integrin $\alpha5\beta1$ and heparan sulphate proteoglycans. Moreover, the fact that the selective suppression of the expression of syndecan-2 with an antisense oligonucleotide for the core protein of this proteoglycan resulted in the failure to form actin stress fibres, indicated that the syndecan-2 is an essential component for the induction of this cytoskeletal organization. These results are consistent with our previous findings that more than 85% of the cell-surface heparan sulphate proteoglycans purified from P29 cells by fibronectin affinity is syndecan-2 [27] and that among these proteoglycans only syndecan-2 has a serine residue(s) in the cytoplasmic portion of the core protein, which is phosphorylated [28].

The highly metastatic LM66-H11 clone derived from the same carcinoma from which the P29 clone was isolated, was established after 66 episodes of an *in vivo* selection on the basis of spontaneous metastatic potential, exhibiting an ECM-dependent tumorigenesis distinctly different from the P29 clone [27]. Thus P29 cells with a capacity to elicit a host-stromal response, exhibit tumorigenesis dependent on a fibronectin-rich interstitial-type matrix generated by the induced stromal cells, whereas the highly metastatic cells, without any detectable capacity to elicit such a stromal response, show tumorigenesis dependent on the well-organized basement membranes formed by tumour cells themselves [29–31]. Therefore in the LM66-H11 tumour, the tumour cells encounter fibronectin only when they are confronted with the basement membrane of tumour blood vessels, whereas P29 cells are constantly interacting with fibronectin in the immediate surroundings. In the present study, we demonstrated that cellular responses of the two clones to adhere on a fibronectin substratum *in vitro* reflected the difference in their ECM dependence in tumorigenesis and the difference of the responses was attributable to the expression level of syndecan-2 on the cells to modify the integrin $\alpha5\beta1$-mediating signal. To determine the ligands which initiate signals and their respective receptors, we used as substrata the fibronectin-relating recombinant polypeptides, RGD-containing cell-binding domain (designated as C-274), C-terminal heparin-binding domain (H-271) and a fusion polypeptide of both (CH-271). Moreover, we demonstrated that overexpression of syndecan-2 in LM66-H11 cells resulted in the formation of stress fibres on fibronectin as did the P29 cells. These clones of epithelial origin do not produce fibronectin [32], thus providing a useful system for this type of analysis without any complications due to synthesis of endogenous fibronectin.

MATERIALS AND METHODS

Materials

Human-plasma fibronectin was purchased from Iwaki Glass (Tokyo, Japan). Three species of fibronectin-recombinant polypeptides (Figure 1), i.e. C-274 (Pro^{1239}-Ser^{1515}) with the RGD-containing Cell-I domain, H-271 (Ala^{1690}-Thr^{1960}) with the C-terminal heparin-binding Hep-II domain and CH-271, a fusion polypeptide of C-274 and H-271 with a methionine residue were generously supplied by TaKaRa Biomedicals (Otsu, Japan). Amino-acid sequences used here are numbered according to the system of Kornblihtt et al. [33]. Goat anti-human integrin $\alpha5\beta1$ antibody (AB1950) was purchased from Chemicon International (Temecula, CA, U.S.A.). Anti-heparan sulphate monoclonal antibody, F58-10E4, was a gift from Dr K. Yoshida of Seikagaku Corp., Tokyo, Japan. The rabbit anti-mouse syndecan-2 antibody (SN2Ab), specific to the ectodomain of syndecan-2, was prepared as described previously [26]. [*Me*-^{3}H]thymidine (3.1 TBq/mmol), [^{35}S]sulphate (carrier-free) and [α-^{32}P]dCTP (111 TBq/mmol) were purchased from DuPont–NEN Research Product (Boston, MA, U.S.A.).

Cell culture

The low-metastatic P29 and highly metastatic LM66-H11 cells cloned from a murine Lewis lung carcinoma 3LL [27] were cultured in Dulbecco's modified Eagle's medium (DMEM) supplemented with 10% (v/v) foetal calf serum (FCS) (Gibco, NY, U.S.A.), streptomycin (100 μg/ml) and penicillin (100 units/ml) at 37 °C in a humidified 5% CO_2 atmosphere. The syndecan-2 transfectants used in the present study were cultured in DMEM supplemented with 10% FCS G418 (800 μg/ml), streptomycin (100 μg/ml) and penicillin (100 units/ml) at 37 °C in a humidified 5% CO_2 atmosphere. The cells were harvested after incubation with 2 mM EDTA in PBS (EDTA/PBS) for 10 min at 37 °C, followed by gentle flushing with a pipette and subcultured twice a week.

Metastasis assay and immunostaining of primary tumour tissues

The metastatic potentials of the clones were measured by injecting single-cell suspensions of 1.0×10^5 or 2.0×10^5 cells in 200 μl of DMEM into the tail vein intravenously or subcutaneously to the right abdominal flank of syngenic C57BL/6 6-week-old male mice, respectively. After 4 weeks, the animals were killed and the number of visible parietal nodules in the lung, fixed in Bouin's solution, were counted.

The subcutaneous primary tumours were excised. Fresh frozen sections of 7 μm thickness were blocked with 1% BSA/PBS and treated with anti-fibronectin or anti-laminin antibodies at room temperature for 1 h. After washing with PBS, the sections were exposed to FITC-conjugated anti-rabbit immunoglobulin and 1.5 μM propidium iodide (Molecular Probes, OR, U.S.A.), and used for nuclear counterstaining. The sections were examined under an OLYMPUS Bx-50 microscope and images were captured using a High Sensitivity Cooled CCD Camera SenSys 0400 (RS-Photometrics, AZ, U.S.A.) and processed using Adobe PhotoShop 4.0.1J software.

Actin-cytoskeleton staining

Cells (5×10^3 cells in 50 μl of 0.2% BSA/DMEM) were inoculated on coverslips that had been coated with fibronectin (50 μg/ml), fibronectin-recombinant polypeptides (100 μg/ml) or combinations of C-274 (500 μg/ml) and antibodies F58-10E4 (15 μg/ml) or SN2Ab (0.7 μg/ml) overnight at 4 °C and blocked with 0.2% BSA/PBS for 30 min at room temperature. The cells were incubated for 1 h and then fixed in 3.7% paraformaldehyde containing 0.1% (v/v) Tween 20 for 5 min at room temperature. Actin filaments were stained with Rhodamine-conjugated phalloidin (Molecular Probes) for 30 min at room temperature and specimens were observed under a fluorescent microscope.

Cell-adhesion assay

Cells growing in a logarithmic phase were incubated with [*Me*-^{3}H]thymidine (74 kBq/ml) for 12 h. After washing thrice with PBS, the cells were harvested with EDTA/PBS. The radiolabelled cells (1×10^4 cells) were suspended in 100 μl of 0.2%

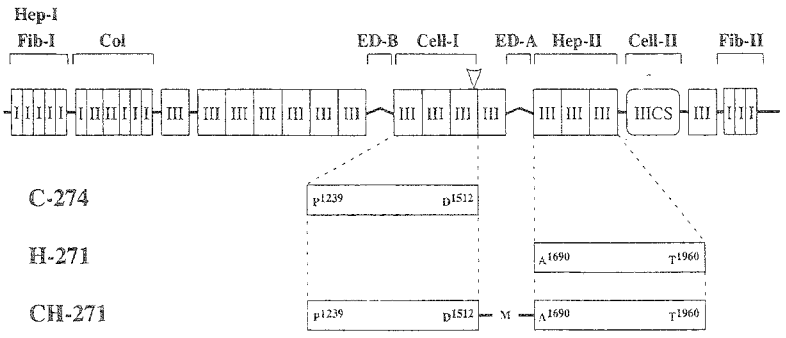

Figure 1 Schematic models of fibronectin and the recombinant polypeptides used as substrata

Homology domain structures in fibronectin are represented by I, II, III and IIICS for type-I, -II, and -III homology units, and type-III homology connecting segment, respectively. Functional heparin-, fibrinogen-, collagen- and cell-binding domains are abbreviated as Hep, Fib, Col and Cell, respectively. The open arrowhead shows the position of the GRGDS sequence. The recombinant polypeptide, C-274, was designed with 8th to 10th type-III homology and H-271 with 12th to 14th. CH-271 is a fusion form of C-274 and H-271 with a methionine residue (M). ED-A and ED-B indicate that extra domains arise from alternative splicing.

BSA/DMEM and inoculated in 96-well plates coated with fibronectin (50 μg/ml) or its recombinant polypeptides (100 μg/ml). After incubation for 1 h at 37 °C, the plates were agitated on a microtube mixer at 1000 rev./min for 2 min to suspend unattached and loosely attached cells. The attached and unattached cells were solubilized separately in 1 % SDS in 0.5 M NaOH. The radioactivity of an aliquot of each sample was measured in a liquid-scintillation counter (Beckman LS-9000).

Flow-cytometric assay

Cells (3×10^5 cells suspended in 50 μl of 0.2 % BSA/DMEM) were incubated with antibodies or respective non-immune sera for 1 h at 4 °C with gentle agitation. After washing thrice with PBS, they were exposed to an FITC-conjugated second antibody for 30 min. The labelled cells were washed and the intensity of fluorescence was measured in a flow cytometer, Ortho Cytoron (Ortho Diagnostic Systems K.K.).

RT (reverse transcription)-PCR and Northern-blot analyses

Poly(A)$^+$ RNAs were isolated from 1×10^7 cells of each clone, using a QuickPrep micro mRNA Purification Kit (Amersham Pharmacia Biotech) and analysed by RT-PCR using a TaKaRa RNA LA PCR Kit (TaKaRa Biomedicals) in a thermal cycler, Gene Amp PCR System 9600-R (PerkinElmer). The amounts of poly(A)$^+$ RNA templates (50 ng) and cycle numbers (28 cycles) for amplification were chosen in quantitative ranges where the reactions proceeded linearly. Temperatures and time periods employed for melting, annealing and extension were 94 °C for 0.5 min, 55 °C for 0.5 min and 72 °C for 1.5 min, respectively. Oligodeoxyribonucleotide primers employed were as follows: 5′-GAGAATTCCACGGCAGACACCTTCCACTTG-3′ (nucleotides 170–191 plus *Eco*RI adapter) and 5′-GACTGCAGGCACCTGTGGCTCCTTCGTC-3′ (complement of nucleotides 709–728 plus *Pst*I adapter) for detection of mouse syndecan-1 mRNA (accession no. Z22532); 5′-GAGGATCCGAGACGAGAACAGAGCTGAC-3′ (nucleotides 487–506 plus *Kpn*I adapter) and 5′-GAGAATTCTTATTCTGTCCGTTTAAACAGATT-3′ (complement of nucleotides 1151–1175 plus *Eco*RI adapter) for mouse syndecan-2 (U00674); 5′-GAGAATTCACCCACAACCGTTATCCAGCC-3′ (nucleotides 370–390 plus *Eco*RI adapter) and 5′-GACTGCAGCAGAAGGGACTCTGGAGTTGGG-3′ (complement of nucleotides 910–931 plus *Pst*I adapter) for mouse syndecan-3 (U52826); 5′-GAGAATTCGCGAGTCGATTCGAGAGACTGAGG-3′ (nucleotides 69–23 plus *Eco*RI adapter) and 5′-GACTGCAGGTACACCAGCAGCAGGATCAGG-3′ (complement of nucleotides 498–520 plus *Pst*I adapter) for mouse syndecan-4 (W51352); and 5′-GTGGGGCGCCCCAGGCACCA-3′ (nucleotides 144–163) and 5′-CTCCTTAATGTCACGCACGATTTC-3′ (complement of nucleotides 683–660) for β-actin [34]. The PCR products were electrophoresed on a 1.5 % agarose gel containing ethidium bromide (5 μg/ml) and visualized under UV light. The RT-PCR products were sequence-verified.

Northern-blot analysis was performed as described previously [35]. In brief, 2 μg each of poly(A)$^+$ RNAs from both clones were electrophoresed on a 1.5 % agarose gel containing 1.1 M formaldehyde, transferred to a Hybond N+ nylon membrane (Amersham Pharmacia Biotech), and hybridized to a cDNA fragment of syndecan-1 (nucleotides 409–967), syndecan-2 (487–1175), syndecan-3 (370–931), or syndecan-4 (92–534), which had been labelled with [α-^{32}P]dCTP by the random labelling method. After hybridization for 14 h at 42 °C, the membranes were exposed to X-ray films and the films were scanned by CanoScan 600 (Canon, Tokyo). The quantification of the bands was performed with the public-domain NIH Image program in 256-grey-scale mode.

Transfection of syndecan-2 cDNA into LM66-H11 cells

The mouse syndecan-2 cDNA containing the entire coding region was amplified by RT-PCR with poly(A)$^+$ RNA form P29 cells as template using 5′-GAGGTACCTCCTTTTATCCGGGTAGGAG-3′ and 5′-GAGAATTCAAAGTTCAGTGCTCTCCTAAATAG-3′, which corresponded to nucleotides 487–506 and 1151–1174 (GenBank® accession no. U00674) respectively as primers. The 5′- and 3′-primers contained *Kpn*I and *Eco*RI sites respectively as indicated with underlines. The amplified cDNA was inserted into the *Kpn*I and *Eco*RI sites of a mammalian expression plasmid vector, pcDNA3 (Promega) at a site downstream of the cytomegalovirus promoter. The nucleotide sequence of the cloned syndecan-2 cDNA was verified with a Hitachi SQ-5500 sequencer (Hitachi, Tokyo, Japan). Recombinant plasmid DNA was purified with a Qiagen plasmid kit (Qiagen, Valencia, CA, U.S.A.) and used for transfection of LM66-H11 cells. After transfection using Tfx-50 reagent (Promega), cells were cultured in the presence of G418, and the

G418-resistant colonies were picked 2 weeks later. Cell clones were expanded individually and clones expressing high levels of syndecan-2 on their surface were selected by flow-cytometric analysis with SN2Ab. A clone (designated as H11-SN2) that expressed syndecan-2 on the cell surface at a similar level to that of P29 cells was used in the present study. LM66-H11 cells transfected only with vector (H11-Vec) were used as control cells.

Affinity chromatography of purified syndecan-2

[^{35}S]Sulphate-labelled syndecan-2 was isolated from both the clones as described below. P29 and LM66-H11 cells were labelled with [^{35}S]sulphate (7.4 MBq/ml) in 10 % FCS/Ham's F-12 for 24 h at 37 °C in a humidified 5 % CO_2 atmosphere. The radiolabelled macromolecules were extracted from the cell layer with 7 M urea/0.5 % (v/v) Triton X-100/0.15 M NaCl/50 mM Tris/HCl, pH 7.3, containing protease inhibitors, 10 mM EDTA/10 mM *N*-ethylmaleimide/1 mM PMSF/0.036 mM pepstatin A, for 12 h on ice. After removal of insoluble materials by centrifugation at 65000 *g* for 30 min at 4 °C, the proteoglycan fraction was obtained on DEAE-Sephacel column chromatography and then applied to an Octyl-Sepharose 4B column. The bound hydrophobic proteoglycans were eluted with a linear-gradient concentration of 0–0.5 % (v/v) Triton X-100 in 4 M guanidinium chloride/50 mM Tris/HCl, pH 7.3. Syndecan-2 was precipitated from this hydrophobic proteoglycan fraction with SN2Ab, as described previously [36]. Briefly, the sample was mixed with SN2Ab in 0.15 M NaCl/0.1 % (v/v) Triton X-100/50 mM Tris/HCl, pH 7.3, for 1 h at room temperature, and 50 % Protein A–Sepharose was added and mixed. One hour later, the beads were precipitated by a centrifugation and washed with 1 M NaCl/0.1 % (v/v) Triton X-100/50 mM Tris/HCl, pH 7.3. Syndecan-2 was eluted by 0.1 % (v/v) Triton X-100/0.1 M glycine/HCl, pH 2.0, followed by neutralization with 1.0 M Tris/HCl, pH 9.0. The ^{35}S-labelled syndecan-2 samples thus obtained were applied to a fibronectin-linked Sepharose 4B column. Elution was with a linear gradient concentration of 0.1–0.5 M NaCl in 0.5 % (v/v) Triton X-100/50 mM Tris/HCl, pH 7.3.

RESULTS

Metastatic potential and tumorigenesis of P29 and LM66-H11 clones

The metastatic potentials of the two clones used in the present study are shown in Table 1. Irrespective of the sites of injection, a significant difference in the number of lung foci was observed between the clones. These clones also exhibited strikingly different patterns in the localization of fibronectin in primary tumours (Figure 2). The low-metastatic P29 cells having a strong ability to induce host-stromal response [31] were immediately surrounded by a fibronectin-rich interstitial-type matrix formed by the induced host-stromal cells (Figure 2A). On the contrary, in the tumour formed by the highly metastatic LM66-H11 cells lacking the capacity to induce the host-stromal response, fibronectin was hardly observed in the extracellular compartment of tumour parenchyma except in the endothelial basement membrane of tumour blood vessels (Figure 2B). The results indicate that each clone grew in quite different microenvironments *in vivo*, especially in the interaction with fibronectin, which was an allogenic ECM component for them.

Table 1 Lung metastatic potentials of P29 and LM66-H11 clones

Clone	Route of injection	No. of cells injected ($\times 10^{-5}$)	Incidence	No. of lung foci	
				Mean	Range
P29	i.v.*	1.0	3/7	0.4	0–1
LM66-H11	i.v.	1.0	7/7	516.2	467–744
P29	s.c.†	2.0	0/7	0	–
LM66-H11	s.c.	2.0	7/7	35.2	23–56

* i.v., intravenous.
† s.c., subcutaneous.

Cellular responses of P29 and LM66-H11 cells to substrata composed of fibronectin and fibronectin-recombinant polypeptides

When inoculated on a fibronectin substratum, the two cloned cells showed distinctly different responses in terms of actin-cytoskeletal organization (Figure 3). P29 cells spread extensively in association with actin stress-fibre formation (Figure 3A), whereas LM66-H11 cells spread to a slightly lesser extent in association with the formation of cortex actin (Figure 3B). We have previously demonstrated that the stress-fibre formation in P29 cells required a dual-receptor system with integrin $\alpha 5\beta 1$ and syndecan-2 and thus selective suppression of syndecan-2 in P29 cells by *in vitro* treatment with its antisense oligonucleotides resulted in the failure to form actin stress fibres; the cells formed cortex actin instead [26], which was indistinguishable from the actin cytoskeleton induced in LM66-H11 cells. Therefore to clarify signalling by individual or co-operative action of the two receptors, we examined the responses of the cells on adhesion to substrata of fibronectin-recombinant polypeptides containing the respective ligands for the two receptors.

On CH-271, the actin cytoskeletons of the two cloned cells on fibronectin were reproduced (Figures 3C and 3D), suggesting that the other portions, except Cell-I and Hep-II domains of fibronectin, were not involved in these responses. Adhesion of both P29 and LM66-H11 cells to C-274 resulted in the formation of a cortex-actin structure (Figure 3E), indicating that cells adhering to fibronectin only by the interaction between integrin $\alpha 5\beta 1$ and the Cell-I domain form cortex actin. The finding that the cortex-actin structure was induced in LM66-H11 cells not only on C-274 (Figure 3F) but also on both fibronectin and CH-271, despite the fact that the latter two substrata contain the ligand (Hep-II domain) for syndecan-2, suggested strongly that syndecan-2 expression on LM66-H11 cells was not sufficient in quality or quantity for co-operation with integrin $\alpha 5\beta 1$. Adhesion of P29 cells to H-271 caused the formation of filopodia (Figure 3G), suggesting that the action of syndecan-2 resulted in the induction of filopodium formation, since the expression levels of other syndecans were similar between the two clones. In contrast, LM66-H11 cells hardly spread on an H-271 substratum and showed rounded shapes with small numbers of filopodia (Figure 3H), suggesting its insufficient expression on cells for their spreading and formation of filopodia.

The cell-adhesion assay demonstrated that, for the P29 clone, more than 90 % of the cells adhering to a fibronectin substratum adhered not only to CH-271 but also to C-274 and H-271, indicating that the cells could adhere to the substratum by either of the receptors (Table 2). In contrast, LM66-H11 cells adhering to H-271 accounted for 68 % of the cells adhering to fibronectin and the significantly lower percentage compared with those adhering to CH-271 or C-274 suggested again an insufficiency of probably syndecan-2 expressed on LM66-H11 cells in quality or quantity. Therefore we examined next the expression level of the two receptors on each of the cloned cell lines.

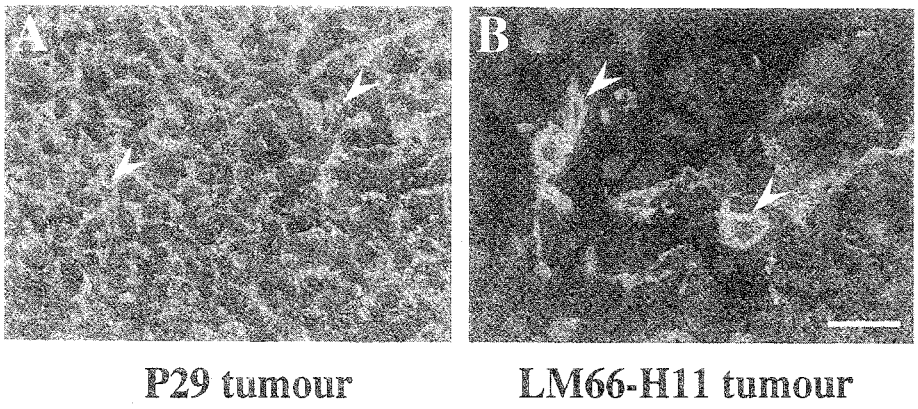

Figure 2 Localization of fibronectin in primary tumours

Primary tumours formed by subcutaneous injection of P29 (**A**) and LM66-H11 (**B**) cells were treated with antibody against fibronectin. The reactive components were visualized by an FITC-conjugated second antibody (green) and the nuclei were counterstained with propidium iodide (red). Arrowheads show basement membranes of tumour blood vessels. Bar, 50 μm.

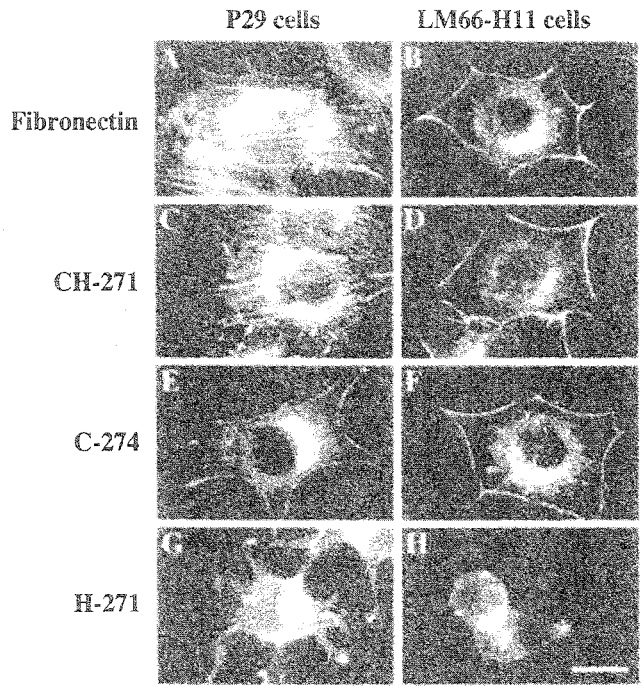

Figure 3 Actin-cytoskeletal organization of P29 and LM66-H11 cells on substrata of fibronectin and fibronectin-recombinant polypeptides

P29 (**A, C, E, G**) and LM66-H11 (**B, D, F, H**) cells suspended in 0.2% BSA/DMEM were inoculated on coverslips coated with fibronectin (**A, B**), CH-271 (**C, D**), C-274 (**E, F**) and H-271 (**G, H**), incubated for 1 h at 37 °C, fixed and stained with Rhodamine-conjugated phalloidin to visualize actin fibres. Bar, 20 μm.

Expression and fibronectin-binding affinity of syndecan-2 produced by P29 and LM66-H11 cells

The cell-surface expression of the two receptors was compared using flow cytometry (Figure 4). As expected, the expression levels of integrin $\alpha5\beta1$ were almost the same in the cloned cell lines (Figures 4A and 4B), whereas that of syndecan-2 on P29 cells was approx. eight times higher in fluorescence intensity than that of LM66-H11 cells (Figures 4C and 4D). To compare the binding ability of the syndecan-2 proteoglycan which was isolated from the two cloned cell lines with fibronectin, [^{35}S]sulphate-labelled syndecan-2 precipitated with SN2Ab from the hydrophobic proteoglycan fractions was subjected to fibronectin-affinity chromatography (Figures 4E and 4F). The syndecan-2 proteoglycan from each of the clones was eluted with 0.22 M NaCl, indicating that the binding abilities of the two samples to fibronectin were the same. These results suggest that the formation of stress fibres in P29 cells, which was induced in co-operation of syndecan-2 and integrin $\alpha5\beta1$, requires a certain threshold of syndecan-2 below which the formation of cortex-actin structure ensues, as observed in LM66-H11 cells in this study and in the antisense-treated P29 cells in the previous study [26].

Table 2 Adhesion of cells to substrata of fibronectin and fibronectin-recombinant polypeptides

[^{3}H]Thymidine-labelled cells were inoculated on 96-well plates coated with fibronectin or the recombinant polypeptides and incubated for 1 h at 37 °C. Cells attached and unattached were separated and dissolved in 0.5 M NaOH. Radioactivity of each fraction was measured. The results show values obtained from two different experiments done in triplicate.

	P29		LM66-H11	
Substratum	% of inoculated cells	Ratio	% of inoculated cells	Ratio
Fibronectin	83.8 ± 1.88	1	81.3 ± 4.38	1
CH-271	81.3 ± 4.38	0.97	72.5 ± 3.75	0.89
C-274	76.3 ± 3.50	0.91	68.8 ± 1.88	0.85
H-271	76.3 ± 3.63	0.91	55.0 ± 5.00	0.68

Participation of syndecan-2 in actin-cytoskeletal organization

Most cells express more than one species of syndecans [37] and our previous study also suggested that P29 cells synthesized cell-surface heparan sulphate proteoglycans other than syndecan-2 [27]. Hence, the expression of mRNAs of all members of the syndecan family was examined in the two clones (Figure 5). The RT-PCR analysis showed that the two clones expressed all members of the syndecan family although the levels of syndecan-3 were extremely low (Figure 5A). Among them, only syndecan-2 exhibited different expression levels between the two clones, i.e. the expression in P29 cells was significantly higher

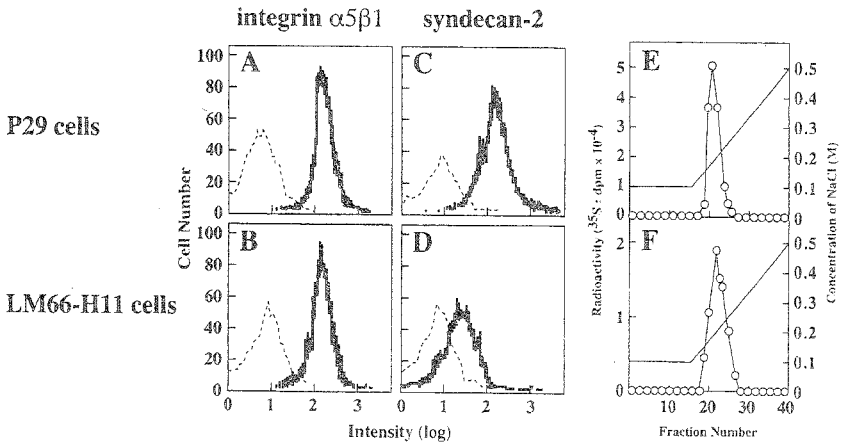

Figure 4 Expression of integrin $\alpha5\beta1$ and syndecan-2 on P29 and LM66-H11 cells

P29 (**A, C**) and LM66-H11 (**B, D**) cells suspended in 0.2% BSA/DMEM were treated with anti-integrin $\alpha5\beta1$ antibody, AB1950 (**A, B**) or anti-syndecan-2 core protein antibody, SN2Ab (**C, D**) for 1 h at 4 °C and then FITC-conjugated second antibodies for 30 min. Intensity of fluorescence was measured with a flow cytometer. Peaks shown with dotted lines are for control samples reacted with non-immune sera as the first antibodies. [^{35}S]Sulphate-labelled syndecan-2 purified from P29 (**E**) and LM66-H11 (**E**) cells was applied to a fibronectin-linked Sepharose 4B column and eluted with a linear-gradient concentration of NaCl to compare the binding affinity of the two samples with fibronectin.

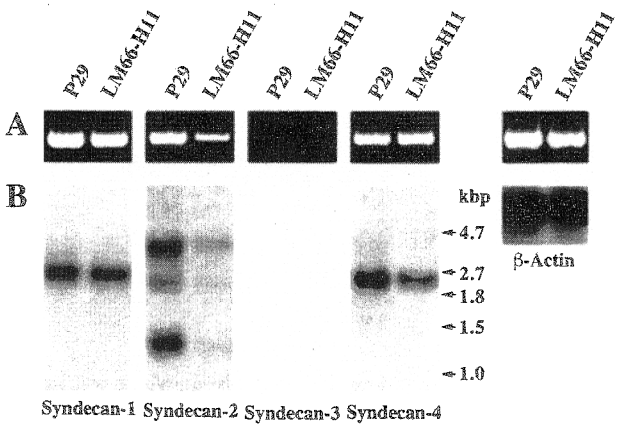

Figure 5 Expression of mRNAs of a syndecan family in P29 and LM66-H11 cells

Expressions of mRNAs of syndecan-1, -2, -3, -4 and β-actin in P29 and LM66-H11 cells were analysed by RT-PCR (**A**) and by Northern blot (**B**). Their levels were normalized by the expression of β-actin.

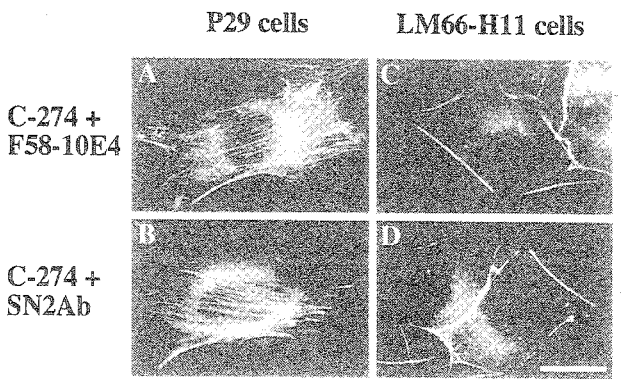

Figure 6 Actin cytoskeletons formed in P29 and LM66-H11 cells on adhesion to substrata comprising a mixture of C-274 and antibody against heparan sulphate (F58-10E4) or syndecan-2 core protein (SN2Ab)

P29 (**A, B**) and LM66-H11 (**C, D**) cells suspended in 0.2% BSA/DMEM were inoculated on coverslips coated with a mixture of C-274 (500 μg/ml) and F58-10E4 (15 μg/ml) (**A, C**) or SN2Ab (0.7 μg/ml) (**B, D**) and incubated for 1 h at 37 °C. Cells were fixed and stained with Rhodamine-conjugated phalloidin. Bar, 20 μm.

than that in LM66-H11 cells. By Northern-blot analysis (Figure 5B), mRNA of syndecan-3 was not detected but that of other syndecans, syndecan-1 (2.4 kb), syndecan-2 (1.2, 2.1 and 3.6 kb) and syndecan-4 (2.3 kb) were detected in both clones. Three syndecan-2 mRNA species of different sizes have been reported in human foetal lung fibroblasts [38] and shown to result from different use of alternative polyadenylation signals. The densities of the bands were quantified using the NIH Image program and normalized with the amount of β-actin. The ratios of the individual densities of the P29 and LM66-H11 cell-derived syndecan-1, -2, and -4 bands were 1.00, 4.47 (ratio of total densities of three bands) and 1.47 respectively demonstrating a significant difference in the expression of syndecan-2 mRNAs.

To confirm the participation of syndecan-2 in actin-cytoskeletal organization, responses of the cells to mixed substrata comprising C-274 and antibodies against two portions of the syndecan-2 proteoglycan, heparan sulphate (F58-10E4) and the ectodomain of core protein (SN2Ab), were assessed (Figure 6). When P29 cells were inoculated on a mixed C-274 and F58-10E4 substratum, they spread extensively in association with the formation of stress fibres (Figure 6A), whereas those pretreated with heparitinase-I did not form stress fibres under the same conditions (results not shown), indicating a necessity for clustering of heparan sulphate proteoglycans, mediated by binding of their glycosaminoglycans to the ligand. Moreover, a mixed substratum of C-274 and SN2Ab exerted similar effects on the organization of the actin cytoskeleton in P29 cells (Figure 6B), whereas heparitinase-I digestion of the cells did not affect the formation of stress fibres (results not shown). These results lead us to speculate that clustering of syndecan-2 on the cell surface

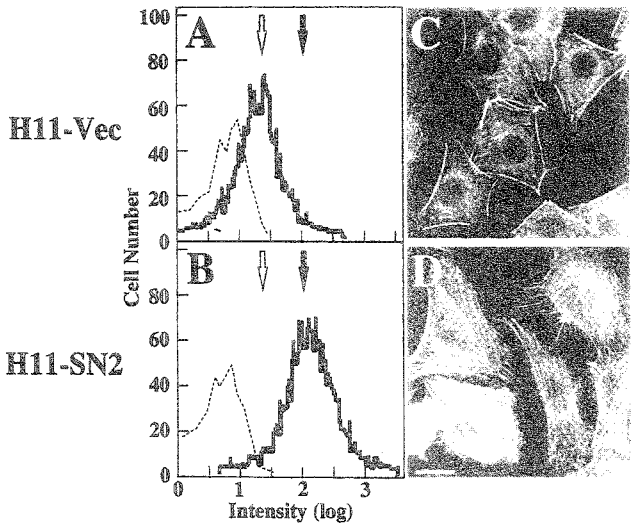

Figure 7 Induction of stress-fibre formation by overexpression of syndecan-2 in LM66-H11

LM66-H11 cells were transfected with syndecan-2 cDNA and the vector only, and the transfectants were cloned and named H11-SN2 and H11-Vec, respectively. The cell-surface expression of syndecan-2 in H11-Vec (**A**) and H11-SN2 (**B**) was measured with a flow cytometer. Peaks shown with dotted lines are for control samples reacted with non-immune sera as the first antibodies. Open and closed arrows show the peak positions of fluorescent intensity due to syndecan-2 expressed on LM66-H11 and P29 cells, respectively. H11-Vec (**C**) and H11-SN2 (**D**) cells were inoculated on a fibronectin substratum and incubated for 1 h at 37 °C. Cells were fixed and stained with Rhodamine-conjugated phalloidin. Bar, 20 μm.

is sufficient to work co-operatively with integrin $\alpha5\beta1$ for signal transduction to induce stress fibre formation, and both glycosaminoglycan- and core protein-mediated clusterings are equivalent in terms of this signal transduction. On the contrary, LM66-H11 cells failed to form stress fibres, but exhibited the formation of cortex actin on these two substrata (Figures 6C and 6D), suggesting that the clustering of syndecan-2 expressed on their surface was not sufficient to form stress fibres under the conditions used, or that the cells lack some components to complete the stress-fibre formation. This possibility has been investigated below.

Induction of stress-fibre formation by overexpression of syndecan-2 in LM66-H11

To confirm that syndecan-2 is specifically involved in the induction of stress-fibre formation in the present system, we inserted a full-length cDNA of the mouse syndecan-2 into LM66-H11 cells with its low expression and obtained a stable clone, H11-SN2, expressing it at a level similar to that of P29 cells (Figure 7B). On the contrary, the clone transfected only with the vector, H11-Vec, expressed syndecan-2 at a level similar to that of the parental LM66-H11 cells (Figure 7A). Its overexpression did not affect the expression of other syndecans and integrin $\alpha5\beta1$ (results not shown). When H11-Vec cells were allowed to adhere to the fibronectin substratum, they formed cortex actin (Figure 7C) as did the parental cells (Figure 3B). On the other hand, H11-SN2 cells spread extensively in association with the formation of stress fibres (Figure 7D). This actin-cytoskeletal organization was indistinguishable from that of P29 cells on the same substratum (Figure 3A). These results indicate that LM66-H11 cells have all the features required for the induction of stress-fibre formation, except the expression of syndecan-2 beneath the threshold.

DISCUSSION

In the present study, using the fibronectin-recombinant polypeptides as substrata, we have clearly demonstrated that signal transduction by (1) integrin $\alpha5\beta1$ alone results in the induction of cortex-actin structure in association with cell spreading; (2) syndecan-2 alone results in the formation of filopodia; and (3) both receptors cause the formation of stress fibres (Figure 8). Increasing evidence suggests that many heparin-binding growth factors are activated by binding to cell-surface heparan sulphate chains, acting as physiological co-receptors before binding to their intrinsic receptors [37,39–41]. Thus it is noteworthy that unlike co-receptors for soluble growth factors, syndecan-2 itself has the potential to induce the formation of filopodia by binding to an immobilized substratum, indicating that ECM-ligand-mediated clustering of syndecan-2 can trigger the cytoplasmic cascade for signalling to rearrange the actin cytoskeleton. Another new finding is that the signals binding to fibronectin by integrin $\alpha5\beta1$ alone induced the formation of cortex actin in the cells used in the present study. In addition, syndecan-2 can act co-operatively with integrin $\alpha5\beta1$ to generate a new signal for the formation of stress fibres, which differs from the respective signals by syndecan-2 or integrin $\alpha5\beta1$ alone. Moreover, the fact that the stress fibre formation was induced in P29 cells on adhesion to a mixed substratum composed of C-274 and not only anti-core protein of syndecan-2 antibody but also anti-heparan sulphate antibody, further corroborates our previous finding that syndecan-2 participates specifically in the induction of stress-fibre formation [26]. However, it remains to be elucidated how syndecan-2 and integrin $\alpha5\beta1$ cross-talk with each other to generate a new signal in terms of the molecular mechanism.

The responses of LM66-H11 cells with low syndecan-2-expression to adhesion substrata indicated that a certain threshold in the expression of syndecan-2 might be required for co-operation with integrin $\alpha5\beta1$. The expression level of syndecan-2 on P29 cells is sufficient to work co-operatively with integrin $\alpha5\beta1$ to induce the formation of stress fibres on fibronectin. Thus an elevated expression of syndecan-2 in LM66-H11 cells by transfection of its cDNA caused the formation of stress fibres in co-operation with integrin $\alpha5\beta1$. This also suggests that LM66-H11 cells have all the features required for the induction of stress fibres, except for a low expression of syndecan-2.

The facts that the mixed substratum composed of C-274 and SN2Ab is sufficient to induce the formation of stress fibres in P29 cells and treatment of P29 cells with the antisense oligonucleotide for syndecan-2 prevents the formation of stress fibres [26], indicate that a certain level of syndecan-2 is not only essential but also sufficient to receive the ECM signals co-operatively with integrin $\alpha5\beta1$ to induce stress-fibre formation. Although the clones used in this study expressed all members of the syndecan family, the molecular species exhibiting specific binding to fibronectin or H-271 was syndecan-2 [26–28]. On the other hand, it has been well established that syndecan-4 signals co-operatively with integrin $\alpha5\beta1$ to result in the assembly of focal adhesions and actin stress fibres in fibroblasts inoculated on to a fibronectin substratum [16,17,42]. The cytoplasmic domain of syndecan-4 binds phosphatidylinositol 4,5-bisphosphate and PKCα at its variable region, and this interaction mediates its own multimerization, with resultant regulation of the intracellular distribution and activity of PKCα [18, 19]. We have recently demonstrated [43] that the cross-talk of syndecan-2 and -4 is

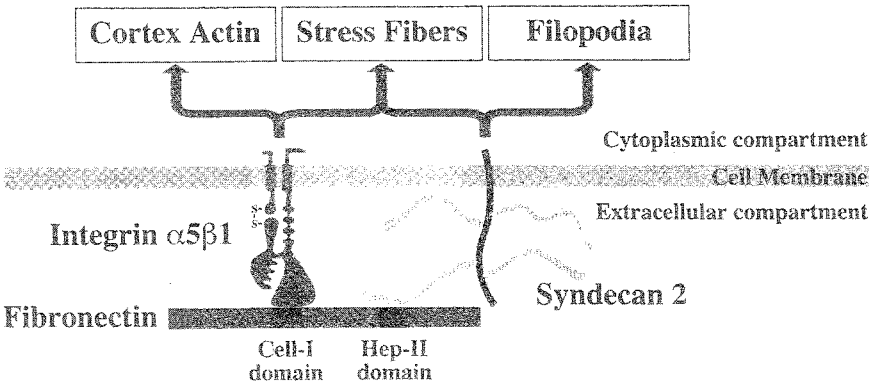

Figure 8 Fibronectin-induced signallings mediated by integrin $\alpha5\beta1$ and/or syndecan-2

The results obtained in this study show that cells adhering to the Cell-I domain of fibronectin by integrin $\alpha5\beta1$ spread and form cortex actin. In contrast, the cells adhering to the Hep-II domain by heparan sulphate side-chains of syndecan-2 spread to a lesser extent and develop filopodia. When they adhere to fibronectin by both receptors, stress-fibre formation is induced. It is also revealed that there is a threshold level for syndecan-2 signalling to form filopodia or regulating integrin $\alpha5\beta1$-mediated signalling to form stress fibres. However, this depends on the ability of a ligand to bind syndecan-2. Therefore, on a fibronectin substratum, P29 cells with high syndecan-2-expression form stress fibres and LM66-H11 cells with low expression form cortex actin.

required for the induction of those cytoskeletons in co-operation with integrin $\alpha5\beta1$. This cross-talk may be explained by a substrate–enzyme interaction, i.e. a phosphorylation reaction at the serine residue(s) of the syndecan-2 cytoplasmic domain, which is catalysed by PKCα bound to the syndecan-4 cytoplasmic domain [20]. However, it should be noted that fibroblasts derived from syndecan-4-null mice have been recently demonstrated to form focal contacts and stress fibres on adhesion to fibronectin as observed in normal fibroblasts [44], indicating that syndecan-4 is not essential and can be compensated for by some other molecule(s). Thus all these results suggest that both syndecans appear to function co-operatively with integrin $\alpha5\beta1$ for the assembly of focal adhesions and actin stress fibres on cell adhesion to the fibronectin substratum.

Finally, it is appropriate to discuss the correlation between the metastatic potential and the expression level of syndecan-2. An *in vivo* selection of different metastatic clones from Lewis lung carcinoma cells on the basis of spontaneous metastatic potential results in the selection of clones with different abilities to induce the host-stromal responses, and also different expressions of syndecan-2. Thus each of the cloned cell lines grow in quite different microenvironments *in vivo* and cells adapt to such a milieu by all the receptors that they express on the cell surface. In consequence, the two cloned cells behave differently. Indeed, the actin cytoskeleton formed in the highly metastatic LM66-H11 cells on adhesion to a fibronectin substratum is indistinguishable from that in the low-metastatic P29 cells whose expression of syndecan-2 is selectively suppressed by *in vitro* treatment with antisense oligonucleotides for its core protein [26]. Moreover, we have recently demonstrated that overexpression of syndecan-2 by transfection of its cDNA into LM66-H11 cells causes the formation of actin stress fibres in the cells on adhesion to fibronectin, which is indistinguishable from the actin cytoskeleton induced in P29 cells on fibronectin and, surprisingly, results in striking suppression of metastasis [43]. The results reported here consistently suggest that syndecan-2 plays a pivotal role in the determination of the degree of metastasis.

This work was supported in part by Grants-in-Aid for Bio-venture Research Center from the Ministry of Education, Culture, Sports, Science and Technology (M.O.), a Grant-in-Aid for Cancer Research (11–12, 11–13) from the Ministry of Health, Labour and Welfare (K.O. and Y. K.), and a grant from the Aichi Cancer Research Foundation (Y.K.). We acknowledge Takara Shuzo Co. (TaKaRa Biomedicals) for generously providing the recombinant fibronectin polypeptides, C-274, H-271 and CH-271. We also thank Dr H. Yonekura, Kanazawa University, Kanazawa, Japan, and Professor Bruce Caterson, Cardiff University, Cardiff, Wales, U.K., for their critical review of the paper.

REFERENCES

1 Grobstein, C. (1955) Tissue interaction in morphogenesis of mouse embryonic rudiments *in vitro*. In Aspects of Synthesis and Order in Growth (Rudunic, D., ed.), pp. 233–256, Princeton University, Princeton, NJ
2 Adams, J. C. and Watt, F. M. (1993) Regulation of development and differentiation by the extracellular matrix. Development **117**, 1183–1198
3 Grinnell, F. (1992) Wound repair, keratinocyte activation and integrin modulation. J. Cell Sci. **101**, 1–5
4 Chiquet-Ehrismann, R. (1993) Tenascin and other adhesion-modulating proteins in cancer. Semin. Cancer Biol. **4**, 301–310
5 Ekblom, M., Klein, G., Mugrauer, G., Fecker, L., Deutzmann, R., Timpl, R. and Ekblom, P. (1990) Transient and locally restricted expression of laminin A chain mRNA by developing epithelial cells during kidney organogenesis. Cell **60**, 337–346
6 Prieto, A. L., Jones, F. S., Cunningham, B. A., Crossin, K. L. and Edelman, G. M. (1990) Localization during development of alternatively spliced forms of cytotactin mRNA by in situ hybridization. J. Cell Biol. **111**, 685–698
7 Damsky, C. H. and Werb, Z. (1992) Signal transduction by integrin receptors for extracellular matrix: co-operative processing of extracellular information. Curr. Opin. Cell Biol. **4**, 772–781
8 Huhtala, P., Humphries, M. J., McCarthy, J. B., Tremble, P. M., Werb, Z. and Damsky, C. H. (1995) Co-operative signalling by alpha 5 beta 1 and alpha 4 beta 1 integrins regulates metalloproteinase gene expression in fibroblasts adhering to fibronectin. J. Cell Biol. **129**, 867–879
9 Pierschbacher, M. D. and Ruoslahti, E. (1984) Cell attachment activity of fibronectin can be duplicated by small synthetic fragments of the molecule. Nature (London) **309**, 30–33
10 Hynes, R. O. (1987) Integrins: a family of cell surface receptors. Cell **48**, 549–554
11 Miyamoto, S., Katz, B. Z., Lafrenie, R. M. and Yamada, K. M. (1998) Fibronectin and integrins in cell adhesion, signaling, and morphogenesis. Ann. N.Y. Acad. Sci. **857**, 119–129
12 Miyamoto, S., Akiyama, S. K. and Yamada, K. M. (1995) Synergistic roles for receptor occupancy and aggregation in integrin transmembrane function. Science **267**, 883–885
13 Miyamoto, S., Teramoto, H., Coso, O. A., Gutkind, J. S., Burbelo, P. D., Akiyama, S. K. and Yamada, K. M. (1995) Integrin function: molecular hierarchies of cytoskeletal and signaling molecules. J. Cell Biol. **131**, 791–805
14 Rapraeger, A. C. (2000) Syndecan-regulated receptor signaling. J. Cell Biol. **149**, 995–998
15 Woods, A. and Couchman, J. R. (1998) Syndecans: synergistic activators of cell adhesion. Trends Cell Biol. **8**, 189–192
16 Couchman, J. R. and Woods, A. (1998) Syndecan-4 and integrins: combinatorial signaling in cell adhesion. J. Cell Sci. **112**, 3415–3420

17 Saoncella, S., Echtermeyer, F., Denhez, F., Nowlen, J. K., Mosher, D. F., Robinson, S. D., Hynes, R. O. and Goetinck, P. F. (1999) Syndecan-4 signals co-operatively with integrins in a Rho-dependent manner in the assembly of focal adhesions and actin stress fibres. Proc. Natl. Acad. Sci. U.S.A. **96**, 2805–2810
18 Oh, E. S., Woods, A. and Couchman, J. R. (1997) Syndecan-4 proteoglycan regulates the distribution and activity of protein kinase C. J. Biol. Chem. **272**, 8133–8136
19 Oh, E. S., Woods, A. and Couchman, J. R. (1997) Multimerization of the cytoplasmic domain of syndecan-4 is required for its ability to activate protein kinase C. J. Biol. Chem. **272**, 11805–11811
20 Oh, E. S., Woods, A., Lim, S. T., Theibert, A. W. and Couchman, J. R. (1998) Syndecan-4 proteoglycan cytoplasmic domain and phosphatidylinositol 4,5-bisphosphate co-ordinately regulate protein kinase C activity. J. Biol. Chem. **273**, 10624–10629
21 Grootjans, J. J., Zimmermann, P., Reekmans, G., Smets, A., Degeest, G., Durr, J. and David, G. (1997) Syntenin, a PDZ protein that binds syndecan cytoplasmic domains. Proc. Natl. Acad. Sci. U.S.A. **94**, 13683–13688
22 Cohen, A. R., Woods, D. F., Marfatia, S. M., Walther, Z., Chishti, A. H., Anderson, J. M. and Wood, D. F. (1998) Human CASK/LIN-2 binds syndecan-2 and protein 4.1 and localizes to the basolateral membrane of epithelial cells. J. Cell Biol. **142**, 129–138
23 Gao, Y., Li, M., Chen, W. and Simons, M. (2000) Synectin, syndecan-4 cytoplasmic domain binding PDZ protein, inhibits cell migration. J. Cell Physiol. **184**, 373–379
24 Ethell, I. M., Hagihara, K., Miura, Y., Irie, F. and Yamaguchi, Y. (2000) Synbindin, a novel syndecan-2-binding protein in neuronal dendritic spines. J. Cell Biol. **151**, 53–68
25 Baciu, P. C., Saoncella, S., Lee, S. H., Denhez, F., Lauthardt, D. and Goetinck, P. F. (2000) Syndesmos, a protein that interacts with the cytoplasmic domain of syndecan-4, mediates cell spreading and actin cytoskeletal organization. J. Cell Sci. **113**, 315–324
26 Kusano, Y., Oguri, K., Nagayasu, Y., Munesue, S., Ishihara, M., Saiki, I., Yonekura, H., Yamamoto, H. and Okayama, M. (2000) Participation of syndecan 2 in the induction of stress fibre formation in co-operation with integrin alpha5beta1: structural characteristics of heparan sulfate chains with avidity to COOH-terminal heparin-binding domain of fibronectin. Exp. Cell Res. **256**, 434–444
27 Itano, N., Oguri, K., Nakanishi, H. and Okayama, M. (1993) Membrane-intercalated proteoglycan of a stroma-inducing clone from Lewis lung carcinoma binds to fibronectin via its heparan sulfate chains. J. Biochem. (Tokyo) **114**, 862–873
28 Itano, N., Oguri, K., Nagayasu, N., Kusano, Y., Nakanishi, H., David, G. and Okayama, M. (1996) Phosphorylation of a membrane-intercalated proteoglycan, syndecan-2, *expressed in a stroma-inducing clone from a mouse Lewis lung carcinoma*. Biochem. J. **315**, 925–930
29 Nakanishi, H., Takenaga, K., Oguri, K., Yoshida, A. and Okayama, M. (1992) Morphological characteristics of tumours formed by Lewis lung carcinoma-derived cloned cell lines with different metastatic potentials: structural differences in their basement membranes formed in vivo. Virchows Arch. A **420**, 163–170
30 Nakanishi, H., Oguri, K., Yoshida, K., Itano, N., Takenaga, K., Kazama, T., Yoshida, A. and Okayama, M. (1992) Structural differences between heparan sulphates of proteoglycan involved in the formation of basement membranes *in vivo* by Lewis-lung-carcinoma-derived cloned cells with different metastatic potentials. Biochem. J. **288**, 215–224
31 Nakanishi, H., Oguri, K., Takenaga, K., Hosoda, S. and Okayama, M. (1994) Differential fibrotic stromal responses of host tissue to low- and high-metastatic cloned Lewis lung carcinoma cells. Lab. Invest. **70**, 324–332
32 Narumi, K., Satoh, K., Isemura, M., Sakai, T., Abe, T., Kikuchi, T., Sindoh, S., Motomiya, M., Oguri, K. and Okayama, M. (1993) Difference in laminin expression between high and low metastatic cell clones derived from murine Lewis lung carcinoma. Cell Struct. Funct. **18**, 183–187
33 Kornblihtt, A. R., Umezawa, K., Vibe-Pedersen, K. and Baralle, F. E. (1985) Primary *structure of human fibronectin: differential splicing may generate at least 10* polypeptides from a signal gene. EMBO J. **4**, 1755–1759
34 Yamamura, M., Uyemura, K., Deans, R. J., Weinberg, K., Rea, T. H., Bloom, B. R. and Modlin, R. L. (1991) Defining protective responses to pathogens: cytokine profiles in leprosy lesions. Science **254**, 277–279
35 Yonekura, H., Migita, H., Sakurai, S., Wang, H., Harada, S., Abedin, M. J., Yamagishi, S. and Yamamoto, H. (1999) Antisense display – a method for functional gene screening: evaluation in a cell-free system and isolation of angiogenesis-related genes. Nucleic Acids Res. **27**, 2591–2600
36 Harlow, E. and Lane, D. (1988) Immunoprecipitation. In Antibodies: A Laboratory *Manual (Cuddihy, J., ed.), pp. 421–470, Cold Spring Harbor Laboratory Press*, New York
37 Bernfield, M., Gotte, M., Park, P. W., Reizes, O., Fitzgerald, M. L., Lincecum, J. and Zako, M. (1999) Functions of cell surface heparan sulfate proteoglycans. Annu. Rev. Biochem. **68**, 729–777
38 Marynen, P., Zhang, J., Cassiman, J. J., Van den Berghe, H. and David, G. (1989) Partial primary structure of the 48- and 90-kilodalton core proteins of cell surface-associated heparan sulfate proteoglycans of lung fibroblasts. Prediction of an integral membrane domain and evidence for multiple distinct core proteins at the cell surface of human lung fibroblasts. J. Biol. Chem. **264**, 7017–7024
39 Mizuno, K., Inoue, H., Hagiya, M., Shimizu, S., Nose, T., Shimohigashi, Y. and Nakamura, T. (1994) Hairpin loop and second kringle domain are essential sites for heparin binding and biological activity of hepatocyte growth factor. J. Biol. Chem. **269**, 1131–1136
40 Filla, M. S., Dam, P. and Rapraeger, A. C. (1998) The cell surface proteoglycan syndecan-1 mediates fibroblast growth factor-2 binding and activity. J. Cell Physiol. **174**, 310–321
41 Pye, D. A., Vives, R. R., Turnbull, J. E., Hyde, P. and Gallagher, J. T. (1998) Heparan sulfate oligosaccharides require 6-O-sulfation for promotion of basic fibroblast growth factor mitogenic activity. J. Biol. Chem. **273**, 22936–22942
42 Echtermeyer, F., Baciu, P. C., Saoncella, S., Ge, Y. and Goetinck, P. F. (1999) Syndecan-4 core protein is sufficient for the assembly of focal adhesions and actin stress fibres. J. Cell Sci. **112**, 3433–3441
43 Okayama, M., Munesue, S., Yoshitomi, Y., Kusano, Y. and Oguri, K. (2001). Elevated level of syndecan-2 expression suppresses the metastatic phenotype of Lewis lung carcinoma cells. XVI International Symposium on Glycoconjugates (The Hague). Abstract, p. 126
44 Ishiguro, K., Kadomatsu, K., Kojima, T., Muramatsu, H., Tsuzuki, S., Nakamura, E., Kusugami, K., Saito, H. and Muramatsu, T. (2000) Syndecan-4 deficiency impairs focal adhesion formation only under restricted conditions. J. Biol. Chem. **275**, 5249–5252

Received 22 October 2001/2 January 2002; accepted 4 January 2002

doi:10.1006/mthe.2002.0587, available online at http://www.idealibrary.com on IDEAL

ARTICLE

Significant Antitumor Effects Obtained by Autologous Tumor Cell Vaccine Engineered to Secrete Interleukin (IL)-12 and IL-18 by Means of the EBV/Lipoplex

Hidetsugu Asada,[1] Tsunao Kishida,[1] Hideyo Hirai,[1] Etsuko Satoh,[1] Suzuyo Ohashi,[2] Minoru Takeuchi,[3] Toshikazu Kubo,[2] Masakazu Kita,[1] Yoichiro Iwakura,[4] Jiro Imanishi,[1] and Osam Mazda[1,*]

Departments of [1]Microbiology and [2]Orthopedics, Kyoto Prefectural University of Medicine, Kyoto 602-8566, Japan
[3]Department of Biotechnology, Faculty of Engineering, Kyoto Sangyo University, Kyoto 603-8555, Japan
[4]Center for Experimental Medicine, Institute of Medical Science, University of Tokyo, Tokyo 108-8639, Japan

**To whom correspondence and reprint requests should be addressed. Fax: +81-75-251-5331. E-mail: mazda@basic.kpu-m.ac.jp.*

The EBV/lipoplex is a nonviral gene delivery system composed of a cationic lipid and Epstein-Barr virus (EBV)-based plasmid vector that carries the EBV oriP and EBV nuclear antigen 1 (EBNA1) gene. Because the EBNA1 supports retention, nuclear localization, and transcriptional upregulation of the oriP-bearing plasmid, cells transfected with the EBV/lipoplex express the transgene at a very high level. We hypothesized that tumor cells genetically manipulated with the EBV/lipoplex may be used as a tumor vaccine without drug selection, strongly contributing to immunotherapy of patients with malignancies. The cytokines interleukin (IL)-12 and IL-18 exert a variety of immune-regulatory functions including interferon (IFN)-γ production and cytotoxic T lymphocyte (CTL) and natural killer (NK) activation. Here, we investigated the possible therapeutic effects of an autologous tumor cell vaccine in the B16 melanoma model. The vaccine was engineered to secrete IL-12 and IL-18 by means of the EBV/lipoplex. B16 cells were subcutaneously implanted into syngenic mice followed by repetitive immunization with irradiated B16 cells that had been transfected 3 days earlier by TFL2-3, a novel cationic lipid, with EBV-plasmid vectors encoding IL-12 and/or IL-18 genes (B16/mIL-12, B16/mIL-18, and B16/mIL-12+mIL-18). The mice vaccinated with B16/mIL-12 underwent strong tumor suppression accompanied by a high IFN-γ production. Both CTL and NK activities were significantly elevated in these mice. When the tumor cell vaccine was prepared by means of conventional (non-EBV) plasmid vectors combined with the same cationic lipid, the therapeutic outcome was not as good, suggesting the superiority of the EBV-based plasmid in engineering these types of tumor vaccines. Vaccination with B16/mIL-18 was not effective in suppressing tumors, whereas B16/mIL-12+mIL-18 showed comparable antitumor therapeutic validity as B16/mIL-12 did. When IFN-γ mutant (*IFN-γ*$^{-/-}$) mice were treated, B16/mIL-12 vaccine did not show any therapeutic activity, suggesting the necessity of IFN-γ in the anti-melanoma immune responses. In contrast, the antitumor effect was not affected by NK depletion in mice that received repetitive injections with anti-asialo GM1 antibody. Furthermore, vaccination with B16/mIL-12 significantly suppressed pulmonary metastases in mice that had been intravenously injected with parental B16. Our results suggest that the EBV/lipoplex is quite useful in generating an autologous tumor cell vaccine and that IL-12 is an important component of the vaccine.

Key Words: gene therapy, tumor vaccine, melanoma, IL-12, IL-18, EBV-based plasmid vector, episomal vector, liposome

Introduction

Various tumor vaccines have been devised as tools for immunotherapy approaches against many types of tumors, including malignant melanoma [1–5], renal cell carcinoma [6], prostate cancer [5,7,8], and colon carcinoma [9,10]. Earlier preclinical studies reported that various vaccination protocols succeeded in inducing some antitumor effect. However, few tumor vaccine protocols have achieved satisfactory clinical validity at the present time.

1525-0016/02 $35.00

doi:10.1006/mthe.2002.0587, available online at http://www.idealibrary.com on IDEAL

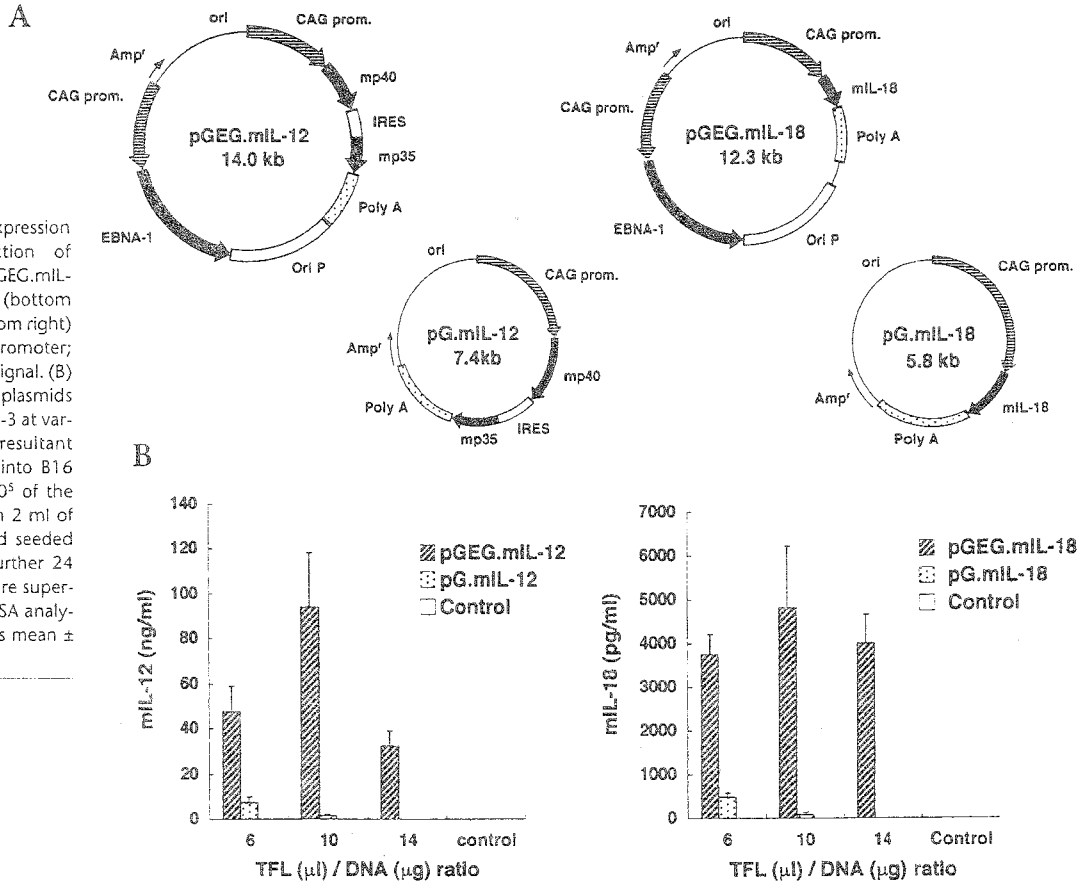

FIG. 1. Cytokine gene expression *in vitro*. (A) Construction of pGEG.mIL-12 (top left), pGEG.mIL-18 (top right), pG.mIL-12 (bottom left), and pG.mIL-18 (bottom right) [21] are shown. Prom, promoter; polyA, poly(A) additional signal. (B) Two μg of the indicated plasmids were combined with TFL2-3 at various ratios, and the resultant lipoplex was transfected into B16 cells. Three days later, 10^5 of the cells were resuspended in 2 ml of new culture medium and seeded into a new flask. After further 24 hours of cultivation, culture supernatant was served for ELISA analyses. Data are presented as mean ± SD (n = 3).

Because of low transduction efficiency of conventional retroviral and nonviral gene transfer systems, tumor cells to be used as vaccine are cultured in the presence of antibiotics following the transduction with these vectors, to establish cells producing high levels of transgene. The selection process not only requires cost and labor but also takes more than several weeks, during which period the patients remain untreated with the vaccine. Even if the drug selection is completed, the resultant drug-resistant cells do not always express the transgene product at a therapeutically relevant level. If a highly efficient gene transfer system is available and transduced cells are used as a vaccine without drug selection, the system may greatly contribute to developing an autologous tumor cell vaccine of clinical validity.

The Epstein-Barr (EBV)-based plasmid vectors carry the EBV EBNA1 (EBV nuclear antigen 1) gene and the oriP sequence [11]. We have previously shown in various animal models that the EBV-based plasmid vectors could become quite powerful tools for nonviral gene therapy [reviewed in 12]. Not only human [13–17] but also rodent [18–22] cells are quite effectively transfected both *in vitro* [13–16,18] and *in vivo* [17–22]. A variety of gene delivery vehicles including cationic polymer [15–17], electroporation [21,23], and gene gun [19] are successfully combined with the EBV-based plasmids. Among them, the EBV-based plasmid/cationic lipid complex vector (the EBV/lipoplex) enables efficient genetic transfer into cancerous [15] and primary [13] cells *in vitro*.

Here, we examined if autologous B16 melanoma cells transfected with IL-12 and IL-18 genes via the EBV/lipoplex successfully induce immune responses against a tumor, resulting in a significant therapeutic outcome. The mechanism of the antitumor immunity is also analyzed.

RESULTS

High-Level Cytokine Secretion from B16 Cells Transfected with EBV/Lipoplex

We first estimated the cytokine production *in vitro* of B16 cells transfected with the novel cationic liposome, TFL2-3. Cells transfected with pG.mIL-12 and pG.mIL-18 secreted low levels of IL-12 and IL-18, respectively, as revealed by ELISA analysis (Fig. 1B). This is not surprising because the transfected cells were not selected with antibiotics and the assay was performed 4 days after the transfection (transient expression). In contrast, transfection

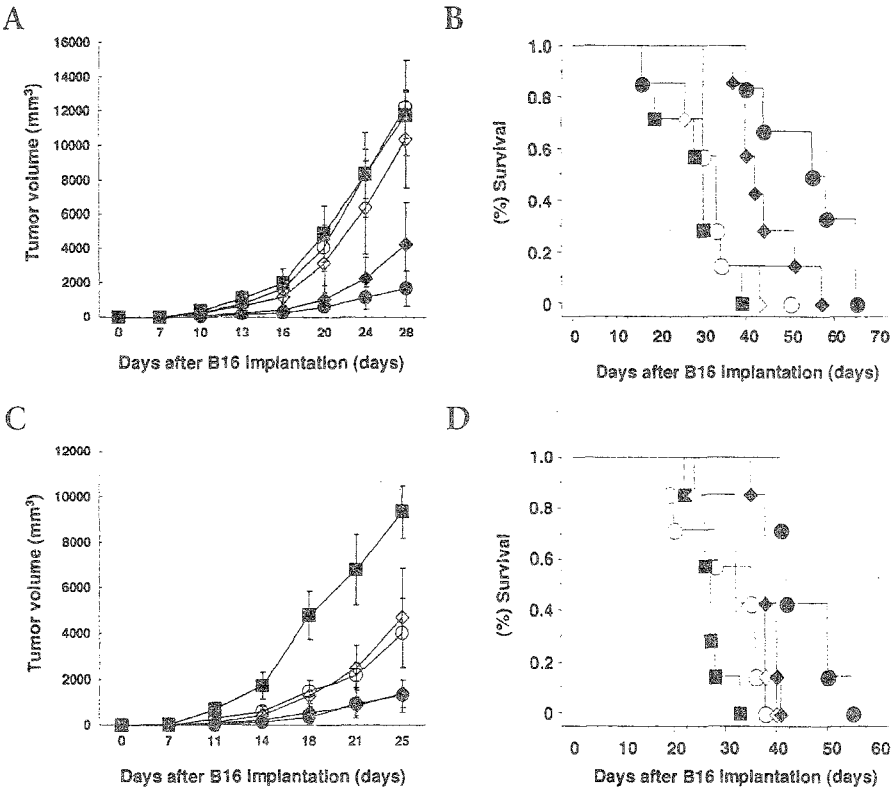

FIG. 2. Therapeutic effect against preestablished subcutaneous tumors. (A) and (B) Mice were injected with 2×10^5 of B16 (day 0), and on days 5, 12, 19 and 26, the animals were vaccinated with 2×10^6 of irradiated B16 (open circle), B16/mIL-12 (filled circle), B16/mIL-18 (open diamond), or B16/mIL-12+mIL-18 (filled diamond). As a control, a group of tumor-implanted mice were not vaccinated (filled square). Tumor volume (A) and percent survival of mice (B) are shown ($n = 7$ in each group). (C) and (D) Tumor-bearing mice were vaccinated with 2×10^6 of irradiated B16/mIL-12 (filled circle), B16/mIL-12+mIL-18 (filled diamond), B16 transfected with pG.mIL-12 (open diamond), or B16 co-transfected with B16/mIL-12 and pG.mIL-18 (open circle) as above. The control mice were not vaccinated (filled square). Tumor volume (C) and percent survival of mice (D) are shown ($n = 7$ in each group).

with pGEG.mIL-12 and pGEG.mIL-18 induced an approximately 10 times higher level of the corresponding cytokine at every DNA:liposome ratio tested. The results are consistent with our previous finding that the EBV-based plasmid vector is superior to a conventional plasmid vector in terms of the transfection efficiency and the expression level of the transgene [14–18,21,22]. The expression levels achieved by TFL2-3 are comparable to those obtained by polyamidoamine dendrimer (Qiagen) or lipofectamine (data not shown).

Autologous Tumor Cell Vaccine Engineered to Secrete IL-12 Efficiently Suppressed Subcutaneous B16 Tumor Growth

Next we used as tumor vaccine genetically modified B16 cells to secrete cytokines by means of the EBV/lipoplex. B16 cells were transfected with pGEG.mIL-12, pGEG.mIL-18, or both, and 3 days later the resultant transfectants (B16/mIL-12, B16/mIL-18, and B16/mIL-12+mIL-18, respectively) were irradiated and inoculated into the animals that had been implanted with parental B16 cells. The vaccination with B16/mIL-12 effectively inhibited the growth of the preestablished tumors ($P < 0.001$ compared with B16-vaccinated group), resulting in substantial prolongation of the survival of the animals ($P < 0.005$ compared with B16-vaccinated group; Figs. 2A and 2B). In contrast, the B16/mIL-18 failed to exhibit antimelanoma activity. The B16/mIL-12+mIL-18 was not more effective than B16/mIL-12 in suppressing tumors, suggesting that IL-18 did not synergize with IL-12 in inducing an antitumor response in this animal model.

Next we compared the vaccines transfected with the EBV-based plasmid vectors with the ones transfected with the conventional plasmid vectors. B16 cells transfected with pG.mIL-12 showed only partial suppressive effects on melanoma growth when inoculated into tumor-bearing mice as vaccine (Fig. 2C). The longevity of the mice was slightly ameliorated (Fig. 2D). Similar results were also observed for B16 cotransfected with pG.mIL-12 and pG.mIL-18 plasmids. This may be ascribed to the poor cytokine production by B16 cells transfected with pG vectors.

Cytokine Production *in Vivo*

To demonstrate cytokine production *in vivo*, sera were collected from vaccinated animals and cytokine concentrations were measured by ELISA analyses. The serum IL-12 level reached its peak on day 1 after the injection with B16/mIL-12 (1049 ± 118 pg/ml; Fig. 3A). Similarly, the serum IL-18 level was highly elevated in mice injected with IL-18 producing vaccine (2145 ± 364 pg/ml on day 3 of injection; Fig. 3B).

As for the B16/mIL-12-vaccinated group, the concentration of interferon (IFN)-γ was substantially increased in the serum (Fig. 3C). Maximum serum IFN-γ levels were 238 ± 54 pg/ml. IL-12 induced endogenous IFN-γ production *in vivo*. In contrast, IFN-γ was not demonstrated at a detectable level in serum of mice given an injection with B16/mIL-18.

doi:10.1006/mthe.2002.0587, available online at http://www.idealibrary.com on IDEAL

CTL and NK Activities Are Augmented by IL-12 Producing Vaccine

To elucidate the mechanisms that mediated the antitumor effects, we assessed the CTL and NK activities in the tumor-bearing mice that had been vaccinated with B16 transfectants. Vaccination with parental B16 elevated neither CTL nor NK activity (Fig. 4). In contrast, strong cytotoxic activity against B16 cells was demonstrated in the tumor-bearing mice treated with B16/mIL-12 or B16/mIL-12+mIL-18 (Fig. 4A). Mice immunized with B16/mIL-18 showed an intermediate level of elevation in CTL activity, suggesting that IL-18 stimulated CTL against the melanoma in the absence of exogenous IL-12. The B16/mIL-12+mIL-18-vaccinated group showed significantly higher CTL activity than the B16/mIL-12 group. The vaccine secreting IL-12, IL-18, or both augmented the NK activity to a similar level because no significant difference was seen in YAC-1 killing activities in groups given injections with B16/mIL-12, B16/mIL-18, and B16/mIL-12+mIL-18 (Fig. 4B).

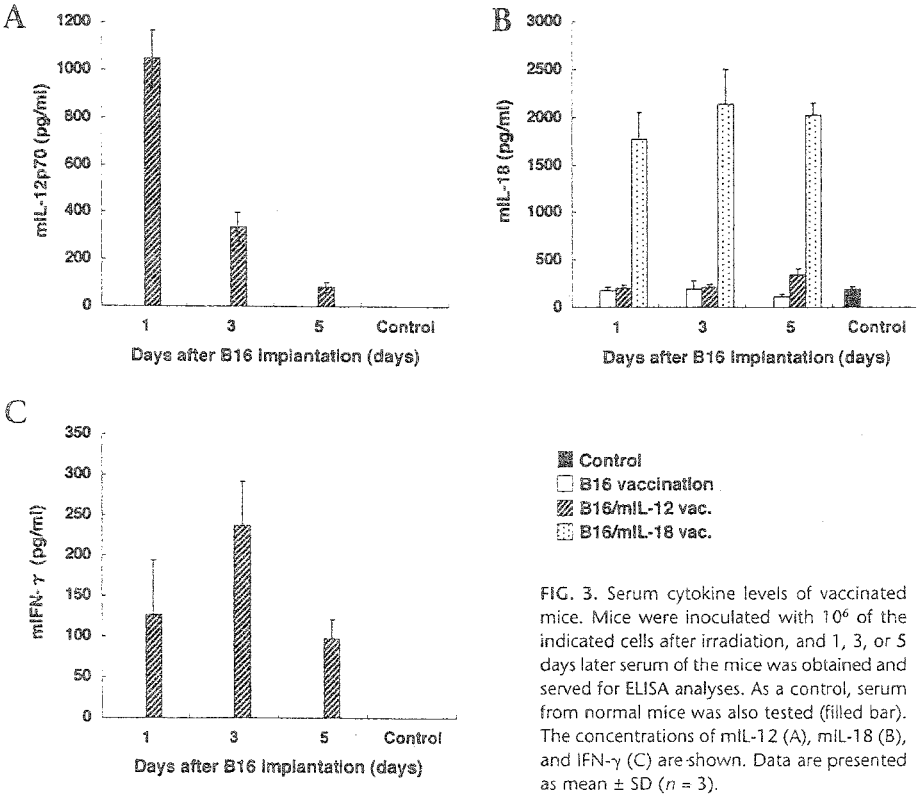

FIG. 3. Serum cytokine levels of vaccinated mice. Mice were inoculated with 10^6 of the indicated cells after irradiation, and 1, 3, or 5 days later serum of the mice was obtained and served for ELISA analyses. As a control, serum from normal mice was also tested (filled bar). The concentrations of mIL-12 (A), mIL-18 (B), and IFN-γ (C) are shown. Data are presented as mean ± SD (n = 3).

Antitumor Effects Were Abrogated by IFN-γ Deficiency

To assess the role of IFN-γ in the antitumor response, we examined whether the vaccine therapy also induces similar responses against B16 tumors in *IFN-γ*$^{-/-}$ mice. Wild-type and *IFN-γ*$^{-/-}$ mice were implanted with the parental melanoma cells followed by immunization with B16 transfectants (Fig. 5). Unlike wild-type animals, *IFN-γ*$^{-/-}$mice showed comparable growth curves of the subcutaneous tumors regardless of the vaccines injected (P values between B16/mIL-12-vaccinated group and control group are $P < 0.0000005$ (wild type) and $P < 0.05$ (*IFN-γ*$^{-/-}$ mice). P values between B16/mIL-12+mIL-18-vaccinated group and control group are $P < 0.00001$ (wild type) and $P = 0.5$ (*IFN-γ*$^{-/-}$ mice)). These results suggest that the IFN-γ production is a prerequisite to direct antitumor effect in our vaccine therapy protocol.

Cytotoxic activities against B16 and YAC-1 cells were also estimated for splenic cells from the *IFN-γ*$^{-/-}$ mice (Figs. 5B and 5C). NK activity in tumor-bearing, non-vaccinated, *IFN-γ*$^{-/-}$ mice was significantly lower than that in tumor-bearing, non-vaccinated, wild-type mice. The treatment with B16/mIL-12 elevated NK and CTL activities only marginally, if at all, in mutant animals. The B16/mIL-12+mIL-18 inoculation significantly elevated the tumoricidal activities, but the degree of elevation is smaller than that in wild-type animals. The results suggest that augmentation of CTL and NK activities in wild-type mice resulted from stimulation of these cells by IFN-γ that was induced by the vaccination.

NK Depletion Did Not Affect the Therapeutic Effect of the Vaccine

We next asked whether the NK cells really contribute to the therapeutic effect of the vaccine. To deprive NK cells, anti-asialo GM1 antibody was systemically administered into mice via the peritoneal cavity. By this treatment, NK activity was completely abrogated in the mice as judged by a cytotoxic assay of spleen cells against YAC-1 (data not shown). Normal and NK-depleted mice showed similar growth rates of tumors as well as comparable survival curves following the treatment with B16/mIL-12 (Fig. 6). The B16/mIL-12+mIL-18 treatment could suppress tumors in NK-depleted mice at a similar level as in normal mice. The results indicate that the augmented NK activity in the vaccinated animals is not indispensable to elicit therapeutic responses against melanoma.

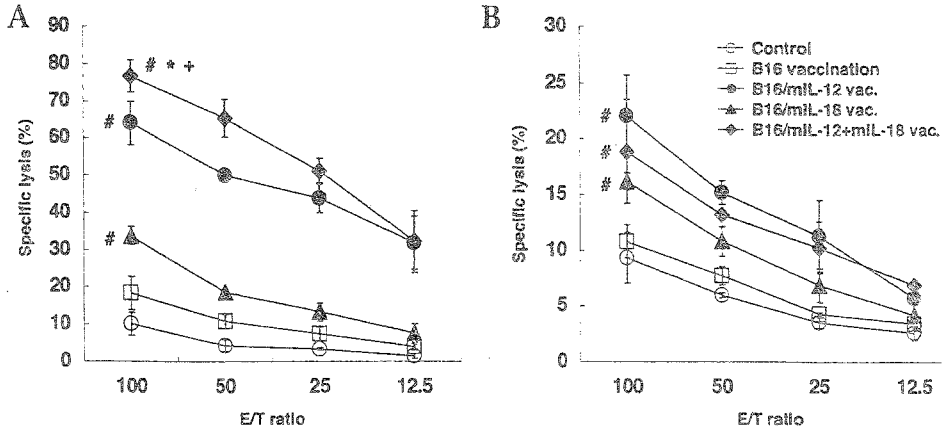

FIG. 4. Elevation in CTL and NK cytotoxic activities induced by vaccination. Tumor-bearing mice were vaccinated with the indicated cells as described in the legend to Fig. 2. On day 29, splenic cells were prepared and cytotoxic activities against B16 (A) and YAC-1 (B) were measured. #$P < 0.01$ compared with B16-vaccinated group; *$P < 0.05$ compared with B16/mIL-12-vaccinated group; +$P < 0.0005$ compared with B16/mIL-18-vaccinated group. Data are presented as mean ± SD ($n = 3$).

Metastatic Pulmonary Tumor Is Also Suppressed by B16/mIL-12 Immunization

To examine whether the immunotherapy strategy also suppresses metastatic tumor outgrowth, pulmonary metastases were established in syngenic mice and the vaccination therapy was conducted as above. Figure 7 shows the number of tumor foci in the lung of the animals. Although parental B16 vaccine partially inhibited the metastatic tumors, further therapeutic results were obtained in mice injected with B16/mIL-12. Vaccination with B16/mIL-12+mIL-18 showed tumor suppression comparable to the B16/mIL-12 vaccination.

DISCUSSION

Here, we have succeeded in devising an effective tumor cell vaccine secreting Th1 cytokines by means of the EBV/lipoplex. The transfected tumor cells were cultured for as short as 3 days in the absence of antibiotics before being used as vaccine. The vaccination induced IFN-γ production and elevation in CTL activity in mice resulting in the growth suppression of preestablished tumors as well as prolonged mean survival time of the animals. The vaccine therapy also significantly suppressed pulmonary metastases of the tumor. This is ascribed to the high cytokine production achieved by the EBV/lipoplex (Fig. 1B).

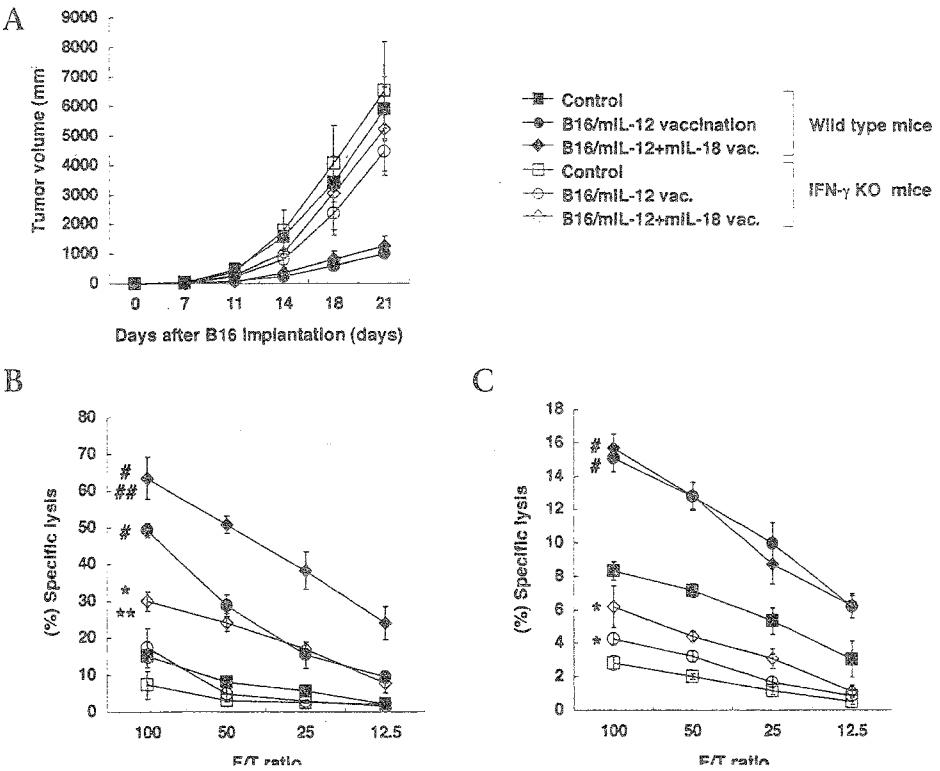

FIG. 5. Therapeutic effects were not obtained in IFN-γ deficient mice. Wild-type or $IFN\gamma^{-/-}$ mice were implanted with 2×10^5 of B16 (day 0) followed by vaccination with 2×10^6 of the indicated cells after irradiation on days 5, 12, and 19. Tumor volume (A) ($n = 7$) and cytotoxic activities against B16 (B) and YAC-1 (C) ($n = 3$) are shown. #$P <$ 0.005 compared with untreated wild-type mice; ##$P < 0.05$ compared with B16/mIL-12-vaccinated wild-type mice; *$P < 0.05$ compared with untreated $IFN\gamma^{-/-}$ mice; **$P < 0.05$ compared with B16/mIL-12-vaccinated $IFN\gamma^{-/-}$ mice.

doi:10.1006/mthe.2002.0587, available online at http://www.idealibrary.com on IDEAL

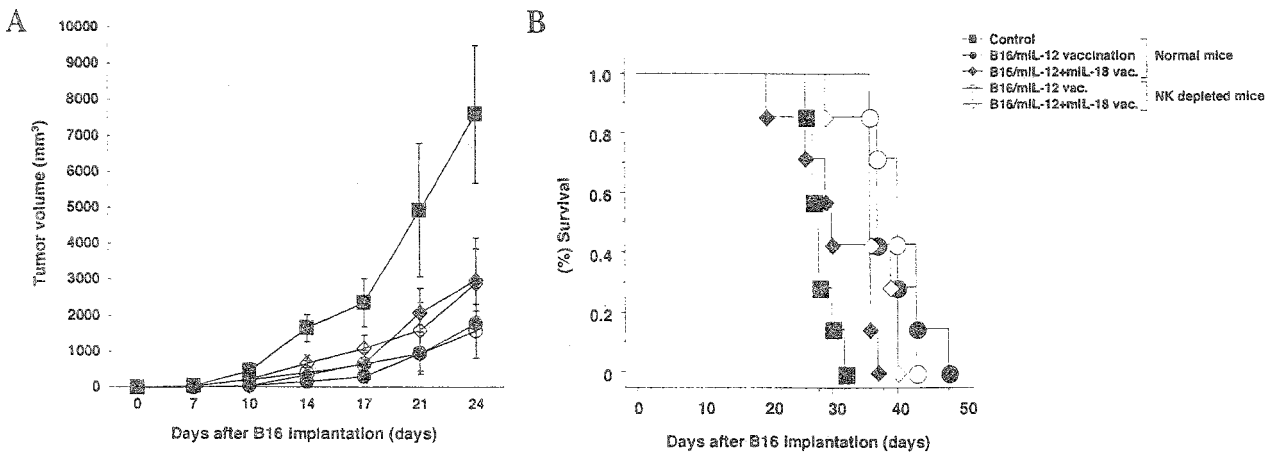

FIG. 6. NK depletion does not affect therapeutic outcome. Normal mice or mice deprived of NK cells were implanted with 2×10^5 of B16 (day 0) followed by vaccination with 2×10^6 of the indicated cells after irradiation on days 5, 12, 19, and 26. Tumor volume (A) and percent survival of mice (B) are shown ($n = 7$ in each group).

Actually, the vaccine manipulated via a conventional plasmid vector was less effective in suppressing tumor growth (Figs. 2C and 2D), consistent with the low cytokine production (Fig. 1B). As far as we know, our report is the first in which an EBV-based plasmid vector was used to produce a tumor vaccine. The novel vaccine strategy may liberate us from drug selection process and virus-related complications.

In some earlier studies, adenovirus vectors were used to establish tumor vaccines [24,25]. Thanks to the high transduction efficiency and abundant expression of the adenovirus vectors, the transduced cells need not be selected before vaccination. But the problems of the adenovirus vectors are their immunogenicity and potential induction of inflammatory responses [26,27]. Repetitive immunization with cells infected with an adenovirus vector may cause immune responses to the viral gene products. Retroviral and nonviral vectors may be less immunogenic, but their transduction efficiency is relatively poor, so a selection process is usually indispensable. In this regard, the EBV/lipoplex could become an alternative tool to genetically manipulate tumor vaccines.

IL-12 is a heteromeric cytokine produced by antigen-presenting cells, phagocytes, and granulocytes [28]. IL-12 plays critical roles in the induction of Th1 immune responses [29]. This cytokine also activates CTL and NK cells and stimulates the production of IFN-γ [30,31]. IL-18 shares similar immune regulatory functions as IL-12. IL-18 not only enhances CTL and NK activities in an IL-12-independent manner, but also synergizes with IL-12 in facilitating the cellular immunity [32,33]. Therefore, transduction of IL-12 and/or IL-18 genes may enhance both innate and adaptive immune responses against a tumor. Earlier reports by Osaki *et al.* showed that intratumoral transduction with an IL-18 adenovirus vector together with systemic administration with recombinant IL-12 resulted in suppression of a subcutaneous fibrosarcoma implant [34]. Gene gun-mediated intratumoral delivery of IL-12, pro-IL-18, and IL-1β converting enzyme genes was shown to be effective in suppressing murine mammary adenocarcinoma [35]. We have recently reported that electroporation-mediated transfection *in vivo* with EBV-based plasmid vectors encoding IL-12 and IL-18 conferred an efficacious antitumor activity against preestablished melanoma in mice [21]. In all of these reports in which IL-12 and IL-18 were delivered *in vivo* as genes or recombinant proteins, the cytokines showed apparent synergism in inducing immune responses to eradicate the tumors. Concerning tumor vaccines, IL-12 producing vaccines were shown to synergize with systemic administration of recombinant IL-18 to induce antitumor immunity against renal cell carcinoma [36] or bladder carcinoma [37].

To our knowledge, there has been no report in which both IL-12 and IL-18 genes were used to genetically manipulate a tumor vaccine. It is noteworthy that no synergistic effect was evident between IL-12 and IL-18 in our experimental protocols. This is not due to failure of pGEG.mIL-18 in expressing active IL-18, because spleen cells cultured with supernatant of B16/mIL-18 secrete as high as 772 ± 148 pg/ml of IFN-γ on day 4 of cultivation (data not shown). B16/mIL-18 inoculation elicited a relatively weak but significant elevation in both CTL and NK tumoricidal activities (Fig. 4). Therefore, unlike *in vivo* delivery of IL-12 and IL-18 genes/proteins, these cytokine genes may not show strong synergism when used as a vaccine *ex vivo*. This may be ascribed to the differences between *in vivo* and *ex vivo* regimens regarding the magnitude, duration, and localization of expression of these cytokines. Recently, Veenstra *et al.* reported that IL-12 stimulates monocytes to produce the IL-18 binding protein a (IL-18BPa), which interferes with IL-18 functions [38]. Such an immune modulatory system may work in vaccinated animals.

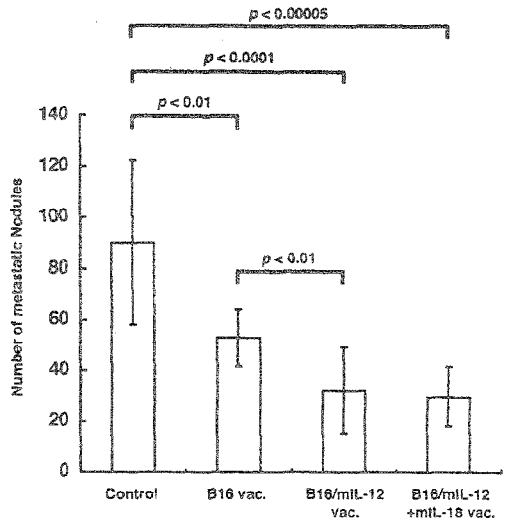

FIG. 7. Therapeutic effects against pulmonary metastases. Mice were intravenously injected into the tail vein with 10^5 of B16 (day 0). At 1, 6, and 11 days later, 10^6 of the indicated cells were inoculated into the flanks and on day 14, the number of tumor foci in the lungs was counted (n = 9 in each group).

IFN-γ has essential roles in the present gene therapy strategy (Fig. 5). Consistent with our finding is the earlier report showing that antitumor activity of a melanoma vaccine secreting GM-CSF was abrogated in *IFNγ*$^{-/-}$ mice [39]. IFN-γ is the Th1 cytokine that has a central role in the induction of cellular immune responses [40,41]. Reportedly, administration with recombinant IFN-γ enhances NK, lymphokine-activated killer (LAK), macrophage, and CTL activities against specific or nonspecific targets [42]. Enhancement of antigen processing and MHC class I and II expression is another important immunoregulatory function of IFN-γ that may trigger effective immune responses against tumor cells [43]. IFN-γ also directly inhibits growth of tumor cells [44]. In contrast, NK cells may not necessarily be required for the overall antitumor effects in the present vaccine therapy (Fig. 6) although their killing activity is enhanced by the B16/mIL-12 inoculation (Fig. 4B).

Our results suggest that the EBV/lipoplex is useful in engineering autologous tumor vaccines of potential clinical use that elicits therapeutic immunity against primary and metastatic tumors.

Materials and Methods

Plasmid vectors. The plasmid vectors have been described [21]. Briefly, the pGEG.mIL-12 is composed of a bicistronic expression cassette with murine IL-12 p35 and p40 genes [34] located between the CAG promoter [45] and the SV40 poly(A) additional signal; EBV oriP (derived from p220.2) [11]; EBV EBNA1 gene (derived from p220.2) under the control of another CAG promoter; the ampicillin resistance gene; and the replication origin for *Escherichia coli* (Fig. 1). pGEG.mIL-18 contains murine IL-18 cDNA fused with the leader sequence of the human parathyroid hormone gene [34]. pG.mIL-12 and pG.mIL-18 were constructed from pGEG.mIL-12 and pGEG.mIL-18, respectively, by deleting both CAG-EBNA1 and oriP. Plasmids were purified using Qiagen Maxiprep Endo-free kits (Qiagen, Hilden, Germany).

Cell lines and mice. The murine melanoma cell line B16 and YAC-1 cells were maintained in RPMI 1640 medium (Nacalai Tesque, Kyoto, Japan) supplemented with 100 U/ml penicillin, 100 μg/ml streptomycin, and 10% fetal bovine serum. Female C57BL/6 mice were purchased from Shimizu Laboratory Suppliers Co, Ltd. (Kyoto, Japan). To deplete NK cells, 200 μg anti-asialo GM1 antibody (Wako, Osaka, Japan) was injected intraperitoneally on days −2, 0, 4, 11, 18, and 25 of tumor cell challenge. *IFNγ*$^{-/-}$ mice were described [46] and maintained in our animal facility. All the animals received humane care in compliance with the Guide to the Care and Use of Laboratory Animals.

Gene transfection. Plasmid DNA (10 μg) was incubated for 10 minutes with the appropriate amount of TFL2-3, a cationic liposome composed of DC-6-14 and DOPE (mol ratio = 5:2). The resultant complex (EBV/lipoplex) was added to the B16 cells that had been seeded in a 175 cm^2 flask a day ago. After 2 hours of incubation in 5% CO_2/95% humidified air (standard condition), cells were washed with PBS (-), added with fresh complete medium, and further cultured for 3 days at the standard condition.

In vivo experiments. To establish subcutaneous tumors, 2×10^5 B16 cells were subcutaneously injected into the right flanks of mice (female, 6–8 weeks of age; day 0). Five days after the tumor cell challenge, 2×10^6 vaccine cells were irradiated at 40 Gy by soft X-ray and subcutaneously inoculated into the opposite flanks. The vaccination was repeated on days 5, 12, and 19, except that in an experiment *IFNγ*$^{-/-}$ and wild-type mice were immunized on days 5, 12, 19, and 26. The diameters of tumors were measured with a digital caliper and the tumor volume was calculated by the formula: $v = a \times b^2 / 2$ mm^3, where a = long diameter and b = short diameter. To establish a lung metastasis model, 10^5 of B16 cells were implanted in mice, and 1, 6, and 11 days later, 10^6 of soft X-ray irradiated B16, B16/mIL-12, or B16/mIL-12+mIL-18 cells were inoculated into the flanks of mice.

ELISA. Sera were obtained from the tail vein of mice that had received an inoculation with 10^6 of soft X-ray irradiated B16, B16/mIL-12, or B16/mIL-18 cells. Cytokine concentration in the culture supernatant or the serum was measured using a mouse IL-12 p70 ELISA kit (R&D Systems Inc.), a mouse IFN-γ ELISA kit (BioSouce International, Camarillo, CA) and a mouse IL-18 ELISA kit (MBL, Nagoya, Japan) according to the supplier's instructions.

Cytotoxicity assays. The standard ^{51}Cr-release assay was carried out as described [21]. Briefly, splenic cells were obtained from the tumor-bearing animals on day 3 of the final vaccination and used as effector cells in a NK cell assay. For the CTL assay, the splenic cells were cocultured with irradiated B16 (40 Gy) in the presence of 10 U/ml of recombinant human IL-2 for 5 days at the standard condition. B16 and YAC-1 cells were used as target cells for CTL and NK cytotoxicity, respectively. The target cells were incubated with 3.70 MBq of [^{51}Cr] sodium chromate for 60 minutes at 37°C. After washing, the cells were seeded into a microtiter plate at a density of 1×10^4/well. The effector cells were added to the microtiter plate at various effector to target ratios (E:T ratio; 100:1, 50:1, 25:1, and 12.5:1). After 4 hours of incubation at the standard condition, supernatants were collected and radioactivity was measured on a gamma counter. Specific ^{51}Cr release was calculated with the standard formula [21].

Statistical evaluation. The Student's t-test was used for the ELISA, cytotoxicity assays, and the comparison of tumor volumes. For the Kaplan-Meier analyses, survival differences between groups were evaluated using the Logrank test.

Acknowledgments

We thank Hiroshi Kikuchi and Norio Suzuki (Daiichi Pharmaceutical, Tokyo, Japan), Jun-Ichi Miyazaki (Department of Nutrition and Physiological Chemistry, Osaka University Medical School), and Hideaki Tahara (Department of Surgery, Institute of Medical Science, University of Tokyo) for the TFL2-3, the CAG promoter, and the IL-12 and IL-18 genes, respectively; and Wilfred T. V. Germeraad (Crucell, Leiden, The Netherlands) for critical reading of the manuscript. This research was supported by a grant-in-aid for scientific research from the Ministry of Education, Science, Sports and Culture, Japan, and a grant from the Japanese Research Foundation for Clinical Pharmacology.

doi:10.1006/mthe.2002.0587, available online at http://www.idealibrary.com on IDEAL

RECEIVED FOR PUBLICATION NOVEMBER 20, 2001;
ACCEPTED MARCH 6, 2002.

REFERENCES

1. Soiffer, R., *et al.* (1998). Vaccination with irradiated autologous melanoma cells engineered to secrete human granulocyte-macrophage colony-stimulating factor generates potent antitumor immunity in patients with metastatic melanoma. *Proc. Natl. Acad. Sci. USA* **95**: 13141–13146.
2. Moller, P., *et al.* (1998). Vaccination with IL-7 gene-modified autologous melanoma cells can enhance the anti-melanoma lytic activity in peripheral blood of patients with a good clinical performance status: a clinical phase I study. *Br. J. Cancer* **77**: 1907–1916.
3. Sun, Y., *et al.* (1998). Vaccination with IL-12 gene-modified autologous melanoma cells: preclinical results and a first clinical phase I study. *Gene Ther.* **5**: 481–490.
4. Mach, N., *et al.* (2000). Differences in dendritic cells stimulated *in vivo* by tumors engineered to secrete granulocyte-macrophage colony-stimulating factor or Flt3-ligand. *Cancer Res.* **60**: 3239–3246.
5. Dummer, R. (2001). GVAX (Cell Genesys). *Curr. Opin. Investig. Drugs* **2**: 844–848.
6. Nishisaka, N., *et al.* (1999). Immunotherapy for lung metastases of murine renal cell carcinoma: synergy between radiation and cytokine-producing tumor vaccines. *J. Immunother.* **22**: 308–314.
7. Nigam, A., *et al.* (1998). Immunomodulatory properties of antineoplastic drugs administered in conjunction with GM-CSF-secreting cancer cell vaccines. *Int. J. Oncol.* **12**: 161–170.
8. Simons, J. W., *et al.* (1999). Induction of immunity to prostate cancer antigens: results of a clinical trial of vaccination with irradiated autologous prostate tumor cells engineered to secrete granulocyte-macrophage colony-stimulating factor using *ex vivo* gene transfer. *Cancer Res.* **59**: 5160–5168.
9. Hanna, M. G., Jr., Hoover, H. C., Jr., Vermorken, J. B., Harris, J. E., and Pinedo, H. M. (2001). Adjuvant active specific immunotherapy of stage II and stage III colon cancer with an autologous tumor cell vaccine: first randomized phase III trials show promise. *Vaccine* **19**: 2576–2582.
10. Yoshimura, K., *et al.* (2001). Successful immunogene therapy using colon cancer cells (colon 26) transfected with plasmid vector containing mature interleukin-18 cDNA and the Igκ leader sequence. *Cancer Gene Ther.* **8**: 9–16.
11. Yates, J. L., Warren, N., and Sugden, B. (1985). Stable replication of plasmids derived from Epstein-Barr virus in various mammalian cells. *Nature* **313**: 812–815.
12. Mazda, O. (2000). Application of EBV and its replication machinery to gene therapy. In *Viral Vectors: Basic Science & Gene Therapy* (A. Garcia-Carranca, and A. Cid-Arregui, Eds.), pp. 325–337. Eaton Publishing, Natick, MA.
13. Satoh, E., *et al.* (1997). Efficient gene transduction by Epstein-Barr-virus-based vectors coupled with cationic liposome and HVJ-liposome. *Biochem. Biophys. Res. Commun.* **238**: 795–799.
14. Mazda, O., Satoh, E., Yasutomi, K., and Imanishi, J. (1997). Extremely efficient gene transfection into lympho-hematopoietic cell lines by Epstein-Barr virus-based vectors. *J. Immunol. Methods* **204**: 143–151.
15. Harada, Y., *et al.* (2000). Highly efficient suicide gene expression in hepatocellular carcinoma cells by Epstein-Barr virus-based plasmid vectors combined with polyamidoamine dendrimer. *Cancer Gene Ther.* **7**: 27–36.
16. Tanaka, S., *et al.* (2000). Targeted killing of carcinoembryonic antigen (CEA)-producing cholangiocarcinoma cells by polyamidoamine dendrimer-mediated transfer of an Epstein-Barr virus (EBV)-based plasmid vector carrying the CEA promoter. *Cancer Gene Ther.* **7**: 1241–1250.
17. Maruyama-Tabata, H., *et al.* (2000). Effective suicide gene therapy *in vivo* by EBV-based plasmid vector coupled with polyamidoamine dendrimer. *Gene Ther.* **7**: 53–60.
18. Tomiyasu, K., *et al.* (1998). Gene transfer *in vitro* and *in vivo* with Epstein-Barr virus-based episomal vector results in markedly high transient expression in rodent cells. *Biochem. Biophys. Res. Commun.* **253**: 733–738.
19. Nishizaki, K., *et al.* (2000). *In vivo* gene transfer into rat hearts with Epstein-Barr virus-based episomal vectors using a gene gun. *Transplant Proc.* **32**: 2413–2414.
20. Tomiyasu, K., *et al.* (2000). Direct intra-cardiomuscular transfer of β2-adrenergic receptor gene augments cardiac output in cardiomyopathic hamsters. *Gene Ther.* **7**: 2087–2093.
21. Kishida, T., *et al.* (2001). *In vivo* electroporation-mediated transfer of interleukin-12 and interleukin-18 genes induces significant antitumor effects against melanoma in mice. *Gene Ther.* **8**: 1234–1240.
22. Cui, F., *et al.* (2001). Highly efficient gene transfer into murine liver achieved by intravenous administration of naked Epstein-Barr virus (EBV)-based plasmid vectors. *Gene Ther.* **8**: 1508–1513.
23. Satoh, E., *et al.* (1998). Successful transfer of ADA gene *in vitro* into human peripheral blood CD34+ cells by transfecting EBV-based episomal vectors. *FEBS Lett.* **441**: 39–42.
24. Bonnet, M. C., *et al.* (2000). Recombinant viruses as a tool for therapeutic vaccination against human cancers. *Immunol. Lett.* **74**: 11–25.
25. Trudel, S., *et al.* (2001). Adenovector engineered interleukin-2 expressing autologous plasma cell vaccination after high-dose chemotherapy for multiple myeloma—a phase I study. *Leukemia* **15**: 846–854.
26. Ginsberg, H. S. (1996). The ups and downs of adenovirus vectors. *Bull. NY Acad. Med.* **73**: 53–58.
27. Zhang, W. W. (1999). Development and application of adenoviral vectors for gene therapy of cancer. *Cancer Gene Ther.* **6**: 113–138.
28. Trinchieri, G. (1995). Interleukin-12: a proinflammatory cytokine with immunoregulatory functions that bridge innate resistance and antigen-specific adaptive immunity. *Annu. Rev. Immunol.* **13**: 251–276.
29. Trinchieri, G. (1994). Interleukin-12: a cytokine produced by antigen-presenting cells with immunoregulatory functions in the generation of T-helper cells type 1 and cytotoxic lymphocytes. *Blood* **84**: 4008–4027.
30. Gately, M. K., *et al.* (1991). Regulation of human lymphocyte proliferation by a heterodimeric cytokine, IL-12 (cytotoxic lymphocyte maturation factor). *J. Immunol.* **147**: 874–882.
31. Gately, M. K., *et al.* (1994). Administration of recombinant IL-12 to normal mice enhances cytolytic lymphocyte activity and induces production of IFN-γ *in vivo*. *Int. Immunol.* **6**: 157–167.
32. Kohno, K., *et al.* (1997). IFN-γ-inducing factor (IGIF) is a costimulatory factor on the activation of Th1 but not Th2 cells and exerts its effect independently of IL-12. *J. Immunol.* **158**: 1541–1550.
33. Micallef, M. J., *et al.* (1996). Interferon-γ-inducing factor enhances T helper 1 cytokine production by stimulated human T cells: synergism with interleukin-12 for interferon-γ production. *Eur. J. Immunol.* **26**: 1647–1651.
34. Osaki, T., *et al.* (1999). Potent antitumor effects mediated by local expression of the mature form of the interferon-γ inducing factor, interleukin-18 (IL-18). *Gene Ther.* **6**: 808–815.
35. Oshikawa, K., *et al.* (1999). Synergistic inhibition of tumor growth in a murine mammary adenocarcinoma model by combinational gene therapy using IL-12, pro-IL-18, and IL-1β converting enzyme cDNA. *Proc. Natl. Acad. Sci. USA* **96**: 13351–13356.
36. Hara, I., *et al.* (2000). Effectiveness of cancer vaccine therapy using cells transduced with the interleukin-12 gene combined with systemic interleukin-18 administration. *Cancer Gene Ther.* **7**: 83–90.
37. Yamanaka, K., *et al.* (1999). Synergistic antitumor effects of interleukin-12 gene transfer and systemic administration of interleukin-18 in a mouse bladder cancer model. *Cancer Immunol. Immunother.* **48**: 297–302.
38. Veenstra, K. G., Jonak, Z. L., Trulli, S., and Gollob, J. A. (2002). IL-12 induces monocyte IL-18 binding protein expression via IFN-γ. *J. Immunol.* **168**: 2282–2287.
39. Winter, H., Hu, H. M., McClain, K., Urba, W. J., and Fox, B. A. (2001). Immunotherapy of melanoma: a dichotomy in the requirement for IFN-γ in vaccine-induced antitumor immunity versus adoptive immunotherapy. *J. Immunol.* **166**: 7370–7380.
40. Nelson, B. E., and Borden, E. C. (1989). Interferons: biological and clinical effects. *Semin. Surg. Oncol.* **5**: 391–401.
41. Itri, L. M. (1992). The interferons. *Cancer* **70**: 940–945.
42. Black, P. L., *et al.* (1993). Antitumor response to recombinant murine interferon γ correlates with enhanced immune function of organ-associated, but not recirculating cytolytic T lymphocytes and macrophages. *Cancer Immunol. Immunother.* **37**: 299–306.
43. Hammerling, G. J., Klar, D., Pulm, W., Momburg, F., and Moldenhauer, G. (1987). The influence of major histocompatibility complex class I antigens on tumor growth and metastasis. *Biochim. Biophys. Acta* **907**: 245–259.
44. Kalvakolanu, D. V. (2000). Interferons and cell growth control. *Histol. Histopathol.* **15**: 523–537.
45. Niwa, H., Yamamura, K., and Miyazaki, J. (1991). Efficient selection for high-expression transfectants with a novel eukaryotic vector. *Gene* **108**: 193–199.
46. Tagawa, Y., Sekikawa, K., and Iwakura, Y. (1997). Suppression of concanavalin A-induced hepatitis in IFN-γ(-/-) mice, but not in TNF-α(-/-) mice: role for IFN-γ in activating apoptosis of hepatocytes. *J. Immunol.* **159**: 1418–1428.

ELSEVIER

Immunology Letters 84 (2002) 49–55

Immunology Letters

www.elsevier.com/locate/

Expression of cytokine mRNAs in mice cutaneously exposed to formaldehyde

Baohui Xu [a,*], Kohji Aoyama [a], Minoru Takeuchi [b], Toshio Matsushita [a,c], Toru Takeuchi [a]

[a] *Department of Environmental Medicine, Faculty of Medicine, Kagoshima University, 8-35-1 Sakuragaoka, Kagoshima 890-8520, Japan*
[b] *Department of Biotechnology, Faculty of Engineering, Kyoto Sangyo University, Kyoto, Japan*
[c] *Kagoshima Occupational Health Promotion Center, Japan Labour Welfare Corporation, 6F, I'm Building, 1–38 Higashisengoku, Kagoshima 892-0842, Japan*

Received 7 May 2002; accepted 14 May 2002

Abstract

In this study, we have investigated the expression of cytokine mRNAs in mice cutaneously exposed to formaldehyde using semiquantitative RT-PCR. We show that formaldehyde induced the long-lasting expression of IL-4 and IFN-γ mRNAs and the transient expression of IL-13 mRNA in mouse spleen and draining lymph nodes. The transient increases in IL-2, IL-15, IL-12p40, IL-15 and IL-18 mRNAs, but long-lasting IL-15 mRNA were only seen in the formaldehyde-exposed mouse spleen. Moreover, a weak contact hypersensitivity (CH) and the significant increases in IL-4 and IFN-γ mRNAs were detected in the ear skin of formaldehyde-cutaneously exposed mice when rechallenged mouse ears. Furthermore, CH as measured by mouse ear swelling response was positively correlated with IL-4 and IFN-γ mRNA levels in the challenged ears. This study thus suggests that the induction of Th1 and Th2 cytokine mRNAs, particularly IL-4 and IFN-γ, are a common immunological feature caused by contact allergens irrespective of strong or weak contact allergens. The analysis of IL-4 and IFN-γ mRNAs may be useful markers in establishing the novel test for predicting chemical sensitizing potentials.

Keywords: Cytokine; mRNA; RT-PCR; Formaldehyde; Mice

1. Introduction

The relation of formaldehyde exposure to respiratory and contact allergy has attracted considerable attention [1,2]. Accumulating epidemiological evidence suggests that formaldehyde is one of the major contact allergens for allergic contact dermatitis [3–5]. Skin sensitizing potential of formaldehyde has also been demonstrated in different systems including guinea pig maximization test, mouse ear swelling test, local lymph node assay and in vitro hapten-specific lymphocyte transformation test, but the immunological basis of contact allergic dermatitis (or contact hypersensitivity, CH) to formaldehyde remains unclear [2,6–8]. On the other hand, cytokines in conjunction with other molecules are considered to play important roles in immune responses. It has been considered that IFN-γ-producing type 1 CD4 cells (Th1) and type 1 CD8 cells acting as effector cells contribute to the pathogenesis of CH, whereas IL-4-producing Th2 cells as negative regulatory cells are involved [9–12]. However, Th2 cytokines especially IL-4 have been shown to be essential in CH depending on contact allergens and the disease stages [13–19]. Using strong skin sensitizers, such as dinitrochlorobenzene (DNCB) and oxazolone, it has been shown that Th1-related cytokines (IL-2, IFN-γ and IL-12) and Th2 cytokines (IL-4, IL-5, IL-10 and IL-13) are coexpressed in draining lymph nodes or/and inflamed skin of mice with CH [20–22]. However, there is no report dealing with in vivo cytokine patterns in animals following cutaneous exposure to formaldehyde.

In this study, we have studied the in vivo expression of Th1 (IL-2, IL-12p40, IL-15, IL-18 and IFN-γ)- and Th2 (IL-4, IL-5, IL-10 and IL-13)-related cytokine mRNAs

* Corresponding author. Tel.: +81-99-275-5291; fax: +81-99-265-8434
E-mail address: xubaohui@m.kufm.kagoshima-u.ac.jp (B.H. Xu).

0165-2478/02/$ - see front matter
PII: S0165-2478(02)00126-8

in mice repeatedly cutaneously exposed to formaldehyde. We demonstrate that, consistent with previous findings on strong skin sensitizers, IL-4 and IFN-γ are induced or enhanced in the draining lymph nodes, spleen and rechallenged mouse skin. Our results imply that increased IL-4 and IFN-r mRNAs may be used as in vivo markers to evaluate chemical skin sensitizing potentials.

2. Materials and methods

2.1. Animals

Female Balb/C mice were purchased from Japan SLC (Hamamatsu, Shizuoka Prefecture, Japan). Mice were housed in the Institute of Experimental Animal, Faculty of Medicine, Kagoshima University and bred with standard diet and tap water ad libitum. Three to five age-matched mice (8–10 weeks) were used in each group.

2.2. Reagents

Moloney Murine Leukemia Virus reverse transcriptase was purchased from GIBCO Life Technologies (Rockville, MD). Oligo-dT_{16} was obtained from Sigma Chemical Co. (St. Louis, MO). Taq DNA polymerase and dNTP mixture were obtained from Roche Diagnostics GmbH (Mannheim, Germany). Agarose and formalin containing 37% formaldehyde were obtained from Nacalai Tesque Inc. (Kyoto, Japan).

2.3. Animal treatment protocol

Mice were skin-painted by three topical applications of 100 μl of 17.5% formaldehyde or distilled water to shaved abdominal skin with 1-day interval. Mice were sacrificed and the spleen and draining lymph nodes were removed on day 3, 5, 7, 9 and 12 after last skin painting. On the other hands, to induce CH to formaldehyde, both sides of mouse ears were challenged with 2% formaldehyde on day 3 following last skin painting. Before ear challenge and 24 h thereafter, mouse ear thickness was measured in triplicate using a dial-thickness gauge (Peacock model G, Ozaki, Japan) and CH was evaluated by the percent increase in mouse ear thickness [(ear thickness after challenge − ear thickness before ear challenge)/(ear thickness before challenge) × 100%]. Mouse lymph nodes, spleen and ears were stored at −80 °C until RNA isolation.

2.4. Semiquantitative detection of cytokine mRNAs using reverse transcription polymerase chain reaction (RT-PCR)

Total RNA from spleen, lymph nodes and ears was extracted by a guanidinium thiocyanate phenol chloroform isoamyl alcohol procedure [23]. RT-PCR analysis of IL-2, IL-4, IL-5, IL-10, IL-12p40, IL-13, IL-15, IL-18, IFN-γ and GAPDH mRNAs has been described previously [21,24]. Briefly, complementary DNA (cDNA) was synthesized by reverse transcribing total RNA with Moloney Murine Leukemia Virus reverse transcriptase using oligo-dT_{16} primer, amplified by PCR in the presence of gene-specific primers on the Mini-Cycler (MJ Research Inc., Watertown, MA). PCR primers were synthesized at Takara Biochemicals (Kyoto, Japan) and the sequences for IL-2, IL-4, IL-5, IL-10, IL-12p40, IL-13, IL-18 and glyceraldehydes-3-phosphate dehydrogenase (GAPDH) have been described previously [21,24]. Primer sequences for IL-15 were 5′-AGG AAT ACA TCC ATC TCG TGC TA (sense) and 5′-GGA GAA AGC AGT TCA TTG CAG TA (antisense). PCR cycling conditions were 1 min at 94 °C, 1 min at 55–60 °C, 2 min at 72 °C, 35 cycles. PCR products were run on 2% agarose gel, stained in ethidium bromide and imaged on Gel Image Freezer System (AE6905N, ATTA Corp., Tokyo, Japan). To analyze cytokine mRNAs semiquantitatively, the band area for individual RT-PCR products was measured using LabImage software (Version 2.6; http://www.labimage.de). The relative amounts of cytokine mRNAs were calculated as the ratio of cytokine to GAPDH band areas.

2.5. Data analysis

One-way analysis of variance (ANOVA) was used to test the difference in increase in cytokine mRNA expression among different time-point groups. Two-way ANOVA was used to test ear thickness among different groups. If $P < 0.05$ was obtained in ANOVA, the Newman–Keuls test was used to test the difference between two groups. $P < 0.05$ was considered to be statistically significant.

3. Results

3.1. Expression kinetics of cytokine mRNAs in spleen and draining lymph nodes following repeatedly cutaneously exposed to formaldehyde

To know the cytokine gene expression patterns in mice following cutaneous exposure to formaldehyde, we comparatively studied the expression of Th1 (IL-2,

IL15, IL-12, IL-18, IFN-γ)-related and Th2 (IL-4, IL-5, IL-10 and IL-13)-related cytokine mRNAs in draining lymph nodes and spleen using semiquantitative RT-PCR.

For the induction of contact hypersensitivity, epidermal Langerhans cells take up and process contact allergens and then migrate to draining lymph nodes, where antigens are presented to naïve T cells and then the development of memory T cells are initiated. Thus, we first examined Th1- and Th2-related cytokine mRNAs in the draining lymph nodes. As shown in Fig. 1, IL-2, IL-4, IL-12p40, IL-15, IL-18 and IFN-γ mRNAs were detected in the draining lymph nodes of control mice. In contrast, IL-4 and IFN-γ mRNAs were obviously induced and lasted for 12 days in the draining lymph nodes from formaldehyde-exposed mice compared with control mice (ANOVA, $P < 0.01$). Similarly, the transiently elevated IL-13 mRNA was seen in the lymph nodes of formaldehyde-exposed mice compared with control mice (ANOVA, $P < 0.05$). However, we did not observe any significant changes in IL-2, IL-12p40, IL-15 and IL-18 mRNAs in the draining lymph nodes of formaldehyde-exposed mice.

On the other hand, at least some memory T cells leave draining lymph nodes and circulate blood, lymph nodes and spleen in CH. We thus tested if same cytokine mRNA profiles are present in the spleen. Fig. 2 shows that IFN-γ, IL-2, IL-12, IL-13 and IL-18 mRNAs were weakly but constitutively expressed, whereas IL-4 and IL-15 mRNAs were undetectable in control mouse

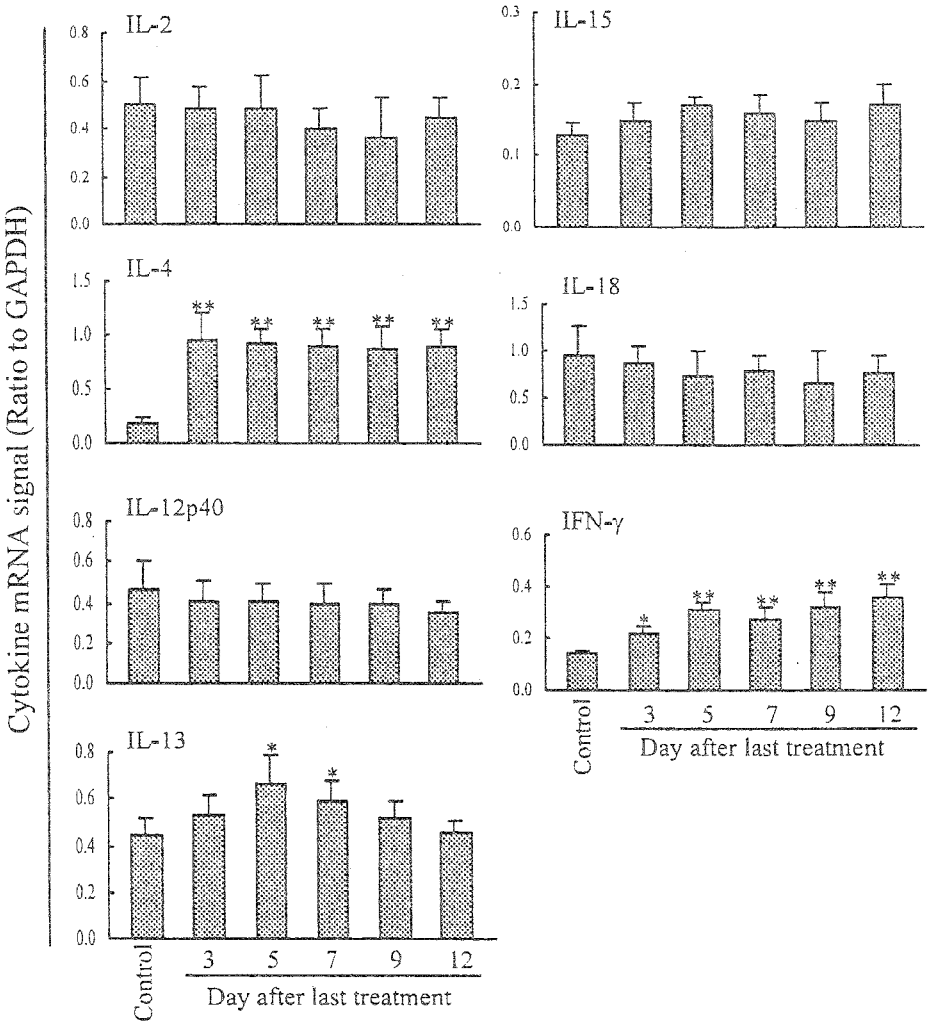

Fig. 1. In vivo expression of Th1- and Th2-related cytokine mRNAs in the draining lymph nodes of mice following repeated cutaneous exposure to formaldehyde. Mice were skin-painted with 17.5% formaldehyde three times. Mouse draining lymph nodes were removed on the indicated days following the last skin painting. The expression of individual cytokine mRNA was analyzed by semi-quantitative RT-PCR, as described in Section 2. mRNA signal for each cytokine was expressed as the ratio of cytokine and GAPDH band areas. Three mice were used for each group. One-way ANOVA, $P < 0.01$ for IL-4 and IFN-γ, $P < 0.05$ for IL-13. Newman–Keuls test, $^{*}P < 0.05$ and $^{**}P < 0.01$ compared with control group.

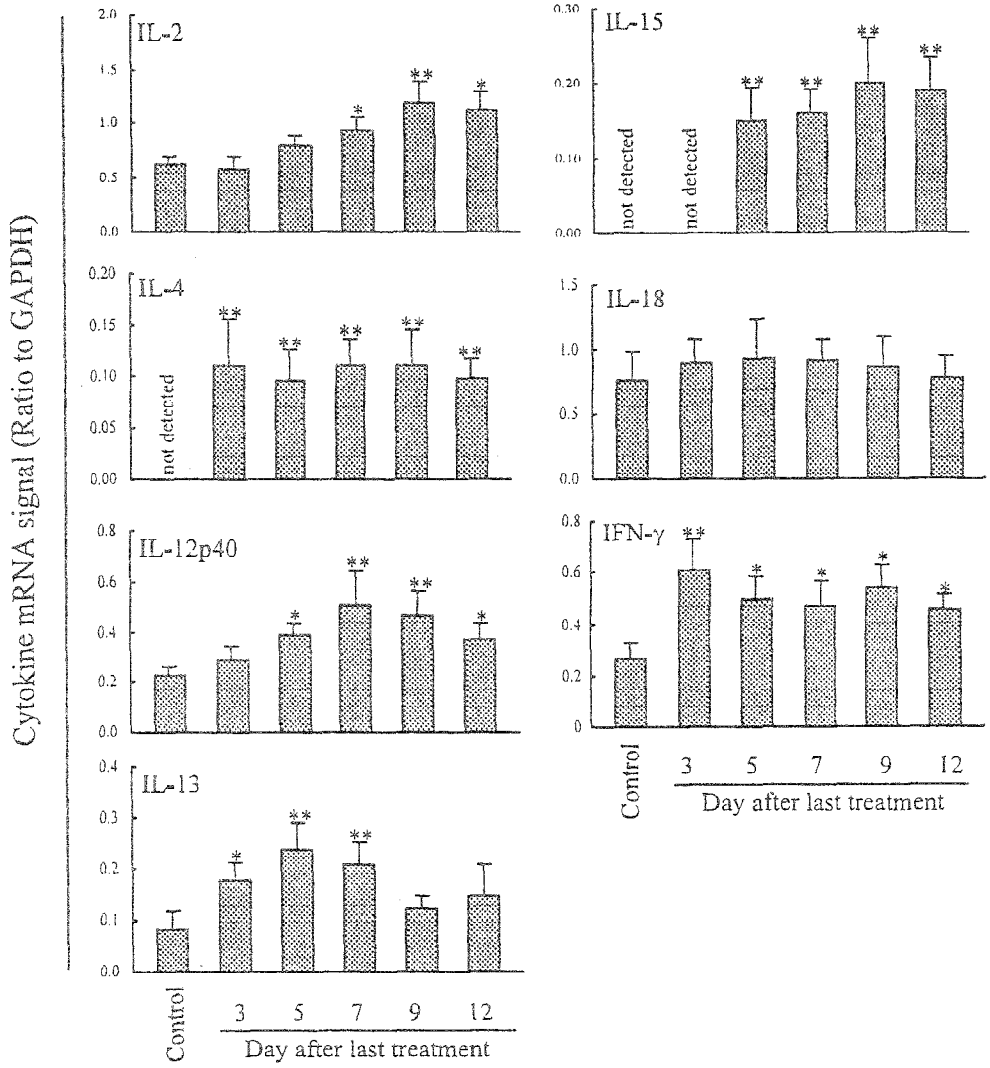

Fig. 2. In vivo expression of Th1- and Th2-related cytokine mRNAs in the spleen of mice following repeated cutaneous exposure to formaldehyde. Mice were skin-painted with 17.5% formaldehyde three times. Mouse spleens were removed on the indicated days following the last skin painting. The expression of individual cytokine mRNA was analyzed by semi-quantitative RT-PCR as described in Section 2. mRNA signal for each cytokine was expressed as the ratio of cytokine and GAPDH band areas. Three mice were used for each group. One-way ANOVA, $P < 0.01$ for IL-2, IL-4, IL-12p40, IL-15 and IFN-γ, $P < 0.05$ for IL-13. Newman–Keuls test, $^{*}P < 0.05$ and $^{**}P < 0.01$ compared with control group.

spleen in our experimental settings. In the mice exposed to formaldehyde, IL-2 and IL-15 mRNAs were significantly induced in the spleen of formaldehyde-painted mice and lasted for a long time after last skin painting ($P < 0.01$). Consistent with the finding in the draining lymph nodes, the expression of IL-4 and IFN-γ mRNAs was markedly enhanced in the spleen of exposed mice compared with control mice (ANOVA, $P < 0.01$). Unlike other cytokines, IL-12p40 and IL-13 mRNAs were transiently but significantly elevated in the exposed mice and then returned to control mouse level.

In addition, we did not detect IL-5 and IL-10 in the spleen and lymph nodes of formaldehyde-exposed or control mice in our experimental conditions (data not shown).

3.2. Expression of cytokine mRNAs in the skin of formaldehyde-exposed mice after rechallenged with formaldehyde

Increased IL-2, IL-4 and IFN-γ mRNAs in mouse spleen and lymph nodes suggest that mice may be sensitized to formaldehyde, we thus challenged both sides of mouse ears with 2% formaldehyde to examine whether CH could be provoked. As expected, a weak CH as indicated by ear swelling response was found observed in previously formaldehyde-exposed mice after ear challenged with formaldehyde again compared with control mice (ANOVA, $P < 0.05$), whereas no CH was observed in formaldehyde-exposed and control mice when challenged with distilled water (Fig. 3A).

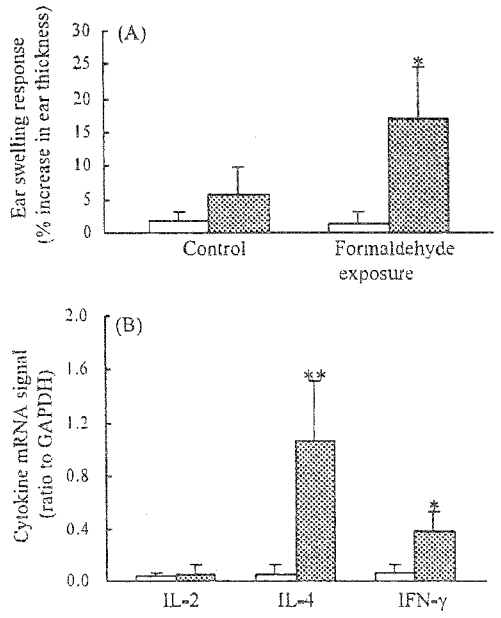

Fig. 3. Ear swelling response and skin cytokine mRNA levels in mice with or without repeated cutaneous exposure to formaldehyde after rechallenged with formaldehyde or solvent. (A) Ear swelling responses in the mice of control or formaldehyde exposure groups 24 h after challenged with solvent (unfilled) or 2% formaldehyde (filled). Formaldehyde challenge provoked significant ear swelling response in formaldehyde-previously exposed mice. $^{*}P < 0.05$ compared with control mice 24 h after allergen challenged. (B) Cytokine mRNAs in the mouse ear skin of control (unfilled) and formaldehyde exposure groups 24 h after challenged with 2% formaldehyde. $^{**}P < 0.01$ for IL-4, $^{*}P < 0.05$ for IFN-γ compared with control mice after challenged with formaldehyde.

Based on previous studies on strong contact allergens and present findings in the spleen and lymph nodes of formaldehyde-exposed mice [20,21], we detected IL-2, IL-4 and IFN-γ mRNAs in the challenged mouse ears. As shown in Fig. 3(B), IL-2, IL-4 and IFN-γ mRNAs were higher in the ears from formaldehyde-exposed and rechallenged mice than those in control mice, but there were only significant differences in IL-4 and IFN-γ mRNAs between two groups ($P < 0.01$ for IL-4, $P < 0.05$ for IFN-γ). We further analyzed the correlationships among ear swelling response and skin cytokine mRNAs using Spearman's rank test. As seen in Table 1, IL-4 and IFN-γ mRNAs were positively correlated with ear swelling response ($r = 0.74$ for IL-4, $r = 0.67$ for IFN-γ, both $P < 0.05$). A positive correlationship was also found between IL-4 and IFN-γ mRNAs in the ears ($r = 0.79$, $P < 0.05$).

Table 1
Correlation coefficients among ear swelling response and skin cytokine mRNA levels in contact hypersensitivity to formaldehyde in mice

Variables	IL-2	IL-4	IFN-γ
Ear swelling	0.50	0.74*	0.67*
IL-2	–	0.39	0.60
IL-4	–	–	0.79*

Coefficients were calculated by Spearman rank test.
* $P < 0.05$.

4. Discussion

In this study, we have investigated the gene expression profiles of Th1 and Th2 cytokines in the spleen, lymph nodes and skin in mice repeatedly cutaneously exposed to formaldehyde using semiquantitative RT-PCR. We show that the repeated cutaneous exposure to formaldehyde induces common cytokine profiles characterized by increases in long-lasting IFN-γ and IL-4 mRNAs in spleen, lymph nodes and rechallenged ears. This cytokine gene expression patterns are in agreement with recent studies conducted in contact allergic patients and animals. For examples, T cell clones established from contact allergic dermatitis produce IL-4 and IFN-γ in vitro upon activation [19,25]. The expression of IL-2, IL-4, IL-5 and IFN-γ are detected in the skin lesions of patients with contact allergic dermatitis using cytokine immunohistochemical staining and RT-PCR [26,27]. The repeated topical application of contact allergen to mice has been shown to induce a mixed expression of both Th1 and Th2 cytokine mRNAs with some time-dependent variations in the draining lymph nodes and local skin [14,28]. Ulrich et al. and we have recently shown that strong contact allergens, such as DNCB and oxazolone, induce a coexpression of Th1 and Th2 cytokine mRNAs, IL-2, IL-4, IL-10 and IFN-γ mRNAs in the draining lymph nodes [20,21]. Taken together, we propose that the induced or enhanced expression of IL-4 and IFN-γ mRNAs may serve as in vivo markers of contact sensitivity to chemicals.

There are only few reports concerning the cytokine profiles in CH to formaldehyde. Dearman et al. have shown that distinct from DNCB-sensitized mouse lymphocytes, unseparated lymph node cells, CD4 or CD8 cells from formaldehyde-skin painted mice produced more IFN-γ with less or without IL-4 production in vitro upon stimulation with Con A [29–31]. In contrast, Ulrich et al. have shown that, in accordance with DNCB- and oxazolone-sensitized mice, lymph node cells from formaldehyde-painted mice secreted both IL-4 and IFN-γ even higher IL-4 in vitro after stimulated with plate coated-anti-CD3 antibody [20]. Using immunohistochemical staining method, Hoefakker et al. have reported an indistinguishable cytokine profiles characterized by significantly higher frequencies of IL-2, IFN-γ and TNF-α-producing cells in the skin lesions between irritant and allergic dermatitis to formaldehyde, but they did not examine Th2 cytokines in particular IL-4 [32]. Overall, neither ex vivo nor in vivo observations on Th1 cytokines can exactly mirror

in vivo status during contact sensitivity to formaldehyde. In our study, we demonstrate a common cytokine profiles, the induced or enhanced mRNA expression of IFN-γ and IL-4, in spleen, lymph nodes and challenged ears of formaldehyde-exposed mice although there are variations in other Th1 and Th2 cytokine mRNAs depending on tissues. Compared with previous studies, our study thus provides more complete in vivo cytokine gene expression profiles in formaldehyde-sensitized mice. Furthermore, the similar expression kinetics of IL-4 and IFN-γ in the draining lymph nodes, significantly positive correlation between ear IL-4 and IFN-γ mRNAs, and the positive correlation of CH to formaldehyde with ear IL-4 and IFN-γ mRNA levels observed in this study suggest that, similar to IFN-γ, IL-4 may be fundamental to the development of CH to formaldehyde. Our proposal is supported by previous studies indicating a crucial role of IL-4 in CH. For examples, anti-IL-4 monoclonal antibody suppresses CH to trinitrochlorobenzene (TNCB) at the effector stage and the passive transfer of CH [16]. CH to DNCB or TNCB is impaired in IL-4-deficient mice and the lymph node cells from IL-4-deficient, sensitized mice fail to transfer CH to wild type mice [15,18,19].

Several points should be addressed concerning the present study. One is the discrepancy in the transient expression of IL-2, IL-12p40, IL-15 and IL-18 mRNAs between lymph nodes and spleen. The identification of cellular source for these cytokines is helpful, but is beyond the scope of this study. This difference between draining lymph nodes and spleen may be in part due to quantitative difference in cellular sources. For example, spleen has more B cells, macrophages, dendritic cells, endothelial cells and natural killer cells compared with lymph nodes. Moreover, since IL-4 is important in IgE production, the question is whether the elevated IL-4 mRNA in formaldehyde-exposed mice could imply the role of IL-4-mediated IgE production in allergy to formaldehyde, such as allergic asthma. Currently, the evidence supporting formaldehyde as an asthmatic substance is particularly from formaldehyde inhalation challenge test in asthma patients [33–38]. However, rare or no specific antibody against formaldehyde is detected in patients with formaldehyde asthma, other formaldehyde-exposed population and even experimental animals [8,34,39–42]. It is therefore unlikely that elevated IL-4 mRNA observed in our study may associate IgE-mediated immediate allergy to formaldehyde. In addition, the limitation of conventional RT-PCR used in this study is that cytokine mRNA expression level is evaluated in a semiquantitative manner compared with real-time and competitive RT-PCR methods. In comparison with the latter two techniques, the conventional method not only needs special PCR machine for real-time PCR, but also omits plasmid construction for competitive RT-PCR, these advantages thus allow analyzing gene expression patterns more routinely.

In summary, we demonstrate here that formaldehyde, a common contact allergen, induces a mixed expression of Th1 and Th2 cytokine mRNAs, particularly IL-4 and IFN-γ in the spleen, lymph nodes and rechallenged ears following repeated cutaneous exposure. Our findings extend the issue that Th1 and Th2 cytokines can be induced in contact hypersensitivity to chemicals and further suggest that IL-4 and IFN-γ mRNAs may be used as in vivo markers for assessing chemical sensitizing potentials.

Acknowledgements

This work was supported by grants from The Japanese Ministry of Education, Culture, Science and Technology, and its publication was supported partly by the Kodama Medical Foundation.

References

[1] Z.T. Handzel, Rev. Environ. Health 15 (2000) 325–336.
[2] E.J.J. Bardana, A. Montanaro, Ann. Allergy 66 (1991) 441–452.
[3] T. Agner, M.A. Flyvholm, T. Menne, Am. J. Contact. Dermat. 10 (1999) 12–17.
[4] M. Maouad, A.B.J. Fleischer, E.F. Sherertz, S.R. Feldman, J. Am. Acad. Dermatol. 41 (1999) 573–576.
[5] J.G. Marks, D.V. Belsito, V.A. DeLeo, J.F.J. Fowler, A.F. Fransway, H.I. Maibach, C.G. Mathias, J.R. Nethercott, R.L. Rietschel, E.F. Sherertz, F.J. Storrs, J.S. Taylor, J. Am. Acad. Dermatol. 38 (1998) 911–918.
[6] Q. Li, Z.Y. Wang, H. Inagaki, Y.J. Li, M. Minami, Toxicology 104 (1995) 17–23.
[7] T. Satoh, J.A. Kramarik, D.J. Tollerud, M.H. Karol, Toxicol. Lett. 78 (1995) 57–66.
[8] J.H. Arts, S.C. Droge, S. Spanhaak, N. Bloksma, A.H. Penninks, C.F. Kuper, Toxicology 117 (1997) 229–234.
[9] T. Biedermann, R. Mailhammer, A. Mai, C. Sander, A. Ogilvie, F. Brombacher, K. Maier, A.D. Levine, M. Rocken, Eur. J. Immunol. 31 (2001) 1582–1591.
[10] H. Xu, N.A. Dilulio, R.L. Fairchild, J. Exp. Med. 183 (1996) 1001–1012.
[11] H. Asada, J. Linton, S.I. Katz, J. Invest. Dermatol. 108 (1997) 406–411.
[12] K.M. Mohler, L.D. Butler, J. Immunol. 145 (1990) 1734–1739.
[13] R.J. Dearman, I. Kimber, Immunology 101 (2000) 442–451.
[14] H. Kitagaki, M. Kimishima, Y. Teraki, J. Hayakawa, K. Hayakawa, S. Fujisawa, T. Shiohara, J. Immunol. 163 (1999) 1265–1273.
[15] F. Dieli, G. Sireci, E. Scire, A. Salerno, A. Bellavia, Immunology 98 (1999) 71–79.
[16] A. Salerno, F. Dieli, G. Sireci, A. Bellavia, G.L. Asherson, Immunology 84 (1995) 404–409.
[17] J.A. Thomson, A.B. Troutt, A. Kelso, Immunology 78 (1993) 185–192.
[18] C. Traidl, F. Jugert, T. Krieg, H. Merk, N. Hunzelmann, J. Invest. Dermatol. 112 (1999) 476–482.
[19] B. Weigmann, J. Schwing, H. Huber, R. Ross, H. Mossmann, J. Knop, A.B. Reske-Kunz, Scand. J. Immunol. 45 (1997) 308–314.

[20] P. Ulrich, O. Grenet, J. Bluemel, H.W. Vohr, C. Wiemann, O. Grundler, W. Suter, Arch. Toxicol. 75 (2001) 470–479.
[21] B.H. Xu, K. Aoyama, A. Kitani, T. Matsuyama, T. Matsushita, Toxicol. Methods 7 (1997) 137–148.
[22] B.H. Xu, K. Aoyama, A. Kitani, S. Yu, T. Matsuyama, T. Matsushita, J. Interfer. Cytokine. Res. 18 (1998) 23–31.
[23] P. Chomczynski, N. Sacchi, Anal. Biochem. 162 (1987) 156–159.
[24] B.H. Xu, K. Aoyama, S. Yu, A. Kitani, H. Okamura, M. Kurimoto, T. Matsuyama, T. Matsushita, J. Interfer. Cytokine Res. 18 (1998) 653–659.
[25] J.D. Ohmen, J.M. Hanifin, B.J. Nickoloff, T.H. Rea, R. Wyzykowski, J. Kim, D. Jullien, T. McHugh, A.S. Nassif, S.C. Chan, J. Immunol. 154 (1995) 1956–1963.
[26] T. Koga, T. Fujimura, S. Imayama, K. Katsuoka, S. Toshitani, H. Hori, Contact. Dermat. 35 (1996) 105–106.
[27] A. Rowe, C.B. Bunker, Contact. Dermat. 38 (1990) 36–39.
[28] H. Kitagaki, N. Ono, K. Hayakawa, T. Kitazawa, K. Watanabe, T. Shiohara, J. Immunol. 159 (1997) 2484–2491.
[29] R.J. Dearman, A. Moussavi, D.M. Kemeny, I. Kimber, Immunology 89 (1996) 502–510.
[30] R.J. Dearman, S. Smith, D.A. Basketter, I. Kimber, J. Appl. Toxicol. 17 (1997) 53–62.
[31] R.J. Dearman, D.A. Basketter, P. Evans, I. Kimber, Clin. Exp. Allergy 29 (1999) 124–132.
[32] S. Hoefakker, M. Caubo, E.H. van't Erve, M.J. Roggeveen, W.J. Boersma, T. van Joost, W.R. Notten, E. Claassen, Contact Dermat. 33 (1995) 258–266.
[33] A. Krakowiak, P. Gorski, K. Pazdrak, U. Ruta, Am. J. Ind. Med. 33 (1998) 274–281.
[34] F. Wantke, M. Focke, W. Hemmer, M. Tschabitscher, M. Gann, P. Tappler, M. Gotz, R. Jarisch, Allergy 51 (1996) 837–841.
[35] J. Smedley, Clin. Exp. Allergy 26 (1996) 247–249.
[36] P.F. Gannon, P. Bright, M. Campbell, S.P. O'Hickey, P.S. Burge, Thorax 50 (1995) 156–159.
[37] L.C. Grammer, K.E. Harris, D.W. Cugell, R. Patterson, J. Allergy. Clin. Immunol. 92 (1993) 29–33.
[38] R. Alexandersson, G. Hedenstierna, Arch. Environ. Health 44 (1989) 5–11.
[39] D.W. Potter, K.S. Wederbrand, Fundam. Appl. Toxicol. 26 (1995) 127–135.
[40] S. Liden, A. Scheynius, T. Fischer, S.G. Johansson, M. Ruhnek-Forsbeck, V. Stejskal, Allergy 48 (1993) 525–529.
[41] M.S. Dykewicz, R. Patterson, D.W. Cugell, K.E. Harris, A.F. Wu, J. Allergy. Clin. Immunol. 87 (1991) 48–57.
[42] J. Hilton, R.J. Dearman, D.A. Basketter, E.W. Scholes, I. Kimber, Food Chem. Toxicol. 34 (1996) 571–578.

ELSEVIER

International Immunopharmacology 2 (2002) 1205–1211

International Immunopharmacology

www.elsevier.com/locate/intimp

Preliminary Study

Effect of hot water extract from *Agaricus blazei* Murill on antibody-producing cells in mice

A. Nakajima [a], T. Ishida [a], M. Koga [a], T. Takeuchi [b], O. Mazda [c], M. Takeuchi [a,*]

[a] *Department of Biotechnology, Faculty of Engineering, Kyoto Sangyo University, Motoyama, Kamigamo, Kita-ku, Kyoto 603-8555, Japan*
[b] *Department of Hygine, Kagoshima University Faculty of Medicine, Kagoshima, Japan*
[c] *Department of Microbiology, Kyoto Prefectual University of Medicine, Kyoto, Japan*

Received 17 May 2002; received in revised form 17 May 2002; accepted 19 May 2002

Abstract

We investigated the immunopotentiating activities of boiled water-soluble extracts from desiccated *Agaricus blazei* Murill (ABM). Effect of ABM extract on antibody production was investigated by method of hemolytic plaque-forming cells (PFC) against sheep red blood cells (SRBC) antigen. ABM extracts significantly ($p<0.01$) increased the number of PFC in spleen with intraperitoneal administration at doses of 25 mg/kg as compared with control group. The populations of Mac-1- or CD25-positive cells significantly ($p<0.01$, $p<0.001$) increased, but in CD19-positive cells, there were no differences in ABM-treated mice as compared with control mice. The expressions of IL-6 and IL-1β mRNA were augmented by ABM extract in both peritoneal macrophages and spleen cells. These results suggested that ABM extract might be an effective stimulator for T cell and macrophage to IL-1β and IL-6 release, resulting in augmentation of antibody production against SRBC antigen.

Keywords: *Agaricus blazei* Murill; Antibody production; Mice

1. Introduction

Attention has been gathering for natural products that have few side effects and an active ingredient, especially antitumor effect, because the chemotherapeutic drugs or synthetic compounds exhibit potent antitumor activity with much side effect [1]. In particular, a large variety of mushrooms have been used as immune potentiator, and many polysaccharides and peptides with antitumor activity have been isolated from mushrooms, such as black mushroom shiitake, *Hericium erinaceum*, *Calvatia caelata* [2–5]. Also, *Agaricus blazei* Murill of them has been much reported for antitumor activity [6–9]. The basidiomycete fungus *A. blazei* Murill has been traditionally used as medicine in Piedade, which is located in the suburbs of Sao Paulo, Brazil. Polysaccharides from *A. blazei* Murill have antitumor activity against Sarcoma 180 and the structure includes β-1,6-glucopyranosyl residues [6]. *A. blazei* extract, mainly (1–4)-α-D-glucan with (1–6)-β branching, has selective tumoricidal activity mediated via natural killer cell activation and apoptosis [7]. In a double-grafted tumor system, peptide glucan from *A. blazei* Murill had a direct cytotoxic action on Meth A tumor cells and an indirect immunopotentiating action on tumor-bearing mice [8]. The polysaccharides from *A. blazei* changed the percentage of splenic Thy1,2-, L3T4-positive cells

* Corresponding author. Tel.: +81-75-705-1926; fax: +81-75-705-1926.
E-mail address: mtakex@cc.kyoto-su.ac.jp (M. Takeuchi).

1567-5769/02/$ - see front matter
PII: S1567-5769(02)00056-5

in the T cell subsets in Agaricus-treated mice [9]. These reports suggest that the polysaccharides from *A. blazei* have cytotoxic action on tumor cells through immunomodulatory activities. Although many reports have been made that a variety of natural products, especially *A. blazei* Murill, possess tumoricidal activity, the immunopotentiating activities are few reported about delayed hypersensitivity or antibody response. It is unclear how Agaricus extract activates the immune system. It has not been reported that *A. blazei* Murill enhances antibody-producing activity. Therefore, in this report, we studied whether Agaricus extract induced antibody production and its mechanism.

2. Materials and methods

2.1. Mice

Female mice of C57BL/6 strain at 8–10 weeks of age were used. Mice were obtained from Japan SLC (Hamamatsu, Japan). Twelve mice were subjected to ABM and control group. Mice were treated according to the ethical guideline of Kyoto Sangyo University animal committee.

2.2. Preparation of A. blazei Murill

The boiled water extracts from *A. blazei* Murill (abbreviated to ABM) were a gift from Kyowa Engineering (Tokyo, Japan). ABM was extracted by the method described by Mizuno et al. [9], with modifications. Briefly, the dried fruiting bodies of ABM were extracted with boiled water. Then, these extracts were centrifuged at 1800×*g* for 10 min and freeze dried, and then redissolved in $Ca2^{+}$, $Mg2^{+}$-free Dulbecco's physiological buffered saline (PBS) (Nissui Pharmaceutical Tokyo, Japan) at concentration of 10 mg/ml and filtered through 0.45 μm membrane filter (Millipore, Bedford, MA) and then stored at 4 °C before use.

2.3. Assay of hemolytic plaque-forming cells (PFC)

Sheep red blood cells (SRBC) were used as antigen and obtained from Nikken Bio-medical laboratory (Kyoto, Japan). SRBC were washed three times with saline. Mice received simultaneous intraperitoneal injection of 1×10^{8} SRBC and ABM extract (25 mg/kg) or PBS as a control. After 4 days, murine spleen cells from these mice were then centrifuged two times at 490×*g* for 5 min and resuspended in 10 ml of Eagle's MEM (Nikken Bio-medical laboratory). Viable cell counts were performed by trypan blue dye exclusion test. The number of PFC against SRBC antigen was determined by the method of Cunningham and Szenberg [10] and reported as PFC per 10^{6} spleen cells or spleen. Briefly, 100-μl aliquots of the spleen cell suspension were mixed with 50 μl of 50% SRBC and 24% complement in final volume of 500 μl. One hundred microliters of these samples was incubated at 37 °C for 1 h in Cunningham's chamber (76×26 mm, Trade Mark, Japan). Hemolytic plaques of SRBC were counted by colony counter (Sekisui Chemical, Osaka, Japan).

2.4. Expressions of IL-1β and IL-6 mRNA

(1) Extraction of RNA. (a) Spleen cells. Mice were intraperitoneally administered with ABM extract (25 mg/kg) or PBS. After 4 days, spleens were isolated and minced on steel mesh and passed through a layer of gauze. Cellular total RNA from spleen cell suspensions was extracted by the method with acid guanidinium thiocyanate–phenol–chloroform (AGPC) [11]. (b) Peritoneal cells. Macrophage cultures were established from peritoneal exudates collected by lavage with 10 ml of cold PBS (−) [12]. The exudates were pooled into plastic tubes, and centrifuged at 250×*g* for 10 min. The pelletted exudates cells were resuspended in RPMI plus 10% fetal bovine serum (FCS) (respectively, Nikken Bio-medical laboratory and JRH Biosciences, Lenexa, KS). Aliquot of peritoneal cells (5×10^{5} cells/0.1 ml/well) were cultured with or without 0.1 or 1 mg/ml ABM extracts in 96-well flat-bottom culture plate (Becton Dickinson, MA, US) at 37 °C in 5% CO_2 humidified atmosphere. After 24 or 48 h, total RNA was isolated by using AGPC method. (2) RT-PCR. Total RNA was transcribed to cDNA with MLV reverse transcriptase (Life Technologies, MD, US). Oligonucleotide primers were used from published cDNA sequences of IL-1β (250 bp), IL-6 (290 bp) and β-actin (268 bp) as a house-keeping gene. PCR was then performed for 30 cycles against IL-1β, 32 cycles against IL-6 using the following

Table 1
Summary for effect of ABM extract on the number of PFC

	The number of PFC[a]		The total number of spleen cells ($\times 10^8$ cells)
	per 10^6 spleen cells	per spleen ($\times 10^4$ cells)	
Control	425.19±283.74[b]	3.86±2.20	0.98±0.20
ABM[c]	897.09±439.78*	10.59±5.63*	1.11±0.29

Asterisks denote significant difference versus control.
[a] PFC assay was performed on day 4 after immunization with SRBC antigens.
[b] Each value represents the mean±S.D. n=12.
[c] SRBC antigen (1×10^8) and ABM extract (25 mg/kg) were intraperitoneally administered.
* $p<0.01$.

primer pairs: β-actin sense (5′-GCATTGTTAC-CAACTGGGAC-3′) and β-actin antisense (5′-TCTC-CGGAGTCCATCACAAT-3′); IL-1β sense (5′-AGC-TACCTGTGTCTTTCCCG-3′) and IL-1β antisense (5′-GTCGTTGCTTGGTTCTCCTT-3′); IL-6 sense (5′-GATGCTACCAAACTGGAGATAATC-3′) and IL-6 antisense (5′-GGTCCTTAGCCACTGCTTCTG-TG-3′). The amplification profile consisted of denaturation at 94 °C for 1 min, primer annealing at 56 °C for 1 min, and extension at 72 °C for 1 min. After final cycle, the extension was performed at 72 °C for 10 min and the reaction was terminated by chilling at 4 °C. PCR products were visualized using ethidium bromide after 30% polyacrylamide gel electrophoresis. These data of the expression in IL-1β and IL-6 mRNA were quantified by Scion Image.

2.5. The analysis of surface antigens

The expression of surface antigens on spleen cells was determined by direct immunofluorescence method as described by Nicholson-Weller et al. [13] with slight modification. Spleen cells (5×10^5 cells/100 μl) treated with or without ABM extract were stained with final 0.5 μg of fluorescein–isothiocyanate (FITC)-conjugated or phycoerythrin (PE)-conjugated mAb at 4 °C for 45 min. The FITC-conjugated anti-CD3, anti-CD4, anti-CD8, anti-CD25, anti-CD11b (Mac-1) mAb, and PE-conjugated anti-CD19 mAb were obtained from PharMingen (San Diego, CA), FITC-conjugated anti-ClassII and anti-B7-1 mAb from Caltag (San Francisco, CA). After incubation, these cells were centrifuged two times at 490×g for 5 min with 1 ml of PBS and resuspended in 0.5 ml of PBS containing 100 μg/ml $CaCl_2$/$MgCl_2$, 0.01% sodium azide and 1% FCS, and then analyzed using a FACScan flow cytometer (Becton Dickinson).

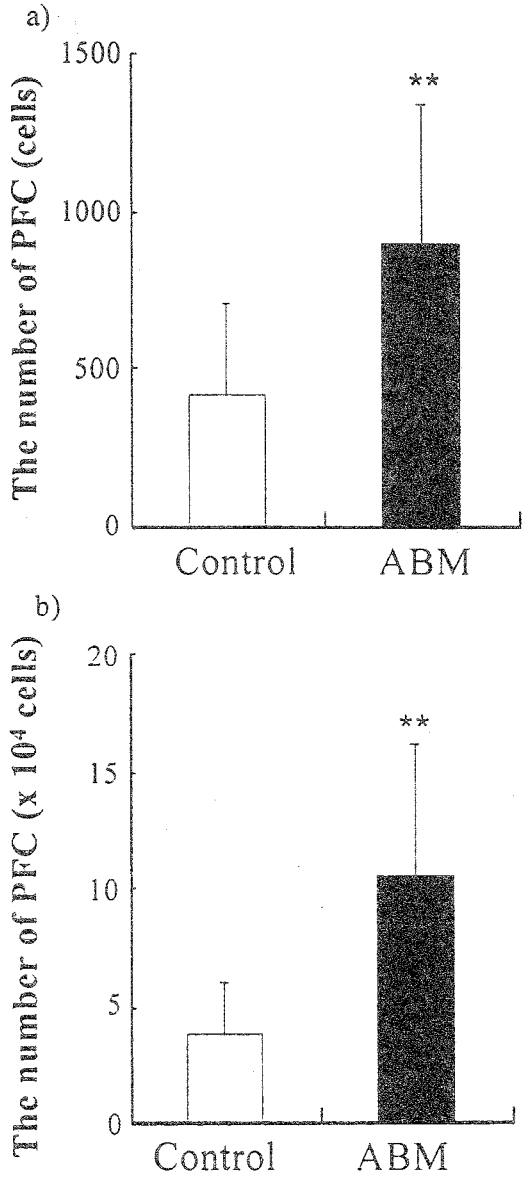

Fig. 1. Effect of ABM extracts on the number of PFC. Mice were intraperitoneally injected with 1×10^8 SRBC and ABM extract (25 mg/kg) or PBS(−) as a control on day 0. On day 4, spleens were harvested and PFC against SRBC antigen were counted by using PFC assay. (a) The number of PFC per 10^6 spleen cells, (b) the number of PFC per spleen. Results are shown as means±S.D. (n=12). **: Statistically significant ($p<0.01$), compared to control.

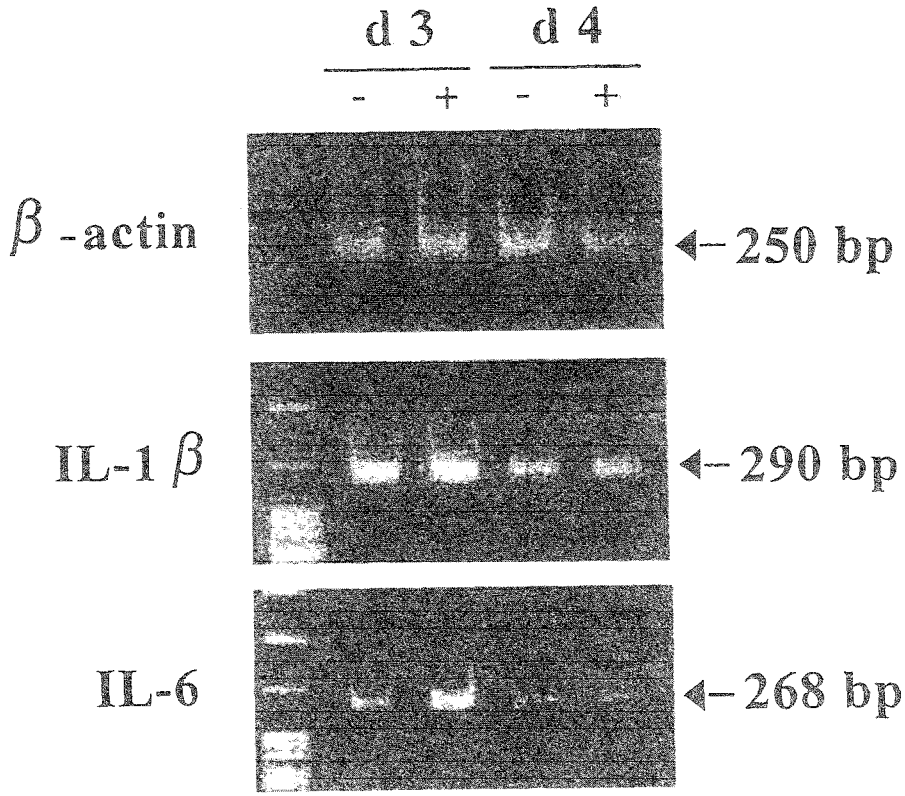

Fig. 2. Effect of ABM extract on expression of IL-1β and IL-6 mRNA in spleen cells. Mice were intraperitoneally injected with ABM extract (25 mg kg) (+) or without ABM extract (−). After 3 or 4 days, spleens were harvested and isolated total RNA by using AGPC method. RT-PCR was then performed for 26 cycles against β-actin, 29 cycles against IL-1β and 32 cycles against IL-6. PCR products were visualized using ethidium bromide after 30% polyacrylamide gel electrophoresis.

2.6. Statistical analysis

All values were expressed as means±S.D. Comparison between Agaricus-treated group and control group was made with Student's *t*-test. Any *p*-value less than 0.05 was considered significant.

3. Results

3.1. Effect of ABM extract on antibody production

We examined the effect of ABM extract on the number of PFC per 10^6 spleen cells and spleen. There was no significant difference in the number of spleen cells between ABM-treated mice ($1.11\pm0.29\times10^8$ cells/spleen; mean±S.D.) and control ($0.98\pm0.20\times10^8$ cells/spleen) as shown in Table 1. Although the number of PFC per 10^6 spleen cells was 425±283 cells in control, that in ABM-treated mice was 897±440 cells (Fig. 1a, Table 1). The number of PFC per spleen was $3.8\pm2.20\times10^4$ cells in the ABM-treated group and $10.5\pm5.63\times10^4$ cells in control (Fig. 1b, Table 1). Therefore, ABM extract resulted in a significant increase on the number of PFC per 10^6 spleen cells and spleen ($p<0.01$).

Table 2
Effect of ABM extract on ratio of IL-1β or IL-6 and β-actin mRNA expressions in spleen cells

	d3[a]		d4	
	(−)[b]	(+)	(−)	(+)
IL-1β	16.52[c]	30.74	8.62	26.69
IL-6	26.83[d]	38.42	10.48	21.72

[a] Three days after injection.
[b] Mice were intraperitoneally injected with ABM extract (25 mg kg) (+) or without ABM extract (−).
[c] Ratio of IL-1β and β-actin mRNA expression.
[d] Ratio of IL-6 and β-actin mRNA expression.

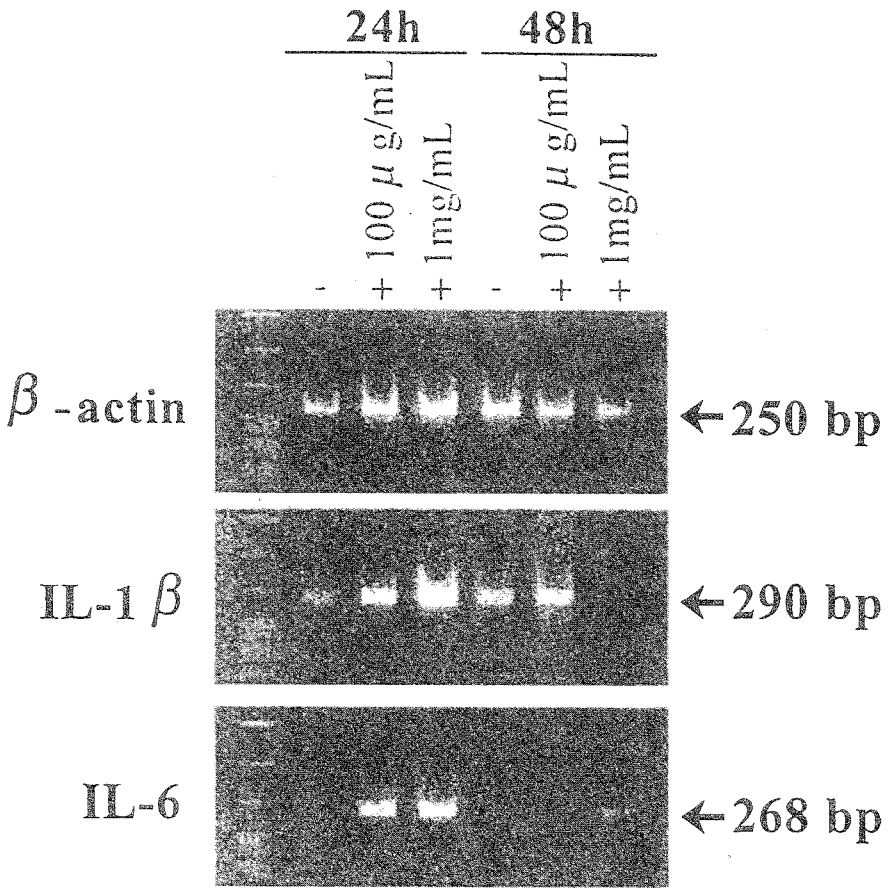

Fig. 3. Effect of ABM extract on expression of IL-1β and IL-6 mRNA in peritoneal macrophages. The peritoneal cells were distributed (5×10^4/0.1 ml/well) in 96-well flat-bottom culture plate with or without 0.1 or 1 mg ml ABM extracts. The cells were incubated for 24 or 48 h at 37 °C in 5% CO_2, and isolated total RNA by using AGPC method. RT-PCR was then performed as described above. PCR products were visualized using ethidium bromide after 30% polyacrylamide gel electrophoresis.

3.2. Effect of ABM extract on expression of IL-1β and IL-6 mRNA in spleen cells or peritoneal macrophages

To investigate how the number of PFC increased with ABM extract, we examined expression of IL-1β and IL-6 mRNA. These cytokines are known as association with B cell-differentiation to antibody-producing cell. It was found that IL-1β and IL-6 mRNA levels were enhanced the most at day 3 after SRBC treatment and ABM extract maintained higher

Table 3
Cell population of spleen cell subsets on day 4 after intraperitoneal administration of ABM extract (25 mg/kg)

	Percentage of positive cells (%)							
	CD3	CD4	CD8	CD19	Mac-1	Class II	B7	CD25
Control	28.94±1.32[a]	18.67±1.73	12.24±0.87	52.20±3.33	16.97±3.55	35.92±9.64	11.92±2.89	13.13±2.23
ABM[b]	28.03±1.21	18.98±0.49	14.39±1.84	53.79±5.28	25.44±1.35*	42.03±2.02	18.68±2.04*	26.90±2.46**

Asterisks denote significant difference versus control.

[a] Each value represents the mean±S.D. (n=5).

[b] ABM extract (25 mg/kg) was intraperitoneally administered on day 4 before FACS analysis.

* p<0.01.

** p<0.001.

expressions up to 4 day than control group (Fig. 2). These quantified data of IL-1β and IL-6 mRNA expressions are shown in Table 2. We examined whether ABM extract activated macrophages. The expression of IL-1β mRNA reached a peak at 24 h after addition of 1 mg/ml ABM extract and receded subsequently (Fig. 3).

3.3. Effect of ABM extract on surface antigens in spleen cells

The percentage of Mac-1, B7-1 or CD25 antigens positive cells were 25.4±1.4, 18.7±2.0 or 26.9±2.5 in ABM-treated mice, and were 17.0±3.6, 11.9±2.9 or 13.1±2.2 in the control, respectively. There were significant increases ($p<0.01$, $p<0.01$ and $p<0.001$, respectively) in the ABM-treated group as compared with control. However, significant difference between control and ABM-treated mice was not shown in the proportion of CD3, CD4, CD8, CD19 or ClassII antigens positive cells (Table 3).

4. Discussion

Although it is generally accepted that *A. blazei* Murill has tumoricidal activities [6–9], there are few reports on its effect for antibody production. The present study demonstrated that ABM extract could augment the immune response. Using PFC assay, we showed effect of ABM extract on antibody production. PFC assay is a typical method for examining humoral immune response [10]. In the present study, the number of PFC in spleen against SRBC antigen increased up to about three times in ABM-treated mice as compared with control, although there were no differences in the population of B cells and the number of splenic cells between ABM-treated and untreated mice. This PFC method can analyze the IgM production. Since the co-administration of ABM enhanced antibody production (mainly IgM), it was possible that elevation of IgG would happen by the isotype class switch of IgM to IgG of immunoglobulin. In spleen from mice on day 4 after immunization, percentage of Mac-1 or CD25 antigens positive cells significantly increased in ABM-treated mice, but the population of CD19 antigen positive cells had no significant difference between ABM extract treated and control mice. Mac-1 antigen is presented on differentiated monocytes/macrophages, granulocytes and activated T lymphocytes [14]. CD25 antigen is on cell surface membrane of activated or differentiated T/B lymphocytes and differentiated monocytes/macrophages [15]. CD19 antigen exists on cell surface membrane of non-activated B lymphocytes [16]. Since ABM extract could increase Mac-1, B7-1 and CD25 stained cells, the augmenting effect of ABM extract on the antibody responses resulted from expansion and differentiation of mainly monocytes and macrophages. T cell subsets were not different by ABM extract. However, antibody production against SRBC antigens was dependent on T cell. It was suggested that ABM extract stimulated on monocytes and macrophages and might elicit on T-cell and B-cell activation unless these numbers change and result in PFC induction. Mizuno et al. [9] showed that the percentage of Thy-1,2, CD4 and CD8 positive cell population was significantly increased in mice orally administered hot water-soluble fraction from *A. blazei* Murill as compared with control. However, we did not find significant differences in the percentages of CD4 and CD8 positive cells. These discrepancies might be due to distinctions of extraction, administration methods and concentration of ABM extract. The B-cell differentiation requires the interaction of various cytokines, which are secreted from macrophages or T cells [17]. It was reported that antibody production to SRBC antigen was reduced in IL-1$^{-/-}$ mice [18]. GM-CSF had been shown to have an effect on mature functional APC and that it causes an augmented response of immune system in vitro by increasing the secretion of IL-1 and expression of Ia antigens [19]. IL-6 has been shown to facilitate terminal differentiation of B cell to antibody-secreting cells and its major producers are monocytes and T cells [20]. The expression of IL-1β and IL-6 mRNA by RT-PCR has higher sensitivity and specificity than secreted analysis. Therefore, we carried out the detection of IL-1β and IL-6 mRNA level instead of protein level in the present study. ABM extract augmented the expression of IL-6 and IL-1β RNA from peritoneal macrophages. In addition, the same result was shown in whole spleen where increasing antibody-producing cells by addition of ABM extract and IL-1β and IL-6 mRNA of splenic cells from ABM-treated mice showed higher expression than control. These results suggested that augmentation of antibody production by

ABM extract might be induced by production of IL-1β and IL-6 from activated T cells and macrophages, resulting in B-cell differentiation. Therefore, the hot water extract from *A. blazei* Murill may be an important substance for augmentation of immune system and prevention of various diseases. Furthermore, it is necessary to investigate about the mechanism of PFC up-regulation by the co-administration of ABM extract.

Acknowledgements

We thank Kyowa Engineering Co. Ltd. (Tokyo, Japan) for their kind provision of extracts from *Agaricus blazei* Murill. This study was supported by a grant-in-aid for Bio-venture project from the Ministry of Education Science, Sports and Culture, Japan.

References

[1] Capelli D, Santini G, De Souza C, Poloni A, Marino G, et al. Amifostine can reduce mucosal damage after high-dose melphalan conditioning for peripheral blood progenitor cellautotransplant: a retrospective study. Br J Haematol 2000;110(2):300–7.

[2] Ooi VE, Liu F. Immunomodulation and anti-cancer activity of polysaccharide–protein complexes. Curr Med Chem 2000;7(7):715–29.

[3] Hamuro J, Rollinghoff M, Wagner H. β(1–3) Glucan-mediated augmentation of alloreactive murine cytotoxic T-lymphocytes in vivo. Cancer Res 1978;38:3080–5.

[4] Mizuno T, Wasa T, Ito H, Suzuki C, Ukai N. Antitumor-active polysaccharides isolated from the fruiting body of *Hericium erinaceum*, an edible and medicinal mushroom called *yamabushitake* or *houtou*. Biosci Biotechnol Biochem 1992;56:347–8.

[5] Lam YW, Ng TB, Wang HX. Antiproliferative and antimitogenic activities in a peptide from puffball mushroom *Calvatia caelata*. Biochem Biophys Res Commun 2001;289(3):744–9.

[6] Ebina T, Kohya H, Yamaguchi T, Ishida N. Antimetastatic effect of biological response modifiers in 'double grafted tumor system'. Jpn J Cancer Res 1986;77:1034–42.

[7] Fujimiya Y, Suzuki Y, Oshima K, Kobori H, Moriguchi K, et al. Selective tumoricidal effect of soluble proteoglucan extracted from the basidiomycete, *Agaricus blazei* Murill, mediated via natural killer cell activation and apoptosis. Cancer Immunol Immunother 1998;46:147–59.

[8] Ebina T, Fujiyama Y. Antitumor effect of a peptide-glucan preparation extracted from *Agaricus blazei* in a double-grafted tumor system in mice. Biotherapy 1998;11:259–65.

[9] Mizuno M, Morimoto M, Minato K, Tsuchida H. Polysaccharides from *Agaricus blazei* stimulate lymphocyte T-cell subsets in mice. Biosci Biotechnol Biochem 1998;62:434–37.

[10] Cunningham AJ, Szenberg A. Further improvements in the plaque technique for detecting single antibody-forming cells. Immunology 1968;14(4):599–600.

[11] Chomczynski P, Sacchi N. Single-step method of RNA isolation by acid guanidinium thiocyanate–phenol–chloroform extraction. Ann Biochem 1987;162:156–9.

[12] Seledtsova GV, Seledtsov VI, Kozlov VA. Triggering effect of BCG vaccine on antitumor and interleukin-1 secretory activity of T cell lymphokine-primed macrophages. Biomed Pharmacother 1995;5:369–74.

[13] Nicholson-Weller A, Russian DA, Austen KF. Natural killer cells are deficient in the surface expression of the complement regulatory protein, decay accelerating factor (DAF). J Immunol Aug 15, 1986;137(4):1275–9.

[14] Papiernik M, el Rouby S. Control of helper-T-cell proliferation by recognition of Ia and Mac-1 antigens on phagocytic cells of the thymic reticulum. Cell Immunol 1988;15(113(1)):95–106.

[15] Ortega G, Robb RJ, Shevach EM, Malek TR. The murine IL 2 receptor: I. Monoclonal antibodies that define distinct functional epitopes on activated T cells and react with activated B cells. J Immunol Oct 1984;133(4):1970–5.

[16] Krop I, Shaffer AL, Fearon DT, Schlissel MS. The signaling activity of murine CD19 is regulated during cell development. J Immunol July 1, 1996;157(1):48–56.

[17] Mitsuzumi H, Kusamiya M, Kurimoto T, Yamamoto I. Requirement of cytokines for augmentation of the antigen-specific antibody responses by ascorbate in cultured murine T-cell-depleted splenocytes. Jpn J Pharmacol 1998;78(2):169–79.

[18] Nakae S, Asano M, Horai R, Sakaguchi N, Iwakura Y. IL-1 enhances T cell-dependent antibody production through induction of CD40 ligand and OX40 on T cells. J Immunol 2001;167(1):90–7.

[19] Morrissey PJ, Bressler L, Park LS, Alpert A, Gillis S. Granulocyte-macrophage colony-stimulating factor augments the primary antibody response by enhancing the function of antigen-presenting cells. J Immunol 1987;15(139(4)):1113–9.

[20] Morgan EL, Hobbs MV, Thoman ML, Janda J, Noonan DJ, et al. Induction of human B cell differentiation by Fc region activators: II. Stimulation of IL-6 production. J Immunol 1990;1(144(7)):2499–505.

Induction of cyclooxygenase-2 in monocyte/macrophage by mucins secreted from colon cancer cells

Takaaki Inaba*, Hajime Sano†, Yutaka Kawahito‡, Timothy Hla§, Kaoru Akita*, Munetoyo Toda*, Ikuo Yamashina*, Mizue Inoue*, and Hiroshi Nakada*¶

*Department of Biotechnology, Faculty of Engineering, Kyoto Sangyo University, Kita-ku, Kyoto 603-8555, Japan; †Division of Rheumatology, Department of Internal Medicine, Hyogo College of Medicine, Nishinomiya, Hyogo 663-8501, Japan; ‡First Department of Internal Medicine, Kyoto Prefectural University of Medicine, Kamigyo-ku, Kyoto 602-8566, Japan; and §Department of Physiology, University of Connecticut School of Medicine, Farmington, CT 06030-3501

Edited by Sen-itiroh Hakomori, Pacific Northwest Research Institute, Seattle, WA, and approved January 6, 2003 (received for review September 5, 2002)

Up-regulation of cyclooxygenase-2 (COX-2) and overproduction of prostaglandins have been implicated in the initiation and/or progression of colon cancer. However, it is uncertain in which cells and how COX-2 is induced initially in the tumor microenvironment. We found that a conditioned medium of the colon cancer cell line, LS 180, contained a factor to induce COX-2 in human peripheral blood mononuclear cells. This factor was purified biochemically and revealed to be mucins. A small amount of mucins (≈100 ng of protein per ml) could elevate prostaglandin E2 production by monocytes. The mucins induced COX-2 mRNA and protein levels of monocytes in a dose- and time-dependent manner, indicating a COX-2-mediated pathway. We also have examined immunohistochemically the localization of COX-2 protein and mucins in human colorectal cancer tissues. It is noteworthy that COX-2-expressing macrophages were located around the region in which mucins were detectable, suggesting that COX-2 also was induced by mucins *in vivo*. These results suggest that mucins produced by colon cancer cells play a critical role in the initial induction of COX-2 in the tumor microenvironment.

Several epidemiological and chemical studies have shown that nonsteroid antiinflammatory drugs can decrease the incidence and mortality of colorectal cancer and induce the regression of adenomas in patients with familial adenomatous polyposis (1, 2). Nonsteroid antiinflammatory drugs are known to inhibit cyclooxygenase (COX) (3). Two isoforms of COX, i.e., COX-1 and COX-2, which are constitutive and inductive enzymes, respectively, have been identified (4, 5). Expression of COX-2 is up-regulated in various types of cancer including gastrointestinal cancers (6–10). Recent studies have led to the recognition of the importance of COX-2 in colorectal tumorigenesis (11–13). Oshima *et al.* (14) reported direct evidence that the formation of intestinal polyps in ApcΔ^{716} knockout mice was dramatically suppressed by crossing them with COX-2 knockout mice. Because such polyps are precursors to cancer, these results indicate that COX-2 acts at a rate-limiting step and contributes at an early stage of colon carcinogenesis. They also showed that COX-2 is not expressed in the colon epithelial cells but in interstitial cells at an early stage, indicating that the interstitial cells are essential for the intestinal polyp formation. There are some reports showing the expression of COX-2 in infiltrated macrophages in tumor tissues (13, 15–17).

Many tumors arising from epithelial tissues produce mucins. They are defined by their characteristic O-glycosylated domains, which contain a repetitive protein backbone with an especially high content of Thr and Ser residues. Upon malignant transformation, many epithelial cells produce mucins in abnormal amounts and/or with abnormal glycosylation patterns (18). A human colon cancer cell line, LS 180, produces MUC2 mucin (19), which has a high number of tandem repeat and is highly glycosylated. Most and about half of O-glycans contained in ovine and bovine submaxillary mucin (OSM and BSM), respectively, are elucidated to be a sialyl Tn antigen (20, 21). It is reported that BSM has a central domain consisting of ≈55 tandem repeats of 329 aa (22). Mucins produced by cancer cells are found in the sera of cancer patients and used as disease markers. There have been many reports that patients with a higher amount of mucins in their bloodstream have a lower 5-year survival rate (23). However, little is known regarding the biological significance of mucins. Mucins readily make contact with various circulating cells of the blood stream in cancer patients or with the infiltrated cells in cancer tissues.

Despite much evidence that COX-2 overexpression is an important early event in adenoma formation and that nonsteroid antiinflammatory drugs have a profound effect on adenoma formation, the mechanism by which COX-2 is induced remains unresolved.

In the present article, we demonstrate that mucins secreted from colon cancer cells could induce COX-2 in monocytes/macrophages.

Materials and Methods

Cells and Materials. A human colon cancer cell line, LS 180, was obtained from the American Type Culture Collection and cultured in Eagle's MEM supplemented with 10% FCS. In some cases, the cells were cultured in the presence of 5 mM phenyl α-GalNAc. Monocytes were obtained from the buffy coat of healthy human donors. The cells were separated on Ficoll-Isopaque centrifugation according to the manufacturer's instructions. The cells (1×10^7 cells per ml) were suspended in RPMI medium 1640 supplemented with 10% FCS and allowed to attach to the culture plate for 1 h. Nonadherent cells were removed by washing the plate with warm RPMI medium 1640, and adherent cells were collected. BSM was obtained from Roche Diagnostics. OSM was prepared as described (24). Murine mAbs MSW 113, MLS 132, and MLS 128, which recognize sialyl Lewis A, sialyl Tn, and Tn antigens, respectively, were prepared as described (25–27). Goat anti-human COX-1 and -2 antibodies and mouse anti-human CD 68 antibody were obtained from Santa Cruz Biotechnology and DAKO, respectively.

Isolation of Mucins from the Conditioned Medium of LS 180 Cells. Mucins were detected by a dot blot analysis with MLS 132 mAb. A concentrated conditioned medium of LS 180 cells was subjected to gel filtration on Sepharose 6B (3 × 105 cm). From the excluded fractions, the mucins were purified according to Baeckstrom *et al.* (28).

This paper was submitted directly (Track II) to the PNAS office.

Abbreviations: COX, cyclooxygenase; PGE2, prostaglandin E2; BSM, bovine submaxillary mucin; OSM, ovine submaxillary mucin; MSR, macrophage scavenger receptor.

¶To whom correspondence should be addressed. E-mail: hnakada@cc.kyoto-su.ac.jp.

www.pnas.org/cgi/doi/10.1073/pnas.0435410100

Purified mucin (5 μg of protein) was subjected to SDS/PAGE (6% gel) according to Laemmli (29), followed by periodate–Schiff and silver stainings. Another sample was transferred to Zeta-probe membrane, and sialyl Lewis A, sialyl Tn, and Tn antigens borne on the mucin core protein were detected by using a mixture of MSW 113, MLS 132, and MLS 128 mAbs. Purified mucin was labeled with [^{125}I]NaI by the chloramine T method (30).

Secretion of Prostaglandin E2 (PGE2) from Monocytes. Monocytes (1×10^5 cells) were cultured in RPMI 1640 medium supplemented with 10% FCS or cocultured with LS 180 cells (1×10^5 cells) for 36 h. LS 180 cells were cultured in the presence or absence of 5 mM phenyl α-GalNAc, whose culture supernatants were used as the conditioned medium. Monocytes (1×10^5 cells) were cultured for 36 h in the presence of the conditioned medium treated or not with phenyl α-GalNAc or the equivalent amount of culture medium of LS 180 cells. Each culture supernatant was collected and assayed for PGE2 by ELISA.

RT-PCR of COX-1 and COX-2 mRNAs. Preparation of total RNA from monocytes (1×10^7 cells) was performed by using Isogen (Nippon Gene, Toyama, Japan) according to the manufacturer's instructions. Reverse transcription and cDNA amplification were performed by using the TaKaRa RNA PCR kit (Takara Shuzo, Otsu, Japan). The forward and reverse primers and the expected product sizes were as follows: COX-1, 5′-TGCCCAGCTCCTGGCCCGCCGCTT-3′ and 5′-GTGCATCAACACAGGCGCCTCTTC-3′, 331 bp; COX-2, 5′-TTCAAATGAGATTGTGGGAAAATTGCT-3′ and 5′-AGATCATCTCTGCCTGAGTATCTT-3′, 305 bp; and β-actin, 5′-ATGGATGATGATATCGC-3′ and 5′-ATAGGAATCCTTCTGACCCA-3′, 291 bp. COX-1 cDNA was amplified for 30 cycles of denaturation at 94°C for 1 min, annealing at 65°C for 1 min, and extension at 72°C for 45 sec. COX-2 cDNA was amplified for 22 or 30 cycles of denaturation at 94°C for 1 min, annealing at 60°C for 1 min, and extension at 72°C for 45 sec. β-Actin cDNA was amplified for 27 cycles of denaturation at 94°C for 45 sec, annealing at 52°C for 30 sec, and extension at 72°C for 30 sec. The amplified cDNAs were run on 2% agarose gel with 0.5 μg/ml ethidium bromide and visualized under UV light.

Northern Blot Analysis. The COX-2 cDNA fragment was prepared as described above. A GAPDH cDNA fragment also was amplified by RT-PCR by using forward primer 5′-CGGGATCCACCACCAGTCCATGCCAT-3′ and reverse primer 5′-CCTTAAGTCCACCACCCTGTTGCTG-3′. pUC 18 ligated with the purified cDNA fragments was introduced into TOP 10F′ cells and amplified according to manufacturer instructions. Purified 310-base *Bam*HI and *Kpn*I DNA fragment (COX-2) and 472-base *Bam*HI and *Eco*RI DNA fragment (GAPDH) were labeled by using a digoxigenin-labeling kit (Roche Diagnostic) according to the manufacturer's instructions.

Total RNA (10 μg) was subjected to electrophoresis on a 1% denaturing formaldehyde/agarose gel and electrotransferred to Hybond N$^+$ nylon membrane (Amersham Pharmacia). After fixation, the membrane was hybridized with digoxigenin-labeled probes at 44°C (COX-2) and 50°C (GAPDH) for 24 h. After incubation with anti-digoxigenin antibody–alkaline phosphatase conjugate and washing, the membrane was visualized by chemiluminescence according to the manufacturer's instructions.

Binding of ^{125}I-Labeled Mucin to Monocytes and Macrophage Scavenger Receptor (MSR) Transfectants. Expression of recombinant MSR (group A, type I) in COS 7 cells was carried out as described (31).

The binding of ^{125}I-labeled mucin was assessed by incubating monocytes (1×10^6 cells) or the MSR transfectants (1×10^6 cells) with ^{125}I-labeled mucin (10 ng/ml) at 4°C for 2 h in the presence of various inhibitors. The inhibitors used were BSM (30 μg protein/ml), fucoidan, polyinosinic acid (poly I), polycytidylic acid (poly C) (100 μg/ml), and orosomucoid (2 μg of protein per ml). After extensive washing with 25 mM Hepes buffer, pH 7.2, and 0.15 M NaCl, the cells were solubilized with 1 M NaOH and the radioactivity was determined.

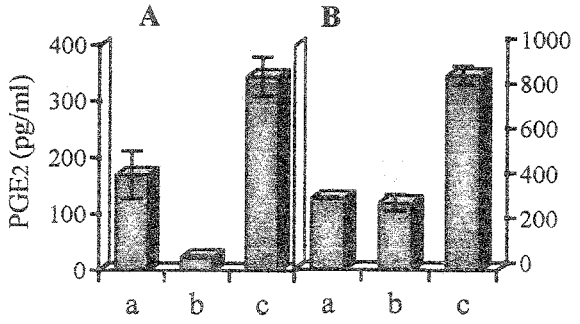

Fig. 1. PGE2 production in monocytes cocultured with LS 180 cells or cultured in the presence of conditioned medium of LS 180 cells. (*A*) Monocytes (1×10^5 cells) (lane a) and LS 180 cells (1×10^5 cells) (lane b) were cultured separately for 36 h. The same number of both cells (lane c) was cocultured for 36 h. (*B*) Monocytes (1×10^5 cells) were cultured for 36 h in the presence of 10% FCS-MEM (lane a) and in the presence of conditioned medium of LS 180 cells treated (lane b) or not (lane c) with 5 mM phenyl α-GalNAc. Each culture supernatant was assayed for PGE2 by ELISA. The data are mean levels ($n = 3$) ± SD of the secreted PGE2.

Immunoblotting. When lysate of monocytes was fractionated to prepare total RNA as described above, another fraction containing proteins was obtained. After dialysis against 50 mM Tris·HCl buffer, pH 7.5, containing 0.2 M NaCl, 1% Triton X-100, 2 mM EDTA, and 1 mM PMSF, COX-2 protein was immunoprecipitated by using goat anti-human COX-2 antibody and protein G-Sepharose. The immunoprecipitate was subjected to SDS/PAGE followed by Western blotting. The COX-2 protein was detected by using the same antibody as described above.

Tissue Specimens and Immunohistochemistry. We examined 15 patients with colorectal cancer (nine males and six females; ages 21–36 years) obtained from surgical resection. Five specimens were obtained from the ascending colon, four from the transverse colon, two from the descending colon, one from the sigmoid colon, and three from the rectum.

Immunohistochemical staining was performed with the Vectastain avidin–biotin peroxidase complex kit (Vector Laboratories) as described (15). Double immunostaining was carried out according to Kawahito *et al.* (32).

Results and Discussion

PGE2 Secreted from Monocytes Cocultured with LS 180 Cells or Cultured in the Presence of Conditioned Medium of LS 180 Cells. Monocytes were cocultured with colon cancer cells, LS 180, for 36 h. Approximately 1.7-fold PGE2 was secreted by coculture when compared with the separate culture of each cell, as shown in Fig. 1*A*. To determine whether or not the activating factor is contained in the conditioned medium, monocytes were cultured in the presence of a concentrated conditioned medium of LS 180 cells. The culture medium itself seems to contain a small amount of the activating factor needed to slightly enhance PGE2 production. However, the conditioned medium clearly elevated PGE2 production, indicating that it contained a high level of the activating factor. When the conditioned medium of LS 180 cells was prepared in the presence of 5 mM phenyl α-GalNAc, the activity of the medium was at the control level, suggesting that mucins were relevant to the activity (Fig. 1*B*).

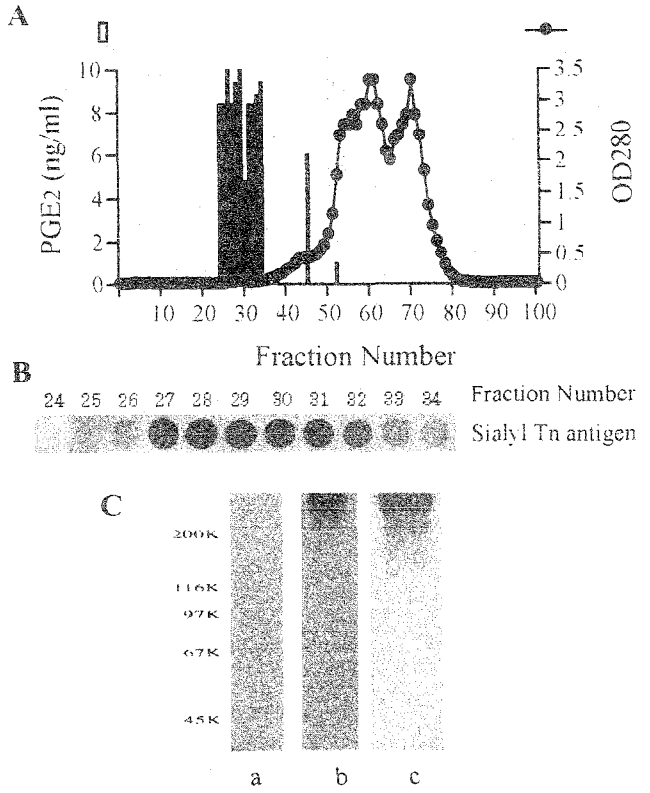

Fig. 2. Isolation of activating factor from conditioned medium of LS 180 cells. The conditioned medium of LS 180 cells was subjected to gel filtration on Sepharose 6B (3.0 × 105 cm) and then eluted with 25 mM sodium phosphate buffer, pH 7.5, and 0.15 M NaCl. (*A*) Fractions of 18.6 ml were collected, and absorbance at OD_{280} was determined. One microgram of protein of each fraction was added to the culture medium of monocytes (1×10^5 cells). After 24 h, secreted PGE2 was assayed by ELISA. (*B*) One hundred microliters of each fraction was loaded on a nylon membrane. Dot blot analysis was performed by using mAb MLS 132. (*C*) Purified mucin (5 μg) was subjected to SDS/PAGE with a 6% running gel, followed by silver (lane a) and periodate–Schiff (lane b) staining. Another sample was subjected to Western blotting after SDS/PAGE, and cancer-associated carbohydrate antigens were detected (lane c) as described in *Materials and Methods*.

Isolation of the Activating Factor from the Conditioned Medium of LS 180 Cells. To isolate the activating factor, the conditioned medium of LS 180 cells was fractionated by gel filtration on Sepharose 6B. One microgram of protein of each fraction was added to the culture medium of monocytes. The excluded fractions elevated the secretion of PGE2 remarkably, as shown in Fig. 2*A*.

A sialyl Tn antigen, one of the typical tumor-associated carbohydrate antigens expressed on mucin core proteins, was detected in the same fractions by dot blot analysis as shown in Fig. 2*B*, suggesting that the activating factor is a mucin. From the excluded fractions, mucins were purified according to Baeckstrom *et al.* (28).

The purity of the mucin was examined by SDS/PAGE followed by both protein and carbohydrate stainings (Fig. 2*C*, lanes a and b). No protein could be detected on silver staining. The same sample was subjected to SDS/PAGE followed by Western blotting. Expression of cancer-associated carbohydrate antigens was demonstrated on the mucins (Fig. 2*C*, lane c).

PGE2 Production Enhanced by Mucins or BSM in a Dose- and Time-Dependent Manner. Mucins and BSM were found to potently increase PGE2 production in monocytes. To examine dose dependency, the monocytes were cultured in the presence of mucins (0–2 μg of protein per ml) or BSM (0–30 μg of protein per ml) for 12 h, and the supernatants were collected for the determination of PGE2 production by ELISA. As shown in Fig. 3*A*, mucins or BSM enhanced PGE2 production in a dose-dependent manner. A small amount of mucins (100 ng/ml) or BSM (3 μg/ml) could induce the production of PGE2.

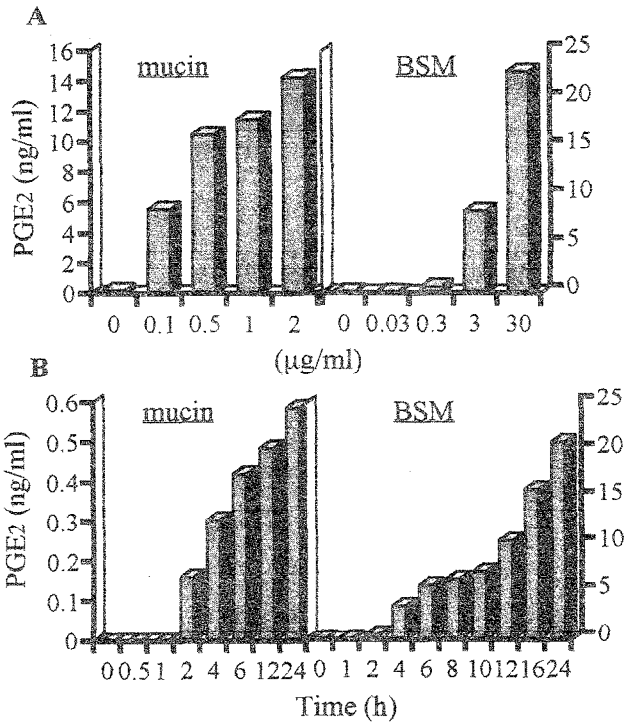

Fig. 3. Dose- and time-dependent PGE2 production in monocytes stimulated with mucin or BSM. (*A*) Monocytes (1×10^5 cells) were cultured in the presence of mucin (0–2 μg of protein per ml) or BSM (0–30 μg of protein per ml) for 12 h. (*B*) Monocytes (1×10^5 cells) were cultured in the presence of mucin (1 μg of protein per ml) or BSM (30 μg of protein per ml) for the time indicated. Each supernatant was assayed for PGE2 by ELISA.

To study the kinetics of PGE2 production by mucins or BSM, monocytes were incubated with mucins (1 μg/ml) or BSM (30 μg/ml) at different time points (0–24 h), and the culture supernatants were assessed for PGE2 by ELISA (Fig. 3*B*). Mucins or BSM enhanced PGE2 production as early as 2 h after incubation. The time and dose dependence of PGE2 production suggests a COX-2-mediated pathway.

Induction of COX-2 mRNA Expression and Protein Synthesis by Mucins or BSM. To determine whether mucin- or BSM-induced production of PGE2 was associated with up-regulation of COX-2, COX-2 mRNA and protein levels in monocytes were determined after treatment with mucins or BSM. At different time points (0–24 h), the monocytes were harvested, and total RNA and protein fractions were prepared.

As shown in Fig. 4*A*, the COX-2 mRNA was not detected in the absence of mucins or BSM, and the level peaked as early as 2 h in response to mucins. In contrast, COX-1 mRNA expression either remained unchanged or declined slightly.

To examine the induction of COX-2 protein in response to mucins or BSM, immunoprecipitation and Western blot analysis were performed. An increase in COX-2 protein synthesis in response to mucins or BSM was demonstrated by the increased intensity of a M_r 70,000 band corresponding to the COX-2

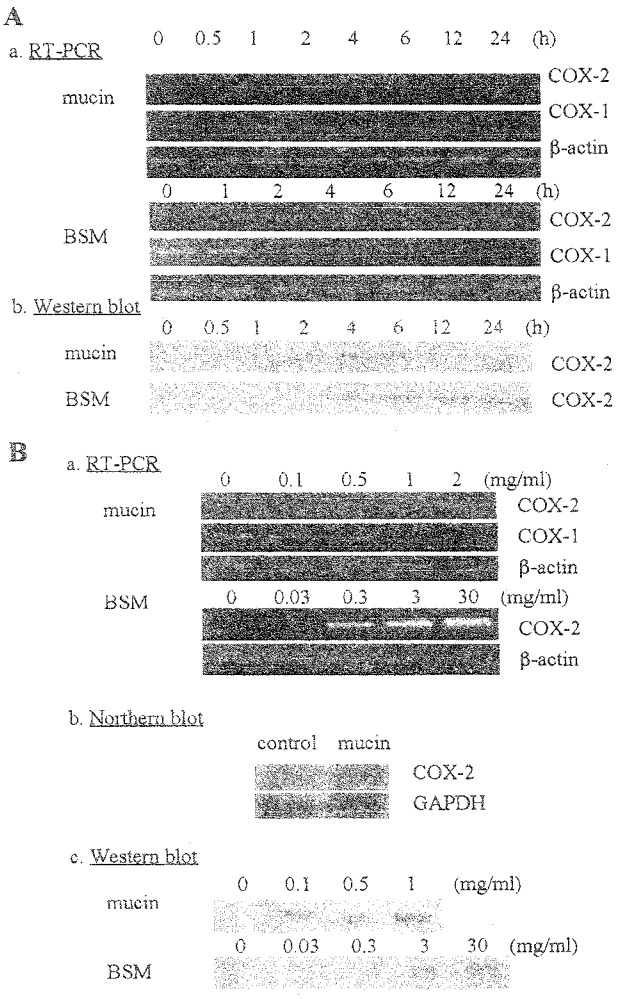

Fig. 4. Induction of COX-2 mRNA and protein in monocytes. (*A*) Monocytes (5×10^6 cells) were cultured in the presence of mucin (1 μg of protein per ml) or BSM (30 μg of protein per ml) for the time indicated. (*a*) Total RNA was prepared, and COX-2 cDNA was amplified for 22 cycles and subjected to agarose gel electrophoresis as described in *Materials and Methods*. (*b*) COX-2 protein was immunoprecipitated by using anti-human COX-2 antibody and detected as described in *Materials and Methods*. (*Ba*) Monocytes (5×10^6 cells) were cultured for 2 h in the presence of mucin (0–2 μg of protein per ml) or BSM (0–30 μg of protein per ml), from which total RNA was prepared. COX-2 cDNA was amplified (mucin-treated monocytes: 22 cycles; BSM-treated monocytes: 30 cycles) and analyzed as described above. (*b*) Monocytes (2×10^7 cells) were cultured for 2 h in the presence of mucin (1 μg of protein per ml). Total RNA was prepared and Northern blot analysis was performed as described in *Materials and Methods*. (*c*) COX-2 protein was prepared from the protein fraction and detected as described above. Representative data of three experiments are shown.

protein. The band was detected as early as 4 h, which is consistent with the fact that the COX-2 mRNA level peaked at 2 h. The doublet seems to be attributed to partial N-glycosylation as reported (33).

The dose dependence of COX-2 mRNA and protein induction was examined. The monocytes were incubated with various concentrations of mucins or BSM for 2 h, and total RNA and protein fractions were prepared. As shown in Fig. 4*B*, a small amount of mucins or BSM induced COX-2 mRNA, the level of which was increased in a dose-dependent manner. Induction of COX-2 mRNA also was confirmed by Northern blot analysis. A similar dose-dependent induction of COX-2 protein also was demonstrated by Western blot analysis.

Binding of Mucins to Monocytes Through MSR. Because monocytes were activated by both mucins and BSM, it appears that the binding sites are carbohydrate moieties but not the core protein. There exist so many types of O-glycans on the mucin core protein that multiple receptors may be responsible for the binding. The mucins contain various tumor-associated carbohydrate antigens such as sialyl Lewis A and sialyl Tn antigens. Treatment with mAbs against these antigens partially reduced the effect (data not shown). Thus, it seems unlikely that specific oligosaccharide chains are responsible for the binding.

Monocytes were incubated with ^{125}I-labeled mucin in the presence or absence of various inhibitors at 4°C for 2 h, and

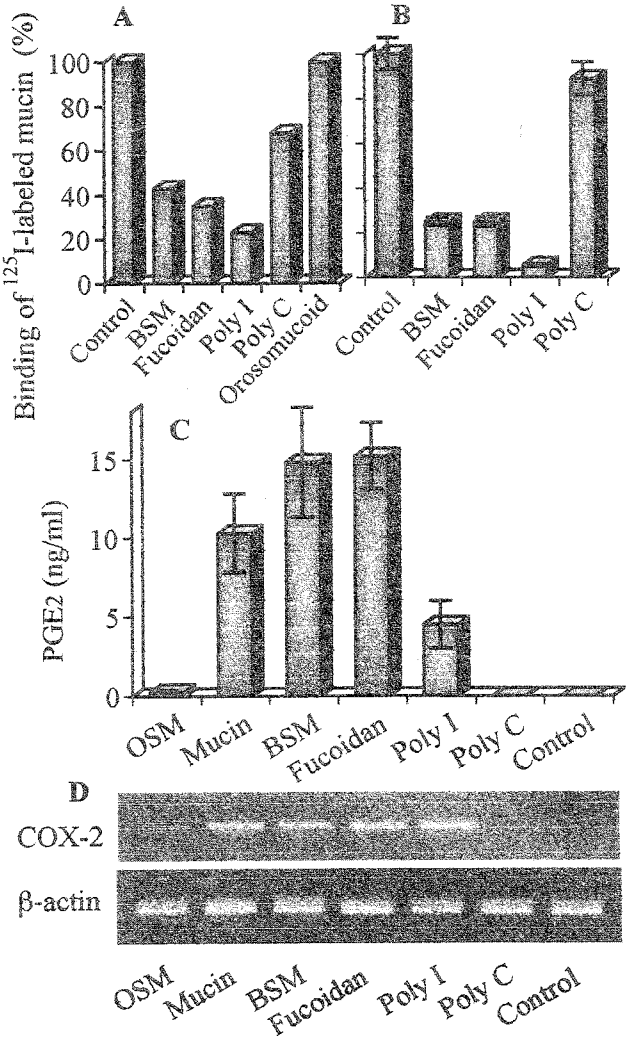

Fig. 5. Binding of mucins to monocytes through MSR. (*A*) Monocytes (1×10^6 cells) were incubated with ^{125}I-labeled mucin at 4°C for 2 h in the presence of various inhibitors. The radioactivity bound to the cell was determined as described in *Materials and Methods* (duplicate experiments). (*B*) Binding of ^{125}I-labeled mucin to the MSR cDNA transfectants (1×10^6 cells) was examined as described above (triplicate experiments). (*C*) Monocytes (1×10^5 cells) were cultured for 36 h in the presence of various ligands. Each culture supernatant was assayed for PGE2 by ELISA. (*D*) Monocytes (5×10^6 cells) were cultured for 2 h in the presence of various ligands, from which total RNA was prepared. COX-2 and β-actin cDNAs were amplified for 30 and 27 cycles, respectively, and analyzed as described above. The amounts of various ligands used are as follows: OSM and BSM, 30 μg of protein per ml; fucoidan, poly I, and poly C, 100 μg/ml; orosomucoid, 2 μg of protein per ml.

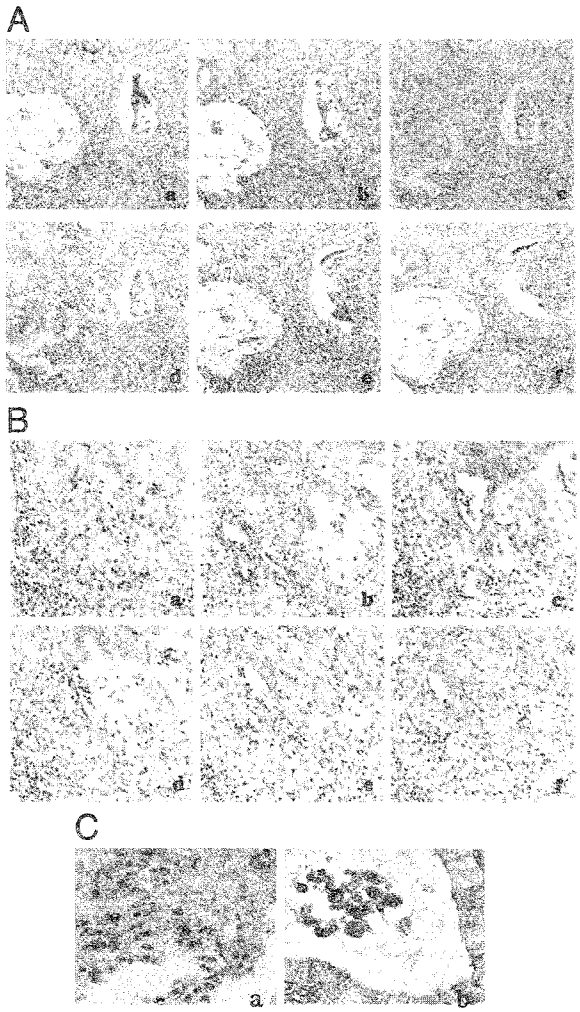

Fig. 6. Immunostaining for CD 68, COX-2, and cancer-associated carbohydrate antigens in colon cancer tissues. Colon cancer tissues were immunostained by using the Vectastain avidin–biotin peroxidase complex kit as described in *Materials and Methods* (*A* and *B*). (*A*) COX-2-positive macrophages were located around the region in which carbohydrate antigens were detectable. (*B*) COX-2 was not expressed in macrophages without carbohydrate antigens around them. (*a*) CD 68; (*b*) COX-2; (*c*) Tn antigen; (*d*) sialyl Tn antigen; (*e*) control (mouse IgG); (*f*) control (goat IgG). (*C*) The same specimens as in *A* were double-stained with anti-CD68 and anti-COX-2 antibodies as described in *Materials and Methods*. Most of CD 68-positive macrophages (brownish-black deposit) were costained with anti-COX-2 antibody (blue deposit). (*a*) Macrophages in cancer tissues; (*b*) macrophages in intraluminal space of adenocarcinoma.

radioactivity of ^{125}I-labeled mucins bound to the cell surface was determined (Fig. 5*A*). The binding was inhibited effectively by poly I, fucoidan, and BSM but slightly by poly C, suggesting that the MSR is included in the binding proteins. It has been reported that the MSR could recognize a pattern of anionic charges on molecules such as acetyl LDL, poly I, fucoidan (34, 35), and LPS (36). Anionic charges due to sialic acid and sulfate borne on O-glycans of mucins may be recognized by the receptor. We also confirmed that ^{125}I-labeled mucins could bind to the MSR cDNA transfectant. As shown in Fig. 5*B*, BSM, fucoidan, and poly I, but not poly C, reduced the binding of ^{125}I-labeled mucin to the MSR transfectants, which is consistent with characteristics of the MSR. The effect of other MSR ligands on PGE2 production and induction of COX-2 mRNA was examined (Fig. 5 *C* and *D*). Expectedly, in addition to mucin and BSM, fucoidan and poly I, but not poly C, could induce COX-2 mRNA and enhance PGE2 production. OSM had weak activity to induce COX-2 mRNA and enhance PGE2 production. The activity was much lower than that of BSM. Different activity among these mucins seems to be due to a different distribution of anionic charges on the molecule but not to the carbohydrate structure itself. LS 180 cells produce MUC 2 mucin (19), which has a high number of tandem repeats. It is reported that BSM also contains a tandem repeat (22). If the tandem repeat unit has one or more binding sites, the mucin has so many binding sites for the receptor that it could bridge many receptors on the cell surface, probably leading to more extensive activation of the monocytes. In addition, orosomucoid had no effect on the binding of the mucin, suggesting that some siglecs present on the monocyte cell surface are not responsible for the binding of the mucin probably from the masking of siglecs.

Immunohistochemical Staining of COX-2 in Colorectal Cancer Tissues. In a previous article (15), we found immunoreactive COX-2 in inflammatory cells, vascular endothelial cells, fibroblasts, and cancer cells. Additionally, we immunohistochemically examined the distribution of cancer-associated carbohydrate antigens such as Tn and sialyl Tn antigens borne on mucin core peptides in colorectal cancer tissues. Itzkowitz *et al.* (37) reported that Tn and sialyl Tn antigens are expressed in 72–81% and 93–96% of colon cancers, respectively.

Interestingly, immunoreactive COX-2 was expressed in CD 68-positive cells infiltrated around the region with an expression of mucins (Fig. 6*A a–d*), whereas COX-2 was not detectable in CD 68-positive cells without mucins in the adjacent tissues (Fig. 6*B a–d*). Double immunostaining clearly indicates that COX-2 is induced in most of CD 68-positive cells (Fig. 6*C a* and *b*).

The other cells around the CD 68-positive cells also expressed COX-2 (Fig. 6 *Ab* and *C a* and *b*), which probably is induced by

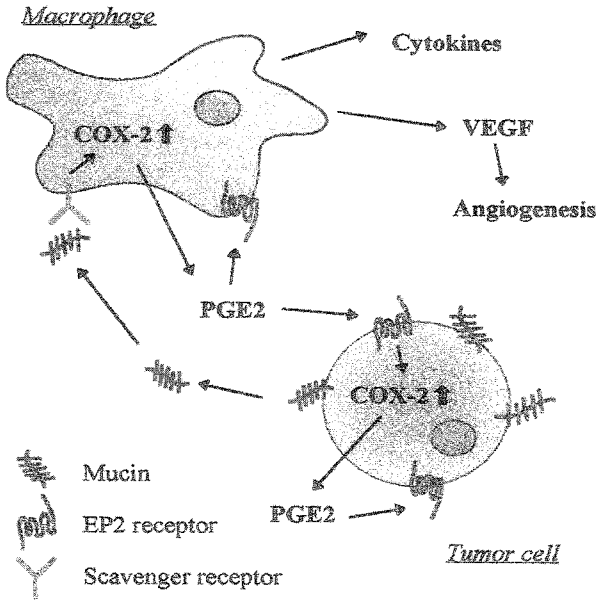

Fig. 7. Possible role of mucins as chemical mediators in the tumor microenvironment. Mucins produced by colon cancer cells induce COX-2 in macrophages, resulting in PGE2 production. PGE2 functions as a mediator in an autocline and/or paracline fashion, leading to vascular endothelial growth factor (VEGF) production.

mediators secreted from activated macrophages. Immunostaining with normal goat serum and normal mouse IgG was completely negative (Fig. 6*A e* and *f*). These immunostaining patterns were observed in other mucin-producing cancer tissues irrespective of differentiation level (unpublished results).

These findings suggest that COX-2 also is induced *in vivo* in tumor-associated macrophages by mucins secreted from the tumor.

Williams *et al.* (38) have indicated that tumor growth implanted in COX-2 null mice, but not in COX-1 null or wild-type mice, is attenuated significantly, suggesting that COX-2 in stroma also has an important role in tumor growth. Recently, Sonoshita *et al.* (39) have demonstrated that COX-2 expression is boosted by PGE2 through the EP2 receptor via a positive feedback loop.

Collectively, these findings strongly suggest that PGE2 exerts a positive effect, inducing the expression of COX-2 in its own and/or nearby cells, resulting in a substantial increase in the capacity of tissues to synthesize and release prostaglandins.

In the present article, we demonstrated that COX-2 in monocytes/macrophages is induced by mucins. We propose the following cascade in the tumor microenvironment as shown in Fig. 7. Mucins are produced by cancer cells. Infiltrated macrophages are activated by the mucins through the MSR. PGE2 secreted from the macrophages binds to EP2 receptor present on cancer cells and/or other cells, and activated cancer cells and macrophages produce vascular endothelial growth factor as reported (39, 40), leading to favorable conditions in epithelial cancer tissues for cancer cell growth.

The buffy coat of human peripheral blood was kindly provided by the Kyoto Red Cross Blood Center. We thank Dr. N. Wakamiya for useful discussion and encouragement. This work was supported by the Foundation for Bio-venture Research Center from the Ministry of Education, Science, and Culture of Japan.

1. DuBois, R. N., Giardiello, F. M. & Smalley, W. E. (1996) *Gastroenterol. Clin. North Am.* **25,** 773–791.
2. Giardiello, F. M., Hamilton, S. R., Krush, A. J., Piantadosi, S., Hylind, L. M., Celano, P., Booker, S. V., Robinson, C. R. & Offerhaus, G. J. (1993) *N. Engl. J. Med.* **328,** 1313–1316.
3. Marnett, L. J. (1992) *Cancer Res.* **52,** 5575–5589.
4. Smith, L. L., Garavito, M. & DoWitt, D. L. (1996) *J. Biol. Chem.* **271,** 33157–33160.
5. Eberhart, C. E. & DuBois, R. N. (1995) *Gastroenterology* **109,** 285–301.
6. Ristimaki, A., Honkanen, N., Jankala, H., Sipponen, P. & Harkonen, M. (1997) *Cancer Res.* **57,** 1276–1280.
7. Hwang, D., Scollard, D., Byrne, J. & Levine, E. (1998) *J. Natl. Cancer Inst.* **90,** 445–460.
8. Wolff, H., Saukkonen, K., Anttila, S., Karjalainen, A., Vainio, H. & Ristrimaki, A. (1998) *Cancer Res.* **58,** 4997–5001.
9. Tucker, O. N., Dannenberh, B. J., Yang, E. K., Zhang, F., Tang, L., Daly, J. M., Soslow, R. A., Masferrer, J. L., Woerner, B. M., Koki, A. T., *et al.* (1999) *Cancer Res.* **59,** 987–990.
10. Klimp, A. H., Hollema, H., Kemipinga, C., Zee, A. G. J., Vries, E. G. E. & Daemen, T. (2001) *Cancer Res.* **61,** 7305–7309.
11. Williams, C. S., Luongo, C., Radhika, A., Chang, T., Lamps, L. W., Nanney, L. B., Beauchamp, R. D. & DuBois, R. N. (1996) *Gastroenterology,* **111,** 1134–1140.
12. Kawamori, T., Rao, C. V., Seibet, K. & Reddy, B. S. (1998) *Cancer Res.* **58,** 409–412.
13. Gupta, R. A. & DuBois, R. N. (1998) *Gastroenterology* **114,** 1095–1098.
14. Oshima, M., Dinchak, J. E., Kargman, S. L., Oshima, H., Hancock, B., Kwong, E., Trzaskos, J. M., Evans, J. F. & Taketo, M. M. (1996) *Cell* **87,** 803–809.
15. Sano, H., Kawahito, Y., Wilder, R. L., Hashiramoto, A., Mukai, S., Asai, K., Kimura, S., Kato, H., Kondo, M. & Hla, T. (1995) *Cancer Res.* **55,** 3785–3789.
16. Hull, M. A., Booth, J. K., Tisbury, A., Scott, N., Bonifer, C., Markham, A. F. & Coletta, P. L. (1999) *Br. J. Cancer* **79,** 1399–1405.
17. Bamba, H., Ota, S., Kato, A., Adachi, A., Itoyama, S. & Matsuzaki, F. (1999) *Int. J. Cancer* **83,** 470–475.
18. Kim, Y. S., Gum, J., Jr., & Brockhausen, I. (1996) *Glycoconjugate J.* **13,** 693–707.
19. McCool, D. J., Forstner, J. F. & Forstner, G. G. (1994) *Biochem. J.* **302,** 111–118.
20. Pigman, W. & Gottschalk, A., eds. (1966) *Glycoproteins* (Elsevier, New York), Vol. 5, pp. 434–445.
21. Tsuji, T. & Osawa, T. (1986) *Carbohydrate Res.* **151,** 391–402.
22. Jiang, W., Gupta, D., Gallagher, D., Davis, S. & Bhavanandan, V. P. (2000) *Eur. J. Biochem.* **267,** 2208–2217.
23. Miyake, M., Taki, T., Hitomi, S. & Hakomori, S. (1992) *N. Engl. J. Med.* **327,** 14–18.
24. Tettamanti, G. & Pigman, W. (1968) *Arch. Biochem. Biophys.* **124,** 41–50.
25. Kitagawa, H., Nakada, H., Numata, Y., Kurosaka, A., Fukui, S., Funakoshi, I., Kawasaki, T., Shimada, K., Inagaki, F. & Yamashina, I. (1998) *J. Biochem.* **104,** 591–595.
26. Tanaka, N., Nakada, H., Inoue, M. & Yamashina, I. (1999) *Eur. J. Biochem.* **263,** 27–32.
27. Numata, Y., Nakada, H., Fukui, S., Kitagawa, H., Ozaki, K., Inoue, M., Kawasaki, T., Funakoshi, I. & Yamashina, I. (1990) *Biochem. Biophys. Res. Commun.* **170,** 802–808.
28. Baeckstrom, D., Hansson, G. C., Nilsson, O., Johansson, C., Gendler, S. J. & Lindholm, L. (1991) *J. Biol. Chem.* **266,** 21537–21547.
29. Laemmli, U. K. (1970) *Nature* **227,** 680–685.
30. Langone, J. J. (1980) *Methods Enzymol.* **70,** 350–375.
31. Inoue, M., Fujii, H., Kaseyama, H., Yamashina, I. & Nakada, H. (1999) *Biochem. Biophys. Res. Commun.* **264,** 276–280.
32. Kawahito, Y., Kondo, M., Tsubouchi, Y., Hashiramoto, A., Bishop-Bailey, D., Inoue, K., Kohno, M., Yamada, R., Hla, T. & Sano, H. (2000) *J. Clin. Invest.* **106,** 189–197.
33. Smith, W. L. & Dewitt, D. L. (1995) *Semin. Nephrol.* **15,** 179–194.
34. Kodama, T., Reddy, P., Kishimoto, C. & Krieger, M. (1988) *Proc. Natl. Acad. Sci. USA* **85,** 9238–9242.
35. Kodama, T., Freeman, M., Rohrer, L., Zabrecky, J., Matsudaira, P. & Krieger, M. (1990) *Nature* **343,** 531–535.
36. Hampton, R. Y., Golenbock, D. T., Penman, M., Krieger, M. & Raetz, C. R. H. (1991) *Nature* **352,** 342–344.
37. Itzkowitz, S. H., Yuan, M., Montgomery, C. K., Kjeldsen, T., Takahashi, H. K., Bigbee, W. L. & Kim, Y. S. (1989) *Cancer Res.* **49,** 197–204.
38. Williams, C. S., Tsujii, M., Reese, J., Dey, S. K. & DuBois, R. N. (2000) *J. Clin. Invest.* **105,** 1589–1594.
39. Sonoshita, M., Takaku, K., Sasaki, N., Sugimoto, Y., Ushikubi, F., Narumiya, S., Oshima, M. & Taketo, M. M. (2001) *Nat. Med.* **7,** 1048–1051.
40. Tsujii, M., Kawano, S., Tsuji, S., Sawaoka, H., Hori, M. & DuBois, R. N. (1998) *Cell* **93,** 705–716.

Review

Involvement of Syndecans in Actin Cytoskeletal Organization and Tumor Metastasis

Kayoko OGURI[1], Seiichi MUNESUE[2], Yuri KUSANO[1], Yasuo YOSHITOMI[2] and Minoru OKAYAMA[2]
[1]Clinical Research Institute, National Nagoya Hospital
[2]Department of Biotechnology, Faculty of Engineering, Kyoto Sangyo University

Received, 11 July 2002; accepted 25 July 2002.

Abstract: Syndecan-2, a transmembrane heparan sulfate proteoglycan, cooperates with integrin $\alpha 5\beta 1$ on cell adhesion to a fibronectin substratum and regulates actin cytoskeletal organization. A signal generated by adhesion of cells to fibronectin through integrin $\alpha 5\beta 1$ alone results in cortex actin formation and through syndecan-2 alone results in a filopodium formation, but through both receptors results in the formation of stress fibers. This regulation depends on the syndecan-2-expression level, and therefore the low expresser does not form stress fibers but cortex actin. Among other syndecans expressed by the cells, syndecan-1 and syndecan-3 do not participate in this signaling, but syndecan-4 seems to function upstream of syndecan-2 in the cascade, suggesting that each syndecan bears functional specificity as a receptor. We have found that there is an inverse correlation between the syndecan-2-expression level and the metastatic potential of Lewis lung carcinoma-derived clones. The fact that overexpression of syndecan-2 causes suppression of metastasis indicates that there is a causal relationship behind this correlation.

Key words: syndecan, integrin, extracellular matrix-receptor, actin cytoskeleton, metastasis

INTRODUCTION

In 1989, Merton Bernfield, who had long studied epithelial-mesenchymal interactions during embryonic mammary gland morphogenesis, cloned cDNA of an integral membrane heparan sulfate proteoglycan from cultured mammary epithelial cells[1] which could bind to various extracellular matrix components through its heparan sulfate chains[2)3)]. He named it "syndecan" from the Greek syndein, 'to bind together', because it was thought to link the cytoskeleton to the interstitial matrix. After that, structurally related syndecans were soon identified[4-6], and this prototype was called syndecan-1. The others were numbered in the order of cDNA cloning[7].

Syndecans comprise a family of four distinct genes in mammals, and are found in many animal species ranging from nematoda to mammals (Table 1). In adult tissues, the distribution of their expression seems to be roughly classified, that is, syndecan-1 locates in epithelia and plasma cells, syndecan-2 in endothelia and fibroblasts, syndecan-3 in the central nerve system, and syndecan-4 ubiquitous on adherent cells. They are composed of a transmembrane core protein and covalently bound extracellular heparan sulfate chains in which binding sites for ligands exist (Fig. 1). The ectodomains of their core proteins are diverse among the members, but have common sites for heparan sulfate attachment and proteolytic cleavage. The transmembrane domains are stable evolutionarily and maintain high homology across members and species. The cytoplasmic domains contain two invariant regions, a membrane proximal common region C1 and a C-terminal common region C2, separated by a region V which is variable in length and composition across members but highly conserved across species[8]. These structural characteristics suggest that each member interacts with the same cytoplasmic proteins by C regions and also with unique proteins by V region. Binding partners for the cytoplasmic domain of syndecans are beginning to be determined. On the other hand, the ligand-binding sites of syndecans exist in their heparan sulfate chains in any case. Because of a structural heterogeneity of heparan sulfate owing to the position and number of sulfate residues[9], syndecans can bind a wide variety of extracellular heparin-binding molecules both soluble and insoluble. In fact they exhibit diverse functions of a participation in the signaling of growth factors and in the organization of cell-matrix adhesion and signaling[10),11)]. However, it has gradually become clear that the ligand-recognition sites of heparan sulfate are considerably restricted by the sulfation pattern[12], and the ligand-redundancy of cell surface heparan sulfate proteoglycans is only now apparent. The recent research suggests that each of them has functional specificity and its own job.

In this review article, on the basis of our recent results, we focused on the function of syndecans as

Reprint requests to: Kayoko Oguri, Clinical Research Institute, National Nagoya Hospital, 4-1-1 Sannomaru, Naka-ku, Nagoya 460-0001, Japan. Tel: 052-951-1111 (ext. 2764), Fax: 052-951-0664, e-mail: ogurik@fbe.freeserve.ne.jp

Table 1. Syndecan family members cloned.

Species	Name	No. of amino acid of core protein	References
Human	syndecan-1	310	J. Biol. Chem. **265**, 6884 (1990)
	syndecan-2	201	J. Biol. Chem. **264**, 7017 (1989)
	syndecan-3	442	J. Cell Biochem. **82**, 246 (2001)
	syndecan-4	198	J. Cell Biol. **118**, 961 (1992)
Mouse	syndecan-1	311	J. Cell Biol. **108**, 1547 (1989)
	syndecan-2	202	Develoment **119**, 841 (1993)
	syndecan-3	442	(accession No. AAB03283)
	syndecan-4	198	J. Biochem. **112**, 17 (1997)
Rat	syndecan-1	313	J. Biol. Chem. **267**, 4870 (1992)
	syndecan-2	201	J. Biol. Chem. **267**, 3894 (1992)
	syndecan-3	442	J. Cell Biol. **117**, 191 (1992)
	syndecan-4	198	J. Biol. Chem. **267**, 4870 (1992)
Hamster	syndecan-1	309	J. Biol. Chem. **270**, 27127 (1995)
Chick	syndecan-2	201	Biochem. J., in press (2002)
	syndecan-3	405	Proc. Natl. Acad. Sci. USA **89**, 3271 (1992)
	syndecan-4	197	J. Biol. Chem. **269**, 696 (1994)
Xenopus	syndecan-1	604	Mech. Dev **59**, 115 (1996)
	syndecan-2	191	Biochem. J. **309**, 69 (1995)
	syndecan-3	390	Mech. Dev. **59**, 115 (1996)
Zebrafish	syndecan-2	208	(accession No. AAK49414)
Drosophila	syndecan	395	Proc. Natl. Acad. Sci. USA **91**, 3334 (1994)
Sea urchin	syndecan	219	Develop. Growth Differ. **42**, 449 (2000)
Ascidian	syndecan	209	Develop. Biol. **211**, 198 (1999)
C. elegans	syndecan	288	Science **282**, 2012 (1998)

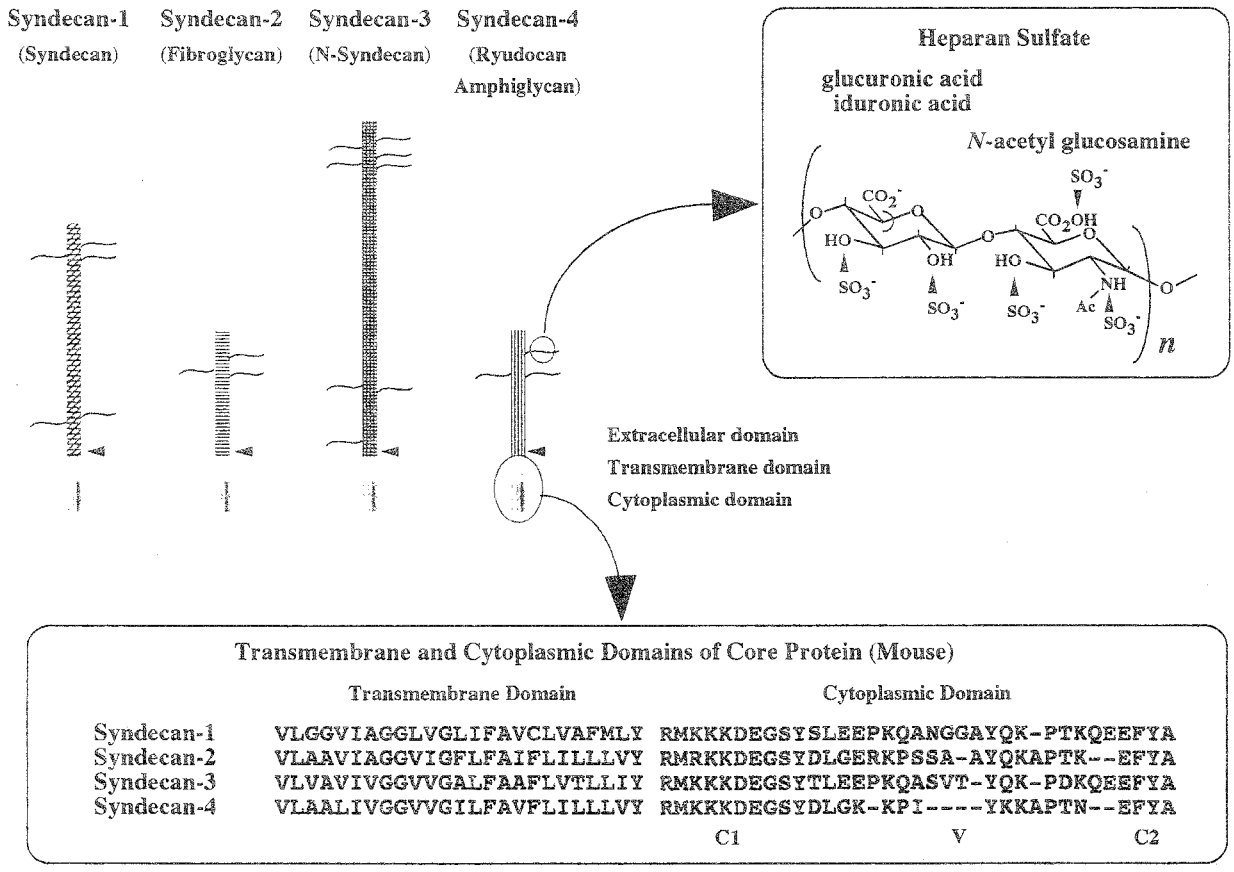

Fig. 1. Schematic depiction of a syndecan family.
Syndecans (original designations are shown in parentheses) are transmembrane heparan sulfate proteoglycans of which ligand-binding sites are located in heparan sulfate side chains. Heparan sulfates exhibit enormous structural heterogeneity due to the number and position of sulfate residues and can bind a number of heparin-binding active molecules. The core proteins consist of three parts, an ectodomain unique to each syndecan, a highly homologous transmembrane domain and a moderately homologous cytoplasmic domain. The cytoplasmic domains are further separated into three, the variable (V) region between the conserved (C1 and C2) regions.

extracellular matrix-receptors, especially on the cooperation of syndecan-2 with integrin $\alpha5\beta1$ for actin cytoskeletal organization. For this purpose, we used mouse Lewis lung carcinoma-derived clones with different metastatic potentials. Interestingly, the selection of the clones by spontaneous metastatic potentials resulted in the selection of the clones with varying levels of syndecan-2 expression. Moreover, we have found that the various phenotypes including cell morphology, growth rate, cellular response to extracellular matrix components, cell migration, and invasion, correlate with the expression level of syndecan-2.

Difference of Actin Cytoskeletal Organizations in Cells on Adhesion to Fibronectin Substrata

The low metastatic P29, intermediate metastatic LM12-3, and highly metastatic LM60-D6 and LM66-H11 clones were established from mouse Lewis lung carcinoma 3LL[13),14)]. Besides metastatic potentials, they exhibited several different characteristics. Among them, the architecture of the extracellular matrices of the primary tumors were strikingly different[15),16)] and the difference was attributable to their stroma-inducing abilities[17)]. In the primary tumors, P29 cells with strong stroma-inducing ability were surrounded by fibronectin-rich interstitial type matrix produced by the induced host stromal cells, whereas LM66-H11 cells with very weak stromal induction grew on basement membrane produced by themselves. This difference was reflected in the *in vitro* responses of the cells adhering to a fibronectin substratum (Fig. 2). P29 cells spread with stress fiber formation (Fig. 2A), whereas LM66-H11 cells form cortex actin (Fig. 2B). It has been reported that integrin $\alpha5\beta1$ mediates fibronectin-signaling to form focal adhesions and stress fibers in fibroblasts[18)], and suggested the participation of syndecan as co-receptor on this signal transduction[19)]. Therefore, the cooperation of a cell surface heparan sulfate proteoglycan with integrin $\alpha5\beta1$ in these clones on cell attachment to a fibronectin substratum was examined. For this, fibronectin recombinant polypeptides were used as substrata (Fig. 2). C-274,

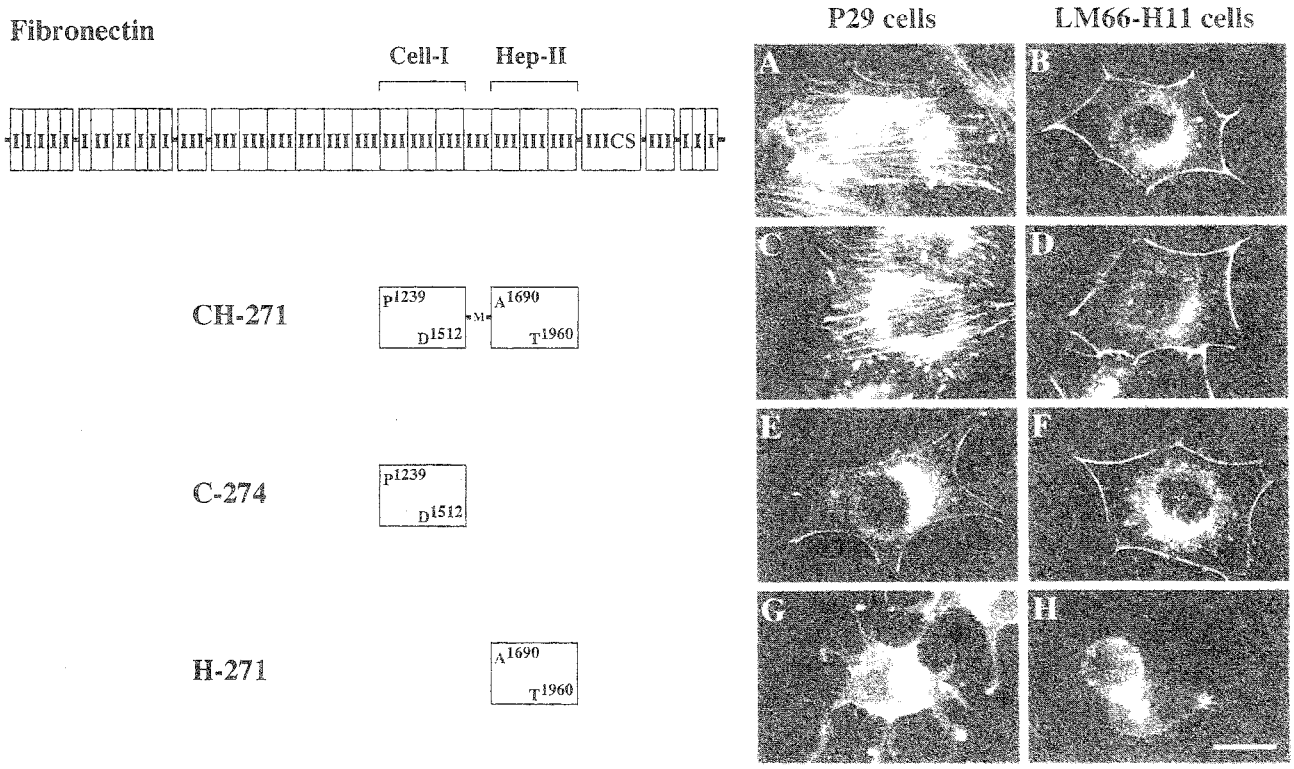

Fig. 2. Actin cytoskeletal organizations of P29 and LM66-H11 cells on substrata of fibronectin and its recombinant polypeptides.
Homology domain structures in fibronectin are presented by I, II and III, and IIICS for type-I, -II, and -III homology units, and type-III homology connecting segment, respectively. Cell-I and Hep-II show functional domains. RGD sequence-containing cell-binding domain and C-terminal cell-binding domain, respectively. P29 (A, C, E, G) and LM66-H11 (B, D, F, H) cells were plated on coverslips coated with fibronectin (A, B), CH-271, a fusion peptide of Cell-I and Hep-II domains with methionine residue (C, D), C-274, a peptide corresponding to Cell-I domain (E, F) and H-271, corresponding to Hep-II domain (G, H). The cells were fixed at 1 h after and stained with Rhodamine-conjugated phalloidin to visualize actin fibers. Bar, 20 μm. (modified from Munesue, S. et al., Biochem. J. **363**, 201-209 (2002) with the permission of the publisher).

which consists of Cell-I domain containing RGD sequence, is a ligand for integrin $\alpha5\beta1$, H-271, which consists of Hep-II domain, is a ligand for heparan sulfate, and CH-271, a fusion peptide of C-274 and H-271 with a methionine residue, has ligands for both receptors. On CH-271, the cytoskeletal organizations of the cells were reproduced those on intact fibronectin, indicating that an existence of the two domains was sufficient to induce these responses in both cells (Fig. 2C, D). On C-274, both the cells formed cortex actin, indicating that the signaling mediated through integrin $\alpha5\beta1$ alone resulted in a formation of cortex actin (Fig. 2E, F). Furthermore, their responses were similar to those of LM66-H11 cells on fibronectin (Fig. 2B) or CH-271 (Fig. 2D) despite the fact that both substrata contain the Hep-II domain, suggesting that H-271-signaling is useless for LM66-H11 cells because of a probable loss of the expression or the function of their cell surface heparan sulfate proteoglycans. This was supported by the response of LM66-H11 cells on H-271 where cells adhered to the substratum but did not spread nor organize actin cytoskeletons at all (Fig. 2H). On the other hand, P29 cells formed filopodia on H-271, indicating that the cell surface heparan sulfate proteoglycan by itself could transduce the signal to organize actin cytoskeletons (Fig. 2G). These results show that the cell surface heparan sulfate proteoglycan as a receptor for fibronectin acts independently or cooperatively with integrin $\alpha5\beta1$, and regulates the cytoskeletal organization of cells. The next question is which cell surface heparan sulfate proteoglycan plays this role.

Syndecan-2 Is the Responsible Receptor Regulating Integrin $\alpha5\beta1$-Signaling to Induce Stress Fiber Formation

Our previous report showed that more than 85% of the cell surface heparan sulfate proteoglycans bound to immobilized fibronectin was syndecan-2[14]. Therefore the cell surface expression levels of syndecan-2 were compared between the two clones. As expected, its expression in LM66-H11 cells is lower than that in P29 cells, and the expression levels of integrin $\alpha5\beta1$ in both clones were very similar (Fig. 3A), suggesting that the cell surface heparan sulfate proteoglycan responsible for this action is syndecan-2. This was also supported by the fact that among syndecans expressed by both clones only the expression level of syndecan-2 was different in mRNA level (Fig. 3B, C) and in cell surface expression level. This supposition was confirmed by the artificial manipulation of the expression levels of the clones (Fig. 4). P29 cells in which the syndecan-2 expression was suppressed by the treatment with antisense oligonucleotide of its mRNA failed to form stress fibers but formed cortex actin (Fig. 4B), whereas the cells treated with its sense oligonuleotide formed stress fibers (Fig. 4A)[20]. Conversely, H11-SN2 cells cloned from LM66-H11 cells transfected with cDNA of syndecan-2 formed stress fibers (Fig. 4D), whereas H11-Vec, a transfectant with the vector only formed cortex actin (Fig. 4C)[21]. We confirmed that these manipulations did not affect the

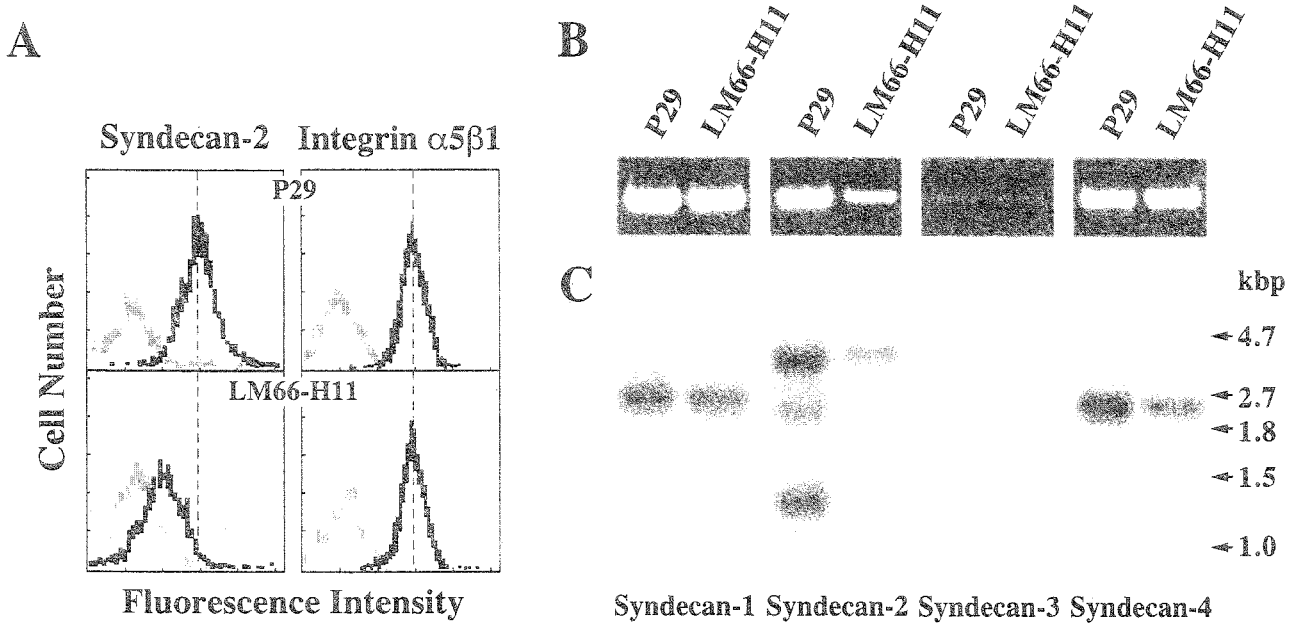

Fig. 3. Comparison of expression of syndecans and integrin $\alpha5\beta1$ between P29 and LM66-H11 cells.
(A) Cell surface expressions of fibronectin receptors were analyzed by flow cytometry using antisera against syndecan-2 and integrin $\alpha5\beta1$ (black lines). Peaks shown with gray lines are for control samples reacted with non-immune sera. Expressions of mRNAs of a syndecan family in both clones were analyzed by RT-PCR (B) and by Northern blot (C). (modified from Munesue, S. et al., Biochem. J. **363**, 201-209 (2002) with the permission of the publisher).

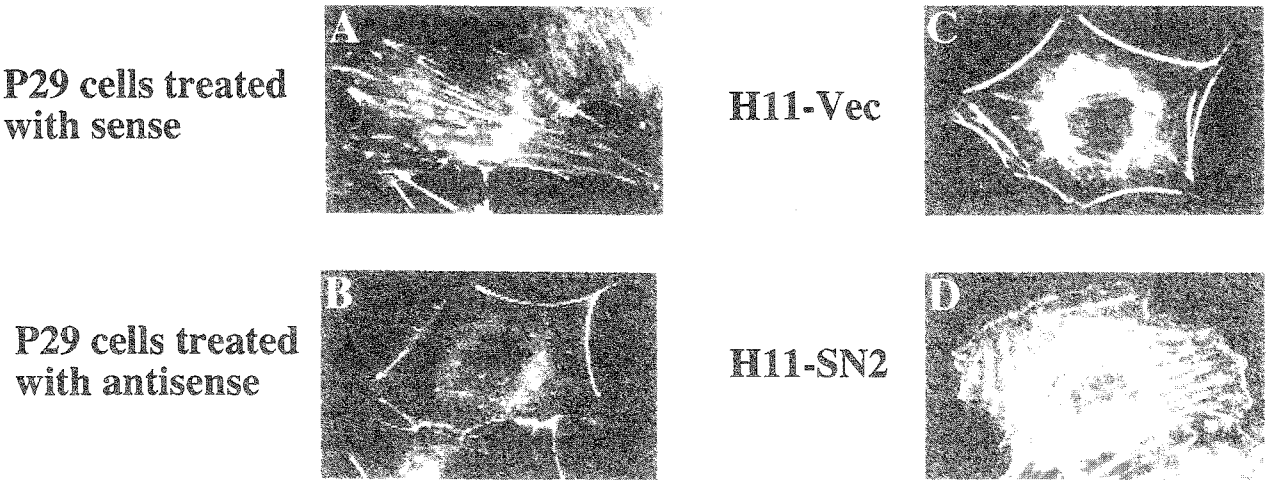

Fig. 4. Actin cytoskeletal organizations of the cells which changed artificially syndecan-2 expressions.
P29 cells were treated with antisense oligonucleotide of syndecan-2 mRNA (B) to suppress their expression. The cells were also treated with the sense oligonucleotide for the control (A). LM66-H11 cells were transfected with syndecan-2 cDNA and the high expresser, H11-SN2, was cloned (D). The clone, H11-Vec, transfected with only the vector was used for the control (C). The cells were plated on fibronectin substrata and the actin cytoskeletal organizations were observed as described in Fig. 2.

expressions of other syndecans and integrin $\alpha5\beta1$. These results clearly show that the stress fiber formation, in other words the modification of integrin $\alpha5\beta1$-mediating signaling, is regulated only by the expression level of syndecan-2. If this is the case, how do other syndecans participate in this signal transduction? To clarify this, the antibodies against the ectodomains of core protein of each syndecan were used as the ligands for the respective syndecans in the mixed substrata with C-274 (Table 2). On a mixed substratum of C-274 and anti-syndecan-2 antibody, the cytoskeletal organizations of the cells were reproduced on fibronectin, indicating that the clustering of syndecan-2 over threshold is required to modify the integrin-signaling to form stress fibers. On the substratum containing anti-syndecan-3, both cells formed cortex actin, as was expected from its extremely low expression. On the other hand, both cells also formed cortex actin on the substratum containing anti-syndecan-1, though they expressed it strongly, indicating that syndecan-1 did not participate in this signal transduction. Interestingly, on the substratum containing anti-syndecan-4, P29 cells formed stress fibers but LM66-H11 cells did not in spite of the similar expression level of syndecan-4. This indicates that the signaling mediated by syndecan-4 to form stress fibers is also regulated by syndecan-2, and suggests that syndecan-4 acts upstream of syndecan-2 in this signal cascade. This is also supported by the result that LM66-H11 cells formed cortex actin on the substratum containing anti-heparan sulfate antibody whereas P29 cells formed stress fibers on the same substratum. These results are summarized in Fig. 5. Couchman and his colleagues have reported that the clustering of syndecan-4 activates protein kinase Cα (PKCα) and activated PKCα recruits cytoplasmic proteins to focal adhesions in fibroblasts[22]. They also suggested that the cytoplasmic domain of

Table 2. Actin cytoskeletons formed in P29 and LM66-H11 cells on adhesion to substrata comprised with a mixture of C-274 and antibodies.

Substratum	Cytoskeleton	
Antibody mixed with C-274	P29 cells	LM66-H11 cells
F58-10E4 (anti-heparan sulfate)	SF	CA
SN1Ab (anti-syndecan-1 core protein)	CA	CA
SN2Ab (anti-syndecan-2 core protein)	SF	CA
SN3Ab (anti-syndecan-3 core protein)	CA	CA
SN4Ab (anti-syndecan-4 core protein)	SF	CA

SF, stress fiber; CA, cortex actin.

syndecan-2 could be a substrate for this activated PKCα[23]. This is consistent with our previous report that serine residue(s) of syndecan-2 cytoplasmic domain was phosphorylated[24]. Together with these results, it is reasonable to consider that the clustering of syndecan-4 stimulates activation of PKCs and the activated PKCs phosphorylate syndecan-2, and finally that this phosphorylation may accelerate syndecan-2-clustering (upper in Fig. 5). However, this PKC activity is not sufficient to induce stress fiber formation in the syndecan-2-low expressers because of the smaller cluster of syndecan-2 below the threshold (lower in Fig. 5). Stress fiber formation in LM66-H11 cells can be induced on fibronectin by treatment with phorbol ester, an activator for PKC, or on the substratum comprised of C-274 and bFGF which has a stronger ability to bind heparan sulfate than Hep-II domain (dashed arrows in Fig. 5). This may be why P29 cells form stress fibers by anti-syndecan-4 stimulation but LM66-H11 cells do not. The scheme is also supported by

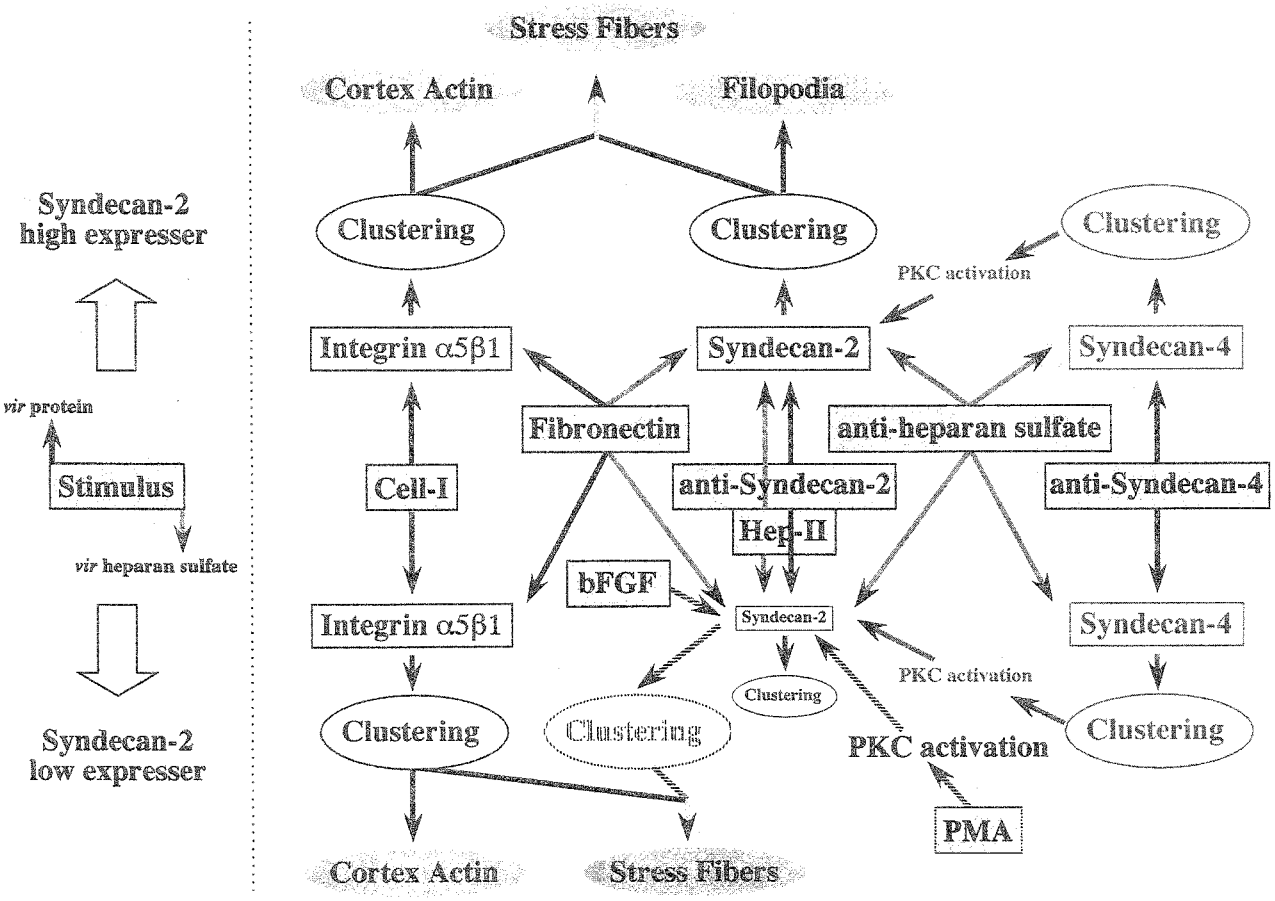

Fig. 5. Fibronectin-induced signalings mediated by integrin $\alpha 5\beta 1$ and/or syndecans.
In the case of syndecan-2 high expressers (upper part), cells adhering to the Cell-1 domain of fibronectin by integrin $\alpha 5\beta 1$ spread and formed cortex actin (the cascade with green arrows). In contrast, cells adhering to the Hep-II domain by heparan sulfate side chains of syndecan-2 spread and developed filopodia (the cascade with red arrows). When they adhere to fibronectin by both receptors, stress fiber formation is induced (the cascade with a yellow arrow). Clustering of syndecan-4 activates protein kinase C (PKC), and the activated enzymes phosphorylate serine residue(s) of syndecan-2 (the cascade with blue arrows), resulting in the acceleration of the clustering of syndecan-2. There is a threshold in syndecan-2 signaling mentioned above. Therefore in the case of the low expresser the same stimulation to syndecan-2 does not show any effect on these signal transductions (lower part). However, stronger stimulations, for example, treatment of cells with phorbol ester (PMA) or of basic fibroblast growth factor (bFGF) as immobilized substratum, decrease this threshold (the cascade with dashed arrows), and under those conditions, even the low expresser can organize stress fibers.

the recent report that fibroblasts isolated from syndecan-4-null mice organize stress fibers on fibronectin[25]. Syndecan members may share different roles with each other and may cooperate with each other.

Correlation between Syndecan-2 Expression Levels and Metastatic Potentials

As described in the beginning, the selection of the different metastatic clones on the basis of spontaneous metastatic potentials resulted in the selection of the clones with a different level of syndecan-2 expression. The expression levels of other syndecans and integrin $\alpha 5\beta 1$ were very similar among the clones. However, only the syndecan-2 expression exhibits an inverse correlation to metastatic potential (data not shown). If this correlation includes a causal relationship, indeed the elevation of syndecan-2 expression must decrease the metastatic potential of the cells. Thus, the metastatic potential of H11-SN2 cells decreases to the level of P29 cells, whereas that of H11-Vec cells does not change from that of the parent cells (Fig. 6). At present, we do not know what mechanism explains this causal relationship.

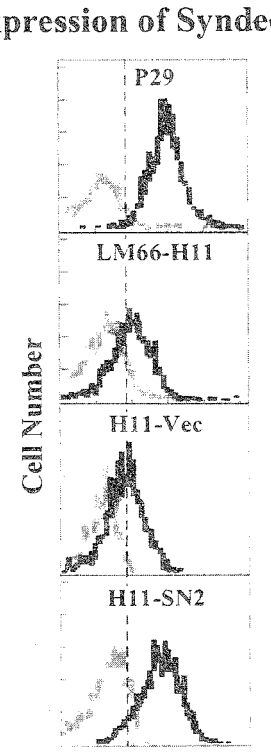

Spontaneous metastasis

Clone	Animals metastasized	Range no. of lung nodules	Mean no. of lung nodules
P29	3/8	0 - 3	0.6
LM66-H11	7/7	3 - 69	29.7
H11-Vec	7/7	4 - 79	32.1
H11-SN2	1/8	0 - 1	0.1

Fig. 6. Inverse correlation of syndecan-2 expressions and metastatic potentials.
Flow cytometrical analyses of syndecan-2 expression of the clones with different metastatic potentials and of syndecan-2 transfectants (left panels) were performed. Metastatic potentials of these clones were determined by counting lung nodules at four weeks after the subcutaneous injection of the cells to form the primary tumor (right-hand table).

CONCLUSION

In this review article, we have demonstrated that when the cells adhere to the same substratum (a fibronectin substratum) by a different combination of receptors (integrin $\alpha5\beta1$ and syndecans), they form different types of actin cytoskeletons. The key molecule deciding the organization of actin cytoskeletons on the substratum is syndecan-2, and the regulation by syndecan-2 depends on its expression level. Among the syndecan family, syndecan-4 acts upstream of syndecan-2 in this signal cascade. However, syndecan-1 does not participate in this signal transduction, indicating that each syndecan has functional specificity and plays a unique role. We do not know whether this is due to the ligand-binding specificity of each syndecan or to a specificity of signal transduction cascade caused by each syndecan. Furthermore, we have observed that there is a reverse correlation between the metastatic potential and syndecan-2 expression of the tumor cells. The elucidation of the mechanisms of signal transduction through syndecans is the next subject.

Acknowledgements: The authors wish to acknowledge Dr. Hayao Nakanishi of the Aichi Cancer Center Research Institute for his contribution to the work on these topics. This research is currently supported by a grant from The Sagawa Foundation for Promotion of Cancer Research (KO), a Grant-in-Aid for Cancer Research (11-12) from the Ministry of Health, Labour and Welfare (YK), and Grants-in-Aid for Bio-venture Research Center from the Ministry of Education, Culture, Sports, Science and Technology (MO).

References

1) Saunders, S., Jalkanen, M., O'Farrell, S., and Bernfield, M. (1989) Molecular cloning of syndecan, an integral membrane proteoglycan. J. Cell Biol. **108**, 1547-1556
2) Koda, J.E., Rapraeger, A., and Bernfield, M. (1985) Heparan sulfate proteoglycans from mouse mammary epithelial cells. Cell surface proteoglycan as a receptor for interstitial collagens. J. Biol. Chem. **260**, 8157-8162
3) Saunders, S. and Bernfield, M. (1988) Cell surface proteoglycan binds mouse mammary epithelial cells to fibronectin and behaves as a receptor for interstitial matrix. J. Cell Biol. **106**, 423-430
4) Marynen, P., Zhang, J., Cassiman, J.J., Van den Berghe, H., and David, G. (1989) Partial primary structure of the 48- and 90-kilodalton core proteins of cell surface-associated heparan sulfate proteoglycans of lung fibro-

blasts. Prediction of an integral membrane domain and evidence for multiple distinct core proteins at the cell surface of human lung fibroblasts. J. Biol. Chem. **264**, 7017 7024

5) Gould, S.E., Upholt, W.B., and Kosher, R.A. (1992) Syndecan 3 : a member of the syndecan family of membrane-intercalated proteoglycans that is expressed in high amounts at the onset of chicken limb cartilage differentiation. Proc. Natl. Acad. Sci. U.S.A. **89**, 3271-3275
6) Kojima, T., Leone, C.W., Marchildon, G.A., Marcum, J. A., and Rosenberg, R.D. (1992) Isolation and characterization of heparan sulfate proteoglycans produced by cloned rat microvascular endothelial cells. J. Biol. Chem. **267**, 4859-4869
7) Bernfield, M., Kokenyesi, R., Kato, M., Hinkes, M.T., Spring, J., Gallo, R.L., and Lose, E.J. (1992) Biology of the syndecans : a family of transmembrane heparan sulfate proteoglycans. Annu. Rev. Cell Biol. **8**, 365-393
8) Zimmermann, P. and David, G. (1999) The syndecans, tuners of transmembrane signaling. FASEB J., **13** Suppl., S91-100
9) Esko, J.D. and Lindahl, U. (2001) Molecular diversity of heparan sulfate. J. Clin. Invest. **108**, 169-174
10) Bernfield, M., Gotte, M., Park, P.W., Reizes, O., Fitzgerald, M.L., Lincecum, J., and Zako, M. (1999) Functions of cell surface heparan sulfate proteoglycans. Annu. Rev. Biochem. **68**, 729-777
11) Rapraeger, A.C. (2000) Syndecan-regulated receptor signaling. J. Cell Biol. **149**, 995-998
12) Gallagher, J.T. (2001) Heparan sulfate : growth control with a restricted sequence menu. J. Clin. Invest. **108**, 357-361
13) Takenaga, K. (1984) Characterization of low- and high-metastatic clones isolated from a Lewis lung carcinoma. Gann **75**, 61-71
14) Itano, N., Oguri, K., Nakanishi, H., and Okayama, M. (1993) Membrane-intercalated proteoglycan of a stroma-inducing clone from Lewis lung carcinoma binds to fibronectin *via* its heparan sulfate chains. J. Biochem. **114**, 862-873
15) Nakanishi, H., Takenaga, K., Oguri, K., Yoshida, A., and Okayama, M. (1992) Morphological characteristics of tumours formed by Lewis lung carcinoma-derived cloned cell lines with different metastatic potentials : structural differences in their basement membranes formed *in vivo*. Virchows Arch. A Pathol. Anat. Histopathol. **420**, 163-170
16) Nakanishi, H., Oguri, K., Yoshida, K., Itano, N., Takenaga, K., Kazama, T., Yoshida, A., and Okayama, M. (1992) Structural differences between heparan sulphates of proteoglycan involved in the formation of basement membranes *in vivo* by Lewis-lung-carcinoma-derived cloned cells with different metastatic potentials. Biochem. J. **288**, 215-224
17) Nakanishi, H., Oguri, K., Takenaga, K., Hosoda, S., and Okayama, M. (1994) Differential fibrotic stromal responses of host tissue to low- and high-metastatic cloned Lewis lung carcinoma cells. Lab. Invest. **70**, 324-332
18) Hynes, R.O. (1987) Integrins : a family of cell surface receptors. Cell **48**, 549-554
19) Couchman, J.R. and Woods, A. (1999) Syndecan-4 and integrins : combinatorial signaling in cell adhesion. J. Cell Sci. **112**, 3415-3420
20) Kusano, Y., Oguri, K., Nagayasu, Y., Munesue, S., Ishihara, M., Saiki, I., Yonekura, H., Yamamoto, H., and Okayama, M. (2000) Participation of syndecan 2 in the induction of stress fiber formation in cooperation with integrin $\alpha 5\beta 1$: structural characteristics of heparan sulfate chains with avidity to COOH-terminal heparin-binding domain of fibronectin. Exp. Cell Res. **256**, 434-444
21) Munesue, S., Kusano, Y., Oguri, K., Itano, N., Yoshitomi, Y., Nakanishi, H., Yamashina, I., and Okayama, M. (2002) The role of syndecan-2 in regulation of actin-cytoskeletal organization of Lewis lung carcinoma-derived metastatic clones. Biochem. J. **363**, 201-209
22) Oh, E.S., Woods, A., and Couchman, J.R. (1997) Syndecan-4 proteoglycan regulates the distribution and activity of protein kinase C. J. Biol. Chem. **272**, 8133-8136
23) Oh, E.S., Couchman, J.R., and Woods, A. (1997) Serine phosphorylation of syndecan-2 proteoglycan cytoplasmic domain. Arch. Biochem. Biophys. **344**, 67-74
24) Itano, N., Oguri, K., Nagayasu, N., Kusano, Y., Nakanishi, H., David, G., and Okayama, M. (1996) Phosphorylation of a membrane-intercalated proteoglycan, syndecan-2, expressed in a stroma-inducing clone from a mouse Lewis lung carcinoma. Biochem. J. **315**, 925-930
25) Ishiguro, K., Kadomatsu, K., Kojima, T., Muramatsu, H., Tsuzuki, S., Nakamura, E., Kusugami, K., Saito, H., and Muramatsu, T. (2000) Syndecan-4 deficiency impairs focal adhesion formation only under restricted conditions. J. Biol. Chem. **275**, 5249-5252

IL-2と癌の遺伝子治療

竹内　実　新屋政春

◉IL-2による癌の遺伝子治療は担癌宿主の免疫機能を増強し，直接的な抗腫瘍作用をもつエフェクター細胞の増殖・分化の誘導と細胞障害活性を強化し，抗腫瘍効果を発揮する。

interleukin-2（IL-2）はcytotoxic T lymphocyte（CTL），natural killer（NK），lymphokine activated killer（LAK）細胞などの抗腫瘍性エフェクター細胞の癌細胞障害活性を増強し，直接癌細胞に対して細胞障害活性を示さないが，広く生体の免疫機能を活性化するサイトカインであることから，癌の遺伝子治療によく用いられている[1]．そのため，IL-2遺伝子を用いた癌の遺伝子治療の報告は，ほかのサイトカイン遺伝子治療に比べ数多く報告されている[2]．最初のIL-2遺伝子を導入した癌治療実験の報告は，マウス大腸癌細胞であるcolon 26細胞にIL-2遺伝子を導入し，抗腫瘍効果を認めている[3]．また，IL-2がT細胞系を増殖・活性化することから，とくにCTLが誘導されやすい高免疫原性癌であるメラノーマ細胞にIL-2遺伝子を導入し，一方でCTLにもIL-2遺伝子を導入しその抗腫瘍効果を認めた報告が多くなされ，現在臨床試験も多数行われている[4]．

ヒト癌では高免疫原性を示す癌は少ないことから，著者らの研究室ではヒト癌のモデルとして免疫原性を示さず，自然に肺転移を起こすLewis lung carcinoma 2（LL 2）腫瘍細胞を用い，マウスに移植後，担癌宿主の免疫機能について研究してきた．LL 2腫瘍は増殖に伴い，担癌宿主の脾臓内に免疫抑制細胞が出現することにより，T細胞サブセット比率が減少し，T細胞のIL-2産生機能が低下し，その結果，おもにT細胞機能低下による宿主の免疫系機能の低下が引き起こされることを報告してきた[5,6]．このように低下した担癌宿主のT細胞機能の回復と抗腫瘍エフェクター細胞の活性の増強を考えてIL-2遺伝子をLL/2腫瘍細胞に導入し，その抗腫瘍効果と担癌宿主の免疫機能の回復について検討している．

本稿では自験成績をもとに実験的IL-2の癌遺伝子治療の効果とその問題点について述べたい．

■遺伝子導入

IL-2の癌遺伝子治療の効果は，用いるベクターと遺伝子の導入法によりその効果が異なることが報告されている．現在使用されているベクターはウイルス性ベクター（レトロウイルス，ア

Minoru TAKEUCHI and Masaharu SHINYA／京都産業大学工学部生物工学科

サイドメモ

IL-2と腫瘍細胞障害性エフェクター細胞

IL-2は，T細胞のなかのおもにヘルパーT細胞のtype 1型（Th1）細胞から産生される分子量15000の可溶性糖蛋白で，T細胞自体の増殖を引き起こす以外に，CTLの分化誘導，NK細胞の増殖・活性化，LAK細胞の誘導，B細胞，マクロファージなどの細胞にも作用するサイトカインである．これらの細胞はIL-2受容体をもっており，IL-2は受容体に結合して細胞内にシグナルを伝える．IL-2により誘導される抗腫瘍性エフェクター細胞としては，おもにCTL，NK，LAK細胞があり，CTLはクラスI拘束性，NKとLAK細胞は非拘束性の腫瘍細胞障害性細胞である．これらの細胞は，IL-2により活性化されると，細胞内からperforinを放出し，癌細胞の膜に結合・重合し，polyperforinによる小孔を形成し，小孔からgranzymeが細胞内に注入され，癌細胞のDNA断片化をきたし，アポトーシスによって標的細胞を死に至らしめる．

デノウイルス，アデノ随伴ウイルスなど）と非ウイルス性ベクター（プラスミドなど）の2つに分けられる．ウイルス性ベクターは，一般的に遺伝子の細胞内への導入効率，核内への移行効率，染色体DNAへの取込み効率がよいことから，導入遺伝子の発現効率が非常に高いのに比べ，プラスミドベクターは導入遺伝子の発現効率が低いが，ウイルス性ベクターのもつ特徴である病原性がないという利点が報告されている[7]．導入方法には，ウイルス性ベクターを用いない場合はリン酸カルシウム共沈法，エレクトロポレーション法，DEAE-デキストラン法，リポソーム法などがあるが，手技的にも簡単で，通常の遺伝子導入実験においていずれの方法も汎用されている方法である．ただし，これらの方法は遺伝子導入発現効率があまりよくないのが欠点である．いずれにしても100%の癌細胞に目的とする遺伝子を安定に導入発現させることは難しいのが現状である．

著者らの研究室では臨床応用を考え，ヒトIL-2（hIL-2）遺伝子を組み込んだ病原性のないプラスミドベクターであるpCMV-Neo-hIL-2を京都府立医大の松田先生より供与していただいてエレクトロポレーション法によりLL 2細胞に導入し，*in vitro*でIL-2の産生を確認後，実験を行っている．

■抗腫瘍効果

IL-2遺伝子導入による抗腫瘍効果に関しては標的とする腫瘍細胞，導入法の違いにより抗腫瘍効果が異なる．IL-2遺伝子導入により程度の差はあるが，一般的には抗腫瘍性が認められている報告が多い．自験成績でもIL-2遺伝子導入LL/2腫瘍細胞（LL/2+IL-2）を5×10^5個/マウスに皮下移植後，その増殖を非導入LL/2細胞と比較し，IL-2遺伝子導入による抗腫瘍効果を検討したところ，有意な腫瘍増殖の抑制が認められた（図1）．生存率に関しても腫瘍移植後50日目の生存率は非導入マウスでは0%であるのに対し，IL-2遺伝子導入では45%で，生存率の延長が認められ，平均生存日数においても有意な延長が認められた（図2，表1）．

移植腫瘍部位のIL-2産生を調べたところ，*in vitro*の培養上清中の濃度よりも低いがIL-2の産生が認められた．また，組織所見においてもIL-2遺伝子導入により腫瘍組織部位に限局したリンパ球浸潤が認められた．しかし，血清中にはIL-2は検出されなかった．これらの成績から，腫瘍周辺部位に限局してIL-2の産生が起こり，エンドクラインではなく，パラクラインに腫瘍組織周辺部位に浸潤あるいは存在しているIL-2反応性細胞が活性化された結果，抗腫瘍性が認められたと考えられる．

腫瘍の完全退縮が認められなかったのは，腫瘍部位でのIL-2の産生濃度が低値であったこと，免疫原性がほとんどない腫瘍細胞を用いたことか

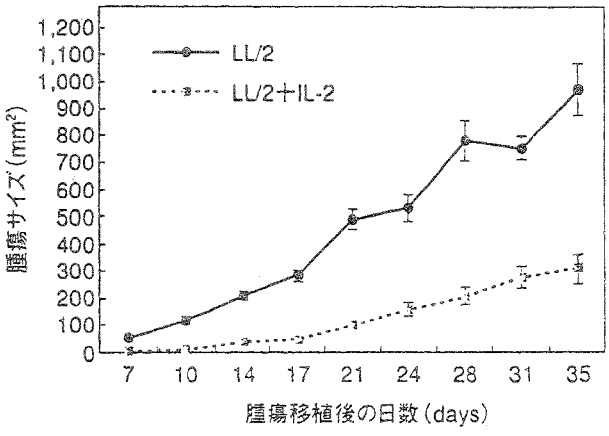

図1　hIL-2遺伝子導入した腫瘍細胞移植による抗腫瘍効果

LL/2およびLL 2+IL-2腫瘍細胞5.0×10^5個をC57BL/6マウスの大腿部皮下に移植し，腫瘍移植後7日目から3～4日ごとに腫瘍サイズを測定し，面積を算出した．

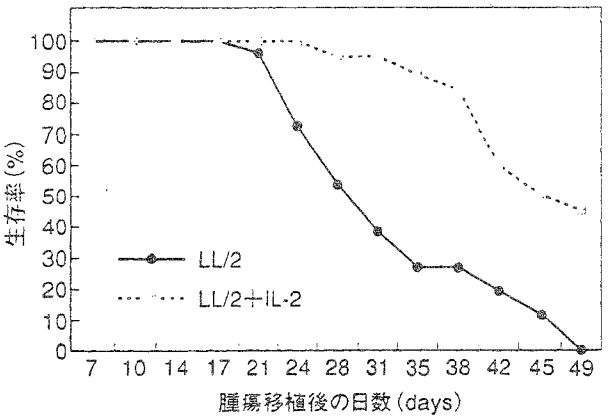

図2　hIL-2遺伝子導入した腫瘍細胞移植による抗腫瘍効果

表 1　hIL-2 遺伝子導入した腫瘍細胞移植による平均生存日数

	平均生存日数（mean±S. E.）
LL/2 腫瘍移植マウス	32.2±1.2 日
LL/2+IL-2 腫瘍移植マウス	52.3±4.0 日

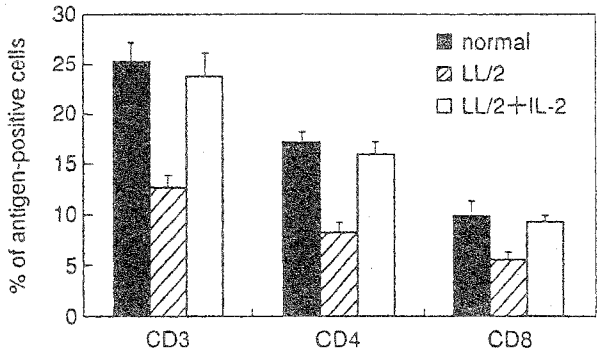

図 3　hIL-2 遺伝子導入した腫瘍細胞移植による担癌宿主の T 細胞サブセット

腫瘍移植後 21 日目のマウス脾細胞の陽性細胞比率を，抗 CD3，CD4，CD8FITC 標識抗体と反応後，FACS により測定した．

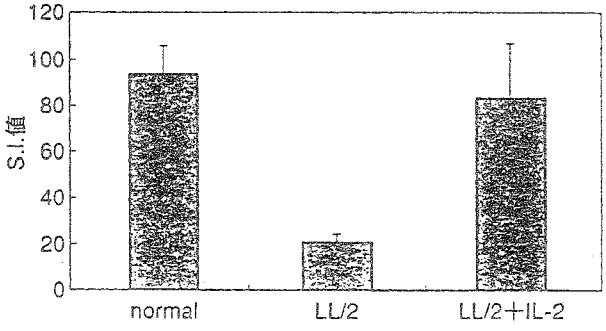

図 4　hIL-2 遺伝子導入した腫瘍細胞移植による担癌宿主の ConA 反応

脾臓は腫瘍移植後 21 日目のマウスから摘出し，ConA（最終濃度 1.0 μg ml）存在下で培養し，^{3}H-thymidine の取込み値を測定した．SI 値は，以下の式から算出した．

SI＝ConA 刺激（cpm）非刺激（cpm）

らとくに抗腫瘍作用の強い CTL の誘導がなされなかったためと思われる．また，腫瘍組織局所にもこれらエフェクター細胞の誘導・集積がうまく行われなかったためと思われる．ほかの IL-2 の遺伝子治療の報告では腫瘍の完全退縮が認められている報告もあるが，その多くは免疫原性の高い腫瘍を用い，IL-2 遺伝子導入腫瘍をワクチンとして投与している[8]．

今後は抗腫瘍免疫の誘導がされにくい低免疫原性腫瘍についても検討を加える必要があると思われる．

■担癌宿主の免疫機能の回復

担癌宿主の免疫機能は低下していることが知られていることから，宿主の免疫機能を回復することは抗腫瘍効果および延命効果を高めるためにも重要な要因である．しかし，IL-2 遺伝子による癌遺伝子治療においては抗腫瘍効果に主眼がおかれ，担癌宿主の免疫機能への影響についてはほとんど報告されていないのが現状である．LL/2 腫瘍移植により担癌宿主の免疫機能のなかで，とくに T 細胞機能が抑制されることから，IL-2 遺伝子導入により T 細胞機能が回復するかどうかについて検討している[9]．

まず，T 細胞サブセット比率に関しては，LL/2 腫瘍担癌マウスでは正常マウスに比較して脾臓の CD3，4 および 8 陽性 T 細胞の比率がそれぞれ約 50％減少するが，IL-2 遺伝子導入によりそれぞれの細胞比率はほぼ正常レベルの値まで回復することが認められた（図3）．また，T 細胞マイトゲンである concanavalin A（ConA）に対する反応（ConA 反応）に関しても，LL/2 腫瘍担癌マウスの脾細胞では正常マウスに比べて反応値の有意な低下が認められたが，IL-2 遺伝子導入により低下した ConA 反応は正常値レベルまでに回復した（図4）．さらに，マウス IL-2（mIL-2）mRNA の発現に関しても，LL/2 担癌マウスの脾細胞では IL-2 mRNA 発現の低下が認められたが，IL-2 遺伝子導入により正常マウスと同レベルまで回復した（図5）．

このように本腫瘍系においては，IL-2 遺伝子導入により T 細胞サブセット比率の回復および T 細胞機能の回復が認められ，その結果，生存率お

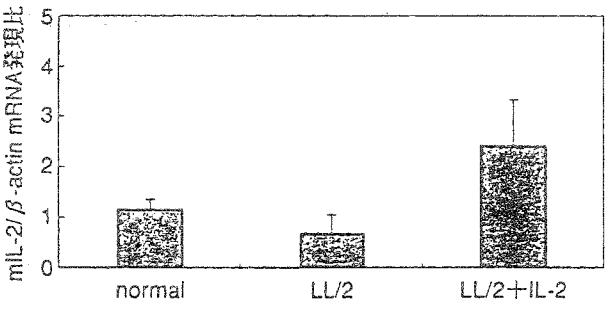

図 5　hIL-2遺伝子導入した腫瘍細胞移植による担癌宿主のmIL-2mRNA発現

脾臓は腫瘍移植後21日目のマウスから摘出し，細切後，AGPC法により全RNAを抽出し，RT-PCRを行いmIL-2mRNA発現を検討した．電気泳動後，検出されたバンドは，NIH imageにより解析し，β-actinとmIL-2mRNA発現比で表示した．

よび生存日数の延長による延命効果が認められたと考えられる．また，LL/2腫瘍増殖に伴い担癌宿主の脾臓中に出現する免疫抑制細胞数の減少もIL-2遺伝子導入により認められた．IL-2遺伝子の癌遺伝子治療による免疫機能の回復については，IL-2遺伝子導入により腫瘍細胞に対する遅延型免疫反応が認められたとの報告がされている程度で，前述したように宿主の免疫機能への影響についてはまだ十分な報告はされていないのが現状である[10]．

おわりに

癌に対するIL-2の遺伝子治療はマウスのモデルでは抗腫瘍効果が認められており，現在臨床試験も行われているが，まだヒトでは十分な抗腫瘍効果は得られていない[11]．これはヒトの癌細胞では腫瘍株の樹立が難しいため，IL-2遺伝子導入腫瘍細胞を作成しにくいこと，さらに腫瘍抗原の発現が少ないため，IL-2遺伝子を導入しても腫瘍抗原特異的なCTLを誘導しにくいことが考えられる．また，マウス，ヒトの場合ともに腫瘍組織への抗腫瘍エフェクター細胞の集積がうまくいかない点があり，ケモカイン遺伝子などを同時に導入し腫瘍局所にエフェクター細胞を集積させる必要がある．いずれにしても1種類のサイトカイン遺伝子導入だけでは十分な抗腫瘍効果を上げるのは難しいと思われ，数種類のサイトカイン遺伝子あるいは主要組織適合抗原などの抗原認識を強め免疫応答を亢進させるような遺伝子を同時に導入することにより，より強い抗腫瘍効果が期待できる．さらに，IL-2遺伝子導入と非特異的な免疫能力を促進するbiological response modifiers (BRM) などとの併用により，腫瘍特異的・非特異的な生体の免疫応答を増強させ，より強い抗腫瘍効果が発揮できると思われる．

一方，IL-2遺伝子の導入効率が動物実験に比べ，ヒトでは低い点も問題であることからIL-2遺伝子治療の効果を高めるには，よりよいベクター，導入システムの開発が必要であり，さらに，安全性の面から考えるとウイルス性ベクターよりも，より安全で導入効率がよい，非ウイルス性のプラスミドベクターの開発も重要な課題である．

文献

1) Krap, S. et al.: *J. Immunol.*, 150: 896-908, 1993.
2) Ohe, Y. et al.: *Int. J. Cancer*, 53: 432-437, 1993.
3) Fearon, E. R. et al.: *Cell*, 60: 397-403, 1990.
4) Gansbacher, B. et al.: *Blood*, 80: 2817-2825, 1992.
5) 塚野千春・他：第55回日本癌学会総会記事，1996，p.511.
6) 塚野千春・他：第56回日本癌学会総会記事，1997，p.493.
7) 小沢敦也：*Mol. Med.*, 36: 602-609, 1999.
8) Qin, H. et al.: *Cancer Gene Ther.*, 3: 163-167.
9) 新屋政春・他：日本免疫学会総会記録，29：153，1999.
10) 谷　憲三郎・他：遺伝子治療開発研究ハンドブック（日本遺伝子治療学会編），1999，pp.188-199.
11) Roth, A. J. et al.: *J. Natl. Cancer Inst.*, 88: 21-39, 1997.

Inhibition of natural killer cell activity by alveolar macrophages in smokers

M. Takeuchi[1], S. Nagai[2] & T. Izumi[2]

[1]Department of Biotechnology, Kyoto Sangyo University, and [2]Kyoto University, Kyoto, Japan

Abstract

We investigated the mechanism of the suppressive effect of alveolar macrophages on the activity of natural killer (NK) cells taken from bronchoalveolar lavage fluid and blood from smokers and non-smokers. The activity of NK cells was very low initially in both non-smokers and smokers. After 24 h in culture, the activity increased significantly in non-smokers but not smokers, and the activity of NK cells in the lung was significantly augmented by addition of interleukin-2, also only in non-smokers. Addition of alveolar macrophages from smokers had a significantly greater inhibitory effect on NK cell activity in blood than those from non-smokers. Indomethacin, catalase and thoiurea did not prevent the suppression of NK cell activity by alveolar macrophages, but superoxide dismutase prevented the inhibition. These results suggest that NK cell activity is suppressed in smokers by the release of oxygen radicals from alveolar macrophages.

Introduction

Cigarette smoking is known to inhibit the immune system, and cigarette smokers have decreased helper:suppressor T-cell ratios, decreased serum immunoglobulin concentrations and suppressed NK cell activity (Ferson *et al.*, 1979). NK cells play an important role in immune surveillance against tumours and viral infections in the lung, but many studies have focused on their activity in peripheral blood (Phillips *et al.*, 1985), while little is known about NK cells in the lung (Bordignon *et al.*, 1982). We reported previously that the NK cell activity in the lungs of smokers is lower than that in non-smokers (Takeuchi *et al.*, 1989). Alveolar macrophages play a major role in pulmonary defence mechanisms, and cigarette smoking induces various changes in the metabolism of these cells (Harris *et al.*, 1970). Alveolar macrophages have been shown to inhibit the expression of NK cell activity (Takeuchi *et al.*, 1989), but little is known about this cell-mediated down-regulation. In this study, we investigated the mechanism of the inhibitory effect of alveolar macrophages on NK cell activity in smokers.

Material and methods

The subjects were 10 healthy men, five of whom were non-smokers (mean age, 35.4 years) and five were cigarette smokers (mean age, 34.2 years). The duration of smoking ranged from 4 to 30 years (mean, 13.4), and the consumption was 15–50 cigarettes per day (mean, 27.0) or 4–50 pack–years (mean, 22.8).

Lung effector cells were obtained by bronchoelveolar lavage and purified with Ficoll-Hypaque on a plastic dish and nylon wool column. The alveolar macrophages were purified by E-rosette methods. NK cell activity was assayed by the ^{51}Cr release method after incubation for 4 or 24 h, with K562 as the target cell (E:T = 10). Alveolar macrophages were added at a final concentration of 5–50% to effector cells in the NK cell assay.

To evaluate a possible role of prostaglandins and oxygen radicals produced by alveolar macrophages in the inhibition of NK cell activity, indomethacin and anti-oxidants were added with 25% alveolar macrophages to a final concentration of 2.5×10^{-7} to 2.5×10^{-5} mmol/l of indomethacin, 1.4–1400 U/ml of catalse, 2.5–25 mmol/L of thiourea or 7.5–750 U/ml of superoxide dismutase.

Results

The NK cell activity in lung tissue from smokers showed little cytotoxicity before or after 24 h of incubation. The activity in lung from non-smokers was initially very low (mean, 1.5%) but increased to a mean of 6.1% after 24 h of incubation ($p < 0.05$); the corresponding values for smokers were 1.3% and 2.9%, the difference being non-significant. When interleukin-2 was added to the cultures at a concentration of 50 U/ml, the activity of NK cells in lung was significantly increased in non-smokers but not in smokers.

When alveolar macrophages from smokers were added at a concentration of 5% to autologous blood samples, they significantly inhibited blood NK cell activity, whereas those from non-smokers did not. The 42% inhibition caused by alveolar macrophages from smokers was not inhibited by indomethacin, catalase or thiourea, but was suppressed by superoxide dismutase, the activity returning to the level observed before the addition of alveolar macrophages.

Discussion

Whereas it has been shown previously that heavy smokers have decreased NK cell activity in their blood (Phillips *et al.*, 1985), we have shown that the activity of NK cells in the lungs of smokers is not increased after 24 h in culture, in contrast to those of non-smokers, and no difference is seen between smokers and non-smokers in NK cell activity in the blood. In an earlier study, NK cell activity was augmented by interleukin-2 (Itoh *et al.*, 1985), but the activity in the lungs of smokers in our study was not increased. Our data show that the function of NK cells in the lungs is damaged by smoking. Robinson *et al.* (1984) showed that alveolar macrophages in bronchoalveolar lavage fluid from healthy non-smokers inhibited blood NK cell activity; we have also shown that alveolar macrophages from smokers and non-smokers can inhibit this activity, but we also observed that alveolar macrophages from smokers inhibit blood NK cell activity to a greater extent than those from non-smokers.

Smokers are known to have an increased number of alveolar macrophages, which release more oxygen radicals than macrophages from non-smokers (Richter *et al.*, 1986). Although it is also known that alveolar macrophages can release superoxide anions, other forms of reduced oxygen species and prostaglandins (Hoidal *et al.*, 1979), we found that only superoxide dismutase prevented the inhibition of NK cell activity. These results suggest that the inhibition of NK cell activity mediated by alveolar macrophages is caused by production of oxygen radicals in smokers. The reduced NK cell activity in the lungs of smokers may contribute to the development and progression of lung cancer and cause greater susceptibility to viral infections.

References

Bordignon, C., Villa, F., Vecchi, A., Giavazzi, R., Introna, M. & Avallone (1982) *Clin. Exp. Immunol.*, 47, 437–444
Ferson, M., Edwards, A., Lint, A., Milton, G.W. & Kersey, P. (1979) *Int. J. Cancer*, 23, 603–609
Harris, J.O., Swenson, E.W. & Johnson, J.E. (1970) *J. Clin. Invest.*, 49, 2086–2096
Hoidal, J.R., Beal, G.D. & Repine, J.E. (1979) *Infect. Immunol.*, 26, 1088–1094
Itoh, K., Shiba, K., Shimizu, Y., Suzuki, R. & Kumagai, K. *J. Immunol.*, 134, 3124–3129
Phillips, B., Marshall, M.E., Brown, S. & Thompson, J.S. (1985) *Cancer*, 56, 2789–2792
Richter, A.M., Abboud, R.T., Johal, S.S. & Fera, T.A. (1986) *Lung*, 164, 233–242
Robinson, B.W.S., Pinkston, P. & Crystal, R.G. (1984) *J. Clin. Invest.*, 74, 942–950
Takeuchi, M., Nagai, S. & Izumi, T. (1989) *Chest*, 94, 688–693

Effect of Smoking on Immunological Functions of Alveolar Macrophages in Mice

M. Takeuchi, A. Nakajima, K. Yoshikawa, M. Shinya, H. Asada, M. Yoshimura, C. Tsuchihara, S. Nagai* and T. Izumi*

Faculty of Engineering, Kyoto Sangyo University, *Department of pulmonary medicine, Kyoto University, Kyoto, JAPAN

ABSTRACT

In previous studies, we demonstrated that the tobacco smoking induces functional changes in alveolar macrophages (AM). However, the effects of smoking on the reactive oxygen species production and antigen presenting activity are not well defined. In the present study, we investigated the effect of smoking on the oxidant productions, cell surface antigen expression and antigen presenting activity of AM in smoking mice. Female C57BL/6 mice were exposed to 20 cigarettes (Coresta Monitor No. 2)/day during 10 days using Hamburg II smoking machine. After 10 days, mice were sacrificed. The AM were obtained by brochoalveolar lavage (BAL). The antigen presenting activity of AM was assayed by mixed lymphocyte reaction (MLR). The reactive oxygen species productions in AM were analyzed by flow cytometry using hydroethidine and dichlorofluorescen (DCFH). The expression of surface antigens (Class II and B7-1) of AM were analyzed by flow cytometry. The antigen presenting activity of AM was significantly ($p<0.01$) decreased in smoked mice compared with non-smoked mice. The O_2^- production of AM was significantly ($p<0.01$) increased in smoked mice, whereas the H_2O_2 production of AM was not difference in both groups. The Class II and B7-1 antigen positive cells in AM were significantly ($p<0.01$) decreased in smoked mice compared with non-smoked mice. These results suggest that the antigen presenting activity, expressions of Class II and B7-1 antigens of the AM may be impaired by O_2^- but not H_2O_2 from AM in smoked mice.

INTRODUCTION

It is generally accepted that prolonged exposure to cigarette smoke is associated with an increased prevalence of a variety of respiratory disease [1], the mechanisms

of which have not been clearly defined. Immune system has long been known to play an essential role in defense mechanisms against infectious disease. Previous studies have shown smoking can impair pulmonary immune function and hence alter resistance to the development of lung disease [2]. The alveolar macrophages (AM) play a major role in lung immune system. Functions of AM are largely classified into phagocytosis, secretory (cytokines, enzymes and reactive oxygen intermediates) and antigen presentation [3]. In previous studies, we demonstrated that the tobacco smoking induces functional changes in AM [4]. However, the global influence of cigarette smoke on the AM functions is not yet fully understood. Therefore, we investigated the effect of smoking on the antigen presentation activity, expression of surface antigens associated with antigen presentation and secretion of reactive oxygen species products by AM.

MATERIALS AND METHODS

C57BL/6 female mice at 8 weeks of age were used. Mice in the smoked group (n=10) were exposed to main stream smoke of 20 filter Monitor No. 2 cigarettes per day during 10 days using Hamburg II smoking machine. Mice in the non-smoked group (n=10) was treated daily exactly like those in the smoked group, except that instead of cigarette smoke. After 10 days, mice were sacrificed. AM were obtained by bronchoalveolar lavage (BAL). Briefly, the lung washed 10 times with 1 ml PBS. The recovered BAL fluids were centrifuged, AM were diluted to the desired final concentration with RPMI 1640 medium. A functional stimulation assay was used to measure the capacity of AM to produce oxidants using hydroethidine and DCFH as a fluorescent indicator and FACScan flow cytometry. Quantification of surface antigens expression of AM was performed using FITC conjugated anti-class II or B7-1 monoclonal antibody by FACScan. Antigen presenting activity of AM was performed using ^{3}H-thymidine by mix lymphocyte reaction (MLR).

RESULTS

The percent of BAL fluid recovery was similar in non-smoked mice group (84.5%) and smoked mice group (84.4%). The total cell count was significantly ($p<0.01$) increased in smoked mice (2.95×10^5 cells/mouse) compared with non-smoked mice (4.02×10^5 cells/mouse). More than 95% of cells in each group were alveolar macrophages by morphology and non-specific esterase staining. In the effect of smoking on antigen presenting activity of AM, the AM in smoked mice caused a 46% inhibition of MLR compared with non-smoked group. This represented significantly ($p<0.01$) decrease in antigen presenting activity of AM in smoked mice compared with non-smoked mice. The positive ratio of expression of class II antigen in AM was 25% in non-smoked mice and 8% in smoked mice. The positive ratio of expression of B7-1 antigen in AM was 35% in non-smoked mice and 15% in smoked mice. The class II or B7-1 antigen expression of AM was significantly decrease in smoked mice compared with non-smoked mice. In the oxidant

productions of AM, O_2^- production of AM was 47% in non-smoked mice and 87% in smoked mice. H_2O_2 production of AM was 64% in non-smoked mice and 71% in smoked mice. O_2^- production of AM was significantly increase in smoked mice. However, there was not difference between non-smoked mice and smoked mice in H_2O_2 production of AM (Table 1).

Table 1 Effect of smoking on immunological functions of AM

	antigen presenting activity (%)	surface antigen (%)		oxidant production (%)	
		Class II	B7-1	O_2^-	H_2O_2
non-smoked mice	100	25.4±4.9[a)]	35.0±2.7	46.9±3.5	63.6±4.9
smoked mice	54**	7.9±2.1*	15.6±2.6**	87.2±1.5**	70.7±6.6

a) : mean ± S.E.
* : significantly difference from non-smoked mice, $p < 0.05$
** : significantly difference from non-smoked mice, $p < 0.01$

DISCUSSION

Cigarette smoking exerts a great influence on the immune system. For example cigarette smokers have increased total white blood cell count, decreased CD4/CD8 T cell ratios, decreased serum immunoglobulin levels and suppressed natural killer activity [5, 6]. The alveolar macrophages (AM) play a major role in lung defense mechanisms. Cigarette smoking induces various changes in the functions of the AM [7]. Results in experimental animals have been controversial, demonstrating both inhibition and enhancement of immune function of AM in smoked mice [8]. As antigen presentation cells, the AM play vital roles in both humoral and cell-mediated immunity. This antigen presentation leads to a specific T cell and B cell immune response against an antigen. Hence, it is possible that the AM in smoked mice have enhanced abilities to present antigens, since AM are directly stimulated by inhaled cigarette smoke. However, the antigen presenting activity of AM was decrease in smoked mice. AM in smoked mice were not particularly potent antigen presenting cells. The ability of macrophages to present antigens to T cells is strictly dependent upon the cell surface antigen expression of class II and B7-1 [9]. In addition, the effect of cigarette smoke exposure on the expression of surface antigens of AM has not been thoroughly evaluated. The expression of class II and B7-1 antigen of AM were inhibited by smoke exposure. The AM also can release reactive oxygen species. It is known that oxygen radicals from human AM can suppress NK cell activity [10]. The O_2^- production of AM were increased in smoked mice, however, H_2O_2 production of AM were similar in both groups. The mechanism responsible for the smoke-induced regional immunosuppression is as yet unclear. In this present study, our data suggest that the suppression of antigen presenting activity and expression of class II and B7-1 antigens of AM in smoked mice may be caused by O_2^- production, but not H_2O_2 from AM by cigarette smoke exposure.

ACKNOWLEDGEMENTS

This research was supported by a grant-in-aid for Scientific Research C (No. 09680537) and bio-venture project of frontier science from The Ministry of Education, Science, and Sports and Culture, Japan.

REFERENCES

1. Finklea JF et al. Cigarette smoking and acute non-influenza respiratory disease in military cadets. Amer. J. Epidemiol., 93 : 457-462, 1971.
2. Felss AOS et al. The alveolar macrophage. J. Appl. Physiol., 60 : 353-369, 1986.
3. Nathan CF. Secretory products of macrophages. J. Clin. Invest., 79 : 319-326, 1987.
4. Nagai S et al. Smoking and interleukin-1 activity released from human alveolar macrophages in healthy subjects. Chest, 94 : 694-700, 1988.
5. Miller LG et al. Reversible alterations in immunoregulatory T cells in smoking. Chest, 82 : 526-529, 1982.
6. Andersen P et al. Serum antibodies and immunoglobulins in smokers and non-smokers. Clin. Exp. Immunol., 47 : 467-473, 1982.
7. Ando M et al. Surface morphology and function of human pulmonary alveolar macrophages from smoker and non-smokers. Thorax, 39 : 850-856, 1984.
8. Barbour SE et al. Tobacco and smoking. Rev. Oral. Biol. Med., 8 : 437–460, 1997.
9. Pankow W et al. Reduction in HLA-DR density on alveolar macrophages of smokers. Lung, 169: 255–262, 1991.
10. Takeuchi M et al. The mechanism of inhibition of alveolar macrophages on autologous blood NK cell activity. Chest, 95 : 383–387, 1989.

Map 2

Biosynthetic Pathways of *O*-Glycans

O-Linked mucin-type oligosaccharides are not preassembled on a dolichol derivative, but every sugar is transferred individually from a specific nucleotide sugar. *O*-Glycans are not processed by glycosidases.

Synthesis of Core Structures

The first step in the biosynthesis of mucin-type *O*-glycans is the enzymatic transfer of GalNAc from UDP-GalNAc to a Ser/Thr residue. The reaction is catalyzed by a family of UDP-GalNAc:polypeptide *N*-acetylgalactosaminyltransferases (GalNAc transferase), which occurs mainly in the *cis*-Golgi. This enzyme is expressed in all mammalian cells and is common to the synthesis of all mucin-type *O*-glycans. It appears that each member of the multiple GalNAc transferases has a slightly different, but overlapping, substrate specificity; and the repertoire of GalNAc transferases expressed in a cell controls the *O*-glycosylation pattern. No general consensus sequence of the peptide backbone for *O*-glycosylation has been found.

Subsequently, stepwise elongation by specific transferases yields eight core structures containing GlcNAc, Gal, or GalNAc substitutions of GalNAc 1α-Ser/Thr. If this elongation does not occur, GalNAc 1α-Ser/Thr, which is often referred to as the Tn antigen, is generated. The Tn antigen may be modified to sialyl Tn antigen by α2,6-SA transferase.

Core 1 is a common core structure in mucins and other secreted and cell surface glycoproteins. The enzyme synthesizing core1, core1β1,3 Gal transferase is a ubiquitous enzyme present in most mammalian cells. Core 1 as a terminal structure, often referred to as the T antigen, is prevalent in cancer cells and their secretions. Core 1 is not usually exposed in glycoproteins but is monosialylated (SAα2→3Galβ1→

Hiroshi Nakada

Department of Biotechnology, Faculty of Engineering, Kyoto Sangyo University, Kamigamo-Motoyama, Kita-ku, Kyoto 603-8555, Japan
Tel. +81-75-705-1897; Fax +81-75-705-1888
e-mail: hnakada@cc.kyoto-su.ac.jp

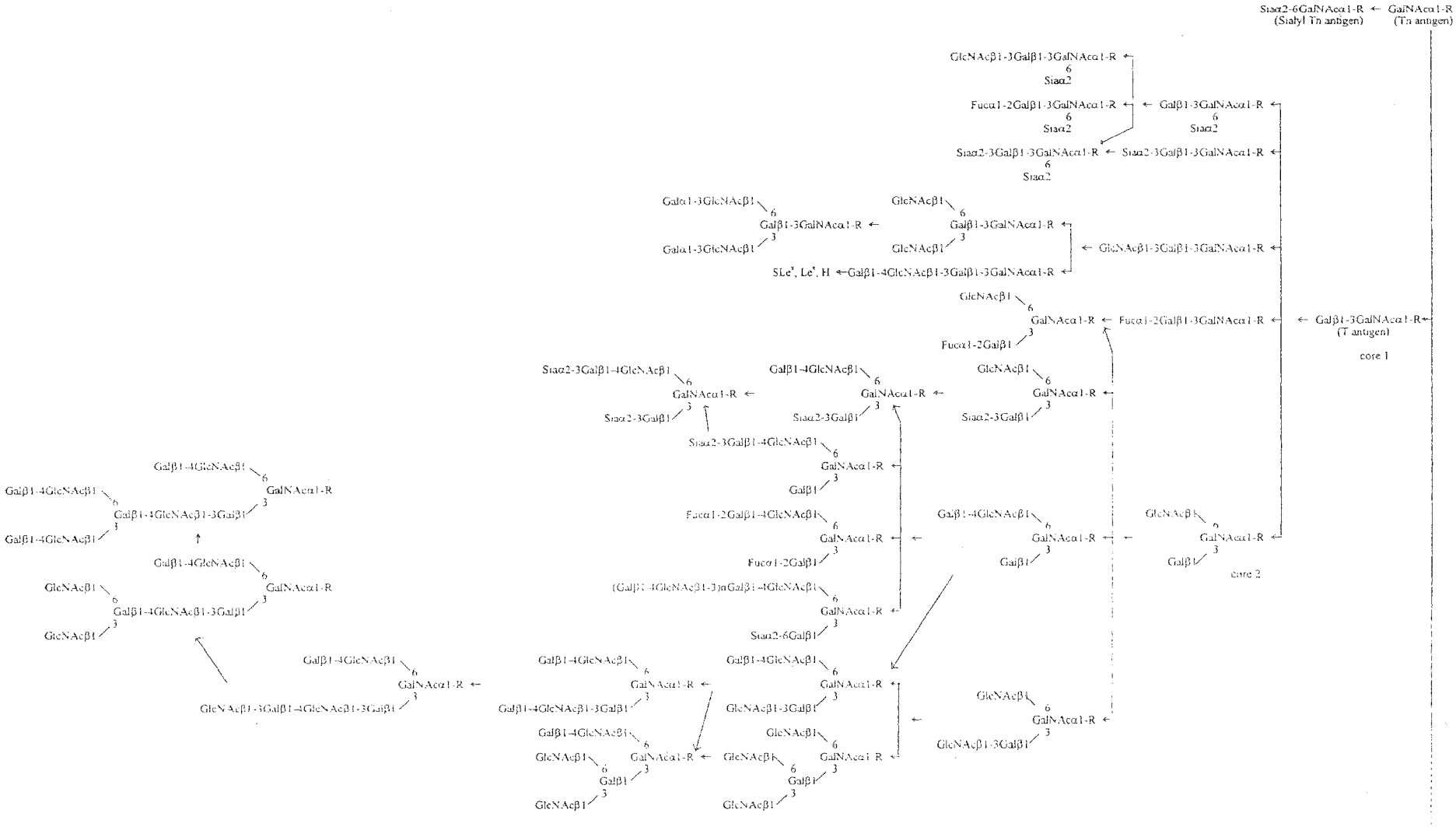
Siaα2-6GalNAcα1-R ← GalNAcα1-R
(Sialyl Tn antigen) (Tn antigen)
GlcNAcβ1-3Galβ1-3GalNAcα1-R
Siaα2
Fucα1-2Galβ1-3GalNAcα1-R ← Galβ1-3GalNAcα1-R
Siaα2 Siaα2
Siaα2-3Galβ1-3GalNAcα1-R ← Siaα2-3Galβ1-3GalNAcα1-R
Siaα2
Galα1-3GlcNAcβ1
Galβ1-3GalNAcα1-R ←
Galα1-3GlcNAcβ1
GlcNAcβ1
Galβ1-3GalNAcα1-R
GlcNAcβ1
← GlcNAcβ1-3Galβ1-3GalNAcα1-R
SLe^a, Le^a, H ←Galβ1-4GlcNAcβ1-3Galβ1-3GalNAcα1-R
GlcNAcβ1
GalNAcα1-R ← Fucα1-2Galβ1-3GalNAcα1-R ← Galβ1-3GalNAcα1-R←
(T antigen)
Fucα1-2Galβ1
core 1
Siaα2-3Galβ1-4GlcNAcβ1
GalNAcα1-R ←
Siaα2-3Galβ1
Siaα2-3Galβ1-4GlcNAcβ1
GalNAcα1-R
Galβ1
Fucα1-2Galβ1-4GlcNAcβ1
GalNAcα1-R ←
Fucα1-2Galβ1
(Galβ1-4GlcNAcβ1-3)nGalβ1-4GlcNAcβ1
GalNAcα1-R
Siaα2-6Galβ1
Galβ1-4GlcNAcβ1
GalNAcα1-R ←
Galβ1-4GlcNAcβ1-3Galβ1
Galβ1-4GlcNAcβ1
GlcNAcβ1-3Galβ1-4GlcNAcβ1-3Galβ1
Galβ1-4GlcNAcβ1
GalNAcα1-R ←
GlcNAcβ1-3Galβ1-4GlcNAcβ1-3Galβ1
Galβ1-4GlcNAcβ1
GalNAcα1-R
Galβ1-4GlcNAcβ1-3Galβ1
Galβ1-4GlcNAcβ1
GlcNAcβ1
Galβ1-4GlcNAcβ1
GalNAcα1-R
Galβ1-4GlcNAcβ1-3Galβ1
GlcNAcβ1
Galβ1
GlcNAcβ1
Galβ1-4GlcNAcβ1
GalNAcα1-R ←
Galβ1
core 2
GlcNAcβ1
GalNAcα1-R
GlcNAcβ1-3Galβ1

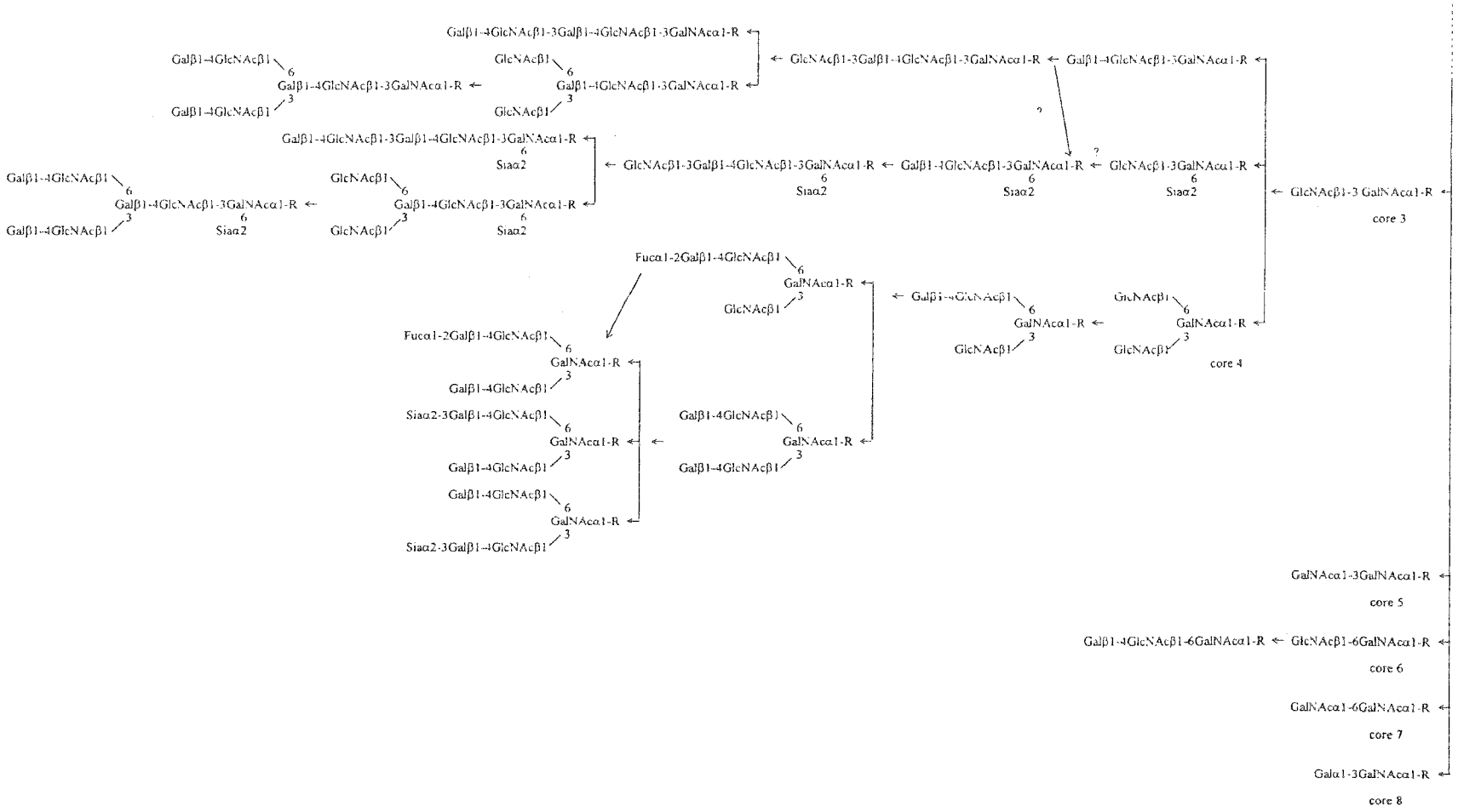

Map 2. Biosynthetic pathways of mucin-type *O*-glycans in mammals

3GalNAcα1→Ser/Thr and SAα2→6[Galβ1→3]GalNAcα1→Ser/Thr) or disialylated (SAα2→6[SAα2→3Galβ1→3]GalNAcα1→Ser/Thr).

Core 2 β6-GlcNAc transferase converts an unsubstituted core 1 to core 2. A number of related β6-GlcNAc transferases appear to exist with distinct substrate specificities. The core 2 β6-GlcNAc transferase does not act when core 1 is elongated, sialylated, sulfated, or fucosylated. The L-type core 2 β6-GlcNAc transferase occurs in leukocytes, leukemia cells, and many cancer cells and catalyzes only the conversion of core 1 to core 2. It is postulated that this enzyme is rate-limiting for biosynthesis of the poly-lactosamine-type structure on *O*-glycans. The enzyme activity is high in leukemia and activated T lymphocytes, and it is often altered in cancer cells. The M-type enzyme may act on three substrates—Gal β1→3GalNAcα1→Ser/Thr, GlcNAc β1→3GalNAcα1→Ser/Thr, and GlcNAc β1→3Galβ→, to form core 2, core 4, and I antigen, respectively. Other types of β1,6 GlcNAc transferase synthesize terminal or internal GlcNAc β1→6 branches as well as linear GlcNAc β1→6Gal/GalNAc structures of cores 2, 4, 6, and I determinants.

Core 3 is synthesized by core 3 β3-GlcNAc transferase. The enzyme activity has been found only in mucin-secreting tissues and is low in colon cancer tissue. Because synthesis of core 3 precedes that of core 4, synthesis of core 4 is limited by low activity and limited tissue distribution of core 3 β3-GlcNAc transferase.

The core 4 β6-GlcNAc transferase activity is found in colonic tissues and a number of cancer cell lines. Occurrence of the core 4 structure is restricted owing to the limiting and tissue-specific activity of core 3 β3-GlcNAc transferase as described above.

The core 5 structure has been found in mucins from several mammalian and human meconia. Core 5 α3-GalNAc transferase activity has been demonstrated in the colonic mucosa of a patient with adenocarcinoma.

Core 6 β6-GlcNAc transferase activity has been found in human ovarian tissues. The enzyme acts on GalNAc without prior substitution of GalNAc by a Gal β1→3 or GlcNAc β1→3 residue. Core 7 and 8 structures have been reported in bovine submaxillary mucin and in human bronchial mucin, respectively.

Synthesis of the core structures regulates the expression of functional terminal carbohydrate structures. Thus control of the biosynthetic pathways at early steps may have a great effect on the structures, properties, and functions of *O*-glycans. When terminal sialic acid or sulfate residues are added to the core structures, further elongation is inhibited, resulting in short acidic *O*-glycans.

Elongation of *O*-Glycans

Elongation β3-GlcNAc transferase catalyzes the elongation of core 1 or core 2 structure with an unsubstituted Gal β1→3 residue. β4-Gal transferase and i β3-GlcNAc transferase act sequentially to synthesize a common backbone structure, repeating Gal β1→4 GlcNAc β1→3 units (type 2 chain), leading to the synthesis of i antigen and poly-*N*-acetyllactosamine. These two enzymes are ubiquitous, and i β3-GlcNAc transferase differs from the elongation β3-GlcNAc transferase and from the core 3 β3-GlcNAc transferase by its tissue distribution and specificity. β4-Gal transferase is ubiquitous, and a number of related β4-Gal transferases exist.

Another backbone structure (i.e., repeating Gal β1→3 GlcNAc β1→3 units, or type 1 chain) may be introduced by a β3-Gal transferase. Thus at least two types of Gal transferase are involved in the synthesis of poly-*N*-acetyllactosamine.

GlcNAc β1→6 branches of the elongated backbone structure, which is referred to as the I antigen, are synthesized by a number of β6-GlcNAc transferases.

Terminal Glycosylation

Terminal sugars include SA, Fuc, Gal, GalNAc, and GlcNAc. *O*-Glycans may carry terminal epitopes such as Lewis-type or ABO-type antigens, which are synthesized probably by the same enzymes as those assembling these antigens on glycolipids and *N*-glycans.

A number of α3-SA transferases with various specificities toward Gal terminal acceptors act on core 1, core 2, and other *O*-glycan structures. Core 1 α3-SA transferase I (ST3GalI) acts on core 1. A family of α6-SA transferases have been cloned. α6-SA transferase I (ST6GalNAc-I) acts on substituted or unsubstituted GalNAc-Ser/Thr. α6-SA transferase II (ST6GalNAc-II) acts on the GalNAc residue of the core 1 structure. SAα2→6GalNAcα1→Ser/Thr is referred to as the sialyl Tn antigen. SAα2→3Galβ1→3GalNAc→R is a substrate for α6-SA transferases III and IV (ST6GalNAc-III and ST6GalNAc-IV).

There are two types of α2-Fuc transferases [i.e., hematopoietic type (FucT-I) and secretory type (FucT-II)] that synthesize the blood group H (O) determinant. A family of α3-Fuc transferases (FucT-III–VII and IX) act on internal GlcNAc residues with slightly different substrate specificities. These enzymes synthesize Lewis determinants in various cell types. α3-Fuc transferase III (FucT-III) has an unusual dual enzyme activity and is capable of synthesizing both Fucα1→3GlcNAc and Fucα1→4GlcNAc linkages. α3-Fuc transferases IV and VII (FucT-IV and -VII) appear to be responsible for the synthesis of sialyl- and sulfo-Le^x ligands for selectins.

特集Ⅰ　環境要因と免疫機能

喫煙と免疫機能*

竹内　実**

Key words：Smoking, Tobacco, Immune functions

はじめに

喫煙用タバコは，ナス科植物の*Nicotiana tabacum*の葉を乾燥，発酵，熟成などの過程を経て作られる．タバコ煙中には約6000種以上の化学物質が含まれているが，物質の状態によりガス相と粒子相にわけられ，それぞれに多種のcarcinogen, tumor initiator, 肺胞上皮細胞傷害物質などを含んでいる．ガス相には，一酸化炭素，二酸化炭素，一酸化窒素，アンモニアガスなどが含まれ，粒子相には，タバコの主成分であるニコチン，cartinogenであるベンツピレン，ジメチルニトロソアミン，ウレタンなどが含まれている．また，直接Ⅰ型肺胞上皮細胞を傷害する成分として，カドミウム，二酸化窒素などが知られている．さらに，タバコ煙は，主流煙，副流煙，成長煙，拡散煙，流出煙，くすぶり煙および主流煙を吸った後に喫煙者から吐き出される吹き出し煙(剰余煙)からなり，副流煙，成長煙，拡散煙，流出煙および剰余煙をまとめて環境タバコ煙と呼ばれている．主流煙，成長煙，流出煙，くすぶり煙および剰余煙は一服の間に生じる煙で，副流煙と拡散煙は一服と一服の間に生じるタバコ煙で，環境タバコ煙の大部分は副流煙と剰余煙からなっている[1]．主流煙は，pHが酸性であるが，副流煙は，アルカリ性で，粘膜に対する刺激性も強い．このようにタバコ煙には多種の有害物質が含まれており，これら有害物質が主に肺から吸入されること，また肺胞領域には免疫細胞であるマクロファージ，リンパ球などが常在しており，タバコ煙が直接これらの細胞に接触することから，喫煙がとくに肺の免疫細胞，免疫機能に影響を及ぼしている可能性が十分考えられる．

喫煙の免疫系に及ぼす影響に関しては，最初の報告は1970年Howellらが非喫煙者に比べて，喫煙者で末梢血白血球数が増加していることを報告している[2]．また実験動物では，1973年Esberらがマウスで喫煙により抗体産生機能が低下することを報告している[3]．それ以来，喫煙の免疫系への影響については，実験動物あるいはヒトのレベルでさまざまな報告がされている[4]．特にヒトでは，Reynoldsらによる気管支肺胞洗浄Bronchoalveolar Lavage(BAL)術の開発によってBAL液から容易に肺胞マクロファージ，リンパ球などの免疫細胞が得られるようになった結果，多くの報告がされるようになった[5][6]．また，肺癌，肺気腫，肺線維症，特発性間質性肺炎などtobacco related diseaseのあることから，臨床のレベルからも特に喫煙と肺疾患については重要な問題となってきている．著者らも以前より，環境分野で重要な問題として取り上げられているタバコ喫煙に着目し，喫煙の肺免疫系への影響をヒトおよびマウスについて研究してきてい

* Smoking and immune functions.

** Minoru TAKEUCHI, D.V.M., M.S.D., Ph.D.: 京都産業大学工学部生物工学科〔〒603-8555 京都市北区上賀茂本山〕; Department of Biotechnology, Faculty of Engineering, Kyoto Sangyo University, Kyoto 603-8555, JAPAN

表1　喫煙による肺胞マクロファージ数への影響

	非喫煙者(35)	喫煙者(29)	
回収率(%)	73.3±7.8*	67.3±11.8	P<0.05
回収細胞数(10^3/ml)	67.9±32.6	286.1±195.1	P<0.001
マクロファージ(%)	85.7±10.7	95.6±3.0	P<0.001
(10^3/ml)	58.7±30.5	274.1±189.6	P<0.001
リンパ球(%)	13.3±10.2	3.5±2.1	P<0.001
(10^3/ml)	8.8±7.9	10.9±11.9	
好中球(%)	0.7±1.1	0.7±1.7	
(10^3/ml)	0.4±0.6	2.4±0.7	

*平均±SD

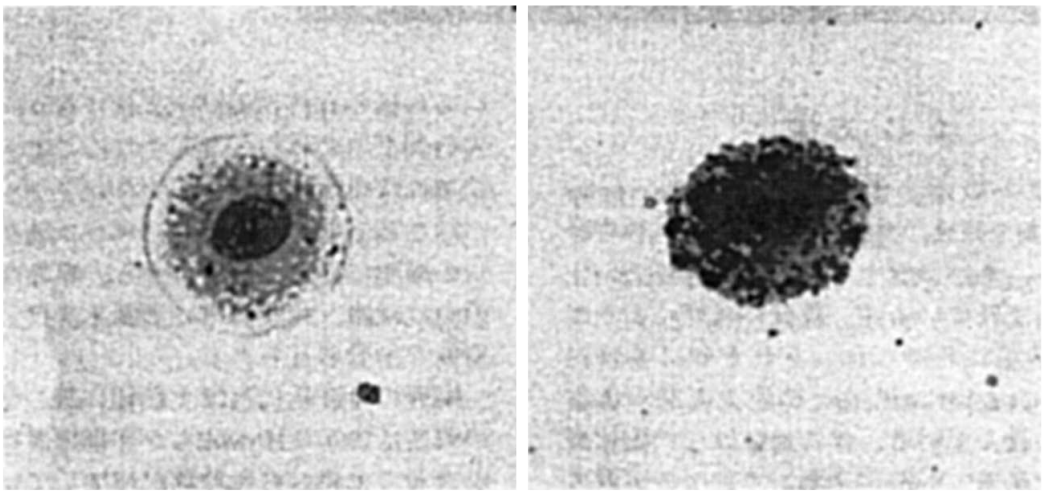

図1　喫煙者と非喫煙者の肺胞マクロファージへの影響
気管支肺胞洗浄(BAL)は，温生理食塩水60ml×5回，計300mlで行い，回収された肺胞マクロファージ．喫煙者の肺胞マクロファージの細胞質内に，タバコ煙粒子の取り込みが認められる．

る．本稿では，タバコ喫煙の免疫細胞機能へ及ぼす影響について，各免疫細胞別に最近の知見と自験成績を含めて解説したい．

マクロファージへの影響

タバコ煙は肺から吸入されるため，肺胞マクロファージがもっとも影響を受ける細胞である．肺胞マクロファージ数は，喫煙者で喫煙本数，年数に比例して増加している[7]．我々の成績でもBALにより回収された細胞は，非喫煙者に比べて，喫煙者で増加を示した(表1)．この細胞数の増加は，タバコ煙中の粒子をクリアランスするため肺でのマクロファージの増殖と末梢血単球が肺に誘導されたためであると考えられる．形態に関しては，喫煙者の肺胞マクロファージは，大型化し，表面の隆起，ラフリング，偽足などの特徴が観察され，細胞内にタバコ煙による色素沈着(図1)，ミトコンドリア，リボゾーム，針状の線維構造をしたリソゾームの増加が認められる[8]．

機能面に関しては，喫煙により貪食能，殺菌能の低下が報告されているが[9]，これはすでにタバコ煙中の粒子を取り込んでいるため，その後の貪食，殺菌能力が十分に発揮できないためである．PGE_2，LTB4の産生に対しては，喫煙により差がない報告と低下する報告があり，血中単球をニコチンで刺激した場合，産生が増強されるなど一定した見解は得られていない[10]．サイトカイン産生に関しては，IL-6，TNFαは抑制されるが，IL-1βに関しては，増強と低下が報告さ

れている[11)12)]，これはIL-1活性にIL-1RA活性が影響しているためであると思われ，マウスでもIL-1βのmRNAレベルでは抑制されている[13)]．表面抗原の発現に関しては，クラスⅡ抗原の低下が報告され，また我々の成績でもマウスにフィルター付きタバコ(タール15mg，ニコチン1.5 mg)を20本/1日，自動喫煙装置により10回喫煙させた肺胞マクロファージのCD11bおよび抗原提示に関係するクラスⅡ，B7-1抗原ともに抑制され，MLRによる抗原提示機能も低下していた(図2)[13)]．抗腫瘍活性に関しては，A549腫瘍細胞に対して，喫煙者では増殖抑制活性が低下していることが報告されている[14)]．一方，活性酸素の産生に関しては，喫煙者で増強され，マウスでも喫煙により増加する．しかし，PMAなどで肺胞マクロファージを試験管内で2次的に刺激すると産生は非喫煙に比べて低下している．つまり，タバコ煙によりすでに一次刺激されているため，二次的な刺激に対する反応性が傷害されていると考えられる．これら肺胞マクロファージ数，機能については，可逆的で一般的に喫煙を中止することにより非喫煙のレベルに戻ることが知られている．

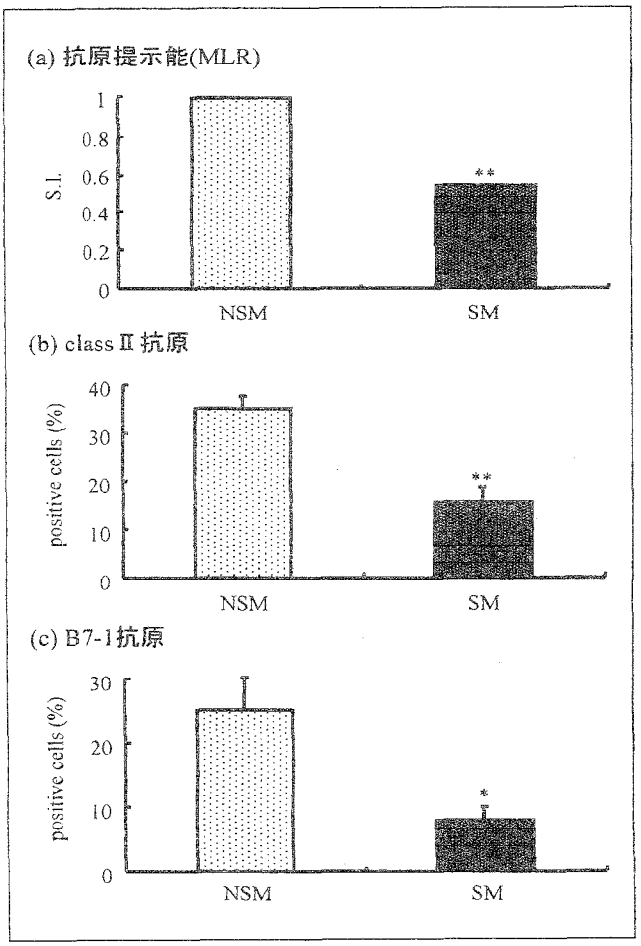

図2　喫煙によるマウス肺胞マクロファージ機能への影響
a：抗原提示能(MLR)
b：class Ⅱ抗原
c：B7-1抗原
喫煙はHamburg Ⅱ自動喫煙装置を用いて，CORESTA No.2タバコを1日20本，10回マウスに喫煙後，BALにより肺胞マクロファージを回収し，MLR反応とFACSにより解析した．
NSM：非喫煙マウス，SM：喫煙マウス，*：$P<0.05$，**：$P<0.01$

T細胞への影響

末梢血の総白血球数は喫煙者で増加している．末梢血のT細胞数に関しては，非喫煙者に比べて喫煙者で，増加する報告と差がない報告がされているが，ヘビースモーカー(50～120pack years)では増加する報告が多い[15)]．末梢血のT細胞サブセットに関しては，CD4とCD8の比率は一定した見解は得られていないのが現状であるが，肺のCD4とCD8の比率は，非喫煙者に比べて喫煙者ではCD4の減少，CD8の増加が知られている[12)]．

機能に関しては，PHA反応は差がないか喫煙者で低下している．動物実験では，急性の喫煙暴露では差がないが，慢性暴露で抑制されることが報告され[16)]，ConA反応の抑制，肺あるいは気管支周囲のリンパ節のT細胞では抗原誘導性の増殖の低下が認められている．T細胞依存性の抗体産生の系で，喫煙により抗体産生が抑制されたことから，ヘルパーT細胞機能が抑制されると報告されている[17)]．しかし，タバコの葉から抽出したタバコグリコプロテイン(TGP)がT細胞を分裂促進することから，喫煙によるT細胞機能の低下はタバコの燃焼産物によるものであると考えられる．抗腫瘍性に関しては，B16メラノーマに対する抗腫瘍性は著しく低下している．これら動物実験での細胞性免疫への喫煙の影響は，喫煙の暴露の期間，喫煙量により異なるが，喫煙量が多く期間が長ければ抑制される報告が多い[4)]．

サイトカインの産生に関しては，IL-4の産生は，

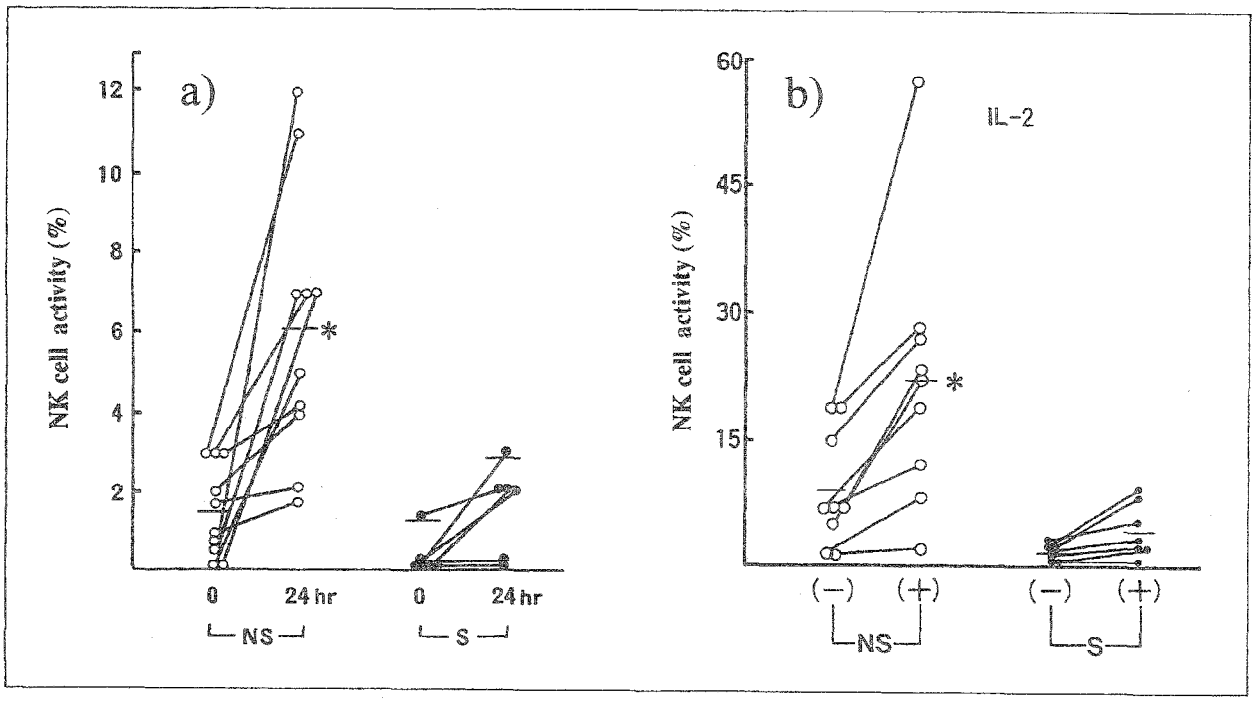

図3　喫煙の肺のNatural Killer(NK)活性に及ぼす影響
a：肺のNK活性，b：肺のNK細胞のIL-2への反応性
BALにより回収された細胞をシャーレ付着，ナイロンウールカラム法により分離し，^{51}Cr標識K562細胞を標的細胞としてNK活性(E/T＝10)を測定した．
NS：非喫煙者，S：喫煙者，(−)IL-2非処理，(＋)IL-2 50u/m*l*処理，＊：$P<0.05$

喫煙者で高く，喫煙者で血清IgEが高い報告と関連している[18]．また，IL-2の産生は，ニコチンを吸入させたラットの脾臓T細胞で増加している報告がある[19]．これはニコチンがT細胞のニコチンレセプターを発現させ，ニコチンがこれらのレセプターに結合しT細胞を活性化させた可能性が考えられ，喫煙者によるT細胞機能の低下と一致していない．しかし，喫煙者で血清中の可溶性IL-2レセプターの値が高いとの報告があることから，産生されたIL-2は可溶性のIL-2レセプターと結合することにより，喫煙者ではT細胞機能が抑制されることが考えられ，またマウスでニコチンがT細胞アネルギーを引き起こす報告もある[20]．

NK細胞への影響

末梢血のNK細胞比率に関しては，非喫煙者に比べて喫煙者で差は認められないが，NK細胞活性に関しては，抑制される報告と差がない報告があり，一定した見解は得られていない[15]．我々の成績でも喫煙による差は認められなかったが，これはライトスモーカー(4～45pack years)では差がないがヘビースモーカー(50～120pack years)では低下している．また，マウスの喫煙実験でも，慢性喫煙(208週以上の暴露)でNK活性が抑制されている[4]．

一方，肺のNK細胞活性は，末梢血に比べ低活性である．非喫煙者では24時間培養することにより，肺のNK活性は増強されるが，喫煙者では増強が認められない．また，IL-2への反応性も喫煙者のNK細胞では低下しており，非喫煙者のようにIL-2によるNK活性の増強は認められず，喫煙により肺のNK細胞は傷害されていることが認められる(図3)．肺のNK細胞活性が末梢血に比べて低い原因は，肺では肺胞マクロファージが多く存在するため，肺胞マクロファージによりNK細胞が影響を受け，さらに喫煙により強い影響を受けていると思われる．その抑制機序について検討を加えたところ，肺胞マクロファージを自己の末梢血NK細胞に添加し，その抑制程度を非喫煙者と喫煙者で比べると，喫煙者の肺胞マクロファージ添加により，非喫煙者に比べ強

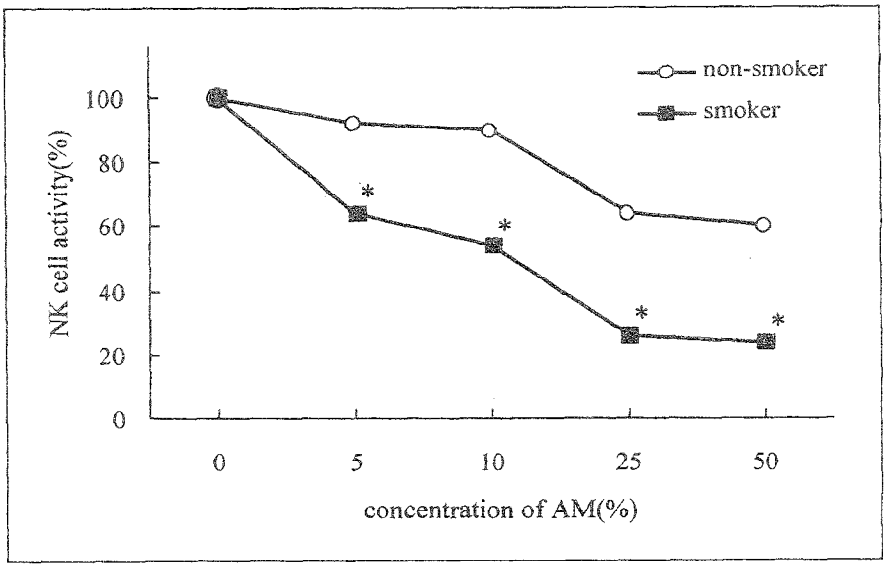

図4　喫煙による肺胞マクロファージ(AM)の自己末梢血NK活性に及ぼす影響
NK活性は，E/T-10にBALにより回収した自己肺胞マクロファージを各種濃度で添加後，AMのNK活性に及ぼす影響をAM非添加のNK活性を100％として検討した．
*：$P<0.05$

いNK活性の抑制が認められ，喫煙者の肺のNK活性抑制に肺胞マクロファージが関与していることが示された(図4)[21]．

肺胞マクロファージは，PGE_2，活性酸素を放出し，特に喫煙者では活性酸素の産生が高いことから，この抑制機序にPGE_2，活性酸素が関与しているか否かについてさらに検討を加えた．肺胞マクロファージと自己の末梢血NK細胞の混合培養系にO_2^-，H_2O_2，OHのスカベンジャーであるSOD，カタラーゼ，チオウレア，PGE_2のインヒビターであるインドメタシンを各種濃度で加え培養後，NK活性を測定した．SOD添加群で肺胞マクロファージ添加によるNK活性の抑制が回復され，喫煙者の肺のNK活性低下は，喫煙により肺胞マクロファージから産生される活性酸素の中のO_2^-によることが認められた(図5)．

B細胞への影響

喫煙者では，血清中のIgG濃度が減少しているが，血清IgAとIgMに関しては減少する報告と非喫煙者と差がない報告があり，一定した見解は得られていない[15]．IgGのサブクラスについては，IgG1，G3の濃度は非喫煙者と差がないが，IgG2濃度は低下していることが報告されていることから[22]，喫煙者の血清IgG濃度の低下は，IgG2の減少によると考えられる．また，B細胞マイトゲンや抗原に対して，喫煙者のB細胞では反応性が低下していることも報告されている[15]．しかし，末梢血のB細胞の比率は非喫煙者と差がないことから，喫煙者の血清IgG濃度の低下はB細胞数の低下によるのではなく，喫煙によりB細胞が機能的に傷害されていることを示している．動物実験でも，喫煙暴露により抗原に対するB細胞機能は抑制されている．しかし，無煙タバコ，TGP，タバコ葉中ポリフェリックタンパクはB細胞の増殖促進活性を示し，IgM，IgG，IgAの産生を刺激促進することがヒトおよびマウスで認められていることから，喫煙によるB細胞機能障害は，T細胞の場合と同様にタバコの燃焼産物によると思われる．

一方，血清IgE濃度に関しては，喫煙者で増加している．この影響は，女性より男性で多い．また，IgEの増加は，喫煙量と相関関係がある[23]．さらに，さい帯血のIgEは，妊娠中母親か両親の喫煙により高くなる．この喫煙者の血清IgE濃度の増加は，喫煙により気管支上皮の透過性が増し，侵入してきたアレルゲンが容易に所属のリンパ組織に侵入し易くなるため生じると思われる．また，IgEの産生を制御しているIL-4，IFN-γについては，非喫煙者に比べて喫煙者のTリン

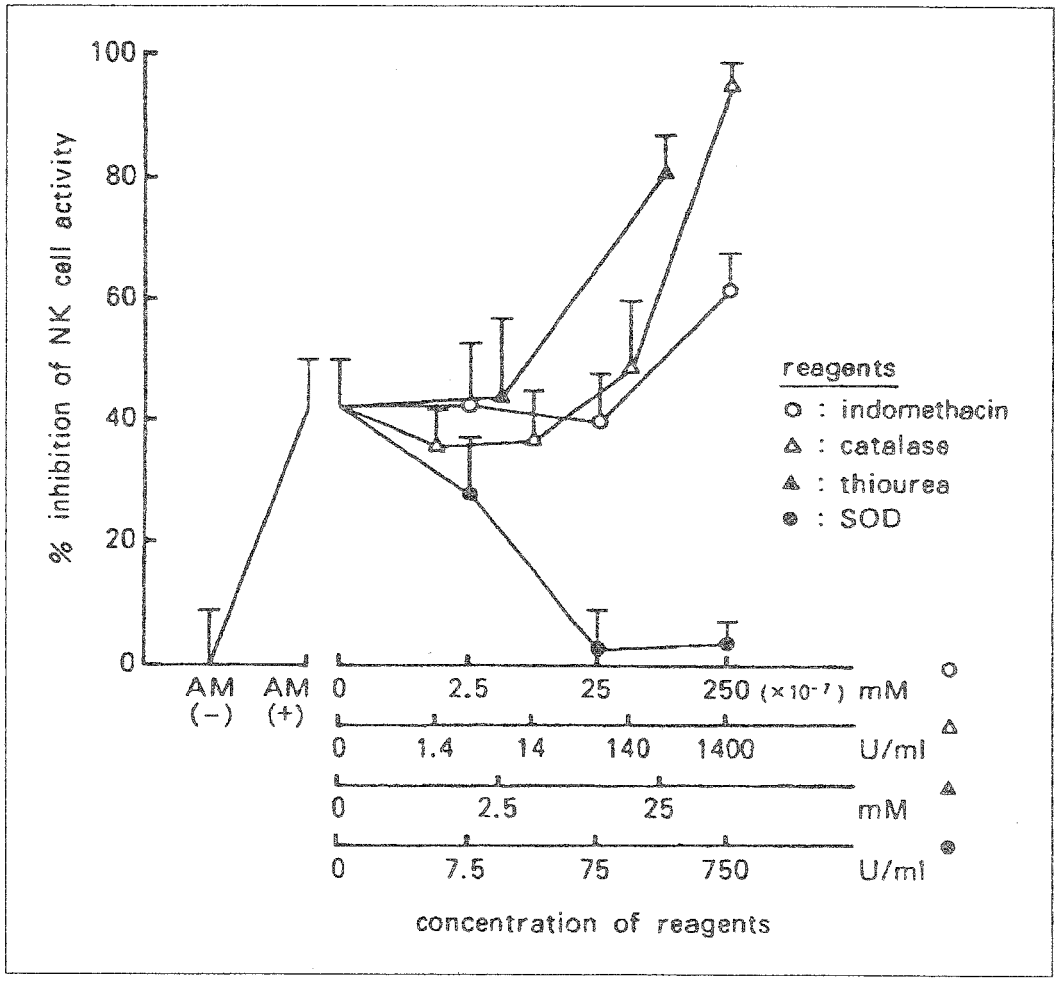

図5　喫煙者の肺胞マクロファージによるNK活性抑制に対する各種スカベンジャーの影響
(−)：AM非添加，(+)：自己末梢血NK活性(E/T=10)に25%濃度でAMを添加後，各種スカベンジャーを加え培養し，NK活性を測定した．NK活性の抑制率(%)は，AM非添加を0%として求めた．

パ球ではIL-4の産生は増加しているが，IFN-γに関しては両者に差がないことから，喫煙によるIL-4の産生増加が関与している可能性がある．

好中球への影響

非喫煙者に比べて，喫煙者では末梢血の好中球数は増加している．特に，ヘビースモーカーでは顕著である．喫煙中は肺毛細血管内での好中球の輸送が遅くなり，タバコ煙はこの好中球を活性化する．また，肺における好中球の流入を管理している補体系の二次経路をタバコ煙は活性化する[24]．補体系の活性化によりC5aが産生され，これにより肺毛細血管の透過性が増し，またC5aは好中球の走化性因子であることから，末梢血で増加した好中球の肺への流入が促進される．さらに，ニコチンにも好中球に対し走化作用がある．その結果，肺では好中球から遊離されるエラスターゼが増加し，またタバコ煙中の酸化物質によりα-1プロテアーゼインヒビター(α-PI)が不活化されるのと相まって，肺組織のエラスチン線維が傷害され，肺気腫が起こる．肺気腫の患者の好中球ではO_2^-の産生が増強されており，このO_2^-によりα-PIが不活化され，エラスターゼ/α-PIのアンバランスが生じ，肺でのエラスターゼの作用がより働き易い状況が出来，肺気腫の病変が形成される．また，この病変形成には，好中球と同様に喫煙により増加した肺胞マクロファージも関与している．最近ではタバコ煙中の発癌物質だけでなく酸化物質およびこれら細胞から産生される活性酸素により気管支肺上皮のDNA損傷が生じることが報告され[25]，タバコ喫煙により生じた活性酸素が，特にp53癌

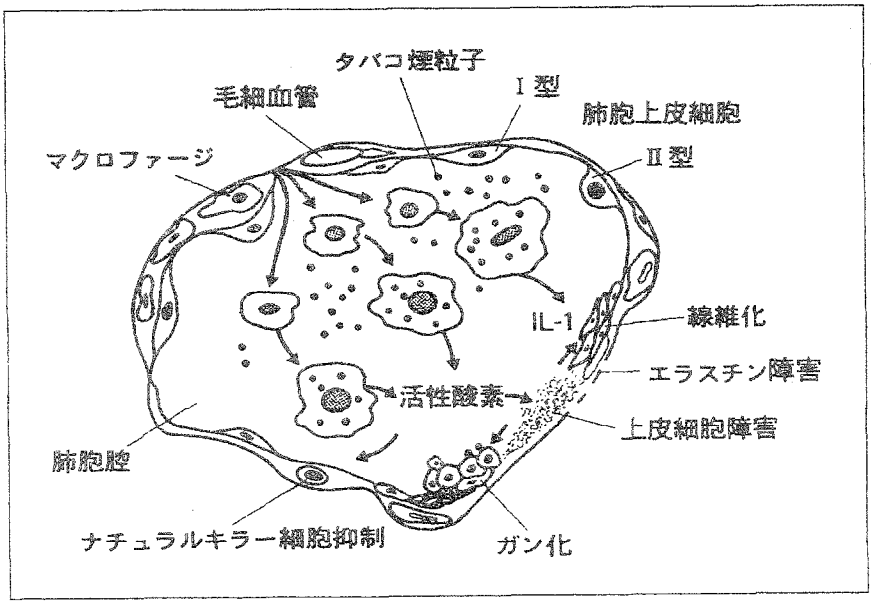

図6　喫煙の肺胞領域への影響

抑制遺伝子に変異を起こし，NK活性の抑制と相まって，喫煙者の気管支上皮癌の高い発生率と関係していることも考えられる．以上の成績をもとに，喫煙による肺胞領域への影響を模式図で示した(図6)．

おわりに

タバコ喫煙の免疫細胞への影響について，ヒトおよびマウスの報告を紹介した．いずれの成績も多くの場合，喫煙量に比例して免疫機能は抑制される．喫煙の正確な影響に関しては，ヒトの場合，タバコの喫煙期間，本数，吸い方，種類などの違いにより喫煙量(喫煙歴)と肺の環境(疾患歴)を一定にして喫煙の影響を評価することが困難なため，研究者により異なった成績がされ，一定した見解が得られないと思われる．そのため，喫煙の影響を正確に評価するには喫煙量を一定に出来，飼育環境も統一出来るため，肺の環境が一定に出来る動物実験の方が，タバコ喫煙による影響をより正確に評価出来ると思われる．喫煙による影響は主流煙の報告が多く，今後，副流煙による影響についても詳細な解明を期待したい．

文　献

1) Stober, W.: The measurement of "Environmental Tobacco Smoke" particulates. Toxicol. Lett., 35 : 125, 1987.
2) Howell, R.W.: Smoking habits and laboratory tests. Lancet, 2 : 152, 1970.
3) Esber, H.J., Menninger, F.F., Bogden, A.E., et al.: Immunological deficiency associated with cigarette smoke inhalation by mice. Arch. Environ. Health, 27 : 99, 1973.
4) Johnson, D.J., Houchens, P.D., Kluwe, M.W., et al.: Effects of mainstream and environmental tobacco smoke on the immune system in animals and humans. Toxicology, 20 : 369, 1990.
5) Reynolds, H.Y.: Bronchoalveolar lavage. Am. Rev. Respir. Dis., 135 : 250, 1987.
6) Merchant, R.K., Schwartz, D.A., Helmers, R.A. et al.: Bronchoalveolar lavage cellularity. Am. Rev. Respir. Dis., 146 : 448, 1992.
7) Takeuchi, M., Nagai, S. & Izumi, T.: Effect of smoking on natural killer cell activity in the lung. Chest, 94 : 688, 1989.
8) Pratt, S.A., Smith, M.H., Lodman, A.J., et al.: The ultrastructure of alveolar macrophage from smokers and non-smokers. Lab. Invest., 24 : 331, 1971.
9) Ortega, E., Barriga, C. & Rodriguez, A.B.: Decline in the phagocytic function of alveolar macrophage from mice exposed to cigarette smoke. Comp.

Immunol. Microbiol. Infect. Dis., 17 : 77, 1994.
10) Payne, J.B., Johnson, G.K., Reinhardt, R.A., et al.: Smokeless tobacco effects on monocyte secretion of PGE2 and IL-1 beta. J. Periodontal., 65 : 937, 1994.
11) Sauty, A., Mauel, J., Philippeaux, M.M., et al.: Cytostatic activity of alveolar macrophages from smokers and nonsmokers : role of interleukin-1 beta, interleukin-6 and tumor necrosis factor alpha. Am. J. Res. Cell. Mol. Biol., 11 : 631, 1994.
12) Nagai, S., Takeuchi, M., Watanabe, K., et al.: Smoking and interleukin-1 activity released from human alveolar macrophages in healthy subjects. Chest, 94 : 694, 1988.
13) Takeuchi, M., Nakajima, A., Yoshikawa, K., et al.: Effect of smoking on immunological functions of alveolar macrophages in mice. In *Tobacco Counters Health* (edited by Varma,A.K.), Macmilan Ltd, India, 2000, p.168.
14) Skold, C.M., Forslid, J., Eklund, A., et al. : Metabolic activity in human alveolar macrophages increase after cessation of smoking. Inflammation, 17 : 345, 1993.
15) Barbour, E.S., Nakashima, K., Zhang, B.J., et al.: Tobacco and smoking. Crit Rev. Oral. Biol. Med., 8 : 437, 1997.
16) Thomas, W.R., Holt, P.G. & Keast, D.: Cellular immunity in mice chronically exposed fresh cigarette smoke. Arch. Environ. Health, 27 : 372, 1973.
17) Thomas, W.R., Holt, P.G. & Keast, D.: Humoral immune response of mice with long-term exposure to cigarette smoke. Arch. Environ. Health, 30 : 78, 1975.
18) Byron, K.A., Varigos, G.A. & Wootton, A.M.: IL-4 production is increased in cigarette smokers. Clin. Exp. Immunol., 95 : 333, 1994.
19) Petro, T.M., Peterson, D.S. & Fung, Y.K.: Nicotine enhances interleukin production of rat splenic T-lymphocytes. Immunopharmacol. Immunotoxicol., 14 : 463. 1992.
20) Geng, Y., Savage, M.S., Johnson, L.J., et al.: Effect of nicotine on the immune response. J. Immunol., 156 : 2384, 1996.
21) Takeuchi, M., Nagai, S., Nakajima, A., et al.: Inhibition of lung natural killer cell activity by smoking. Respiration, 68 : 262, 2001.
22) Quinn, S.M., Zhang, I., Gunsolley, J.C., et al.: Influence of smoking and race on immunoglobulin G subclass concentrations in early-onset periodontitis patients. Infect. Immun., 64 : 2500, 1996.
23) Jensen, E.J., Pedersen, B., Schmidt, E., et al.: Serum IgE in nonatopic smokers, nonsmokers, and recent exsmokers. Allergy, Clin. Immunol., 90 : 224, 1992.
24) Robbins, R.A., Nelson, K.I., Gossman, G.L., et al.: Complement activation by cigarette smoke. Am. J. Physiol., 260 : L254, 1991.
25) Howard, D.J., Briggs, L.A. & Pritsos, C.A.: Oxidative DNA damage in mouse heart, liver and lung tissue due to acute side-stream tobacco smoke exposure. Arch. Biochem. Biophys., 352 : 293, 1998.

第3章

中田 博

ムチンおよびムチン型糖鎖の多様性とその意義

ムチンは消化管や気道の内膜を被う高分子の粘液性糖タンパク質である．ムチンは分泌型と膜結合型に分類され，前者はゲルを形成し粘膜を保護する．後者は情報伝達や細胞間接着を制御する分子としての機能が示唆されている．セリン，スレオニン，プロリンで全アミノ酸の50％以上を占め，一定のアミノ酸配列の繰り返し構造（タンデムリピート）をもつ．また，糖含量が全体の50％以上を占め，癌性変化に伴い癌関連糖鎖抗原を発現する．また，上皮細胞以外にも，コアタンパク質の全体もしくは一部にセリン，スレオニンに富むムチン様領域をもつムチン様糖タンパク質が産生され，その生物学的機能が明らかになりつつある（概略図）．

【キーワード&略語】
ムチン，O-グリカン，癌関連糖鎖抗原，タンデムリピート
MAN：Mannose（マンノース）
SA：Sialic acid（シアル酸）
Gal：Galactose（ガラクトース）
GalNAc：N-Acetylgalactosamine（N-アセチルガラクトサミン）
GlcNAc：N-Acetylglucosamine（N-アセチルグルコサミン）
GlyCAM-1：Glycosylation dependent cell adhesion molecule-1
PSGL-1：P-selectin glycoprotein ligand-1
MAdCAM-1：Mucosal addressin cell adhesion molecule-1
VWF：von-Willebrand factor（フォン・ビルブラント因子）
Fuc：Fucose（フコース）

1 ムチン

1）コアタンパク質の構造

ムチンには多数の糖鎖が結合し，タンパク質レベルでのアミノ酸配列の解析はきわめて困難であり，ほとんどのムチンのアミノ酸配列は塩基配列より決定された．現在，部分配列も含めると十数種のムチン遺伝子が報告されている[1]．特徴的な性質としては，ほとんどのムチンが複数の反復配列（タンデムリピート）をもつことである．その反復配列の反復数の違いにより遺伝的多型を示す．表1に示すように，反復配列一単位のアミノ酸の数はそれぞれのムチンにより異なるが，セリン（Ser），スレオニン（Thr）のいずれかあるいは両方のアミノ酸に富み，O-グリカン*の結合する部位となっている．MUC2，5AC，5B，6などのムチン遺伝子は分泌型ムチンをコードし，染色体11p15.5にクラスターで存在する．これらのムチンは，通常ゲルの状態で粘膜を覆っている．最も研究されているヒト小腸ムチン（MUC2ムチン）は，4,500個以上のアミノ酸残基からなるコアタンパク質をもち，2つの異なるスレオニンに富む

＊O-グリカン
アミノ酸の水酸基と結合している糖鎖をO-グリカンと総称するが，結合している糖残基の種類により分類される．そのなかで，GalNAcがセリン，スレオニンと結合しているものをムチン型糖鎖と呼ぶ．そのほか，マンノース（Mannose：Man）やGlcNAcがセリン，スレオニンと結合しているもの，Galがヒドロキシリジンに結合しているものなどがある．

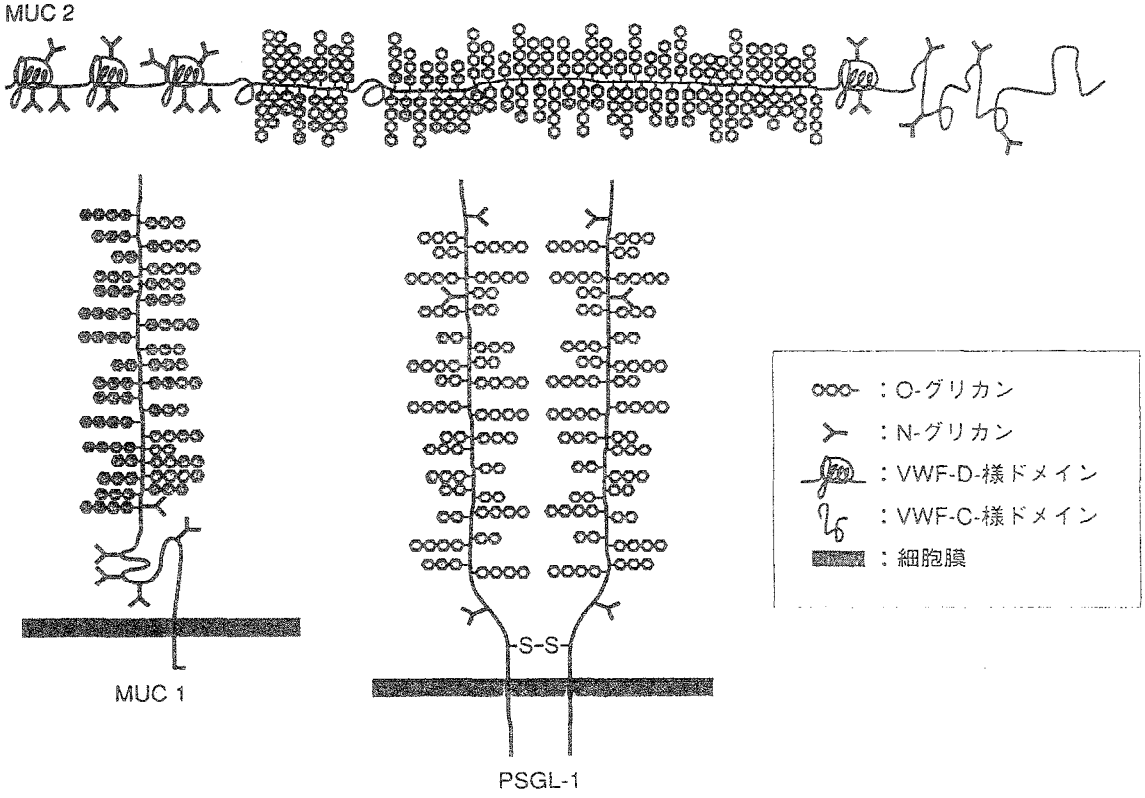

概略図 ムチンおよびムチン様糖タンパク質

上皮細胞の産生するムチンには，MUC1やMUC2のようなそれぞれ膜結合型と分泌型が存在する．一定のアミノ酸配列の繰り返し構造（タンデムリピート）をもち，セリン，スレオニンを多く含みGalNAcを介してO-グリカンで修飾されている．糖含量は全体の50％以上を占める．癌性変化に伴い癌関連糖鎖抗原を発現する．上皮細胞以外にもコアタンパク質の全体もしくは一部にセリン，スレオニンに富むムチン様領域をもつムチン様糖タンパク質が見出されている．PSGL-1（P-selectin glycoprotein ligand-1）のようにセレクチンのリガンド糖鎖をもつ分子として同定されたものが多い．〔VWF（von-Willebrand factor：フォン・ビルブラント因子*）については用語解説参照〕

反復配列ドメイン，システインに富む4つの繰り返しドメインで構成されている．C末端側に存在する反復配列のユニットは23アミノ酸残基からなり，そのうちスレオニンが14残基存在する．反復配列を100～115単位含み多型性を示す．一方，MUC1，3，4，12，16は膜結合型ムチンで，多くの上皮細胞や種々の癌細胞に存在する．MUC3，11，12遺伝子は染色体7q22に局在している．MUC1分子では，分子の中央部に20アミノ酸残基からなる反復配列が存在し，高度の多型性を示す．MUC1タンパク質の細胞質ドメインは比較的種差が少ない．乳腺腫瘍細胞ではMUC1分子は微絨毛に局在し，細胞骨格と結合していることが示唆されている．

2）ムチンの糖鎖

i）ムチン型糖鎖の構造

ムチンにはN-グリカンも少量存在するが，大半の糖鎖はO-グリカンで，単糖から20個以上の糖からなるオリゴ糖で構成され，多様である．糖鎖の構造は，母核構造，Galactose（Gal）

＊VWF（フォン・ビルブラント因子）
血管内皮細胞や骨髄巨核球で産生され，N末端のS-S結合により多量体を形成する．血小板との接着に関与し，止血初期にかかわる．また，血液凝固Ⅷ因子と複合体を形成し，Ⅷ因子を安定化する．

表1 ◆ムチンの反復配列のアミノ酸配列

ムチン	アミノ酸配列
MUC1	PGSTAPPAHGVTSAPDTRPA (20)
MUC2	PTTTPITTTTTVTPTPTPTGTQT (23)
MUC3	HSTPSFTSSITTTETTS (17)
MUC4	TSSASTGHATPLPVTD (16)
MUC5AC	TTSTTSAP (8)
MUC5B	SSTPGTAHTLTVLTTTATTPTATGSTATP (29)
MUC6	SPFSSTGPMTATSFQTTTTYPTPSHPQTTLPTHVP-PFSTSLVTPSTGTVITPTHAQMATSASIHSTPTGT-IPPPTTLKATGSTHTAPPMTPTTSGTSQAHSSFST-AKTSTSLHSHTSSTHHPEVTPTSTTTITPNPTSTG-TSTPVAHTTSATSSRLPTPFTTHSPPTGS (169)
MUC7	TTAAPPTPSATTPAPPSSSAPPE (23)
MUC8	TSCPRPLQEGTPGS (14)
MUC9	GAMTMTSVGHQSMTP (15)
MUC11	SGLSEESTTSHSSPGSTHTTLSPASTTT (28)

ムチンのコアタンパク質にみられる典型的なタンデムリピートのアミノ酸配列を示す．（ ）はアミノ酸残基数を示す

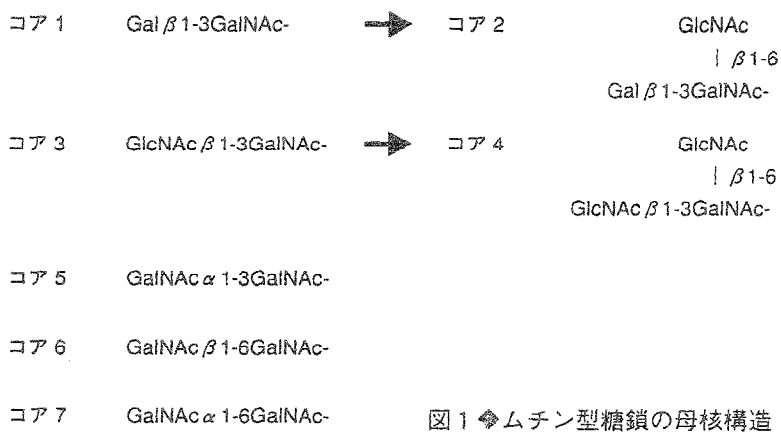

図1 ◆ムチン型糖鎖の母核構造
ムチン型糖鎖の母核構造は8つの型に分類される（詳細は本文参照）

とN-Acetylglucosamine（GlcNAc）の繰り返し構造からなる基幹構造．それにSialic acid（SA）やFucose（Fuc）の結合した修飾構造の部分から成り立っている．母核構造は生合成の中間体であり，図1に示すように，コアタンパク質のセリンまたはスレオニン残基に結合したN-Acetylgalactosamine（GalNAc）とこの糖に直接結合した1個あるいは2個の糖からなり，コア1～8の8種類が知られている．GalとGlcNAcの繰り返し構造からなる基幹構造には，Galβ1-3GlcNAc（タイプ1糖鎖）とGalβ1-4GlcNAc（タイプ2糖鎖）の2種類が存在する．末端の修飾構造には，GalNAc，Gal，Fuc，SAなどが結合した構造がある．

ii）癌関連糖鎖抗原

ヒト上皮性癌細胞を免疫原として，癌関連糖鎖抗原を認識するモノクローナル抗体を作製すると，その大半がムチンのO-グリカン上の糖鎖を認識する抗体であることがわかった．ム

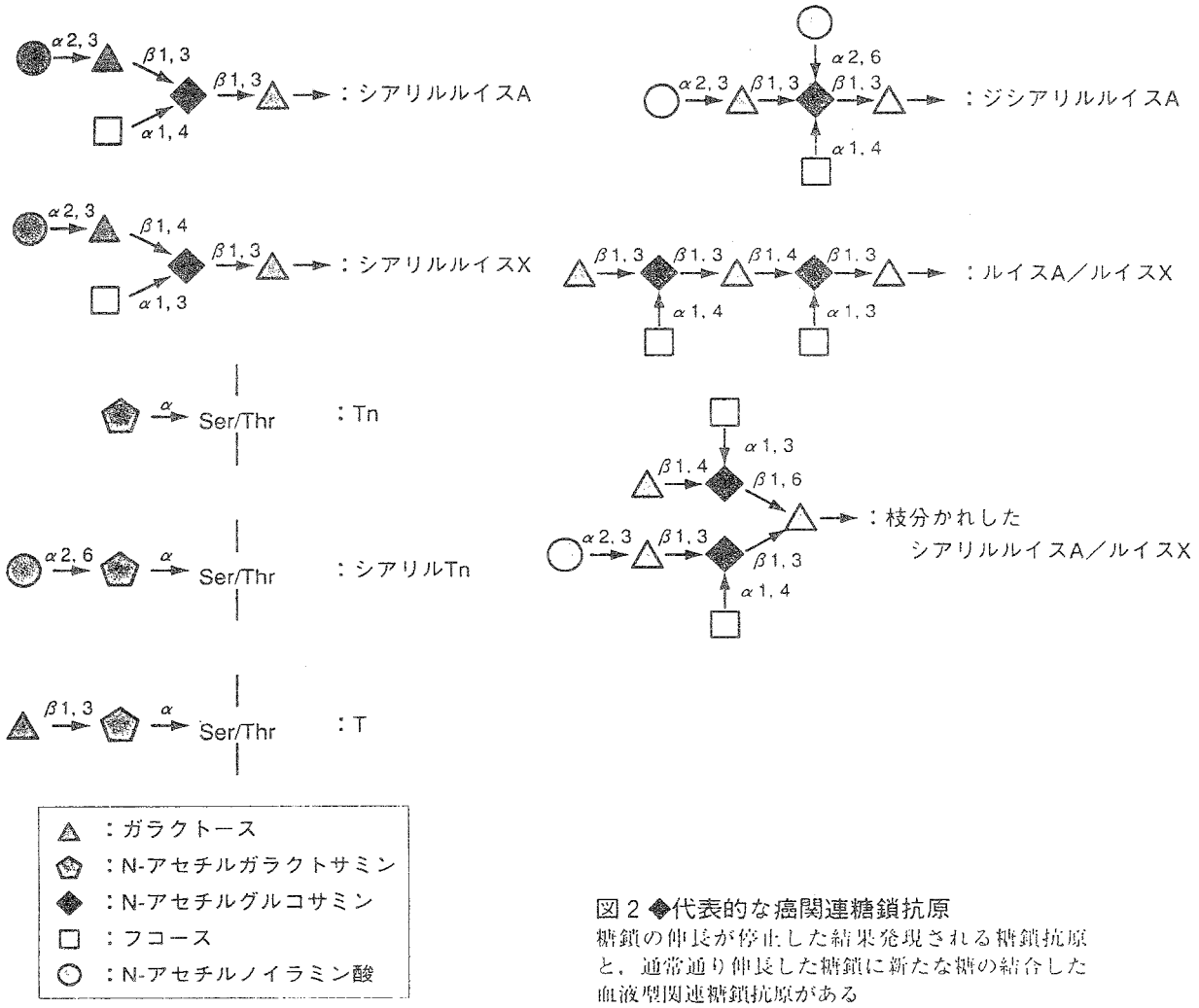

図2 ◆代表的な癌関連糖鎖抗原
糖鎖の伸長が停止した結果発現される糖鎖抗原と，通常通り伸長した糖鎖に新たな糖の結合した血液型関連糖鎖抗原がある

チン上の糖鎖の解析は，このようなモノクローナル抗体のエピトープの構造を明らかにすることで発展してきた．ムチン型糖鎖にみられる癌性変化は，大別して2つに分類される．すなわち，糖鎖の伸長が停止した，いわゆる“糖鎖不全”による異常な糖鎖と通常の血液型抗原にさまざまな糖が結合した糖鎖に大別される．図2に代表的な癌関連糖鎖抗原を示す．Tn抗原，T抗原（1型コア）およびTn抗原からの伸長がシアル酸の結合により停止したシアリルTn抗原は，大腸癌などにおいて高い発現を示す．これらの癌関連糖鎖抗原のエピトープの構成単位としては，図2に示す通りであるが，実際の強い抗原性をもつ構造としては，これらの構成単位のクラスターである可能性が高い．われわれの調製したモノクローナル抗体MLS128，132は，それぞれGalNAc-Ser/Thr，SA-GalNAc-Ser/Thrが3個および4個連続した糖ペプチドを認識する[2)3)]．消化器系の癌患者の血液中に頻度高く検出されるシアリルルイスA抗原は，タイ

＊癌関連糖鎖抗原
正常細胞にも見出されるが，癌細胞では量的に著しく多く発現したり，発現部位が異なっているような糖鎖抗原をいう．糖鎖抗原は糖タンパク質や糖脂質に発現される．癌性変化に伴って，糖鎖不全（T抗原やTn抗原）により生じた糖鎖抗原と，コア構造より糖鎖が伸長しポリラクトサミン上にシアル酸やフコースなどが付加することにより生じた血液型関連抗原が存在する．

プ1糖鎖にシアル酸とフコースの結合した構造である．タイプ2糖鎖をもつ糖鎖抗原としてはルイスX抗原などがある．本抗原は，肺癌や卵巣癌の患者の血液中に多く見出されるとともに，胎児性糖鎖抗原でもある．また，癌細胞に発現しているMUC1ムチンには，コアタンパク質中のPro-Asp-Thr-Arg-Proのスレオニンに GalNAc残基が結合していないケースがしばしばみられ，この構造が抗原性をもつ．癌患者より分離されたキラーT細胞の中にこのコアタンパク質抗原を認識するものがしばしば認められる．

iii）ムチン型糖鎖の生合成

N-グリカンの生合成とは異なり，ドリコール中間体#1の関与や生合成の過程でのグリコシダーゼによるプロセシングを受けない．すなわち，1つ1つの糖が糖ヌクレオチドよりそれぞれの酵素により転加される．生合成は，UDP-GalNAc（ポリペプチドGalNAcトランスフェラーゼ）によりペプチド鎖のセリン/スレオニン残基へのGalNAcの転加により開始される．本酵素の遺伝子はすでに十数種報告されている．O-グリコシル化されるセリン/スレオニン残基周辺のペプチドのコンセンサス配列はないとされている．それぞれの酵素は多少オーバーラップしているが，少しずつ違う基質特異性をもっている．個々の細胞におけるこれらのアイソザイムの発現パターンの違いにより，O-グリコシル化のパターンが決められていると考えられている．また，これらの酵素はシスゴルジ体*に局在している．われわれは，前項で述べた糖鎖のクラスターを形成するには，本酵素のアイソザイムのうちどの酵素が関与しているかを検討した．MUC2のタンデムリピートのユニットに相当するペプチドを基質として検討した結果，3個連続したスレオニン残基にGalNAcを転加しうる酵素はUDP-GalNAc（ポリペプチドGalNAcトランスフェラーゼ）3であることを明らかにした[1]．また，本アイソザイムのmRNAの発現は，ヒト腸癌組織で著しく亢進していることも示した．前述したように，GalNAc1α-Ser/ThrにGlcNAc，GalまたはGalNAcがそれぞれの酵素により転加されるとコア1～8の構造物が合成される．注目される酵素は，コア1からコア2を合成するコア2β6-GlcNAcトランスフェラーゼであるが，本酵素にも数種のアイソザイムが存在する．白血病細胞や活性化Tリンパ球などで高い活性を示すLタイプコア2β6-GlcNAcトランスフェラーゼは，O-グリカン上のポリラクトサミン鎖を合成するうえで律速酵素となっている．ポリラクトサミン鎖の修飾構造の中に，前述した血液型糖鎖抗原が合成されることから，本酵素の重要性は明らかである．末端の修飾構造を形成する糖は，SA，Fuc，GalNAcそれにGlcNAcであるが，この場合も同じ糖を同じ結合様式で転加する酵素でもアクセプターに対しさまざまな特異性をもつ複数の酵素集団からなるケースが多い．例えば，α3Fucトランスフェラーゼも複数の酵素が存在し，FucT-ⅣとⅦはセレクチン*のリガンドであるシアリルルイスXやスルホルイスXを合成する．

#メモ1：ドリコール中間体

ポリプレノールで，N-グリカンの生合成過程で糖を運搬する中間体として働く．

*シスゴルジ体

ゴルジ体の層板は，凸面から凹面にかけて順番にシス部（cis），中間部（medial），トランス部（trans）に分けられる．粗面小胞体でつくられたタンパク質はシスゴルジ体へ運ばれる．ムチンコアタンパク質へのGalNAcの付加は，主にここでなされる．

*セレクチン

糖鎖を認識するタンパク質，すなわちレクチン（基本編-第7章，UP TO DATE-6，参照）の1つである．白血球に構成的に発現しているL-セレクチン，炎症性サイトカインなどの刺激により血管内皮上に発現するE-セレクチン，ヒスタミンなどの刺激により血管内皮や血小板に発現するP-セレクチンの3つの糖結合膜タンパク質をセレクチンファミリーという．構造としては，N末端よりCa^{2+}依存的に糖を認識するC型レクチン様ドメイン，EGF様ドメイン，補体結合タンパク質様ドメインを共通にもつ．白血球のローリング現象，リンパ球のホーミング，癌の転移（トピックス編-2，参照）などに関与している．

3）ムチンの機能

粘膜上皮を覆ってゲルを形成する分泌型ムチンは，上皮の乾燥を防ぎ表面を潤滑に保つ．消化管では，胃酸，消化酵素や細菌から防御する．また，気道では外来の異物や細菌から保護する働きをする．近年，このような物理的なバリヤー以外の機能も報告されつつある．A. Velcichらは胃腸で最も多量に存在するMUC2ムチンの欠損マウスを作製した[5]．1年後には小腸と大腸において，それぞれ47％と21％に発癌が認められた．小腸上皮細胞の増殖の亢進，アポトーシスの減少，細胞移動の増加などの現象の結果と考えられているが，上記のムチンの物理的保護の欠失に伴う現象なのかその他の原因によるものかは明確でない．膜結合型ムチンについては，細胞表面に突出した構造をとることから，免疫系による攻撃を回避させたりする働きがあると考えられている．MUC1ムチンは，上皮細胞のアピカル側に局在し，その細胞質部分は，細胞骨格と連携しているといわれている．また，細胞質側のチロシンがリン酸化され，SH2含有タンパク質[#メモ2]がリクルートされ情報伝達分子として機能する．また，MUC4に相当するラットのムチンであるASGP2（Ascites sialoglycoprotein 2）は，EGF（Epidermal growth factor）様ドメインを介してErbB2受容体[*]と相互作用し，ErbB2チロシンキナーゼの活性を高める．これは癌の進展に関与する因子の1つと考えられている[6]．

2 ムチン様糖タンパク質

前項までに述べたムチンのほかに，上皮細胞以外の細胞にもコアタンパク質の多くの部分あるいは一部にセリン，スレオニンに富む領域（ムチン様領域）をもつ糖タンパク質が数多く見出されている．これらの膜タンパク質を総称してシアロムチンファミリーとも呼ぶ．このファミリーに属する糖タンパク質は，セレクチンのリガンド糖鎖をもつ分子として同定されたものが多い．

1）GlyCAM-1

GlyCAM-1（Glycosylation dependent cell adhesion molecule-1）は，末梢リンパ節の高内皮細静脈に特異的に存在し，L-セレクチンのリガンドをもつタンパク質として同定された．分子量50 kDで分子内にセリン，スレオニンに富む2つの領域があり，O-グリカンが結合している．そのO-グリカン上に6′-硫酸化シアリルルイスX構造をもち，L-セレクチンと結合する．

2）PSGL-1

PSGL-1（P-selectin glycoprotein ligand-1）は，好中球細胞表面に存在し，P-セレクチン結合タンパク質として同定された．ほとんどのエクトドメイン（細胞膜貫通型タンパク質の細胞外に露出した部分）がセリン，スレオニンに富むムチン様ドメインからなり，O-グリカンが結合している．細胞表面ではジスルフィド結合によりホモダイマーとして存在する．P-セレクチンとの結合には，O-グリカン上のシアリルルイスX構造に加えて，N末端付近の硫酸化さ

＃メモ2：SH2（src homology 2）
リン酸化チロシンを認識する部位．

＊ErbB2受容体
EGF受容体はトリ赤芽球症ウイルス（erythroblastosis virus）の癌遺伝子*v-erbB*と高い相同性がある．また，いくつかのEGF受容体様似の分子が存在し，これらには*v-erbB-2*，*-3*，*-4*があり，いずれも受容体チロシンキナーゼである．

＊パイエル板
哺乳動物の主に回腸に存在するリンパ小節のかたまりで，リンパ球や形質細胞を含む．腸内細菌に対する生体防御に関与する．

＊インテグリン
α，β鎖からなるヘテロダイマーで，コラーゲン，ラミニン，フィブロネクチンなどと結合する．少なくとも16種類のαサブユニットと8種類のβサブユニットが存在する．

れたチロシンが必要である．PSGL-1は好中球のほかに単球やリンパ球にも広く発現している．炎症部位における白血球のローリング（UP TO DATE-5，参照）は，このPSGL-1上の糖鎖とE-セレクチンの結合も関与している．

3) MAdCAM-1

MAdCAM-1（Mucosal addressin cell adhesion molecule-1）は，パイエル板*や腸間膜リンパ節に発現し，リンパ球と結合する分子として同定された．3つの免疫グロブリン様ドメインをもち，第2，第3免疫グロブリン様ドメインの間にムチン様領域をもつ．糖鎖を介してL-セレクチンと結合するほかに，インテグリン$\alpha 4\beta 7$とも結合する．

おわりに

ムチンは巨大分子で，コアのポリペプチド鎖は遺伝的多型性を示し，糖鎖は多様であることからその研究は困難をきわめた．しかし，遺伝子レベルの研究も加わり次第にその概要がわかってきた．機能的な分子としてのムチンは，むしろ比較的解析の容易なムチン様分子から先鞭がつけられた．PSGL-1などを代表として，ムチン型糖鎖が情報認識分子として機能することがわかった．ムチン上の糖鎖は，癌関連糖鎖抗原も含めてより多様であり，その多様性が情報認識に機能していることは十分に考えられる．特に，その多くが癌のマーカーとして研究の対象とされてきた癌関連糖鎖抗原についても機能的側面を示唆する結果が報告されつつある．

参考文献

1) Dekker, J. et al.：The MUC family. an obituary TRENDS in Biochemical Science, 27：126-131, 2002
2) Nakada, H. et al.：Epitopic structure of Tn glycophorin A for an anti-Tn antibody (MLS 128). Proc. Natl. Acad. Sci. USA, 90：2495-2499, 1993
3) Tanaka, N. et al.：Binding characteristics of an anti-Sia α 2-6GalNAc α -Ser/Thr (sialyl Tn) monoclonal antibody (MLS 132). Eur. J. Biochem., 263：27-32, 1999
4) Inoue, M. el al.：High density O-glycosylation of the MUC2 tandem repeat unit by N-acetylgalactosaminyltransferase-3 in colonic adenocarcinoma extracts. Cancer Res., 61：950-956, 2001
5) Velcich, A. et al.：Colorectal cancer in mice genetically deficient in the mucin Muc 2. Science, 295：1726-1729, 2002
6) Carraway Ⅲ, K. L. et al.：An intramembrane modulator of the ErbB2 receptor tyrosine kinase that potentiates Neuregulin signaling. J. Biol. Chem., 274：5263-5266, 1999

参考図書 ……もう少し詳しく知りたい人に

- 「糖とタンパク質との接点」福田 稹，『糖鎖の多様な世界』（木幡 陽 他/編），グリコバイオロジーシリーズ①：1-48，講談社，1993
- 「ムチンの癌性変化とムチン型糖鎖の異常」五艘行信，堀田恭子，『グリコパソロジー』（箱守 仙一郎 他/編），グリコバイオロジーシリーズ⑥，：65-75，講談社，1993
- 「シアロムチンファミリー」神田英伸 他，『細胞工学：接着分子ハンドブック』（宮坂昌之/編）：130-138，秀潤社，2000
- 「Pathways of O-glycan biosynthesis in cancer cells.」Brockhausen, I.，『Biochemica. Biophysica. Acta.』，1473：67-95，Elsevier Science，1999

１）研究成果要旨

〈岡山〉

「糖鎖シグナルと生体防御」の研究プロジェクト実施期間中に、岡山らは、マウス・ルイス肺癌由来の転移能の異なるいくつかのクローン性株細胞を樹立し、それを用いて、シンデカン-2（以下 SN2 と省略）の発現量と転移能との間に逆相関の存在することを明らかにし、その背後に、（１）SN2 が、血管新生制御能を持つこと、（２）SN2 がインテグリン$\alpha 5\beta 1$ との協調下でアクチン細胞骨格形成制御に関与していること、及び（３）SN2 とマトリックス・メタロプロテアーゼ（MMP）-2 活性化受容体（MT1-MMP/TIMP 複合体分子）との間で proMMP-2 の競合的奪い合いを介した MMP-2（癌転移への直接的関与が示されている）活性化制御能を持つことを明らかにした。更には、新規物質硫酸化ジェランが強い転移抑制活性を示すことを発見し（特許申請中：出願番号：特がん 2004-244405）、抗転移剤としての臨床的応用の可能性を示した。

〈中田〉

１）上皮性癌細胞の産生するムチンの生物学的意義について；上皮性癌細胞の産生するムチンと免疫系細胞との相互作用を解析し、癌組織におけるムチンの生物学的意義について明らかにしてきた。ムチンに結合しうる免疫系細胞上の受容体を検索した結果、単球／マクロファージ上のスカベンジャーリセプター（SCR）や種々の免疫系細胞上のシグレックファミリー（シグレック 2, 3, 7）についてムチンと結合しうることがわかった。SCR を介した系では、ムチンの結合によりシクロオキシゲナーゼ 2 が誘導され、PGE2 の産生が亢進した。PGE2 により免疫系のバランスが Th2 に偏ること、血管新生因子の産生亢進などを通して、癌細胞の増殖・進展に有利な環境を整えていることがわかった。シグレックについても、B 細胞のシグナル伝達の抑制や NK 細胞の細胞障害活性のムチンによる抑制などが明らかになった。

２）マウス脳に存在するシンデカン-3 の生物学的意義について；マウス胎児における癌胎児性糖鎖抗原の発現を検討する過程で、脳特異的に Tn 抗原が発現することを見いだした。コアタンパク質はシンデカン-3 であることを示すとともに、ニューロカンと結合することを見いだした。また、この相互作用は小脳顆粒細胞の神経突起の形成に関与することを見いだした。

〈竹内〉

喫煙による肺胞マクロファージの免疫機能、遺伝子損傷、ガン細胞の肺転移への影響とその機構についてマウスに一定量、一定期間シガッレトタバコ主流煙を曝露し検討した。喫煙により、肺胞マクロファージの抗原提示機能の低下、LPS による B 細胞増殖反応の低下が認められ、その低下機構には喫煙により産生増強された活性酸素により抗原提示に関係した肺胞マクロファージのクラス II、B7-1 と LPS に対する CD14 などの細胞表面抗原発現、また IL-1β、TNA-αの mRNA 発現が抑制されたことが示された。さらに、これらの発現低下は、肺胞マクロファージの DNA 損傷による可能性が示唆された。また、肺転移に関しては、喫煙マウスで肺転移が促進され、肺毛細血管に ICAM-1 の発現が認められた結果より、ガン細胞が毛細血管壁に接着し易くなり肺転移が促進された可能性が示唆された。これらの成績より、喫煙により肺の免疫機能は低下し、特に肺胞マクロファージを介した B 細胞反応系が強く抑制されていたことから、喫煙により肺感染が起こり易い状況が引き起こされていると考えられる。

２）評価

本プロジェクトは糖鎖生物学と癌免疫学の第一線の研究者をそろえ、多角的視野からプロジェクトを推進できる優れた組織体制が組まれている。研究内容は癌の進展における糖鎖の役割の研究に焦点が良く絞られている。研究成果のうち、岡山らによるヘパラン硫酸シンデカン-2 の癌転移抑制作用は画期的な発見である。岡山らはさらに微生物や海藻由来の多糖であるジェランを化学的に硫酸化したものに転移抑制作用があることを見いだしており、臨床応用が十分に期待できる。中田らは癌細胞の産生するムチンが単球・マクロファージのスカベンジャーリセプターに結合し、COX2 および PGE2 の産生を誘導することにより癌細胞の増殖・進展を促進することを見いだした。癌細胞の産生するムチンはシグレックとも結合し免疫抑制を惹起することを見いだした。これらの研究は今後がんの診断・治療への応用が期待できる。竹内らは喫煙が発癌のみならず癌の肺転移にも密接に関与することを解明しており、転移防止に役立つ発見と考えられる。総じて、研究期間内に臨床応用可能な有意義なシーズが多数得られており、これらの成果はバイオベンチャー開発拠点の整備事業として高く評価できる。

１）研究成果要旨

〈岡山〉

「糖鎖シグナルと生体防御」の研究プロジェクト実施期間中に、岡山らは、マウス・ルイス肺癌由来の転移能の異なるいくつかのクローン性株細胞を樹立し、それを用いて、シンデカン-２（ヘパラン硫酸糖鎖を持つプロテオグライカン）の発現量と転移能との間に逆相関の存在することを明らかにし、その背後に、（１）シンデカン-２が、血管新生制御能を持つこと、（２）シンデカン-２がインテグリン $\alpha5\beta1$ との協調下でアクチン細胞骨格形成制御に関与していること、及び（３）シンデカン-２とマトリックス・メタロプロテアーゼ（MMP）-２活性化受容体（MT1-MMP/TIMP 複合体分子）との間で proMMP-2 の競合的奪い合いを介した MMP-2（癌転移への直接的関与が示されている）活性化制御能を持つことを示し、これらの実験系における糖鎖シグナルの役割を明らかにした。更には、新規物質のヘパラン硫酸糖鎖ミメティクスである硫酸化ジェランが強い癌転移抑制活性を示すことを発見し（特許申請中：出願番号：特がん 2004-244405）、抗癌転移剤としての臨床的応用の可能性を示した。

〈中田〉

１）上皮性癌細胞の産生するムチン（糖タンパク質）の生物学的意義について；上皮性癌細胞の産生するムチンと免疫系細胞との相互作用を解析し、癌組織におけるムチンを介した糖鎖シグナルの生物学的意義について明らかにした。ムチンに結合しうる免疫系細胞上の受容体を検索した結果、単球／マクロファージ上のスカベンジャーリセプター（SCR）や種々の免疫系細胞上の糖鎖結合タンパクであるシグレックファミリー（シグレック 2，3，7）についてムチンと結合しうることがわかった。SCR を介した系では、ムチンの結合によりシクロオキシゲナーゼ２が誘導され、プロスタグランジン E_2 の産生が亢進した。プロスタグランジン E_2 により免疫系のバランスが Th2 に偏ること、血管新生因子の産生亢進などを通して、癌細胞の増殖・進展に有利な環境を整えていることがわかった。シグレックについても、B 細胞のシグナル伝達の抑制や NK 細胞の細胞障害活性のムチンを介した糖鎖シグナルによる抑制などが明らかになった。

２）マウス脳に存在するシンデカン-3 の生物学的意義について；マウス胎児における癌胎児性糖鎖抗原の発現を検討する過程で、脳特異的に Tn 抗原が発現することを見いだした。コアタンパク質はシンデカン-3 であることを示すとともに、ニューロカンと結合することも見いだした。また、この糖鎖シグナルを介した分子間相互作用は小脳顆粒細胞の神経突起の形成に関与することを見いだした。

〈竹内〉

喫煙による肺胞マクロファージの免疫機能低下、遺伝子損傷、癌細胞の肺転移への影響とその機構についてマウスに一定量、一定期間シガッレトタバコ主流煙を曝露し検討した。喫煙により、肺胞マクロファージの抗原提示機能の低下、LPS による B 細胞増殖反応の低下が認められ、その低下機構には喫煙により産生増強された活性酸素により抗原提示に関係した肺胞マクロファージのクラス II、B7-1 と LPS に対する CD14 などの細胞表面抗原発現低下、また IL-1β、TNA-α の mRNA 発現が抑制されたことが示された。さらに、これらの発現低下は、肺胞マクロファージの DNA 損傷による可能性が示唆された。また、肺への癌転移に関しては、喫煙マウスで肺への癌転移が促進され、肺毛細血管に ICAM-1 の発現が認められた結果より、癌細胞が毛細血管壁に接着し易くなり肺への転移が促進された可能性が示唆された。これらの成績から、喫煙により肺の免疫機能は低下し、特に肺胞マクロファージを介した B 細胞反応系が強く抑制され、肺感染が起こり易い状況が引き起こされていると考えられる。

２）評価

本プログラム、「糖鎖シグナルと生体防御」、はタンパク質、核酸とともに第三の生命の鎖とされている糖鎖の生命現象における意義を解明し、「生体防御」という基礎医学的観点からその具体的医学応用の方向を探索することを目指したものである。本プログラムは、ヒトゲノムが事実上完全に解明された現在、タンパク質、遺伝子、糖鎖の生物学的機能の詳細を基盤に生命現象を研究する 21 世紀初頭の「ポストゲノム」研究の最先端に位置づけることができる生命科学研究分野であると言えよう。また糖鎖の持つ分子シグナルを臨床医学で重要な課題である発癌メカニズム、免疫機構といった生体防御機構の解析に結びつける研究方向性も意義が大きい。本研究プログラムを中心的に遂行した、岡山、中田、竹内らはそれぞれプロテオグライカン、ムチン型糖鎖、肺癌発生過程におけるマクロファージの役割に関する研究分野で多くの業績を持ち世界的に認められた研究者であったが、プログラム期間中にはさらに学外の共同研究者とも活発な研究情報交換や共同研究がなされ、プログラムの遂行にととまらず、将来に継続できる共同研究の基盤が形成されたと考えられ

る。期間中に各研究者はそれぞれ計画された研究課題にそった着実な研究業績をあげ、その要旨は上記項目(1)に示した。この間（平成15年5月現在の中間報告までにおいて）国際誌に発表した英文原著論文数14報をはじめとして、著書7編、学会発表54報等があり、平成14年度には同表題の公開セミナーも開催するなど活発な研究活動を展開した。特に意義の大きい発見として評価できるのは、(岡山ら)(1)シンデカン-2の発現と癌転移能との間には逆相関があることを示し、その背後にシンデカン-2が、(a) 血管新生制御能、及び、(b) 癌転移への直接的関与が示されているMMP-2の活性化制御能を有することが深く関連していることを示した点。更には、MMP-2活性化制御へのシンデカン-2へパラン硫酸糖鎖の関与の機構として、MMP-2の活性化受容体（細胞膜型マトリックスメタロプロテアーゼ-1：MT1-MMPとTIMPとの複合体分子）とシンデカン-2のヘパラン硫酸鎖との間におけるproMMP-2の奪い合いの機構を新しい機構として提唱した点。(2)新規物質硫酸化ジェランによる癌転移抑制にも成功した点であろう。本物質は微生物や海藻由来の多糖、ジェラン、を化学合成反応で硫酸化したもので、生体に対して毒性を持たず、動物臓器由来でないためウイルスやプリオン等の混入の危険性が無く、又、安価で大量製造が可能である等、臨床医学応用に適した物質であることが提唱された。(中田ら)(1)単球／マクロファージ上のスカベンジャーリセプターにムチンが結合することを示し、この糖鎖シグナルを介して(2)同細胞でシクロオキシゲナーゼ2の誘導、プロスタグランジンE_2の産生が亢進することを示した。さらに糖鎖シグナルは(3)プロスタグランジンE_2の血管新生の誘導やTh2バランスへの偏りなどを通して、癌細胞の増殖・進展に有利な環境をつくることを示した。また、(4)実際の担癌患者の血清中のムチンでも、末梢血単球を活性化することを示した。(5)シグレック2，3，7などがムチンに結合し、その糖鎖シグナルが免疫抑制にかかわることを見いだした。(6)マウス胎児期脳に発現しているシンデカン-3にTn抗原が発現していることを見いだした。(7)シンデカン-3はヘパラン硫酸糖鎖を介してニューロカンに結合することを見いだし、ニューロカンではC末側のEGF様ドメインが結合に必須であることがわかった。(8)シンデカン-3を介した糖鎖シグナルはニューロカンとの分子間相互作用を通じて小脳顆粒細胞の神経突起形成に関与していることがわかった。(竹内ら) 肺胞マクロファージの免疫機能は、喫煙により生じた活性酸素により肺組織、肺胞マクロファージのDNA損傷が引き起こされた結果、機能低下となり、さらに染色体、遺伝子の異常が引き起こされ、肺癌の発生、癌細胞の肺転移にこれら要因が密接に関係していることが見出された。喫煙による免疫機能の低下、活性酸素の増加、DNA損傷、染色体異常と肺癌の発生、癌細胞の肺転移に関しての系統だった研究はこれまでほとんど行われておらず、その意味でも意義ある発見であった。また竹内の確立した喫煙を介した肺胞マクロファージの免疫機能の低下と肺癌発生を関連付ける実験系は、岡山、中田らの解析したプロテオグライカン、ムチン型糖鎖による糖鎖シグナルと癌発生機構の関連性の解析に使用できる可能性をもち、将来にわたってプログラム内での新しい共同研究課題として発展することも期待される。

以上。

バイオベンチャー研究開発拠点整備事業　プロジェクト１

「糖鎖シグナルと生体防御」

平成１７年４月

発行　京都産業大学

〒603-8555　京都市北区上賀茂本山

印刷　株式会社 田中プリント

KYOTO SANGYO UNIVERSITY